The Dissertation Committee for Farhad Ahmadi Koutalan certifies that this is the approved version of the following dissertation:

Displacement-based Seismic Design and Tools for Reinforced Masonry Shear-Wall Structures

Committee:

Richard E. Klingner, Supervisor

James O. Jirsa

Sharon Wood

Joseph A. Yura

Stelios Kyriakides

Displacement-based Seismic Design and Tools for Reinforced Masonry Shear-Wall Structures

by

Farhad Ahmadi Koutalan, B.S., M.S.

Dissertation

Presented to the Faculty of the Graduate School of
The University of Texas at Austin
in Partial Fulfillment
of the Requirements
for the Degree of

Doctor of Philosophy

The University of Texas at Austin
December 2012

Dedication

I dedicate this dissertation to my loving wife, Roxana,
who followed me halfway around the world in the pursuit of a dream.

To my parents, for their infinite love and support.

Acknowledgements

I would like to express my most sincere thanks and appreciation to Dr. Richard E. Klingner for his advice, guidance, and support throughout my PhD program at UT Austin. I am also pleased to acknowledge the financial support provided by the National Institute of Standards and Technology (NIST). Deep thanks are also due to Brazos Masonry Inc. for their financial support and help in constructing the masonry shear walls at the University of Texas at Austin.

Many thanks are due to Dr. Benson Shing, Dr. David McLean, Dr. Stavridis, and Marios Mavros for their valuable assistance and guidance. I want to express my special gratitude to Jaime Hernandez and Geoff Scheid for their hard work, which made it possible to carry out our test program successfully. Special thanks are given to the staff of Phil M. Ferguson Laboratory and all the people who worked together on the project, "Displacement-based Seismic Design and Tools for Reinforced Masonry Shear-Wall Structures." My sincerest thanks are extended to my UT Austin colleagues involved with this joint project, Juan Rodriguez, Saleh Alogla, Steven Blair, Nick David, and Whitney Lee, who participated in different stages of the construction and testing of the masonry walls.

Besides all the support I had from my professor and colleagues, I cannot ignore my family's generous love and support during my PhD program at the University of Texas At Austin. My heartfelt gratitude goes to my wife, parents, family and friends for their support, encouragement, and love. I cannot imagine my life without them.

Farhad Ahmadi Koutalan

December 2012

Displacement-based Seismic Design and Tools for Reinforced Masonry Shear-Wall Structures

Publication No. ____________

Farhad Ahmadi Koutalan, Ph.D.
The University of Texas at Austin, 2012

Supervisor: Richard E. Klingner

The research described here is part of a multi-university project on "Performance-based Seismic Design Methods and Tools for Reinforced Masonry Shear-Wall Structures." Within the context of that project, the objective of the research described in this dissertation was to develop and validate a specific displacement-based seismic design methodology for masonry structures. Experimental work consisted of reversed cyclic loading tests of reinforced masonry wall segments with different boundary conditions, aspect ratios, axial loads, and reinforcement detailing. Analytical work consisted of developing analytical models for in-plane concrete masonry shear wall segments; calibrating those models using reversed cyclic test data; and using those models to successfully predict the nonlinear seismic response of two full-scale, multi-story reinforced masonry specimens tested on the shake-table at the University of California at San Diego. Design work consisted of the force-based and displacement based design of those specimens. Based on the results, provisions for displacement-based seismic design are proposed for inclusion in United States design codes.

Table of Contents

CHAPTER 8 Shake-Table Performance of Full-Scale, Two-Story Specimen (September 2012) 232

List of Figures

List of Tables

CHAPTER 1

Introduction

1.1 OUTLINE OF OVERALL PROJECT

From June 2010 through December 2012, the United States National Institute for Standards and Technology (NIST) sponsored a research project, “Performance-based Seismic Design Methods and Tools for Reinforced Masonry Shear-Wall Structures.” That project used shaking-table facilities at the University of California at San Diego, provided by the United States National Science Foundation’s Network for Earthquake Engineering Simulation (NSF NEES). In addition to direct funding and equipment support from the NIST and NSF NEES program, this project received financial and in-kind support from many segments of the masonry industry.

The overall objectives of this project were to develop and validate an innovative displacement-based design procedure for masonry shear walls; to produce much-needed experimental data to improve current design requirements; and to develop effective ways of confining boundary elements in flexure-dominated walls. This project consisted of the following major tasks:

- develop displacement-based design methods for reinforced masonry structures;
- conduct reversed cyclic load tests on masonry wall segments;
- improve analytical models for reinforced masonry shear walls; and
- use full-scale shake-table tests to check displacement-based seismic design;

Project participants included the following:

- The University of Texas at Austin (Richard E. Klingner, Farhad Ahmadi, Jaime Hernandez Barredo, Juan Diego Rodriguez, and Saleh Alogla);
- The University of California at San Diego (Benson Shing, Marios Mavros, and Andreas Stavridis, now at the University of Texas at Arlington); and
- Washington State University (David McLean, Jake Sherman, Christina Duncan Kapoi, and Will Cyrier).

The experimental work carried out in this project consisted of the following:

- conduct in-plane, reversed cyclic loading tests of cantilever wall segments with different levels of prescriptive detailing, axial loads, and aspect ratios;
- conduct in-plane, reversed cyclic loading tests of cantilever wall segments with detailing based on displacement-based design principles;
- conduct in-plane, reversed cyclic loading tests of fixed-fixed wall segments with different levels of prescriptive detailing, axial loads, and aspect ratios;
- conduct shaking-table tests of a full-scale, 3-story reinforced masonry specimen with a regular configuration of openings; and
- conduct shaking-table tests of a full-scale, 2-story reinforced masonry specimen with an irregular configuration of openings.

The analytical work carried in this project consisted of the following:

- develop analytical models for in-plane shear-wall segments of reinforced concrete masonry, and calibrate the models using reversed cyclic load test data;
- use those models to predict the nonlinear seismic response of complex, reinforced masonry structures;
- use those models to verify limit-design provisions of the draft 2013 Masonry Standards Joint Committee (MSJC) *Code*; and
- use those models as part of a systematic framework for displacement-based seismic design of masonry structures.

The experimental and analytical work centered around two full-scale, shake table specimens: a 3-story reinforced masonry specimen with a regular configuration of openings (Figure 1.1); and a 2-story reinforced masonry specimen with an irregular configuration of openings (Figure 1.2).

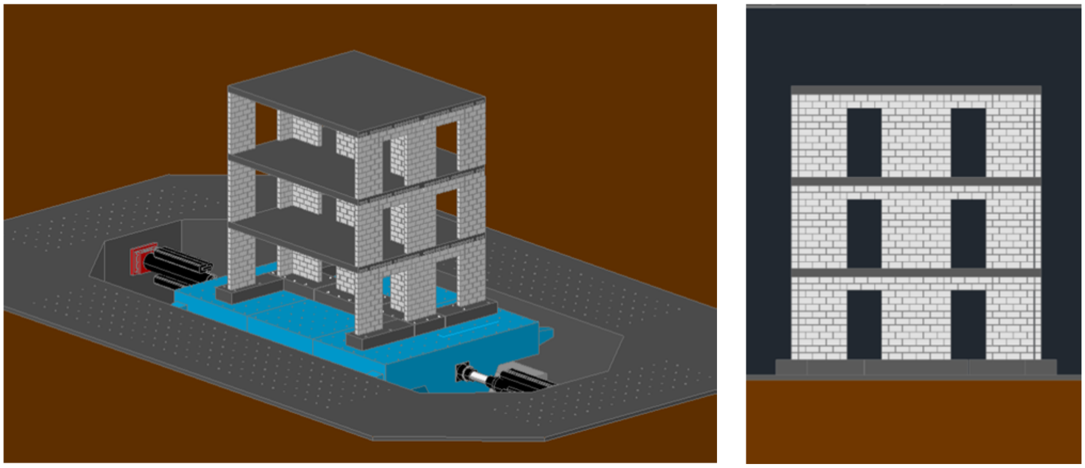

Figure 1.1 Schematic views of full-scale, 3-story reinforced masonry specimen

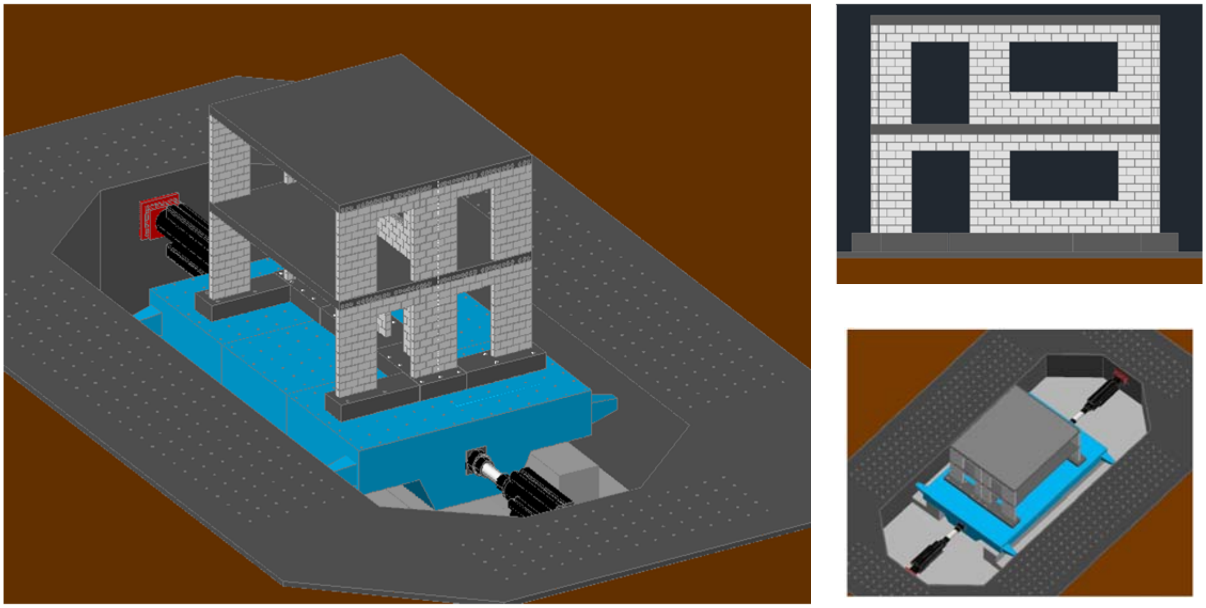

Figure 1.2 Schematic views of full-scale, 2-story reinforced masonry specimen

1.2 OBJECTIVES AND SCOPE OF THIS DISSERTATION WITHIN THE PROJECT

The research described by this dissertation was conducted as part of the project outlined in Section 1.1: experimental work, analytical work and development of refined displacement-based design provisions. The primary objective of this dissertation is to develop systematic procedures for displacement-based seismic design of masonry shear-wall structures. This dissertation also provides a comprehensive validation of a specific displacement-based seismic design procedure for reinforced masonry structures. The procedure produces structures that behave reliably in strong earthquakes. It is more consistent and transparent than current force-based seismic design procedures. It can be used for structures with irregular configurations of openings that are difficult or practically impossible for force-based design, and that are commonly encountered in practice. This design procedure is suitable for experienced design offices. The research described in this dissertation also has the following secondary objectives:

- study the seismic performance of reinforced masonry shear-wall segments;
- study the inelastic behavior of low-rise reinforced concrete masonry structures with different configurations of openings; and
- refine and validate MSJC draft limit-design provisions for reinforced concrete shear-wall structures.

The experimental work of this dissertation included the following:

- design, construct, and conduct reversed cyclic load tests of cantilever and fixed-fixed concrete masonry wall segments with different design parameters;
- evaluate the results of those tests;
- design two full-scale specimens using force-based and displacement-based methods;
- participate in the shake-table testing of those two specimens; and
- evaluate the results of those shake-table tests.

The analytical work of this dissertation included the following:

- develop analytical models for in-plane concrete masonry shear wall segments, and calibrate the models using reversed cyclic load test data;
- use those models to predict the nonlinear seismic response of complex, reinforced masonry structures; and
- use those models to verify limit-design provisions of the draft 2013 Masonry Standards Joint Committee (MSJC) *Code*; and
- use those models as part of a systematic procedure for displacement-based seismic design of reinforced masonry structures.

1.3 ORGANIZATION

Details of the work completed to meet the previously described objectives are presented in the following chapters. In Chapter 2, the current force-based design approach to the design of reinforced masonry shear-wall structures is briefly described, and its historical basis is reviewed. Deficiencies inherent in that approach are outlined, and those deficiencies are used as a way of introducing other design approaches, based on deformations rather than forces. Chapter 3 addresses the overall project reversed cyclic testing program; the wall specimens and test setups used at UT Austin; construction procedures; testing procedures; and material properties. Test results and test results evaluation for cantilever shear walls and fixed-fixed shear-walls tested at UT Austin are discussed in Chapter 4 and Chapter 5, respectively. Chapter 6 presents a detailed description of the 3-story full-scale specimen's design, shake-table testing, observations and results from the shake-table tests, and overall structural performance. Chapter 7 deals with the development and verification of effective and reliable approaches for displacement-based seismic design of masonry structures. In Chapter 7, the proposed analytical models for masonry shear-wall structures are checked against the reversed cyclic load test results of the CMU wall specimens described in Chapters 4 and Chapter 5, and against the shake-table test results of the 3-story, full-scale, CMU building described in Chapter 6. Finally, as the heart of this dissertation, in Chapter 8, the technical basis for a specific displacement-based seismic design procedure is developed for multi-story masonry shear-wall structures. In Chapter 8, that proposed procedure is applied to the seismic design of full-scale, 2-story reinforced masonry shear-wall system with a complex configuration of openings, and is validated using shake-table tests of that specimen. Based on the results, displacement-based seismic design is proposed for inclusion in United States design codes for masonry structures.

CHAPTER 2

Background

In this chapter, the current force-based design approach to the design of reinforced masonry shear-wall structures is briefly described, and its historical basis is reviewed. Deficiencies inherent in that approach are outlined, particularly as applied to reinforced masonry structures designed using the MSJC *Code* (2011) and ASCE/SEI 7 (2010). Those deficiencies are used as a way of introducing other design approaches, based on deformations rather than forces. In that context, the limit-design procedure included in the draft 2013 MSJC *Code* is briefly discussed, followed by a review of displacement-based design for masonry structures.

2.1 FUNDAMENTAL BASIS FOR SEISMIC DESIGN OF CONCRETE MASONRY IN THE UNITED STATES

The seismic design of masonry shear-wall structures in the United States is based on the premise that reinforced masonry structures can perform well in earthquakes, provided that they meet the following conditions (Bozorgnia and Bertero 2004):

1) They must have engineered lateral force-resisting systems, generally consisting of reinforced masonry shear walls distributed throughout their plan area, and acting

in both principal plan directions. The typical seismic response of a low-rise reinforced masonry shear-wall structure with reinforced concrete diaphragms is shown schematically in Figure 2.1, for shaking parallel to a principal plan direction of the structure.

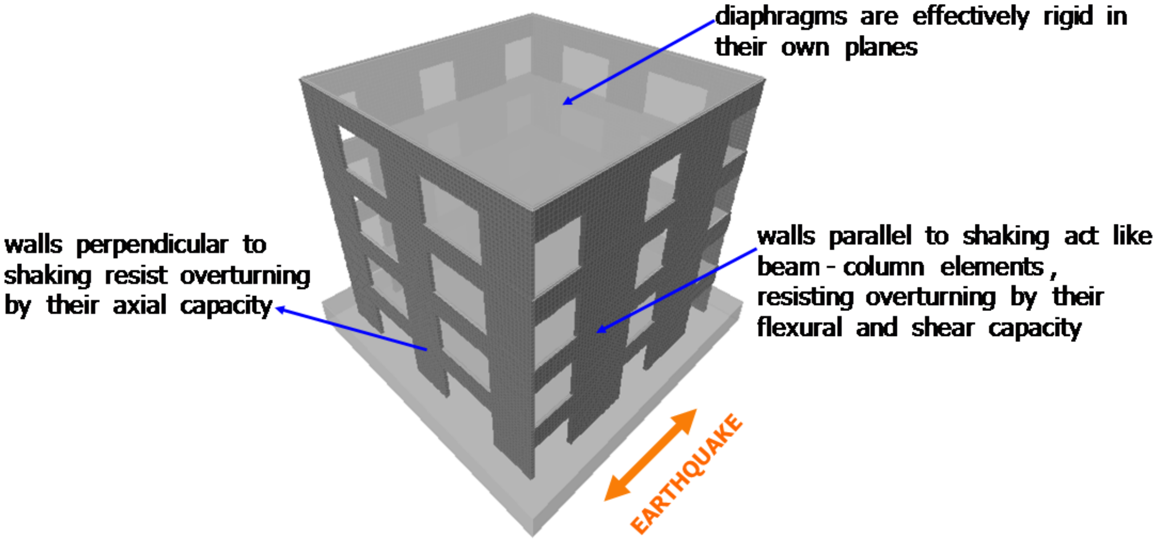

Figure 2.1 Seismic behavior of reinforced masonry shear-wall structure

2) Walls oriented perpendicular to the direction of shaking (out-of-plane walls) behave as vertically spanning beams, transfer the lateral loads to the foundation and the diaphragms, and resist overturning by their axial capacity. Diaphragms are effectively rigid in their own planes, and transfer lateral loads to the shear walls oriented parallel to the direction of shaking. Walls oriented parallel to the direction of shaking (in-plane walls) transmit the diaphragm reactions at the floor levels to the foundation. The construction joints present at each end of the lintels partially or completely uncouple the in-plane walls connected by the lintels (Jo 2010).

3) Structural load-displacement characteristics under cyclic reversed loading must be consistent with the assumptions used to develop their design loadings (Bozorgnia and Bertero 2004):

   a) If shear walls are intended to behave elastically, they must be provided with sufficient strength to resist elastic lateral forces.

   b) If shear walls are intended to behave inelastically, they must be detailed and proportioned to be capable of resisting the effects of the reversed cyclic deformation demands.

2.2 FORCE-BASED SEISMIC DESIGN OF BUILDINGS

Current United States seismic design provisions (ASCE/SEI 7-10 2010), including those for masonry structures, are force-based. In this section, the background of those provisions is reviewed, and their inherent limitations are noted.

2.2.1 Background on Seismic Design Provisions for Masonry in the United States

The traditional approach to force-based seismic design of buildings is to define the load applied to the building; to carry out a preliminary design of each element of the building; to analyze the building as designed; and to verify that each element, and the entire building, satisfies requirements for stress or force (Ghobarah 2001).

Prior to the 1980s, masonry design provisions in the United States were a combination of allowable-stress design and empirical design, and did not address the possibility of inelastic behavior. A very significant step in the evolution of US masonry design provisions was the research carried out by the Technical Coordinating Committee for Masonry Research (TCCMAR), supported by the National Science Foundation and the masonry industry. The TCCMAR program began in February 1984 and lasted for 10 years. Its main objective was to define and perform the analytical and experimental research necessary to improve masonry structural technology, and to provide the technical basis for strength design provisions of masonry structures (Bozorgnia and Bertero 2004).

The TCCMAR program comprised many research tasks. Assis *et al.* (1989) addressed basic stress-block parameters for flexural behavior. Shing (1991b) reaffirmed basic design principles for flexure-dominated and shear-dominated masonry shear-wall segments. Leiva and Klingner (1991) studied seismic behavior and design of low-rise masonry shear wall structures with openings. He and Priestley (1992) addressed flanged shear-wall segments, and proposed effective flange widths for them. Finally, Seible *et al.* (1992, 1994a, 1994b) addressed the structural performance and design of masonry wall structures, and tested a full-scale, five-story reinforced masonry structure, using pseudo-dynamic testing to simulate earthquake ground motions. Their specimen showed good inelastic behavior under overall drift ratios exceeding 1%, confirming that reinforced masonry structures can exhibit significant ductility, and verifying field observations and previous TCCMAR laboratory testing (Bozorgnia and Bertero 2004). Results of the TCCMAR program were then applied to the force-based seismic design of masonry structures (Bozorgnia and Bertero 2004).

Limited shaking-table tests have been conducted on reinforced masonry structures built using typical modern US practice. A series of single-story, one-third scale masonry structures were constructed and subjected to shake-table testing (Gulkan *et al.* 1990a and 1990b). The main objective of the testing was to verify prescriptive reinforcement details for reinforced masonry shear walls in moderate seismic zones (Gulkan *et al.* 1990a and 1990b). Two, three-story, quarter-scale reinforced masonry structures were tested to validate small-scale testing (Abrams and Paulson 1991). Cohen (2001) tested two low-rise, half-scale reinforced masonry buildings with flexible roof diaphragms subjected to shake-table testing, and compared test results with the results of static testing and analytical predictions. Results of these tests generally support field observations of satisfactory behavior of modern reinforced masonry structures in earthquakes.

As a part of a recent NSF NEES project, concrete masonry wall segments with clay masonry veneer were tested under reversed cyclic out-of-plane and in-plane loading (Jo 2010). Identical wall segments also were tested on a shaking table, and a full-scale, one-story structure was tested on a shaking table. That research program showed that low-rise reinforced concrete masonry buildings with clay masonry veneer, designed and constructed according to the requirements of the 2008 MSJC *Code* and *Specification* for SDC E, can resist earthquakes above Maximum Considered Earthquake (MCE) without collapse (Jo 2010).

2.2.2 Review of Force-Based Seismic Design

Current United States seismic design provisions (ASCE/SEI 7-10, MSJC 2011) use force-based seismic design for structures, including reinforced masonry structures. In the US, ASCE/SEI 7-10 first prescribes seismic design loads in terms of a building's geographic location, its function, and the characteristics of the underlying soil. These three descriptors define the building's "seismic design category." For example Seismic Design Category A corresponds to a low level of ground shaking, typical use and typical underlying soil. Increasing levels of ground shaking, increasingly essential nature of the facility, and unknown or undesirable soil types correspond to higher seismic design categories, with Seismic Design Category F being the highest.

The sequence of operations required in force-based seismic design can be summarized as follows:

The masonry building is assigned a seismic design category (SDC). That SDC corresponds to a list of permitted lateral resisting systems, each with its force-reduction *R*-factor representing a combination of probable system ductility and system over-strength. Generally the *R*-factor is specified by ASCE/SEI 7, and is not a design choice. Although the designer may elect to use a lower value than the code-specified one, the required wall type must be used. Masonry buildings in seismic design categories D and higher are required to have seismic force-resisting systems composed of so-called "special" reinforced masonry shear walls. Such structural systems are assigned a seismic force-reduction factor (*R*-factor) of 5, consistent with an expected displacement ductility of about 3.5 and an assumed structural over-strength of about 1.5.

The assignment of a building to a particular seismic design category requires, in addition to the seismic forces noted above, compliance with four types of prescriptive requirements, whose severity increases as the building's seismic design category increases from A to F (Bozorgnia and Bertero 2004):

- Seismic-related restrictions on materials;
- Seismic-related restrictions on design methods;
- Seismic-related requirements for connectors; and
- Seismic-related requirements for locations and minimum percentages of reinforcement.

Because seismic design forces depend on the calculated fundamental period of vibration of the structure, the fundamental period of the structure is calculated, using elastic stiffnesses based on preliminary estimates of member sizes. For masonry elements, cracked transformed stiffnesses are permitted to be used, reflecting expected flexural cracking in the elastic range. In ASCE/SEI 7 (2010) a default formula is also provided for calculating the fundamental period of masonry structures based on building height only, independent of member stiffness, mass distribution, or structural geometry.

Based on the initial cracked elastic structural period, and using elastic response spectrum reduced by the *R*-factor, the design base shear force is calculated and is distributed among masonry shear-wall segments according to their relative stiffnesses. Each masonry shear wall segment must be provided with sufficient flexural (longitudinal) reinforcement to resist its factored design moments and axial forces, and sufficient transverse reinforcement to resist its factored design shears. Segments of “special” reinforced masonry shear walls also must be designed for the shears consistent with the flexural capacity of the segment (capacity design for shear). Finally, each segment must meet prescriptive requirements for percentages and spacing of reinforcement. For segments of “special” reinforced masonry shear walls, the total reinforcement percentage (horizontal and vertical) must be at least 0.002, with at least one-third of this placed in each direction.

The maximum percentage of flexural reinforcement is limited to that consistent with a strain gradient varying from the maximum useful masonry strain at the extreme compression fiber to a factor α times the specified steel yield strain in the extreme-fiber tension reinforcement. The factor α depends on the expected ductility demand on the element, and is equal to 4 for the in-plane design of segments of special reinforced masonry shear walls. Although designers are offered the alternative of using confined boundary elements, no design procedures are yet available for such elements.

After wall segments are designed, inelastic seismic design displacements are calculated as the elastic displacements (cracked sections), multiplied by the displacement amplification factor (C_d). The resulting inelastic displacements must meet code limits.

2.3 LIMITATIONS OF FORCE-BASED SEISMIC DESIGN FOR MASONRY BUILDINGS

Although forced-based design has been used extensively in the last century and remains the basis for current seismic design codes, it has many limitations for typical masonry buildings. These limitations are discussed below.

2.3.1 Fixed-Valued Seismic Design Factors Are Inherently Inconsistent

The seismic design factors R, C_d, and over-strength factor (Ω_0) are intended to represent the inelastic behavior of classes of structures. They were developed primarily based on the response of long-period structures, and were further modified by engineering judgment. They are not consistently related to real structural behavior. In addition, the current requirement for higher levels of available displacement ductility in higher seismic design categories is not well justified. While some inelastic deformation capacity is required to reduce the probability of collapse under extreme ground motions, arbitrarily high levels of ductility (such as a required R-factor of 5 for the special reinforced masonry shear walls required in SDC D and higher) are not necessary. Post-earthquake reconnaissance studies of modern reinforced masonry buildings show that in strong earthquakes, buildings are much stronger and ductility demands are much lower than commonly assumed in design (Klingner 1994). Based on this observation, modern reinforced masonry buildings with high plan densities of walls can successfully resist seismic forces consistent with lower R-factors. This should be a design decision, not a code requirement. More stringent prescriptive detailing requirements for masonry walls do not necessarily result in higher available displacement ductility for a building composed of those walls, because the displacement ductility of a masonry structure also depends on the plan layout and the aspect ratios (ratios of height to plan length) of its walls.

The seismic force-reduction factor, R, represents a combination of displacement ductility and overstrength, both at the level of an entire structure. When MSJC design provisions based on that *R* are applied to the reinforced masonry walls comprising the structure's seismic force-resisting system, their net effect is to ensure that each wall (and each wall segment within a perforated wall) is flexure-dominated, with an available local rotational ductility consistent with the overall structural displacement ductility demand on which *R* is based. Whether or not the local rotational ductility implied by *R* is actually achievable depends on the aspect ratio (ratio of shear span to depth) each wall, and of each wall segment comprising a perforated wall. For example a typical low-rise masonry building with high plan densities of walls and low aspect ratio of wall segments is shown in Figure 2.2. This building will not achieve high ductility required R-factor for special shear walls, and even can successfully resist seismic forces consistent with lower R-factors. Current force-based seismic design codes (ASCE/SEI 7-10 and the 2011 MSJC *Code*) do not control the aspect ratios of walls or wall segments. As a result, for example, it is possible for a code-compliant special reinforced masonry shear wall to be incapable of ductile behavior.

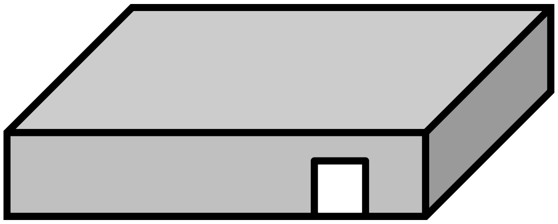

Figure 2.2 A typical low-rise masonry building with high plan densities of walls and low aspect ratio of wall segments

For many cantilever shear-wall buildings of reinforced masonry, code drift limits are consistent with actual ductility levels that are lower than those corresponding to the seismic design factors, making those factors irrelevant to design (Priestley 1993). This essentially requires an extra level of iteration in a conventional design using initial stiffness, because the strength and hence the stiffness cannot be fully defined until the behavior factor appropriate for the code drift limit can be determined (Priestley *et al.* 2007, Priestley 1993).

Evaluation of low-rise, masonry wall structures has shown that *R*-factors should be period-dependent. Future force-based seismic design codes in the US will probably be modified to address the above limitations. Requirements for higher available ductility in higher seismic design categories will be relaxed, and wall aspect ratios will be taken into account.[1]

2.3.2 Emphasis on Forces instead of Deformations is Misguided

Force-based seismic design improperly ignores deformation-related limit states. Limiting deformations is paramount for reinforced masonry shear-wall structures, because most structural and nonstructural damage to masonry buildings in recent earthquakes has been associated with excessive lateral displacements (Priestley et al. 2007). As shown in the curve of base shear versus lateral displacement of Figure 2.3, damage to a wall-type structure increases as deformations increase. In contrast, damage is poorly described by forces, which increases only slightly with increasing displacements. Therefore, seismic design should emphasize deformations instead of forces.

---

[1] Private communication, J. Daniel Dolan (member, Provisions Update Committee, Building Seismic Safety Council), March 2012.

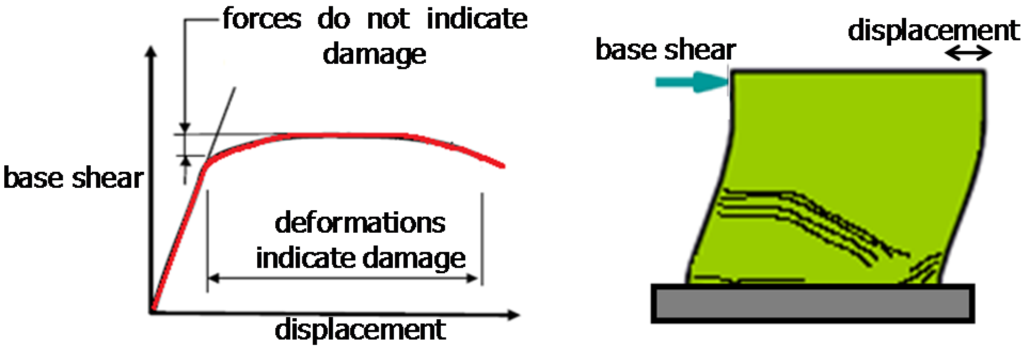

Figure 2.3 Schematic load-displacement curve and associated damage

2.3.3 Force-based Design Requires Incorrect Estimates of Initial Stiffness

In current force-based seismic design, the fundamental period of the structure is estimated using empirical equations provided by design codes, or is calculated using a cracked elastic stiffness. That fundamental period is then used to calculate seismic design base shear using a smoothed design response spectrum that includes the effects of inelastic response. Once the design seismic base shear has been determined, that same initial stiffness is also used to distribute that base shear among structural elements.

In seismic design of structures, if the dimensions of structural elements are known, the global stiffness and the fundamental period of the structure can be estimated with sufficient accuracy for calculating lateral base shear. This calculated base shear is independent of strength. Required global strength then depends on the assumed local and global stiffnesses, and the required strength of each seismic force-resisting element depends on that initial cracked stiffness (Priestley *et al.* 2007). When masonry shear walls are the primary seismic force-resisting elements, the assumption of stiffness being independent of strength is invalid.

2.3.4 Force-based Design Incorrectly Applies the Principle of Equivalent Displacements to All Structures

Based on the elastic initial structural period and using a smoothed elastic response spectrum reduced by the *R*-factor, the design base shear is calculated. This reduction is based on the principle that the maximum displacement of an inelastic structure is equal to the maximum displacement of an otherwise identical elastic structure. This principle is based on the work of Newmark and Hall (1982) for single-degree-of-freedom, elasto-plastic systems, and is generally valid for long-period structures. However, it is not valid for short-period structures such as low-rise masonry shear-wall structures (Priestley *et al.* 2007, Priestley 1993).

In applying the principle of equivalent displacements, it is common to specify a level of elastic damping (typically 5% of the critical damping of the structure) to represent damping in the initial stages of response, before inelastic damping is activated. There are a number of methods to specify this elastic damping, but the principal difference is whether the damping force is related to the initial or to the tangent stiffness. In initial-stiffness elastic damping, the damping force is always related to the initial stiffness, while in tangent-stiffness damping, the damping force reduces when the stiffness reduces as a consequence of onset of the inelastic response (Priestley *et al.* 2007).

Choosing initial-stiffness or tangent-stiffness damping has significant importance in procedures based on the principle of equivalent displacements. Inelastic displacements predicted using initial-stiffness versus tangent-stiffness elastic damping differ by as much as 50% (Priestley and Grant 2005). Such differences increase at low initial periods, high ductility ratios, and with hysteresis models with low energy dissipation capability (Priestley 2007).

2.3.5 Force-Based Seismic Design is Difficult for Perforated Walls

The problems underlying the design of perforated walls are neither simple nor new. Masonry wall configurations are most frequently proportioned by enclosure and function requirements; for these walls, structural performance is an afterthought. Masonry design provisions need to anticipate a wide variety of wall configurations; however, the overall behavior of perforated wall configurations cannot be easily distinguished, ductile from non-ductile, simply by analysis of the force distribution to the various wall segments of which it consists, particularly if those forces were determined using conventional linear-elastic methods of analysis. Masonry buildings in zones of high seismic risk are commonly composed of masonry shear walls with openings. Design of those walls leads to specific examples of the general shortcomings noted above.

A squat wall without openings (Figure 2.4a) is difficult or impossible to design for ductile behavior, regardless of prescriptive reinforcement requirements. Design for ductility must include wall aspect ratio, not just wall detailing. It would be feasible to design this wall for limited ductility and shear-dominated behavior, but that option is prohibited by current code provisions. The wall shown in Figure 2.4b is a taller wall. Its aspect ratio permits it to be designed for ductile, flexure-dominated behavior using current MSJC provisions. It is not realistic in many cases; however, because most shear walls have openings. The wall shown in Figure 2.4c is the same wall, but with openings arranged in a regular manner over the height of the wall. In many configurations, it cannot be sensibly designed using the current code. Consider, for example, the small wall segment to the left of the door in Figure 2.4c. Under in-plane lateral load, that segment is subjected primarily to axial compression and axial tension. It should not have to be designed for flexural ductility. The alternative of confined boundary elements is not practical. While the plastic hinge regions of the shear wall need to be carefully detailed, it is unnecessary and counter-intuitive to require uniform seismic detailing for the entire wall.

Finally, consider the wall of Figure 2.4d, with irregularly located openings. The available ductility of each wall segment depends on its aspect ratio, flexural reinforcement, detailing, and capacity design for shear. Current code requirements will not result in predictable inelastic behavior for this wall.

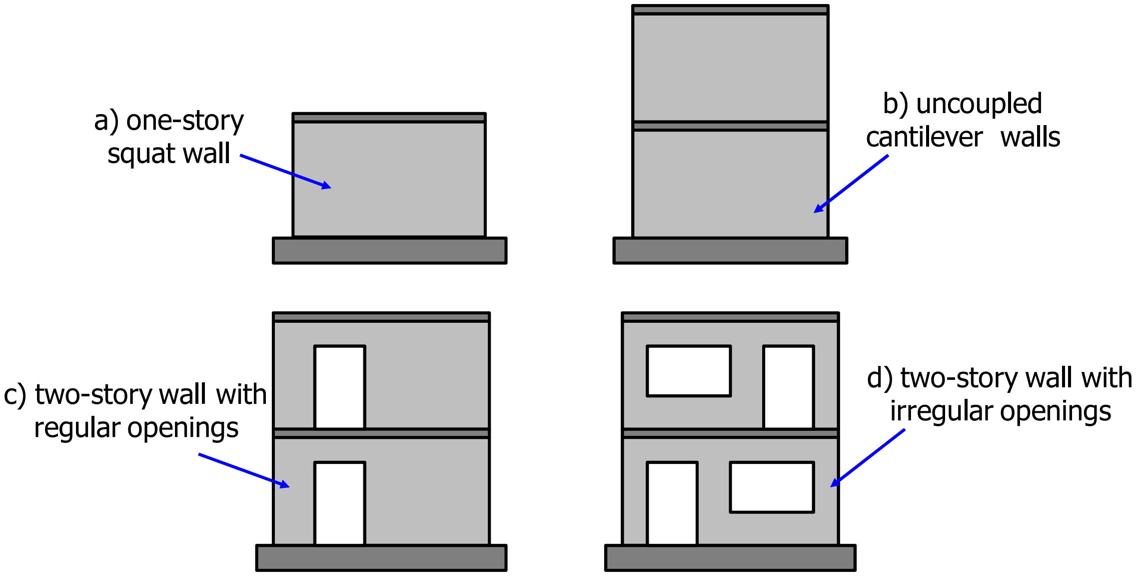

Figure 2.4 Reinforced masonry shear walls

2.3.6 Force-based Design Uses Technically Questionable Requirements for Prescriptive Reinforcement

Current prescriptive reinforcement requirements for special reinforced masonry shear walls are potentially wasteful and irrational. They can provide ductility where it is not required, and can provide insufficient ductility where it is actually required. They do not address shear-dominated wall segments, and they require uniform prescriptive detailing even in wall segments that are so strong that they will never yield.

Ductile detailing should be required only in wall segments where inelastic deformations are expected, such as flexural hinge zones. Current prescriptive reinforcement requirements for special reinforced masonry shear walls are in many cases unrealistic and irrational. Reinforcement requirements for out-of-plane load can lead to vertical reinforcement that exceeds the maximum permitted reinforcement ratio for the prescribed wall designation, even though the actual in-plane ductility demand on the wall is less than implied by that calculation. The designer is not permitted to trade increased strength for decreased ductility. This problem is especially difficult in walls with irregularly located openings, because the wall segments defining window and door openings can easily experience maximum out-of-plane moment and maximum in-plane moment at about the same locations. Furthermore, because the designer is not required or encouraged to check directly the load-deformation response of the wall segments comprising the special masonry shear wall, code requirements are not linked as directly as they might be to particular modes of behavior. Because prescriptive requirements are triggered by the shear wall designation rather than the expected performance of each wall segment, some segments may be under-detailed, and others may be over-detailed. They are primarily force-based, with overlays of prescriptive requirements (reinforcement percentage and spacing), ρ_{max} requirements, and capacity-design requirements. Current MSJC requirements for special reinforced masonry shear walls do not require consistent checks for the start of local inelastic deformation that generally causes concentrated damage and may cause collapse.

Despite this criticism, current force-based seismic design, when combined with capacity design principles and careful structural element detailing, generally provides safe seismic designs for reinforced masonry structures. However, the degree of protection provided against damage under a given seismic hazard level can vary from structure to structure (Priestley 2007).

2.4 IMPROVED SEISMIC DESIGN METHODS

New seismic design methods, representing improvements to force-based seismic design, have been proposed for concrete and masonry shear-wall structures. These methods can be categorized as “Deformation Calculation-based Design” and “Deformation Specification-based Design” (Priestley *et al.* 2007). An abstract of each method is provided below.

2.4.1 Deformation Calculation-based Design

Deformation Calculation-based Design relates the detailing of plastic hinging regions to calculated local deformation demands under seismic loads. Strength is related to force-based design method with specified seismic design parameters such as force-reduction factors and displacement-amplification factors. Nonlinear analytical tools such as inelastic push-over analyses can determine local deformation demands, typically in the form of flexural plastic hinge rotations or shear hinge deformation ratios. Reinforcing details are then determined from state-of-the-art relationships between reinforcing details and local deformation demands. Initial work on this procedure was related to bridges, and was followed by work on reinforced concrete and masonry structures. These approaches can produce structures with a uniform risk of collapse, but not a uniform risk of local damage (Priestley *et al.* 2007).

One new proposed Deformation Calculation-based Design approach for reinforced masonry structures, the 2013 MSJC Limit Design Method, is presented in more detail in Section 2.5.

2.4.2 Deformation Specification-based Design

In last decade, a number of seismic design approaches have been developed whose goal is to achieve a specified local deformation level under design earthquakes.

These approaches provide more philosophically satisfying seismic design methods than current force-based methods, because damage can be directly related to local inelastic deformations. For this reason, designing structures to achieve a specified global displacement (or specified local deformation) limit implies designing for a specified risk of damage. Structures designed by this method provide a uniform risk of damage, rather than the variable risk associated with current force-base design methods and with deformation calculation-based design methods (Priestley *et al.* 2007).

Different procedures have been proposed and validated to achieve specified local deformations under specified hazard levels. One of these procedures uses the secant stiffness to maximum displacement, based on a "Substitute Structure" characterization and an equivalent elastic representation of hysteretic damping at maximum response (Gulkan and Sozen 1974, Shibata and Sozen 1976). These methods generally require some iteration to achieve the specified displacement. They are known as Displacement-based Design (DBD) methods (Priestley *et al.* 2007), and they are discussed further in Section 2.6.

2.5 2013 MSJC LIMIT DESIGN

Although future seismic design provisions for masonry will probably include displacement-based procedures, their development and implementation will take time, because they will require modifications to both the MSJC *Code* and the national load standard, ASCE/SEI 7. For this reason, Limit Design has been proposed as an intermediate step in the draft 2013 MSJC *Code* (Lepage *et al.* 2011).

The draft 2013 MSJC Limit Design procedure provides alternative design provisions for special reinforced masonry shear walls subjected to in-plane seismic loading, and it is considered to be particularly useful for perforated wall configurations for which a representative yield mechanism can be determined. The procedures have not been approved, but are published as part of the public comment period for the 2013 edition of the MSJC *Code*[2]. Limit design requires the following steps, evaluated in each principal plan direction of the structure:

1) Design base shear is calculated by current force-based procedures of ASCE/SEI 7, along with the corresponding elastic displacement, δ_e . The designer must use the seismic loading condition that produces the maximum base shear demand along the line of resistance (ASCE/SEI 7).

2) The controlling yield mechanism must be determined. In many cases, such as cantilever walls, this determination is simple. In others, such as perforated walls, it may be more complicated and pushover analysis can be used.

3) The design mechanism displacement, δ_u, is defined using $C_d \delta_e$ for a target displacement at the developed mechanism. The required inelastic deformations are calculated by a rigid-plastic analysis or an inelastic analysis.

4) Each wall segment that undergoes inelastic deformation is evaluated for shear-limited behavior. The moment capacity of a flexural hinging region is not permitted to exceed to that corresponding to the development of a shear at most one-half the shear strength of the wall segment. This stratagem effectively reduces the strength of the controlling yield mechanism involving wall segments vulnerable to shear failure[2].

5) The designer must verify that the selected mechanism is the critical one. If yielding is detected away from the selected plastic hinge locations, the designer has the choice of changing the selected plastic hinge location to recognize that

---

[2] draft 2013 MSJC Code, circulated as part of the public comment period, September 2013.

yielding, or of placing additional reinforcement at the section where yielding is detected.

6) The inelastic deformation demands calculated in Step 3 above are compared with inelastic deformation capacities. Flexural deformation capacities are based on ultimate curvatures in hinging regions, ignoring elastic deformations away from the hinges. Shear-critical wall segments are assigned a default drift capacity of 1/200, which is increased to 1/100 if the segment has at least a 0.1% reinforcement ratio in the longitudinal and transverse directions. These drift capacities are based on published research results, combined with engineering judgment.

2.6 DISPLACEMENT-BASED SEISMIC DESIGN

In this section, displacement-based seismic design is reviewed. Displacement-based seismic design explicitly calculates a building's probable seismic response under a specified design earthquake, and designs the building so that its inelastic deformation capacity equals or exceeds the inelastic deformation demand associated with that design earthquake.

2.6.1 Background on Displacement-based Design of Buildings

Displacement-based design was first introduced in the 1990s (Moehle 1992, Priestley 1997). Displacement-based design characterizes a structure as an equivalent single-degree-of-freedom (SDOF) system at its peak displacement response, rather than by its initial elastic characteristics. Moehle (1992) presents a general methodology for displacement-based design of reinforced concrete; Thomsen and Wallace (1995) propose a new code format for seismic design of reinforced concrete structural walls. Priestley (1997) describes an assessment procedure for existing reinforced concrete structures, based on displacement-based design and using effective stiffness and effective viscous damping.

A methodology for displacement-based seismic design of wall structures was proposed by Sullivan *et al.* (2006). The methodology starts with computation of a design displacement profile, using the properties of the equivalent single-degree-of-freedom system to obtain the height of the inflection point in the wall. Calvi and Sullivan (2009) propose a Model Code for displacement-based seismic design of structures. The essence of that model code relies on Priestley *et al.* (2007).

A displacement-based design method for the seismic design of reinforced concrete shear wall buildings is presented by Humar *et al.* (2011). For preliminary design, the yield and failure displacements and deformations are estimated approximately, from current practical relations, and then the ductility and deformations demands are kept within ductility and deformation capacities, and the inter-story drifts are limited to the code specified inter-story drift limits. Humar *et al.* (2011) converts multi-story structures to an equivalent single-degree-of-freedom system using an assumed first mode deformed shape, and then determines the required inelastic lateral strength of the structure from the inelastic demand spectrum corresponding to the assumed ductility demand.

2.6.2 Overview of Displacement-Based Seismic Design

This section deals with fundamental aspects of displacement-based seismic design that are common to all materials and structural systems. The key steps are shown in Figure 2.5, adapted from Filiatrault and Folz (2002).

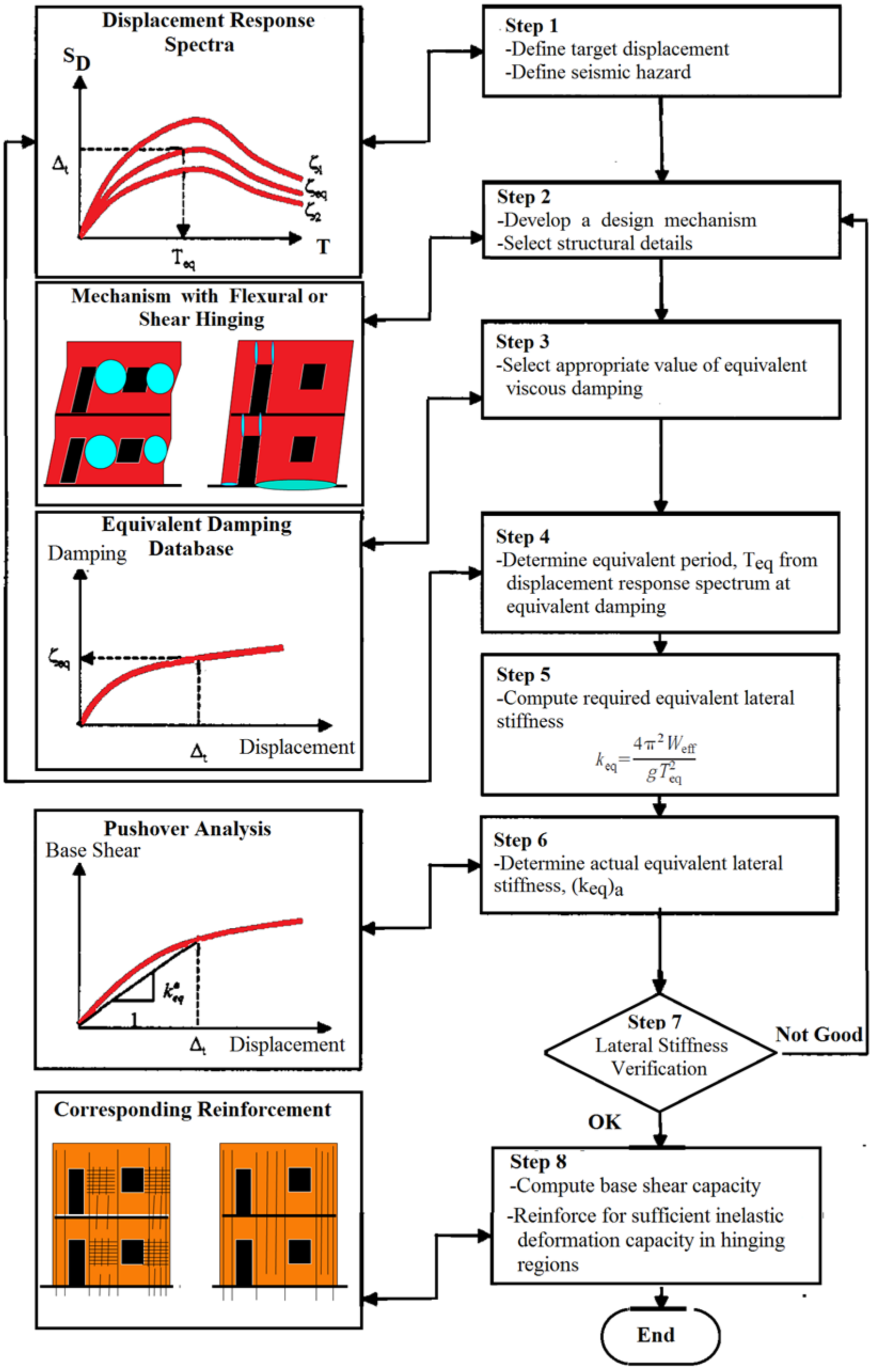

Figure 2.5 Modified flowchart of displacement-based design method for reinforced masonry shear-wall structures (Filiatrault and Folz 2002, Priestley et al. 2007)

1) The first step is the selection of a design level of seismic hazard and the corresponding target displacement (corresponding to local deformation limit). For each level of seismic hazard, the target displacement is described by a relative displacement response spectrum.

2) Once the design seismic hazard and associated target displacement have been defined, a design mechanism consistent with that target displacement must be developed, and structural elements must be detailed appropriately for the deformations associated with that mechanism displacement.

3) To capture the energy dissipation characteristics of the structure at the target displacement, an equivalent damping must be determined. For this purpose, a damping database must be established for the selected structural system from the global hysteretic behavior of the structure. Equivalent viscous damping can then be estimated as the sum of elastic and hysteretic damping, using some relations depending of the structural components displacement levels and ductility.

4) Once the design displacement has been defined, and the corresponding damping estimated from the expected ductility demand, the effective structural period at target displacements can be determined directly from the elastic response spectrum, reduced for the corresponding level of damping.

5) Using the effective period at the target displacement, and representing the building as an equivalent linear SDOF system, the required equivalent lateral stiffness can be obtained at the target displacement.

6) The actual stiffness can be determined from the results of a nonlinear static pushover analysis.

7) The actual equivalent lateral stiffness of the building is compared to the required equivalent lateral stiffness. If these values differ substantially, the seismic force-resisting resisting system of the building must be modified. If the values are sufficiently close, the design is completed by comparing the inelastic local deformation demands calculated in nonlinear analysis with inelastic deformation capacities.

8) Using the local deformation demands, the wall segments are detailed for sufficient inelastic shearing deformation capacity in shear hinging regions, and for sufficient inelastic rotation capacity in flexural hinging regions. The required base shear capacity of the building is computed at the target displacement, and is then used to design the structural elements that are intended to behave elastically. These elements must be provided with sufficient strength to resist the required actions.

2.7 PERFORMANCE-BASED SEISMIC DESIGN

Although buildings designed using force-based seismic design provisions have generally performed well from a life-safety perspective during recent earthquakes, the level of damage to structures, economic losses due to the loss of use and the cost of repair have sometimes been unexpectedly high (Ghobarah 2001). In response, in the past two decades, performance-based design concepts have been developed. Although the term "performance-based design" has many definitions, it generally refers to a methodology in which structural design criteria for different levels of seismic excitation are expressed in terms of a set of performance objectives. These performance objectives may be a level of stress not to be exceeded, a load, a target displacement, a limit state or a target damage state (Ghobarah 2001, Jo 2010).

To develop performance-based seismic design guidelines for new and existing buildings in US, the Federal Emergency Management Agency (FEMA) contracted in September 2001 with the Applied Technology Council (ATC) to carry out the ATC-58 Project. During the past decade, significant progress has been made in performance-based structural design methods.

2.7.1 Theoretical Background of Performance-based Design

In Section 2.6, displacement-based seismic design is reviewed. That design approach is normally applied using design-basis earthquakes or maximum considered earthquake. The same procedure can be extended to the design of structures in which damage is limited at each of a number of different levels of seismic input. These are specific applications of performance-based design.

Performance-based design is described in ATC-40 (1996), FEMA 356 (2000), and ASCE/SEI 41 (2006). The first two of those documents rely on nonlinear static analysis procedures for prediction of structural demands. Both involve the development of a “pushover” curve to predict the inelastic force-deformation behavior of the structure, by methods that differ slightly. ATC-40 (1996) uses the Capacity-Spectrum Method, in which modal displacement demand is determined from the intersection of a capacity curve (derived from the pushover curve) with a demand curve based on a smoothed response spectrum for the design ground motion, modified for hysteretic damping. FEMA 356 (2000) uses the Coefficient Method, in which displacement demand is estimated by modifying elastic predictions of displacement demand. The two procedures often give different estimates for displacement demand for the same building. FEMA 440 (2005) was developed in an effort to resolve this discrepancy. ASCE/SEI 41 (2006) is the latest in a series of documents developed to assist engineers with the seismic assessment and rehabilitation of existing buildings (FEMA 273, 1997; FEMA 356, 2000). Computer software such as PERFORM 3D (CSI 2007) has also been developed as a tool for performance-based design. In the remainder of this section, each of these is discussed.

2.7.2 Capacity-Spectrum Method (CSM)

The Capacity Spectrum Method (ATC-40 1996) is based primarily on the work of Freeman *et al.* (1975). This method combines inelastic seismic demand with structural capacity to predict the seismic displacement of a nonlinear structure. Inelastic seismic demand is represented by a linear response spectrum with varying values of damping, each associated with a corresponding value of ductility. Structural capacity is represented by a push-over curve of the building model. For different displacement values along the push-over curve, bilinear approximations are fit to the curve, and a corresponding equivalent yield displacement is defined for the structure. The point at which the demand and the capacity curves cross defines the expected performance of the structure, and is referred to as the "Performance Point." The principal elements of the capacity-spectrum method are shown in Figure 2.6 (FEMA-440 2005).

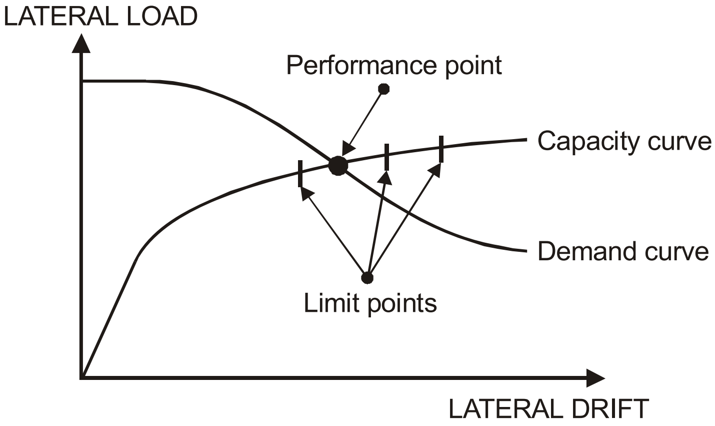

Figure 2.6 Idealized Capacity-Spectrum plot (FEMA-440 2005)

2.7.3 Displacement-Coefficient Method

The determination of the target displacement in the simplified nonlinear static procedure (NSP) using the displacement Coefficient Method is described primarily in ASCE/SEI 41 (2006). According to that document, the “Target Displacement”, δ_t, can be estimated as

$$\delta_t = C_0 C_1 C_2 C_3 S_a \frac{T_e^2}{4\pi^2} g \qquad \textit{Equation 2-1}$$

where C_0 is modification factor to relate spectral displacement of an equivalent SDOF system to the roof displacement of the building MDOF system;

C_1 is a modification factor to relate the expected maximum displacements of an inelastic SDOF oscillator with elasto-plastic hysteretic properties to the linear elastic response displacements;

C_2 is a modification factor to represent the effect of pinched hysteretic shape, stiffness degradation, and strength deterioration on the maximum displacement response;

C_3 is a modification factor to represent increased displacements due to dynamic effects;

T_e is the effective fundamental period of the building; and

S_a is response spectral acceleration at the effective fundamental period and damping ratio of the building.

2.7.4 Computer-based Tools for Performance-based Design

Performance-based design relies on nonlinear analysis procedures that account for local and global inelastic behaviors. Two most practical procedures are nonlinear static analysis (“pushover”) and nonlinear dynamic analysis (time history). In these procedures, a building is modeled, analyzed, and evaluated as an assembly of elements and components. These nonlinear models are available in many computer programs such as the commercial program PERFORM 3D (CSI 2007) and the open-source program OpenSees (PEER 2006). Commercial programs are in general more fully automated, and have a wider range of input and output interfaces.

CHAPTER 3

Development of Reversed Cyclic Shear-wall Specimens

As part of the NIST "Performance-based Seismic Design Methods and Tools for Reinforced Shear Wall Structures" project, twenty-one reinforced concrete masonry shear-wall specimens were tested quasi-statically at the Ferguson Structural Engineering Laboratory of The University of Texas at Austin. Fifteen cantilever wall segments and six fixed-fixed wall segments were tested under in-plane cyclic loading. The primary objective of these tests was to evaluate the relationship between key design parameters and the nonlinear hysteretic response of masonry wall segments. The secondary objective was to provide experimental data to calibrate analytical models for in-plane flexural and shear response of reinforced masonry shear walls, for use in displacement-based seismic design.

This chapter addresses the overall project's reversed cyclic load testing program; the wall specimens and test setups used at UT Austin; construction procedures; testing procedures; and material properties. Test results are discussed in the following chapter.

3.1 OVERVIEW OF CYCLIC TESTING PROGRAM

One of the main tasks of this research program was to conduct an extensive series of cyclic tests on wall segments with different design parameters and loading conditions. The objective of this task was to evaluate the relationship between the most important design parameters (aspect ratio, axial load, percentage and arrangement of reinforcement, boundary condition, and confinement of boundary elements) and the nonlinear hysteretic behavior of concrete masonry unit (CMU) wall segments, especially with respect to ductility, plastic-hinge length, flexural and shear capacities, and deformation ratios. To this end, a total of 43 wall segments were tested at The University of Texas at Austin (UT Austin) and Washington State University (WSU). The wall segments ranged from 4.67- to 12-ft tall and 2.67- to 8-ft. long. They were constructed of fully grouted concrete masonry. Axial loads were applied using a load maintainer. Different boundary conditions were used at the wall top in order to produce different failure modes. Cantilever walls were used to investigate mainly flexure-dominated wall response, and fixed-fixed walls were used to investigate mainly shear-dominated wall response. A few walls had lap splices of longitudinal reinforcement in plastic hinge regions; the rest did not (Sherman 2011).

Table 3-1 shows the test matrix used for shear-wall specimens tested at UT Austin and Washington State University (WSU). The specimens had different types of detailing: current levels of prescriptive detailing; other levels of detailing intended for possible use with displacement-based design; detailing with confined boundary elements; and detailing based on that required for shear-dominated elements under the limit-design provisions of the draft 2013 MSJC *Code*.

Table 3-1 Overview of CMU wall specimens (UT Austin and WSU)

specimen type	specimen number	nominal length, in	nominal height ,in.	aspect ratio	P/(f_m' A_g)	end condition
Current Detailing	**WSU-Wall 1A**	40	80	2	0.0625	cantilever
	WSU-Wall 1B	40	80	2	0.0625	cantilever
	WSU-Wall 2A	40	80	2	0.125	cantilever
	WSU-Wall 2B	40	80	2	0.125	cantilever
	WSU-Wall 3	72	72	1	0	cantilever
	WSU-Wall 4	72	72	1	0.0625	cantilever
	WSU-Wall 5	72	56	0.78	0	cantilever
	WSU-Wall 6	72	56	0.78	0.0625	cantilever
	UT-W-13	48	144	3	0.05	cantilever
	UT-W-14	48	144	3	0.1	cantilever
	UT-W-15	48	144	3	0.1	cantilever
	UT-W-16	48	144	3	0.15	cantilever
	UT-W-17	32	144	4.5	0.05	cantilever
	UT-W-18	32	144	4.5	0.1	cantilever
	UT-W-19	32	144	4.5	0.1	cantilever
	UT-W-20	32	144	4.5	0.15	cantilever
Detailing for Confined Boundary Elements	**WSU-Wall 7**	40	80	2	0	cantilever
	WSU-Wall 8	40	80	2	0.0625	cantilever
	WSU-Wall 9	40	80	2	0.0625	cantilever
	WSU-Wall 10	72	56	0.78	0.0625	cantilever
	WSU-Wall 11	72	72	1	0.0625	cantilever
	WSU-Wall 31	56	112	2	0	cantilever
	WSU-Wall 32	56	112	2	0	cantilever

specimen type	specimen number	nominal length, in	nominal height ,in.	aspect ratio	P/(f_m' A_g)	end condition
Detailing for Displacement-based Design Elements	**UT-PBF-05**	32	144	4.5	0	cantilever
	UT-PBS-03	96	96	1	0	cantilever
	UT-PBS-04	96	96	1	0	cantilever
	UT-PBS-04G*	96	96	1	0	cantilever
	UT-PBS-11	96	96	1	0.1	cantilever
	UT-PBS-12	96	96	1	0.1	cantilever
	UT-PBS-12G*	96	96	1	0.1	cantilever
	WSU-Wall 33	56	112	2	0.0625	cantilever
	WSU-Wall 21	56	112	2	0	cantilever
	WSU-Wall 23	56	112	2	0	cantilever
	WSU-Wall 24	56	112	2	0	cantilever
	WSU-Wall 21	56	112	2	0.0625	cantilever
	WSU-Wall 13	72	56	0.78	0	cantilever
	WSU-Wall 14	72	72	1	0	cantilever
Detailing for Shear Dominated Elements	**UT-PBS-01**	72	72	0.5	0	fixed-fixed
	UT-PBS-02	72	72	0.5	0.10	fixed-fixed
	UT-PBS-05	72	72	0.5	0.05	fixed-fixed
	UT-PBS-06	72	72	0.5	0.05	fixed-fixed
	UT-PBS-09	72	72	0.5	0.1	fixed-fixed
	UT-PBS-10	72	72	0.5	0.1	fixed-fixed

*Was built using “Green blocks” (made of recycled materials)

The first group of cantilever wall specimens was detailed according to 2011 MSJC *Code* requirements. Specimens had two levels of detailing (special and intermediate), five aspect ratios (0.78, 1.0, 2.0, 3.0, and 4.5), and six levels of axial load ratio, P/P_0 (0, 0.05, 0.0625, 0.10, 0.125, and 0.15), for a total of 16 specimens. Aspect ratio is the ratio of height to plan length of the wall segment, and P_0 is the axial capacity of a wall in pure compression ($f_m' A_g$).

The second group of cantilever wall specimens was provided with confined boundary elements, and was tested at Washington State University (Cyrier 2012). Results will be used to develop analytical models for the in-plane response of reinforced masonry shear walls with confined boundary elements.

The third group of cantilever wall specimens, designated "PBF" and "PBS," was used to investigate the performance of shear-wall segments with the wider range of reinforcement contents that are envisioned for use with displacement-based design, and do not meet MSJC *Code* requirements. Walls had different aspect ratios, levels of applied axial stress, and longitudinal and transverse reinforcement ratios Some of these wall segment were tested at Washington State University to examine the effects of concentrated reinforcement at the ends of the walls (jambs) compared with evenly distributed reinforcement on shear wall performance (Kapoi 2012).

The fourth group of wall specimens represented wall segments in perforated wall systems. These wall specimens were tested with fixed-fixed boundary conditions and constant axial load, using coupled servo-controlled hydraulic actuators.

3.2 DETAILS OF SHEAR-WALL SPECIMENS TESTED AT UT AUSTIN

3.2.1 Cantilever Shear-Wall Specimens

The testing program for reinforced masonry shear walls at the Ferguson Structural Engineering Laboratory (FSEL) consists of two phases. The first phase consists of a suite of cantilever shear wall specimens subject to lateral cyclic in-plane loading. Fifteen masonry shear-wall specimens, each representing a segment of a perforated shear wall, were constructed and tested. The first eight cantilever specimens were detailed according to the requirements of the 2011 MSJC *Code*, and were intended to represent special and intermediate reinforced masonry shear walls whose behavior was controlled by flexure. The remaining seven cantilever wall specimens were tested to investigate the response of masonry shear walls with the wider range of reinforcement contents that are envisioned for displacement-based design.

The specimens used nominal 8- x 8- x 16-in. lightweight concrete masonry units (ASTM C90); coarse grout by proportion (ASTM C476); and ASTM C270 Type S cement-lime mortar by proportion. The overview of these wall specimens is provided in Table 3-2 and the design drawings are shown in Appendix A. The geometry, horizontal and vertical reinforcement details, and the applied axial load ratios for each shear wall specimen are summarized in Table 3-2. These segments were designed and tested to refine current MSJC Code design formulas for flexural capacity, to provide experimental data to develop analytical models to predict the behavior of flexure-dominated CMU shear walls under earthquake ground motions, and to define appropriate limiting drift ratios and displacement ductility capacities for CMU shear walls.

The geometry, axial force, and flexural reinforcement for each flexure-dominated specimen were selected to force flexural behavior. The wall geometry for the flexure-dominated specimen was selected to represent the aspect ratio (height divided by plan length) of walls of potential CMU structures whose behavior is dominated by flexure. The axial force in those specimens was varied to represent the range of compressive stresses found in shear walls in typical reinforced masonry structures.

Table 3-2 Overview of cantilever CMU shear-wall specimens tested at UT Austin

specimen number	nominal length, in	nominal height ,in.	aspect ratio	$P/(f_m'A_g)$	vertical reinforcement	horizontal reinforcement
UT-W-13	48	144	3	0.05	#6 @ 8 in.	#4 @ 16 in.
UT-W-14	48	144	3	0.1	#4 @ 8 in.	#4 @ 16 in.
UT-W-15	48	144	3	0.1	#6 @ 8 in.	#4 @ 16 in.
UT-W-16	48	144	3	0.15	#4 @ 8 in.	#4 @ 16 in.
UT-W-17	32	144	4.5	0.05	#6 @ 8 in.	#4 @ 8 in.
UT-W-18	32	144	4.5	0.1	#4 @ 8 in.	#4 @ 8 in.
UT-W-19	32	144	4.5	0.1	#6 @ 8 in.	#4 @ 16 in.
UT-W-20	32	144	4.5	0.15	#4 @ 8 in.	#4 @ 16 in.
UT-PBF-05	32	144	4.5	0	#8@ 8 in.	#4 @ 8 in.
UT-PBS-03	96	96	1	0	#4 @8	#4 @8
UT-PBS-04	96	96	1	0	#4 @16	#4 @16
UT-PBS-04G	96	96	1	0	#4 @16	#4 @16
UT-PBS-11	96	96	1	0.1	#4 @8	#4 @8
UT-PBS-12	96	96	1	0.1	#4 @16	#4 @16
UT-PBS-12G	96	96	1	0.1	#4 @16	#4 @16

3.2.2 Design of Test Setup for Cantilever Wall Specimens at UT Austin

The components comprising each cantilever wall specimen and test setup are shown in Figure 3.1. The loading system consisted of a lateral loading system, a gravity loading system, and an out-of-plane bracing system.

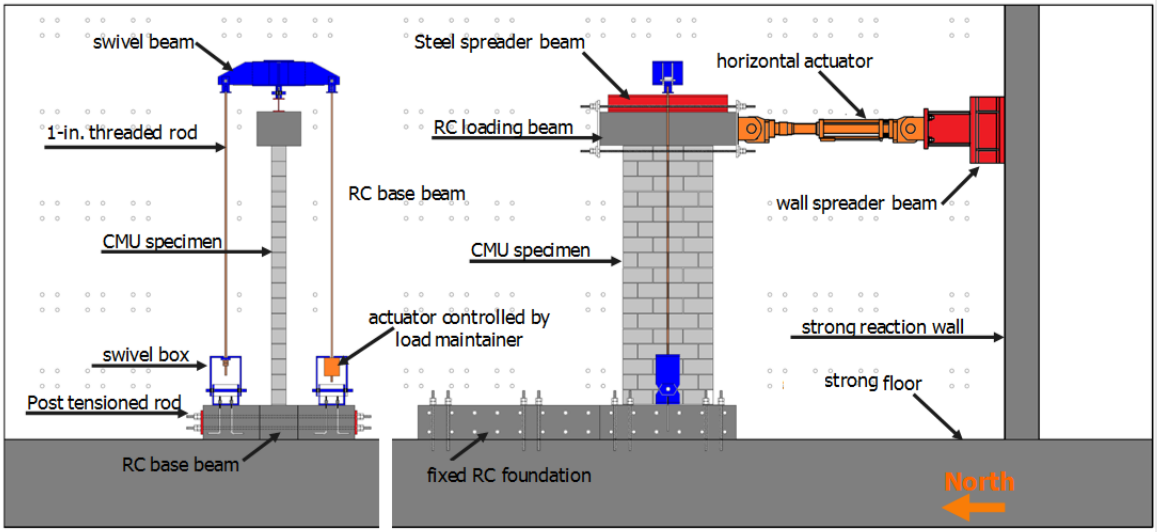

Figure 3.1 Components comprising test setup for cantilever shear-wall specimens

The lateral load system consisted of a hydraulic ram connected to the loading beam of the specimen and reacting against a strong wall. The ram was connected to a hydraulic pump, which was controlled manually. The ram had a maximum capacity of 130 kips in tension and 192 kips in compression, and a total stroke of 18 in. This actuator was bolted at one end to a reinforced concrete loading beam connected to the specimen, and at the other end to a steel beam attached to the strong reaction wall of FSEL. The reinforced concrete loading beam was connected along the top of each specimen using conventional cement-lime masonry mortar conforming to ASTM C270, Type S by proportion.

Axial loads in the wall segments due to gravity load were reproduced by applying a constant axial load to the specimen. The axial loading system consisted of a swivel beam attached to the loading beam and connected to the foundation through threaded rods, as shown in Figure 3.1. Each set of two threaded rods in front of and behind the specimen was placed in tension using a small ram installed over the foundation, as shown in Figure 3.2. In this figure, two threaded rods are connected at one end to a steel swivel beam connected to a steel spreader beam, and at the other end to a swivel steel box bolted to the base beam. The loading system allowed both horizontal and vertical displacements in the wall. The total axial load for each of those specimens was defined by the sum of the axial load applied using the hydraulic actuators and the self-weight of the concrete loading beam.

Figure 3.2 Axial load system for cantilever shear-wall specimens (UT Austin)

Specimens were braced laterally out of plane using two steel channels bolted to two steel columns and clamped to a steel beam on the loading beam. Teflon® (tetrafluoroethylene) sheets were placed in the surface of contact between channels and the steel beam to reduce friction. The out-of-plane bracing system is shown in Figure 3.3.The specimens were built on a precast concrete base beam, on top of a leveling bed of cement-lime mortar conforming to ASTM C270, Type S by proportion. To prevent the base beam from sliding or uplifting, as shown in Figure 3.3 it was tied to the strong floor using 1.5-in threaded rods, post-tensioned to 75 kips each. An elevation of the test setup is presented in Figure 3.4.

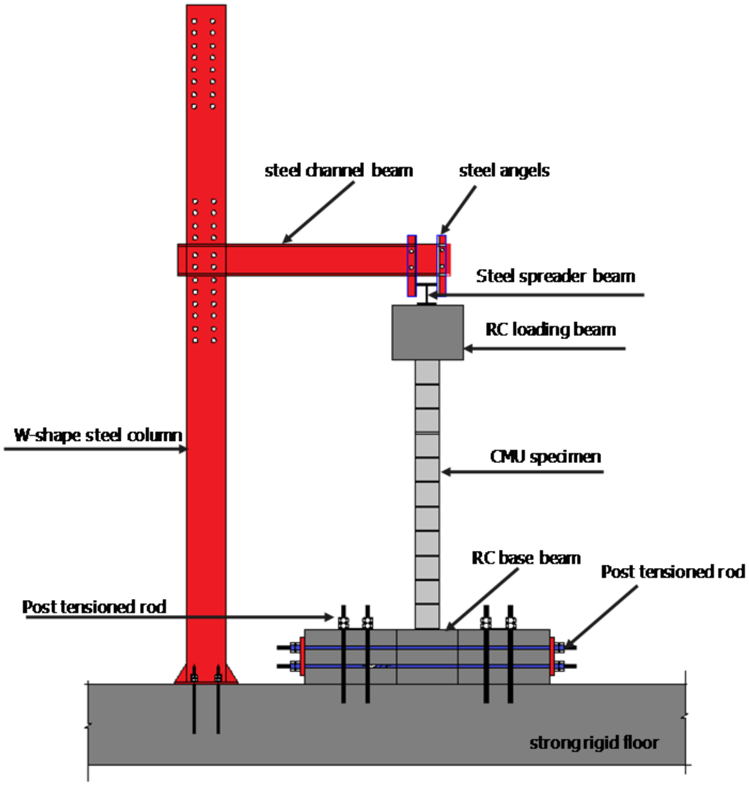

Figure 3.3 Out-of-plane bracing system for cantilever shear-wall specimens

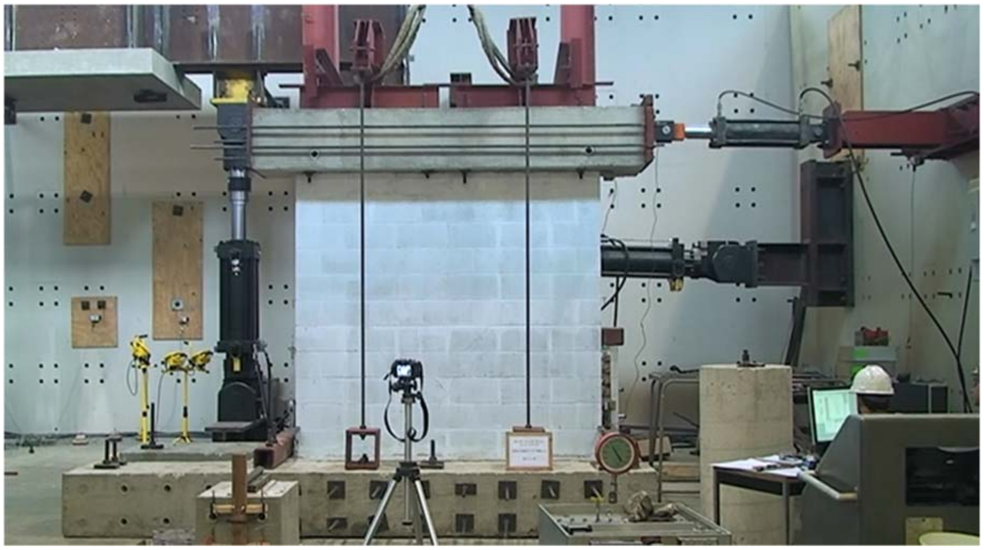

Figure 3.4 Elevation view of test setup for cantilever shear-wall specimens

3.2.3 Fixed-fixed Shear-Wall Specimens

The second phase of experimental studies at UT Austin consists of a suite of fixed-fixed shear-wall specimens subject to lateral cyclic in-plane loading. Six masonry shear-wall specimens, each representing a segment of a perforated shear wall, were constructed and tested at the FSEL. The fixed-fixed specimens used nominal 8- x 8- x 16-in. lightweight concrete masonry units (ASTM C90); coarse grout by proportion (ASTM C476); and ASTM C270 Type S cement-lime mortar by proportion. An overview of these wall specimens is provided in Table 3-3.

Table 3-3 Overview of fixed-fixed CMU wall specimens tested at UT Austin

specimen number	nominal length, in	nominal height ,in.	aspect ratio	$P/(f_m'A_g)$	vertical reinforcement	horizontal reinforcement
UT-PBS-01	72	72	0.5	0	#6 @ 8 in.	#4 @ 8 in.
UT-PBS-02	72	72	0.5	0.10	#6 @ 16 in.	#4 @ 16 in.
UT-PBS-05	72	72	0.5	0.05	#4 @ 8 in.	#4 @ 8 in.
UT-PBS-06	72	72	0.5	0.05	#4 @ 16 in.	#4 @ 16 in.
UT-PBS-09	72	72	0.5	0.1	#4 @ 8 in.	#4 @ 8 in.
UT-PBS-10	72	72	0.5	0.1	#4 @ 16 in.	#4 @ 16 in.

The geometry, horizontal and vertical reinforcement details, and the applied axial load ratios for each shear wall specimen are summarized in Table 3-3. The geometry, flexural and horizontal reinforcement, and axial force for each shear-dominated specimen were selected to force shear-dominated behavior. The wall geometry for the fixed-fixed specimen was selected to represent the aspect ratio of walls of potential CMU structures whose behavior is dominated by shear or sliding shear. The axial force in those specimens was varied to represent the range of compressive stresses found in shear walls in typical reinforced masonry structures. The axial load was varied in some cases among the fixed-fixed specimens to determine the influence of the axial force on the capacity of shear walls as governed by web-shear cracking and shear sliding.

3.2.4 Design of Test Setup for Fixed-fixed Wall Specimens at UT Austin

To reduce the time and expense of testing, the fixed-fixed wall specimens at UT Austin were tested at FSEL using an existing testing frame, originally designed and fabricated by Leborgne (2012) for tests of fixed-ended reinforced concrete columns. The testing frame uses three actuators, controlled simultaneously using an MTS FlexTest 60® closed-loop controller to maintain the desired axial load while preventing in-plane rotation at the top of the wall. This control system is discussed in more detail later in this section.

The L-shaped steel test frame was designed to meet the shear and moment requirements associated with a 200-kip force applied by the horizontal actuator in the north direction (Figure 3.5). The vertical movement of the test frame is limited by the out-of-plane bracing as shown in Figure 3.6. The out-of-plane bracing system consists of three steel tubes with swivels at each end. Each tube and swivel assemblage was designed to have a capacity of 30 kips. The arc traced by the swivels as the specimens undergo lateral displacements leads to negligible out-of-plane motion of the test frame (Leborgne, 2012).

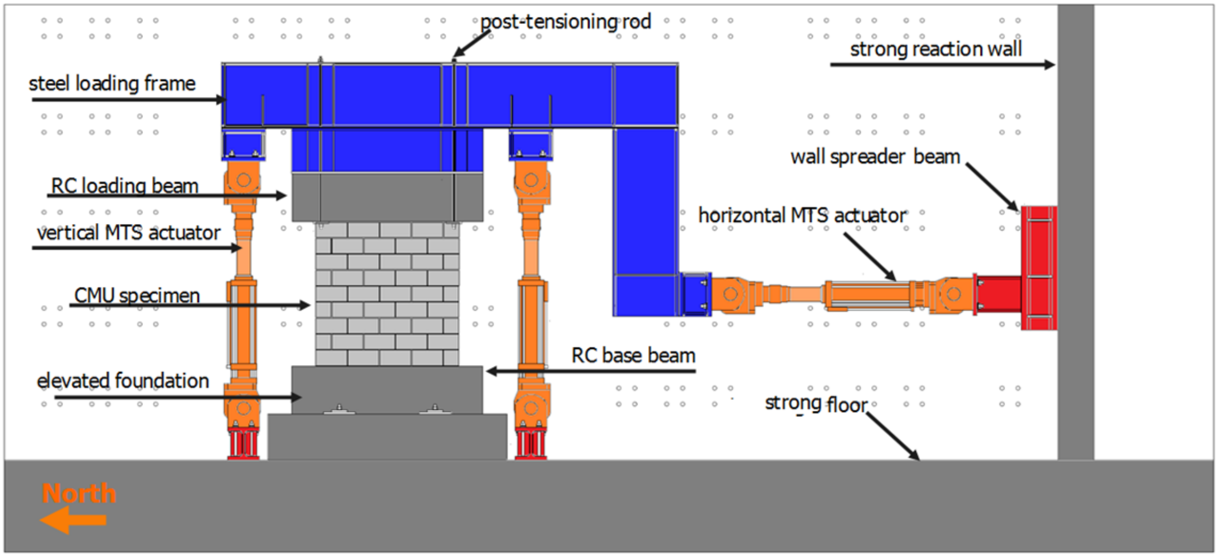

Figure 3.5 Components of test setup for fixed-fixed shear-wall specimens

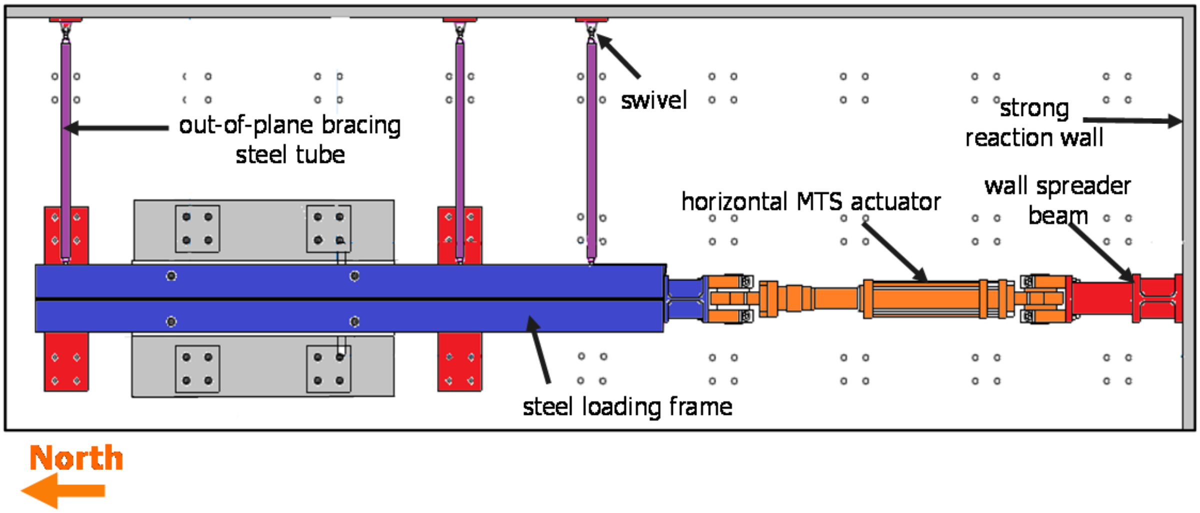

Figure 3.6 Plan view of test setup and out-of-plane bracing system for fixed-fixed shear-wall specimens

The horizontal actuator had a maximum capacity of 220 kips in tension and 320 kips in compression. It was post-tensioned at one end to the L-shaped steel loading frame, and at the other end to a steel beam attached to the strong reaction wall of FSEL. The steel loading frame was post-tensioned to a reinforced concrete loading beam with eight 1.5-in threaded rods tensioned to 75 kips each, and rods located close to the ends of the wall and the loading beam.

The horizontal and vertical loading systems are controlled using an MTS FlexTest 60 controller equipped with three channels, one for each actuator. The controller is programmed using the MTS 793 control software with custom enhancements developed by FSEL staff using the MTS Computer Simulation Interface and Configurator (CISC) application programming interface. The software maintains a constant vertical load and zero rotation of the horizontal loading beam while incrementally applying cyclic lateral displacement. This is accomplished by repeating the following sequence: The desired axial load is applied by moving the vertical actuators through equal vertical displacements. Cyclic lateral displacements are then imposed by moving the horizontal actuator by a small displacement step; reading the load from the vertical actuators; and adjusting the vertical load by extending or retracting the vertical actuators by small equal amounts, thereby maintaining zero rotation of the loading beam. The software checks user-programmable safety limits at each loading step.

The reinforced concrete loading beam was connected along the top of the wall specimen using cement-lime mortar conforming to ASTM C270, Type S by proportion. The specimens were built on a precast concrete base beam, on top of a leveling bed of cement-lime mortar conforming to ASTM C270, Type S by proportion. To prevent the base beam from sliding or uplifting, it was tied to the elevated foundation floor using eight 1.5-in threaded rods, post-tensioned to 75 kips each. An elevation of the test setup is presented in Figure 3.7, and another view is presented in Figure 3.8. A detail of the connection between the L-shaped steel loading frame and the concrete loading beam is presented in Figure 3.9.

Figure 3.7 Elevation view of test setup for fixed-fixed shear-wall specimens

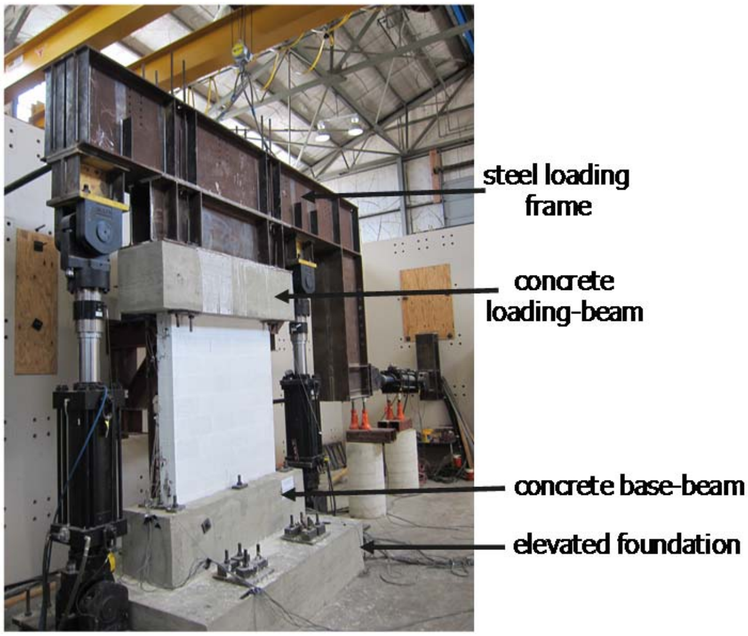

Figure 3.8 North view of test setup for fixed-fixed shear-wall specimens

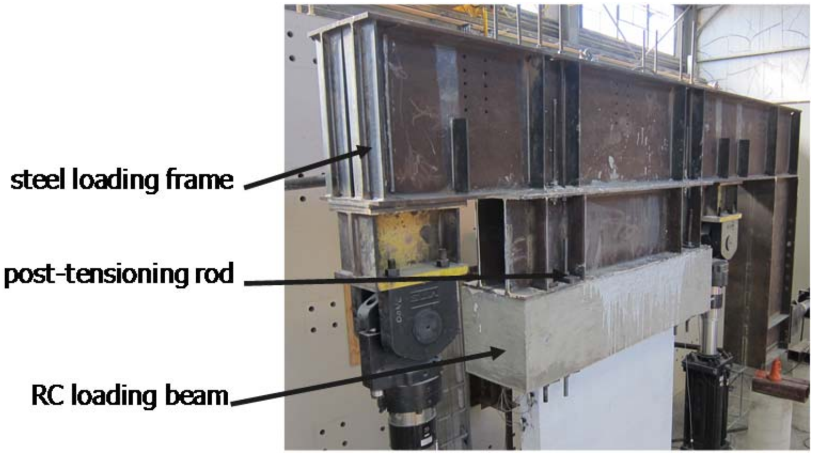

Figure 3.9 Connection between L-shaped loading frame and fixed-fixed shear-wall specimens

3.3 CONSTRUCTION PROCEDURE FOR WALL SPECIMENS

Shear-wall specimens were constructed at the Ferguson Structural Engineering Laboratory by professional masons. In this section, construction procedures used for the test setup and reinforced concrete masonry are briefly described. The purpose is to provide background on the construction of such masonry in general, and on the construction of the specimens tested here in particular.

3.3.1 Construction of Base Beam, Loading Beam and Foundation Beam

Most steps in constructing each beam were the same. Small differences in the function of the beams were considered without changing the construction process. Construction of beams began with the construction of the formwork. Each side of wooden formwork consisted of a piece of plywood over a 2- x 4-in. frame with 2- by 4-in. bracing. As shown in Figure 3.10, holes were drilled in lateral form members for subsequent insertion of PVC tubes. When all formwork sides were ready, they were placed on the wooden casting platform; aligned; squared; and screwed to the platform and to the adjacent sides. Joints between the formwork sides and the platform were sealed to prevent leakage and consequent voids or segregation of concrete. As the formwork was constructed, cages of reinforcement were assembled as shown in Figure 3.11. Transverse bars were tied to the longitudinal bars to prevent interference with the locations of the horizontal and vertical PVC tubes.

Figure 3.10 Construction of formwork for beams

Figure 3.11 Assembling reinforcement cages for beams

Figure 3.12 Typical beams before casting

Figure 3.13 Beam casting

Reinforcement cages were placed inside the formwork; PVC tubes were placed in holes; and gaps between the tubes and formwork were sealed. The tops of the vertical PVC tubes were covered and braced with lengths of wooden 2- by 4-in. boards, screwed to lateral formwork. Dowels were attached to the cage for the base beams and loading beams. For foundation beams, three pairs of coil-rod inserts were attached to the cage. Figure 3.12 shows typical beams before casting. Beams were cast as shown in Figure 3.13, with using concrete with a specified compressive strength of 4000 psi and specified slumps between 8 and 9 in. The foundations were not intentionally roughened, but were cleaned with compressed air and pre-wetted before construction of masonry walls.

3.3.2 Construction of Masonry Walls

Masonry walls were constructed using the following sequence. The first course of masonry units were placed on bedding mortar on the base beam, creating a bond with the base beam, and with mortar joints between units (Figure 3.14). Cleanouts were cut into the masonry units in the lowest course (Figure 3.15), and the cut pieces were replaced in position before grouting (Figure 3.19). When necessary, webs were partially removed to permit the placement of horizontal reinforcement.

As shown in Figure 3.16, special care was taken to locate the extreme vertical reinforcement inside of the 180-degree hook at each end of the horizontal bars (Figure 3.17). Additional courses were constructed using the same procedure. Masonry units were placed level, plumb, and true (Figure 3.18). When the wall segment was complete, the required vertical reinforcement was placed in the appropriate cells, and was checked using the cleanouts, which were then sealed (Figure 3.20). The loading beam was lifted, inverted from its casting position so that the dowels would point down, and checked for alignment by placing it temporarily on top of the wall segment (Figure 3.21). The loading beam was then lifted by crane, and the cells of the masonry wall segments were filled to the top with grout (Figure 3.22). The grout had a specified slump of 8 to 11 in., and was vibrated during pouring (Figure 3.23). The loading beam was again placed and aligned on top of the wall (Figure 3.24). Finally, grout was poured through vertical PVC tubes next to the dowels in the loading beam to fill the cells at the top of the wall (Figure 3.25).

Figure 3.14 Base foundation with dowel bars

Figure 3.15 Cleanouts in the lowest course of masonry units

Figure 3.16 Placement of horizontal reinforcement

Figure 3.17 Detail of horizontal reinforcement and knocked-out webs

Figure 3.18 Hollow concrete masonry units being laid

Figure 3.19 Replacing cut face shells pieces in cleanouts before grouting

Figure 3.20 Placement of vertical reinforcement in cells of units

Figure 3.21 Checking alignment of inverted loading beam

Figure 3.22 Grouting concrete masonry

Figure 3.23 Vibrating grout

Figure 3.24 Placing loading beam on the wall after grouting

Figure 3.25 Pouring grout through vertical PVC tubes in loading beam

3.4 LOADING PROTOCOL FOR SHEAR-WALL SPECIMENS

For all shear-wall tests at the University of Texas at Austin and at Washington State University, a common testing protocol was established, consisting of a series of reversed cycles to monotonically increasing maximum load or displacement amplitudes. At the beginning of each test, target load values were used; after web-shear cracking or yielding of the flexural reinforcement, target displacement values were used. The predetermined target values were based on the loads that were calculated to produce significant changes in the behavior of the specimen (for example, flexural cracking or web-shear cracking). After web-shear cracking or yielding of the flexural reinforcement, the test was controlled by displacements; two reversed cycles were applied at each displacement. The testing protocol for each specimen adhered to the following steps:

1. The expected maximum lateral capacity of the wall specimen was calculated using expected values of f_y and f_m' as shown in Section 3.5.

2. The horizontal load that produces the maximum lateral load predicted for the specimen was calculated.

3. A preliminary test which consisted in two reversed cycles of 25, 50 and 75% of the expected maximum load was conducted.

4. The value of the lateral displacements at +75% and -75% of the expected maximum load at the first cycle was averaged and considered equal to $\Delta_{75\%}$.

5. The lateral displacement for 100% the expected maximum load, $\Delta_{100\%}$, was then obtained by extrapolating from $\Delta_{75\%}$ ($\Delta_{100\%} = 4/3 * \Delta_{75\%}$). This value was considered as the yield displacement, Δ_y.

6. Two reversed cycles of 1, 2, 4, 6, 8, 10, 12, 14, 16 and $20\Delta_y$ were defined as the next steps in the testing protocol.

7. The test was ended when the maximum load dropped to less than 20% of its peak (capping) value.

Figure 3.26 shows a typical testing protocol for the specimens that are part of this dissertation.

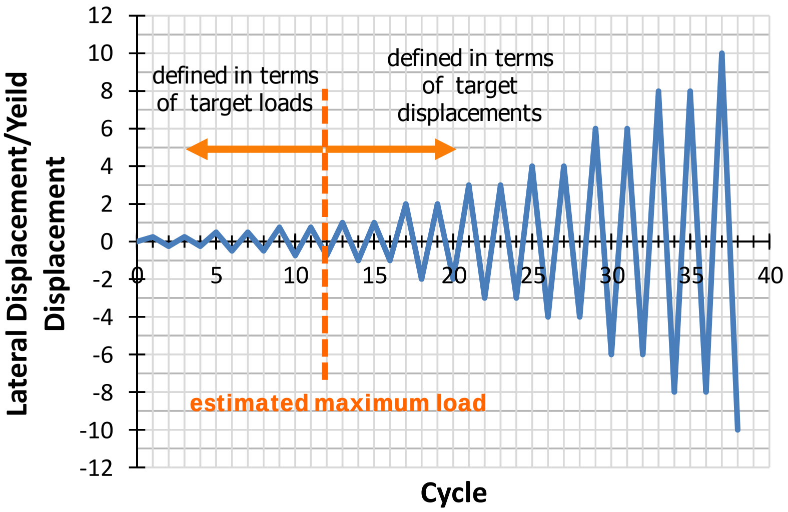

Figure 3.26 Typical cyclic testing protocol

3.5 MATERIAL PROPERTIES AND TESTING

Materials used to construct the wall specimens were tested at the Ferguson Structural Engineering Laboratory and Concrete Durability Center at the University of Texas at Austin. Material tests included compressive strength of mortar; compressive strengths of concrete masonry units; compressive strength of grout; compressive strength of concrete masonry prisms; and yield and tensile strength of reinforcement.

The material specimens were constructed at the same time as the corresponding wall specimens. The reinforcing bar specimens were taken from the same heats as the bars used for construction. In this section, each material test is described, and the corresponding results are presented.

3.5.1 Properties of Concrete Masonry Units (CMU)

The properties of three samples of nominal 8- x 8- x 8-in. concrete masonry units (CMU) for each phase of construction were evaluated in accordance with ASTM C140-09. Wall segments described in part of this dissertation were constructed with two different types of concrete masonry units: “Gray blocks” and “Green blocks” (made of recycled materials). Half blocks were nominal 8- x 8-x 8-in. hollow CMU meeting ASTM C90-11. Compressive strengths and dimensions of these specimens were obtained according to ASTM C140-09 (Figure 3.27). Results are shown in Table 3-4. The average net compressive strength of the 8- x 8- x 8-in. “Gray” units was 3480 psi; and the average width, height and length were 7.68 in., 7.58 in. and 7.65 in., respectively. Also, the average net compressive strength of the 8- x 8- x 8-in. “Green” units was 2850 psi; and the average width, height and length were 7.65 in., 7.62 in. and 7.64 in., respectively. The both 8- x 8- x 8-in. “Gray” and “Green” units met the compressive strength and dimensional requirements of ASTM C90-11.

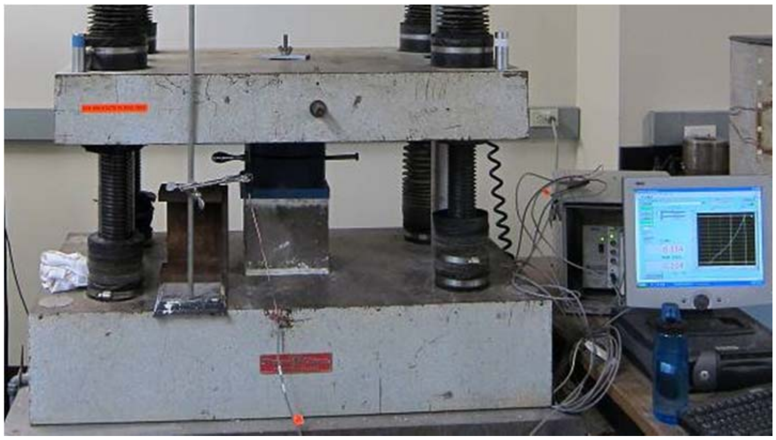

Figure 3.27 Compressive-strength testing of concrete masonry units

Table 3-4 Dimensions and compressive strengths of concrete masonry units

CMU specimen	corresponding wall specimens	width (in.)	height (in.)	length (in.)	thickness (in.)	compressive strength (ksi)	average (ksi)
"Gray" #1	UT-W-13 to UT-W-18, UT-PBF-05, UT-PBS-03,04,11, and 12	7.68	7.58	7.65	1.40	3.55	3.48
"Gray" #2						3.55	
"Gray" #3						3.35	
"Green" #1	UT-PBS-04G and UT-PBS-12G	7.65	7.62	7.64	1.38	2.80	2.85
"Green" #2						2.75	
"Green" #3						3.05	
"Gray" #4	UT-PBS01,02,05, 06,09, and 10	7.63	7.65	7.61	1.42	3.45	3.50
"Gray" #5						3.70	
"Gray" #6						3.35	

3.5.2 Compressive Strengths of Mortar

Compressive strengths of 2-in. mortar cubes were determined according to ASTM C780-11, which refers in turn to ASTM C109-11. Mortar conformed to ASTM C270-12, cement-lime, Type S by proportion. Results for cement-lime mortar are summarized in Table 3-5. Four sets of six cement-lime mortar cubes were prepared corresponding to four phases of specimen construction, and all cubes but three were tested. One set of three mortar cubes, representing the mortar of Specimens UT-W-13, UT-PBS-3, UT-PBS-11, and UT-PBF-5, was not well constructed and was not tested. Figure 3.28 shows a photo of compressive testing of a typical mortar cube. The average compressive strengths were 2281 psi for cement-lime mortar cubes. Even though those strengths were evaluated using job flow rather than the laboratory flow required by the property specification of ASTM C270-12, the compressive strengths exceeded the required property-specified strength of 1800 psi, and sand can be inferred to have met the "use" requirements of ASTM C144-11.

Table 3-5 Compressive strengths of cement-lime mortar cubes

corresponding wall specimens	UT-W-14,15,16 UT-W-19,20	UT-W-17,18 UT-PBS-04,04G UT-PBS-12,12G	UT-W-13 UT-PBS-03,11 UT-PBF-05	UT-PBS-01,02 UT-PBS-05,06 UT-PBS-09,10
construction date	**June 2011**	**August 2011**	**September 2011**	**January 2012**
Cube 1 (psi)	2348	2144	1974	2541
Cube 2 (psi)	2909	1923	2061	2403
Cube 3 (psi)	2968	2242	2081	2520
Cube 4 (psi)	2463	1864	-	2159
Cube 5 (psi)	2556	1951	-	2268
Cube 6 (psi)	2631	1950	-	2685
average (psi)	**2645**	**2012**	**2038**	**2429**
	2281			

Figure 3.28 Compressive testing of a typical mortar cube

3.5.3 Compressive Strength of Grout

Grout specimens measuring 4 x 4 x 8 in. were constructed using the same grout as in the wall specimens, and were tested in accordance with ASTM C1019-11. Four sets of three grout specimens each were prepared, corresponding to four sequences of CMU specimen construction, and all specimens were tested. Figure 3.29 shows a photo of compressive testing of a typical grout specimen. Results are listed in Table 3-6. The average net compressive strength of grout was 5064 psi.

Figure 3.29 Compressive testing of a typical grout specimen

Table 3-6 Compressive strengths of grout specimens

corresponding wall specimens	**UT-W-14,15,16 UT-W-19,20**	**UT-W-17,18 UT-PBS-04,04G UT-PBS-12,12G**	**UT-W-13 UT-PBS-03,11 UT-PBF-05**	**UT-PBS-01,02 UT-PBS-05,06 UT-PBS-09,10**
construction date	**June 2011**	**August 2011**	**September 2011**	**January 2012**
Grout 1 (psi)	5200	4635	5114	5706
Grout 2 (psi)	4896	4585	4379	6481
Grout 3 (psi)	5228	4321	4518	5719
average (psi)	**5108**	**4513**	**4670**	**5968**
	5064			

3.5.4 Compressive Strength of CMU Prisms

Compressive strengths of CMU prisms were determined according to ASTM C1314-11. Twelve grouted concrete masonry prisms were tested. Grouted prisms measured 8 x 8 x 8 in. Each prism was constructed using two concrete masonry half-units. As shown in Table 3-7, three replicates were constructed and tested for each wall-specimen construction sequence. Results are summarized in the same table. The prisms were capped with high-strength hydrostone. The capping plates used satisfied the thickness required by ASTM C140-12, which refers to ASTM C1552-9 for capping. A 600-kip capacity universal testing machine was used to test the CMU prism specimens (Figure 3.30).

Table 3-7 Compressive strengths of CMU prisms

corresponding wall specimens	**UT-W-14,15,16** **UT-W-19,20**	**UT-W-17,18** **UT-PBS-4,4G** **UT-PBS-12,12G**	**UT-W-13** **UT-PBS-3,11** **UT-PBF-5**	**UT-PBS-1,2** **UT-PBS-5,6** **UT-PBS-9,10**
construction date	**June 2011**	**August 2011**	**September 2011**	**January 2012**
Prism 1 (psi)	3560	4798	4870	2666
Prism 2 (psi)	3095	3615	4170	3044
Prism 3 (psi)	1754*	-**	4302	3629
average (psi)	**3328**	**4206**	**4447**	**3113**
	3773			

* The strength of this prism was not included in the average.

** The compressive strength of this prism exceeded the capacity of the compression test machine, so they could not been tested completely and they were discarded.

Figure 3.30 Compressive strength testing of masonry prisms

3.5.5 Tensile Testing of Reinforcement

Tensile properties of reinforcement (No. 4, No. 6, and No 8 bars) were determined according to ASTM A370-12. Strains were measured using an 8-in. extensometer to capture yielding and ultimate strains. For No. 4 bars, yield strength and tensile strength were 63.2 ksi and 100.5 ksi, respectively; for the No. 6 bars, they were 61.1 ksi and 101.9 ksi, respectively; and for the No. 8 bars, they were 64.0 ksi and 105.1 ksi, respectively. Results are listed in Table 3-8. In Figure 3.31 is shown a photo of tensile testing of a typical reinforcing bar.

Table 3-8 Tensile properties of reinforcement

wall specimens	reinforcement direction	Bar diameter	average yield strength (ksi)	average tensile strength (ksi)
UT-W-13,15,17,19	**vertical**	**No. 6**	61.1	101.9
	horizontal	**No. 4**	65.0	102.3
UT-W-14, 16,18,20	**vertical**	**No. 4**	65.0	102.3
	horizontal	**No. 4**	65.0	102.3
UT-PBS-03, 04,04G,12,12G,03,11	**vertical**	**No. 4**	61.4	98.7
	horizontal	**No. 4**	61.4	98.7
UT-PBF-05	**vertical**	**No. 8**	64.0	105.1
	horizontal	**No. 4**	61.4	98.7
UT-PBS-01,02	**vertical**	**No. 6**	63.2	102.7
	horizontal	**No. 4**	62.4	100.5
UT-PBS-05,06 UT-PBS-09,10	**vertical**	**No. 4**	62.4	100.5
	horizontal	**No. 4**	62.4	100.5

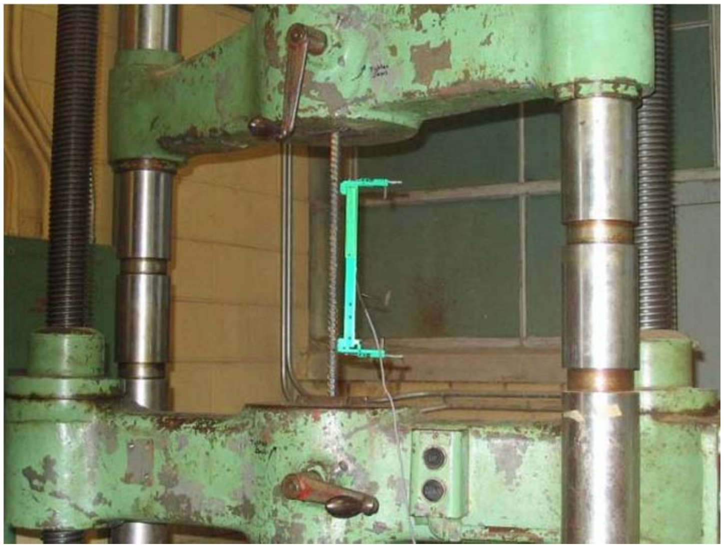

Figure 3.31 Tensile testing of a typical reinforcing bar

CHAPTER 4

Cyclic Tests of Cantilever CMU Wall Specimens

4.1 INTRODUCTION

The first phase of experimental studies at UT Austin consists of a suite of cantilever CMU shear-wall specimens subject to reversed cyclic in-plane loading. Fifteen cantilever specimens, each representing a segment of a perforated shear wall, were constructed and tested. The first eight cantilever specimens were detailed according to the requirements of the 2011 MSJC *Code*, and intended to represent special and intermediate detailed reinforced masonry shear walls whose behavior was controlled by flexure. The remaining seven cantilever wall specimens were tested to investigate the response of masonry shear walls with the wider range of reinforcement contents that are possible for displacement-based design whose behavior was controlled by flexure. They were intended to provide experimental data to develop analytical models for flexure-dominated CMU wall segments subjected to earthquake ground motions. These specimens were also intended for use in refining current MSJC *Code* design formulas for flexural capacity, and to define appropriate values of drift ratio limits and displacement ductility capacities for CMU shear walls.

The geometry, flexural reinforcement, and axial force for each of the cantilever specimens were selected to force flexural behavior. The wall geometry for the cantilever specimens was selected to represent the aspect ratio of walls of potential CMU structures. The axial force in those specimens was varied to represent the range of compressive stresses found in typical reinforced masonry structures. Two photos of the test setup for this group of specimens are shown in Figure 4.1.

The main objective of this chapter is to summarize the experimental results from each cantilever shear wall tested at UT Austin. This chapter also includes the design objectives for each specimen, axial and lateral loading histories, observed major events during the test, and the hysteretic behavior. A full description of testing and the experimental results of the six of the cantilever shear wall (aspect ratio of 1.0), is given in Appendix C as written by Hernandez (2012).

Figure 4.1 Typical cantilever shear-wall specimens tested at UT Austin

4.2 SUMMARY OF DETAILS OF CANTILEVER SHEAR-WALL SPECIMENS AT UT AUSTIN

The cantilever shear-wall specimens tested at UT Austin used nominal 8- x 8- x 16-in. lightweight concrete masonry units (ASTM C90); coarse grout by proportion (ASTM C476); and ASTM C270 Type S cement-lime mortar by proportion. The geometry, aspect ratio, and applied axial load ratio for each shear wall specimen are summarized in Table 4-1, and the design calculation and drawings are shown in Appendix A.

Table 4-1 Overview of cantilever CMU wall specimens tested at UT Austin

specimen number	nominal length, in.	nominal height, in.	aspect ratio	axial load ratio
UT-W-13	48	144	3	0.05
UT-W-14	48	144	3	0.1
UT-W-15	48	144	3	0.1
UT-W-16	48	144	3	0.15
UT-W-17	32	144	4.5	0.05
UT-W-18	32	144	4.5	0.1
UT-W-19	32	144	4.5	0.1
UT-W-20	32	144	4.5	0.15
UT-PBF-05	32	144	4.5	0
UT-PBS-03	96	96	1	0
UT-PBS-04	96	96	1	0
UT-PBS-04G	96	96	1	0
UT-PBS-11	96	96	1	0.1
UT-PBS-12	96	96	1	0.1
UT-PBS-12G	96	96	1	0.1

4.3 DESIGN OF CANTILEVER WALL SPECIMENS AT UT AUSTIN

The design of the cantilever wall specimens at UT Austin involved the following steps:

1) select intended behavior and failure mode (for this group, flexure-dominated);
2) propose horizontal and vertical reinforcement for the wall specimen;
3) prepare an interaction diagram for the wall specimen showing the predicted in-plane capacity as a function of axial load;
4) select the axial load based on that interaction diagram; and
5) check shear capacity and shear sliding capacity for the specimen.

In this section, the process for selecting the wall geometry, reinforcement and axial load for one typical specimen (Specimen UT-W-13) is discussed. The selection of the wall geometry and reinforcement for the remaining specimens is included with the design of each specimen as presented in Appendix A. Specimen UT-W-13 has a height of 12 ft and a plan length of 4.0 ft (aspect ratio 3.0), reinforcement corresponding to MSJC *Code* requirements for special reinforced masonry shear walls, and a normalized axial load ratio $P / (f_m{}' A_g) = 0.05$.

4.3.1 Preliminary Check of Prescriptive Reinforcement Requirements for Specimen UT-W-13

Wall Specimen UT-W-13 was required to meet prescriptive reinforcement requirements. In accordance with the 2011 MSJC *Code*, the total reinforcement percentage (horizontal and vertical) shall be at least 0.002, with at least one-third of this placed in each direction. The corresponding steel area per foot is 0.002 x 7.63 in. x 12 in. = 0.2 in.^{2} per foot. These requirements will be re-checked as the design proceeds.

4.3.2 Computation of $\rho_{\max}$ for Specimen UT-W-13 based on Axial Load

Now check ρ_{max} , considering the wall as a special reinforced masonry shear wall ($R = 5$, $\alpha = 4$).

$$\rho_{\max} = \frac{0.64\, f_m^{'} \left(\dfrac{\varepsilon_{mu}}{\alpha\, \varepsilon_y + \varepsilon_{mu}} \right) - \dfrac{N_{critical}}{bd}}{f_y \left(\dfrac{\alpha\, \varepsilon_y - \varepsilon_{mu}}{\alpha\, \varepsilon_y + \varepsilon_{mu}} \right)}$$

$$N_{critical} = 0.05\, f_m^{'}\, A_g = 0.05 \times 2.5\, ksi \times 48\, in. \times 7.625\, in. = 45.75 \text{ kips}$$

$$\rho_{\max} = \frac{0.64 \times 2500\, psi \left(\dfrac{0.0025}{4 \times 0.00207 + 0.0025} \right) - \dfrac{45750\, lb}{7.625\, in. \times 48\, in.}}{60000\, psi \left(\dfrac{4 \times 0.00207 - 0.0025}{4 \times 0.00207 + 0.0025} \right)}$$

$$\rho_{\max} = \frac{1600\, psi\,(0.231) - 125}{60000\, psi\,(0.536)} = \frac{369.6 - 125}{32160}$$

$$\rho_{\max} = 0.0076$$

This maximum reinforcement is greater than the minimum vertical reinforcement (0.0007), so a design solution is possible.

4.3.3 Computation of Flexural Capacity of Specimen UT-W-13

Specimen UT-W-13 has a plan length of 4.0 ft, and an axial load (see above) of 45.75 kips. The nominal interaction diagram for Specimen UT-W-13 is shown in Figure 4.2. At an axial load of 45.75 kips, the nominal moment capacity of the wall is 306 kip-ft.

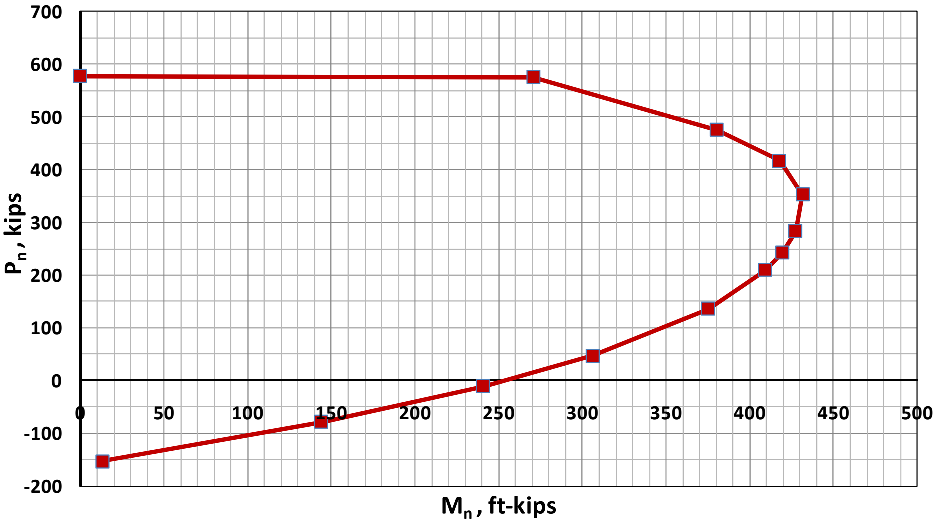

Figure 4.2 Strength moment-axial force interaction diagram for Specimen UT-W-13

4.3.4 Capacity Design for Shear, Specimen UT-W-13

Now check Code Section 3.1.3 (capacity design for shear) for Specimen UT-W-13. The wall is a special reinforced masonry shear wall, so the capacity design requirements of MSJC *Code* Section 1.17.3.2.6.1.1 apply. At an axial load of 45.75 kips, the nominal flexural capacity of this wall is 306 kip-ft. That corresponds to an applied shear of 306 kip-ft divided by the height of the wall (12 ft), or 25.5 kip. Including the additional factor of 1.25, the required nominal shear capacity is,

$$\phi V_n \geq 1.25\ V_u$$

$$V_n \geq \frac{1.25}{\phi} V_u = \frac{1.25}{0.8}\ V_u = 1.56\ V_u = 1.56 \times 25.5\ kips = 39.8\ kips$$

Now check shear capacity. From the 2011 MSJC *Code*, Section 3.3.4.1.2.1,

$$V_{nm} = \left[4.0 - 1.75\left(\frac{M_u}{V_u\, d_v}\right)\right] A_n \sqrt{f'_m} + 0.25P_u$$

Because the wall is a cantilever,

$$\frac{M_u}{V_u\, d_v} = \frac{H}{d_v} = \frac{12\ ft}{4\,ft} = 3.0$$

However, this quotient need not be taken greater than 1.0, so set it equal to that value:

$$V_{nm} = [4.0 - 1.75\,(1.0)]A_n\sqrt{f'_m} + 0.25P_u$$
$$V_{nm} = 2.25 \times 7.63\,in. \times 43.63\,in. \sqrt{2500} psi + 0.25 \times 45{,}750\,lb$$
$$V_{nm} = 52.3\,kips$$

The shear capacity of the wall is sufficient without shear reinforcement. Nominal reinforcement is sufficient. Prescriptive reinforcement requirements must be met. Required horizontal shear reinforcement is at least 0.0007. Use No. 4 bars at 16 in. horizontally.

$$\rho_{horizontal} = \frac{A_s}{bt} = \frac{0.2\ in.^2}{7.625 \times 16\ in.^2} = 0.0016$$

From the 2011 MSJC *Code*, Section 3.3.4.1.2.2,

$$V_{ns} = 0.5\left(\frac{A_v}{s}\right) f_y d_v$$

$$V_{ns} = 0.5\left(\frac{0.2\ in.^2}{16\ in.}\right) \times 60ksi \times 43.63\ in.$$

$$V_{ns} = 16.4\ kip$$
$$V_n = V_{nm} + V_{ns} = 52.3 + 16.4 = 68.7\ kip$$

This exceeds the required nominal shear capacity of 39.8 kips, and the design is satisfactory for shear.

4.3.5 Sliding-shear Capacity, Specimen UT-W-13

Sliding failure can occur in wall segments with low levels of axial load. Because the 2011 MSJC *Code* does not have general shear-friction provisions, the sliding-shear capacity of specimen was estimated using the shear-friction provisions of Section 11.6.4 of ACI 318-11. The coefficient of friction, μ, was considered equal to 1.0 when specimens were designed at the beginning of this study. As explained subsequently, based on the results of the wall tests, a coefficient of friction of 0.68 is recommended for use in design of surfaces that have not been intentionally roughened.

$$V_s = \mu\left(P + A_s f_y\right)$$
$$V_s = 1.0(45.75\ kip + 2.64\ in.^2 \times 60\ ksi) = 204.1\ kip$$

This exceeds the required nominal shear capacity of 39.8 kips, and the design is satisfactory for sliding shear.

4.3.6 Summary of Design, Specimen UT-W-13

Use No. 6 vertical bars at 8 in. (6 bars total) and No. 4 horizontal bars at 16 in., as shown in Figure 4.3. Using the same procedure for each of the other cantilever shear wall specimens, the intended failure mode and lateral capacities are summarized in Table 4-2.

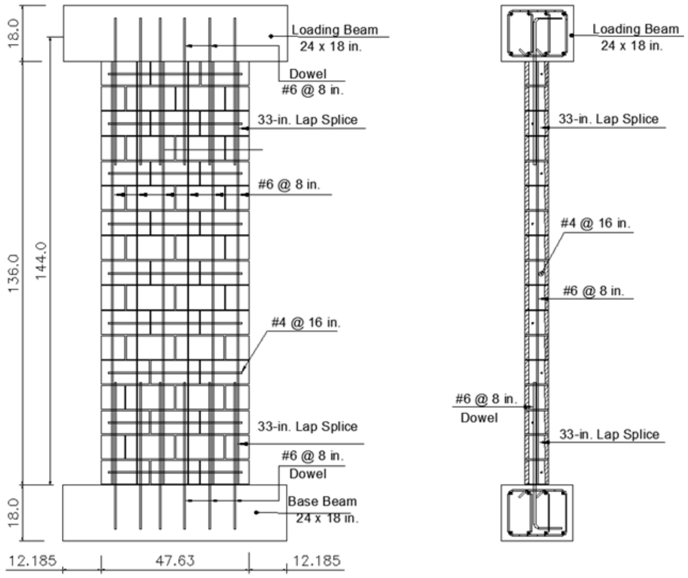

Figure 4.3 Reinforcement details for Specimen UT-W-13

Table 4-2 Test matrix for cantilever wall specimens at UT Austin

specimen number	vertical reinforcement	horizontal reinforcement	axial load ratio	flexural capacity, kips	shear capacity, kips	shear sliding, kips
UT-W-13	#6 @ 8 in.	#4 @ 16 in.	0.05	25.50	68.7	204.1
UT-W-14	#4 @ 8 in.	#4 @ 16 in.	0.1	21.25	80.0	163.5
UT-W-15	#6 @ 8 in.	#4 @ 16 in.	0.1	28.90	80.0	249.9
UT-W-16	#4 @ 8 in.	#4 @ 16 in.	0.15	25.10	91.4	209.3
UT-W-17	#6 @ 8 in.	#4 @ 8 in.	0.05	11.55	55.4	136.1
UT-W-18	#4 @ 8 in.	#4 @ 8 in.	0.1	9.10	63.1	109.0
UT-W-19	#6 @ 8 in.	#4 @ 16 in.	0.1	12.75	52.7	166.6
UT-W-20	#4 @ 8 in.	#4 @ 16 in.	0.15	11.10	60.36	139.5
UT-PBF-05	#8@ 8 in.	#4 @ 8 in.	0	14.58	47.8	189.6
UT-PBS-03	#4 @8	#4 @8	0	60.11	154.3	144.0
UT-PBS-04	#4 @16	#4 @16	0	31.43	118.3	72.0
UT-PBS-04G	#4 @16	#4 @16	0	31.43	118.3	72.0
UT-PBS-11	#4 @8	#4 @8	0.1	119.89	200.1	327.0
UT-PBS-12	#4 @16	#4 @16	0.1	98.06	164.1	255.0
UT-PBS-12G	#4 @16	#4 @16	0.1	98.06	164.1	255.0

4.4 INSTRUMENTATION AND DATA ACQUISITION FOR CANTILEVER SHEAR-WALL SPECIMENS (UT AUSTIN)

Each cantilever shear-wall specimen at UT Austin was instrumented with a variety of strain gauges, linear potentiometers, wire potentiometers, linear variable differential transformers, and load cells. These are described in detail below.

The reinforcement of each specimen was instrumented with strain gauges at critical locations, particularly where yielding was anticipated. Strain gauges were attached to base-beam dowels, extreme vertical reinforcements, and horizontal reinforcement (labeled as D, B, and H respectively in Figure 4.4). Base-beam dowels included one strain gauge at the base of the wall in every interior dowel, two strain gauges at the base of the wall (north and south), and single strain gauges every 8 in. from the base for exterior dowels. Extreme vertical reinforcements included four strain gauges every 8 in. from the base. In addition, four strain gauges were attached to horizontal bars: one strain gauge at each end of the horizontal reinforcement in the first course, and one strain gauge at the center of the horizontal reinforcement in the third and ninth courses from the bottom.

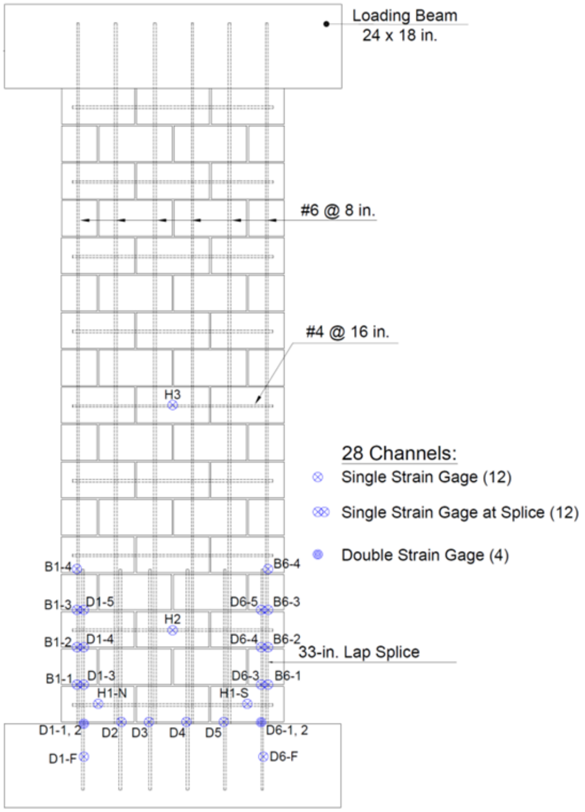

Figure 4.4 Typical locations of strain gauges in cantilever wall specimens (Specimen UT-W-13)

Linear potentiometers were located on the specimen to monitor lateral deformations, shear deformations, incremental vertical deformations at the ends of the specimen, axial deformations, sliding between base beam and shear wall panel, sliding between loading beam and shear wall panel, and any potential slip between the specimen and loading frame. As an example, locations of linear potentiometers are shown in Figure 4.5 for Specimen UT-W-13. Before each test, the end points of the instrument locations were measured so strains and local deformations could be accurately calculated during the test. The applied lateral force was measured using a load cell between the ram and clevis. The applied axial load was measured using a load cell in the rams of the axial load system.

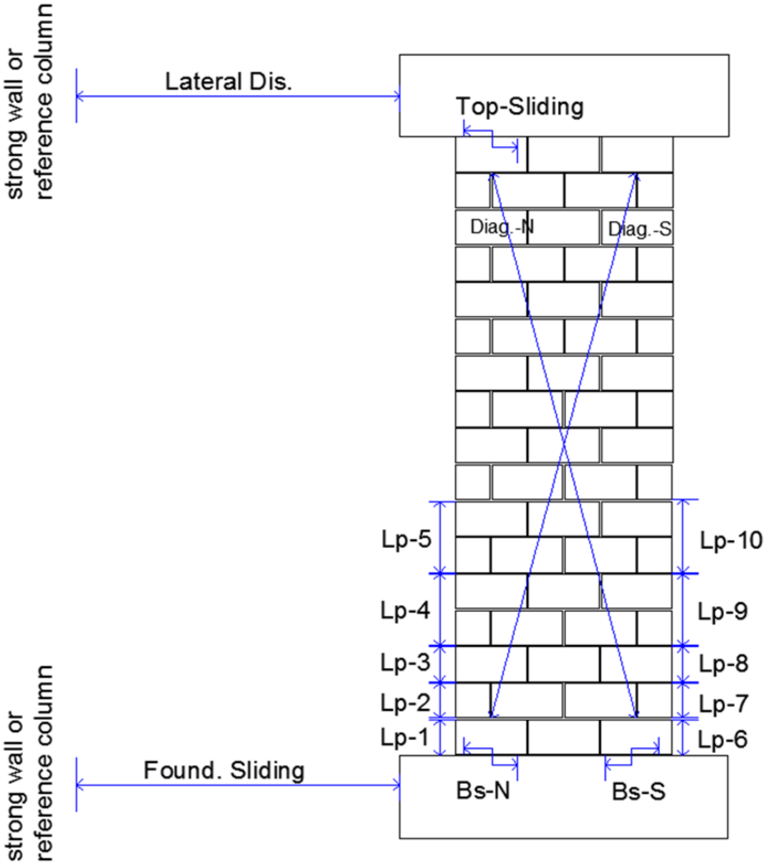

Figure 4.5 Locations of potentiometers on cantilever wall specimens (Specimen UT-W-13)

The data acquisition system (DAQ) consisted of a power supply, a HP-3852 data acquisition unit, and a PC computer with custom data acquisition software written in National Instruments LabView® programming system. The power supply provided an excitation voltage of 2V for strain gauges, and 10V for load cell and linear and string potentiometers. The HP-3852 data acquisition unit measured the analog signal (voltage) from the transducers. The transducers were connected in three different configurations. Strain gauges used a quarter-bridge circuit. Load cells were full-bridge circuits. Linear and string potentiometers used a voltage divider circuit. An analog-to-digital converter, also included in the HP-3852, provided the digital data that was processed in the LabView® program.

4.5 TEST RESULTS FROM CANTILEVER WALL SPECIMENS

In this section, test results for cantilever wall Specimen UT-W-13 are discussed. Detailed test results for the remaining cantilever shear-wall specimens are presented in Appendix B, and summaries of information from Hernandez (2012) are given in Appendix C.

Specimen UT-W-13 was detailed according to the requirements of the 2011 MSJC *Code*. It has a height of 12 ft and a plan length of 4 ft (aspect ratio 3.0), required prescriptive reinforcement for an Intermediate Reinforced Masonry Shear Wall (2011 MSJC Code), and a normalized axial load ratio P / ($f_m' A_g$) of 0.05. The vertical reinforcement ratio was 0.0072, with No. 6 reinforcing bars at 8 in. (every cell); and the horizontal reinforcement ratio was 0.0016, with No. 4 bars at 16 in. The specimen used cement-lime mortar conforming to the proportion specification for Type S of ASTM C270, and grout conforming to the strength specification of ASTM C476. A photo of the specimen before testing is shown in Figure 4.6, and details for the specimen are shown in Figure 4.7.

Figure 4.6 Specimen UT-W-13 before testing

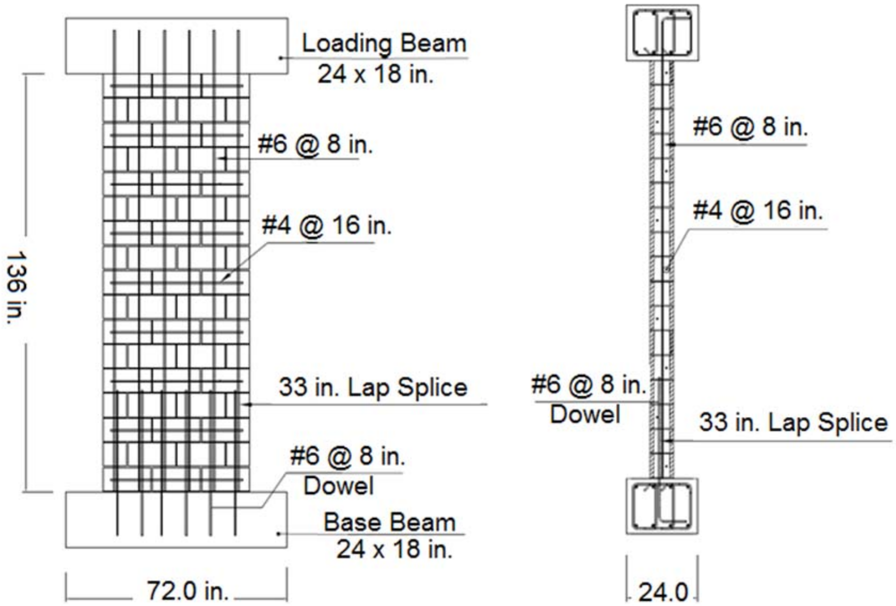

Figure 4.7 Details for Specimen UT-W-13

4.5.1 Loading History for Specimen UT-W-13

Specimen UT-W-13 was first subjected to a preliminary test phase to estimate the yield displacement, Δ_y. A moment-curvature analysis of the specimen was used to estimate the maximum flexural capacity, which was then converted to a peak horizontal load capacity. The specimen was subjected to two reversed cycles of load of ±25%, ±50%, and ±75% of that peak horizontal load capacity. The displacement from the first cycle to 75% of that peak horizontal load capacity was used to establish the probable Δ_y, by extrapolating the displacement at 75% of the maximum load to the displacement at 100% of the maximum load (displacement at 100% maximum load equals 4/3 times displacement at 75% maximum load).

Specimen UT-W-13 was loaded at a maximum rate of 0.3 in./min. to two cycles of reversed displacements of ±1, 2, 3, 4, 6, and 8 times that predicted yield displacement. It was then loaded to a half-cycle to a displacement of 10 times that predicted yield displacement. The planned in-plane loading history for base shear in the specimen is shown in Figure 4.8. The test was stopped when the peak capacity dropped to 20% or less of the experimentally observed peak capacity (capping point). The testing took about 8 hours. In this test the specimen was loaded first to the north and then to the south.

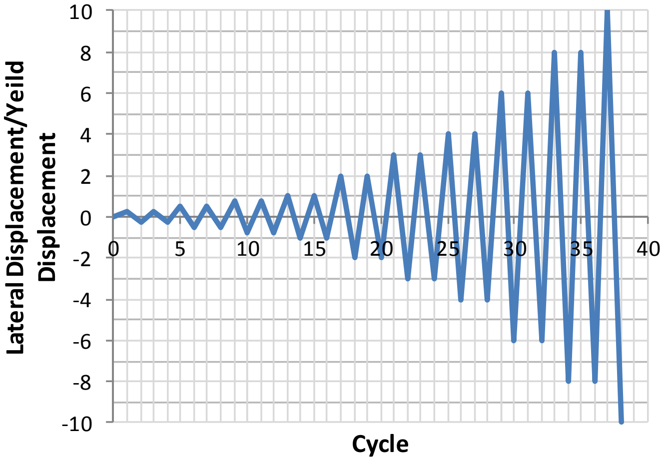

Figure 4.8 Proposed loading history for Specimen UT-W-13

4.5.2 Major Observations from Testing, Specimen UT-W-13

The behavior of Specimen UT-W-13 was controlled by flexure. The value of Δ_y calculated in the preliminary phase of the test was 0.75 in., equivalent to a drift ratio of 0.52 %. Flexural cracks (horizontal cracks in the bed joints) started early in the test before $1\Delta_y$, followed by shear cracks which propagated at $2\Delta_y$ displacement (1.04 % drift ratio) as presented in Figure 4.9a. As shown in Figure 4.10, evidence of toe crushing was found first at the south end at $2\Delta_y$ (1.04% drift ratio) and then at the north end at $3\Delta_y$ (1.56% drift). As shown in Figure 4.9b, the vertical bar at the north end began to buckle at the first cycle to $8\Delta_y$ (4.16% drift ratio), causing extensive spalling. There was no evidence of fracture or buckling of the vertical bars at the south end.

Figure 4.11 shows Specimen UT-W-13 upon completion of the test. As shown in Figure 4.12, reversed cyclic loading caused toe crushing and severe spalling in the compression toes at the base of the specimen. The transverse reinforcing bars, hooked around the longitudinal bar splices, kept the spliced bars at the north toe from coming apart after spalling there.

(a) Cycle 2Δy ***(a) Cycle 8Δy***

Figure 4.9 Flexural and shear cracking and buckling of longitudinal bars, Specimen UT-W-13

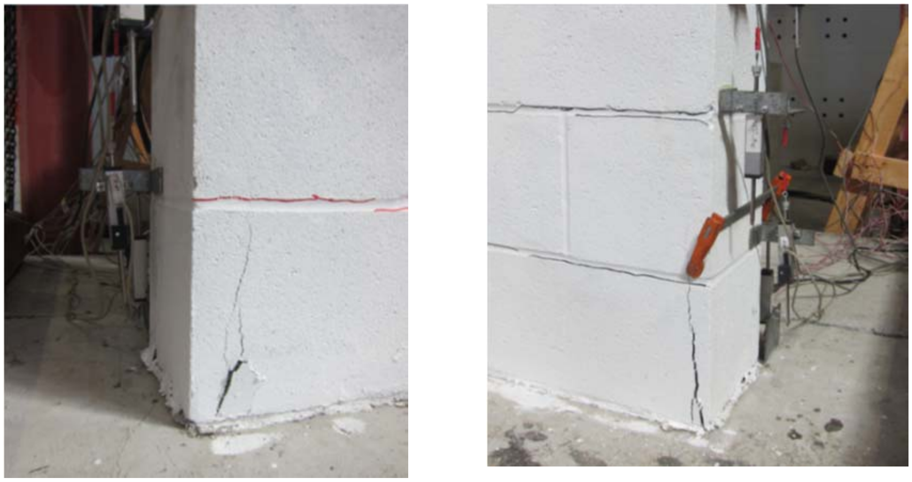

North toe ***South toe***

Figure 4.10 Onset of toe crushing, Specimen UT-W-13

Figure 4.11 Specimen UT-W-13 at end of test

North toe ***South toe***

Figure 4.12 Detail of toe crushing at end of test, Specimen UT-W-13

4.5.3 Load-Displacement Behavior for Specimen UT-W-13

The load-displacement relationship of Specimen UT-W-13 is presented in Figure 4.13 in terms of the lateral tip displacement, which references five major events during testing:

1) first yield of the extreme vertical reinforcement ($\varepsilon_y = 0.0021$);
2) the maximum useful strain in the masonry ($\varepsilon_{mu} = 0.0025$);
3) maximum capacity (capping point);
4) onset of toe crushing; and
5) decrease in capacity to 20% of peak capacity.

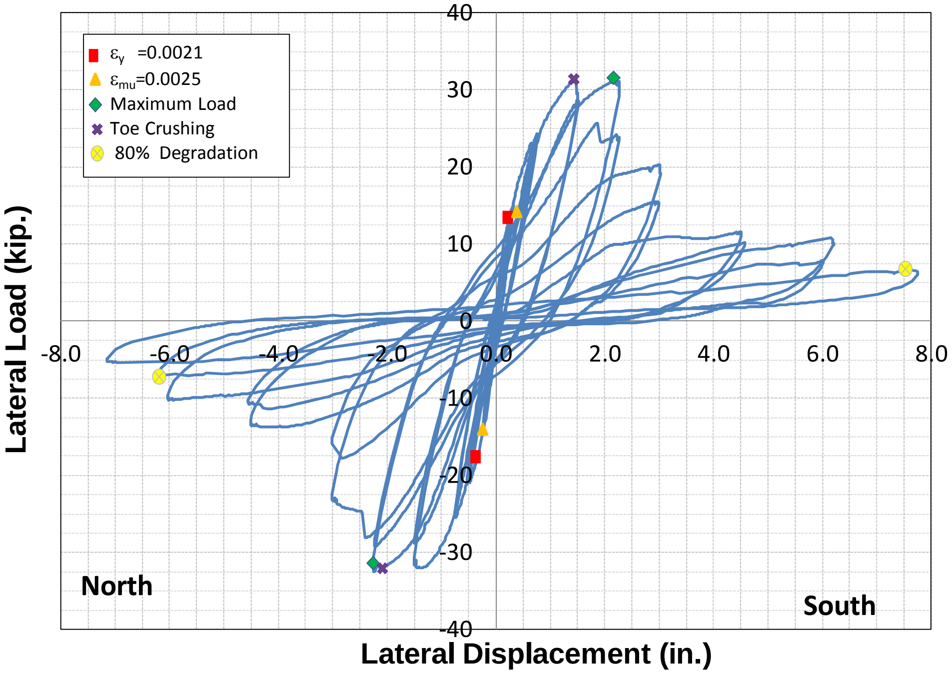

Figure 4.13 Load versus top displacement, Specimen UT-W-13

Curvatures were determined over the wall height based on strain profiles, and are shown in Figure 4.14. The strain profiles were calculated using five potentiometers along the inside edge of the wall (this was mirrored on the opposite side). The curvatures were determined for the first cycle to each displacement. Due to spalling of the face shells at the wall toes and detachment of the displacement potentiometer anchors, these displacement measurements were discontinued at later stages of testing. Therefore, strains and curvatures at larger displacements were not available.

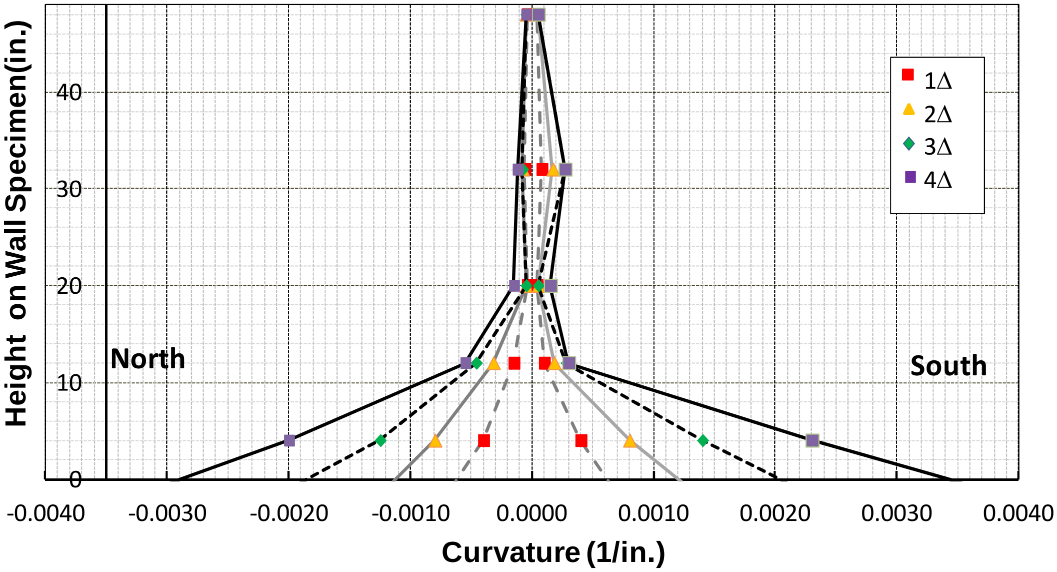

Figure 4.14 Wall Curvature of Specimen UT-W-13

4.5.4 Displacement Ductility, Specimen UT-W-13

The displacement ductility of Specimen UT-W-13 is defined using an elasto-plastic approximation (shown in the Figure 4.15), which is based on the actual area under the load-displacement envelope using the trapezoidal rule. The load-displacement envelope was composed of the peak loads of the first cycle at each displacement until 80% of peak capacity was reached (ultimate load). For a cantilever shear wall, the displacement ductility is determined from Equation 4-1.

$$\mu_{\Delta} = \frac{\Delta_u}{\Delta_y}$$ ***Equation 4-1***

Where:

μ_{Δ}= displacement ductility

Δ_u= displacement at ultimate load (in.)

Δ_y = equivalent yield displacement of elasto-plastic approximation (in.)

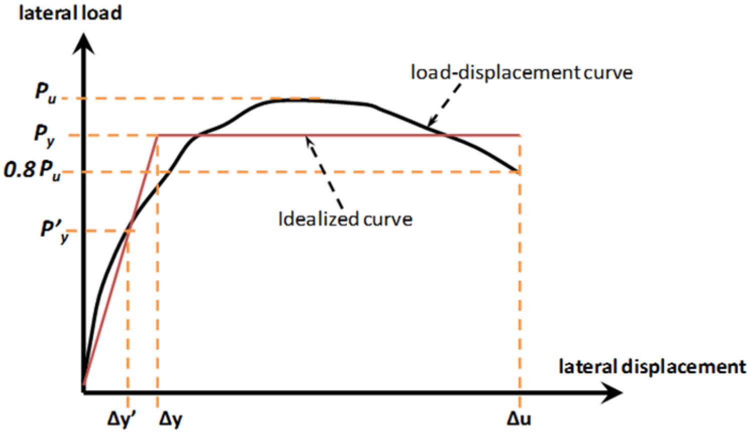

Figure 4.15 Elasto-plastic Approximation

The ultimate displacement in the equation above is defined at the ultimate load (80% of the capping capacity). The displacement of elasto-plastic approximation was defined as the intersection of the secant stiffness through the first yield of the extreme tensile reinforcement to the yield force of the elasto-plastic approximation. The equivalent yield force of the elasto-plastic approximation was determined from Equation 4-2.

$$P_y = \left(\frac{P'_y}{\Delta'_y}\right)\Delta_y$$ ***Equation 4-2***

Where:

P_y = yield force for elasto-plastic approximation (kips)

P'_y = force at first yield of tensile reinforcement (kips)

Δ_y = yield displacement for elasto-plastic approximation (in.)

Δ'_y = displacement at first yield of tensile reinforcement (in.)

The values obtained for the displacement ductility are presented in Table 4-3. The results are presented for both load directions (push to the North and pull to the South) and then averaged.

Table 4-3 Calculated displacement ductilities for Specimen UT-W-13

Direction of Load	**Load and Displacement Parameters**					
	P'_y (kips)	Δ'_y (in.)	Δ_u (in.)	P_y (kips)	Δ_y (in.)	μ_Δ
Push (North)	17.30	0.33	2.75	26.35	0.59	4.66
Pull (South)	12.63	0.22	2.52	27.55	0.48	5.25
					Average	4.95

The curvature ductility of Specimen UT-W-13 was also determined using a similar process as above and was determined from Equation 4-3.

$$\mu_\phi = \frac{\phi_u}{\phi_y}$$ ***Equation 4-3***

Where:

μ_ϕ = curvature ductility

ϕ_u = ultimate curvature at ultimate load (1/in.)

ϕ_y = curvature of elasto-plastic approximation (1/in.)

The elasto-plastic approximation for the curvature ductility was based on the actual area under the moment-curvature envelope, calculated using the trapezoidal rule. The values obtained for the curvature ductility are presented in Table 4-4. The results are presented for both load directions: push in the North and pull in the South, and then averaged between the two.

Table 4-4 Calculated curvature ductilities for Specimen UT-W-13

Direction of Load	**Moment and Curvature Parameters**					
	M'_y (kip-in.)	ϕ'_y (in.$^{-1}$)	ϕ_u (in.$^{-1}$)	M_y (kip-in.)	ϕ_y (in.$^{-1}$)	μ_ϕ
Push (North)	2491	0.00010	0.0031	3794	0.00015	20.3
Pull (South)	1818	0.00011	0.0037	3967	0.00024	15.2
					Average	17.7

4.5.5 Calculation of Plastic Hinge Lengths, Specimen UT-W-13

4.5.5.1 Method 1 (Bohl and Adebar 2011 and Shedid et al. 2010)

The height of the yielded length ($L_{yielded}$), as shown in Figure 4.16, is taken as the height above the foundation at which the curvature is equal to the yield curvature, and l_p is the corresponding plastic hinge length assuming a uniform inelastic curvature, ϕ_u.

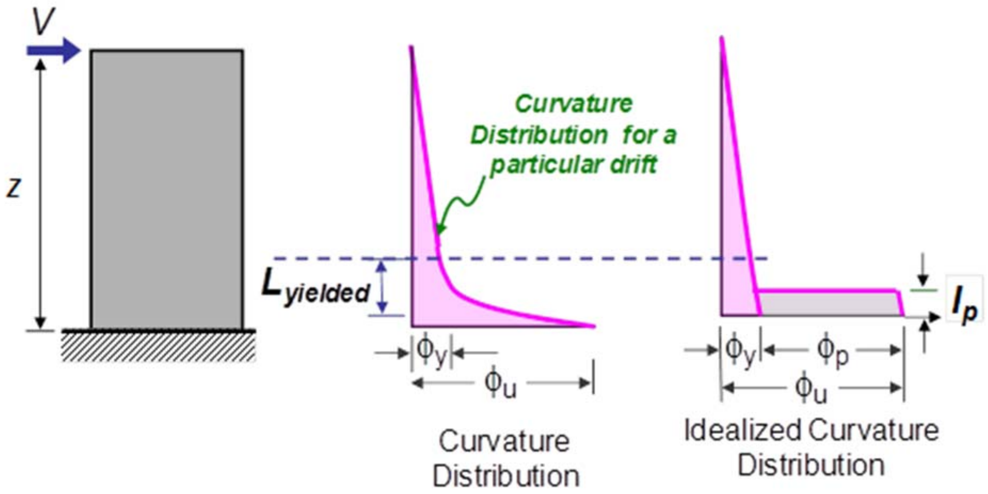

Figure 4.16 Definitions of yielded length and plastic hinge length

In Table 4-5, the calculated yielded lengths are presented as a function of drift ratio for each load direction, and are then averaged between the two directions. In the last line of the table, the calculated yielded lengths are expressed in terms of L_w , the plan length of the wall. Although this representation may not the most useful for masonry walls, it is used for reinforced concrete beams.

Table 4-5 Yielded lengths of Specimen UT-W-13

Drift Ratio (Displacement)	**Yielded Lengths, $L_{yielded}$ (in.), for Different Drift Ratios**			
	0.52% (Δ_y)	**1.04% ($2\Delta_y$)**	**1.56% ($3\Delta_y$)**	**2.08% ($4\Delta_y$)**
Push North	12.5	16.5	18.0	20.5
Pull South	9.5	13.0	15.5	17.5
Average	11.0	14.75	16.75	19.0
$L_{yielded}/L_w$	22.9%	30.7%	34.9%	39.6%

In practice, the non-uniform inelastic curvatures in the yielded length are idealized as a uniform curvature equal to ϕ_u , over an equivalent calculated plastic hinge length, l_p. That plastic hinge length l_p can be calculated using the condition that the calculated tip displacement must be the same whether the yielded length or the plastic hinge length is used in the calculation. Alternatively and more simply, the plastic hinge length can be assumed equal to one-half the yielded length. If the plastic hinge length l_p is assumed equal to 0.5 $L_{yielded}$, then the resulting plastic hinge lengths are as shown in Table 4-6 for each drift ratio.

Table 4-6 Calculation of plastic hinge lengths of Specimen UT-W-13

Drift Ratio (Displacement)	**Plastic Hinge Lengths, l_p (in.), for Different Drift Ratios**			
	0.52% (Δ_y)	**1.04% ($2\Delta_y$)**	**1.56% ($3\Delta_y$)**	**2.08% ($4\Delta_y$)**
Yielded Length	11.0	14.75	16.75	19.0
Plastic Hinge Length (l_p)	5.5	7.38	8.38	9.5
l_p/L_w	11.45%	15.35%	17.45%	19.8%

4.5.5.2 Method 2 (Shedid et al. 2010 and Dazio 2009)

In this method, the plastic hinge length (l_p) is determined by rearranging Equation 4-4, which represents the tip displacement of the wall at different drift ratios.

$$\Delta_u = \Delta_y + (\emptyset - \emptyset_y) l_p \left(h_w - \frac{l_p}{2}\right)$$

Equation 4-4

In this equation, h_w is the height of the wall. The first term represents the displacement at first yield of the extreme tension reinforcement, and the second term represents the plastic displacement corresponding to the idealized curvature profile over the wall height. By solving the displacement of Equation 4-4 for l_p, the plastic hinge length is expressed by Equation 4-5.

$$l_p = h_w - \sqrt{{h_w}^2 - 2\left(\frac{\Delta_u - \Delta_y}{\emptyset - \emptyset_y}\right)} \qquad \textit{Equation 4-5}$$

The equivalent plastic hinge lengths for both load directions at different drift ratios are calculated as shown in Table 4-7.

Table 4-7 Equivalent plastic hinge length of Specimen UT-W-13

Drift Ratio (Displacement)	**Plastic Hinge Lengths, l_p (in.), for Different Drift Ratios**			
	0.52% (Δ_y)	**1.04% ($2\Delta_y$)**	**1.56% ($3\Delta_y$)**	**2.08% ($4\Delta_y$)**
Push North	12.8	13.3	12.9	10.6
Pull South	10.7	12.1	10.7	8.8
Average	11.75	12.7	11.8	9.7
l_p/L_w	24.5%	26.5%	24.6%	20.2%

4.5.5.3 Method 3 (Bohl and Adebar 2011)

A different approach to predict the plastic hinge length is by using moments; that is, the yield moment determined from the force-displacement envelope defines the length of the plastic hinge. For a linear bending moment like the one shown in Figure 4.17, the length where the yielding moment is exceeded can be determined from Equation 4-6.

$$\boldsymbol{L_{yielded} = z\left(1 - \frac{M_y}{M_{max}}\right)} \qquad \textit{Equation 4-6}$$

In that figure, z is the shear span (distance from maximum to zero bending moment), M_y is the bending moment at first yield of the reinforcement, and M_{max} is the maximum bending moment. The load-displacement curve is used to calculate M_y and M_{max} .

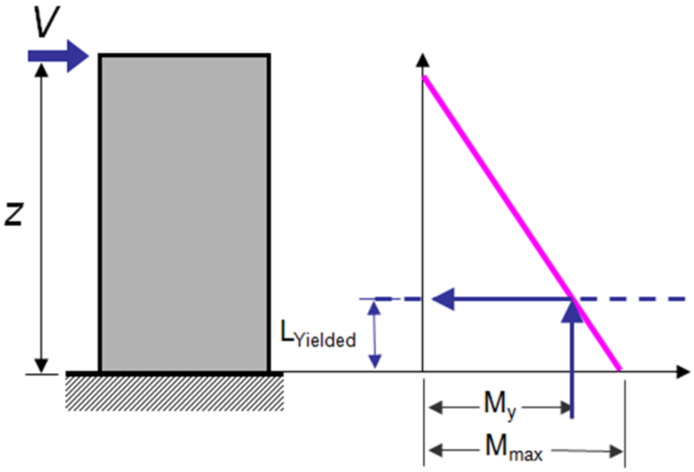

Figure 4.17 Bending moment diagram for a cantilever element

As mentioned previously, in Method 1, the plastic hinge length l_p over which curvatures can be assumed to be uniform is equal to 0.5 $L_{yielded}$, because the same inelastic tip displacement results if the maximum inelastic curvature is uniform over a height l_p = 0.5 $L_{yielded}$. The calculated (using Equation 4-6) plastic hinge lengths were determined for both load direction: push in the North, and pull in the South. The results are shown in Table 4-8.

Table 4-8 Predicted plastic hinge lengths for Specimen UT-W-13

Direction of Load	**Moment and Plastic Hinge Parameters**					
	M_y (kip-in.)	M_{max} (kip-in.)	z (in.)	$L_{yielded}$ (in.)	$l_p = 0.5L_{yielded}$ (in.)	l_p/L_w
Push (North)	2491	4674	144	67.2	33.6	0.70
Pull (South)	1818	4534	144	86.2	43.1	0.90
				Average	38.3	0.80

4.5.6 Contributions to Displacements for Specimen UT-W-13

The total lateral displacements of the wall were the combination of flexural, sliding, and shear displacements. The total in-plane lateral displacement was measured with a linear potentiometer attached to an external reference frame at the level of the loading beams. Linear potentiometers recorded the average sliding displacements between the wall base and the base beam. Shear displacements were measured with two diagonally-oriented linear potentiometers and were calculated based on a previous study by Massone and Wallace (2004). Load-displacement curves for total sliding and shear component of total tip displacement are given in Figure 4.18 and Figure 4.19, and total displacement and shear deformation are compared in Figure 4.20.

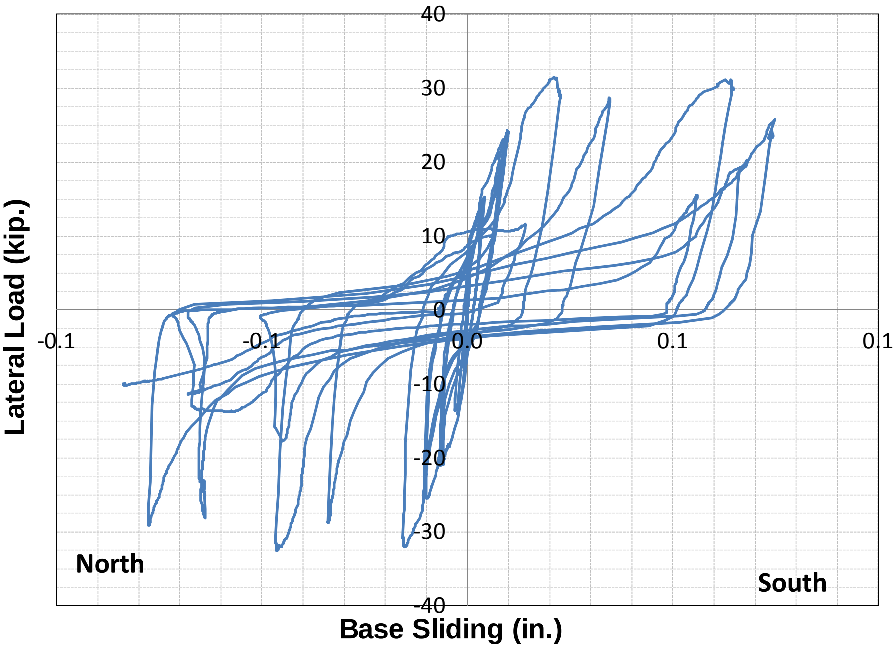

Figure 4.18 Base sliding, Specimen UT-W-13

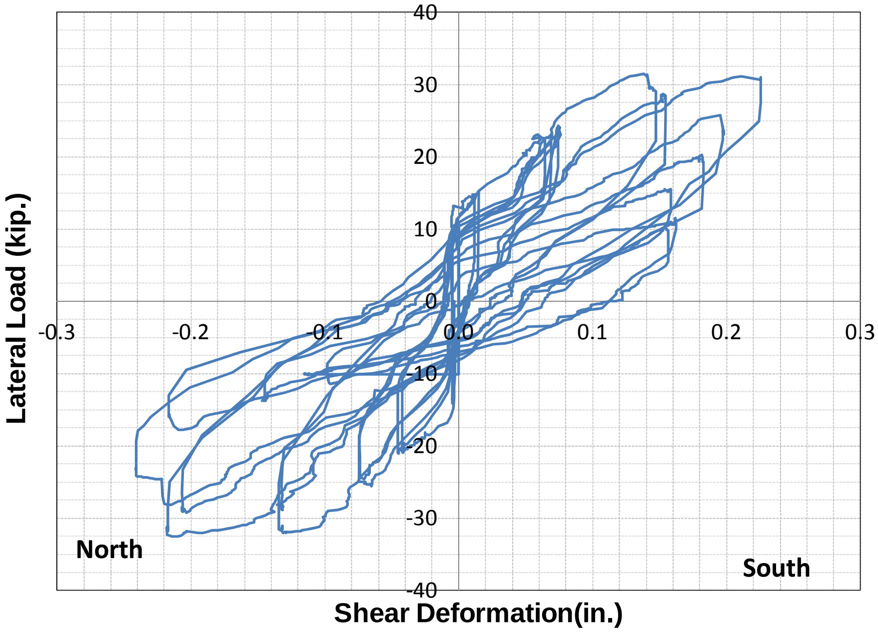

Figure 4.19 Shear deformation, Specimen UT-W-13

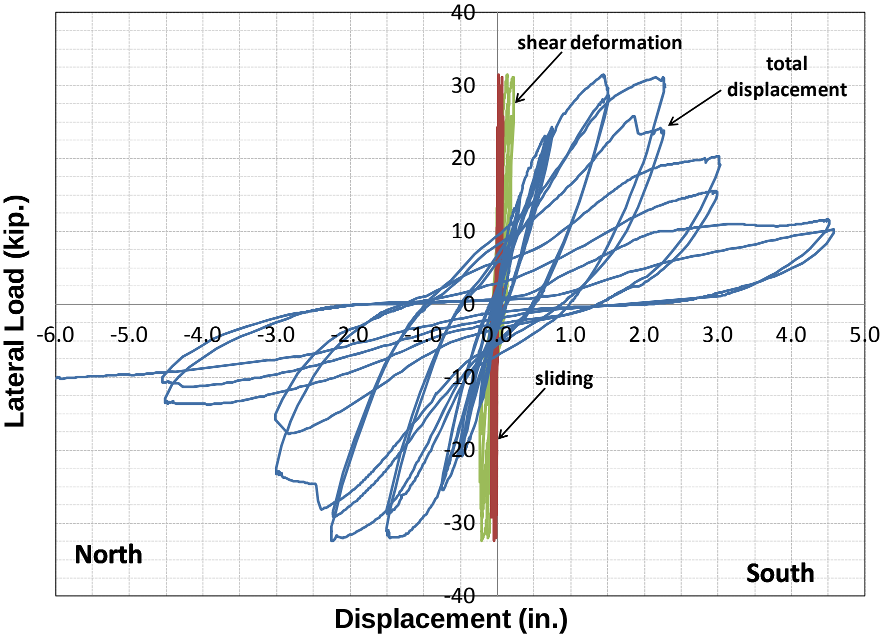

Figure 4.20 Components of displacements for Specimen UT-W-13

4.6 SUMMARY OF EVALUATION OF RESULTS FOR CANTILEVER SHEAR WALLS

In this section, the test results for all fifteen cantilever specimens are summarized and evaluated. Computed capacity is compared with experimental capacity. The contribution of deformation components, load-displacement curve, displacement ductility, height of plasticity, and plastic hinge length are summarized and correlated with the level of axial load and the vertical reinforcement ratio of each specimen.

4.6.1 Observed versus Computed Flexural Capacities

In Table 4-9, nominal flexural capacities based on the 2011 MSJC *Code* are compared with the average experimental peak load (averaged for both loading directions) are for each wall specimen. Maximum loads in the test ranged from 3% to 49% higher than the predicted capacities. Specimens UT-W-18 and UT-PBS-12G provided the closest results to the predicted. Excluding Specimens UT-W-18 and UT-PBS-12G, test results ranged from 14% to 57% higher than the predicted capacities.

On average, calculated nominal capacities based on the MSJC *Code* underestimated the observed capacities by about 24% for all axial load levels. In general, for cantilever reinforced elements the relationship between tested capacities and nominal capacities depends on the strain demand in the reinforcement; increased strain demand results in increased capacity. Strain-hardening in vertical reinforcement is maintained to a peak capacity that typically is about 1.25 times the nominal capacity. In an earlier study, Vaughan (2010) reports that the predicted load capacities underestimated experimental capacities by about 7%, and Sherman (2011) reports experimental peak capacities from the reversed cyclic testing that were about 23% and 10% more than the nominal capacities of the 2011 MSJC *Code*.

Table 4-9 Comparison of nominal and experimental capacities for cantilever wall specimens

Specimen	Average Experimental Capacity (kips)	Nominal Capacity from 2011 MSJC Code (kips)	Ratio of Experimental Capacity Divided by Nominal Capacity
UT-W-13	31.97	25.50	1.25
UT-W-14	24.17	21.25	1.14
UT-W-15	35.96	28.90	1.24
UT-W-16	27.20	25.10	1.08
UT-W-17	14.50	11.55	1.26
UT-W-18	9.38	9.10	1.03
UT-W-19	17.52	12.75	1.37
UT-W-20	14.15	11.10	1.27
UT-PBF-05	17.75	14.58	1.22
UT-PBS-03	81.98	60.11	1.36
UT-PBS-04	47.12	31.43	1.50
UT-PBS-04G	41.74	31.43	1.33
UT-PBS-11	153.28	119.89	1.28
UT-PBS-12	113.69	98.06	1.16
UT-PBS-12G	102.11	98.06	1.04

4.6.2 Relative Contributions from Flexural, Shearing, and Sliding Deformations

Relative drift contributions from flexural, shearing, and sliding deformations for all specimens are summarized in Table 4-10. Flexural deformation dominated in all specimens at maximum load and at ultimate load (80% of maximum load). Shearing deformations contributed more at maximum load than at ultimate loads because of large inelastic deformations at the base of wall segments at ultimate. Walls with an aspect ratio of 1.0 had more drift contributions from sliding and shear than walls with height-to-length aspect ratios of 3.0 and 4.5. Shearing deformations contributed between 5% and 22% of the total displacements. As shown in Table 4-10, walls with an aspect ratio of 1.0 and zero axial load had sliding that accounted for between 23% and 35% of the total displacements. These were significantly higher than the walls with aspect ratios of 3.0 and 4.5, for which sliding deformations contributed from 1% to 4%. This shows that sliding deformation was more important for walls with zero axial load and lower aspect ratio. Specimen UT-PBS-04, with a wall aspect ratio of 1.0 and no axial load, exhibited the largest sliding deformations at 35% of the total.

4.6.3 Lateral Drift Ratios for Cantilever Wall Specimens

The average total drift for each cantilever wall is presented in Table 4-11 at two limit states: maximum observed lateral load and ultimate load (80% of the maximum load).

At maximum load, walls with aspect ratio of 1.0 (excluding UT-PBS-04 and UT-PBS-04G specimen results) had an average drift of approximately 0.67%; walls with aspect ratio of 3.0 had drifts of approximately 1.5%; and walls with aspect ratio of 4.5 had drifts of approximately 2.6%. Results showed higher drift capacity for specimens UT-PBS-04 and UT-PBS-04G; this can be also attributed to the contribution of sliding in the lateral displacement, especially at ultimate load (Hernandez 2012). The average total drift at ultimate load ranged from 1.31% to 4.51%. Sherman (2011) reports values for average total drift at ultimate lateral load ranging from 0.9% to 2.8% for walls with aspect ratios of 0.78, 1.0, and 2.0 designed with 2011 MSJC *Code* provisions. Maximum drift ratios were not affected by vertical reinforcement, but did increase with increasing aspect ratio.

Table 4-10 Relative contributions from flexural, shearing, and sliding deformation for all specimens

Specimen	**Aspect Ratio**	**Vertical Rein. Ratio**	**Axial Load Ratio**	**Maximum Load**			**Ultimate Load**		
				Flexure	Shear	Sliding	Flexure	Shear	Sliding
UT-W-13	3.0	0.72%	0.05	89%	9%	2%	90%	8%	2%
UT-W-14	3.0	0.33%	0.10	78%	21%	1%	83%	16% **	1%
UT-W-15	3.0	0.72%	0.10	84%	15%	1%	87%	12% **	1%
UT-W-16	3.0	0.33%	0.15	81%	18%	1%	-*	-*	-*
UT-W-17	4.5	0.72%	0.05	84%	4%	2%	-*	-*	-*
UT-W-18	4.5	0.33%	0.10	91%	5%	4%	-*	-*	-*
UT-W-19	4.5	0.72%	0.10	90%	9%	1%	-*	-*	-*
UT-W-20	4.5	0.33%	0.15	82%	16%	2%	85%	12%**	3%
UT-PBF-05	4.5	1.29%	0	92%	7%	1%	93%	6%**	1%
UT-PBS-03	1.0	0.33%	0	64%	13%	23%	60%	14%	26%
UT-PBS-04	1.0	0.16%	0	54%	11%	35%	66%	4%	30%
UT-PBS-04G	1.0	0.16%	0	54%	22%	24%	57% **	20% **	23% **
UT-PBS-11	1.0	0.33%	0.10	-*	-*	-*	-*	-*	-*
UT-PBS-12	1.0	0.16%	0.10	81%	13%	6%	77% **	13% **	10% **
UT-PBS-12G	1.0	0.16%	0.10	80%	14%	6%	93% **	5% **	2% **

* Instrumentation failed, ** calculated based on the results in one direction

Table 4-11 Average drift ratios for maximum and ultimate load, cantilever wall specimens

Specimen	Aspect Ratio	Vertical Reinforcement (ratio)	Axial Load Ratio	Average Drift Ratio	
				at Maximum Load	at Ultimate Load
UT-W-13	3.0	#6 @ 8 in. (0.72)	0.05	1.56%	1.841%
UT-W-14	3.0	#4 @ 8 in. (0.33)	0.10	1.93%	2.91%
UT-W-15	3.0	#6 @ 8 in. (0.72)	0.10	1.17%	2.11%
UT-W-16	3.0	#4 @ 8 in. (0.33)	0.15	1.27%	2.10%
UT-W-17	4.5	#6 @ 8 in. (0.72)	0.05	3.00%	4.51%
UT-W-18	4.5	#4 @ 8 in. (0.33)	0.10	2.61%	3.14%
UT-W-19	4.5	#6 @ 8 in. (0.72)	0.10	2.79%	3.42%
UT-W-20	4.5	#4 @ 8 in. (0.33)	0.15	1.65%	2.83%
UT-PBF-05	4.5	#8 @ 8 in. (1.29)	0	3.39%	4.47%
UT-PBS-03	1.0	#4 @ 8 in. (0.33)	0	0.84%	1.66%
UT-PBS-04	1.0	#4 @ 16 in. (0.16)	0	1.76%	2.52%
UT-PBS-04G	1.0	#4 @ 16 in. (0.16)	0	1.78%	2.77%
UT-PBS-11	1.0	#4 @ 8 in. (0.33)	0.10	0.76%	1.31%
UT-PBS-12	1.0	#4 @ 16 in. (0.16)	0.10	0.54%	1.36%
UT-PBS-12G	1.0	#4 @ 16 in. (0.16)	0.10	0.52%	1.72%

4.6.4 Displacement Ductilities for Cantilever Wall Specimens

Displacement ductility in both directions and their averages are shown in Table 4-12 for all cantilever wall specimens. Excluding walls with an aspect ratio of 1.0 which had slip in lap splices (Hernandez, 2012), higher displacement ductilities were found for specimens with higher aspect ratios and lower axial load ratios. Under the same axial load ratio, displacement ductility decreased with increasing vertical reinforcement ratio. This is expected.

Table 4-12 Displacement ductilities, cantilever wall specimens

Specimen	Aspect Ratio	Vertical Reinforcement (percentage)	Axial Load Ratio P/ (Ag fm')	Displacement Ductility		
				North	South	Average
UT-W-13	3.0	#6 @ 8 in. (0.72)	0.05	4.66	5.25	4.66
UT-W-14	3.0	#4 @ 8 in. (0.33)	0.10	5.02	4.96	4.99
UT-W-15	3.0	#6 @ 8 in. (0.72)	0.10	3.80	3.60	3.70
UT-W-16	3.0	#4 @ 8 in. (0.33)	0.15	5.00	5.03	5.02
UT-W-17	4.5	#6 @ 8 in. (0.72)	0.05	6.20	6.37	6.28
UT-W-18	4.5	#4 @ 8 in. (0.33)	0.10	11.57	7.16	9.36
UT-W-19	4.5	#6 @ 8 in. (0.72)	0.10	5.57	4.08	4.96
UT-W-20	4.5	#4 @ 8 in. (0.33)	0.15	5.64	5.57	5.60
UT-PBF-05	4.5	#8 @ 8 in. (1.29)	0	6.30	4.70	5.50
UT-PBS-03	1.0	#4 @ 8 in. (0.33)	0	19.71	12.88	16.29
UT-PBS-04	1.0	#4 @ 16 in. (0.16)	0	11.23	5.53	8.38
UT-PBS-04G	1.0	#4 @ 16 in. (0.16)	0	19.31	14.76	17.04
UT-PBS-11	1.0	#4 @ 8 in. (0.33)	0.10	8.01	6.59	7.30
UT-PBS-12	1.0	#4 @ 16 in. (0.16)	0.10	12.75	9.39	11.07
UT-PBS-12G	1.0	#4 @ 16 in. (0.16)	0.10	10.52	6.81	8.66

4.6.5 Yielded Lengths for Cantilever Wall Specimens

Using Method 1 (Bohl and Adebar (2011) and Shedid *et al.* (2010)), the ratio of the yielded length to the plan length of the wall specimen is presented in Table 4-13 for all the cantilever wall specimens. Average values ranged from 35% to 83%. Shedid et al. (2010) report ratios of yielded length to wall plan length ranging from 43% to 78%. Sherman (2011) concludes that the yielded length is about 16% to 75% of the wall plan length. The yielded length was not influenced by vertical reinforcement ratio or axial load; however, higher the yielded lengths were found for specimens with higher aspect ratios.

Table 4-13 Yielded lengths at drift ratio of 1.5%, cantilever wall specimens

Specimen	Aspect Ratio	Vertical Reinforcement (percentage)	Axial Load Ratio P/ (Ag f'm)	Height of plasticity (%Lw)		
				North	South	Average
UT-W-13	3.0	#6 @ 8 in. (0.72)	0.05	37%	33%	35%
UT-W-14	3.0	#4 @ 8 in. (0.33)	0.10	58%	61%	59%
UT-W-15	3.0	#6 @ 8 in. (0.72)	0.10	81%	86%	83%
UT-W-16	3.0	#4 @ 8 in. (0.33)	0.15	57%	59%	58%
UT-W-17	4.5	#6 @ 8 in. (0.72)	0.05	36%	38%	37%
UT-W-18	4.5	#4 @ 8 in. (0.33)	0.10	38%	40%	39%
UT-W-19	4.5	#6 @ 8 in. (0.72)	0.10	81%	72%	76%
UT-W-20	4.5	#4 @ 8 in. (0.33)	0.15	68%	75%	71%
UT-PBF-05	4.5	#8 @ 8 in. (1.29)	0	95%	46%	71%
UT-PBS-03	1.0	#4 @ 8 in. (0.33)	0	42%	40%	41%
UT-PBS-04	1.0	#4 @ 16 in. (0.16)	0	-*	-*	-*
UT-PBS-04G	1.0	#4 @ 16 in. (0.16)	0	51%	31%	41%
UT-PBS-11	1.0	#4 @ 8 in. (0.33)	0.10	31%	39%	35%
UT-PBS-12	1.0	#4 @ 16 in. (0.16)	0.10	48%	49%	48%
UT-PBS-12G	1.0	#4 @ 16 in. (0.16)	0.10	58%	22%	40%

* Instrumentation failed

4.6.6 Plastic Hinge Lengths for Cantilever Wall Specimens

Using Method 1 (Bohl and Adebar 2011 and Shedid *et al.* 2010), the ratio of plastic hinge length to the plan length of the wall is presented in Table 4-14 for the cantilever wall specimens. Average values ranged from 17% to 41%. Shedid *et al.* (2010) reported drift ratios of the plastic hinge length to wall length that ranged from 17% to 37%. Sherman (2011) concludes that plastic hinge length is about 15% to 64% of the wall plan length. Eikanas (2003) and Paulay and Priestley (1992) found smaller plastic hinge lengths at larger aspect ratios. However, aspect ratio does not have a significant effect on the plastic hinge length for this group of walls, nor for those studied by Sherman (2011) and Shedid et al. (2010). The test results also show that plastic hinge length was not influenced by vertical reinforcement ratio or axial load.

Table 4-14 Plastic hinge length at drift ratio of 1.5%, cantilever wall specimens

Specimen	Aspect Ratio	Vertical Reinforcement (percentage)	Axial Load Ratio P/ (Ag f'm)	Plastic Hinge Length (%Lw)		
				North	South	Average
UT-W-13	3.0	#6 @ 8 in. (0.72)	0.05	19%	17%	18%
UT-W-14	3.0	#4 @ 8 in. (0.33)	0.10	29%	30%	29%
UT-W-15	3.0	#6 @ 8 in. (0.72)	0.10	40%	41%	41%
UT-W-16	3.0	#4 @ 8 in. (0.33)	0.15	29%	30%	29%
UT-W-17	4.5	#6 @ 8 in. (0.72)	0.05	18%	19%	19%
UT-W-18	4.5	#4 @ 8 in. (0.33)	0.10	19%	20%	20%
UT-W-19	4.5	#6 @ 8 in. (0.72)	0.10	40%	36%	38%
UT-W-20	4.5	#4 @ 8 in. (0.33)	0.15	34%	36%	35%
UT-PBF-05	4.5	#8 @ 8 in. (1.29)	0	47%	23%	35%
UT-PBS-03	1.0	#4 @ 8 in. (0.33)	0	21%	20%	21%
UT-PBS-04	1.0	#4 @ 16 in. (0.16)	0	-*	-*	-*
UT-PBS-04G	1.0	#4 @ 16 in. (0.16)	0	26%	15%	21%
UT-PBS-11	1.0	#4 @ 8 in. (0.33)	0.10	15%	19%	17%
UT-PBS-12	1.0	#4 @ 16 in. (0.16)	0.10	24%	25%	25%
UT-PBS-12G	1.0	#4 @ 16 in. (0.16)	0.10	29%	11%	20%

* Instrumentation failed

4.6.7 Effect of Key Parameters on Load-displacement Curves, Cantilever Wall Specimens

The following sections address the relationship between key design variables (wall aspect ratio, applied axial load, and reinforcement quantity) and the overall load-displacement behavior of the cantilever wall specimens tested at UT Austin. In these sections, the normalized load-displacement curves (backbone) for all comparable specimens are plotted in terms of the lateral drift ratio and the ratio of experimental capacity of the walls over the MSJC nominal capacities.

4.6.7.1 Effect of Aspect Ratio on Hysteretic Response of Cantilever Wall Specimens

The relationship between the wall aspect ratio and shear wall load-displacement behavior is evaluated through testing Specimens UT-W-14, UT-W-16, UT-W-18, UT-W-20, UT-PBS-03, and UT-PBS-11 for three different aspect ratios. The relevant design parameters for these six specimens are given in Table 4-15. The normalized load-displacement backbone curves for this group of walls are given in Figure 4.21.The lateral initial stiffness of the wall specimens increased as the aspect ratio decreased. For all but one specimen, the ratio of observed versus nominal flexural capacities of wall specimens also increased as the aspect ratio decreased. Walls with aspect ratio of 1.0 experienced more rapid strength degradation than did walls with aspect ratios of 3.0 and 4.50. As shown in Figure 4.21 the lateral drift ratio at ultimate load (80% of peak capacity) increased with increasing aspect ratio.

Table 4-15 Evaluation of aspect ratio effect on load-displacement curve

specimen number	**aspect ratio**	**axial force ratio**	**vertical reinforcement**	**horizontal reinforcement**
UT-W-14	3	0.1	#4 @ 8 in.	#4 @ 16 in.
UT-W-16		0.15	#4 @ 8 in.	#4 @ 16 in.
UT-W-18	4.5	0.1	#4 @ 8 in.	#4 @ 8 in.
UT-W-20		0.15	#4 @ 8 in.	#4 @ 16 in.
UT-PBS-03	1	0	#4 @ 8 in.	#4 @ 8 in.
UT-PBS-11		0.1	#4 @ 8 in.	#4 @ 8 in.

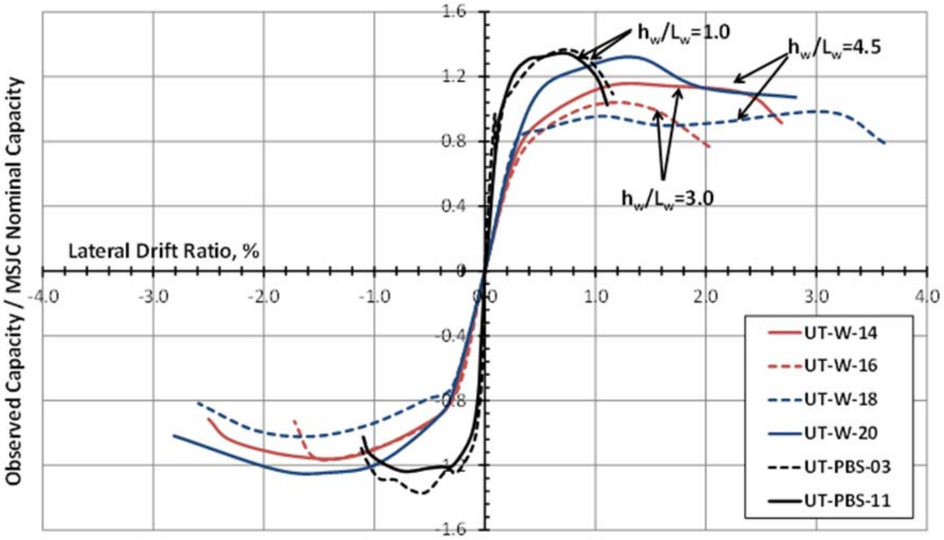

Figure 4.21 Normalized load-displacement backbones for aspect ratio comparison, cantilever wall specimens

4.6.7.2 Effect of Axial Load on Hysteretic Response of Cantilever Wall Specimens

In this section, the effect of axial compressive force on load-displacement behavior is evaluated using results of two groups of walls. Table 4-16 contains the parameters associated with this group of comparable walls for aspect ratios of 1.0 and 4.50. The load-displacement backbones for these groups of specimens are given in Figure 4.22 and Figure 4.23. As shown in these figures, walls with lower axial force ratios are generally less stiff than walls with higher axial force ratios. This is supported by findings from Shedid *et al.* (2008) and Sherman (2011). The results show higher lateral drift ratio at ultimate load for walls with lower axial load ratios in both groups of walls, again corroborating results from Shedid *et al.* (2008) and Sherman (2011). In addition, results show that walls with higher axial load ratios experienced more rapid strength degradation than did walls with lower axial load ratios.

Table 4-16 Evaluation of axial load effects on load-displacement curves of cantilever wall specimens

specimen		aspect ratio	axial load ratio	vertical reinforcement	horizontal reinforcement
group 1	UT-W-17	4.5	0.05	#6 @ 8 in.	#4 @ 8 in.
	UT-W-18		0.1	#4 @ 8 in.	#4 @ 8 in.
	UT-W-19		0.1	#6 @ 8 in.	#4 @ 16 in.
	UT-W-20		0.15	#4 @ 8 in.	#4 @ 16 in.
group 2	UT-PBS-03	1.0	0	#4 @ 8 in.	#4 @ 8 in.
	UT-PBS-04		0	#4 @16 in.	#4 @ 16 in.
	UT-PBS-04G		0	#4 @16 in.	#4 @16 in.
	UT-PBS-11		0.1	#4 @ 8 in.	#4 @ 8 in.
	UT-PBS-12		0.1	#4 @ 16 in.	#4 @ 16 in.
	UT-PBS-12G		0.1	#4 @ 16 in.	#4 @ 16 in.

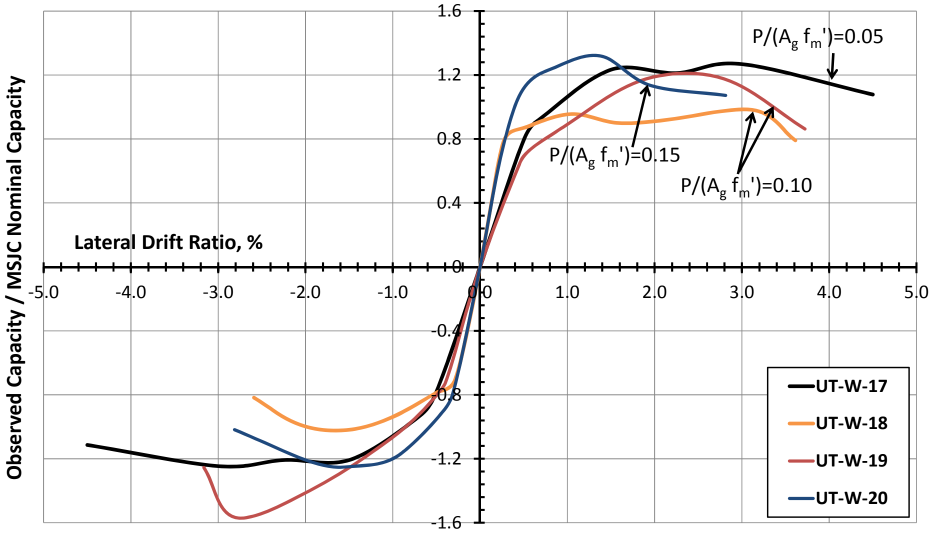

Figure 4.22 Load-displacement backbones for aspect ratio comparison, for cantilever walls with aspect ratio of 4.5

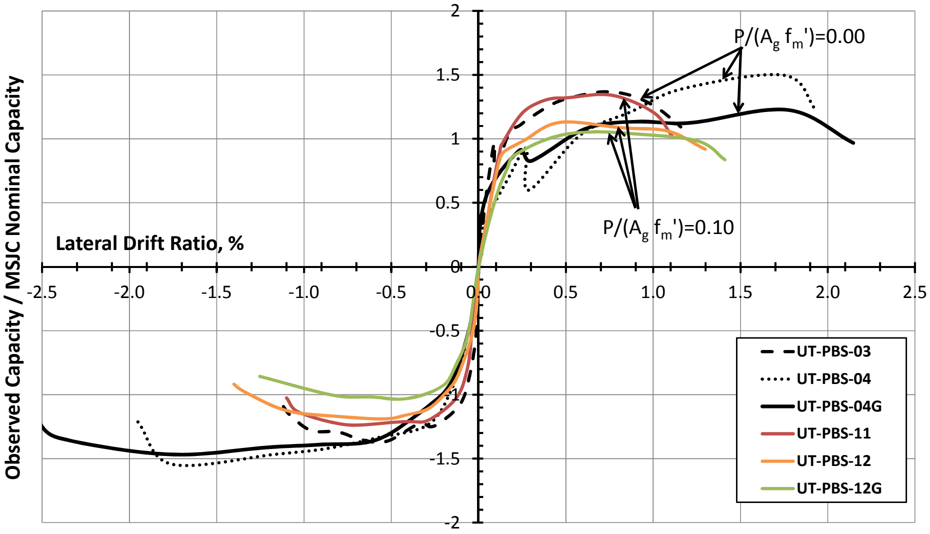

Figure 4.23 Load-displacement backbones for aspect ratio comparison, for cantilever walls with aspect ratio of 1.0

4.6.7.3 Effect of Vertical Reinforcement Ratio on Hysteretic Curves for Cantilever Wall Specimens

The effect of vertical reinforcement ratio on wall behavior is evaluated in this section. Table 4-17 contains the parameters associated with each group of comparable walls. The normalized load-displacement envelope curves for the considered walls are given in Figure 4.24 through Figure 4.27. In general, the initial stiffness of the walls increased with increasing vertical reinforcement ratio, corroborating results from Shedid *et al*. (2008) and Sherman (2011). As shown in the results the drift ratio at the ultimate load decreased as the vertical reinforcement ratio increased; this is supported by findings from Shedid *et al*. (2008) and Sherman (2011).

Table 4-17 Evaluation of vertical reinforcement ratio effect on load-displacement curve

specimen		**aspect ratio**	**axial load ratio**	**vertical reinforcement ratio**
group 1	**UT-W-14**	3	0.1	#4 @ 8 in.
	UT-W-15			#6 @ 8 in.
group 2	**UT-W-18**	4.5	0.1	#4 @ 8 in.
	UT-W-19			#6 @ 8 in.
group 3	**UT-PBS-03**	1	0	#4 @ 8 in.
	UT-PBS-04			#4 @16 in.
	UT-PBS-04G			#4 @16 in.
group 4	**UT-PBS-11**	1	0.1	#4 @ 8 in.
	UT-PBS-12			#4 @ 16 in.
	UT-PBS-12G			#4 @ 16 in.

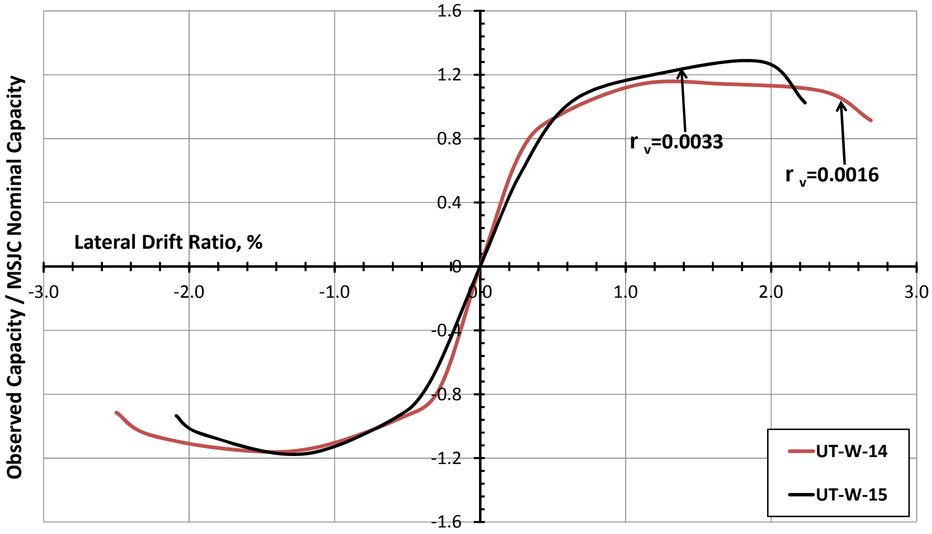

Figure 4.24 Load-displacement backbones for vertical reinforcement ratio comparison, for cantilever walls with aspect ratio of 3.0 and axial load ratio of 0.10

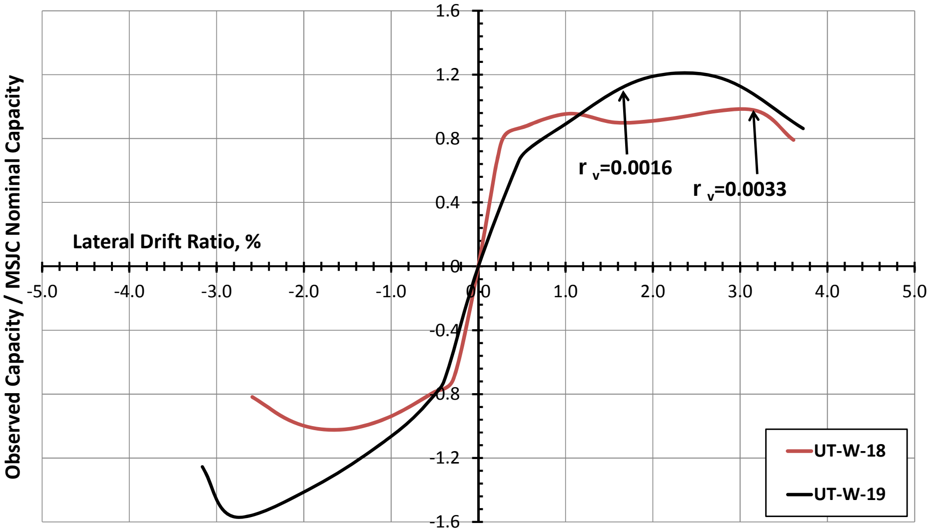

Figure 4.25 Load-displacement backbones for vertical reinforcement ratio comparison, for cantilever walls with aspect ratio of 4.5 and axial load ratio of 0.10

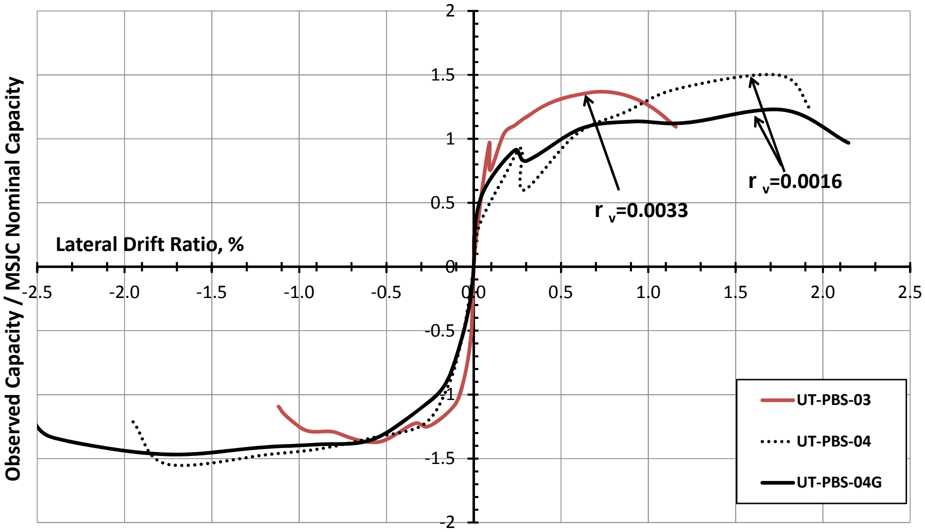

Figure 4.26 Load-displacement backbones for vertical reinforcement ratio comparison for cantilever walls with aspect ratio of 1.0 and zero axial load ratio

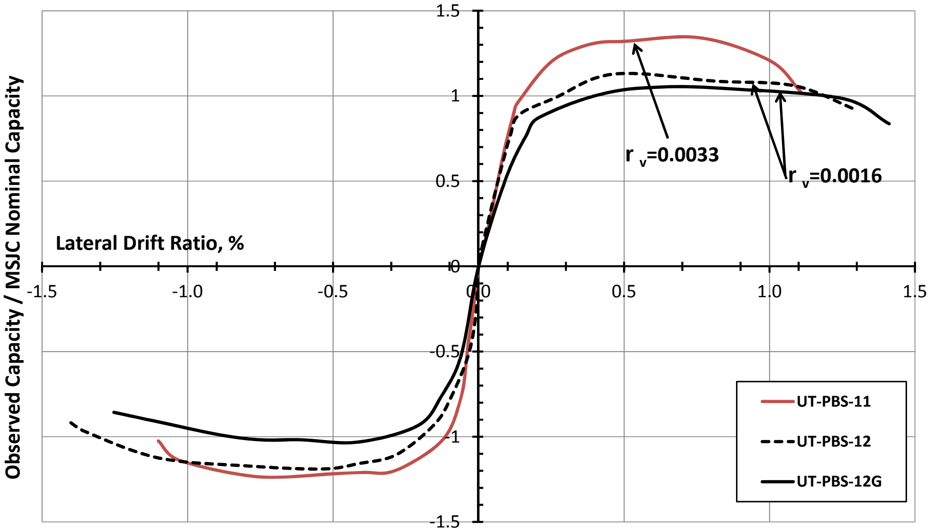

Figure 4.27 Load-displacement backbones for vertical reinforcement ratio comparison, for cantilever walls with aspect ratio of 1.0 and axial load ratio of 0.10

4.6.8 Conclusions from Reversed Cyclic Tests of Cantilever Walls

The cantilever wall specimens referred to here exhibited predominantly flexural behavior, as expected. Specimens exhibited flexural cracking, minor shear cracks, yielding of vertical reinforcement, degradation of the compression toe, inelastic buckling of vertical reinforcement near the base, spalling of the toe regions, and in some cases fracture of the vertical reinforcement. Specimens exhibited high displacement ductility as expected for flexure-dominated shear wall specimens.

Specimen behavior was in good agreement with that reported in previous research work. The provisions of the 2011 MSJC *Code* (MSJC 2011a) gave conservative (low) predictions of nominal flexural capacity. The average ratio of observed flexural capacity to nominal capacity was 1.24 for all axial load levels, corresponding almost exactly to the ratio of 1.25 that the 2011 MSJC *Code* uses in calculating expected flexural capacity for capacity design of special reinforced shear walls. As expected, flexural capacity and initial stiffness increased with increasing axial load and vertical reinforcement ratio. Displacement ductility decreased with increasing axial load.

Walls with lower aspect ratios exhibited larger deformations from sliding. In addition, walls with lower axial loads exhibited larger contributions from sliding and shear deformations. The specimens with no axial load experienced the largest contributions from sliding and shear deformations. Larger aspect ratios increase displacement ductility. Walls with lower aspect ratios experienced more rapid strength degradation than did walls with higher aspect ratios, and the displacement at ultimate loads (80% of maximum loads) increased as the aspect ratio increased.

In this research the specimens were tested under low axial load ratios (the axial load ratio of 0.00 to 0.15). However, axial load ratio had no evident effects on displacement ductility. This does not agree with results from previous studies, perhaps because of the limited number of varying levels of axial load evaluated in this study. More information in this regard can be obtained by comparing the test results of Sherman (2011), Kapoi (2012), and Shedid *et al.* (2010). Displacement ductility varies inversely with axial load, and increasing axial load is associated with lower ductility. Stiffness increases with increasing axial load ratio. This is obviously consistent with the expected flexural stiffness of the cracked, transformed section. The drift ratio at the ultimate load increases as axial load ratio decreases.

The vertical reinforcement ratio influenced the displacement ductility in specimens tested in this research. Specimens tested with low vertical reinforcement ratio developed higher displacement ductility than those tested with high vertical reinforcement ratio. This agrees with results from previous studies. More information in this regard could be obtained by considering the test results of Sherman (2011), Kapoi

(2012), and Shedid *et al.* (2010). Stiffness increases with increasing vertical reinforcement ratio. This is obviously consistent with the expected flexural stiffness of the cracked, transformed section. The drift ratio at the ultimate load decreased as the vertical reinforcement ratio increased.

Although the plastic hinge length was found to be dependent on reinforcement ratio and axial load in previous studies, this study showed no significant effects. There are consistent trends in relation to wall aspect ratio and plastic hinge length. Results correlate to a reduction in the plastic hinge length for the specimens with lower aspect ratios. In this study, the plastic hinge length for the cantilever wall specimens ranged from 17% to 41% of the plan length of the wall.

CHAPTER 5

Cyclic Tests of Fixed-fixed CMU Wall Specimens

5.1 INTRODUCTION

The second phase of the experimental program at The University of Texas at Austin consisted of testing six fixed-fixed CMU wall specimens. These specimens were designed and tested at the Ferguson Structural Engineering Laboratory, and were subjected to reversed cyclic in-plane loads. They were intended to provide experimental data to develop analytical models for shear-dominated CMU wall segments subjected to earthquake ground motions. This group of wall specimens represented wall segments in perforated wall systems, with in-plane rotational fixity at each end. Results of this group of wall segments are used to relate their behavior to key design parameters. A photo of the test setup for these specimens is shown in Figure 5.1. The most obvious part of the setup is the large, L-shaped steel loading frame.

The main objective of this chapter is to summarize the experimental results from each fixed-fixed CMU shear wall tested at UT Austin. This chapter also includes the design objectives for each specimen, axial and lateral loading histories, observed major events during the test, the history of crack formation, and the hysteretic behavior. The sequence of behavior based on the interaction diagram justifies the geometry and prescriptive reinforcement for each shear wall specimen. The sequence of damage in the wall is presented for each specimen, along with quantification of observed versus predicted behavior. Further information on all fixed-fixed specimens is presented in Appendix D.

Figure 5.1 Typical fixed-fixed wall specimen tested at UT Austin

5.2 SUMMARY OF DETAILS OF FIXED-FIXED WALL SPECIMENS

The shear-wall specimens tested at UT Austin used nominal 8- x 8- x 16-in. lightweight concrete masonry units (ASTM C90); coarse grout by proportion (ASTM C476); and ASTM C270 Type S cement-lime mortar by proportion. The geometry, horizontal and vertical reinforcement, and applied axial load ratios for each shear wall specimen, summarized in Table 5-1, were selected to force shear behavior. The reinforcement detailing of each wall specimen is shown in Figure 5.2.

Table 5-1 Overview of fixed-fixed CMU wall specimens

Specimen	Nominal Length, in.	Nominal height, in.	Aspect Ratio	Axial Load Ratio	Vertical Reinforcement	Horizontal Reinforcement
UT-PBS-01	72	72	0.5	0.01	#6 @ 8 in.	#4 @ 8 in.
UT-PBS-02	72	72	0.5	0.075	#6 @ 16 in.	#4 @ 16 in.
UT-PBS-05	72	72	0.5	0.06	#4 @ 8 in.	#4 @ 8 in.
UT-PBS-06	72	72	0.5	0.05	#4 @ 16 in.	#4 @ 16 in.
UT-PBS-09	72	72	0.5	0.1	#4 @ 8 in.	#4 @ 8 in.
UT-PBS-10	72	72	0.5	0.1	#4 @ 16 in.	#4 @ 16 in.

The wall geometry for the fixed-fixed specimens was selected to represent the aspect ratio (height divided by plan length) of walls of typical CMU walls whose behavior is dominated by shear or sliding shear. The range of axial loads in the specimens was selected to represent the range of compressive axial forces found in shear walls in typical reinforced masonry structures. In some cases, axial load was varied from one fixed-fixed specimen to another to refine our current understanding of the role of axial force in the capacity of CMU walls as governed by shear and by sliding shear.

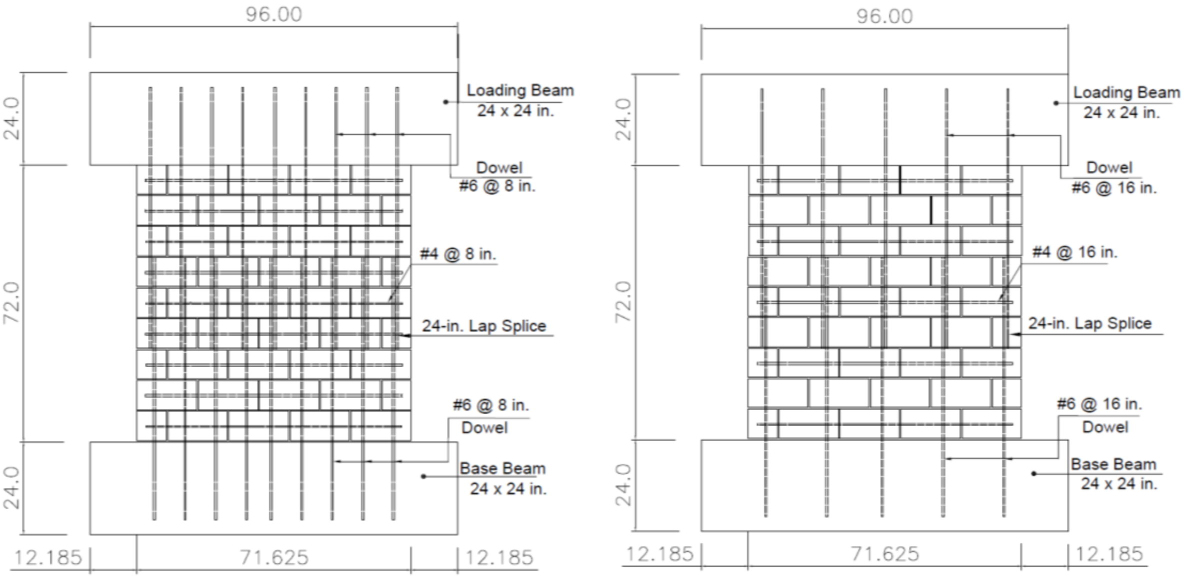

UT-PBS-01 ***UT-PBS-02***

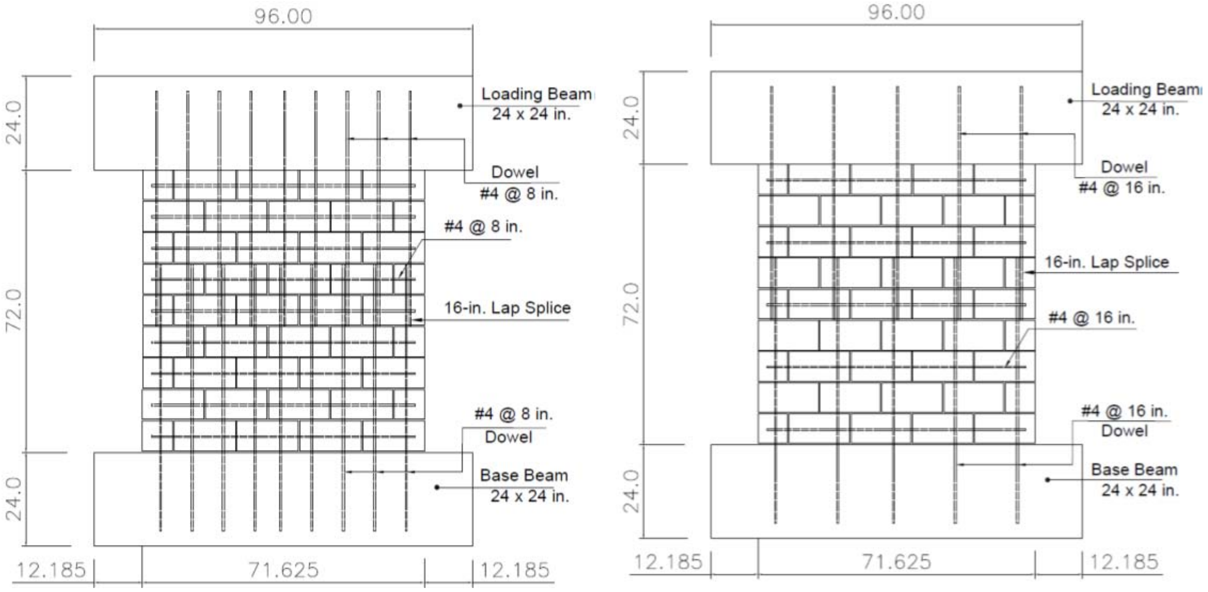

UT-PBS-05 and UT-PBS-09 ***UT-PBS-06 and UT-PBS-10***

Figure 5.2 Reinforcement details for fixed-fixed wall specimens tested at UT Austin

5.3 DESIGN OF FIXED-FIXED WALL SPECIMENS AT UT AUSTIN

The design of the fixed-fixed wall specimens tested at UT Austin involved the following steps:

1) select shear failure as the intended behavior mode;
2) propose horizontal and vertical reinforcement for the wall specimen; and
3) prepare an interaction diagram for the wall showing the in-plane capacity as governed by each possible failure mode, as a function of axial load.

In this section, the process for selecting the wall geometry, reinforcement and axial load for Specimen UT-PBS-01 is discussed. The selection of the wall geometry and reinforcement for the remaining specimens is included with the results of each specimen are given in Appendix D.

The predicted behavior of Specimen UT-PBS-01 is shown in the interaction diagram of Figure 5.3. The curves in that figure show the combinations of axial load and applied in-plane shear associated with nominal capacities as governed by web-shear cracking, shear in masonry plus shear reinforcement, sliding shear, and flexure. Each nominal capacity is calculated using specified material strengths and relevant strength design equations from the 2011 MSJC *Code* or ACI 318-11. The moment capacity was calculated according to the design assumptions of the 2011 MSJC *Code* (MSJC 2011a), Section 3.3.2. The nominal masonry shear strength, V_{nm} , was calculated according to Section 3.3.4.1.2.1 of the 2011 MSJC *Code* (MSJC 2011a), and the nominal shear strength provided by reinforcement, V_{ns} , was calculated according to Section 3.3.4.1.2.2 of 2011 MSJC *Code* (MSJC 2011a).

Because the 2011 MSJC *Code* does not have general shear-friction provisions, the sliding-shear capacity of specimen was estimated using the shear-friction provisions of Section 11.6.4 of ACI 318-11. The coefficient of friction, μ, was considered equal to 1.0.

In addition, for relative interface displacements greater than the characteristic roughness of the interface, to calculate sliding-shear capacity, the contribution from shear friction is calculated using a coefficient of friction of 1.0, and the contribution from dowel action is based on yield in pure shear using the von Mises criterion. Based on the results of testing in this research, a shear-friction mechanism is later proposed with reinforcement in tension and a coefficient of friction of 0.68.

The level of axial load used in this test (20 kips) is shown in this figure by a dashed horizontal line. At that axial load, the expected capacities during testing in order are web-shear cracking, and then shear in masonry plus shear reinforcement.

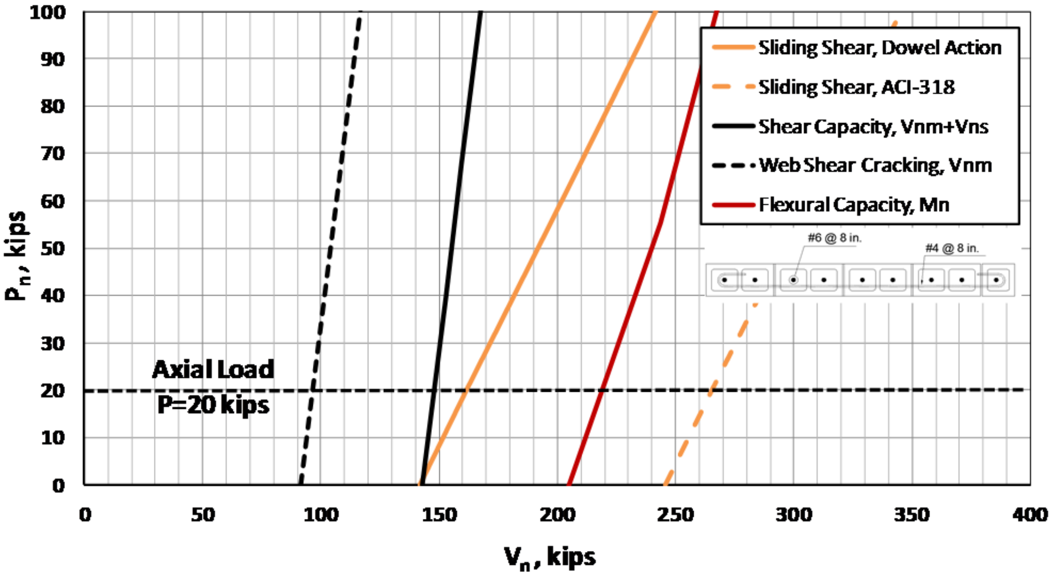

Figure 5.3 Strength interaction diagrams for Specimen UT-PBS-01

Using the same procedure for each of the six fixed-fixed shear wall specimens, the intended failure modes and lateral capacities are summarized in Table 5-2.

Table 5-2 Test matrix for fixed-fixed wall specimens tested at UT Austin

specimen	vertical reinforcement	horizontal reinforcement	axial load, kips	flexural capacity, kips	shear capacity, kips	sliding-shear capacity, kips
UT-PBS-01	#6 @ 8 in.	#4 @ 8 in.	20.0	220	147	161
UT-PBS-02	#6 @ 16 in.	#4 @ 16 in.	103.0	204	142	181
UT-PBS-05	#4 @ 8 in.	#4 @ 8 in.	81.2	168	163	146
UT-PBS-06	#4 @ 16 in.	#4 @ 16 in.	68.3	121	132	103
UT-PBS-09	#4 @ 8 in.	#4 @ 8 in.	136.6	206	177	201
UT-PBS-10	#4 @ 16 in.	#4 @ 16 in.	136.6	171	150	171

5.4 INSTRUMENTATION AND DATA ACQUISITION FOR FIXED-FIXED SHEAR-WALL SPECIMENS

Each specimen was instrumented with a variety of strain gauges, linear potentiometers, wire potentiometers, linear variable differential transformers, and load cells. These are described in detail below.

The reinforcement of each specimen was instrumented with strain gauges at critical locations, particularly where yielding was anticipated. Strain gauges were attached to loading-beam dowels, base-beam dowels, and horizontal reinforcement (labeled as TD, BD, and H respectively in Figure 5.4). Loading-beam and base-beam dowels included one strain gauge at the base of the wall in every interior dowel, two strain gauges at the base and top of the wall (north and south), and two strain gauges every 8 in. from the base for exterior dowels. In addition, six strain gauges were attached to horizontal bars: one strain gauge at each end of the horizontal reinforcement in the bottom and top courses, and one strain gauge at the center of the horizontal reinforcement in the third and seventh courses from the bottom.

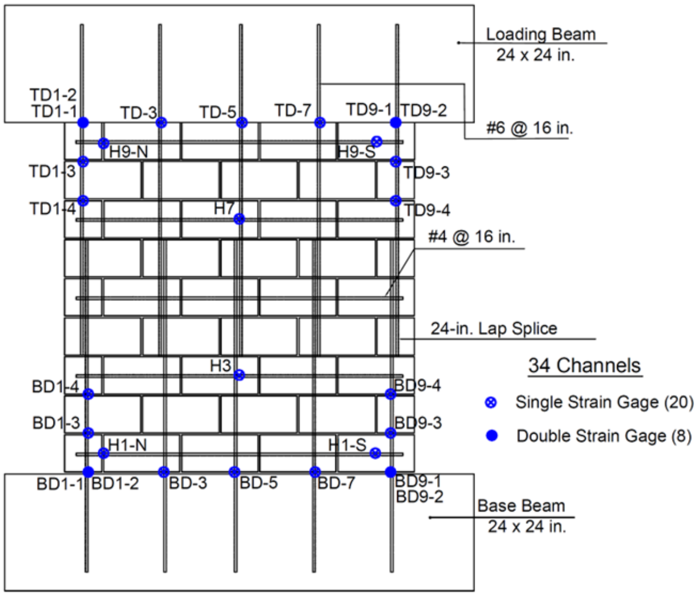

Figure 5.4 Typical locations of strain gauges in fixed-fixed shear-wall specimens

Linear potentiometers were located on the specimen to monitor lateral deformations, shear deformations, incremental vertical deformations at the ends of the specimen, axial deformations, sliding between base beam and shear wall panel, sliding between loading beam and shear wall panel, and any potential slip between the specimen and loading frame. Locations of linear potentiometers are shown in Figure 5.5. Before each test, the end points of the instrument locations were measured so strains and local deformations could be accurately calculated during the test. In addition, linear variable differential transformers and load cells were monitored on each actuator.

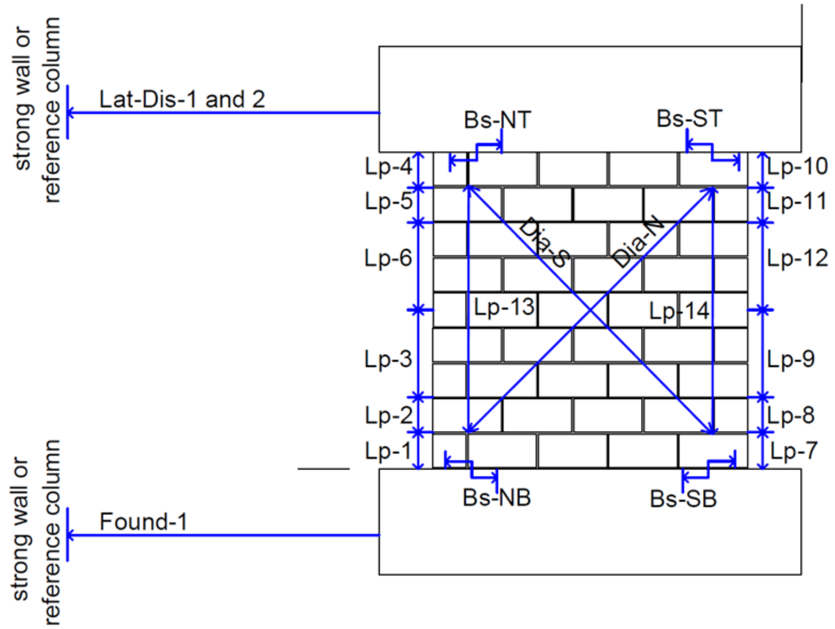

Figure 5.5 Locations of potentiometers on fixed-fixed shear-wall specimens

The data acquisition system (DAQ) consisted of a precision power supply, a HP-3852 data acquisition unit, and a PC computer with custom data acquisition software written in National Instruments LabView® programming system. The power supply provided an excitation voltage of 2V for strain gauges, and 10V for load cell and linear potentiometers. The HP-3852 data acquisition unit measured the analog signal (voltage) from the transducers. Analog-to-digital conversion was carried out by a National Instruments card in a Windows-based microcomputer, running under Measure, a National Instruments add-on for Microsoft Excel®. Once in Excel, data were plotted conventionally.

5.5 TEST RESULTS OF FIXED-FIXED CMU WALL SPECIMENS

In this section, results for typical Specimen UT-PBS-01 are discussed. Detailed test results for the remaining fixed-fixed specimens are presented in Appendix D and in

Alogla (2012). An interaction diagram for base shear capacity as a function of axial load for Specimen UT-PBS-01 is presented in Figure 5.3. The axial load applied to Specimen UT-PBS-01 was 20.0 kips. At this level of axial load the following major events are predicted in order of occurrence: web-shear cracking; shear yielding; shear sliding (based on shear dowel action); and flexural yielding. This specimen was expected to fail by shear before reaching its nominal flexural capacity. Specimen UT PBS-01 before testing is shown in Figure 5.6.

Figure 5.6 Specimen UT-PBS-01 before testing

5.5.1 Loading History and Major Events for Specimen UT-PBS-01

Specimen UT-PBS-01 was first subjected to a preliminary test phase to estimate the yield displacement, Δ_y. A moment-curvature analysis of the specimen was used to estimate the maximum moment capacity, which was then converted to a peak horizontal load capacity. The specimen was subjected to two reversed cycles of load of ±25%, ±50%, and ±75% of that peak horizontal load capacity. The displacement from the first cycle to 75% of that peak horizontal load capacity was used to establish the probable Δ_y, by extrapolating the displacement at 75% of the maximum load to the displacement at 100% of the maximum load (displacement at 100% maximum load, equal to 4/3 times displacement at 75% maximum load. Lateral yield displacement was determined as 0.06 in.

Specimen UT-PBS-01 was loaded two cycles of reversed displacements of ±1, 2, 3, 4, 8, 10 and 12 times that predicted yield displacement. It was then loaded to a half-cycle to a displacement of 14 times that predicted yield displacement. The test was stopped when the peak capacity dropped to 20% of the experimentally observed peak capacity (capping point). The testing took about 12 hours. The actual lateral loading and lateral displacement histories for Specimen UT-PBS-01 are presented in Figure 5.7 and Figure 5.8. Loading to the north is considered positive; loading to the south, negative. In this test the specimen was loaded first to the north and then to the south.

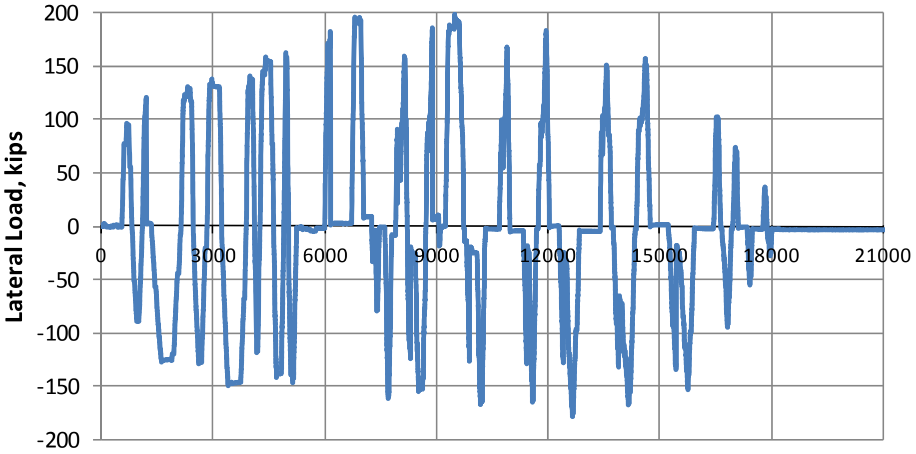

Figure 5.7 Actual lateral loading history for Specimen UT-PBS-01

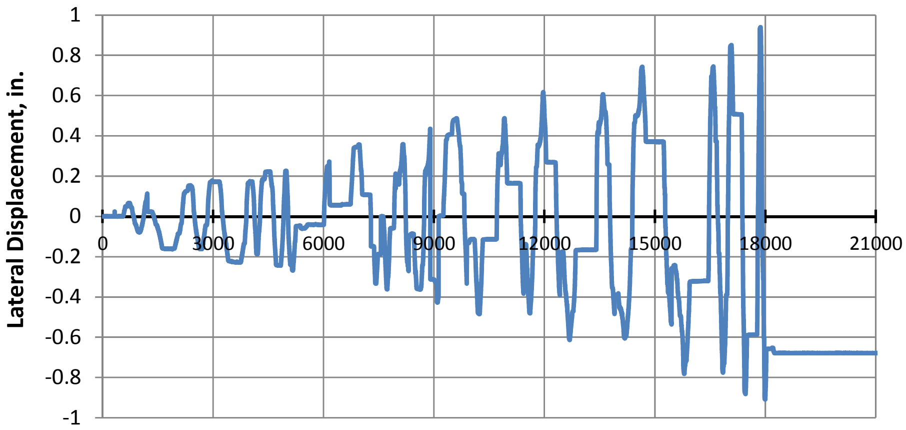

Figure 5.8 Actual lateral displacement history for Specimen UT-PBS-01

5.5.2 Sequence of Crack Formation for Specimen UT-PBS-01

The sequence of crack formation in Specimen UT-PBS-01 is described in terms of major events: drift ratios during the test when the condition of the specimen changed (for example, flexural cracking or shear cracking). Table 5-3 lists the major events and the drift ratio at which they occurred. In the following figures, where crack maps are presented for some of the major events, cracks that formed on loading to the north are shown in black, and cracks that formed on loading to the south are shown in red.

Table 5-3 Description of major events for Specimen UT-PBS-01

major event	lateral drift ratio	physical description
1	0.17%	flexural cracking and web-shear cracking, loading north
2	0.17%	flexural cracking and web-shear cracking, loading south
3	0.32%	additional web-shear cracking, loading north
4	0.32%	additional web-shear cracking, loading south
5	0.50%	additional web-shear cracking and opened diagonal cracks, loading north
6	0.50%	additional web-shear cracking, loading south
7	0.67%	opened diagonal cracks, loading south
8	1.30%	wide opened diagonal cracks combined with crushing and spalling of diagonal struts, spalling at toes
9	1.30%	wide opened diagonal cracks combined with crushing and spalling of diagonal struts, spalling at toes
10	end of test	shear failure and axial collapse

5.5.2.1 Flexural and web-shear cracking in Specimen UT-PBS-01

Major Events 1 and 2, as shown in Figure 5.9, correspond to flexural cracking and web-shear cracking. At the drift ratio of 0.17%, flexural cracks and web-shear cracks formed while loading to the north and south at a load of 97.0 kips. A web-shear crack formed along the entire height of the wall while loading to the north at a base shear and drift ratio of 97.0 kips and 0.17%, respectively. In addition, while loading to the south, parallel smaller web-shear cracks formed along the wall at the same base shear and drift ratio. The predicted nominal capacity in web-shear cracking based on MSJC 2011 Code at the corresponding axial load is 96.1 kips. The ratio of observed to predicted web-shear cracking capacity is 1.00.

5.5.2.1 Additional web-shear cracking in Specimen UT-PBS-01

Major Events 3 and 4 correspond to the development of additional web-shear cracks in the specimen. The base shears were 158 kips and 145 kips for loading north and loading south and the drift ratio was 0.32% for both loading directions. Damage in the specimen at the end of Major Event 4 is shown in Figure 5.10.

5.5.2.2 Distributed open web-shear cracking in Specimen UT-PBS-01

Figure 5.11 shows how shear cracks had opened in wall segment in Major Event 5, while loading north at a drift ratio of 0.50%. In this event, distributed web-shear cracks formed, and a 0.1-in. gap opened in the web-shear cracks along the entire length of diagonal cracks that formed in both directions, as shown in Figure 5.11. Major Event 6 was distributed web-shear cracks at a drift ratio of 0.50%. At Major Event 7, as the load continued to increase to the south, shear cracks started opening at a drift ratio of 0.67%.

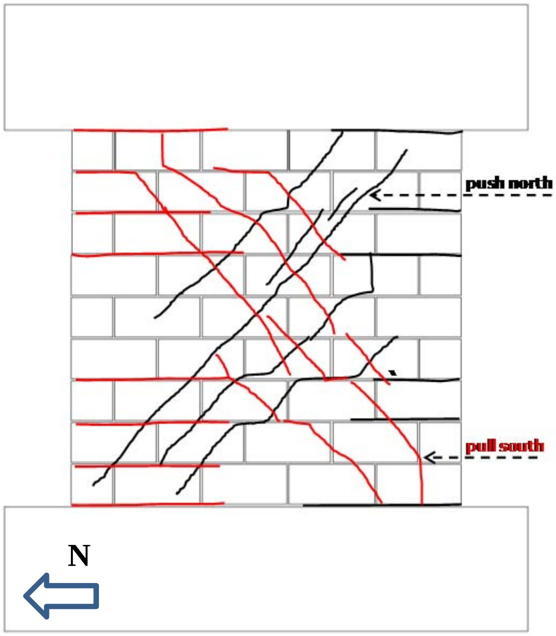

Figure 5.9 Flexural cracking and web-shear cracking at 0.17% drift ratio (UT-PBS-01)

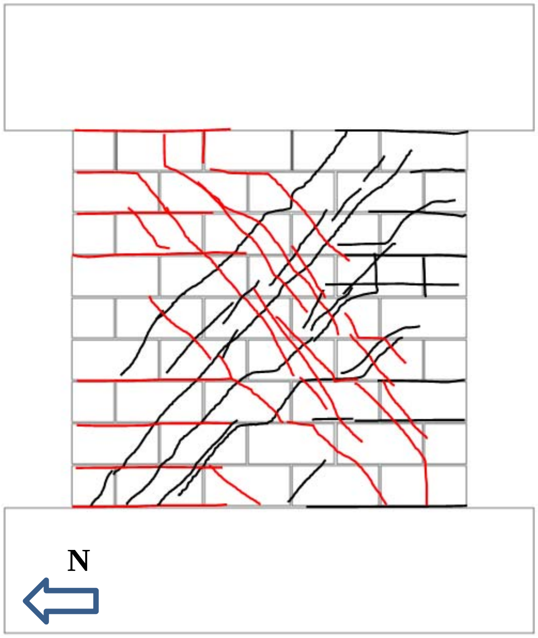

Figure 5.10 Additional web-shear cracking at 0.32% drift ratio (UT-PBS-01)

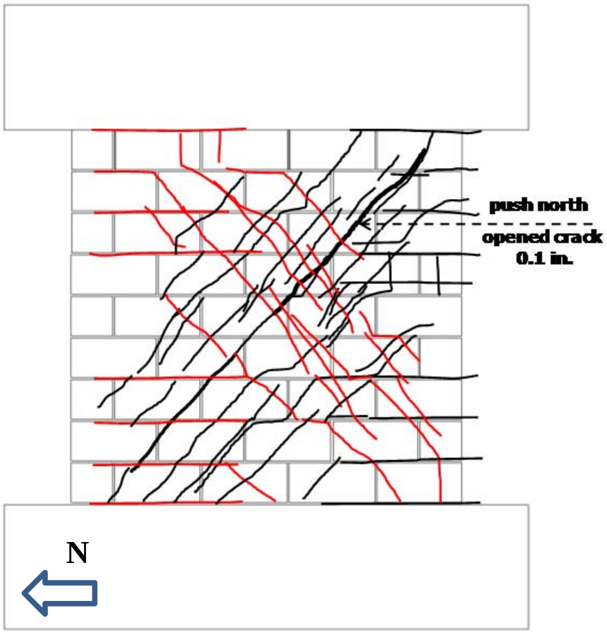

Figure 5.11 Distributed open web-shear cracks at 0.50% drift ratio (UT-PBS-01)

5.5.2.3 Wide diagonal cracks and crushing of the compression toe and diagonal struts in Specimen UT-PBS-01

In the last two cycles of the test, in Major Events 8 and 9, wide diagonal cracks formed, diagonals crushed, and compression toes showed severe spalling and crushing at a drift ratio of 1.30% for northward loading. In addition, in Major Event 9 vertical cracks were observed at the upper north corner while loading to the south. The test was discontinued after Major Event 9 due to crushing of the lower north and south compression toes, significant spalling of the diagonal strut face shells, and opening of a 2.0-in. web-shear crack. Damage at the end of the test is shown in Figure 5.12 and Figure 5.13. As shown in Figure 5.13, reversed cyclic loading caused diagonal strut crushing, vertical cracking, toe crushing, and spalling of the specimen.

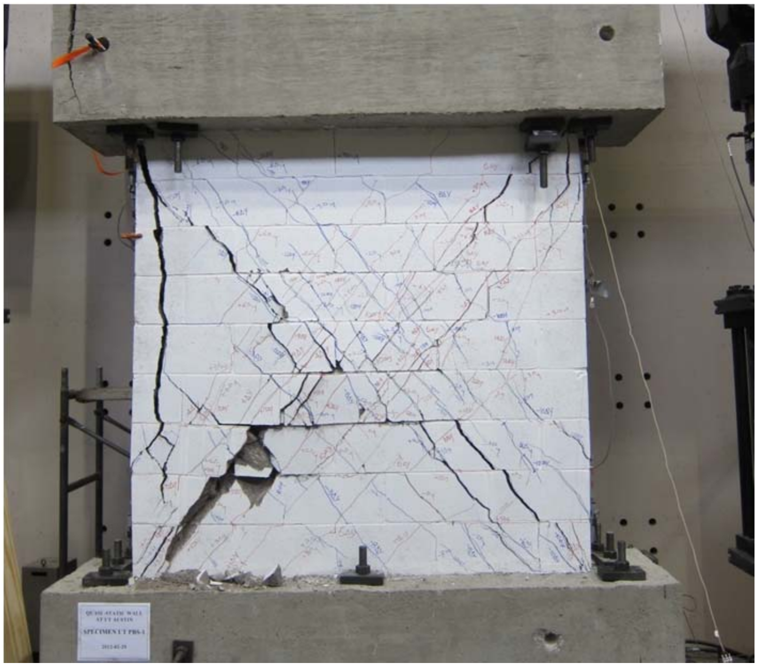

Figure 5.12 Crushing and spalling of compression toe and diagonal struts at 1.30% drift ratio (UT-PBS-01)

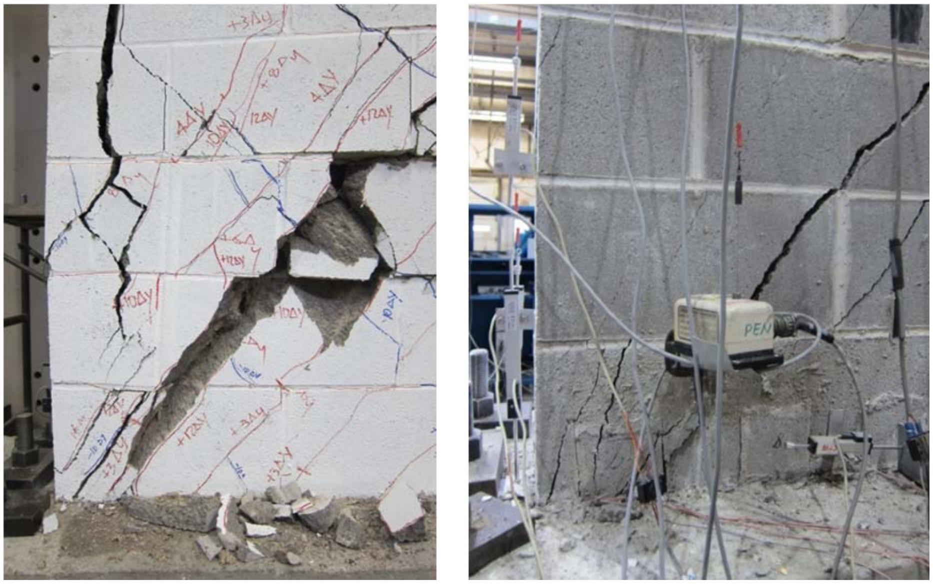

Figure 5.13 Crushing and spalling of compression toe and diagonal struts at end of test (UT-PBS-01)

5.5.3 Load-Displacement Behavior for Specimen UT-PBS-01

The load-displacement relationship of Specimen UT-PBS-01 is presented in Figure 5.14 in terms of the non-dimensional drift ratio, which references seven major events during testing:

1) first web-shear cracking
2) first yield of the extreme vertical reinforcement ($\varepsilon_y = 0.0021$);
3) first yield of the horizontal reinforcement ($\varepsilon_y = 0.0021$);
4) the maximum useful strain in the masonry ($\varepsilon_{mu} = 0.0025$);
5) maximum capacity (capping point);
6) onset of crushing of toes or diagonal struts; and
7) 50% of observed peak capacity

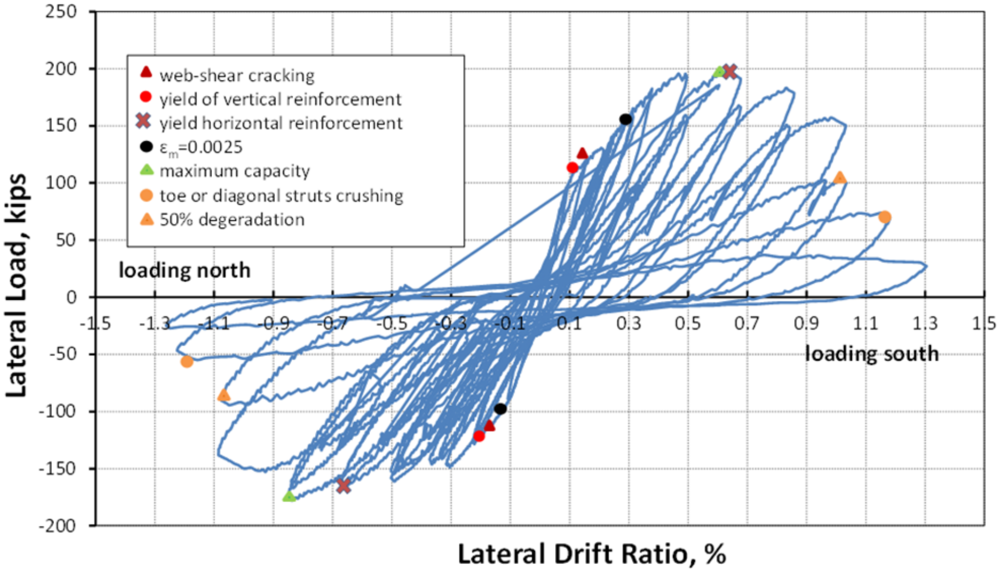

Figure 5.14 Lateral load versus top drift ratio (UT-PBS-01)

5.5.4 Components of Displacements and Drifts for Specimen UT-PBS-01

The lateral displacements of Specimen UT-PBS-01 were determined as total, flexural, sliding, and shear displacements. The total in-plane lateral displacement was measured with a linear potentiometer attached to an external reference frame at the level of loading beams. Linear potentiometers recorded the average sliding displacements between the wall base and the base beam. Sliding was also measured between the top of the wall and the top concrete beam. These load-sliding curves for the top and the base of wall are shown in Figure 5.15.

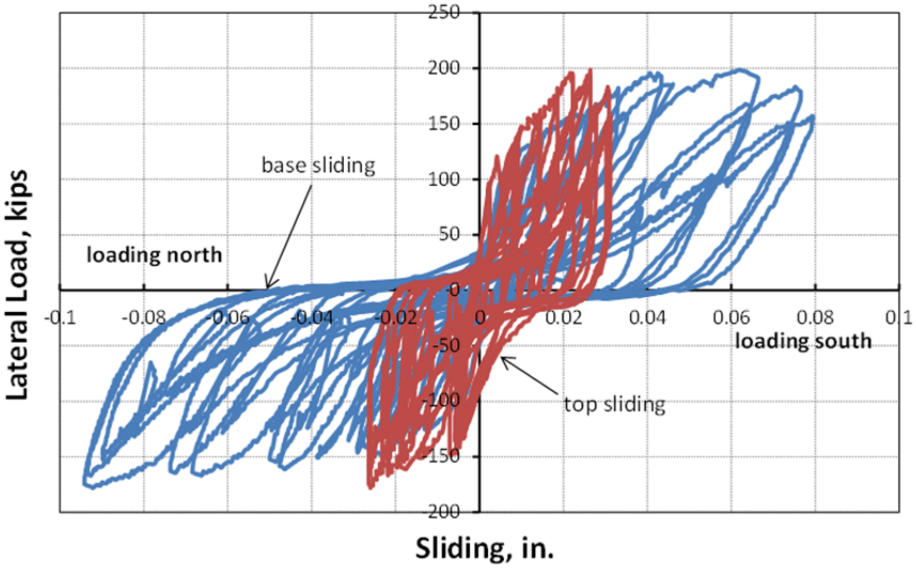

Figure 5.15 Top and base curves of load versus sliding (UT-PBS-01)

Shear displacements were measured with two diagonally oriented and two vertically oriented linear potentiometers, and were calculated as proposed by Massone and Wallace (2004) and shown in Figure 5.16. In that figure, the dashed lines represent the original, undeformed wall; the shaded rhomboid represents the shear deformation; and the combined shear and flexural deformations are shown in solid lines (Massone and Wallace 2004, Sherman 2011).

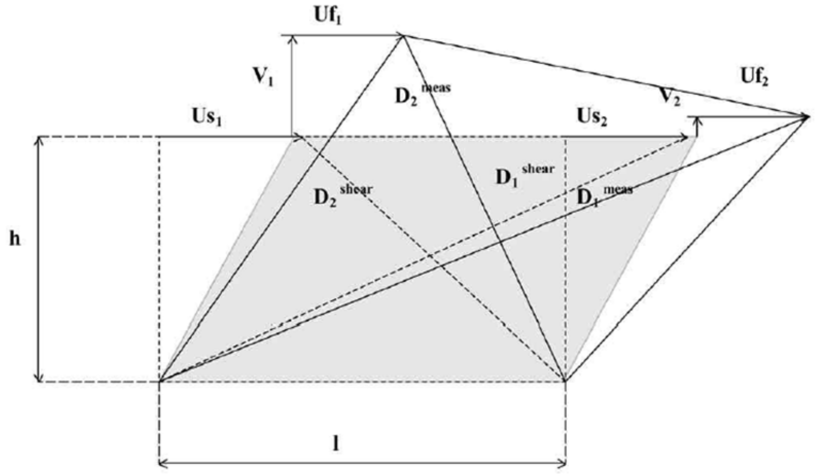

Figure 5.16 Flexural and shear deformation (Massone and Wallace 2004)

The average shear displacements based on contributions from shear and flexural deformations were derived from Figure 5.16 as (Massone and Wallace 2004):

$$\Delta_{sh} = \frac{\sqrt{(D_1)^2 - h^2} - \sqrt{(D_2)^2 - h^2}}{2} - (\frac{1}{2} - \alpha)\left(\frac{V_1 - V_2}{l}\right)h \qquad \textbf{\textit{Equation 5-1}}$$

where Δ_{sh} is average shear displacement;

$D_{1,2}^{meas}$ are diagonal lengths for the deformed X configuration;

h is height of diagonal pattern;

α is distance from the top of wall to the center of rotation;

$V_{1,2}$ are measured displacements from vertical potentiometers (in.); and

l is width of diagonal pattern (in.).

An α value of 0.5 based on assuming the center of rotation occurred at the middle of the wall height. The first term in Equation 5-1 represents the shear displacements from shear deformation, and the second term represents the shear displacements from flexural deformations. Load-displacement curves for total sliding and shear component of total tip displacement are given in Figure 5.17 and Figure 5.18, and comparison among total displacement, sliding, and shear deformation is shown Figure 5.19.

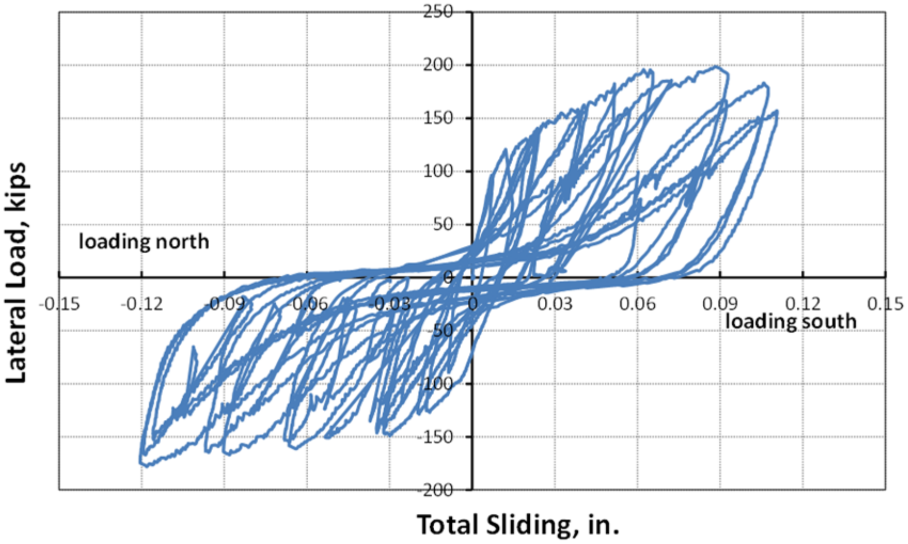

Figure 5.17 Total sliding versus lateral load (UT-PBS-01)

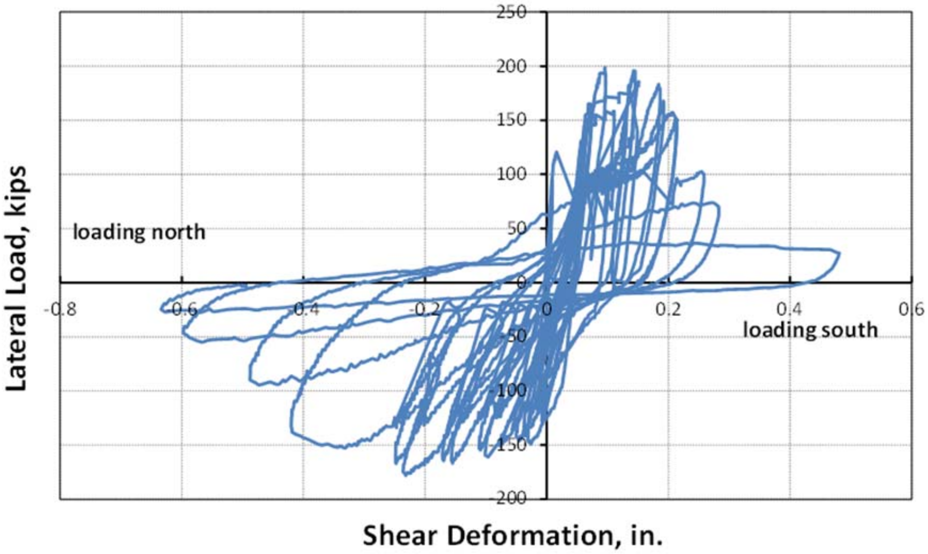

Figure 5.18 Shear deformation versus lateral load (UT-PBS-01)

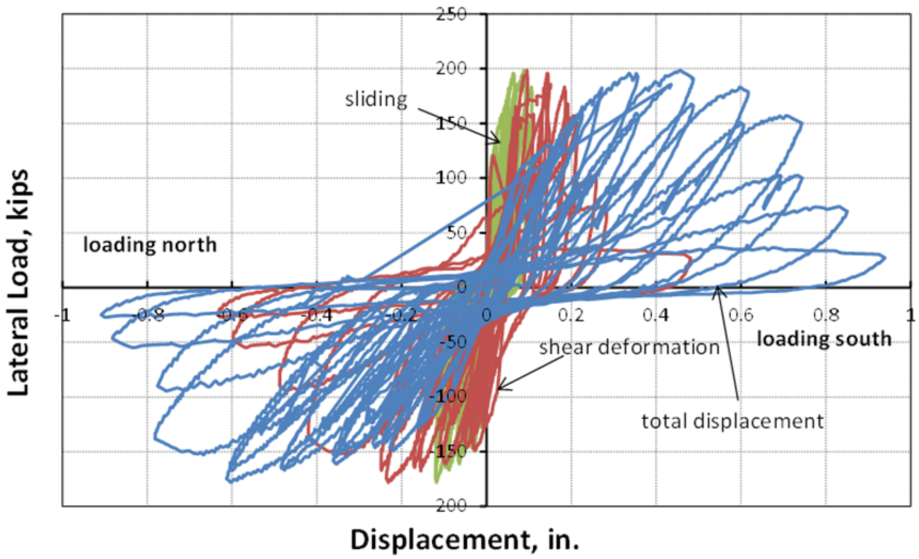

Figure 5.19 Components of displacements and drifts (UT-PBS-01)

5.6 SUMMARY OF EVALUATION OF RESULTS FOR FIXED-FIXED SPECIMENS

Test results for the 6 fixed-fixed reinforced masonry shear walls are summarized in Table 5-4. In this section, computed nominal shear and sliding capacities are compared with experimental capacities. Relative contributions of different deformations to overall drift ratios are summarized, and are correlated with the level of axial load and vertical and horizontal reinforcement ratio of each specimen.

Table 5-4 Results from fixed-fixed shear walls tested at UT Austin

Wall Specimen	V_{test} (kip)	V_n (kip)	(V_{test} / V_n)
UT-PBS-01	198.71	155.97	1.27
UT-PBS-02	165.43	154.92	1.06
UT-PBS-05	153.30	171.47	0.88
UT-PBS-06	115.53	140.23	0.81
UT-PBS-09	186.42	193.44	0.96
UT-PBS-10	169.67	165.54	1.02

5.6.1 Sliding Shear Capacity of Fixed-fixed Wall Specimens

Sliding shear can be the governing failure mechanism for reinforced masonry shear walls with low aspect ratio and low axial load. Because the general strength-design provisions of the 2011 MSJC *Code* do not address sliding, walls are designed either ignoring sliding, or considering it and making assumptions regarding its effect on seismic performance (Centeno 2012). It is useful to develop shear-sliding provisions for inclusion in design codes, including the 2011 MSJC *Code*.

Sliding behavior is well documented for reinforced masonry walls (Shing *et al.* 1990), particularly those with light axial loads and light vertical reinforcement (Seible *et al.* 1994a, b). The flexural and shear capacities of 22 masonry shear wall specimens were studied by Shing *et al.* (1990), and three of those specimens, with zero axial loads, exhibited base sliding. The sliding contribution to displacement increased with increasing displacement demands, reaching up to 50% of the total tip lateral displacement at the end of the test. Voon and Ingham (2007) studied the relationship between design parameters and the shear capacity of reinforced masonry shear walls, and observed significant sliding displacement at larger displacement demands. Hernandez (2012) studied the relationship between design parameters and the seismic performance of six cantilever masonry shear walls with an aspect ratio of 1.0, tested under reversed cyclic loading. Three specimens with zero axial loads experienced sliding, which contributed 23% to 30% of the total lateral displacement at the end of testing. Vertical reinforcement also fractured in those specimens. Shake-table tests of a one-story reinforced concrete masonry building specimen have demonstrated that the seismic performance of low-rise reinforced concrete masonry buildings, designed and constructed according to the requirements of the MSJC Code, can be controlled by the sliding at the base of the in-plane reinforced masonry shear walls (Jo 2010).

5.6.1.1 Background Information for Sliding-Shear Capacity

As shown in Figure 5.20, a reinforced masonry shear wall slides on its interface with the underlying foundation when the shear force at the interface exceeds the shear sliding capacity. The deformation limit for sliding-shear behavior modes may be governed by the fracture of bars (dowels) crossing the sliding plane, crushing of the base course of masonry, or degradation of the shear and flexure transfer mechanisms in the flexural compression zone of the wall as the wall slides beyond its support. After sliding occurs, as shown in Figure 5.20, shear capacity is given by the product of the coefficient of friction across the interface, and the force acting perpendicular to the interface. In ACI 318, this mechanism is referred to as "shear friction," and has two components: the frictional resistance from the axial load on the wall, and the frictional resistance from the clamping force provided by the reinforcement crossing the sliding plane.

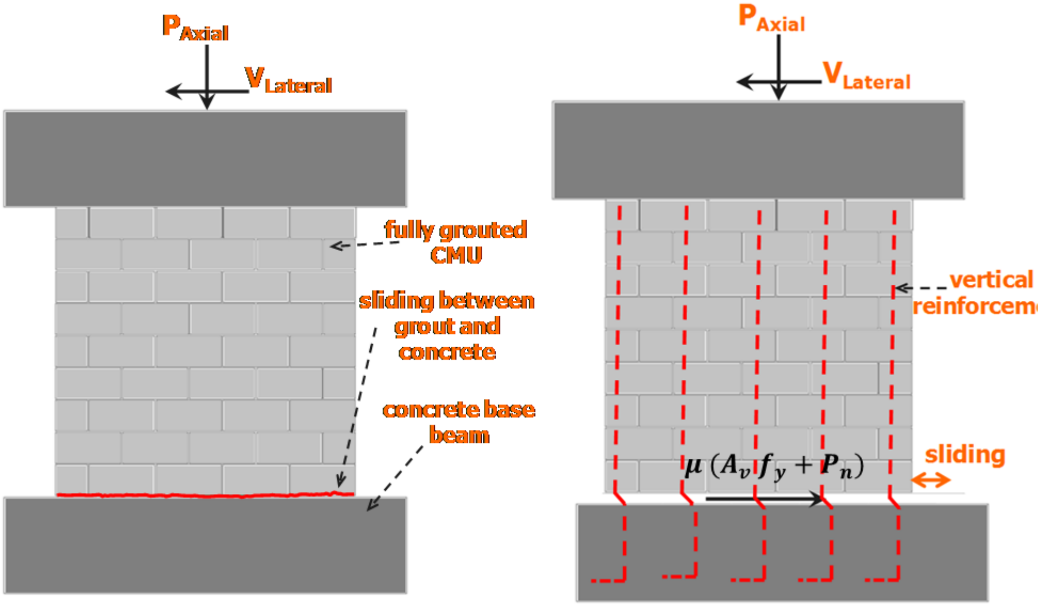

a) Base sliding ***b) Shear friction***

Figure 5.20 Base sliding and shear friction

Neglecting the contribution of the vertical reinforcement to the sliding-shear capacity, and also neglecting dowel action, sliding–shear capacity is given by Equation 5-2. Atkinson et al. (1988) determined an average expected value of 0.70 for μ (FEMA 306 1999).

$$V_n = \mu \, P_n$$

Equation 5-2

The ACI 318 shear-friction concept assumes that reinforcement crossing the sliding plane produces additional resistance to sliding. As shown in Figure 5.20, reinforcement perpendicular to the interface provides a clamping force $A_s f_y$ across the interface, and the resulting resistance can be calculated using Equation 5-3. The same equation was used in the initial design of the fixed-fixed wall specimens tested at UT Austin, using a coefficient of friction, μ, of 1.0.

$$V_s = \mu \ (A_v \, f_y + \ P_n)$$

Equation 5-3

Changes in the sliding-shear formula can be made by changing the assumed coefficient of friction or the assumed contribution of the reinforcement crossing the interface. For sliding displacements greater than the characteristic roughness of the interface, the sliding-shear capacity can be interpreted as the same Equation 2, modifying the assumed coefficient of friction and interpreting the term involving reinforcement as due to dowel action. Tanner *et al.* (2005) tested a group of shear-dominated autoclaved aerated concrete (AAC) shear walls to verify proposed design formulas and found that the effectiveness of the dowel action decreases as the level of damage around a dowel increases. The shear strength and stiffness contribution due to dowel action in reinforced masonry walls depends on the interaction between the vertical reinforcement and the surrounding grout, and can be derived from three possible mechanisms: the flexure of vertical reinforcement; the shear across the vertical reinforcement; and the kinking of the reinforcement as shown in Figure 5.21.

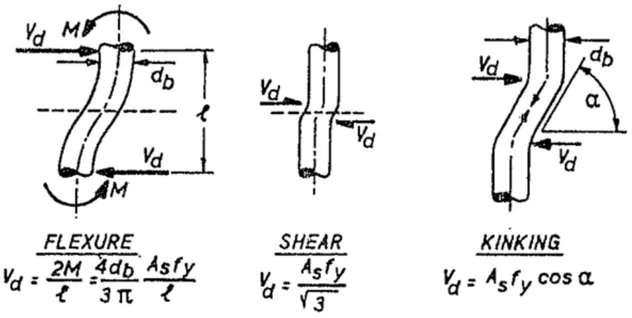

Figure 5.21 Possible dowel action mechanisms (Park and Paulay 1975)

As presented in Equation 5-4, and assuming that dowel action is controlled by shear, the sliding shear capacity can be computed based on shear yielding using the von Mises criterion.

$$V_s = \frac{A_v\, f_y}{\sqrt{3}} + \mu\, P_n \qquad \textit{Equation 5-4}$$

For relative movement less than about 0.01 in., shear friction still seems to be a reasonable mechanism. Larger relative movements are more likely resisted by dowel action, but the computed contribution from reinforcement is still some constant times $A_v f_y$. Priestley and Bridgeman (1974) determined a maximum dowel shear resistance of 0.30 $A_v f_y$, and Paulay, Priestley, and Synge (1982) report a value of 0.40 $A_v f_y$ (Centeno *et al.* 2012).

5.6.1.2 Failure Modes for Fixed-fixed Shear-wall Specimens Tested at UT Austin

Test results for the 6 fixed-fixed reinforced masonry shear walls are summarized in Table 5-5, along with the observed failure mode and the contribution of sliding to the total lateral displacement at the end of the test. As shown in Table 5-5, the capacities of Specimens UT-PBS-01 and UT-PBS-02 were limited by distributed web-shear cracking and shear failure, and did not show significant sliding. These two specimens are therefore excluded from the statistical evaluation. In Specimen UT-PBS-10, distributed web-shear cracks combined with significant sliding at the base and top of the specimen; however, at the end of the test the specimen failed by shear. That specimen is included in this evaluation of sliding shear. The behavior and capacities of the remaining three specimens (UT-PBS-05, UT-PBS-06, and UT-PBS-09) were governed by sliding shear, and those specimens were also included in the evaluation of sliding shear, for a total of four.

Table 5-5 Sliding displacement contribution to total displacement and failure for fixed-fixed specimens

Specimen	**Experimental capacity (V_{test}), kips**		**Sliding displacement contribution of total displacement at the end of test**	**Failure mode at the end of test**
	Push-north	**Pull-south**		
UT-PBS-01	198	178	11%	Shear
UT-PBS-02	162	165	7%	Shear
UT-PBS-05	153	152	63%	Sliding
UT-PBS-06	115	108	46%	Sliding
UT-PBS-09	186	183	52%	Sliding
UT-PBS-10	169	161	55%	Shear and Sliding

5.6.1.3 Sliding-shear Capacities of Fixed-fixed Shear-wall Specimens Tested at UT Austin

Figure 5.22 through Figure 5.25 present shear-dominated hysteretic curves for reversed cyclic loading, including lateral force versus total lateral displacement, and lateral force versus total sliding, for the 4 shear-wall specimens tested at UT Austin that experienced significant sliding at the end of the test. The two lateral displacements in these graphs are almost identical, indicating that most of the measured displacement was due to sliding rather than to deformation of the wall segment itself. The average of the observed sliding shear capacities (north and south) for each specimen is also presented on the hysteretic curves.

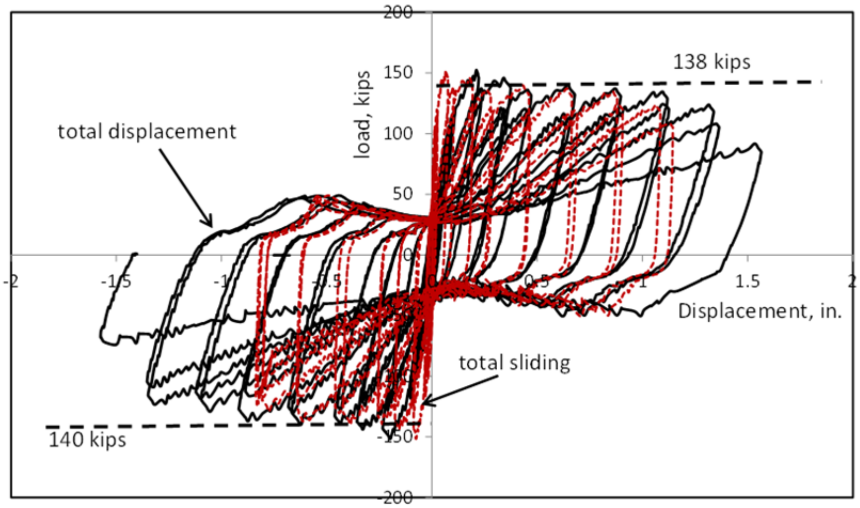

Figure 5.22 Lateral force versus total lateral displacement, and lateral force versus total sliding (Specimen UT-PBS-05)

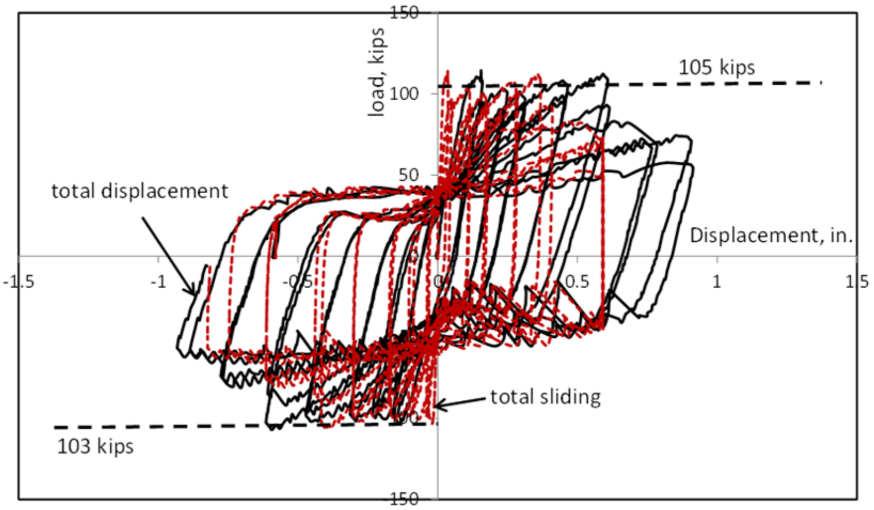

Figure 5.23 Lateral force versus total lateral displacement, and lateral force versus total sliding (Specimen UT-PBS-06)

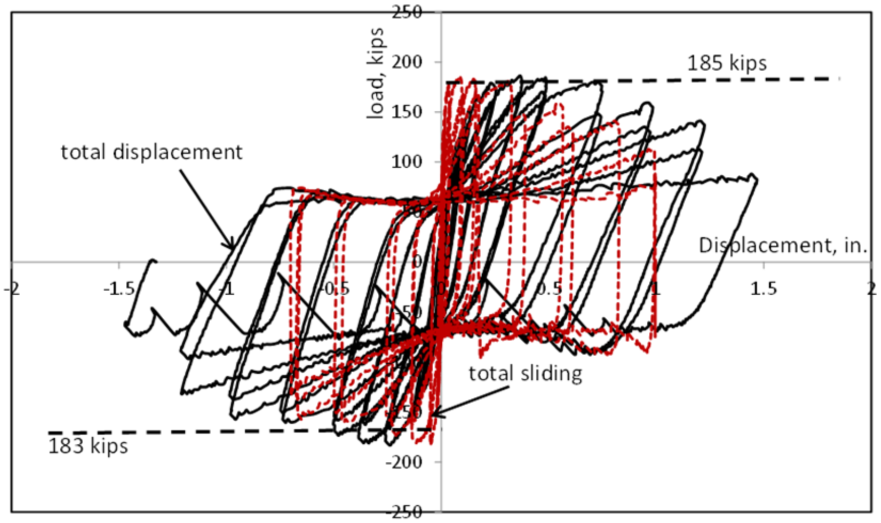

Figure 5.24 Lateral force versus total lateral displacement, and lateral force versus total sliding (Specimen UT-PBS-09)

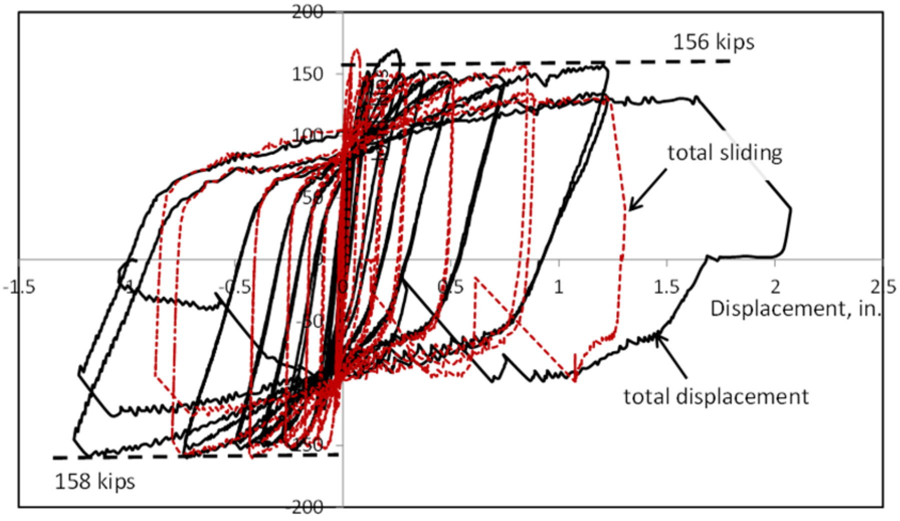

Figure 5.25 Lateral force versus total lateral displacement, and lateral force versus total sliding (Specimen UT-PBS-10)

In the four specimens that experienced significant sliding, the first few cycles showed important diagonal shear cracks and horizontal cracking across the entire plan length of the top and the base of the reinforced masonry walls. Early in the next few cycles, the lateral capacity dropped without propagation of either shear or flexural cracks. This decrease in lateral capacity was due to sliding at the base (or top) of the specimen, which began to dominate the hysteretic load-displacement curves. Dowel action of vertical reinforcement was initially effective, but became less effective as damage increased in the masonry around the dowels. After many additional reversed cycles, some of the longitudinal bars fractured at the sliding interface. Predicted sliding capacity based on the ACI 318 provisions along with the observed maximum loads in both directions are summarized in Table 5-6. As shown in this table, the maximum loads in the UT Austin specimens experienced or governed by base or top sliding ranged from 11% to 25% lower than the nominal sliding-shear capacities of ACI 318. Motivated by this discrepancy, researchers examined the same kind of information previously reported for other reinforced masonry walls failing in sliding shear.

Table 5-6 Comparison of observed and predicted sliding-shear capacities for fixed-fixed specimens tested at UT Austin and showing significant sliding

Specimen	Observed Capacity (kips)		Nominal sliding-shear capacity by ACI 318-11 (kips)
	Push-North	Pull-South	
UT-PBS-05	153	152	189
UT-PBS-06	115	108	128
UT-PBS-09	186	183	244
UT-PBS-10	169	161	196

5.6.1.4 Sliding-shear Capacities of Walls Tested by Other Researchers

The data set of masonry shear walls tested by other researchers and showing significant sliding include cantilever walls of concrete masonry tested by Shing *et al.* (1990), Voon and Ingham (2007), and Hernandez (2012). All those masonry shear walls were fully grouted, and were constructed on a concrete base or foundation. The data set also includes AAC masonry shear walls tested by Tanner *et al.* (2005). This last group showed sliding at the interface between conventional masonry grout (in cells of AAC units) and a concrete foundation. Because their sliding mechanism was fundamentally similar to that of the concrete masonry walls, those tests are also included in this evaluation. In Table 5-7 are shown the observed sliding-shear capacities of reinforced masonry shear walls as reported by other researchers, along with the relevant parameters necessary to develop the constants for a shear-friction equation. Specimen 1 of Tanner *et al.* (2005) had external reinforcement that did not cross the sliding interface. In Table 5-7, that external reinforcement is not counted as vertical reinforcement, but is included in the axial load. Because those two contributions are handled identically in the proposed shear-friction formula, this distinction does not affect the final result.

Table 5-7 Observed sliding-shear capacities of reinforced masonry walls as reported by other researchers

Researcher and Specimen		Observed sliding shear capacities, kips	Axial Load, kips	Vertical Reinforcement	Reinforcement yield strength, ksi
Shing *et al.* (1990)	Specimen-6	+52, -47	0	5 No. 5 bars	64
	Specimen-8	+50, -47	0	5 No. 5 bars	64
Tanner *et al.* (2005)	Specimen-1	+118, -119	140	no reinforcement	-
	Specimen-4	+92, -88	89	5 No. 5 bars	77
Voon and Ingham (2007)	Specimen-3	+48, -47	0	5 D20 wires	46
Hernandez (2012)	Specimen UT-PBS-03	+82, -81	0	12 No. 4 bars	62
	Specimen UT-PBS-04	+48, -46	0	6 No. 4 bars	62
	Specimen UT-PBS-04G	+46, -39	0	6 No. 4 bars	62

5.6.1.5 Development of Proposed Equation for Sliding-shear Capacity

Assuming a shear-friction capacity as given by shear friction equation, and using the reported shear-friction capacities and other parameters shown in Table 5-6 and Table 5-7, the coefficient of friction can be calculated as shown in Table 5-8. The average calculated coefficient of friction is 0.68, with a COV of 18%. In Figure 5.26, the calculated coefficient of friction is also shown as the slope of a best-fit line with experimental sliding-shear capacity on the vertical axis, and the summation of ($A_s f_y + P_n$) on the horizontal axis. Results are reasonably consistent, and are also consistent with the value of 0.70 previously reported by Atkinson (1988) and noted in FEMA 306 (1999).

Table 5-8 Calculation of the coefficient of friction using results of UT Austin fixed-fixed specimens plus previously reported specimens

Researcher and Specimen		**Area of vertical reinforcement, in.^{2}**	**Axial load, kips**	**$A_s f_y$, kips**	**Observed sliding capacity, kips**	**Calculated coefficient of friction, μ**
UT Austin fixed-fixed specimens	UT-PBS-05	1.80	81.2	112.3	138	0.71
					140	0.72
	UT-PBS-06	1.00	68.3	62.38	105	0.80
					103	0.79
	UT-PBS-09	1.80	136.6	112.3	185	0.74
					183	0.73
	UT-PBS-10	1.00	136.6	62.38	156	0.78
					158	0.79
Shing *et al.* (1990)	Specimen-6	1	0	64	52	0.81
					47	0.73
	Specimen-8	1	0	64	50	0.78
					47	0.73
Tanner *et al.* (2005)	Specimen-1	0	140	0	118	0.84
					119	0.85
	Specimen-4	1	89	77	92	0.55
					88	0.53
Voon and Ingham (2007)	Specimen-3	2.35	0	108.1	48	0.44
					47	0.43
Hernandez (2012)	Specimen UT-PBS-03	2.4	0	148.8	82	0.55
					81	0.54
	Specimen UT-PBS-04	1.2	0	74.4	48	0.64
					46	0.61
	Specimen UT-PBS-04G	1.2	0	74.4	46	0.61
					39	0.52
					Average	0.68
					COV	18%

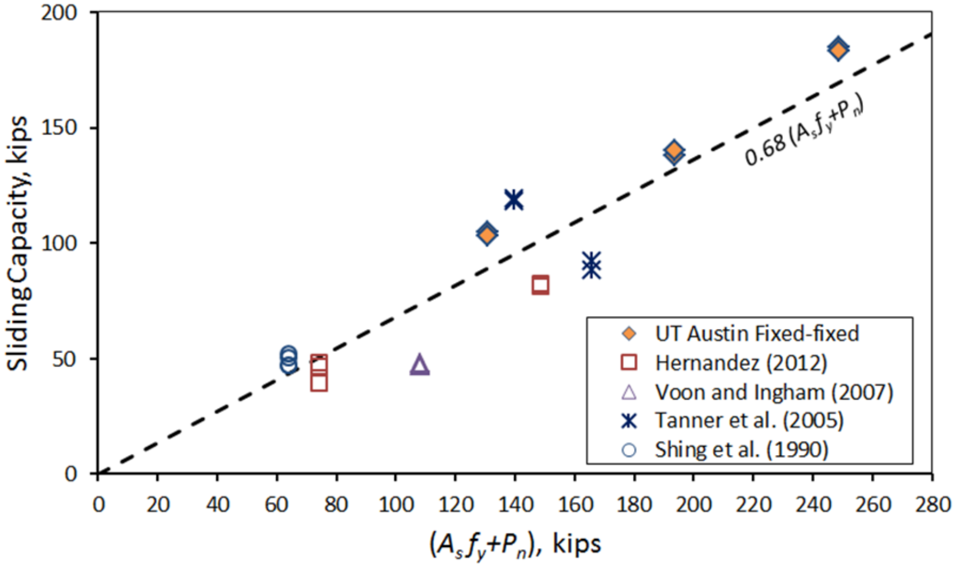

Figure 5.26 Comparison of sliding shear capacity calculated using proposed shear-friction equation (μ = 0.68) with measured sliding shear capacities

These results are also reasonably independent of the degree of roughening of the foundation. In the fixed-fixed shear-wall specimens tested at UT Austin and reported here, and in the cantilever shear-wall specimens tested at UT Austin and reported by Hernandez (2012), the foundations were not intentionally roughened, but were cleaned with compressed air and pre-wetted. Tanner *et al.* (2005) roughened the top of the concrete base or foundation by light bush-hammering, cleaned with compressed air, and pre-wetted. In the specimens reported by Shing *et al.* (1990), to increase base shear friction, ten minutes after the base beam was cast the concrete was roughened by a high-pressure water jet to have approximately a 1/4 in. amplitude of the aggregated exposed. No data are available for the condition of bed joints in Voon and Ingham (2007).

In examining Table 5-8, the values of the calculated coefficient of friction are relatively high for one group of specimens with intentionally roughened interfaces (Shing *et al.* 1990). They are equally high, however, for another group of specimens without intentionally roughened interfaces (fixed-fixed, UT Austin, reported here). For the other specimens of Table 5-8, the values of the calculated coefficient of friction show no clear relationship to interface roughness. In summary, the reported coefficient of friction of 0.68 seems valid whether or not the interface is intentionally roughened.

5.6.2 Shear Capacity of Fixed-fixed Wall Specimens

Based on fixed-fixed reversed cyclic test results, the reliability of the shear capacity equations of the strength provisions of the 2011 MSJC *Code* was evaluated and presented by Alogla (2012). That examination used test data from 62 fully grouted, reinforced-masonry shear walls. That database comprises 56 walls previously evaluated by Davis *et al.* (2010) and 6 walls tested at the University of Texas at Austin. As shown in Table 4, the capacities of Specimens UT-PBS-01 and UT-PBS-02 were limited by distributed web-shear cracking and shear failure and did not show sliding. Those specimens were included in the statistical evaluation of this paper. In Specimen UT-PBS-10, distributed web-shear cracks combined with significant sliding at the base and top of the specimen; however, at the end of the test the specimen failed by shear. This specimen was also included in this evaluation of shear strength, for a total of three. The behavior and capacities of the remaining three specimens (UT-PBS-05, UT-PBS-06, and UT-PBS-09) were governed by sliding shear, and these shear walls were therefore excluded from the statistical evaluation of this section.

Alogla (2012) concludes that for reinforced masonry shear walls meeting the requirements of the 2011 MSJC *Code* for ordinary and intermediate reinforced masonry shear walls, strength-design equation for nominal shear capacity should be reduced by a factor of 0.89, so that ratios of (V_{test} / V_n) would have a lower 5% fractile of 1.0. For reinforced masonry shear walls meeting the requirements of the 2011 MSJC *Code* for special reinforced masonry shear walls, there is no need to reduce the strength-design equation for nominal shear capacity, because the additional requirements for capacity design in effect impose an additional factor of safety of 1.56 for such walls (Alogla 2012).

Table 5-9 Comparison of predicted and experimental shear capacities for fixed-fixed shear-wall specimens

Specimen	**Experimental capacity (V_{test}), kips**		**Nominal shear capacity by MSJC 2011 *Code* (V_n) kips**	**Failure mode at the end of test**
	Push-North	**Pull-South**		
UT-PBS-01	198	178	155	Shear
UT-PBS-02	162	165	154	Shear
UT-PBS-05	153	152	171	Sliding
UT-PBS-06	115	108	140	Sliding
UT-PBS-09	186	183	193	Sliding
UT-PBS-10	169	161	165	Shear and Sliding

CHAPTER 6

Shake-Table Performance of Full-Scale, Three-Story Specimen (January - February 2011)

6.1 INTRODUCTION

As part of the NIST masonry project, a full-scale three-story reinforced concrete masonry shear-wall system was tested in January and February 2011 on the large outdoor shake-table at the Englekirk Structural Engineering Center of the University of California, San Diego (UCSD). This chapter first presents a detailed description of the specimen's design, materials, detailing, construction, testing protocol, test setup, and instrumentation. Observations from the shake-table tests are then presented, along with details of the damage progression and collapse mechanism. Finally, overall structural performance is summarized. Additional details will be provided in the PhD dissertation now being prepared by Marios Mavros, doctoral candidate at UCSD.

The main objectives of shake-table testing of the 3-story CMU building specimens were as follows:

- Examine the overall and local behaviors of low- and mid-rise reinforced concrete masonry buildings designed using force-based procedures;

- Evaluate the performance of special reinforced masonry walls designed and detailed according to 2011 MSJC *Code* provisions;
- Assess the behavior and failure mechanism of a real wall system (loaded uni-directionally) as compared to the idealized system assumed in design;
- Use data from dynamic tests of a full-scale structure to extend, refine, and validate analytical models;
- Observe and report on:
  - (1) the coupling action of floor and roof diaphragms;
  - (2) the performance of lap splices of longitudinal reinforcement in plastic hinge zones;
  - (3) the performance of T-wall with web in compression as governed by maximum reinforcement limits of the MSJC *Code*; and
  - (4) the effective plastic hinge length for flexure.

Construction took place in fall 2010, and lasted seven weeks. After the specimen was constructed and while of the masonry walls and slab toppings were cured, the instrumentation was installed on the specimen in four weeks. Testing took place in January and February 2011, and included recordings of ambient vibrations, low-level white noise tests, and seismic base excitations using scaled historical ground motion records. During the tests the research team monitored the behavior of the structure at increasing maximum levels of seismic input, using 489 sensors measuring accelerations, displacements, and strains at various locations on the specimen.

6.2 PLAN AND ELEVATION OF PROTOTYPE BUILDING

Key requirements for the 3-story shake-table specimen included the following: (1) the specimen must be extracted from a realistic prototype structure; (2) the specimen must be reasonably simple to design, construct, and test; and (3) the specimen must test the limits of reinforced concrete masonry design and must use realistic reinforcement details and representative building materials, similar to those in the prototype building. With those goals in mind, the prototype building was conceived as a three-story regularly-shaped concrete masonry building with a footprint of approximately 3500 ft^2 and story heights of 8.75 ft, located in San Diego, California. The plan and elevation of the prototype building are shown in Figure 6.1 and Figure 6.2.

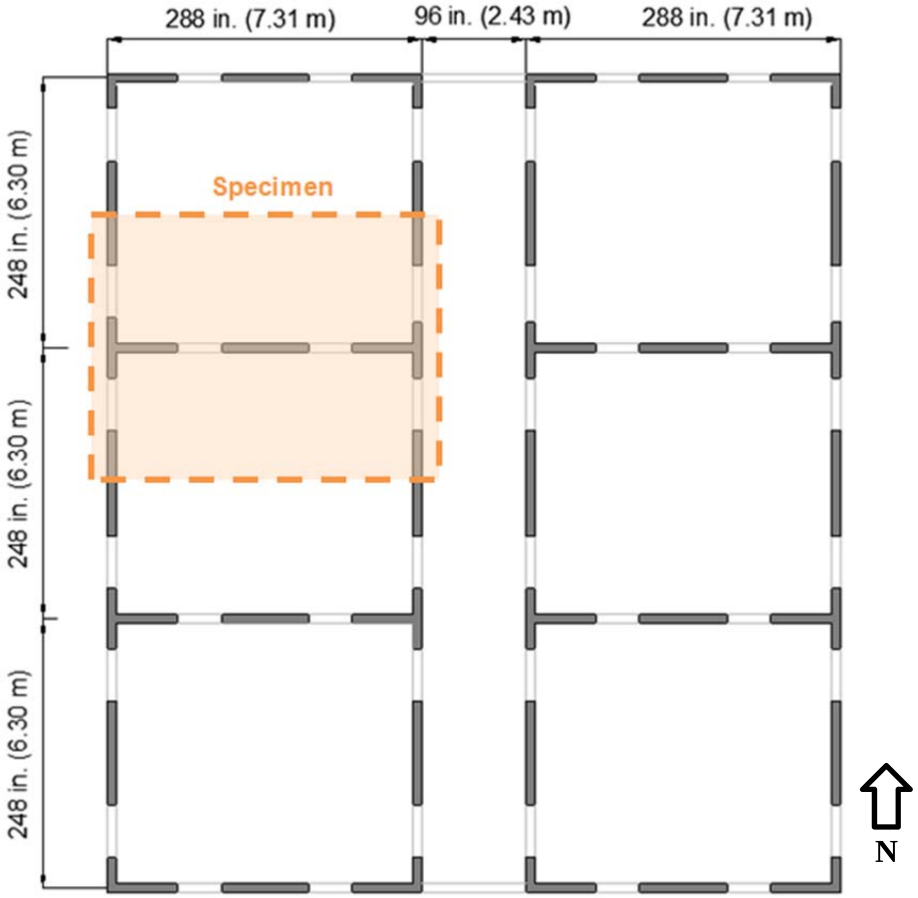

Figure 6.1 Plan view of typical floor of three-story prototype building

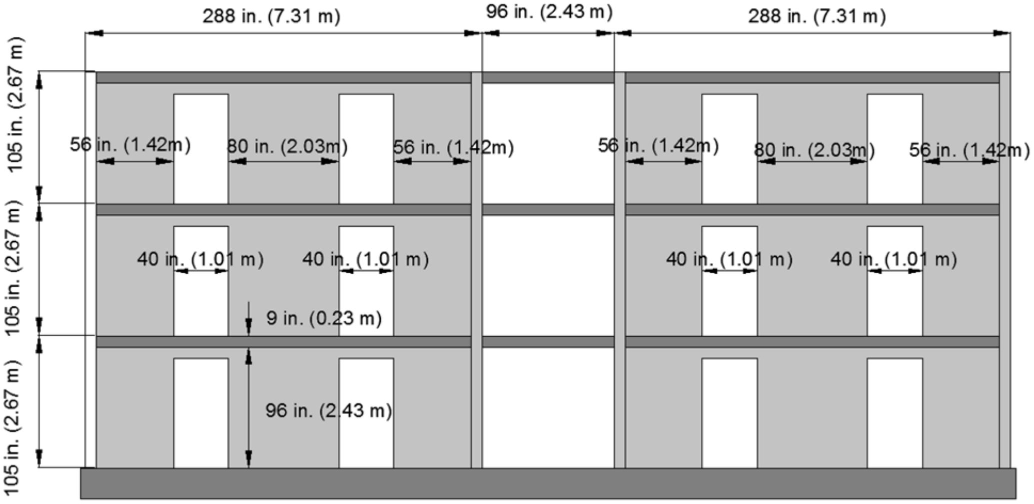

Figure 6.2 Elevation of three-story prototype building

The building is intended to be a typical apartment or office. The proposed prototype building has the following desirable characteristics:

- it is typical, and has repeating modules for the gravity and lateral resisting systems;
- it has a credible configuration of shear walls and openings;
- it has similar plan lengths of shear walls in both principal plan directions; and
- the plan lengths of its walls in the longitudinal direction can be varied to control response in that direction.

6.3 OVERALL DESCRIPTION OF 3-STORY CMU SPECIMEN

The 3-story CMU specimen was intended to represent a portion of the prototype building. The dashed rectangle in the plan view on the left-hand side of Figure 6.1 shows the plan area of the specimen. For simplicity and symmetry, the vertical shafts that would have been required for stairs and mechanical ducts were not included in this specimen. The specimen is simple, and capable of testing the performance of reinforced masonry.

The proposed plan for this specimen has a simple arrangement of walls in the direction of shaking, and a symmetrical arrangement of walls perpendicular to direction of shaking.

The specimen was designed according to ASCE 7-05 and the 2008 MSJC *Code* for Seismic Design Category D, and was thus considered a special reinforced-masonry bearing-wall system. It was detailed in accordance with 2008 MSJC *Code* requirements, including prescriptive reinforcement requirements for special reinforced masonry shear walls. The specimen was constructed by professional masons using common practice. The main structural system consisted of two T-walls, one rectangular wall parallel to the direction of shaking, four walls perpendicular to the shaking direction, and precast hollow core planks with cast-in-place reinforced concrete topping for the floor and roof diaphragms. Schematic views of 3-story, full-scale masonry specimen on the shake-table are illustrated in Figure 6.3.

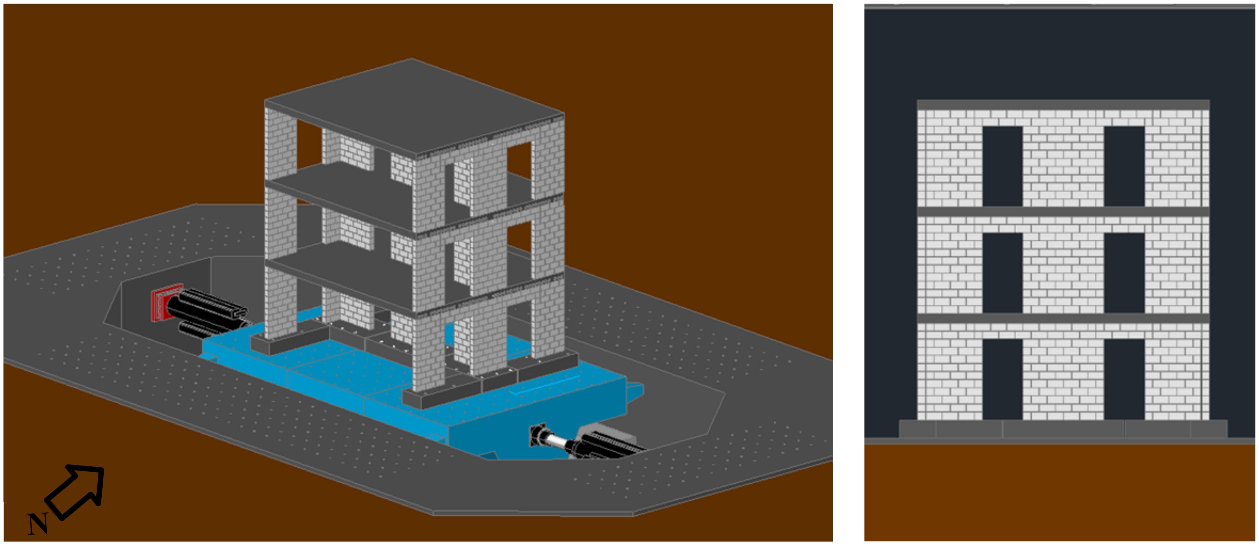

Figure 6.3 Schematic views of 3-story, full-scale reinforced masonry specimen

As shown in Figure 6.4, the specimen was rectangular in plan with out-to-out dimensions of 24 ft in the direction of the shaking, and 20.67 ft perpendicular to the direction of shaking. In the specimen, the walls parallel to the direction of shaking are two symmetrical T-walls and one lineal wall (a wall without flanges). The walls perpendicular to the direction of shaking are four lineal half-walls. As shown in Figure 6.4, Walls W-1 and W-3 are T-shaped flanged walls, whose webs are 64-in. long in plan parallel to the direction of loading, and whose flanges have a width (plan length) of 56 in. perpendicular to the direction of shaking.

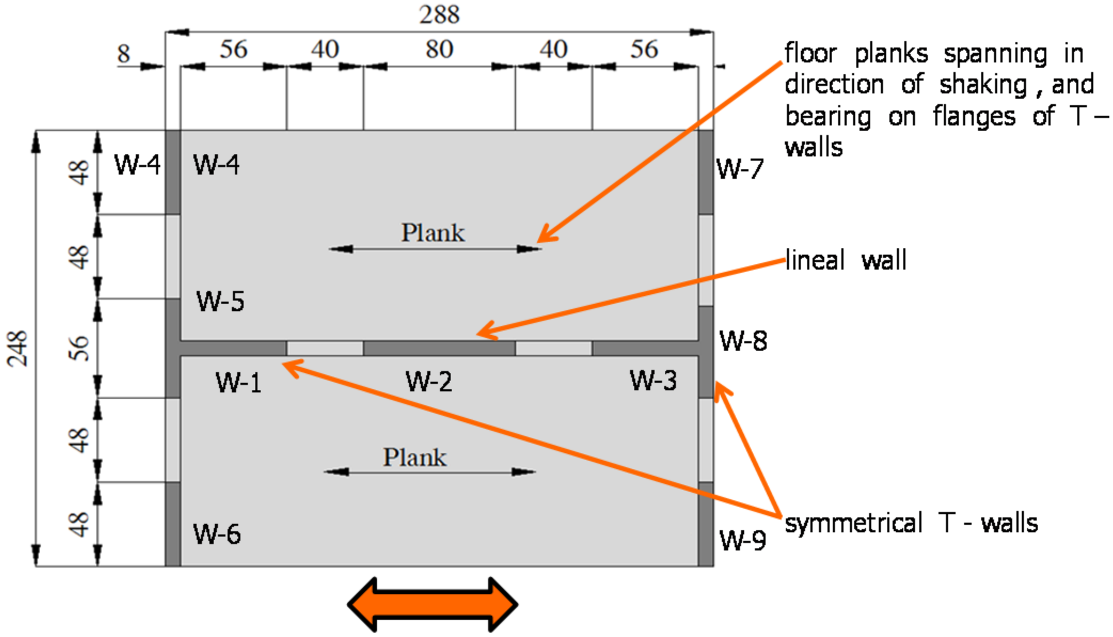

Figure 6.4 Plan view of typical floor of three-story specimen

The specimen used nominal 8- x 8- x 16-in. lightweight concrete masonry units (ASTM C90); ASTM C270 Type S cement-lime mortar by proportion for the CMU walls; and ASTM C476 coarse grout by proportion. Concrete masonry units (CMU) were H-units throughout, with knock-out units at wall ends. The CMU walls were fully grouted. Vertical control joints were located at the ends of the reinforced lintels. The roof diaphragm was composed of prestressed 6-in. concrete planks, spanning parallel to the direction of shaking, bearing on the out-of-plane lineal walls and the flanges of the T-walls. After the installation of the planks, their connections were grouted a 3.0 in. reinforced concrete topping, which had deformed reinforcement consisting of No. 4 bars at 16 in. in both directions, was added. Two No. 4 perimeter bars were placed at the level of the planks to act as a bond beams. This is not required by the 2008 MSJC Code, but is considered good practice in many west-coast design offices. The 3-story, full-scale masonry specimen as constructed on the shake-table is shown in Figure 6.5.

Figure 6.5 Three-story, full-scale specimen as constructed on the UCSD shake-table

6.4 SUMMARY OF FORCE-BASED SEISMIC DESIGN OF 3-STORY SPECIMEN

Design earthquake loads are calculated according to Section 1613 of the 2009 *International Building Code*. That section essentially references ASCE 7-05 (Supplement). Seismic design criteria are given in Chapter 11 of ASCE 7-05. The seismic design provisions of ASCE 7-05 (Supplement) begin in Chapter 12, which prescribes basic requirements (including the requirement for continuous load paths) (Section 12.1); selection of structural systems (Section 12.2); diaphragm characteristics and other possible irregularities (Section 12.3); seismic load effects and combinations (Section 12.4); direction of loading (Section 12.5); analysis procedures (Section 12.6); modeling procedures (Section 12.7); and specific design approaches. Four procedures are prescribed: an equivalent lateral force procedure (Section 12.8); a modal response-spectrum analysis procedure (Section 12.9); a simplified alternative procedure (Section 12.14); and a seismic response history procedure (Chapter 16 of ASCE7-05). The equivalent lateral-force procedure was used here, because it is relatively simple, and is permitted in most situations. The simplified alternative procedure is permitted in only a few situations. The other procedures are permitted in all situations, and are required in only a few situations. Because the equivalent lateral force procedure is being considered, the response spectrum curve is not required. Nevertheless, for completeness, it is shown in Figure 6.6 for a typical site in the San Diego area with soil condition of D, which is considered for the design of the test specimen.

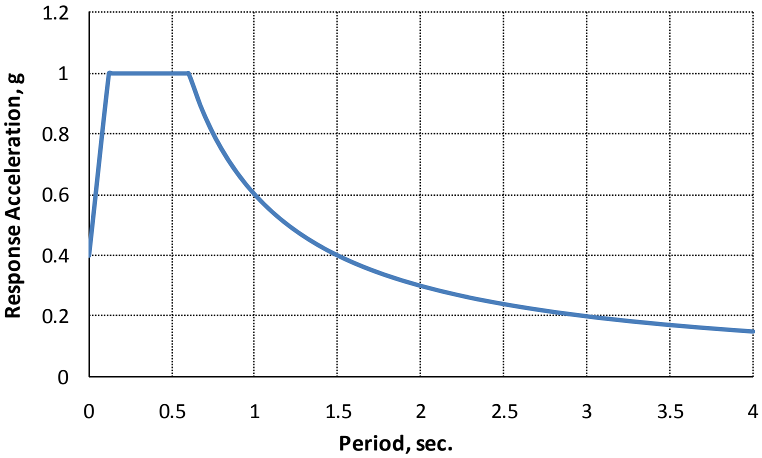

Figure 6.6 Design response spectrum for San Diego, California

Principal design parameters for the 3-story CMU building specimen are presented in Table 6-1. The design process using the principal design parameters in Table 6-1 is summarized below, and principal design parameters values are summarized for each wall segment. Detailed design calculations for each wall segment are provided in Appendix E.

Table 6-1 Principal design parameters for 3-story specimen

Wall Segment	W-1 and W-3	W-2	W-4 and W-5
	In-plane		Out-of-plane
Required Spacing of Reinforcement (2008 MSJC Section 1.17.3.2.6)			
Vertical: No. 4 bar ≤ $l/3$, $h/3$, 48 in.	$h/3$ = 19 in.	$l/3$ = 26 in.	$l/3$ = 16 in.
Horizontal: No. 4 bar when required to resist shear ≤ $l/3$, $h/3$, 48 in.	$h/3$ = 19 in.	$l/3$ = 26 in.	$h/3$ = 16 in.
other cases ≤ 48 in.	48 in.	48 in.	48 in.
Check of Capacity Design Requirement (2008 MSJC Section 1.17.3.2.6.1.1)			
selected vertical reinforcement based on required spacing above	No. 4 bars at 8 in., plus one additional No. 4 bar in the end cell of the web, and 5 No. 4 bars. in the flange	10 No.4 bars	4 No. 4 bars
selected horizontal reinforcement to satisfy capacity design requirement	No. 4 bars @ 16 in.	No. 4 bars @ 16 in.	No. 4 bars @ 16 in.
$\frac{\phi V_n}{V(M_n)} \geq 1.25$	$\frac{69.5\ kips}{31.9\ kips} = 2.17$	$\frac{76.8\ kips}{20.1\ kips} = 3.82$	-
Check of Required Ratio of Reinforcement (2008 MSJC Section 1.17.3.2.6)			
Vertical (ρ_v) ≥ 0.0007, $\rho_h/3$	0.0032	0.0032	0.0016
Horizontal (ρ_h) ≥ 0.0007	0.0016	0.0016	0.0016
Sum (ρ_v+ ρ_h) ≥ 0.002	0.0048	0.0048	0.0032

1. Select the vertical reinforcement for CMU wall segments based on prescriptive requirements for special reinforced masonry shear walls (2008 MSJC *Code* Section 1.17.3.2.6). Make a preliminary selection of horizontal reinforcement based on prescriptive reinforcement requirements. This is preliminary because it is not known in the beginning whether or not horizontal reinforcement will be required for shear.

2. Using moment-axial force interaction diagrams, 2008 MSJC *Code* equations for shear, and the specified material strengths (2500 psi for masonry, 60 ksi for reinforcement), select transverse reinforcement in all wall segments to satisfy the capacity-design requirement for special reinforced masonry shear walls (2008 MSJC *Code* Section 1.17.3.2.6.1.1). For each T-wall segment, the critical case is achieved when the effective flange is in tension (2008 MSJC *Code* Section 1.9.4.2.3). Symbolically, this check is expressed by the following equation, where $V(M_n)$ is the shear associated with the formation of plastic hinges (flexural capacity M_n) at each end of the segment:

$$\frac{\phi V_n}{V(M_n)} \geq 1.25 \qquad \textbf{\textit{Equation 6-1}}$$

Gravity load from the roof diaphragm was assumed to be distributed to out-of-plane walls and T-walls according to tributary area, so that the transverse lineal wall segments and the T-wall flanges would each support a tributary length of 12.33 ft. As shown in Table 6-1, the required spacing of transverse (horizontal) reinforcement needed to meet capacity-design requirements governs over the prescriptive spacing requirements for each wall segment.

3. Walls W-1 and W-3 are T-shaped flanged walls, whose webs are 64-in. long in plan parallel to the direction of loading, and whose flanges have the effective width (plan length) prescribed by the 2008 MSJC *Code*, which differs in tension and compression (MSJC 2008a). The axial load of each wall due to self-weight is assumed to act through the plan centroid of the wall, which is essentially the same as the plastic centroid, because the cross-sectional area of reinforcement is small. The axial load due to the reaction from the floor planks is assumed to act at the center of the flange of each T-wall. The moment-axial force interaction diagrams for each wall are based on the plastic centroid for that wall.

4. The effect of openings on wall stiffness depends on the size, shape, and distribution of those openings. While finite element methods are more accurate, approximate methods can be used to estimate the stiffnesses of walls with openings. The specimen was designed neglecting the coupling effect of the floor and roof slabs. This greatly simplifies the design, and is generally conservative. The three walls are conservatively assumed to be uncoupled, so that each functions as an independent cantilever (Figure 6.7).

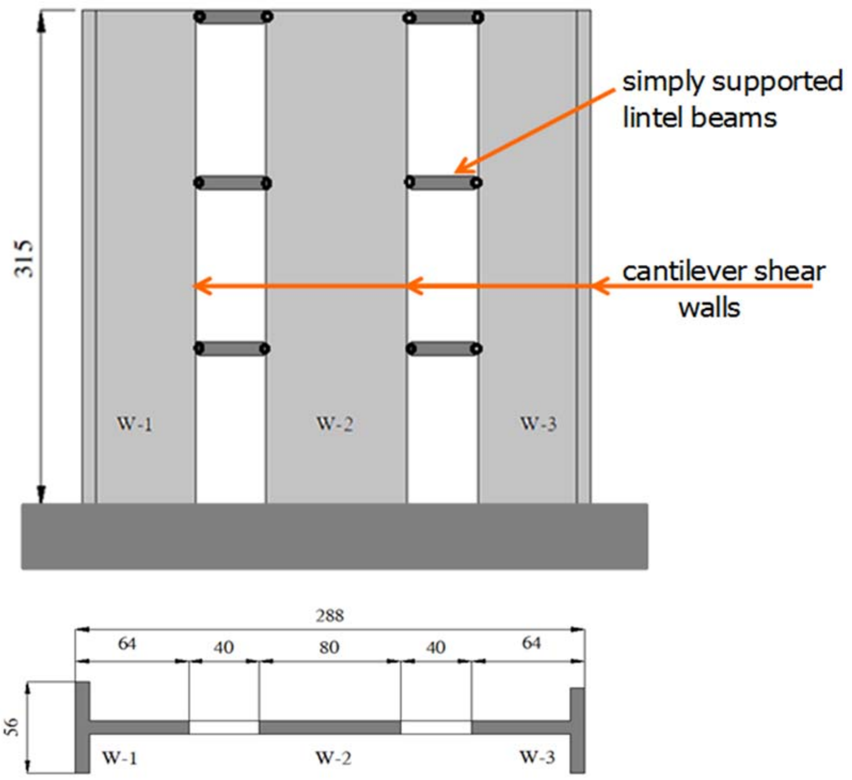

Figure 6.7 Idealization with zero coupling, used in computing stiffnesses of shear walls

6.4.1 Select Vertical Reinforcement and Estimate Horizontal Reinforcement for Each Wall Segment based on Prescriptive Requirements

6.4.1.1 Prescriptive Reinforcement for W-1 and W-3 T-wall segments

For T-wall segments, vertical and horizontal reinforcement must be spaced at the least of $l/3$, $h/3$, and 48 in. The governing (least) dimension is $l/3 = 19$ in.

6.4.1.2 Prescriptive Reinforcement for W-2 lineal wall segment

For the lineal wall segment, vertical and horizontal reinforcement must be spaced at the least of $l/3$, $h/3$, and 48 in. The governing (least) dimension is $l/3 = 26$ in.

6.4.1.3 Prescriptive Reinforcement for W-4 and W-5 out-of-plane wall segments

For the out-of-plane lineal wall segments, vertical and horizontal reinforcement must be spaced at the least of $l/3$, $h/3$, and 48 in. The governing (least) dimension is $l/3 = 16$ in.

6.4.2 Select Horizontal Reinforcement to Meet MSJC Capacity Design Requirements

Using moment-axial force interaction diagrams computed by spreadsheet, 2008 MSJC equations for shear, and specified material strengths (2500 psi for masonry, 60 ksi for reinforcement), select horizontal reinforcement in all wall segments to satisfy the capacity design requirement for special reinforced masonry shear walls (2008 MSJC *Code* Section 1.17.3.2.6.1.1). The strength values associated with MSJC capacity design requirement for the Wall W-1 when the flange is in tension are summarized in Table 6-1 ($\frac{\phi V_n}{V(M_n)} \geq 1.25$, or $\frac{69.5\ kips}{31.9\ kips} = 2.17$). Each of those values corresponds to the final selected bar size and spacing of vertical and horizontal reinforcement for each wall segment. Table 6-1 does not show the process by which those values were determined, because that process is given in detail in Appendix E, along with corresponding calculations and values for Walls W-2 and W-3.

6.4.3 Design Summary

Wall segments were designed and detailed to meet the requirements of the 2008 MSJC Code for special reinforced masonry walls, including capacity design for shear. As shown in Figure 6.8 for T-walls W-1 and W-3, the web required flexural reinforcement consisting of No. 4 bars at 8 in., plus one additional No. 4 bar in the end cell of the web. The flanges also had 5 additional No. 4 longitudinal bars. Transverse reinforcement consisting of No. 4 horizontal bars at 16 in. was used in the webs and flanges. Lineal Wall W-2 had longitudinal reinforcement consisting of No. 4 bars at 8 in., and transverse reinforcement consisting of No. 4 horizontal bars at 16 in. Detailed drawings and reinforcing details for the three-story specimen are provided in Appendix F.

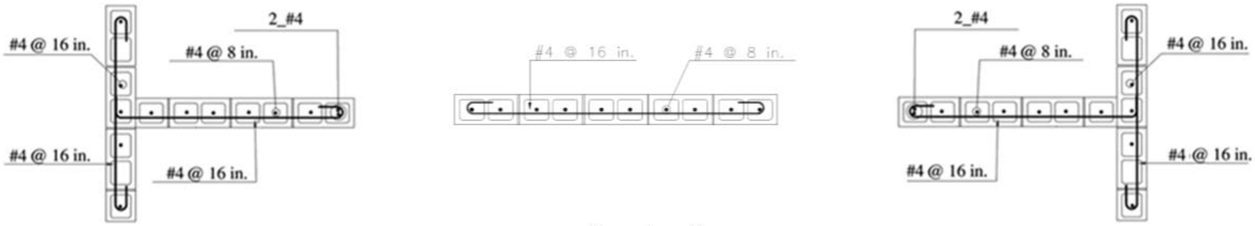

T-wall
(W-1)

lineal wall
(W-2)

T-wall
(W-3)

Figure 6.8 Reinforcement in each wall segment of 3-story specimen

As shown in Figure 6.9, Wall W-1 had vertical reinforcement spliced at the mid-height of the ground story, while Wall W-3 had vertical reinforcement spliced at the base, in a potential plastic hinge zone. The former complies with the requirement of ASCE 7-05, while the latter is permitted by the MSJC *Code*. Walls were not provided with shear keys. Horizontal reinforcement in walls was placed starting in the lowest course. Control joints were introduced on each side of the lintel beams above door openings, and the flexural reinforcing bars in the lintels were de-bonded in regions beyond the control joints to reduce the coupling moments transmitted to the wall elements. The location of splices in vertical reinforcement and control joints in the ground level are shown in Figure 6.10.

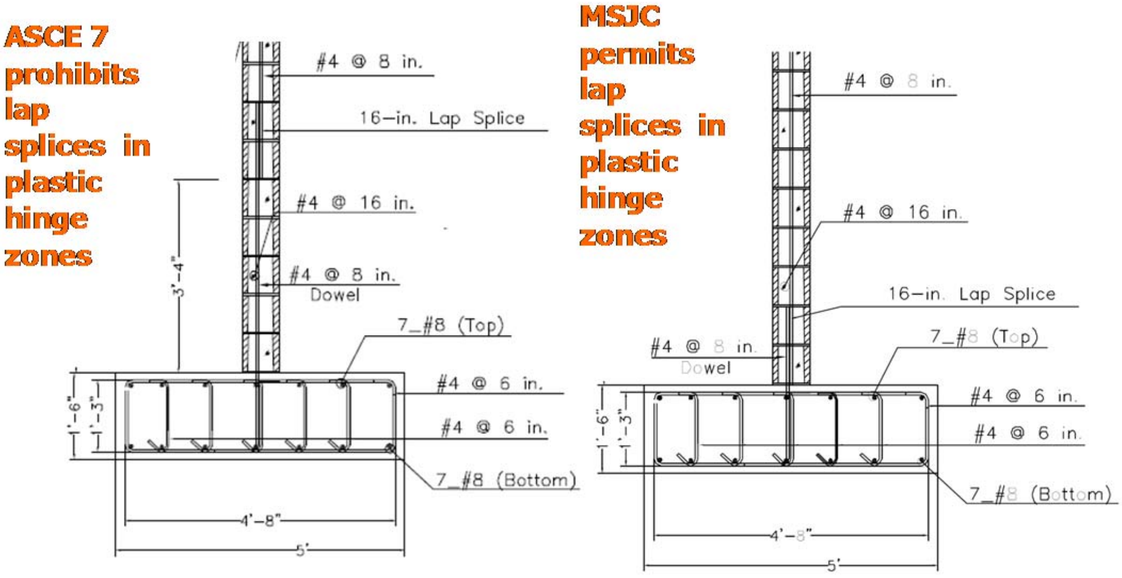

W-1 **W-3**

Figure 6.9 Detail of ground-floor splices

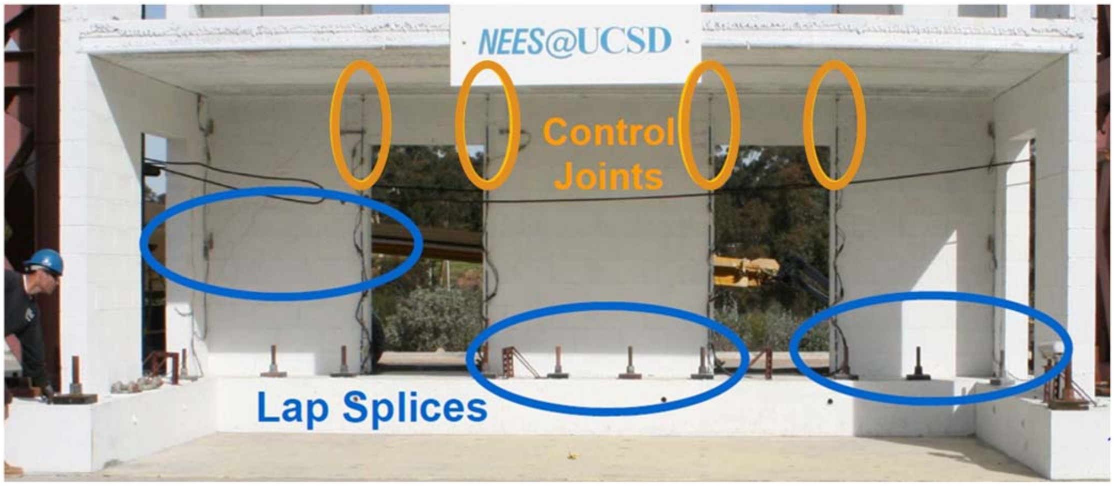

Figure 6.10 Control joints and lap splices at ground story of 3-story specimen

6.5 CONSTRUCTION OF 3-STORY SPECIMEN

The construction of the structure lasted seven weeks in fall 2010. Figure 6.11 to Figure 6.26 present pictures taken during the construction of the 3-story specimen. They show the construction sequence and the different components of the specimen, and clarify some details that might have not been clear in the specimen description in this chapter.

Figure 6.11 Footing formwork and reinforcement ready for casting

Figure 6.12 Casting of reinforced concrete footing

Figure 6.13 Laying hollow CMU

Figure 6.14 Placing horizontal reinforcement

Figure 6.15 Detail of horizontal reinforcement in T-walls

Figure 6.16 Laying lintels

Figure 6.17 Placing horizontal reinforcement in bond beams

Figure 6.18 De-bonding of longitudinal reinforcement at lintel beam control joints

Figure 6.19 Placement of vertical reinforcement in cells of units

Figure 6.20 Placing prestressed concrete planks on walls after grouting

Figure 6.21 Sealing gap between planks before placing topping

Figure 6.22 Reinforcement for concrete topping

Figure 6.23 Casting concrete topping

Figure 6.24 Constructing second story

Figure 6.25 Constructing third story

Figure 6.26 Casting roof topping

6.6 MATERIAL PROPERTIES

Materials used to construct the 3-story specimen were tested to determine their strengths. Reinforcement, mortar, grout and prisms were tested at the University of California at San Diego.

6.6.1 Tensile Testing of Reinforcement

Tensile properties of reinforcement (No. 4 and No. 6 bars) used in the 3-story CMU specimen were determined according to ASTM A370-12. For No. 4 bars, yield strength and tensile strength were 62.9 ksi and 104.1 ksi respectively; and for the No. 6 bars, those values were 64.1 ksi and 88.90 ksi, respectively. Results are listed in Table 6-2. In Figure 6.27 and Figure 6.28 are shown measured stress-strain curves for No. 4 and No. 6 bars.

Table 6-2 Average properties of reinforcing bars of 3-story specimen

Bar Size	Type	Nominal Diameter mm (in.)	Yield Stress MPa (ksi)	Yield Strain	Tensile Strength MPa (ksi)	Strain at Fracture
No. 4	deformed	12.70 (0.50)	433.7 (62.9)	2.30E-3	717.7 (104.1)	1.72E-1
No. 6	deformed	19.05 (0.75)	441.9 (64.1)	2.29E-3	612.9 (88.9)	1.96E-1

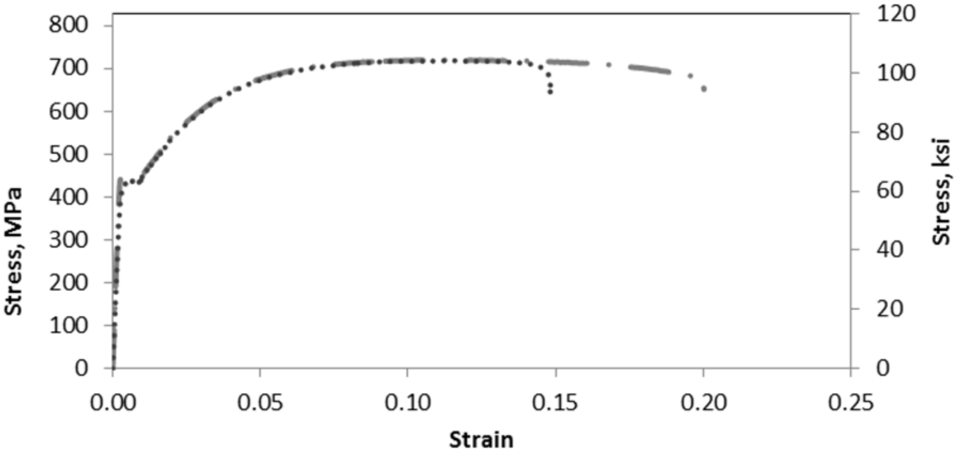

Figure 6.27 Tensile stress-strain curve for No. 4 bars (3-story specimen)

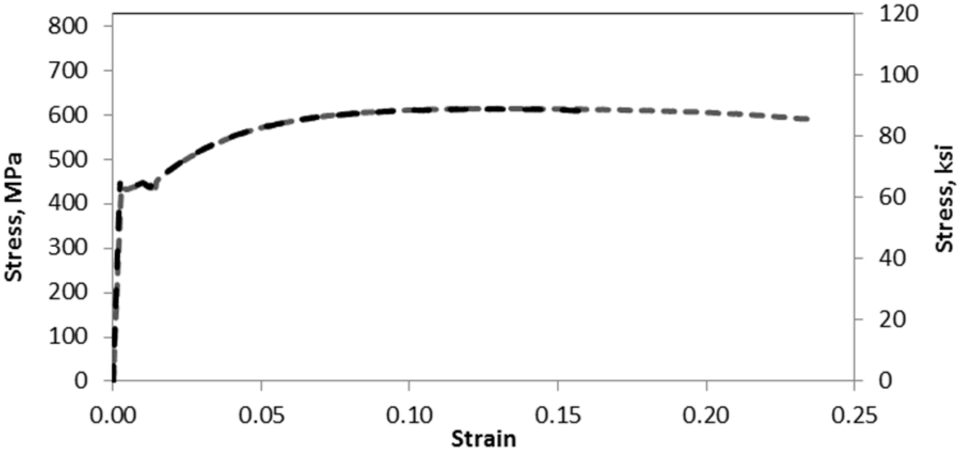

Figure 6.28 Tensile stress-strain curve for No. 6 bars (3-story specimen)

6.6.2 Compressive Strength of Grout

Grout specimens measuring 4 x 4 x 8 in. and 4 x 4 x 4 in. were constructed and tested to determine compressive strength in accordance with ASTM C1019-11. For each first story and second story two sets of grout specimens were prepared, and all specimens were tested. Results are listed in Table 6-3. The average net compressive strengths of grout for the first story were 3.82 and 3.98 ksi.

Table 6-3 Average grout properties measured on the day of the first major test (3-story specimen)

Story	4x8 in. Cylinders			4x4 in. Cubes	
	Elastic Modulus	Compressive Strength	Strain at Peak Stress	Compressive Strength	Elastic Modulus
	GPa (ksi)	MPa (ksi)		MPa (ksi)	GPa (ksi)
1st Story	10.6 (1535.7)	26.3 (3.82)	0.0051	27.4 (3.98)	11.0 (1590.0)
2nd Story	11.4 (1658.1)	24.4 (3.54)	0.0067	25.6 (3.71)	8.57 (1243.6)

6.6.3 Compressive Strength of Mortar (3-story specimen)

Compressive strengths of 2- x4-in. mortar cylinders and 4-in. mortar cubes were determined according to ASTM C780-11, which refers in turn to ASTM C109-11. Results for cement-lime mortar are summarized in Table 6-4. Even though those strengths were evaluated using job flow rather than the laboratory flow required by ASTM C270-12, because the compressive strengths exceeded the required property-specified strength of 1800 psi, the sand can be inferred to have met the "use" requirements of ASTM C144-11.

Table 6-4 Average mortar properties measured on the day of the first major test (3-story specimen)

Story	2- x 4-in. Cylinders			4-in. Cubes	
	Elastic Modulus	Compressive Strength	Strain at Peak Stress	Compressive Strength	Elastic Modulus
	GPa (ksi)	MPa (ksi)		MPa (ksi)	GPa (ksi)
1st Story	6.86 (995.3)	35.5 (5.12)	0.0065	42.7 (6.19)	10.6 (1537.6)
2nd Story	7.54 (1093.4)	33.5 (4.86)	0.0074	*	*

* data are not available

6.6.4 Compressive Strength of CMU Prisms (3-story specimen)

Compressive strengths of CMU prisms were determined according to ASTM C1314-11. Twelve grouted concrete masonry prisms were tested according to ASTM C1314. Grouted prisms were 8 x 8 x 8 in., and were constructed using two concrete masonry half-units. Results are summarized in Table 6-5. The prisms were capped, and the capping plates used satisfied the thickness required by ASTM C140-12, which refers to ASTM C1552-9 for capping.

Table 6-5 Average prism properties measured on the 28-day and day of the first major test (3-story specimen)

Story	28-day Strength MPa (ksi)	Day of First Major Test		Last Day of Test	
		Age Days	Strength MPa (ksi)	Age Days	Strength MPa (ksi)
1st Story	17.5 (2.53)	79	21.0 (3.05)	121	21.4 (3.10)
2nd Story	17.9 (2.59)	71	18.4 (2.66)	113	21.0 (3.05)
3rd Story	15.8 (2.29)	*	*	100	14.9 (2.16)

* data are not available

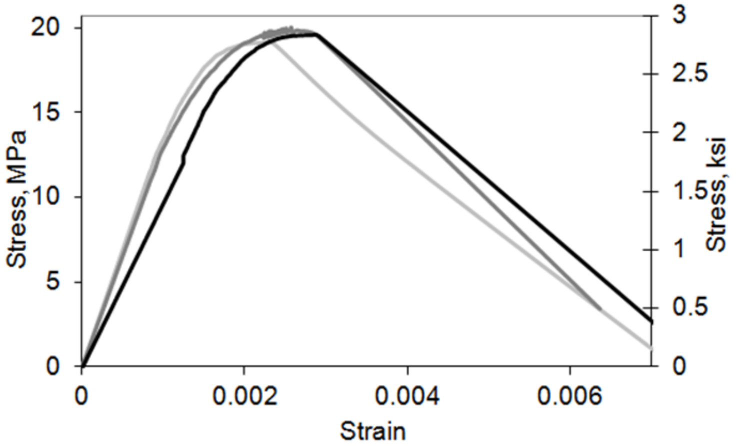

Figure 6.29 Typical compressive stress-strain behavior of masonry prisms for first story of 3-story specimen

6.7 INSTRUMENTATION FOR SHAKE-TABLE TESTS OF 3-STORY SPECIMEN

An array of 489 sensors (266 strain gauges, 133 displacement transducers, and 90 accelerometers) was deployed on the specimen to measure accelerations, displacements, and strains at various locations of the specimen. Displacement transducers were used to monitor the wall segment deformations and floor displacements with respect to the table. The interstory lateral deformations were measured with the use of aluminum reference frames which had very small mass and high stiffness so that their deformations were negligible as compared to displacements they would measure (Stavridis 2009). In addition the specimen was instrumented with a variety of strain gauges, linear potentiometers, string potentiometers, linear variable differential transformers (LVDT). The reinforcement of the specimen was instrumented with strain gauges at critical locations. Emphasis was given at the lap-splice regions and at the locations where yielding was anticipated. Linear potentiometers were located on the specimen to monitor local shear and flexural deformations, incremental vertical deformations at the ends of the wall segments, axial deformations, sliding between foundation and shear wall panels, control joints, and any potential sliding between floors and shear wall panel. The instrumentation scheme for the 3-story CMU building specimen is shown in Appendix G. Figure 6.30 shows some examples of the instrumentation scheme for the specimen in the first story.

Figure 6.30 First-story instrumentation of 3-story specimen

6.8 SUMMARY OF SHAKE-TABLE TESTS AND TEST RESULTS FOR 3-STORY SPECIMEN

Between January 12 and February 8, 2011, the 3-story specimen was subjected to an extended series of ground motions. In this section, the test history and specimen response are first summarized, and the significance of that response is then discussed. Detailed descriptions of the shake-table testing and the test results will be provided in the Stavridis *et al.* (2012).

6.8.1 Test Setup for 3-story Specimen

The structure was tested on the outdoor shaking table at the University of California at San Diego. The table has plan dimensions of 7.60 m x 12.20 m (25 ft x 40 ft) and is capable of carrying a maximum payload of 20 MN (450 kips). The two hydraulic actuators controlling the table motion have a stroke of ± 0.75 m (29.5 in.), and are capable of driving the table to a maximum velocity of 1.80 m/sec (70 in. /sec). The reinforced concrete foundation was tied to the table by post-tensioned threaded steel rods. Figure 6.31 shows the completed structure on the shaking table.

Figure 6.31 Three-story specimen on UCSD shake-table

6.8.2 Overall Summary of Shake-table Tests

The shake-table tests used a series of ground-motion records, factored (scaled) as discussed below. The records were obtained from the Pacific Earthquake Engineering Research (PEER) center; their characteristics are summarized in Table 6-6.

In Figure 6.32, the response spectra for those ground motions are compared with design response spectra at the DBE and MCE levels. The initial fundamental period of the structure was 0.09 sec. In ASCE7-05, the Design Basis Earthquake (DBE) corresponds to an event with a return period of 476 years, and in ASCE 7-10 is now referred to as the "Design Earthquake." The Maximum Considered Earthquake (MCE) corresponds to an event with a return period of about 2500 years.

Table 6-6 Ground-motion records used for shake-table testing of 3-story specimen

Earthquake	Year	Magnitude	Motion	PGA (g)	PGV (cm/sec.)	Duration (sec.)	Time-step (sec.)
Imperial Valley	1979	7.0	El Centro	0.519	46.9	39.285	0.005
Imperial Valley	1940	6.5	El Centro#5	0.313	29.9	40	0.01
Northridge	1994	6.7	Sylmar	0.843	129.3	40	0.02
Northridge	1994	6.7	Rinaldi	0.838	166.1	14.95	0.005
Chi Chi	1999	7.6	TCU129	1.01	60.0	70	0.05

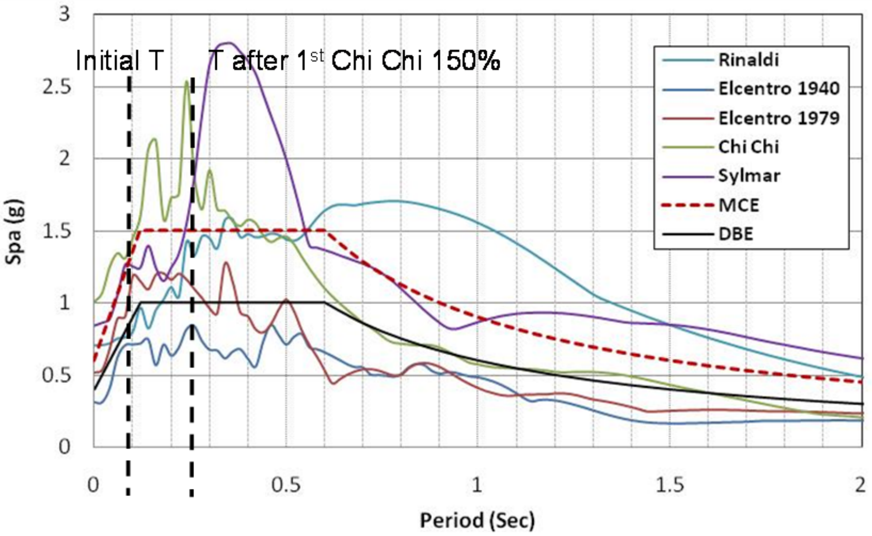

Figure 6.32 Three-story specimen ground motion spectra before scaling

In Table 6-7, the sequence of ground motions used to test the 3-story specimen is summarized, along with the Peak Ground Acceleration (PGA) measured from the table. Before and after each seismic test, white-noise excitations and ambient vibration recordings were used to assess the increase in periods of the specimen due to the induced damage. The white noise had a root-mean-squared acceleration of 0.03 g, and swept a frequency range of 1 – 33 Hz.

Table 6-7 Test sequence for 3-story specimen

Date	**Test**	**Measured Peak Ground Acceleration (PGA)**
Friday, 11 January 2011	10 min ambient vibration 10 min ambient vibration 5 minutes “white” noise **20% of El Centro 1979** 5 minutes “white” noise 10 min ambient vibration	**0.103 g**
Monday, 12 January 2011	10 min ambient vibration 5 minutes “white” noise **45% of El Centro 1979** 5 minutes “white” noise 10 min ambient vibration	**0.234 g**
Thursday, 13 January 2011	**90% of El Centro 1979** 5 minutes “white” noise 10 min ambient vibration	**0.493 g**
Monday, 18 January 2011	10 min ambient vibration 5 minutes “white” noise **120% of El Centro 1979** 5 minutes “white” noise 10 min ambient vibration **150% of El Centro 1979** 5 minutes “white” noise 10 min ambient vibration	**0.623 g** **0.778 g**

Wednesday, 19 January 2011	10 min ambient vibration	
	5 minutes “white” noise	
	180% of El Centro 1979	**0.934 g**
	5 minutes “white” noise	
	5 minutes “white” noise	
	10 min ambient vibration	
	250% of El Centro 1979	**1.295 g**
	5 minutes “white” noise	
	5 minutes “white” noise	
	10 min ambient vibration	
	250% of El Centro 1940	**0.782 g**
	5 minutes “white” noise	
	5 minutes “white” noise	
	10 min ambient vibration	
Thursday, 20 January 2011	10 min ambient vibration	
	5 minutes “white” noise	
	5 minutes “white” noise	
	125% of Sylmar	**1.053 g**
	5 minutes “white” noise	
	5 minutes “white” noise	
	10 min ambient vibration	
Tuesday, 26 January 2011	10 min ambient vibration	
	5 minutes “white” noise	
	5 minutes “white” noise	
	160% of Sylmar	**1.349 g**
	5 minutes “white” noise	
	5 minutes “white” noise	
	10 min ambient vibration	
	140% of Rinaldi	**1.173 g**
	5 minutes “white” noise	
	5 minutes “white” noise	
Tuesday, 8 February 2011	10 min ambient vibration	
	5 minutes “white” noise	
	5 minutes “white” noise	
	100% of Chi Chi	**1.010 g**
	5 minutes “white” noise	
	5 minutes “white” noise	
	10 min ambient vibration	
	150% of Chi Chi	**1.515 g**
	5 minutes “white” noise	
	5 minutes “white” noise	
	10 min ambient vibration	
	150% of ChiChi	**1.515 g**
	5 minutes “white” noise	
	10 min ambient vibration	

6.8.3 Overall Test Results of 3-story Specimen

Key behaviors of the 3-story specimen are listed in Table 6-8. In this table the level of excitations were selected based on spectral ordinates corresponding to the fundamental period of the specimen at the beginning of each run. Most visible damage took place during the first run to 100% Chi Chi. During the first run to 150% Chi Chi, the specimen experienced base sliding of Wall W-2, and wide diagonal cracks in Walls W-1 and W-3. During the second run to 150% Chi Chi, severe damage occurred in the first floor, as shown in Figure 6.33.

Figure 6.33 Severe damage in first story after second run to 150% Chi Chi

Table 6-8 Summary of test history and specimen response

Ground Motion	Level of Excitation	Observations
20% El Centro 1979		No visible damage was observed. Structural period T before and after test = 0.09 sec
45% El Centro 1979		No visible damage was observed.
90% El Centro 1979	Expected DBE based on original ground motion record	Hairline cracking was observed at the bases of the CMU walls in- and out-of-plane, indicating flexural cracking of the in-plane walls and the out-of-plane walls
120% El Centro 1979	Realized DBE based on table motion	Flexural cracks developed at ends of lintel beams near control joints
150% El Centro 1979	Slightly below MCE	Flexural cracks developed at wall base; vertical reinforcement in flange of Wall W-1 (west T-wall) reached tensile strain of 0.01; similar strain level for bars in Wall W-2 (middle wall)
180% El Centro 1979	Slightly above MCE	
250% El Centro 1979		Wall W-2 (middle wall) had very minor base sliding; fine diagonal shear cracks developed on Wall W-1 (west T-wall); max. 1st story drift = 0.25%; after test T = 0.2 sec
300% El Centro 1940		Max. 1st story drift = 0.14%; after test T = 0.2 sec
125% Sylmar	Slightly above MCE	Diagonal shear cracks extended in Wall W-1 (west T-wall); horizontal flexural cracks develop near top of 1st and 2nd story walls; max. 1st story drift = 0.23%
160% Sylmar	Above MCE	Diagonal shear cracks extended in Wall W-1 (west T-wall); flexural cracks observed on top of 2nd story slab close to edges of door openings; max. 1st story drift = 0.38%
140% Rinaldi	Slightly above MCE	After test T= 0.22 sec
100% Chi Chi	Above MCE	Flexural –shear cracks developed near bottom of T-walls; cracks on top of 2nd story slab extended throughout the entire width (10ft); max. 1st story drift = 0.35%
1st 150% Chi Chi	About 2 times MCE	Severe diagonal shear cracks developed in both 1st story T-walls; residual shear crack width of 0.06 in. (1.54 mm.); Wall W-2 (middle wall) slid on the base; max. 1st story drift = 0.73%; after test T = 0.25 sec
2nd 150% Chi Chi	About 2 times MCE	Structure was severely damaged; residual shear crack width of 0.38 in. (9.6 mm.); signs of toe crushing in webs of T walls; max. 1st story drift = 1.52 %

6.8.4 Overall Behavior of 3-story Specimen

Initial response of the 3-story specimen was marked by the appearance of flexural cracks at the bases of Walls W-1, W-2, and W-3, and by the appearance of cracks at the control joints at both ends of the lintels connecting Walls W-1 and W-2. Although the longitudinal reinforcement passing through the lintels had been de-bonded on one side of each control joint, the strong connection between the precast planks and the wall segments caused the lintels to move with the planks rather than the walls, and caused some lintel cracking. The strut action of the lintels also tended to reduce the effective heights of the wall segments.

As shown in Figure 6.34 and Figure 6.35, more severe shaking caused the start of shear cracks at the bases of Walls W-1 and W-3, and produced some minor base sliding of Wall W-2.

Figure 6.34 Shear cracking of Wall W-1 after 100% Chi Chi

Figure 6.35 Shear cracking of Wall W-3 after 100% Chi Chi

As shown in Figure 6.36 and Figure 6.37, still stronger shaking increased the observed flexural and shear cracking.

Figure 6.36 Base of Wall W-2 after 100% Chi Chi

Figure 6.37 Wall W-3 after first run of 150% Chi Chi

As shown in Figure 6.38 through Figure 6.43, still stronger shaking produced additional shear cracking at the bases of Walls W-1 and W-3, and out-of-plane flexural cracking at the bases of the out-of plane walls.

Figure 6.38 Wall W-2 after first run of 150% Chi Chi

Figure 6.39 Wall W-1 after first run of 150% Chi Chi

Figure 6.40 East out-of-plane wall after first run of 150% Chi Chi

Figure 6.41 Specimen after second run of 150% Chi Chi

As shown in Figure 6.42 through Figure 6.47, continued shaking caused crushing at the corner of a door opening due to the rocking of the lintel beam, the widening of shear cracks at the bases of Wall W-1 and Wall W-3, and the crushing of the toe of Wall W-3. Of particular significance is the splice region at the compression toe of base of Wall W-3, shown in Figure 6.47. The lowest transverse reinforcing bar, hooked around the splice, probably helped keep the spliced bars from coming apart.

Figure 6.42 Base of Wall W-1 after second run of 150% Chi Chi

Figure 6.43 Base of Wall W-3 after second run of 150% Chi Chi

Figure 6.44 Corner of first-story lintel beam after second run of 150% Chi Chi

Figure 6.45 Base of Wall W-1 after second run of 150% Chi Chi

Figure 6.46 Toe at base of Wall W-3 after second run of 150% Chi Chi

Figure 6.47 Toe at base of Wall W-3 after second run of 150% Chi Chi

Finally, at the end of the test, Figure 6.48 shows how wide shear cracks had opened in Wall W-1 and Wall W-3 at the ground level. As shown in Figure 6.49, bed-joint cracks near the top of Wall W-2 in the second story, probably due to flexure, indicated that the floor planks were still acting as stiff, strong coupling elements.

Figure 6.48 Shear crack on ground story of Wall W-1 after second run of 150% Chi Chi

Figure 6.49 Wall W-2 at second story after second run of 150% Chi Chi

6.9 SIGNIFICANCE OF RESULTS FROM 3-STORY SPECIMEN

Test results show that the in contrast to the uncoupled condition assumed in design, the walls of the 3-story specimen were actually coupled by the floor slabs. The coupling moments developed by the slabs contributed to the high lateral stiffness and strength of the structure. The coupling helped to prevent toe crushing in the web of the T-walls by alleviating the compressive stress when the web was subjected to flexural compression. The rotational restraints introduced at the top of the bottom-story walls by the floor slab reduced the effective shear-span ratio of the walls and eventually led to the shear failure of the T-walls. Towards the end of testing, the middle wall began to slide, and did not contribute much to the lateral load resistance. Most of the lateral resistance came from the T-wall on the leeward side (the T-wall acting in compression).

For the reasons noted above, the specimen was stiffer and stronger than anticipated in design. It successfully resisted repeated ground motions well in excess of MCE (maximum considered earthquake). Its response was a validation of 2008 MSJC *Code* requirements for the design and detailing of special reinforced masonry shear walls. The 2008 MSJC *Code* permits splices of vertical reinforcement in potential plastic hinge zones, and does not require shear keys at wall bases. ASCE 7-05, in contrast, prohibits splices in plastic hinge zones, and requires shear keys. In this specimen, Wall W-1 (the west wall) had its vertical reinforcement spliced at mid-height, while Wall W-3 (the east wall) had its vertical reinforcement spliced at the base. No difference in performance was observed, even though both splices were subjected to demanding histories of reversed cyclic loading. The response of this specimen may argue for the validity of the MSJC requirements over those of ASCE 7-05. The performance of lap splices in plastic hinge zones requires further investigation. This was studied in cyclic tests of wall segments at Washington State University (Sherman 2011).

Response of the specimen validates 2008 MSJC *Code* requirements that transverse (horizontal) reinforcement be hooked around extreme-fiber vertical reinforcement. It also suggests that horizontal reinforcement should be placed in the lowest course, to protect lap splices there from degradation. In addition the 90-degree hook at the intersection of the shear walls and the perpendicular walls (for T-wall segments) was effective in keeping the intersecting walls together even under shaking in excess of MCE. Response of the specimen validates the 2008 MSJC *Code* requirements for capacity design for shear of special reinforced masonry shear walls. Because of the unexpected strength of the coupling slabs, the walls in the direction of shaking had lower ratios of shear span to depth (*M/Vd*) than anticipated in design, and were therefore subjected to greater shears than anticipated in design. Nevertheless, they continued to be effective in resisting shear, with no visible signs of fracture of transverse reinforcement.

The 2008 MSJC *Code* and Specification deals with only shear and flexure, and does not address base sliding. As shown by the sliding behavior of Wall W-2, the MSJC *Code* needs to address sliding at interfaces. It would be useful for the MSJC to develop shear-friction provisions, and to limit base sliding at DBE and at MCE. Criteria should be developed to limit sliding-induced story drift that might lead to the collapse of other elements in the structure, including gravity systems and walls deflecting out-of-plane.

6.10 SUMMARY AND CONCLUSIONS FROM SHAKE-TABLE TESTING OF 3-STORY SPECIMEN

In early 2011, a 3-story, full-scale, reinforced masonry shear-wall specimen was tested on the large outdoor shake-table at the University of California at San Diego. The specimen was designed and constructed using then-current United States requirements for the seismic design and construction of reinforced masonry. The specimen was very strong and stiff, and suffered little damage when subjected to ground motions with intensities exceeding the maximum considered earthquake (MCE) level. Its performance validates the requirements of the 2008 Masonry Standards Joint Committee (MSJC) *Code* (used throughout the USA) for design and detailing of special reinforced masonry shear walls. The shake-table tests of the CMU building specimen have demonstrated that a concrete masonry building designed and constructed according to the requirements of the 2008 MSJC *Code* and Specification for SDC D, can resist earthquakes above MCE without collapse.

CHAPTER 7

Analytical Tools for Displacement-based Seismic Design of Masonry Structures

7.1 INTRODUCTION

This dissertation deals with the development and verification of effective and reliable approaches for displacement-based seismic design of masonry structures. In this chapter, PERFORM 3D (CSI 2007) models for masonry shear-wall structures are checked against the reversed cyclic test results of the CMU wall specimens described in Chapters 4 and Chapter 5, and on the shake-table test results of the 3-story, full-scale, CMU building described in Chapter 6.

Reinforced masonry wall segments and structures are idealized using the General Wall Element (a "macro-element") of PERFORM 3D (CSI 2007). Input parameters for that element are based on tested mechanical characteristics of masonry and reinforcement, and were refined by comparing analytical predictions against the results of reversed cyclic load tests on reinforced masonry wall segments with varying shear-span ratios, axial loads, and longitudinal reinforcement. The calibrated analytical models were then used to evaluate the response of the three-story specimen tested on the UCSD shake table in early 2011, and to predict the response of the two-story shaking table specimen tested at UCSD in Fall 2012.

7.2 BACKGROUND ON ANALYTICAL MODELING OF REINFORCED MASONRY SHEAR WALLS AND BUILDINGS

Prediction of the nonlinear response of reinforced masonry structures is fundamental to their displacement-based design. Various analytical models have been proposed for this purpose. Four types of models were considered in this overall NIST project. Each has advantages and disadvantages in terms of level of sophistication, suitability for specific wall configurations, computational efficiency, and probable suitability for use in an experienced design office.

7.2.1 Beam-Column Models

A common approach for modeling the nonlinear hysteretic behavior of masonry wall elements uses beam-column elements aligned with the centroidal axes of horizontal and vertical wall elements, and connected with rigid links (Figure 7.1). A single-component beam-column element is most often used, consisting of an elastic flexural element with a nonlinear rotational spring at each end to account for the inelastic behavior of critical regions. Fixed-end rotations at any connection interface can be taken into account by an additional nonlinear rotational spring. To more realistically model walls, beam-column models have been refined with multiple springs (Takayanagi and Schnobrich 1976), varying inelastic zones (Keshavarzian and Schnobrich 1984), and specific inelastic shear behavior (Aristizabal 1983). However, inelastic response of structural walls subjected to horizontal loads is dominated by large tensile strains and fixed-end rotations due to bond slip, both of which are associated with shifting of the neutral axis. This behavior cannot be modeled directly by beam-column models, which assume that rotations occur along the centroidal axis of the element. Therefore, the beam-column element disregards important features of experimentally observed behavior (Shing 2008), including shifting of the neutral axis of the wall cross-section, rocking of the wall, and interaction with the frame members connected to the wall (Kabeyasawa *et al.* 1983).

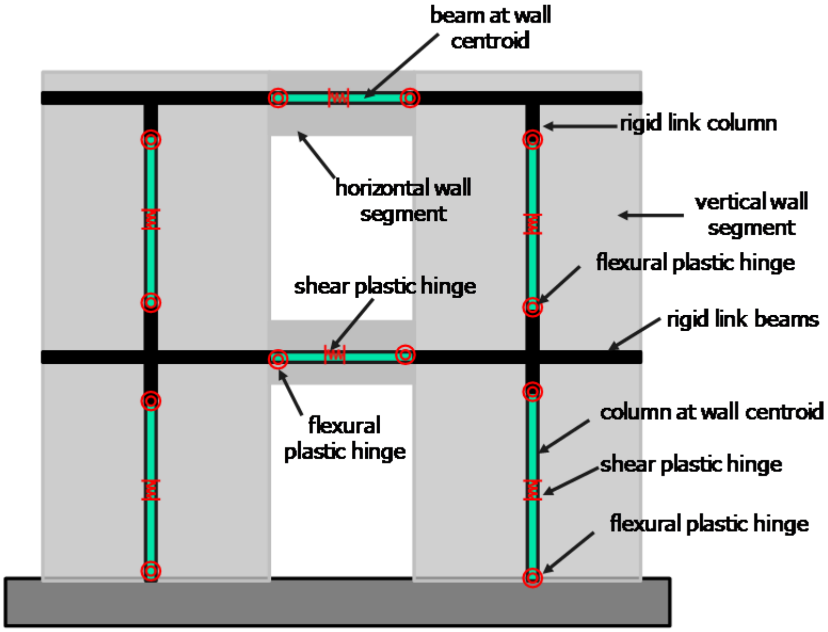

Figure 7.1 Modeling of a masonry wall using beam-column elements and rigid end links

One of the main challenges in using beam-column models is that no reliable method is currently available to estimate the effective plastic hinge length for reinforced masonry shear walls. The empirical formula proposed by Paulay and Priestley (1993) for reinforced concrete members does not correlate well with experimental observations for reinforced masonry shear walls (Shing *et al.* 1990, Shedid *et al.* 2008). However, beam-column models can be useful if calibrated against experimental data for plastic hinge lengths for wall segments.

Another challenge for the use of beam-column elements is the coupling of axial and flexural deformations due to cracking of the concrete or masonry at a wall section. In dynamic analyses, flexural cracking in beam-column elements can induce significant pulses of axial velocity and acceleration. The resulting damping and inertial effects can lead to large fluctuations of the computed axial force in a wall segment, significantly influencing the wall's flexural capacity. Even though some rocking-induced vertical acceleration is expected to occur in a real shear wall, no experimental data or field evidence substantiates the large fluctuations in axial forces predicted by beam-column models.

7.2.2 Fiber-element Models

Fiber-element models are computationally efficient and well suited for flexure-dominated walls with regular openings. As shown in Figure 7.2, in these models, the stress-strain relation of each fiber is governed by a uniaxial constitutive law. These models are available in commercial programs such as PERFORM 3D (CSI 2007), and in the open-source program, *OpenSees* (PEER 2006), developed at the Pacific Earthquake Engineering Research Center (PEER). They naturally account for the axial load-moment interaction phenomenon of a wall section, and can therefore closely simulate the flexure-dominated behavior of a reinforced concrete and masonry shear wall (Koutromanos and Shing 2009). These models have also been extended by replacing the uniaxial stress-strain relation of a fiber with a multi-axial constitutive law to capture the linear and nonlinear shear behavior of a reinforced concrete section (Petrangeli *et al.* 1999, Rose *et al.* 2002). While these models can capture axial-flexural-shear interaction, they idealize shear failure as developing at a section level, and do not represent a diagonal shear crack realistically. More often, shear behavior can be modeled simplistically by incorporating a nonlinear empirical shear behavior (Marini and Spacone 2006).

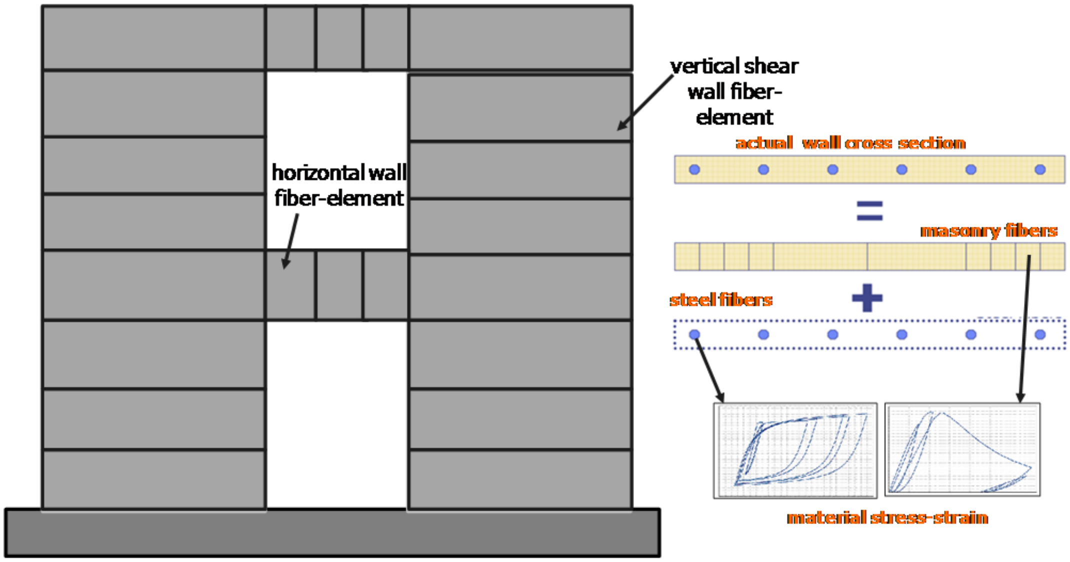

Figure 7.2 Modeling of a masonry wall using fiber elements

One challenge for fiber-element models is their tendency to localize plastic deformation in a single element in the case of a displacement-based element formulation, or at a single Gauss point in the case of a force-based element formulation, as the moment-curvature relation enters the strain-softening regime. This causes numerical results to depend on element size (non-objectivity), and leads to erroneous post-peak behavior if the elements in the plastic zone are not properly sized. To circumvent this problem, Coleman and Spacone (2001) propose a fracture-energy-based regularization method, in which the post-peak stress-strain or moment-curvature relation are adjusted based on the relationship between element size and the expected effective plastic hinge length in an element.

7.2.3 Strut-and-tie Models

Strut-and-tie models have generally been used for walls with irregularly located openings and shear-dominated behavior. They have been used to analyze reinforced masonry shear walls with openings (Voon and Ingham 2008), and reinforced concrete shear walls with irregularly located openings (Yanez *et al.* 1991). Their main challenge is the assumptions necessary to determine the location, orientation, and size of the equivalent compression struts. Even though some guidelines are provided in ACI 318-11, applying these models to walls with irregularly located openings requires additional research.

7.2.4 Finite-element Models

Nonlinear finite-element models based on smeared and discrete crack formulations are the most general analysis method for any wall type, but may require much more computational effort than the models discussed above. Smeared-crack models have two main challenges. The first is their sensitivity to element size (Bazant and Oh 1983), similar to that mentioned above for fiber-section beam-column models. The other is stress-locking (Lotfi and Shing 1991, Rots 1988), which is an over-stiff response in the softening of the plastic zone, not allowing for the full release of the stress (Ehrlich 2005). This stress-locking can lead to a significant over-estimation of the shear capacity of an element. These challenges can be addressed by supplementing smeared-crack models with cohesive crack interface models, to capture cracks in a discrete manner. The introduction of strong discontinuities represented by discrete cracks will remove the stress-locking problem, and also to a certain extent the mesh-size dependence, by concentrating the release of fracture energy in line interface elements. Discrete and smeared-crack modeling approaches have been successfully applied in combination to the modeling of non-ductile reinforced-concrete frames with clay masonry infills (Stavridis and Shing 2008).

7.3 PERFORM 3D WALL ELEMENT MODELING

The components of a shear wall can interact in complex ways, involving vertical and horizontal bending in plane, shearing deformation, and diagonal compression. In Figure 7.3 is shown a simplified wall structure, taken from the users' guide to PERFORM 3D (CSI 2007). The left part of the wall structure is essentially a vertical cantilever. The central part of the wall structure has well-defined vertical and horizontal wall segments, approximating a frame. The right part of the wall structure has staggered openings, and carries load by strut-and-tie action.

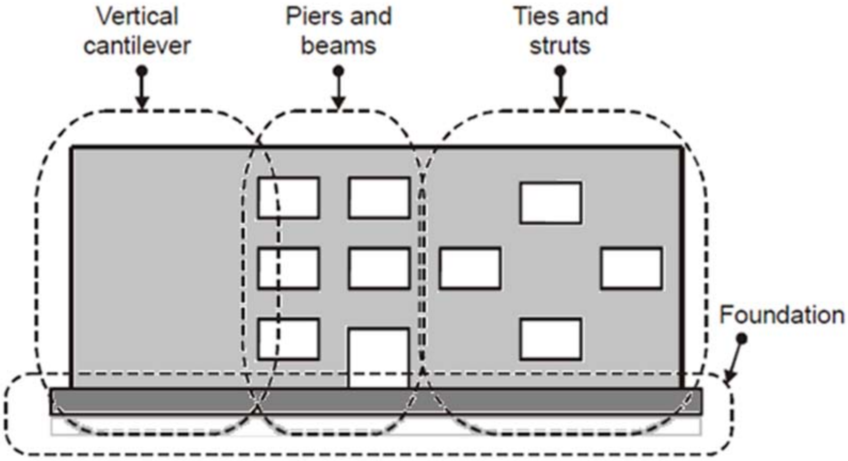

Figure 7.3 Sample wall structure with distinct parts (CSI 2007)

An analytical model for shear-wall structures must capture essential stiffnesses and strengths for each of these different types of behavior. The main requirements for the results of an analysis under seismic loads are as follows (CSI 2007).

1. For static push-over analysis the overall strength should be calculated correctly. The stiffnesses along the curve should be essentially accurate, since they affect the calculated period of vibration, and hence can affect the calculated base shear and drift demands.

2. If a dynamic analysis is carried out, the cyclic behavior and energy dissipation should also be essentially correct.

The modeling approach evaluated in this study used the macro elements implemented in PERFORM 3D (CSI 2007). With this program shear walls can be either modeled with Shear Wall Element or with the General Wall Element. The Shear Wall Element was not used in this research, and is not discussed further here. The General Wall Element is discussed in the next section.

7.4 MAIN FEATURES OF GENERAL WALL ELEMENT OF PERFORM 3D

7.4.1 Nodal Displacements of General Wall Element

Each General Wall Element has 4 nodes and 24 nodal displacements. Of those 24 displacements, eight are associated with in-plane deformations of the element, as shown in Figure 7.4. These are the most important deformation modes. Out-of-plane bending deformations also exist, but are less important. The eight in-plane displacements correspond to five deformation modes and three rigid-body modes.

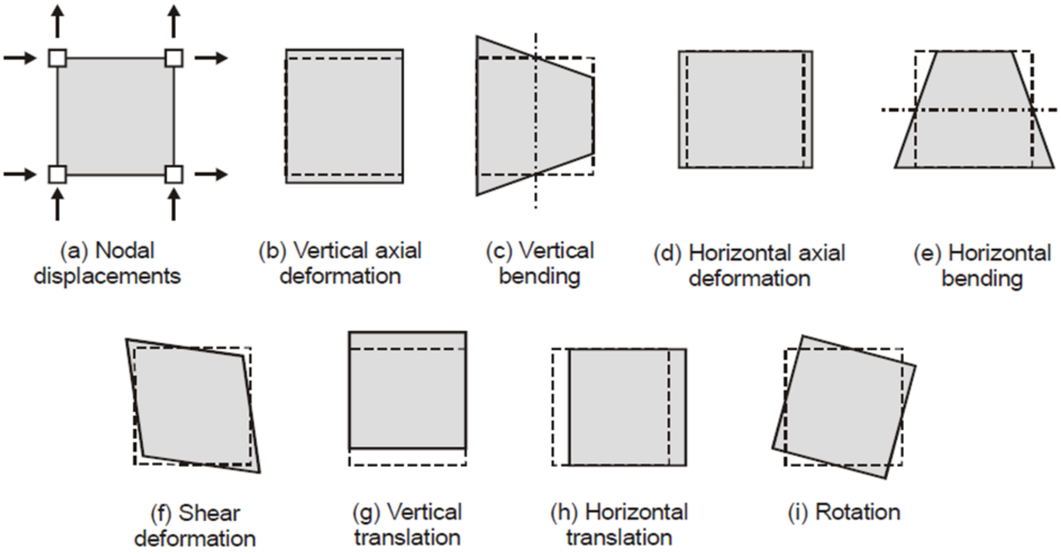

Figure 7.4 In-plane deformation modes of General Wall Element of PERFORM 3D (CSI 2007)

7.4.2 Bending, Shear and Diagonal Layers of General Wall Element

To model bending, shear and diagonal compression behavior, the General Wall Element of PERFORM 3D consists of five layers acting in parallel. These layers are shown in Figure 7.5, and are described as follows (CSI 2007).

1. The axial-bending layer for the vertical axis, shown in Figure 7.5(a), is composed of vertical fibers. It has a uniform bending deformation (uniform curvature), based on the bending moment at the mid-height of the element (CSI 2007).
2. The axial-bending layer for the horizontal axis, shown in Figure 7.5(b), is composed of horizontal fibers, and has a uniform bending deformation based on the bending moment at the mid-length of the element.

3. The conventional shear layer, shown in Figure 7.5(c), has a uniform shear strain and a uniform thickness. Its properties are based on the contribution of the concrete or masonry to its shear stiffness and strength.
4. The diagonal compression layer for the downward diagonal, shown in Figure 7.5(d), has uniform diagonal compression stress and uniform wall thickness. Its slope is usually but not necessarily 45 degrees. Through interaction with the axial-bending layers, it transmits shear and accounts for the contribution of the reinforcing steel to the shear strength. The diagonal layers are intended mainly to model strut-and-tie action.
5. The diagonal compression layer for the upward diagonal, shown in Figure 7.5(e), is analogous to the diagonal compression layer for the upward diagonal.

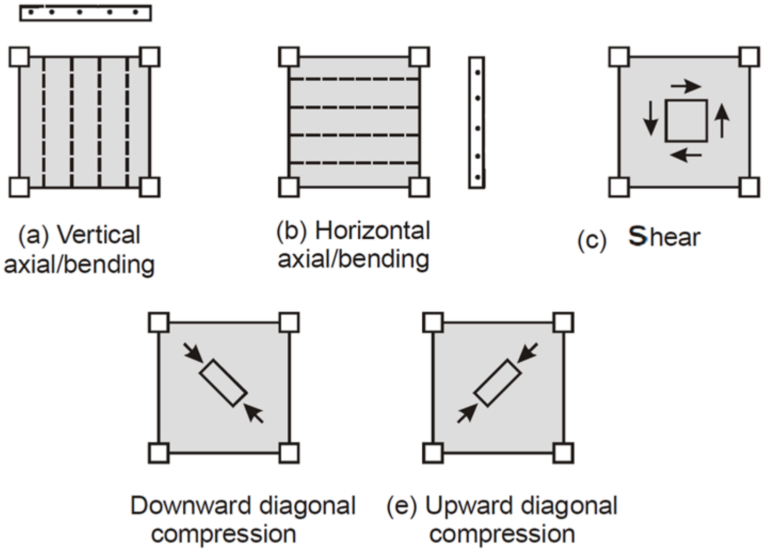

Figure 7.5 Parallel layers comprising the General Wall Element (CSI 2007)

Each layer behaves distinctly; the layers interact because they are connected at the nodes; and their combined behavior defines the behavior of the General Wall Element. For modeling most walls with PERFORM 3D, it is customary to ignore the diagonal layers, and to use only the two bending layers and the shear layer. One reason for this is that strut-and-tie behavior is complex, and a model that includes this behavior can over-estimate the shear strength of a wall. According to PERFORM 3D's developer, the diagonal-compression layers have computational problems, and should be used only for shear-dominated squat walls, and then with caution[3].

7.4.3 Principal Simplifications of the PERFORM 3D General Wall Element

In this section, two principal simplifications of the PERFORM 3D General Wall Element are discussed. The first principal simplification of the General Wall Element is that multi-axial stress states are not considered. The various aspects of behavior are separated into layers, each of which has only uniaxial stress. Some consequences of this simplification are as follows (CSI 2007).

1. The axial-bending layers account for vertical and horizontal compressive stresses in the masonry or concrete, and the diagonal layers account for diagonal compression stresses. In an actual member, these stresses interact directly. For example, instead of crushing vertically under a large vertical stress, the presence of a diagonal stress might cause the concrete or masonry to crush along an inclined direction, at a lower vertical stress than if the diagonal stress were not present. This type of interaction is not considered in the element. The axial-bending layers interact with the diagonal layers because they are connected at the element nodes, but this interaction is not the same as that associated with multi-axial stresses.

---

[3] Personal communication, Prof. Graham Powell, December 2011.

2. When masonry or concrete are subjected to combined compression and shear, their shear strength is increased, essentially because of internal friction. The General Wall Element does not account for this frictional behavior. The shear strength in the masonry or concrete shear layer is assumed to be independent of other stresses.

The second principal simplification of the General Wall Element is that the axial strain, shear strain and curvature are assumed to be uniform along the element dimension, corresponding to the bending moment at the mid-height or mid-length of the element. Hence, the axial/bending element is of lower order than a typical beam element, in which curvature is assumed to linearly along the element length. Figure 7.6 shows a consequence of this for the case of an elasto-plastic cantilever wall with a concentrated load applied at its tip.

o As shown in Figure 7.6a, moments in the real wall increase linearly from tip to base, and the wall yields when the moment at the base reaches the wall's plastic moment capacity.

o As shown in Figure 7.6b, if the wall segment is modeled with a single element extending the entire wall height, moments and curvatures are calculated at that mid-height (Figure 7.6b), where the moment is one-half its value at the base. This wall will be calculated to yield when the moment at mid-height reaches the wall's yield capacity. The load required to produce this calculated yield will be twice that of the real wall.

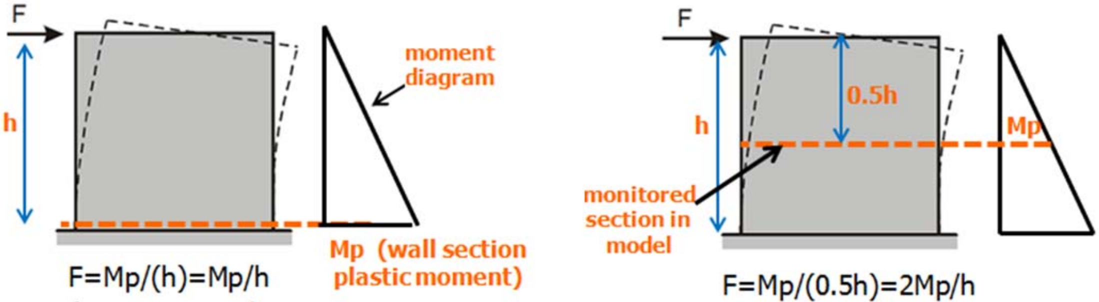

F=Mp/(h)=Mp/h

a) exact strength

F=Mp/(0.5h)=2Mp/h

b) model with single element

F=Mp/(0.75h)=1.33Mp/h

c) model with two elements

F=Mp/(0.875h)=1.14Mp/h

d) model with four elements

Figure 7.6 Error in flexural strength resulting from the uniform-curvature simplification of the General Wall Element of PERFORM 3D (CSI 2007)

o As shown in Figure 7.6c and Figure 7.6d, this error can be reduced by increasing the number of elements used over the height of a wall, or over the length of a beam. If two elements are used (Figure 7.6c), the cantilever wall's capacity is over-estimated by a factor of 1.33. If four elements are used (Figure 7.6d), its capacity is over-estimated by a factor of 1.14.

To address this issue in general, and to more accurately model the strain demand at the ends of a wall segment, the General Wall Element should be used in a finer mesh, with more elements along the axis of the member in plastic hinge zones. For wall segments known to hinge at top or bottom only, mesh refinement can take the form of thinner layers, as in Figure 7.6. As shown in Figure 7.7, for wall segments that could hinge at top and bottom (in vertical wall elements) or left and right (in horizontal wall elements), mesh refinement must take the form of smaller element rectangles.

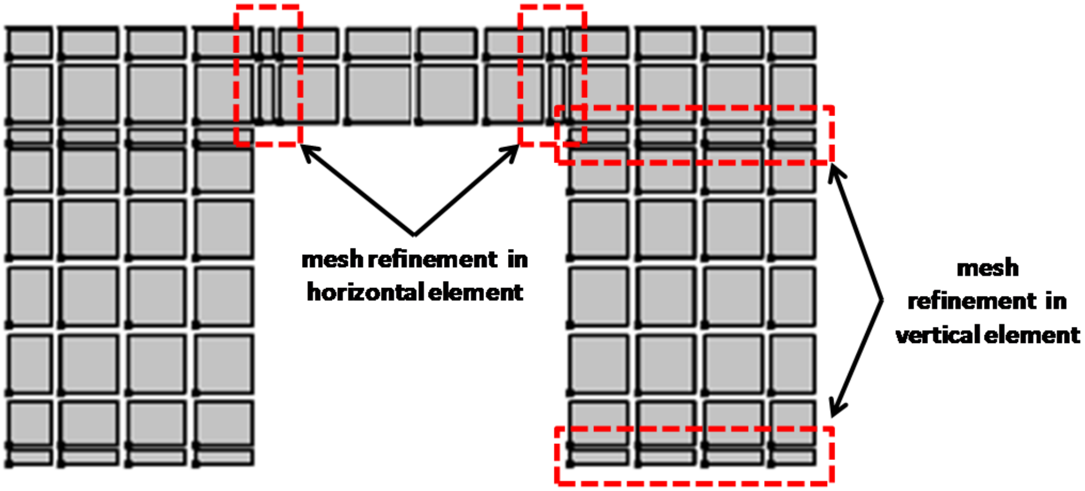

Figure 7.7 Mesh refinement in plastic hinge zones

7.5 VERIFICATION OF PERFORM 3D USING EXPERIMENTAL RESULTS FROM CANTILEVER WALL SEGMENTS

In this section, analytical predictions using the General Wall Element are compared with data from 10 reversed cyclic tests on cantilever wall segments conducted at UT Austin and Washington State University (Table 4-2). Specimens have 4 different aspect ratios (1.0, 2.0, 3.0, and 4.5), different levels of axial load, and the typical reinforcing details shown in Figure 7.8.

Table 7-1 Cantilever wall specimens used to verify and calibrate General Wall Element

Specimen	nominal length, in.	nominal height, in.	aspect ratio	axial load ratio	vertical reinf.	horizontal reinf.
WSU-W-1A	40	80	2	0.0625	#6 @ 8	#4 @ 8
WSU-W-2A	40	80	2	0.125	#4 @ 8	#4 @ 8
UT-W-13	48	144	3	0.05	#6 @ 8	#4 @ 16
UT-W-14	48	144	3	0.1	#4 @ 8	#4 @ 16
UT-W-17	32	144	4.5	0.05	#6 @ 8	#4 @ 8
UT-W-20	32	144	4.5	0.15	#4 @ 8	#4 @ 16
UT-PBS-03	96	96	1	0	#4 @ 8	#4 @ 8
UT-PBS-04	96	96	1	0	#4 @ 16	#4 @ 16
UT-PBS-11	96	96	1	0.1	#4 @ 16	#4 @ 16
UT-PBS-12	96	96	1	0.1	#4 @ 16	#4 @ 16

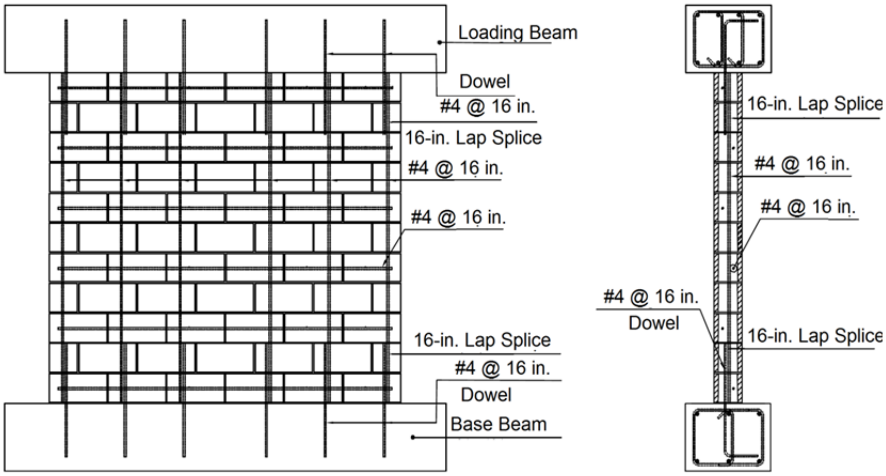

Figure 7.8 Typical details for cantilever wall specimens tested at UT Austin

7.5.1 Mesh and Fiber Geometry for Modeling Wall Specimens

To model the strain demand at the base of the walls realistically, the wall specimens are modeled using 8- × 8-in. General Wall Elements, whose properties are specified as follows:

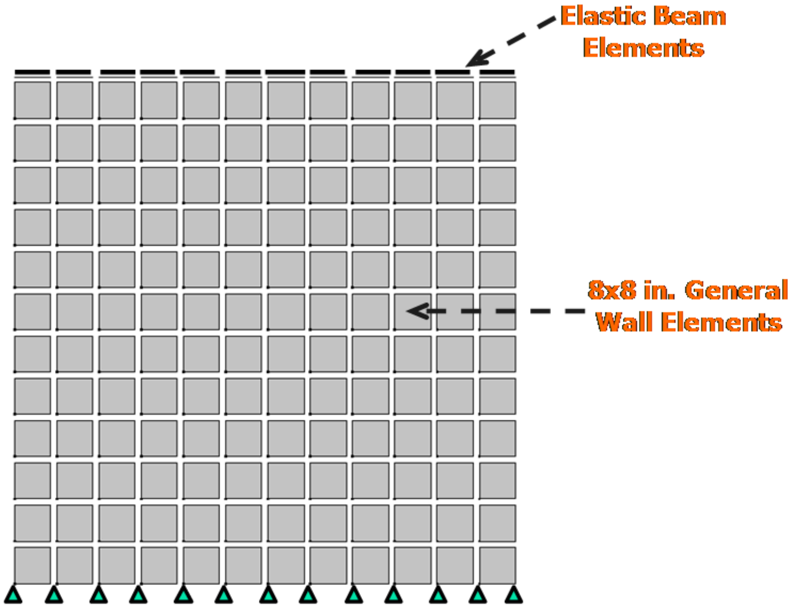

Figure 7.9 Typical detail of PERFORM 3D model and meshing for wall specimens

1. Define properties for the steel material and masonry material components;
2. Define the fiber cross-section components, using defined inelastic materials;
3. Define General Wall compound components, assigning one fiber section to the vertical axial/bending layer and the second fiber section to the horizontal axial/bending layer;
4. Assign conventional shear layer, based on the contribution of the masonry and horizontal reinforcement to the shear strength; and
5. Assign a General Wall compound component to each wall elements.

In wall cross-sections modeled using vertical fibers, masonry crushes fiber by fiber, and progresses discontinuously into the cross-section. Because masonry crushing is important in these analyses, it had to be modeled accurately. The depth of crushing was estimated for each wall segment, and a sufficient number of masonry fibers were placed in that depth as shown in Figure 7.10.

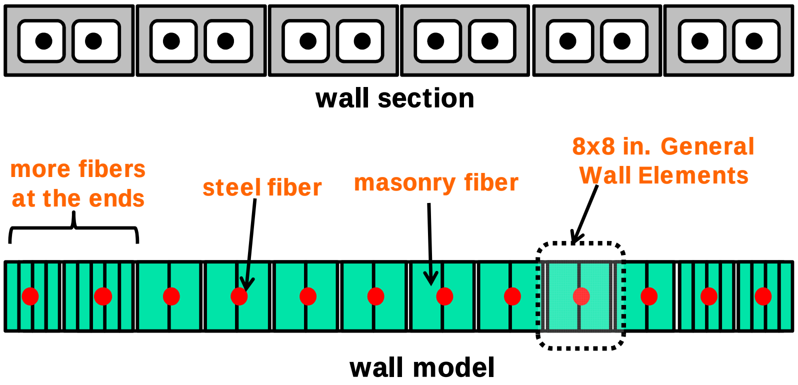

Figure 7.10 Detail of steel and masonry fibers at a typical wall section

7.5.2 Material Parameters Used to Model Wall Specimens

The vertical and horizontal reinforcing bars used in the wall specimens were modeled using the general uniaxial model of shown in Figure 7.11. An elastic modulus of 29000 ksi was used, and tensile yield and ultimate strength were based on the results of material tests. In this model, the buckling strength of steel reinforcing bars (f_{cr}) under compression was initially assumed to be 20% of their ultimate strength in tension, and was subsequently refined by trial and error.

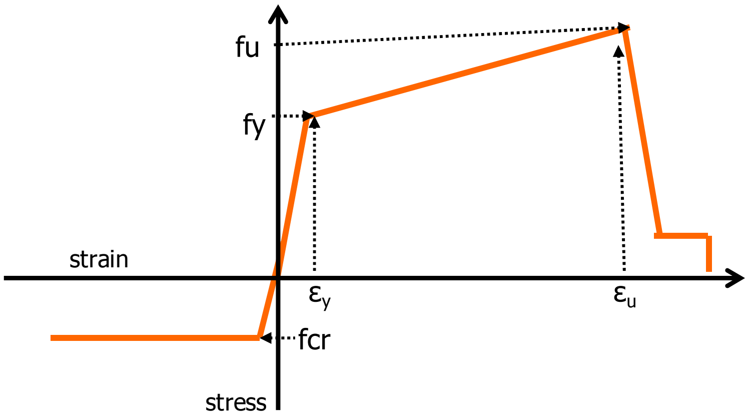

Figure 7.11 Typical steel reinforcement stress-strain relation used to model wall specimens

Masonry fibers were modeled using the uniaxial stress-strain behavior shown in Figure 7.12. Tensile strength and stiffness were neglected, and compressive behavior was based on the results of monotonic stress-strain tests of CMU prisms.

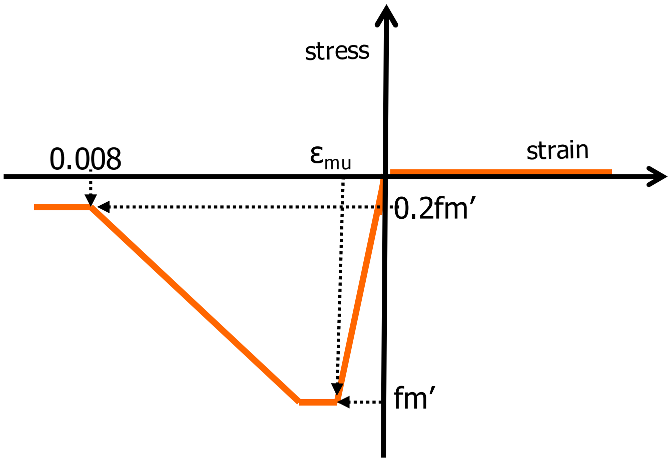

Figure 7.12 Typical masonry stress-strain relation used to model wall specimens

7.5.3 Cantilever Model Predictions and Comparison with Experimental Results

In this section, results from the nonlinear models of the cantilever wall specimens (push-over analysis and time-history analysis) are compared with experimental results from reversed cyclic loading under displacement control.

7.5.3.1 Comparison of Predicted Push-over Results with Measured Responses

Figure 7.13 through Figure 7.16 compare the predicted push-over responses (lateral load versus top displacement) with the measured responses for the cantilever wall specimens with an aspect ratio of 1.0. The predicted responses are quite close to the envelopes of the measured responses. However, stiffness and strength are overestimated at drift ratios below 0.50%. This is probably because the analytical predictions are for monotonic loading, whereas the tests results are for reversed cyclic loading, which would be expected to cause degradation of stiffness and strength.

The sudden reductions in lateral capacity in the analytically predicted responses are due to sequential crushing of masonry and buckling of steel reinforcement. As shown in the results, the model provides a good prediction of the lateral strength and stiffness of the wall specimen for most of the displacement history.

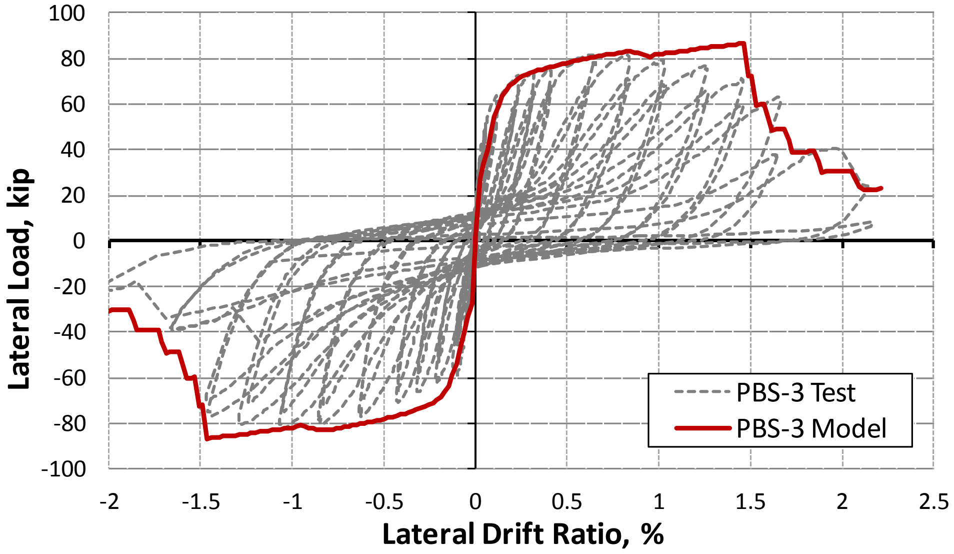

Figure 7.13 Measured versus predicted load-displacement responses for UT-PBS-03 (aspect ratio 1.0)

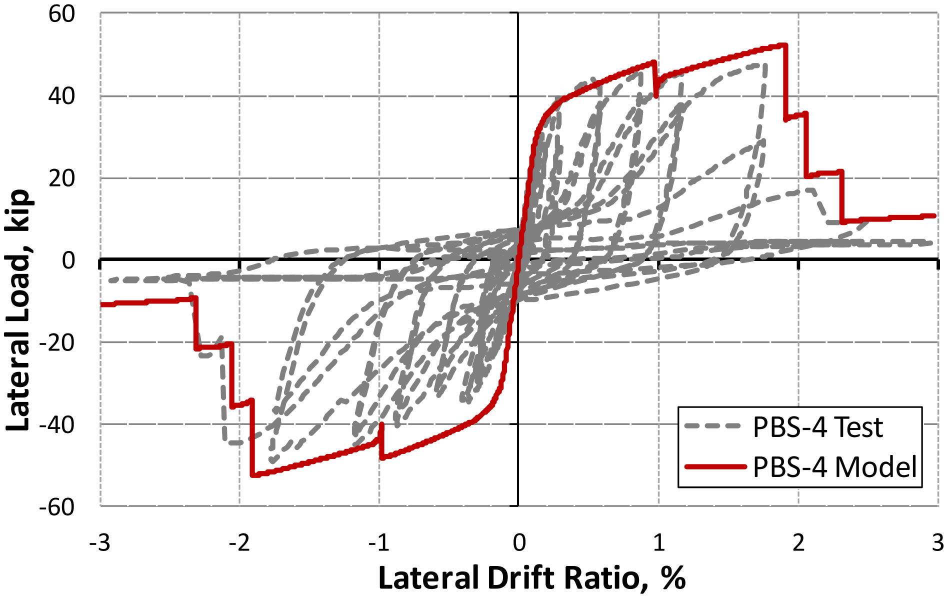

Figure 7.14 Measured versus predicted load-displacement responses for UT-PBS-04 (aspect ratio 1.0)

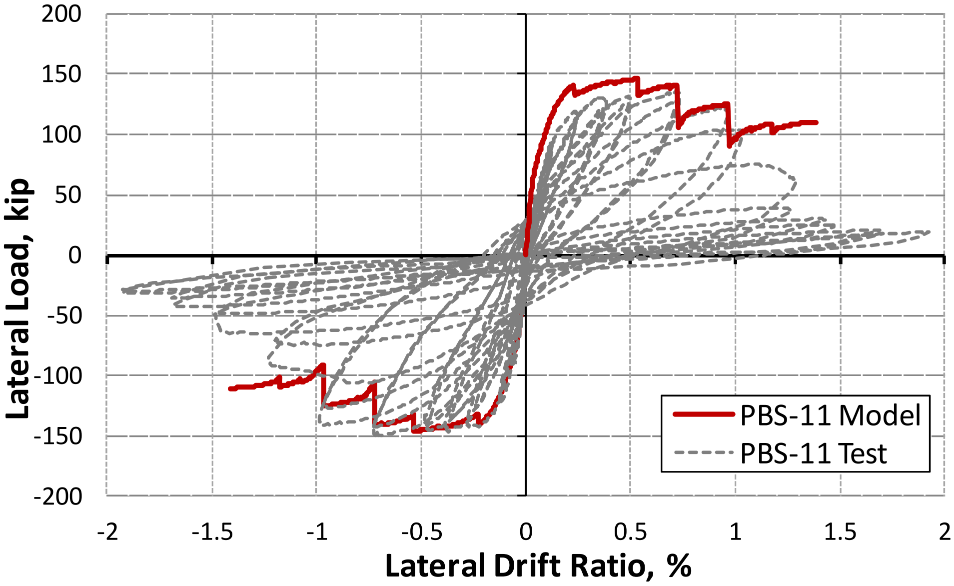

Figure 7.15 Measured versus predicted load-displacement responses for UT-PBS-11 (aspect ratio 1.0)

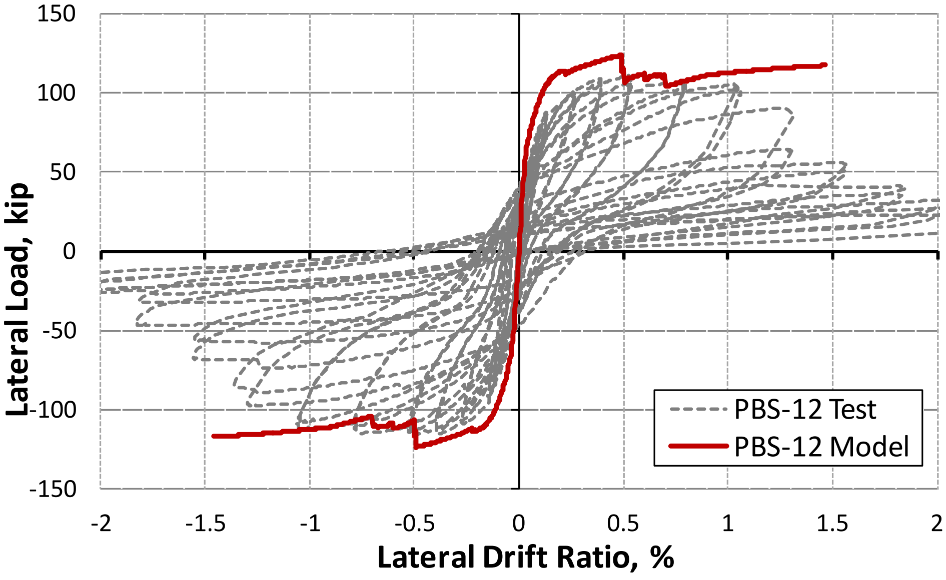

Figure 7.16 Measured versus predicted load-displacement responses for UT-PBS-12 (aspect ratio 1.0)

In Figure 7.17 through Figure 7.22 are shown the same comparisons for wall segments with aspect ratios of 2.0, 3.0, and 4.5. Again, the model accurately predicts the measured responses.

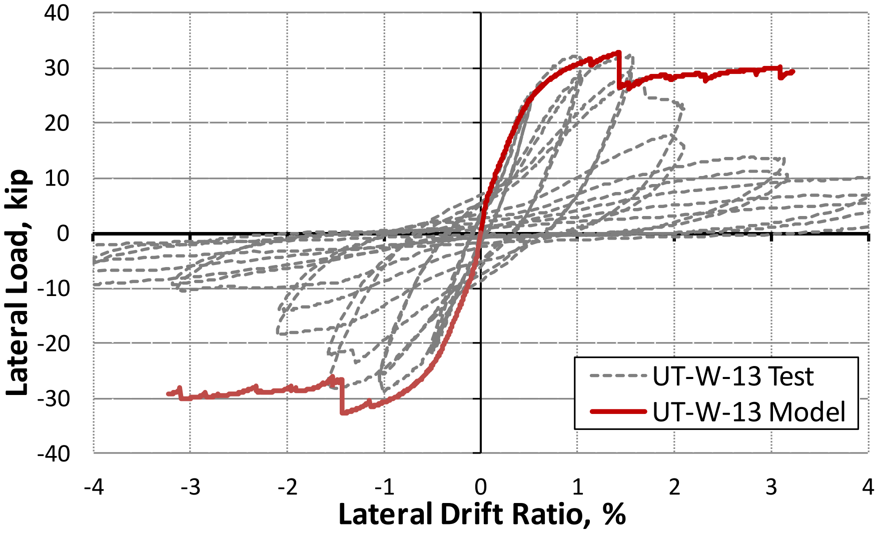

Figure 7.17 Measured versus predicted load-displacement responses for UT-W-13 (aspect ratio 3.0)

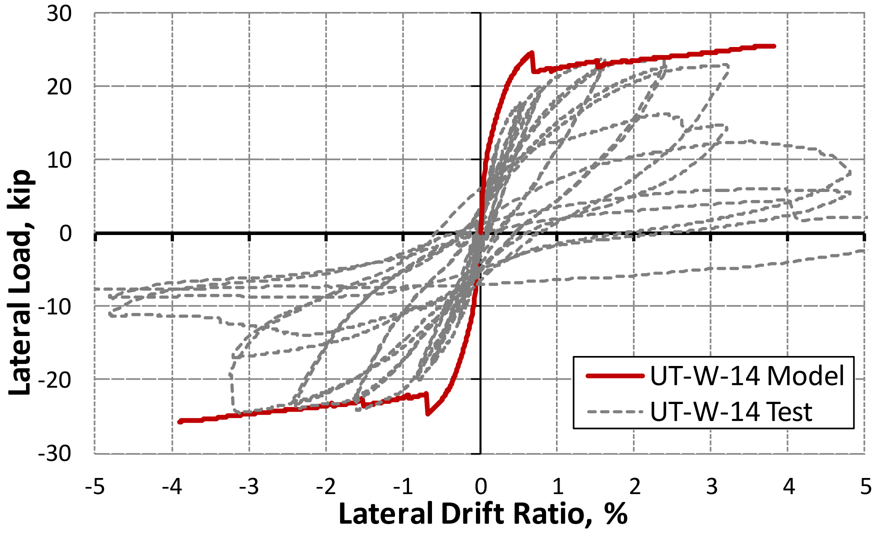

Figure 7.18 Measured versus predicted load-displacement responses for UT-W-14 (aspect ratio 3.0)

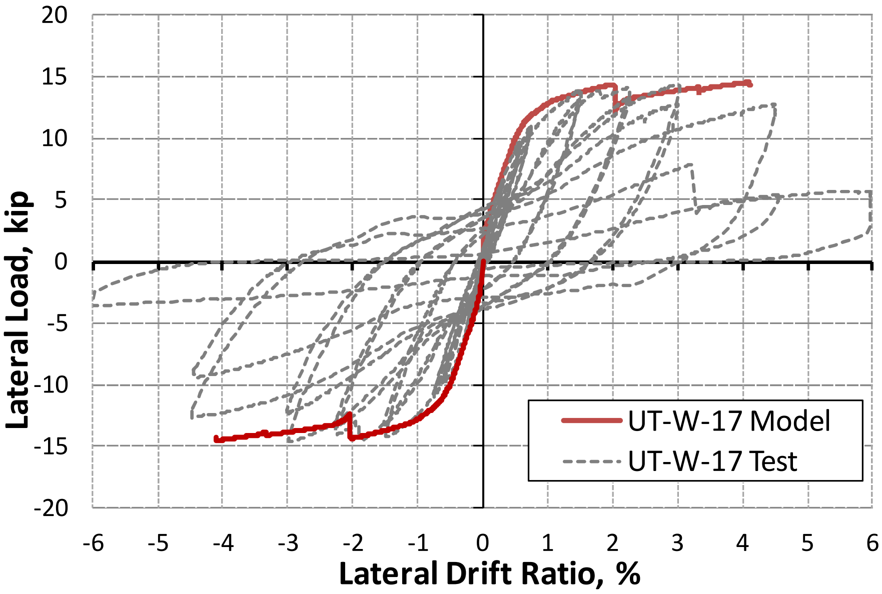

Figure 7.19 Measured versus predicted load-displacement responses for UT-W-17 (aspect ratio 4.5)

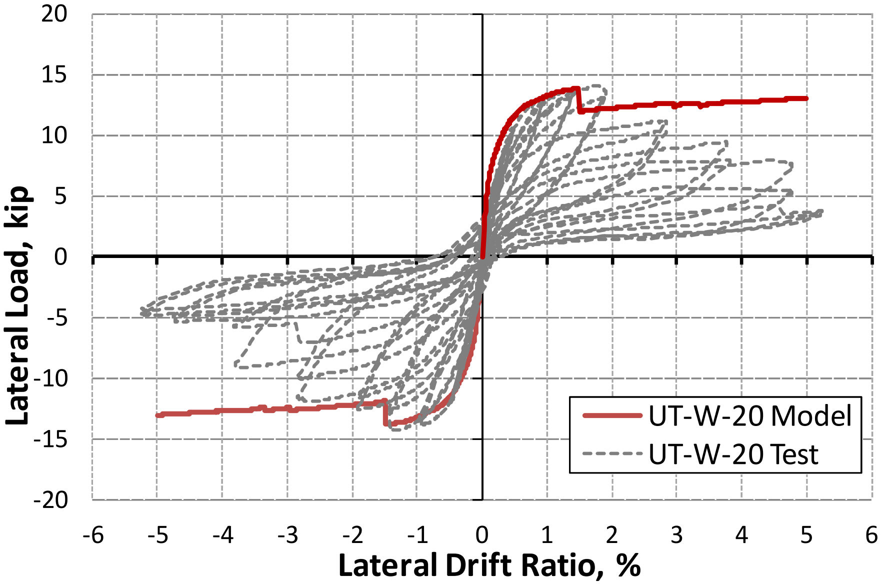

Figure 7.20 Measured versus predicted load-displacement responses for UT-W-20 (aspect ratio 4.5)

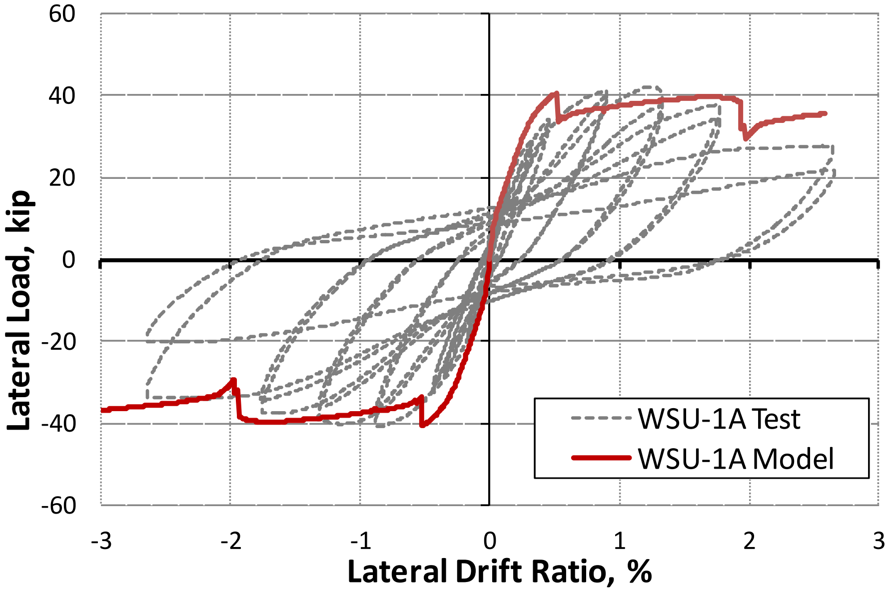

Figure 7.21 Measured versus predicted load-displacement responses for WSU-1A (aspect ratio 2.0)

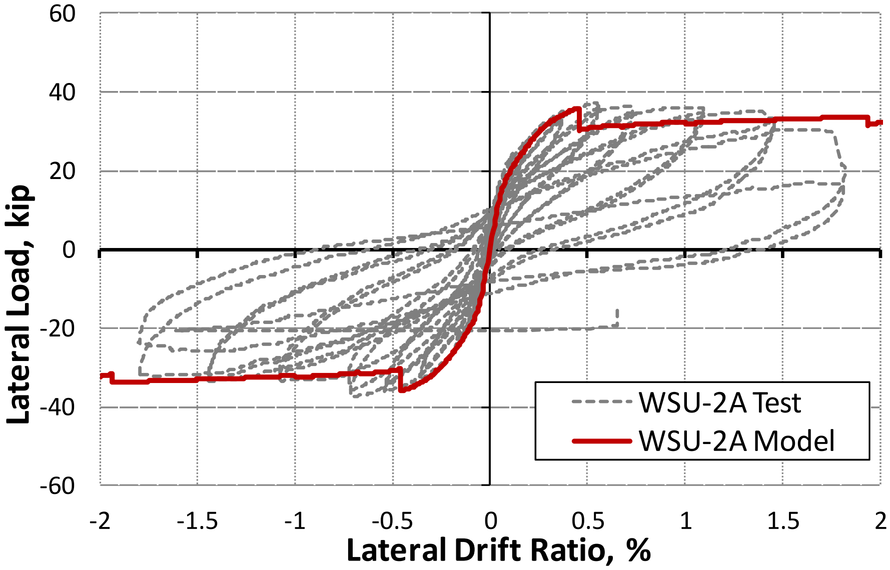

Figure 7.22 Measured versus predicted load-displacement responses for WSU-2A (aspect ratio 2.0)

7.5.3.2 Comparison of Predicted Cyclic Responses with Measured Responses

For further verification, analytical predictions of response under reversed cyclic displacements are compared with test results from cantilever walls under reversed cyclic load. Each analytical model was subjected to the same displacement history as the corresponding test specimen. Gravity load was first applied, followed by a series of static push-over analyses. Each push over-analysis represented a half-cycle of the prescribed lateral displacement history. Each push-over analysis was begun using the material degradation parameters corresponding to the end of the previous push-over analysis, so that the sequence of push-over analyses could attempt to reflect the increasing degradation of the test specimen. Graphs for the analytically predicted responses were obtained by transferring the results of each push-over analysis to a single spreadsheet, and plotting them sequentially.

In Figure 7.23 through Figure 7.26, predicted and measured response histories are compared for Specimen UT-PBS-03 (aspect ratio 1.0), Specimen WSU-1A (aspect ratio 2.0), Specimen UT-W-13 (aspect ratio 3.0), and Specimen UT-W-17 (aspect ratio 4.5). The analytical model captures the measured response quite well, including capacities, stiffnesses, stiffness degradation, hysteretic shape, residual displacements, and pinching.

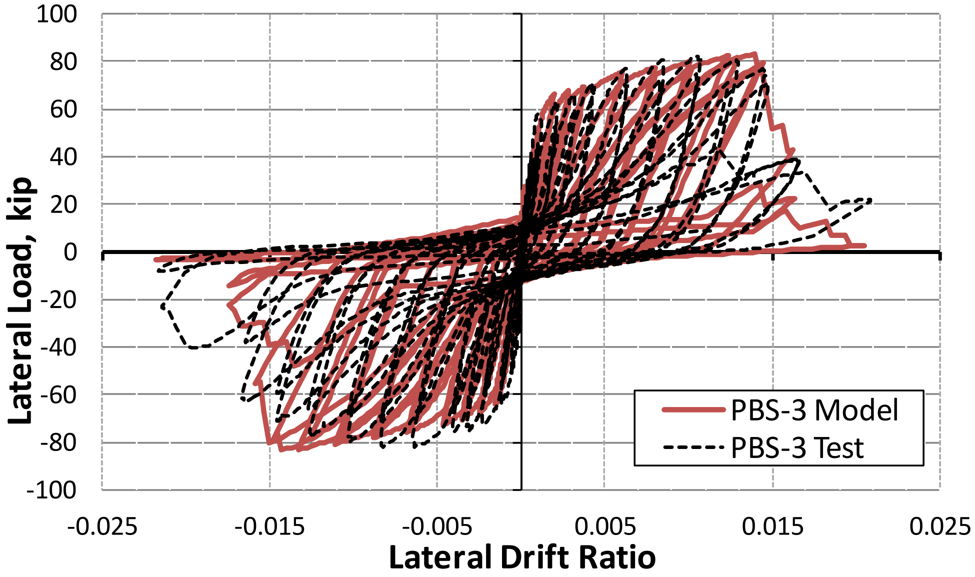

Figure 7.23 Predicted versus measured load-drift responses for UT-PBS-03 (aspect ratio 1.0)

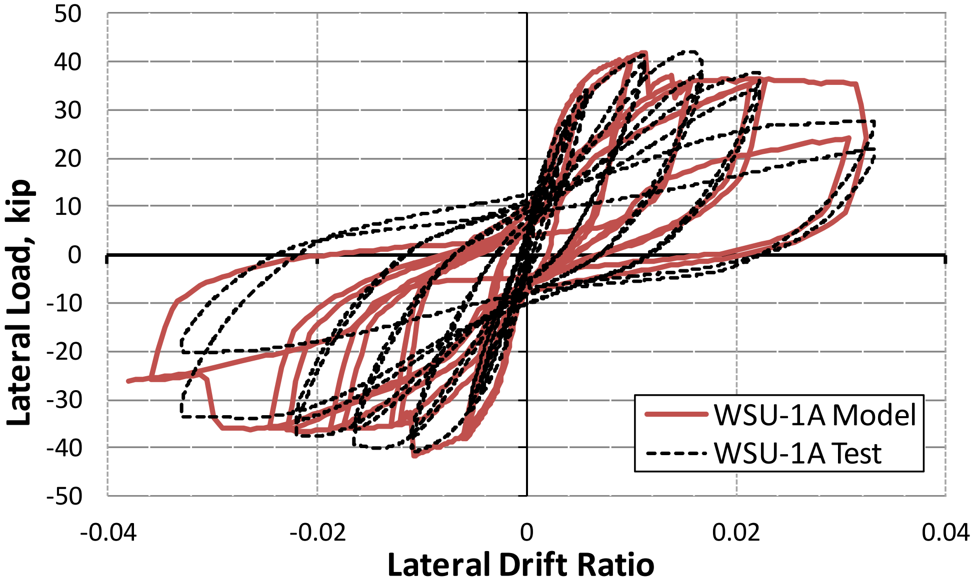

Figure 7.24 Predicted versus measured load-drift responses for WSU-1A (aspect ratio 2.0)

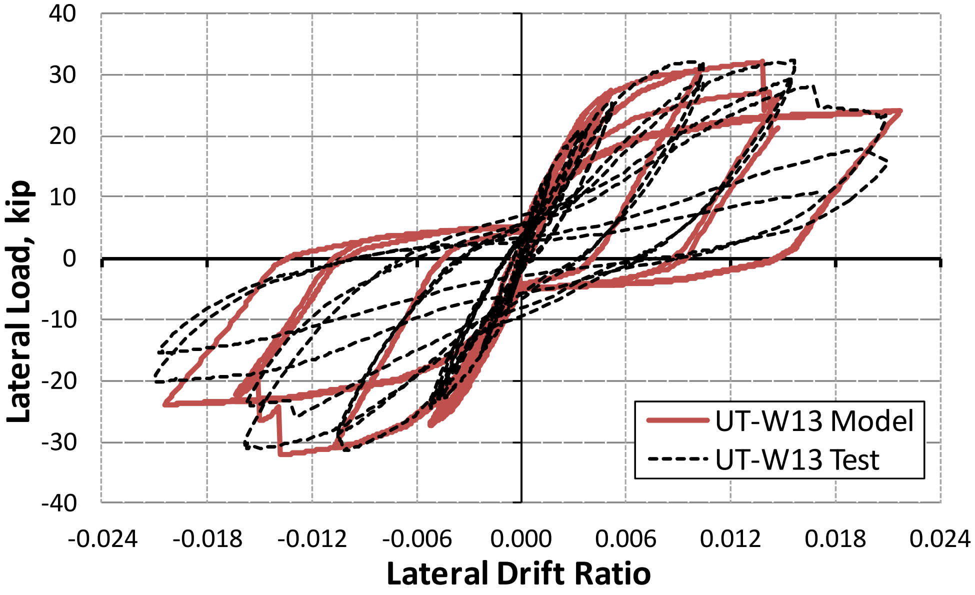

Figure 7.25 Predicted versus measured load-drift responses, for UT-W-13 (aspect ratio 3.0)

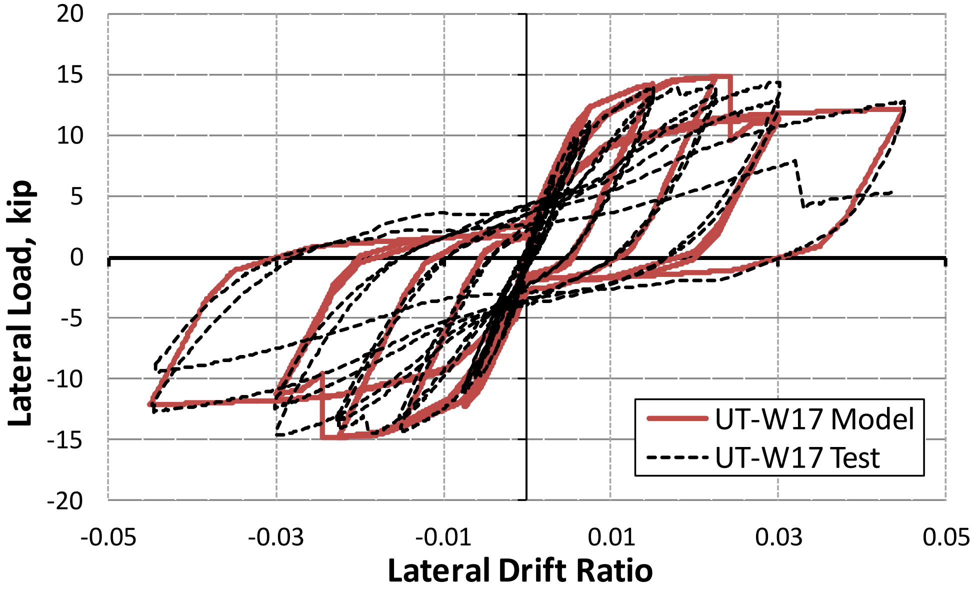

Figure 7.26 Predicted versus measured load-drift responses, for UT-W-17 with (aspect ratio 4.5)

7.5.4 Summary of Comparisons between Predicted and Measured Responses of Wall Specimens

The objective of this section was to investigate the effectiveness of PERFORM 3D's General Wall Element for predicting the inelastic response of reinforced masonry structural wall elements by comparing the predicted and measured responses of representative cantilever wall specimens tested at UT Austin and at Washington State University. For cantilever wall specimens with aspect ratios greater than or equal to 1.0, the analytical models provide very accurate predictions of stiffness, strength, and hysteretic behavior.

7.6 COMPARISON OF ANALYTICAL PREDICTIONS WITH EXPERIMENTAL RESULTS FOR THREE-STORY SPECIMEN TESTED AT UCSD

In this section, the response as predicted by the verified PERFORM 3D General Wall Element model is compared with that observed from shake-table testing of the 3-story specimen tested at UCSD in early 2011. Using PERFORM 3D, a three-dimensional model of the specimen is created, and is used for non-linear static analysis and nonlinear time-history analyses under the same series of input motions used in the test.

7.6.1 Nonlinear Modeling of 3-Story Specimen using PERFORM 3D

As shown in Figure 7.27, a non-linear model of the 3-story specimen was developed using PERFORM 3D (CSI 2007). The in-plane wall segments (vertical and horizontal) are modeled with the General Wall Element, permitting in-plane inelastic response anywhere within the perforated multi-story wall. As shown in Figure 7.27, the out-of-plane wall segments are modeled using PERFORM 3D column elements with biaxial (P-M-M) plastic hinges at each end. The hinges are rigid-plastic, and use yield surfaces calculated based on the nominal capacities given by the 2011 MSJC *Code* provisions for axial and bending interaction for out-of-plane behavior. An effective flexural stiffness of 0.50 EI_o is used for the out-of-plane wall segments (ASCE 41 2007).

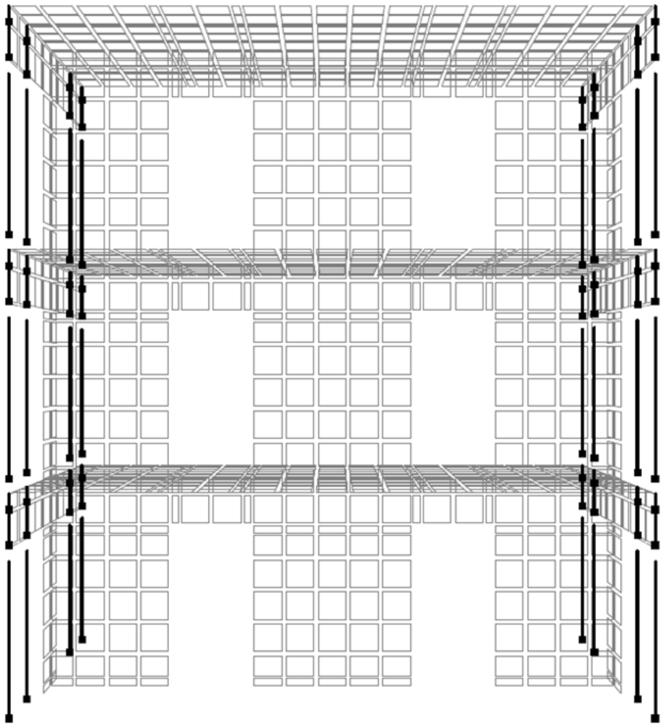

Figure 7.27 Three-dimensional view of PERFORM 3D model of 3-story specimen

The floor slabs are modeled using 4-node, elastic slab/shell elements with membrane (in-plane) and plate bending (out-of-plane) stiffnesses. The slab thickness is uniform over each element, but can be different for membrane and bending effects. Effective stiffness values including the effects of flexural cracking are used for the elastic components of the wall and slab elements. For the wall in flexure, the fiber element properties determine the effective initial stiffness. An effective flexural stiffness of 0.50 EI_o is used for floor slabs (ASCE 41 2007).

The model shown in Figure 7.27, and in more detail (for a typical story) in Figure 7.28, was developed considering the following points:

1) Because the General Wall Element is rectangular only (no triangles), and because displacement compatibility is enforced at corner nodes only, the element mesh must have continuous vertical and horizontal element boundaries.

2) In the interior of each vertically or horizontally oriented wall segment, roughly square elements are used, resulting in a 16- x 16-in. element mesh for most of Walls W-1, W-2, and W-3. To better model the regions at the tops and bottoms of vertically oriented wall segments, where flexural plastic hinges are expected to form, 4-in. deep elements are used there. A similarly refined mesh is used at the ends of horizontally oriented segments (lintels).

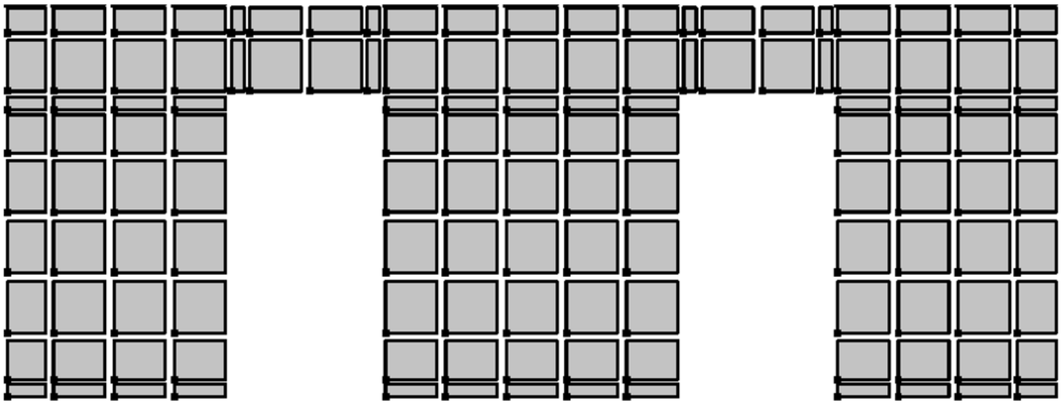

Figure 7.28 Detail of PERFORM 3D mesh at a single floor, longitudinal wall of three-story specimen

In this model, inelastic material models are incorporated into each layer of each element. For most layers, this is routine, and is described below.

a) For each element, combinations of flexural and axial behavior in the vertical and horizontal directions were modeled using one vertical flexural-axial layer and one horizontal flexural-axial layer. Each layer was further subdivided into fibers.

Reinforcing bars were modeled as individual fibers. In these layers, the stress-strain behavior of masonry was based on uniaxial test data, with a low tensile strength and nonlinear compressive strength, including a descending branch. Data were obtained from tests of reinforcement and prisms at the University of California at San Diego.

b) For each element, shearing behavior dominated by diagonal tension was modeled by one elasto-plastic masonry shear layer whose stiffness was calculated using a shearing modulus equal to $0.4E_m$, and whose strength was set equal to V_n from the 2011 MSJC *Code,* including the effects of axial load. For analyses at the DBE level, for which little hysteretic shear degradation is expected, V_n is taken equal to V_{nm} plus V_{ns} , because the masonry would not have experienced degradation. V_{nm} is computed using axial loads from gravity loads only. The justification for this is that seismic overturning increases axial loads on one side of the specimen while decreasing them on the other side, so that the net effect of seismic overturning on base shear capacity is essentially zero.

c) In PERFORM 3D, shearing behavior is modeled using a shear layer only, rather than the diagonal-compression layers, for the reasons discussed in Section 7.4.2.

7.6.2 Material Parameters for Nonlinear Modeling of 3-story Specimen

The material stress-strain relations used to model the reinforcement in the 3-story specimen, shown in Figure 7.29, are based on monotonic stress-strain tests of concrete masonry prisms at the University of California at San Diego. The elastic modulus was taken as 29,000 ksi; tensile yield, 62 ksi; and ultimate, 100 ksi. To account for low-cycle fatigue, the fracture strain (ε_u) for the longitudinal and transverse reinforcement was taken as 0.06. This limit was used based on the analytical and experimental work of

Waugh and Sritharan (2010) on a 7-story, reinforced-concrete-shear wall structure tested on the same shake table.

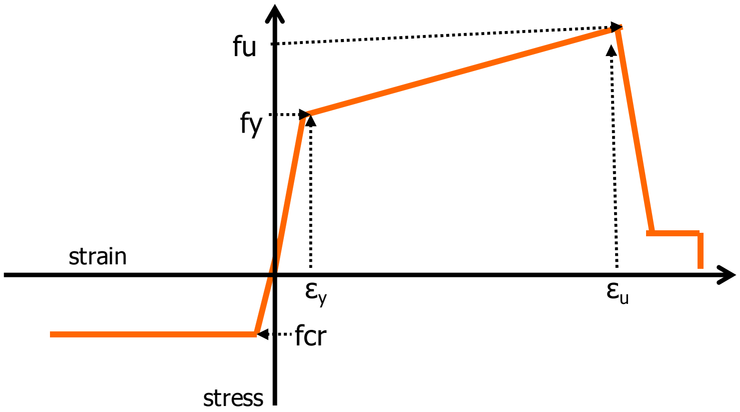

Figure 7.29 Stress-strain relations (tension and compression) used to model reinforcement in 3-story specimen

The envelope curve used to model the masonry in compression, shown in Figure 7.30, is based on monotonic stress-strain tests of concrete masonry prisms. It was used for the masonry fibers of the axial/bending layers of each element.

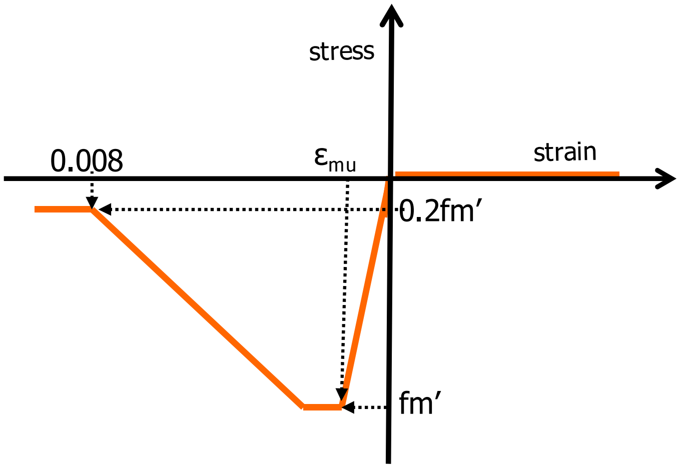

Figure 7.30 Stress-strain relations used to model masonry in 3-story specimen

For time-history dynamic analyses, hysteretic degradation and energy dissipation are important and must be accounted for directly. In PERFORM 3D, this is done by specifying hysteretic degradation factors for inelastic components. These factors include the reduction in swept area between the original hysteretic loop and the degraded loop, and also include changes in the form of the loops, including pinching (CSI 2007). In Figure 7.31a and Figure 7.31b, respectively, are shown the hysteretic response characteristics of the steel and masonry material models, along with their corresponding hysteretic degradation factors.

7.6.3 Model Restraints for 3-story Specimen

The 3-story specimen was fixed to the shake-table, and the analytical model included fixed supports at that level.

7.6.4 Damping Model for 3-story Specimen

In nonlinear dynamic analysis, equivalent viscous damping is customarily used to account for elastic energy dissipation. If the structural analysis is conducted using the natural modes of vibration, it is possible to assume modal damping. In this case, however, modal analysis is not used, and the common assumption of Rayleigh damping is invoked. The structural damping matrix, $\underline{C}$, is assumed to be given by a linear combination of the structures mass and stiffness matrices (CSI 2007):

$$\underline{C} = \alpha \underline{M} + \beta \underline{K}$$

where $\underline{M}$ is the structure mass matrix, $\underline{K}$ is the initial elastic stiffness matrix, and α and β are multiplying factors. When this approach is implemented in PERFORM 3D (CSI 2007), equivalent viscous damping ratios are specified at two period ratios, T_A / T_1 and

T_B / T_1, and the corresponding values of α and β are calculated automatically. In this case, an equivalent viscous damping ratio of 5% was assumed to apply at the initial fundamental period of the structure T_1, and at $0.2T_1$ (CSI 2007).

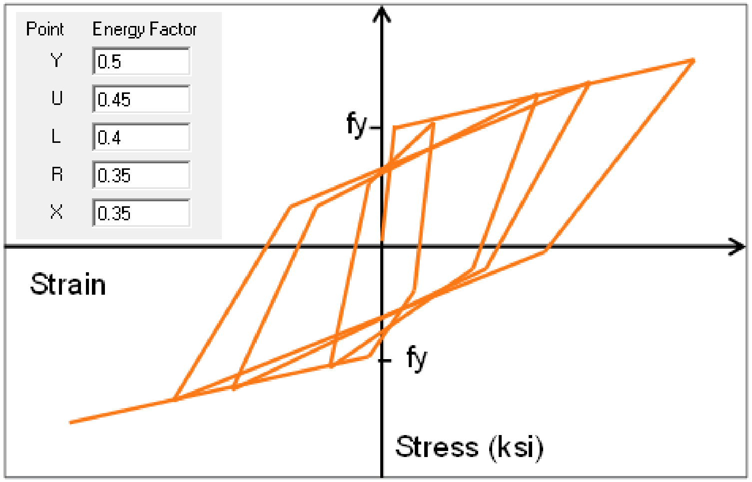

Point	Energy Factor
Y	0.5
U	0.45
L	0.4
R	0.35
X	0.35

a) Degradation factors used in modeling reinforcement of 3-story specimen

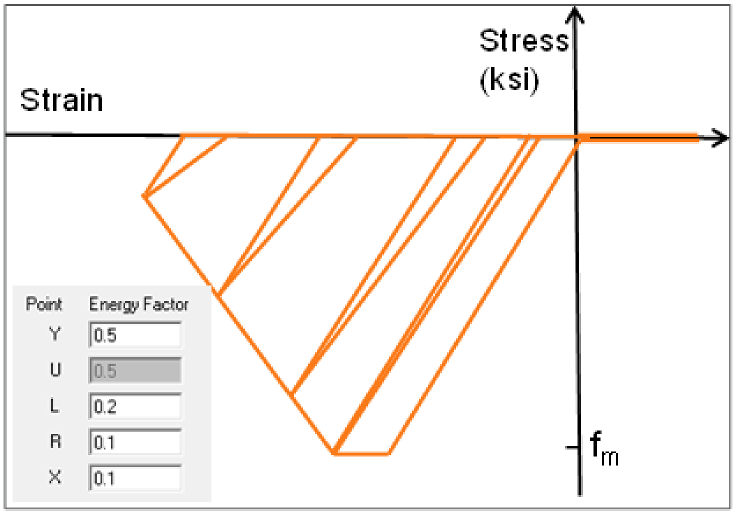

Point	Energy Factor
Y	0.5
U	0.5
L	0.2
R	0.1
X	0.1

b) Degradation factors used in modeling masonry of 3-story specimen

Figure 7.31 Degradation factors used in PERFORM 3D model of 3-story specimen

7.6.5 Pushover Analysis of Three-Story UCSD Model

Monotonic pushover analyses were performed on the analytical model of the 3-story UCSD specimen to determine the envelope of base shear versus lateral drift ratio at the center of the first floor. The first step in the pushover analyses is the selection of a lateral load vector. ASCE 41 (2007) recommends either uniform distribution or a triangular distribution over the building height. A uniform distribution usually corresponds to a uniform acceleration over the building height, so that the load at any floor level is proportional to the mass at that level. Similarly, a triangular distribution usually corresponds to a linearly increasing acceleration over the building height. In the inelastic range of response, low-rise wall structures usually have an approximately uniform distribution of acceleration over the building height, and therefore a uniform distribution was used for the 3-story specimen. The loading was applied until first floor in the building reached an inter-story drift of 0.8 in. (maximum observed drift at the first floor). Figure 7.32 and Figure 7.33 present the deformed shape and the load-deflection curves, respectively, for the 3-story specimen. Because the specimen is symmetrical, the analytical pushover response is identical in each direction. The observed shake-table response is not symmetrical, because response in each direction is affected by response in the other direction.

7.6.6 Comparison of Pushover Analysis with Experimental Results, 3-story Specimen

In Figure 7.33, the predicted response envelope of base shear versus first-floor lateral drift is compared with the response predicted by PERFORM 3D for the 3-story specimen tested at UCSD. The analytical model captures the measured responses reasonably well. However, as observed in Figure 7.33, the lateral load capacity and the lateral stiffness of specimens are underestimated in the -X direction (to the left in the figure), particularly at larger drifts. This underestimation can be attributed to the fact that analysis results for monotonic loading are compared to cyclic test results. To investigate the effects of hysteretic degradation of masonry, the above analysis must be extended to time-history nonlinear analyses.

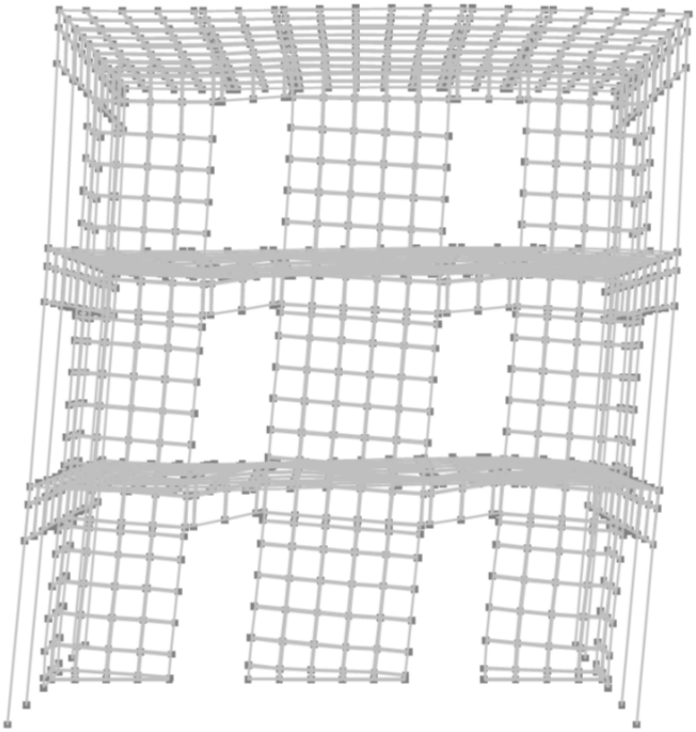

Figure 7.32 Deflected shape from pushover analyses for 3-story specimen at 0.8-in. inter-story drift in first story

7.6.7 Nonlinear Time-history Analysis of 3-story Specimen

In this section, four ground motion records of the shake-table test are used to as input for nonlinear time-history analyses. The sequence of input motions and scaling factors is shown in Table 7-2, and the ground motions before scaling are shown in Figure 7.34.

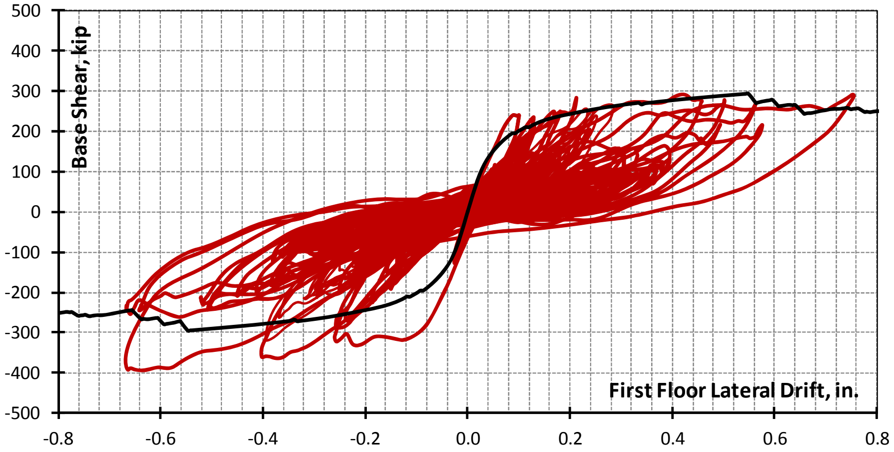

Figure 7.33 Load-displacement results from pushover analysis of 3-story specimen, first-floor drift

Table 7-2 Sequence of input motions used for time-history analyses of 3-story specimen

order	ground motion	scaling factor
1	El Centro 1979	+0.20
2	El Centro 1979	+0.45
3	El Centro 1979	+0.90
4	El Centro 1979	+1.20
5	El Centro 1979	+1.50
6	El Centro 1979	+1.80
7	El Centro 1979	-2.50
8	El Centro 1940	+3.0
9	Sylmar 1994	+1.25
10	Sylmar 1994	+1.60
11	Chi Chi 1999	+1.0
12	Chi Chi 1999	+1.50

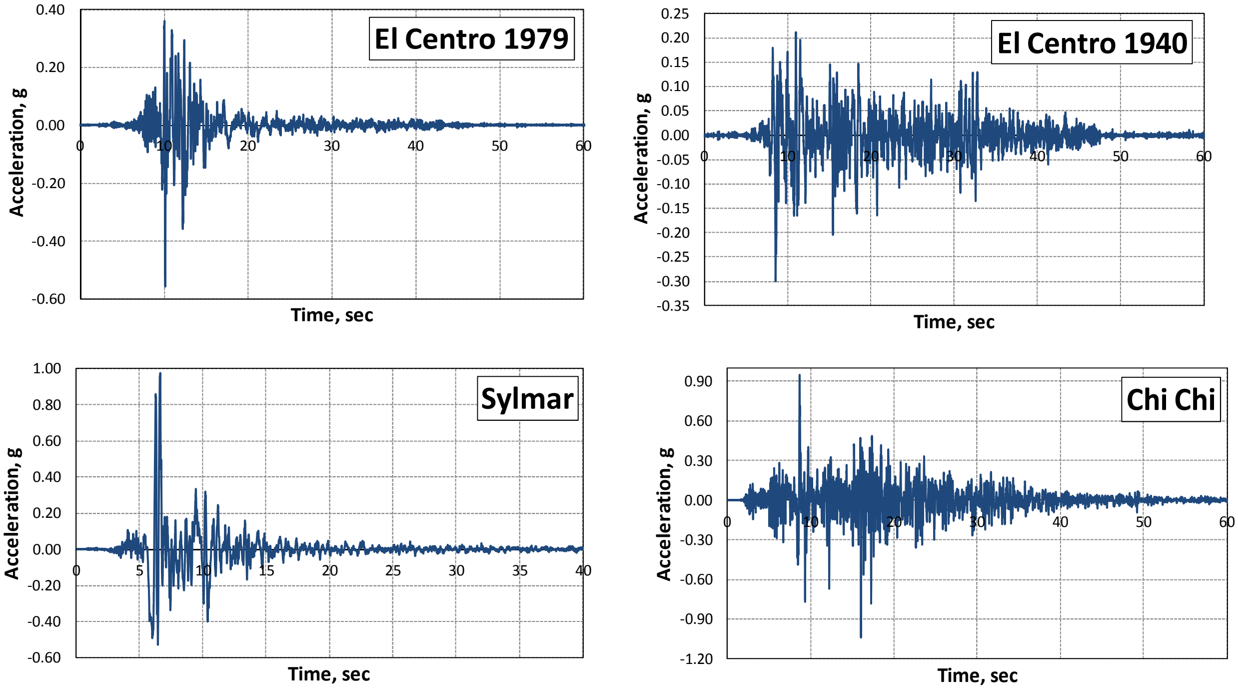

Figure 7.34 Ground-motion records used for time-history analyses of 3-story specimen, before scaling

The input accelerations shown in Figure 7.34 were applied to the base of the building model in the direction of shaking. The analysis was conducted at an initial time step of 1/60 sec to limit the amount of output that would have to be post-processed. If the analysis failed to converge, 100 sub-steps were carried out at time steps of 1/6000 sec to find a solution, after which the time step was increased back to 1/60 sec. To account for the effects of accumulated structural degradation on the response of the test building, the selected ground motion records were applied as a sequence of 13 separate input motions, with 2 sec of zero ground acceleration between each to allow the structure to come to rest prior to the next input motion. The low accelerations at the end of each ground motion, combined with the 2 sec of zero acceleration, were adequate for the structure to return to rest after each record. Modeling of this structure took about 18 hours, and the entire sequence of response (13 input motions) took approximately 48 hours on a 3.0 GHz PC running Windows XP.

Before applying this sequence of input motions to the analytical model, the fundamental frequency of the model and the test specimen was 11.0 Hz. After testing, the fundamental frequency of the model and the test specimen was 4.0 Hz. Because the fundamental frequency of the specimen was well predicted, the analytical model was able to track the response of the specimen with good accuracy, even as damage accumulated.

7.6.8 Comparison of Time-History Analyses with Experimental Results, 3-story Specimen

In this section, time-history analyses are compared with experimental results for the 3-story specimen in terms of three key response parameters: first-floor displacement versus time; base shear versus time; and load-displacement hysteresis loops. In the interest of space, those comparisons are discussed here for only four of the 13 input motions:

- 120% El Centro 1979;
- 180% El Centro 1979;
- 250% El Centro 1979; and
- 160% Sylmar 1994.

7.6.8.1 Response to 120% El Centro 1979

In the input sequence of Table 7-2, an input motion of 120% El Centro 1979 corresponds to the Design Basis Earthquake (DBE) based on recorded table accelerations.

7.6.8.1.1 First-Floor Displacements versus Time (120% El Centro 1979)

Under 120% El Centro 1979, the first-floor displacement time-history is shown in Figure 7.35. Elastic response of the specimen was well captured. Peak displacements were predicted within 10%. In general, agreement between predictions and experiment is quite good.

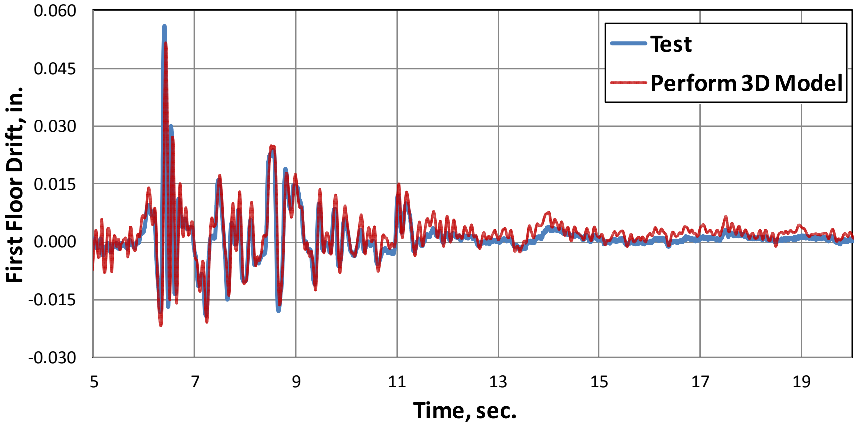

Figure 7.35 First-floor displacement time-history for 3-story specimen (120% El Centro 1979)

7.6.8.1.2 Base Shears versus Time (120% El Centro 1979)

Predicted base shear was determined by summing the calculated shears at the base of the wall segments, and is shown in Figure 7.36. As with displacements, elastic response was well captured. Peak values are within 5% of the measured values. In general, agreement between prediction and analysis is quite good for a complex structure with significant degradation.

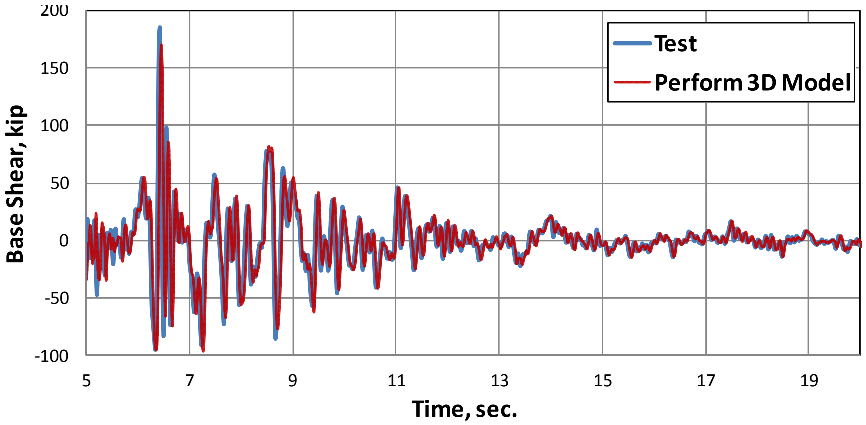

Figure 7.36 Base shear time-history for 3-story specimen (120% El Centro 1979)

7.6.8.1.3 Load-displacement Hysteresis Loops (120% El Centro 1979)

Hysteresis loops of base shear versus first-floor displacement at 120% El Centro are shown in Figure 7.37. Because the histories of first-floor displacements and base shears were accurately predicted, it is not surprising that the hysteresis loops also compare well. However, the analytical model shows less degradation and nonlinearity than the experimental response.

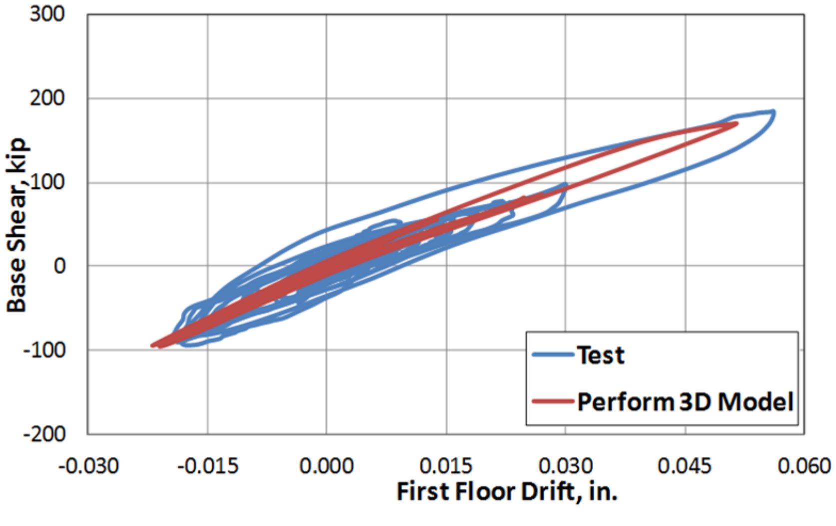

Figure 7.37 Load-displacement hysteresis loops for 3-story specimen (120% El Centro 1979)

7.6.8.2 Response to 180% El Centro 1979

In the input sequence of Table 7-2, the input motion of 180% El Centro corresponds to the Maximum Considered Earthquake (MCE).

7.6.8.2.1 First-Floor Displacement versus Time (180% El Centro 1979)

Under 180% El Centro 1979, the first-floor displacement time-history is shown in Figure 7.38. The response of the specimen was well captured. Peak displacements were predicted within 15%. In general, agreement between predictions and experiment is quite good.

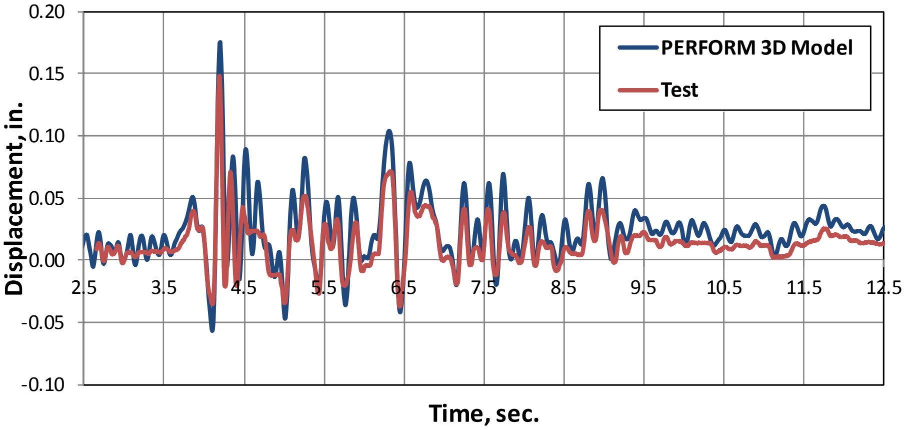

Figure 7.38 First-floor displacement time-history for 3-story specimen (1.80 El Centro 1979)

7.6.8.2.2 Base Shear versus Time (180% El Centro 1979)

Predicted base shear was determined by summing the calculated shears at the base of the wall segments, and is shown in Figure 7.39. As with displacements, the response was well captured, even as the structure degraded. Peak values are within 10% to 15% of the measured values. In general, agreement between prediction and analysis is quite good for a complex structure with significant degradation.

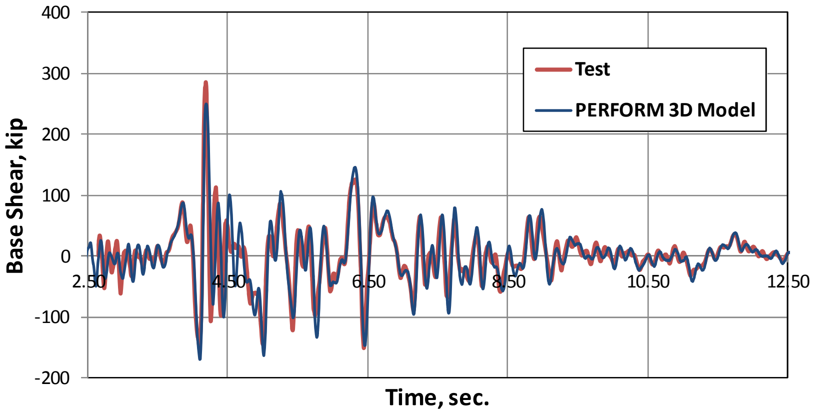

Figure 7.39 Time history of base shear, 3-story model (180% El Centro 1979)

7.6.8.2.3 Load-displacement Hysteresis Loops (180% El Centro 1979)

Hysteresis loops of base shear versus first-floor displacement are shown in Figure 7.40. Because the histories of first-floor displacements and base shears were accurately predicted, it is not surprising that the hysteresis loops also compare well.

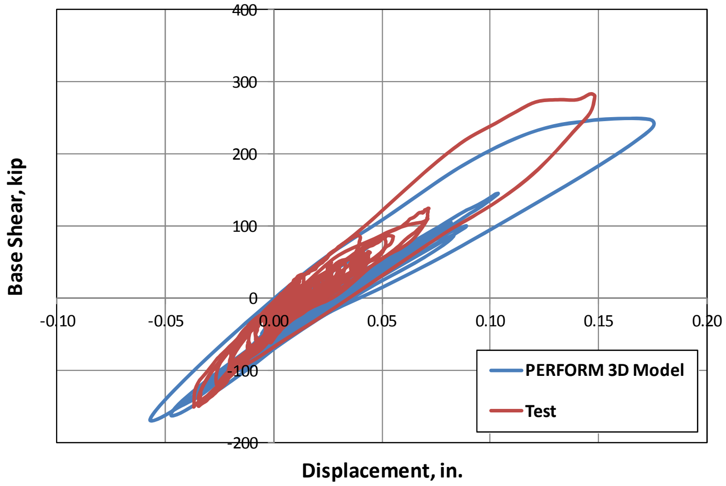

Figure 7.40 Load-displacement hysteresis loops, 3-story specimen (180% El Centro 1979)

7.6.8.3 Response to 250% El Centro 1979

In the input sequence of Table 7-2, the input motion of 250% El Centro corresponds to the Maximum Considered Earthquake (MCE).

7.6.8.3.1 First-Floor Displacement versus Time (250% El Centro 1979)

Under 250% El Centro 1979, the first-floor displacement time-history is shown in Figure 7.41. The response of the specimen was well captured. Peak displacements were predicted within 15%. In general, agreement between predictions and experiment is quite good.

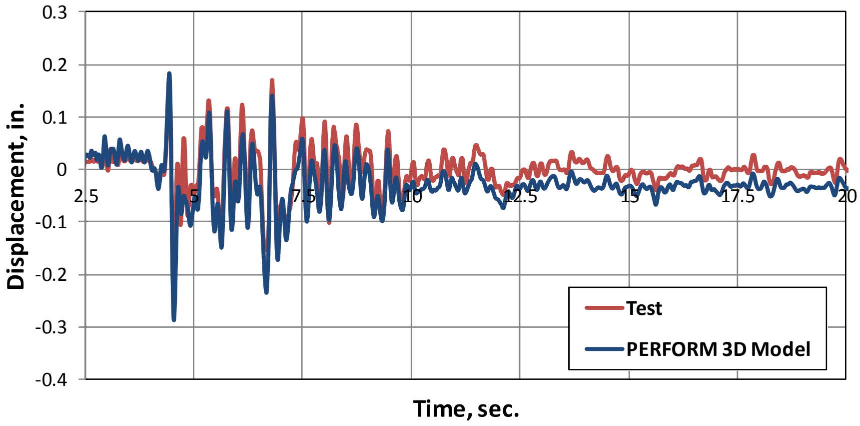

Figure 7.41 Time history of first-floor displacement, 3-story specimen (250% El Centro 1979)

7.6.8.3.2 Base Shear versus Time (250% El Centro 1979)

Predicted base shear was determined by summing the calculated shears at the base of the wall segments, and is shown in Figure 7.42. As with displacements, the response was well captured, even as the structure degraded. Peak values are within 10–15% of the measured values. In general, agreement between prediction and analysis is quite good for a complex structure with significant degradation.

7.6.8.3.3 Load-displacement Hysteresis Loops (250% El Centro 1979)

Hysteresis loops of base shear versus first-floor displacement are shown in Figure 7.43. Because the histories of first-floor displacements and base shears were accurately predicted, it is not surprising that the hysteresis loops also compare well.

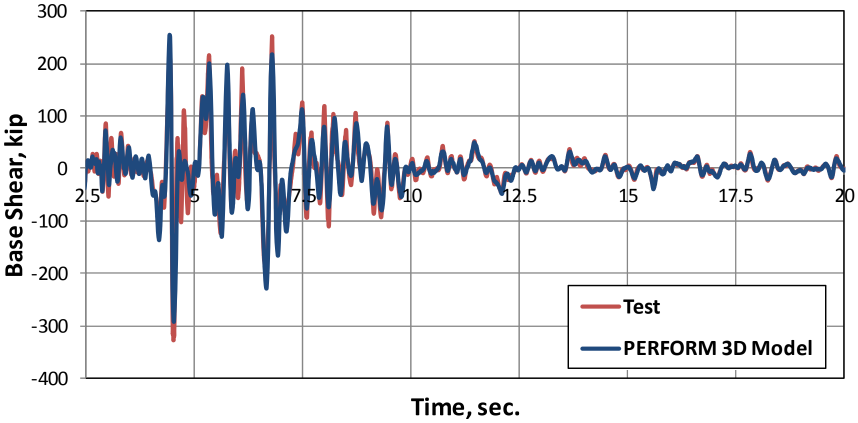

Figure 7.42 Time history of base shear (250% El Centro 1979)

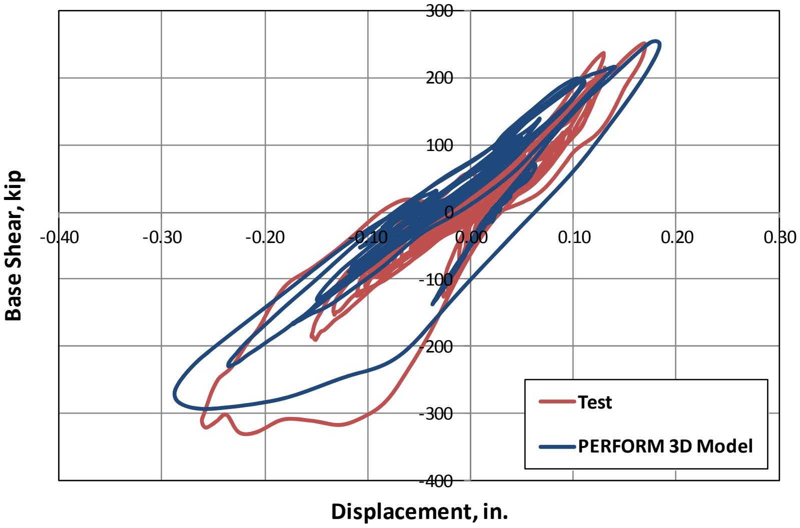

Figure 7.43 Load-displacement hysteresis loops, 3-story specimen (250% El Centro 1979)

7.6.8.4 Response to 160% Sylmar 1994

In the input sequence of Table 7-2, the input motion of 160% Sylmar 1994 corresponds to about 1.5 times the Maximum Considered Earthquake (MCE).

7.6.8.4.1 First-Floor Displacements versus Time (160% Sylmar 1994)

Under 160% Sylmar 1994, the first-floor displacement time-history is shown in Figure 7.44. The response of the specimen was well captured. Peak displacements were predicted within 10-15%. In general, agreement between predictions and experiment is quite good.

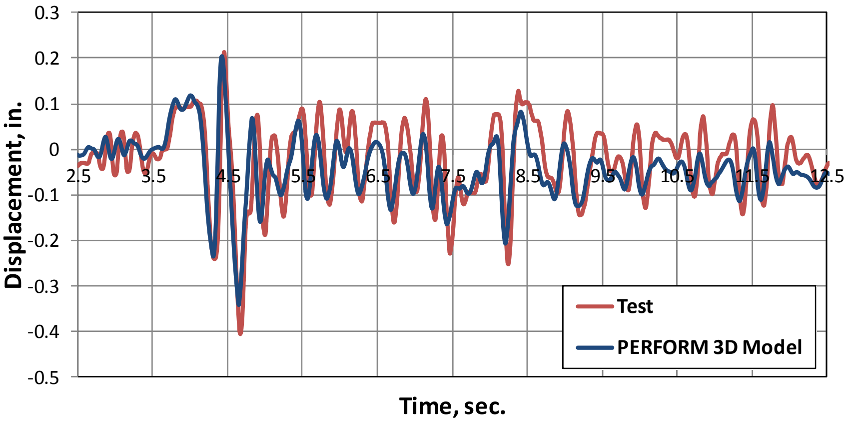

Figure 7.44 Time history of first-floor displacement, 3-story specimen (160% Sylmar 1994)

7.6.8.4.2 Base Shears versus Time (160% Sylmar 1994)

Predicted base shear was determined by summing the calculated shears at the base of the wall segments, and is shown in Figure 7.45. As with displacements, the response was well captured, even as the structure degraded. Peak values are within 15% of the measured values. In general, agreement between prediction and analysis is quite good for a complex structure with significant degradation.

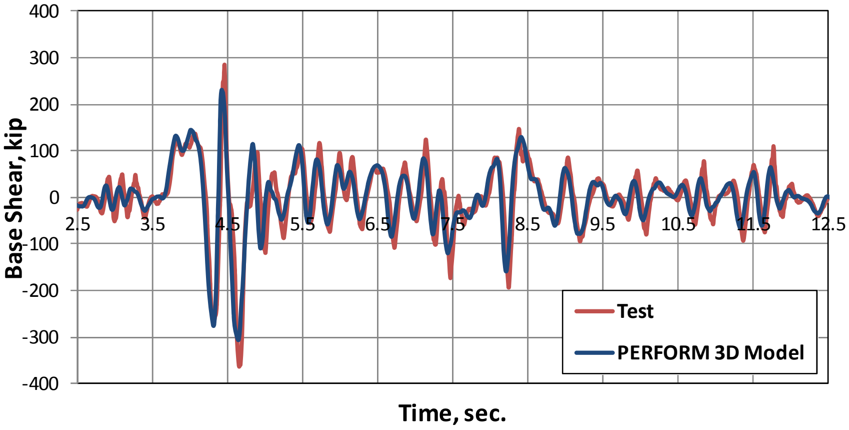

Figure 7.45 Time history of base shear, 3-story specimen (160 Sylmar 1994)

7.6.8.4.3 Load-displacement Hysteresis Loops (160% Sylmar 1994)

Hysteresis loops of base shear versus first-floor displacement are shown in Figure 7.46. Because the histories of first-floor displacements and base shears were accurately predicted, it is not surprising that the hysteresis loops also compare well.

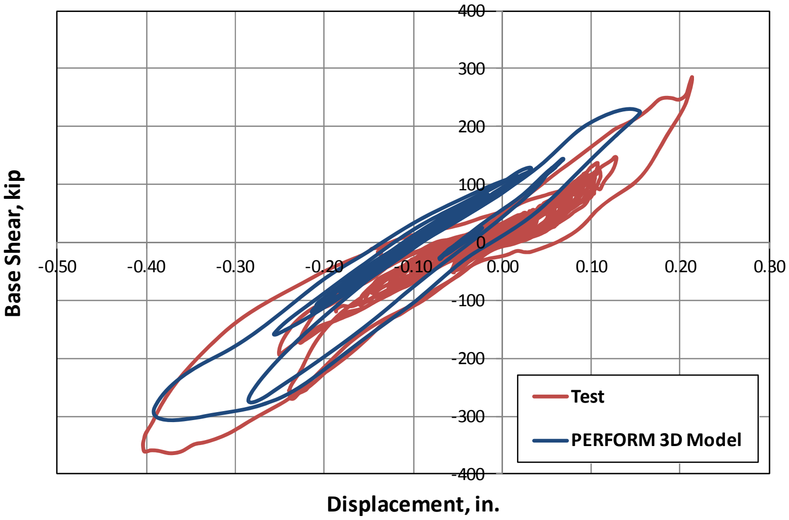

Figure 7.46 Load-displacement hysteresis loops, 3-story specimen (160% Sylmar 1994)

7.6.9 Summary of Comparison between Predicted and Observed Responses, 3-story Specimen

In this section, the 3-story specimen is modeled using PERFORM 3D (CSI 2007), whose General Wall Element provides a reasonable compromise between ease of modeling, quality of results, and computational effort. Nonlinear dynamic analyses were conducted using a single element mesh; a single set of material parameters, selected based on tested material properties; and degradation parameters based on comparisons with the results of reversed cyclic load tests. The analytical model was subjected to a sequence of 13 input motions, very close to the sequence used with the real specimen. Degradation was accounted for continuously throughout that sequence. For inputs at DBE level, MCE level, and above MCE level within that sequence, the analytical model gave good predictions of first-floor displacement versus time, base shear versus time, and hysteresis loops of base shear versus first-floor displacement.

7.7 CONCLUSIONS REGARDING ANALYTICAL MODELING OF REINFORCED MASONRY STRUCTURES

In this chapter, analytical models for masonry shear-wall structures were developed using PERFORM 3D (CSI 2007). Those models were refined and verified based on results of reversed cyclic tests on masonry wall specimens tested at The University of Texas at Austin and at Washington State University. The models were then used, without further modification, to predict the response of the full-scale, 3-story specimen tested in January and February of 2011 on the shake-table at the University of California at San Diego. The predictions agree quite well with the observed responses. This shows that such analytical models can be used to predict the nonlinear response of masonry wall structures with different configurations of openings. These models can be used as part of a systematic framework for displacement-based seismic design provisions for US structural design standards.

The analytical model discussed in this chapter could be refined. The rotational flexibility of the foundation and the shaking-table could be modeled using linear elastic beam elements, and more sophisticated material models could be used, with more accurate unloading and reloading paths. Nevertheless, a model simple enough for use by a sophisticated design office is quite capable of producing very good results.

CHAPTER 8

Shake-Table Performance of Full-Scale, Two-Story Specimen (September 2012)

8.1 INTRODUCTION

As part of the NIST masonry project, a full-scale two-story reinforced concrete masonry shear-wall system with a complex configuration of openings was tested in September 2012 at the large outdoor shake-table on the Englekirk Structural Engineering Center of the University of California, San Diego (UCSD). This chapter first presents an overview of the proposed displacement-based design, and then a detailed description of the specimen's design, materials, detailing, construction, testing protocol, test setup, and instrumentation. Observations from the shake-table tests are presented, along with details of the damage progression and collapse mechanism. Finally, overall structural performance is summarized. Additional details will be provided in the PhD dissertation now being prepared by Marios Mavros, doctoral candidate at UCSD.

The shake-table testing of the full-scale, two-story specimen had the following main objectives:

- Examine the global and local behaviors of low-rise concrete masonry buildings designed by the proposed displacement-based procedures and subjected to strong ground motion;
- Use data from shake-table tests of a full-scale reinforced masonry structure to extend and refine analytical models;
- Develop, refine, and validate systematic procedures for displacement-based design; and
- Evaluate the performance of masonry wall segments reinforced in conformance with the limit-design requirements of the draft 2013 MSJC limit-design provisions.

Construction took place in summer 2012, and lasted four weeks. During curing of the masonry walls and slab toppings, the instrumentation was installed in three weeks. Testing took place in September 2012, included tests using ambient vibrations, low-level white noise, and scaled historical ground motions. During the tests, the research team monitored the behavior of the structure at increasing maximum levels of seismic input, using about 400 sensors measuring accelerations, displacements, and strains at various locations on the specimen.

8.2 OVERALL DESCRIPTION OF FULL-SCALE, TWO-STORY SPECIMEN

The full-scale, two-story specimen tested at UCSD in September 2012 was intended to represent a typical two-story apartment or office building. Schematic views of the specimen on the shake-table are shown in Figure 8.1. The proposed plan has a single wall with a complex arrangement of openings in the direction of shaking, and a symmetrical arrangement of walls perpendicular to direction of shaking. The specimen was designed using the displacement-based design procedure proposed in this research, and was checked and detailed in accordance with the draft limit-design requirements of the 2013 MSJC *Code*, including reinforcement requirements for shear- and flexural-critical reinforced masonry shear wall elements. It did not meet requirements for prescriptive reinforcement in the body of the 2011 MSJC *Code* for special reinforced masonry shear walls.

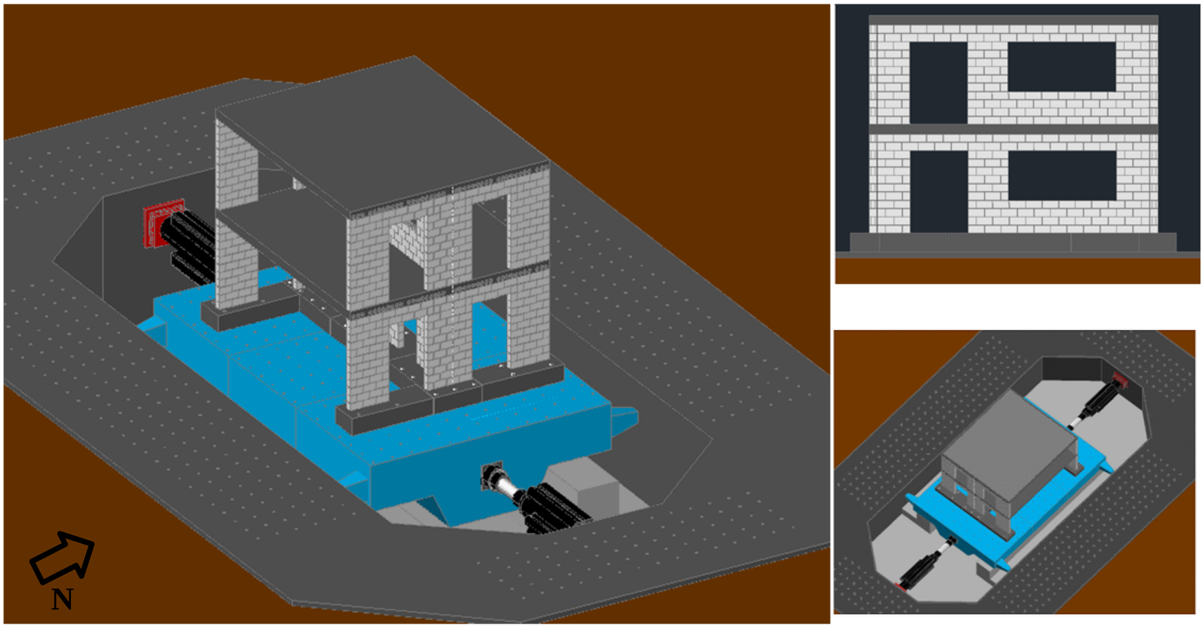

Figure 8.1 Schematic views of full-scale, two-story specimen on UCSD shake table

As shown in Figure 8.2, the specimen was rectangular in plan, with out-to-out dimensions of 22.67 ft in the direction of shaking and 20.67 ft perpendicular to the direction of shaking. The wall in the direction of shaking consists of two T-wall segments (Walls W-1 and W-3) and one lineal wall segment (a wall without flanges, Wall W-2). The walls perpendicular to the direction of shaking are two lineal half-walls. As shown in Figure 8.2, Walls W-1 and W-3 have webs 40-in. long in plan parallel to the direction of shaking, and flanges with a plan length of 24 in. perpendicular to the direction of shaking. Figure 8.3 shows an elevation view of the specimen in the direction of shaking, indicating the locations and the configuration of the openings. As shown in Figure 8.3, control joints were introduced on each side of the lintel beams above door openings.

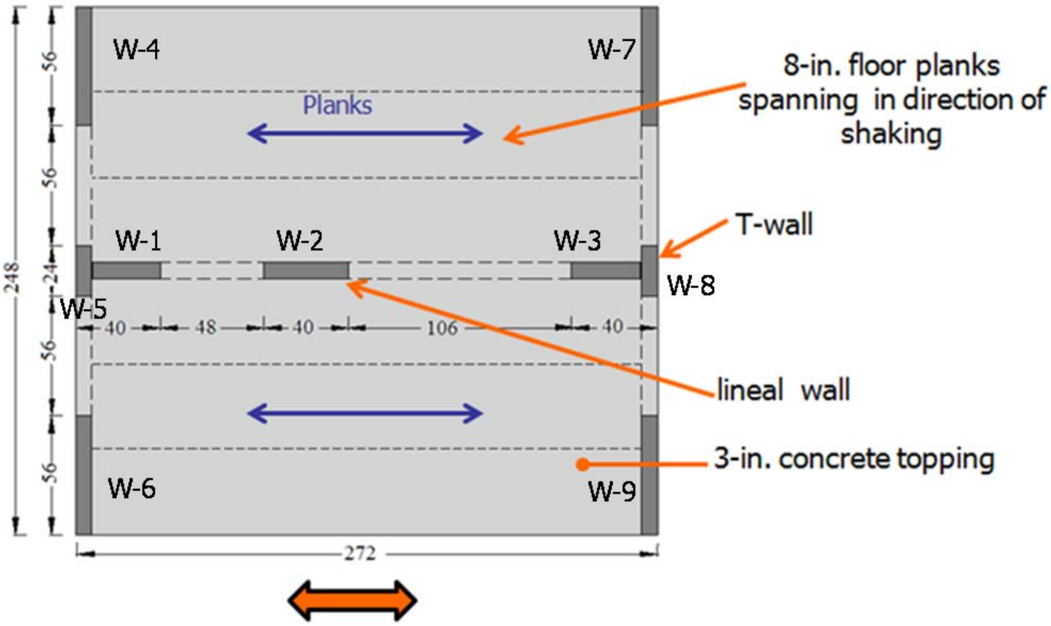

Figure 8.2 Plan view of typical floor of full-scale, two-story specimen

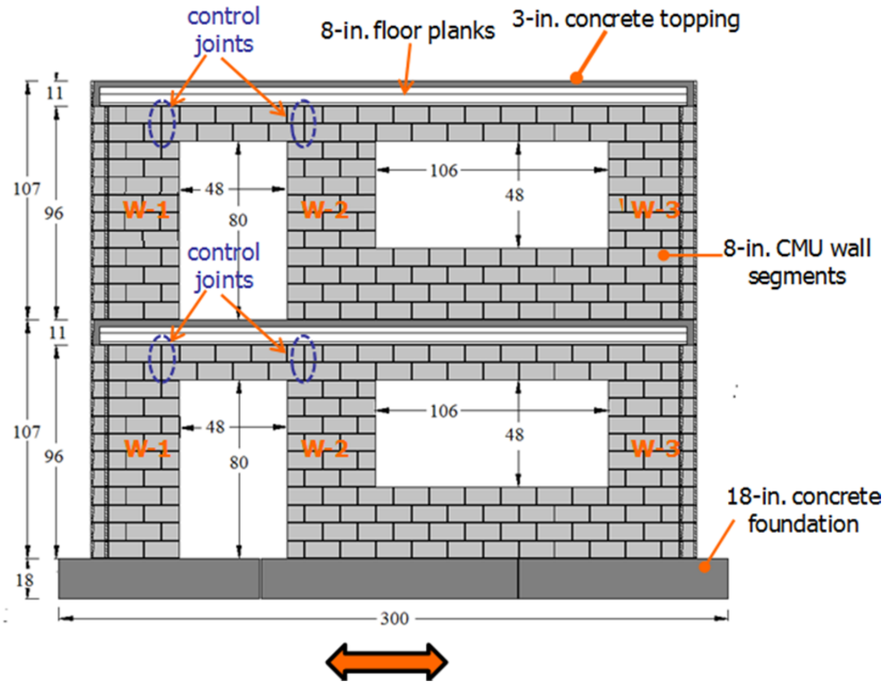

Figure 8.3 Elevation view of the full-scale, two-story specimen in direction of shaking

The specimen used nominal 8- x 8- x 16-in. lightweight concrete masonry units conforming to ASTM C90; ASTM C270 Type S cement-lime mortar by proportion; and ASTM C476 coarse grout by proportion. Concrete masonry units (CMU) were A-units throughout, with knock-out units at wall ends. Walls were fully grouted. The roof diaphragm was composed of prestressed 8-in. concrete planks, spanning parallel to the direction of shaking, bearing on out-of-plane lineal walls and on flanges of T-walls, and covered by 3 in. of concrete topping, reinforced with No. 4 bars at 16 in. in both directions. Two No. 4 perimeter bars were placed at the level of the planks to act as a bond beam. The specimen was constructed by professional masons using common practice, and is shown in Figure 8.4 as constructed on the shake-table.

Figure 8.4 Two-story, full-scale specimen as constructed on the UCSD shake-table

8.3 OVERVIEW OF DISPLACEMENT-BASED SEISMIC DESIGN

The basic elements of the proposed displacement-based seismic design procedure are briefly summarized in this section. The objective of this approach is that the structure be capable of reaching its predicted target displacements and local deformation limits under the considered seismic hazard levels. For this purpose, the structure is idealized as a single-degree-of-freedom (SDOF) system characterized by a secant stiffness at maximum displacement and by equivalent viscous damping that includes elastic and hysteretic contributions. The steps of displacement-based seismic design are summarized in the flow chart of Figure 8.5, and are described briefly below (Filiatrault and Folz 2002, Priestley *et al.* 2007).

Step 1: Define Seismic Hazard and Target Displacement

The first step in displacement-based seismic design is the selection of a design level of seismic hazard, and the corresponding target displacement (or local deformation limits). For each level of seismic hazard, the target displacement is described by a relative displacement response spectrum. The code design spectral accelerations for a given seismic design category $S_{A\ Code}$ can be transformed into corresponding spectral displacement values $S_{D\ Code}$.

$$\boldsymbol{S_{D\ Code} = \frac{T_{eq}^2}{4\pi^2} S_{A\ Code}} \qquad \textbf{\textit{Equation 8-1}}$$

In the above equation, T_{eq} is the equivalent elastic period of the building at the target displacement (or local deformation limits).

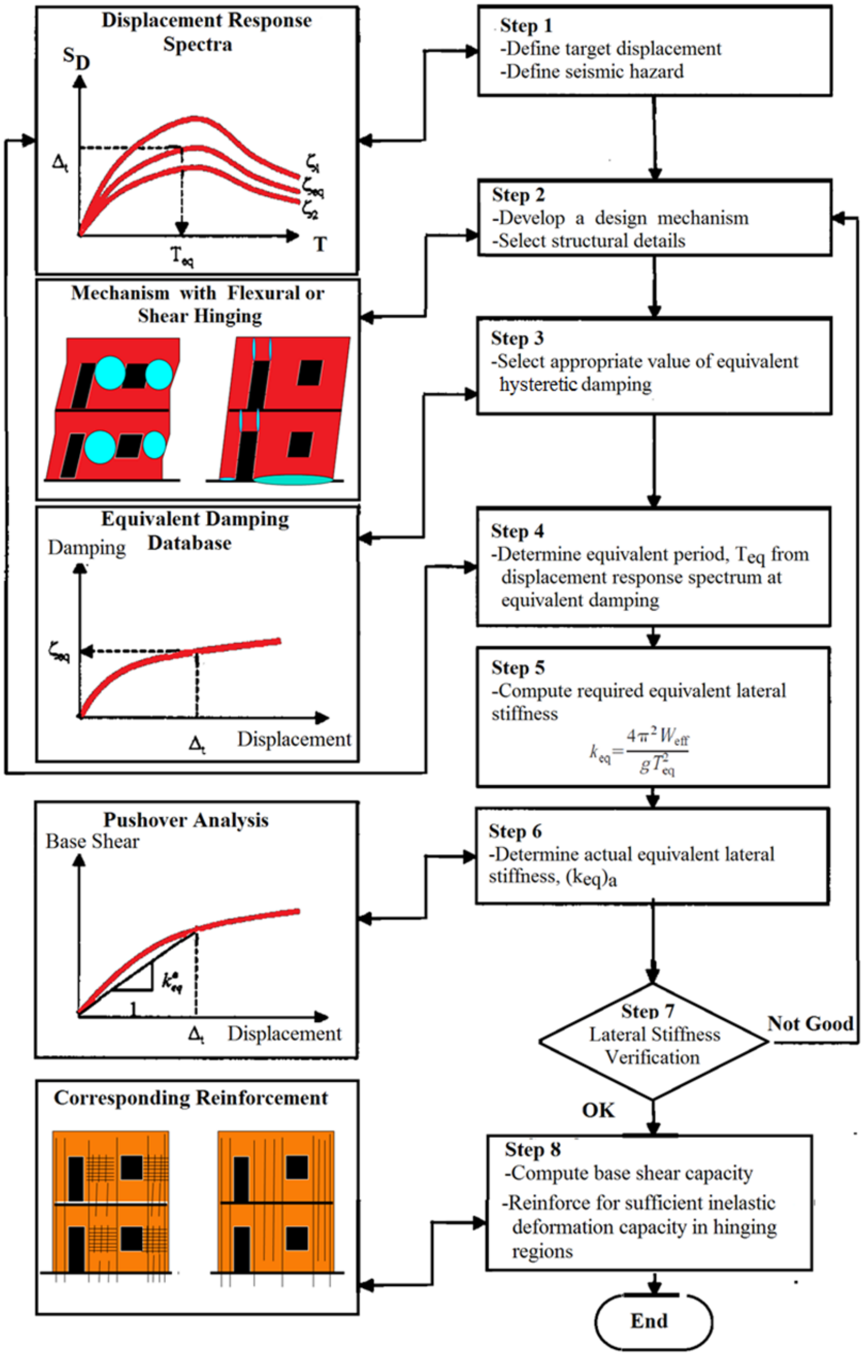

Figure 8.5 Modified flowchart of displacement-based seismic design for reinforced masonry shear-wall structures (Filiatrault and Folz 2002, Priestley et al. 2007)

Code spectral accelerations typically correspond to equivalent viscous damping equal to 5% of critical, and are modified independently for the effects of inelastic response. The spectral displacement values corresponding to the total equivalent viscous damping of the structure including inelastic response, $S_{D\ \xi eq}$, are obtained through empirical modification factors such as those of Equation 8-2 (Priestley *et al.* 2007).

$$\boldsymbol{S_{D\,\xi eq}} = \sqrt{\frac{\mathbf{0.07}}{\mathbf{0.02} + \boldsymbol{\xi_{eq}}}}\boldsymbol{S_{D\,Code}} \qquad \textit{Equation 8-2}$$

Step 2: Conduct Inelastic Analysis and Develop Design Mechanism

Once the design seismic hazard and associated target displacement (local deformation ratio limits) have been defined, a design mechanism consistent with that target displacement must be developed, and elastic and inelastic structural elements must be detailed and reinforced appropriately for the strengths and deformation demands associated with that assumed mechanism displacement. For perforated wall structures, elements with "shear hinging" (distributed inelastic shearing deformations) and elements with flexural hinging (concentrated inelastic rotations) are possible. For this purpose, inelastic procedures facilitate a better understanding of possible mechanisms and actual lateral performance. An important simplification to detailed structural models is what has become known as "pushover" or "capacity" curves. These curves are generated by subjecting a detailed structural model to one or more lateral load patterns (vectors) and then increasing the magnitude of the total load to generate a nonlinear inelastic force-deformation relationship for the structure at a global level (FEMA-440 2005).

For displacement-based design, it is necessary to represent a multi-story structure by an equivalent single-degree-of-freedom (SDOF) system. In deriving an equivalent SDOF structure, the main task is to identify an appropriate deformed shape and the load-displacement characteristic of the equivalent SDOF structure that can be obtained from a static pushover analysis. Pushover analysis converts multi-degree-of-freedom (MDOF) models to equivalent SDOF structural models. In this procedure, the global deformation demand (elastic and inelastic) on the structure is computed from the response of an equivalent SDOF system having the load-deformation properties determined from the pushover analysis (FEMA-440 2005). In this section, four methods for deriving such an equivalent SDOF system are presented and compared.

1. Method of Mehrabi and Shing (2003)

To derive an equivalent SDOF structure, Mehrabi and Shing (2003) obtained the deformed shape (for a single natural mode) and the corresponding capacity curve from a static pushover analysis. For further simplification, they replaced the capacity curve from the pushover analysis by an idealized linear elastic, perfectly plastic curve. For displacement-based design, they conclude that global target displacement and the effective mass for the equivalent SDOF structure can be obtained from Equation 8-3 and Equation 8-4.

$$u_d = u_N$$ ***Equation 8-3***

$$W_{eff} = \frac{\sum W_i u_i}{u_d}$$ ***Equation 8-4***

where u_d and W_{eff} are the target displacement and effective mass for the equivalent SDOF structure. In this approach, the W_i and u_i are the weights and displacements of the i weight locations, and u_N is the inelastic roof displacement.

2. Method of Calvi and Kingsley (1995) and of Priestley *et al.* (2007)

Calvi and Kingsley (1995) assume that the base shear induced by inertial forces is the same for the multi-story structure and the equivalent SDOF system for the elastic first mode shape, and that the work done by the inertial forces of the multi-story structure is the same as that done by the inertial force of the equivalent SDOF system. With these assumptions, they conclude that global target displacement and the effective mass for the equivalent SDOF structure can be obtained from Equation 8-5 and Equation 8-6.

$$u_d = u_N \qquad \textbf{\textit{Equation 8-5}}$$

$$W_{eff} = \frac{\sum W_i {u_i}^2}{\sum W_i u_i} \qquad \textbf{\textit{Equation 8-6}}$$

3. Method of ASCE 41 (2005)

In the Coefficient Method of ASCE 41 (2006), the global parameters are normally base shear and roof displacement. As shown in Figure 8.6, in this approach, the linear elastic response of the equivalent SDOF system is modified by multiplying it by a series of coefficients C_0 through C_3 to generate an estimate of the maximum global displacement (elastic and inelastic), which is termed the target displacement. The coefficients are typically derived empirically from a series of nonlinear response history analyses of SDOF oscillators with varying periods and strengths. The coefficient C_0 is a shape factor (often taken as the first-mode participation factor) that simply converts the spectral displacement to the displacement at the roof. The other coefficients each account for a separate inelastic effect. The coefficient C_0 can be calculated using the first modal participation factor at the level of the control node (FEMA-440 2005).

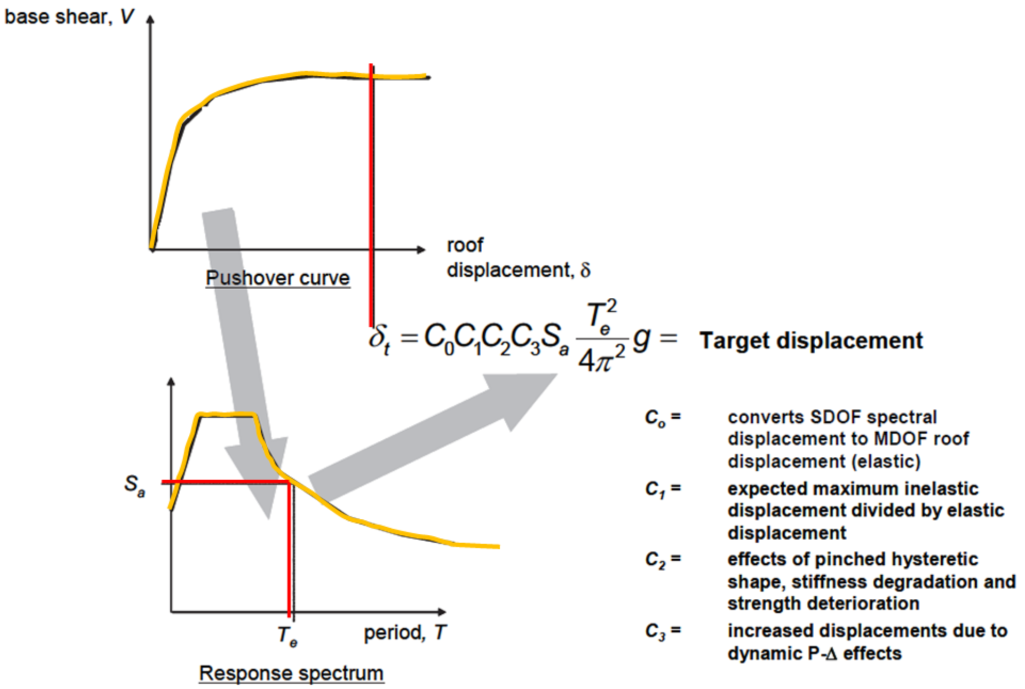

Figure 8.6 Schematic illustration of Coefficient Method (FEMA-440 2005)

4. Method Used in this Research

In this research, the basic approach is that proposed by Filiatrault and Folz (2002), with some modification. To derive an equivalent SDOF structure, the floor displacements are represented by the inelastic pushover deformed shape rather than the elastic first-mode shape. In this approach, inelastic pushover analysis was used to estimate the maximum global displacement at the roof level (which is termed the target displacement) and to calculate the effective stiffness in displacement-based design. However, this global displacement can be modified to convert the displacement at the roof level to the spectral displacement in the equivalent SDOF system.

$$u_d = u_N \qquad \textit{Equation 8-7}$$

In this approach, the effective mass corresponding to the inelastic first mode shape is given by Equation 8-8. This procedure is used consistently in displacement-based design throughout this dissertation.

$$W_{eff} = \frac{(\sum W_i u_i)^2}{W_i {u_i}^2} \qquad \textbf{\textit{Equation 8-8}}$$

Step 3: Determine Equivalent Hysteretic Damping

To capture the energy-dissipation characteristics of the structure at the target displacement, an equivalent hysteretic damping ratio ξ_{eq} must be determined. For this purpose, a damping database must be established for the selected structural system from the global hysteretic behavior of the structure, using Equation 8-9 (Clough and Penzien 1993).

$$\xi_{eq} = \frac{E_{D\Delta_t}}{2\pi\, k_{eq}\Delta_t^2} + \xi_0 \qquad \textbf{\textit{Equation 8-9}}$$

In Equation 8-9, $E_{D\Delta t}$ is the energy dissipated per cycle at the target displacement Δ_t, and k_{eq} is the equivalent lateral secant stiffness of the building at that target displacement. The nominal equivalent viscous damping ratio, ξ_0, is considered to account for the elastic energy dissipation characteristics of *other* structural and nonstructural elements, and is reasonably taken as 5% of critical (Priestley *et al.* 2007).

Step 4: Determine Equivalent Elastic Period

Knowing the target displacement (or displacement related to local deformation ratio limits) and the equivalent viscous damping (including inelastic effects) ξ_{eq} of the building at that target displacement, the equivalent elastic period of the building T_{eq} can be obtained directly from the design displacement response spectrum.

Step 5: Compute Required Equivalent Lateral Stiffness

Representing the building as an equivalent linear SDOF system, the required equivalent lateral stiffness $(k_{eq})_r$ can be obtained using Equation 8-10 (Clough and Penzien 1993).

$$\left(k_{eq}\right)_r = \frac{4\pi^2 W_{eff}}{gT_{eq}^2} \qquad \textbf{\textit{Equation 8-10}}$$

where W_{eff} is the effective weight, calculated from the first mode deflected shape. Several expressions are available for W_{eff}. The required equivalent lateral stiffness and effective weight (or mass) of the substitute structure depend on the target displacement (or local deformations) of the most critical story (or structural member) of the real structure, and a inelastic displaced shape for the structure at that target displacement. This displaced shape is that corresponding to the inelastic first mode shape at the design level of seismic hazard (Priestley 2007). Representing the displacement by the inelastic rather than the elastic first mode shape is consistent with characterizing the structure by secant stiffness to maximum response (Priestley 2007). The effective mass corresponding to the inelastic first mode shape can be given by Equation 8-11.

$$W_{eff} = \frac{(\sum W_i u_i)^2}{W_i {u_i}^2} \qquad \textbf{\textit{Equation 8-11}}$$

where W_i and u_i are the weights and displacements of the i weight locations. For multi-story structure, these will be at the i floors of the structure.

Step 6: Determine Actual Equivalent Lateral Stiffness

The actual equivalent lateral stiffness of the building $(k_{eq})_a$ at the target displacement Δ_t can be determined from a static pushover analysis.

Step 7: Verify Lateral Stiffness

The actual equivalent lateral stiffness of the building must be compared to the required equivalent lateral stiffness. If these two stiffness values differ substantially, the seismic force-resisting system of the building must be modified by returning to Step 2.

Step 8: Compute Design Base Shear and Perform Structural Detailing

If the actual lateral stiffness of the building is sufficiently close to the required lateral stiffness, the design is completed by computing the required base shear capacity Vb of the building using Equation 8-12.

$$V_b = \left(k_{eq}\right)_a \Delta_t \qquad \textbf{\textit{Equation 8-12}}$$

This base shear is then used to design the other elements of the structure. Using this base shear the wall segments are reinforced with the detailing required for sufficient inelastic shearing deformation capacity in shear hinging regions, and for sufficient inelastic rotation capacity in flexural hinging regions.

8.4 DISPLACEMENT-BASED DESIGN OF FULL-SCALE, TWO-STORY SPECIMEN

The steps outlined above are now applied to the displacement-based design of the full-scale, two-story specimen tested on the UCSD shake-table.

8.4.1 Step 1: Define Seismic Hazards and Target Drifts for Two-Story Specimen

Seismic hazard levels for design of new structures have traditionally been a Design Basis Earthquake (DBE) with a probability of exceedance of 10% in 50 years; and Maximum Considered Earthquake (MCE) with a probability of exceedance of 2% in 50 years. Although in ASCE7-10 these traditional definitions are modified to produce “risk-targeted” ground motions with uniform probabilities of collapse, rather than uniform probabilities of exceedance, the basic principle remains essentially the same. In this work, approximately those same seismic hazard levels are used. The target drifts for masonry wall segments must be based on experimentally determined deformation capacities, discussed in the following section.

To investigate structure performance under a particular seismic hazard level, the inter-story drift ratio (relative lateral displacement between floors, divided by the height of the story), and local deformation ratios (relative lateral displacement between ends of each wall segment, divided by the height of that segment) must be checked with target inter-story drift ratio and local deformation capacity ratio limits of the structure. The experimental determination of those limits is discussed below.

8.4.1.1 Limiting Deformation Ratios for Wall Segments

Typical load-displacement loops for of two flexure-controlled wall segments with an aspect ratio of 1.0, tested under reversed cyclic loading at UT Austin, are shown in Figure 8.7. Those loops can be used to obtain limiting deformation-capacity ratios for DBE and MCE hazard levels, assuming reasonable strength loss and damage for each level. As shown in Figure 8.7, this research group has proposed that flexure-controlled wall segments be assigned a maximum local deformation capacity of 0.8% at the DBE level, and 1.5% at the MCE level. The same DBE-level deformation limit is recommended by Priestley *et al.* (2007). In addition, elements detailed in accordance with 2013 MSJC limit-design requirements should be detailed to have inelastic deformation capacity of 0.8% for flexure-dominated elements. Those local deformation capacities consist primarily of flexural deformations (end hinging), but also include some shearing deformations.

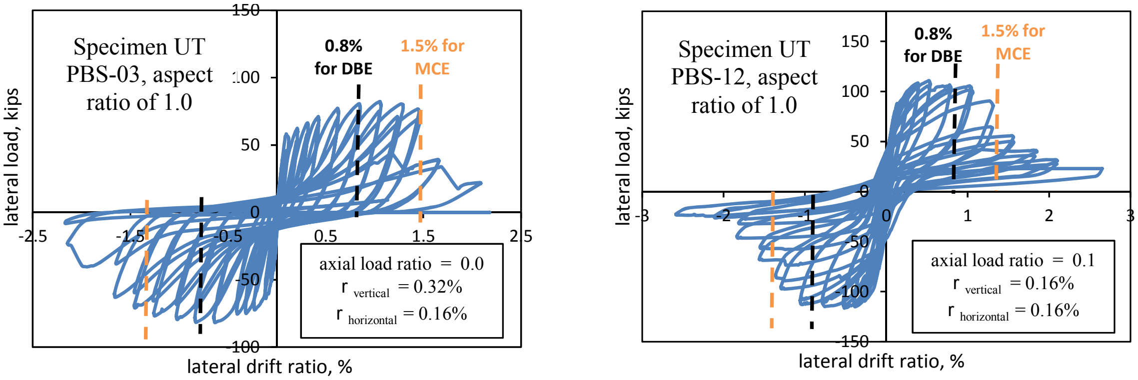

Figure 8.7 Typical lateral load-displacement loops for flexure-controlled wall segments with aspect ratio of 1.0

Typical load-displacement loops for two shear-dominated, fixed-fixed wall segments with an aspect ratio of 1.0, tested at UT Austin, are shown in Figure 8.8. As shown in Figure 8.8, this research group has proposed that shear-controlled wall segments be assigned a maximum local deformation capacity of 0.5% at the DBE level, and 1.0% at the MCE level. Almost the same DBE-level deformation limit (0.4-0.5%) is recommended by Priestley *et al.* (2007). In addition, elements detailed in accordance with 2013 MSJC limit-design requirements should be detailed to have inelastic deformation capacity of 0.5% for shear-dominated elements. Those local deformation capacities consist primarily of shearing deformations, but may also include some elastic and inelastic flexural deformations. They do not include sliding deformations.

8.4.1.2 Inter-story drift ratio limits

In this research, inter-story drift limits will be used as an index to check the seismic performance of 2-story specimen in nonlinear analyses. The relationship between the wall deformation capacity ratios and the inter-story drift limits can be calculated based on the relationship between wall dimension and height of the story. Walls W-2 and

W-3 are the most critical, and their height is 0.5 times the story height. The limiting deformation capacities of the wall segments can then be converted into inter-story drift limits by multiplying the calculated deformation capacities for these segments, to the height of wall over height of the story ratio, 0.5. Based on limiting deformation capacity ratios for shear-controlled segments, the two-story specimen is designed using target inter-story drifts of 0.3% for DBE and 0.7% for MCE level.

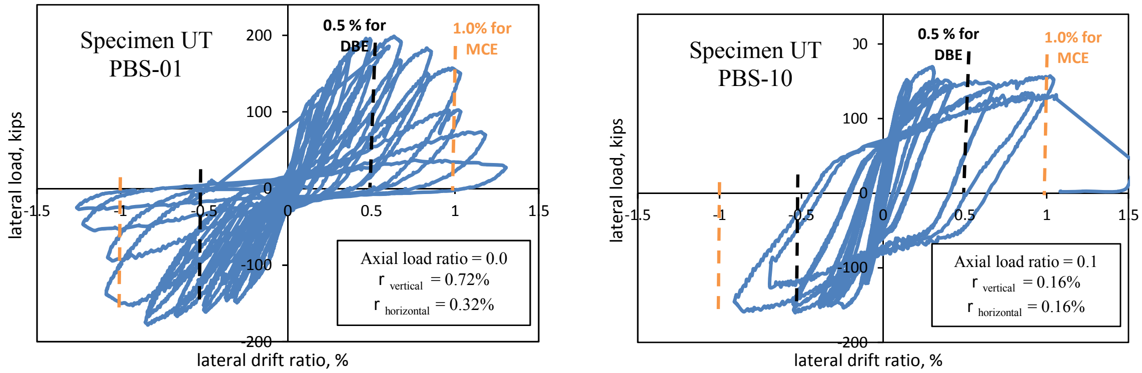

Figure 8.8 Typical lateral load-displacement loops for shear-controlled wall segments with aspect ratio of 1.0 (after removing sliding deformations)

8.4.1.3 Design Response Spectra

Design response spectra are calculated according to ASCE/SEI 7 (2010). For DBE level, assume that the structure is to be constructed in a region of high seismicity, corresponding to $S_S = 1.50$ g, and $S_1 = 0.60$ g, and assume Site Class D (stiff soil). Then the maximum considered short-period response acceleration is:

$$S_{MS} = F_a \times S_S = 1.0 \times 1.5 \text{ g} = 1.5 \text{ g}$$

and the maximum considered 1-second response acceleration is:

$$S_{M1} = F_v \times S_1 = 1.5 \times 0.6\ \text{g} = 0.9\ \text{g}$$

The design response acceleration is two-thirds of the maximum considered acceleration. Then the design response acceleration for short periods is:

$$S_{DS} = \frac{2}{3} S_{MS} = \frac{2}{3} \times 1.5\ \text{g} = 1.0\ \text{g}$$

and the design response acceleration for a 1-second period is:

$$S_{D1} = \frac{2}{3} S_{M1} = \frac{2}{3} \times 0.9\ \text{g} = 0.6\ \text{g}$$

The elastic displacement spectrum is computed from the acceleration, considering that the relationship between acceleration and displacement is:

$$S_{D\,Code} = \frac{T^2}{4\pi^2} S_{A\,Code}$$

The ASCE/SEI 7 (2010) response acceleration and displacement spectra for the design-basis earthquake are shown in Figure 8.9.

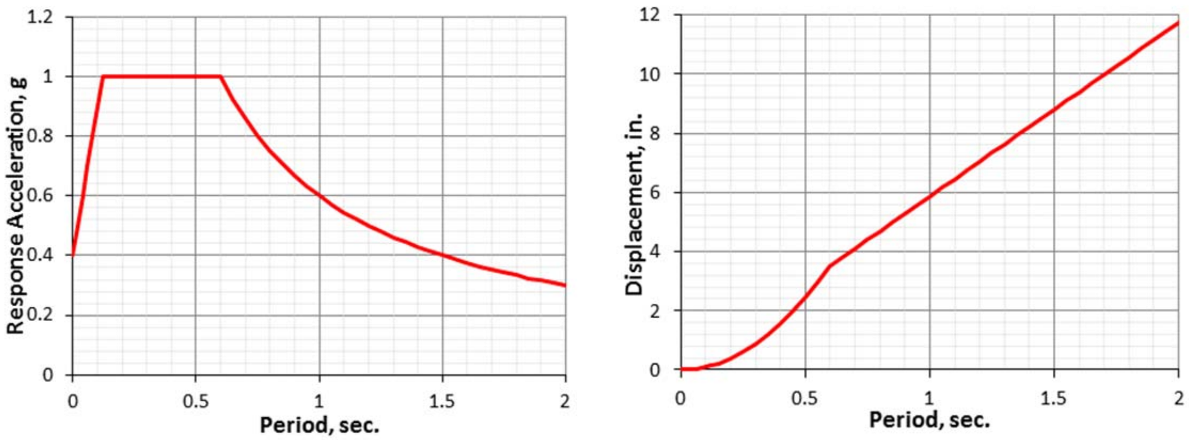

Figure 8.9 Design acceleration and displacement response spectra for DBE

The spectral displacement values corresponding to the different equivalent hysteretic damping levels of the building, $S_{D\ \xi eq}$, can be obtained through empirical modification factors. Figure 8.10 represents the inelastic relative displacement response spectrum for different equivalent viscous damping ratios, using Equation 8-13 (Priestley *et al.* 2007).

$$S_{D\ \xi eq} = \sqrt{\frac{0.07}{0.02 + \xi_{eq}}} S_{D\ Code} \qquad \textbf{\textit{Equation 8-13}}$$

A similar procedure is used to modify the design displacement response spectrum for different equivalent hysteretic damping ratios for the MCE level, as shown in Figure 8.11.

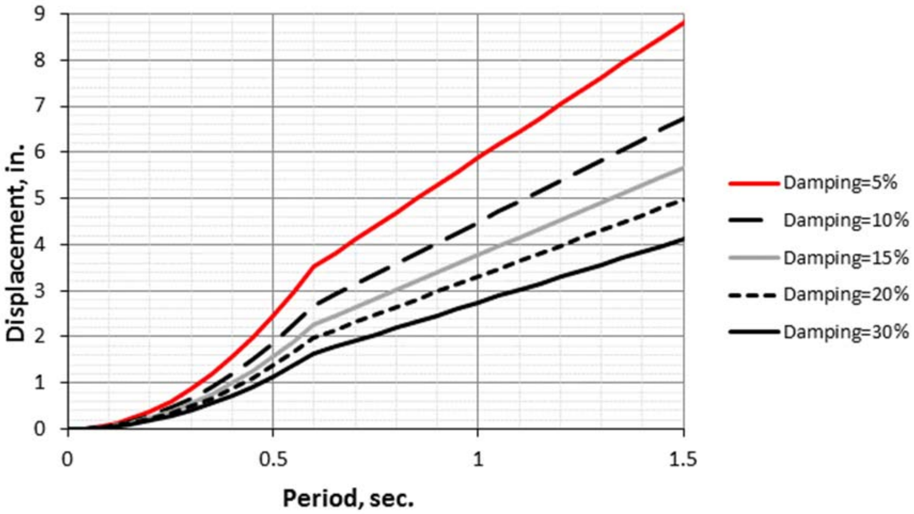

Figure 8.10 Nonlinear displacement response spectra for different equivalent damping ratios at DBE level

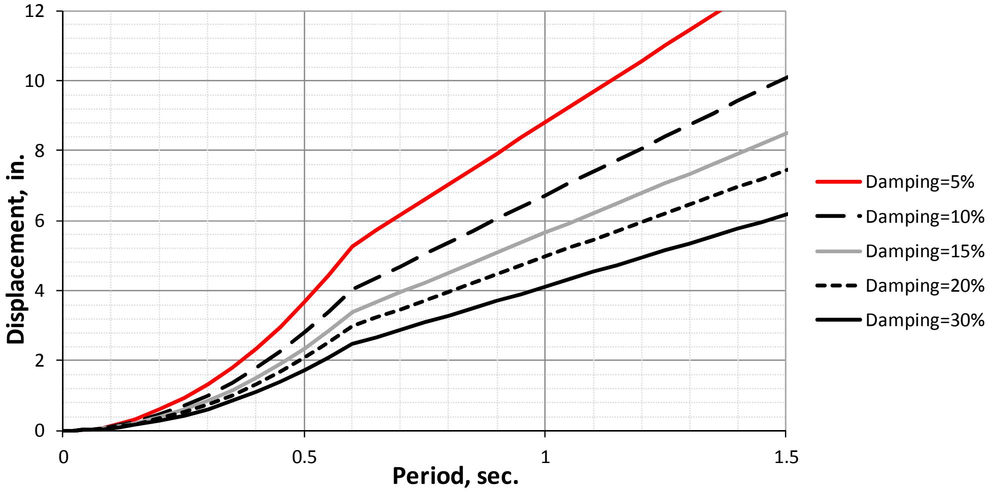

Figure 8.11 Nonlinear displacement response spectra for different equivalent damping ratios at MCE level

8.4.2 Step 2: Conduct Inelastic Analysis and Develop Design Mechanism for Two-Story Specimen

The nonlinear analytical model was composed of General Wall Elements using PERFORM 3D (CSI 2007). A three-dimensional model of the specimen is used for nonlinear static analysis. In this section, details of modeling and analysis results are presented for the two-story UCSD specimen.

8.4.2.1 Nonlinear Modeling of 2-Story Shake-table Specimen using PERFORM 3D

As shown in Figure 8.12, a non-linear model of the 2-story shake-table specimen was developed using PERFORM 3D (CSI 2007). The in-plane wall segments (vertical and horizontal) are modeled with the General Wall Element, permitting in-plane inelastic response anywhere within the perforated multi-story wall. As shown in Figure 8.12, the out-of-plane wall segments are modeled using PERFORM 3D column elements with biaxial (P-M-M) plastic hinges at each end. The hinges are rigid-plastic, and use a yield surface appropriate for reinforced masonry. An effective flexural stiffness of 0.50 EI_o is used for the out-of-plane wall segments (ASCE-41 2007).

The floor slabs are modeled using 4-node, elastic slab/shell elements with membrane (in-plane) and plate bending (out-of-plane) stiffnesses. The slab thickness is uniform over each element, but can be different for membrane and bending effects. Effective stiffness values including the effects of flexural cracking are used for the elastic components of the wall and slab elements. For the wall in flexure, the fiber element properties determine the effective initial stiffness. An effective flexural stiffness of 0.50 EI_o is used for floor slabs (ASCE-41 2007). The model shown in Figure 8.12, and in more detail (for a typical story) in Figure 8.13, was developed considering the following points:

1) Because the General Wall Element is rectangular only (no triangles), and because displacement compatibility is enforced at corner nodes only, the element mesh must have continuous vertical and horizontal element boundaries.

2) In the interior of each vertically or horizontally oriented wall segment, roughly square elements are used. To better model the regions at the tops and bottoms of vertically oriented wall segments, where plastic hinges are expected to form, 4-in. deep elements are used there. A similarly refined mesh is used at the ends of horizontally oriented segments (lintels).

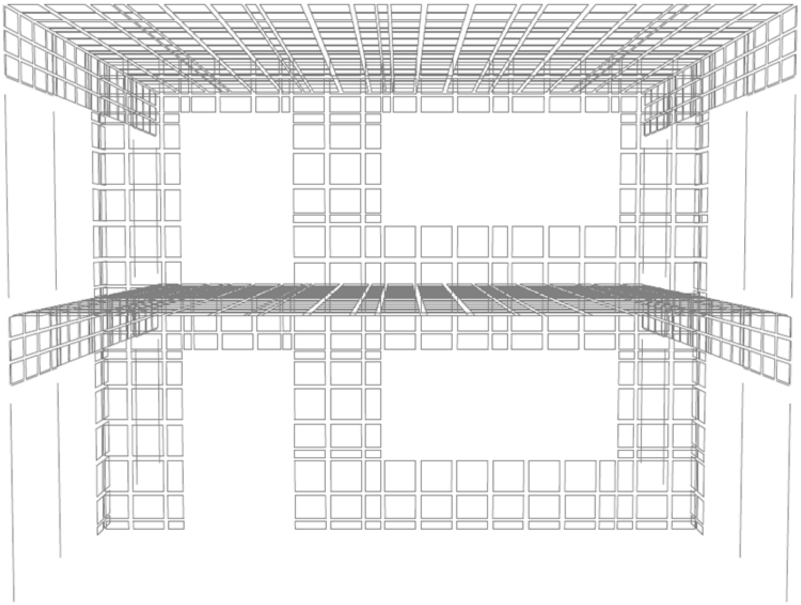

Figure 8.12 Three-dimensional view of PERFORM 3D model of 2-story specimen

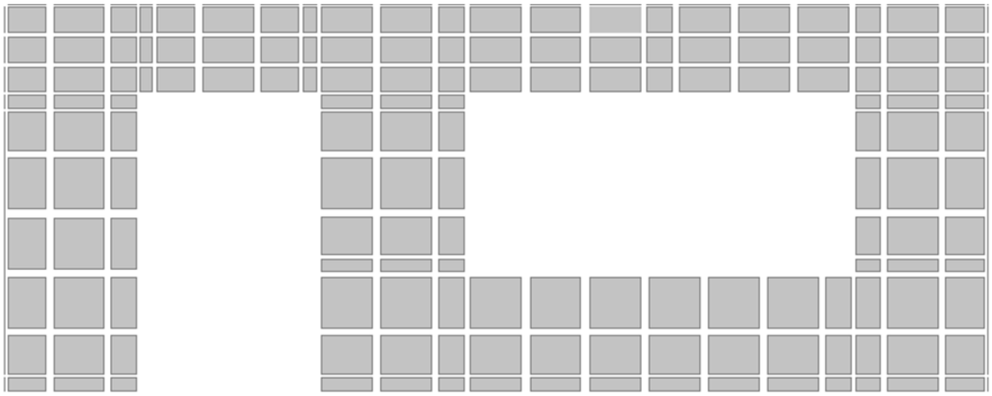

Figure 8.13 Detail of PERFORM 3D mesh at a single floor, longitudinal wall of full-scale, two-story specimen

In this model, inelastic material models are incorporated into each layer of each element. For most layers, this is routine.

a) For each element, combinations of flexural and axial behavior in the vertical and horizontal directions were modeled using one vertical flexural-axial layer and one horizontal flexural-axial layer. Each layer was further subdivided into fibers. Reinforcing bars were modeled as individual fibers. In these layers, the stress-strain behavior of masonry was based on uniaxial test data, with a low tensile strength and nonlinear compressive strength, including a descending branch.

b) For each element, shearing behavior dominated by diagonal tension was modeled by one elasto-plastic masonry shear layer whose stiffness was calculated using a shearing modulus equal to $0.4E_m$, and whose strength was set equal to V_n from the 2011 MSJC *Code,* including the effects of axial force. For analyses at the DBE level, for which little hysteretic shear degradation is expected, V_n is taken equal to V_{nm} plus V_{ns} , because the masonry would not have experienced degradation. V_{nm} is computed using axial loads from gravity loads only. The justification for this is that seismic overturning increases axial loads on one side of the specimen while decreasing them on the other side, so that the net effect of seismic overturning on base shear capacity is essentially zero.

c) In PERFORM 3D, shearing behavior is modeled using a shear layer only, rather than the diagonal-compression layers. Reasons for this are discussed in Section 7.6.1.

8.4.2.2 Material Parameters for Nonlinear Modeling of 2-Story Specimen

The vertical and horizontal reinforcement used in the specimen was modeled using the general uniaxial model shown in Figure 8.14. An elastic modulus of 29000 ksi was used, and tensile yield and ultimate strength were based on the results of material tests at the University of California at San Diego. In this model, the buckling strength of steel reinforcement bars (f_{cr}) under compression was taken as 20% of the specified ultimate specified strength in tension. To account for low-cycle fatigue, the fracture strain for reinforcement was conservatively taken as 0.06.

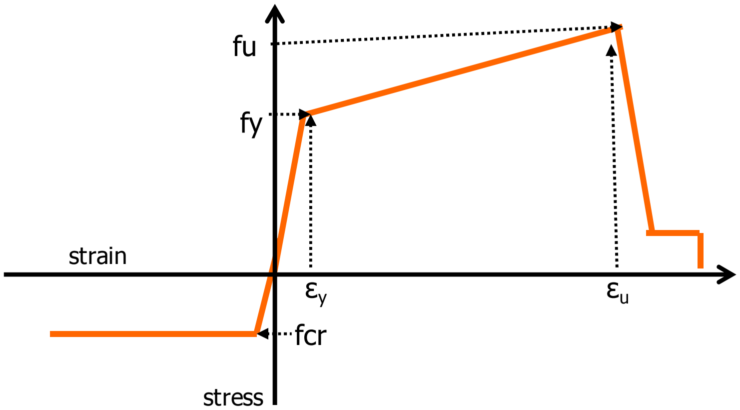

Figure 8.14 Stress-strain relation used to model reinforcement in full-scale, two-story specimen

Masonry fibers were modeled using the uniaxial stress-strain behavior shown in Figure 8.15. Tensile strength and stiffness were neglected, and compressive behavior was based on the results of monotonic stress-strain tests of grouted CMU prisms at the University of California at San Diego. That compressive behavior was used to model the masonry fibers of the axial/bending layers and the shear layer of each element.

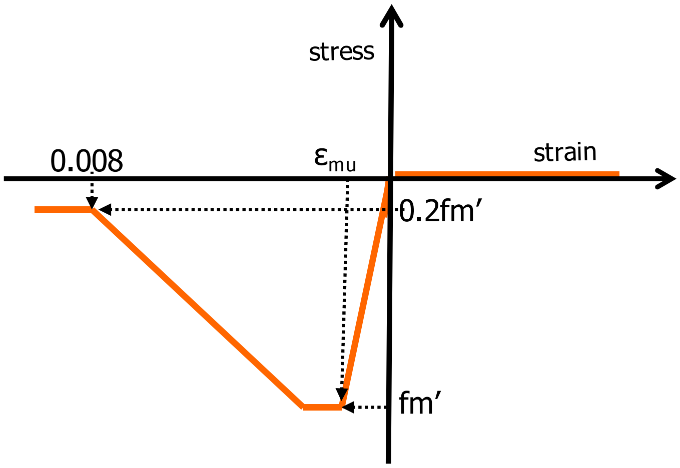

Figure 8.15 Stress-strain relations used to model masonry in full-scale, two-story specimen

For time-history dynamic analyses, hysteretic degradation and energy dissipation are important and must be accounted for directly. In PERFORM 3D, this is done by specifying hysteretic degradation factors for inelastic components. These factors include the reduction in swept area between the original hysteretic loop and the degraded loop, and also include changes in the form of the loops, including pinching (CSI 2007).

8.4.2.3 Model Restraints for 2-Story Specimen

The 2-story specimen was fixed to the shake-table, and the analytical model included had fixed supports at that level.

8.4.2.4 Pushover Analysis of Full-scale, Two-story Specimen

Monotonic pushover analyses were performed to determine the envelope of base shear versus lateral drift ratio at the center of the first floor. The first step in the pushover analyses is the selection of a lateral load vector. ASCE 41 (2007) recommends either uniform distribution or a triangular distribution over the building height. A uniform distribution usually corresponds to a uniform acceleration over the building height, so that the load at any floor level is proportional to the mass at that level. Similarly, a triangular distribution usually corresponds to a linearly increasing acceleration over the building height. In the inelastic range of response, low-rise wall structures usually have an approximately uniform distribution of acceleration over the building height, and therefore a uniform distribution was used for the 2-story specimen. Pushover analysis was conducted using a uniform distribution of load over the height of the structure, applied until the building reached an overall drift ratio of 1.5%. In Figure 8.16 and Figure 8.17 are presented the deformed shapes and target mechanisms for DBE and MCE levels, and the capacity curve, respectively.

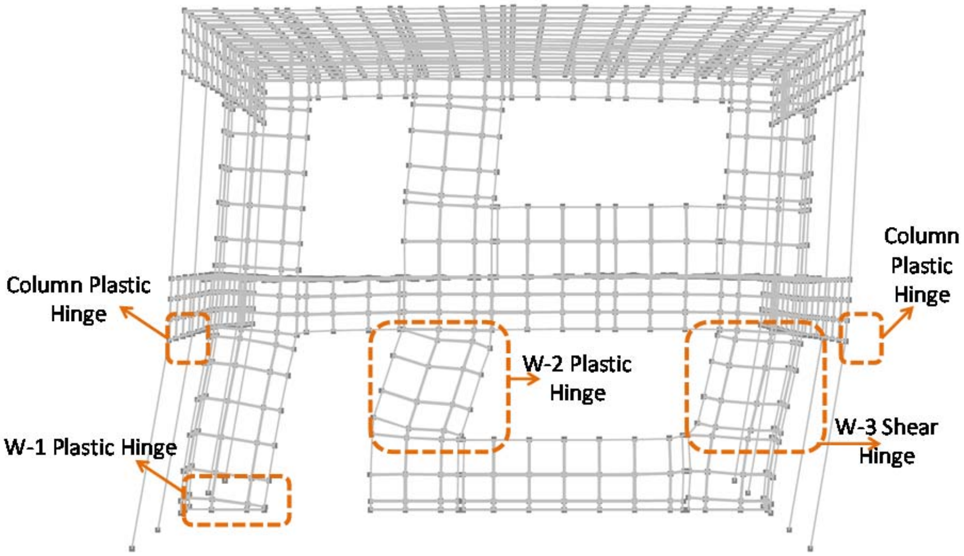

a) Target Mechanism at DBE

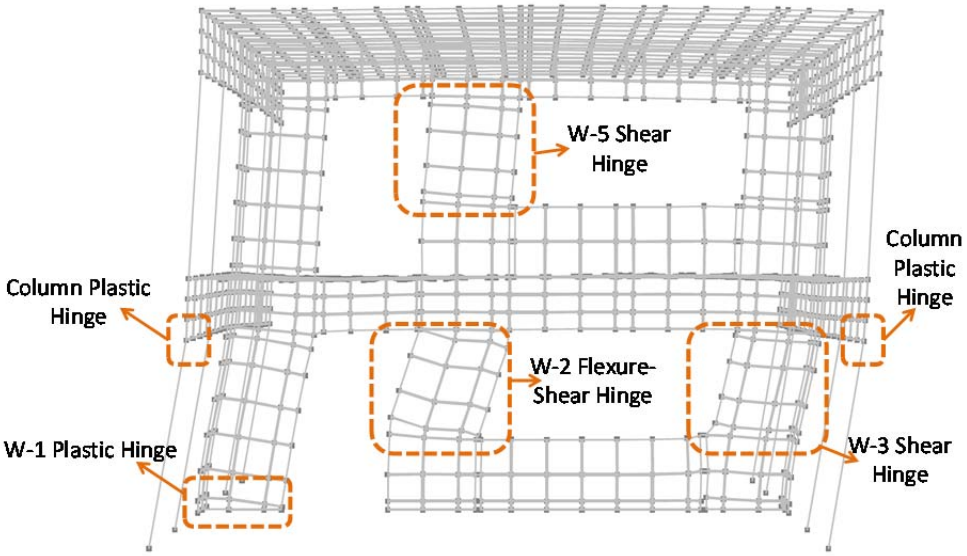

b) Target Mechanism at MCE

Figure 8.16 Deflected shapes and target mechanisms from pushover analyses for the two-story specimen in the direction of shaking

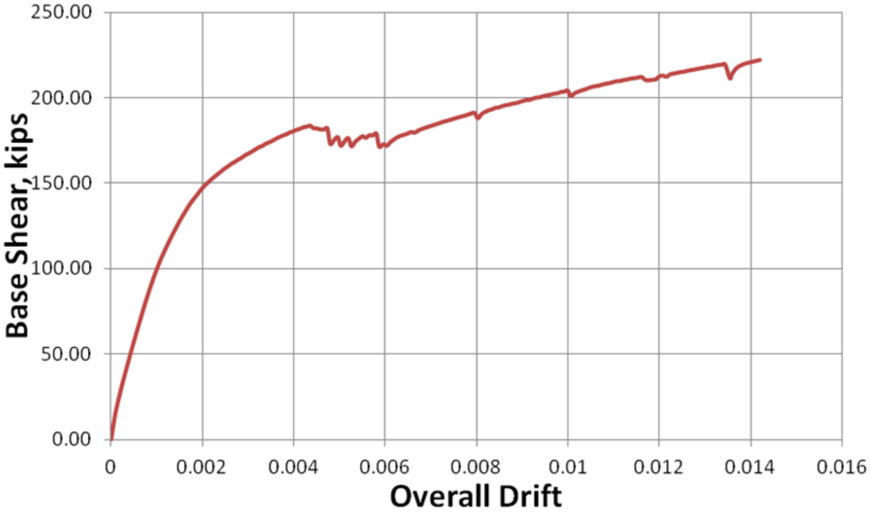

Figure 8.17 Capacity curve for full-scale, two-story specimen in direction of shaking

8.4.3 Step 3: Establish Equivalent Viscous Damping for Two-Story Specimen

The NIST test results for cantilever wall segments are used to establish a damping database for the selected structural system from the global hysteretic behavior of the structure. Test results from cantilever wall specimens are applied for each loop to construct a database of equivalent hysteretic damping ratio ξeq as a function of lateral drift ratio. To capture the energy-dissipation characteristics of the structure at the target displacement, an equivalent viscous damping ratio ξeq must be determined, using Equation 8-14.

$$\xi_{eq} = \frac{E_{D\Delta_t}}{2\pi\, k_{eq}\Delta_t^2} + \xi_0 \qquad \textbf{\textit{Equation 8-14}}$$

From previous work, ξ_0=5% of critical appears reasonable for this purpose (Priestley 2007). The equivalent hysteretic damping for each wall specimen is presented in Table 8-1. The displacements were chosen to be as close to 0.6% and 1.5% drift as possible.

The drift for the first displacement ranged from 0.5% to 0.7%, and the drift for the second displacement ranged from 1.2% to 1.8%. The average equivalent hysteretic damping at approximately 0.6% and 1.5% drift were 16% and 21%, respectively.

Table 8-1 Equivalent hysteretic damping

			about 0.6% drift ratio	**about 1.5% drift ratio**
specimen	**aspect ratio**	**axial load ratio**	**equivalent hysteretic damping (%)**	**equivalent hysteretic damping (%)**
UT-PBS-03	1.0	0	17%	19%
UT-PBS-04	1.0	0	22%	22%
UT-PBS-04G	1.0	0	20%	22%
UT-PBS-11	1.0	0.10	19%	16%
UT-PBS-12	1.0	0.10	18%	18%
UT-PBS-12G	1.0	0.10	19%	24%
WSU-C1	2.0	0	12%	22%
WCU-C2	2.0	0.0625	16%	17%
WSU-C3	2.0	0.0625	11%	20%
WCU-C4	0.78	0.0625	15%	23%
WSU-C5	1.0	0.0625	19%	23%
WCU-C6	2.0	0	12%	20%
WSU-C7	2.0	0	11%	21%
WSU-C8	2.0	0.0625	11%	20%

For structures with shear damage, a total equivalent damping of $\xi_{eq=}$15% is recommended by Priestley *et al.* (2007) for a local deformation ratio of 0.4%. For structures with flexural damage, a total equivalent damping ratio of $\xi_{eq=}$10% was assumed for a local deformation ratio of 0.8% (Priestley *et al.* 2007). In displacement-based design of this specimen, equivalent hysteretic damping of 10% is assumed for DBE, and 15% for MCE.

8.4.4 Step 4: Equivalent Natural Period for Two-Story Specimen

To calculate the equivalent natural period of the two-story specimen for displacement-based design, a family of displacement spectra is used for DBE and MCE levels.

8.4.4.1 Equivalent Natural Period at DBE

Using the DBE response spectrum for 10% damping at the target roof displacement associated with an inter-story drift limit of 0.3%, an equivalent natural period can be obtained. As shown in Figure 8.18, at an inter-story drift ratio of 0.3%, the overall displacement is 0.57 in.

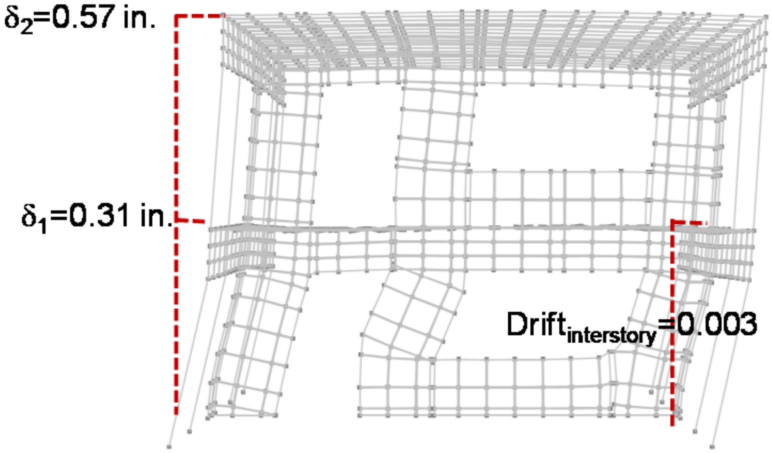

Figure 8.18 Overall displacemnt at target drift of 0.3% for DBE

As shown in Figure 8.19, using the overall displacement of 0.57 in., an equivalent natural period of 0.27 sec. can be determined from the displacement response spectrum.

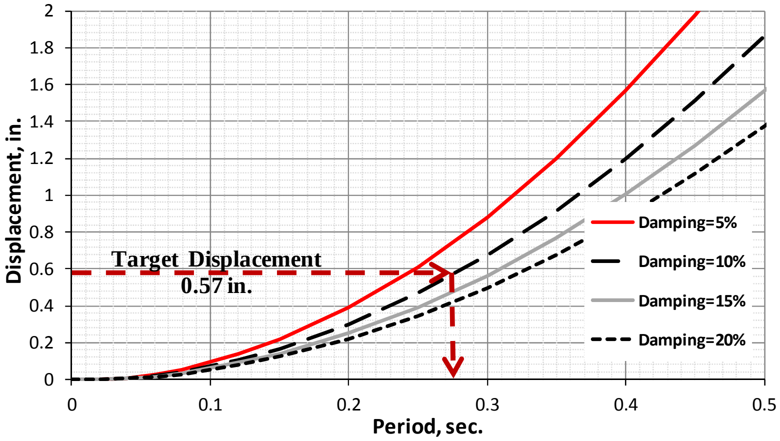

Figure 8.19 Equivalent natural period of two-story specimen at DBE

8.4.4.2 Equivalent Natural Period at MCE

Using the MCE response spectrum for 15% damping at the target roof displacement associated with a 0.7% inter-story drift limit, an equivalent natural period can be obtained. As shown in Figure 8.20, with 0.7% inter-story drift ratio, the overall displacement is 1.16 in.

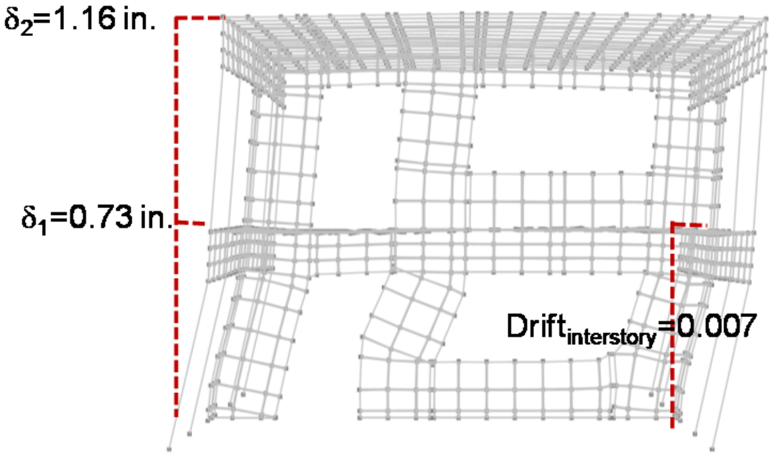

Figure 8.20 Overall displacement at target drift ratio of 0.7% for MCE

As shown in Figure 8.21, using the overall displacement of 1.16 in., an equivalent natural period of 0.35 sec. can be determined from the displacement response spectrum.

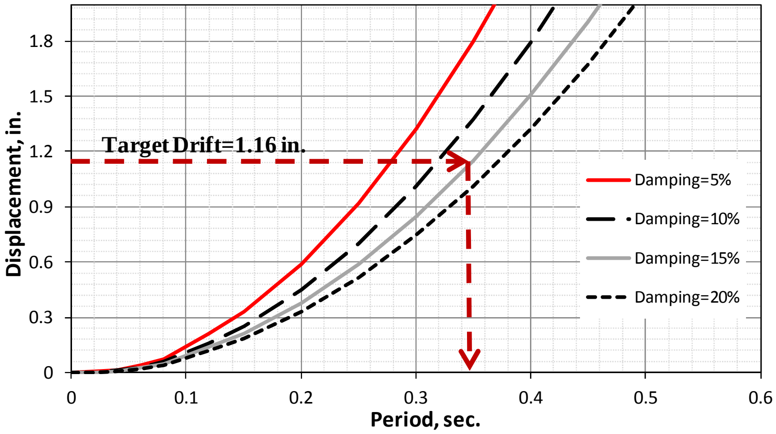

Figure 8.21 Equivalent natural period of two-story specimen at MCE

8.4.5 Step 5: Required Equivalent Lateral Stiffness for UCSD Two-Story Specimen

Representing the specimen as an equivalent linear SDOF system, the required equivalent lateral stiffness $(k_{eq})_r$ can be obtained, using the equivalent natural periods calculated in the previous step, and the specimen's effective seismic mass. The two-story specimen has a gravitational and inertial mass M. The specimen's effective mass in this step is calculated using an increased inertial mass of 1.7M, with the increased inertial mass accounted for by adding more inertial mass to the specimen and scaling the gravity loads in the nonlinear pushover model.

8.4.5.1 Required equivalent lateral stiffness at DBE

The required equivalent lateral stiffness and the required base shear can be calculated using

$$\left(k_{eq}\right)_r = \frac{4\pi^2 W_{eff}}{\mathrm{g}T_{eq}^2}$$

where W_{eff} is the effective weight, can be calculated from the deflected shape in Figure 8.18 in Step 4.

$$W_{eff} = \frac{(\sum W_i u_i)^2}{W_i {u_i}^2}$$

Detailed calculations of the applied floor gravity loads modified with inertial mass scaling factor of 1.7 for the specimen are presented in Appendix H. Based on the gravity load calculations, total weight of the roof level and the ground floor are 105.4 and 131.9 kips, respectively.

$$W_{eff} = \frac{(131.9\ kip \times 0.31\ in. + 105.4\ kip \times 0.57\ in.)^2}{(131.9\ kip \times 0.31^2\ in.^2 + 105.4\ kip \times 0.57^2\ in.^2\ )}$$

$$W_{eff} = 217\ kip$$

The required stiffness is

$$\left(k_{eq}\right)_r = \frac{4\pi^2 W_{eff}}{\mathrm{g}T_{eq}^2} = \frac{4\pi^2 \times 217\ kip}{386.09\ in./sec^2 \times 0.27^2\ sec^2} = 304\ \frac{kip}{in.}$$

and the required base shear is

$$(V_{base})_r = 304\ \frac{kip}{in.} \times 0.57\ in. = 173\ kip$$

8.4.5.2 *Required equivalent lateral stiffness at MCE*

The required equivalent lateral stiffness and the required base shear can be calculated using

$$\left(k_{eq}\right)_r = \frac{4\pi^2 W_{eff}}{\mathrm{g}T_{eq}^2}$$

where W_{eff} is the effective weight, calculated from the deflected shape in Figure 8.20 in Step 4.

$$W_{eff} = \frac{(\sum W_i u_i)^2}{W_i {u_i}^2}$$

$$W_{eff} = \frac{(131.9\ kip \times 0.73\ in. + 105.4\ kip \times 1.16\ in.)^2}{(131.9\ kip \times 0.73^2\ in.^2 + 105.4\ kip \times 1.16^2\ in.^2\ )}$$

$$W_{eff} = 225\ kip$$

The required stiffness is

$$\left(k_{eq}\right)_r = \frac{4\pi^2 W_{eff}}{\mathrm{g}T_{eq}^2} = \frac{4\pi^2 \times 225\ kip}{386.09\ in./sec^2 \times 0.35^2\ sec^2} = 187\ \frac{kip}{in.}$$

and the required base shear is

$$(V_{base})_r = 187\ \frac{kip}{in.} \times 1.16\ in. = 217\ kip$$

8.4.6 Step 6: Actual Equivalent Lateral Stiffness for Two-Story Specimen

In this step, the capacity curve from a static pushover analysis and target displacements is used to calculate actual equivalent lateral stiffnesses (at the target displacements) at DBE and MCE levels. Using the capacity curves obtained from the PERFORM 3D program and shown in Figure 8.17, the actual equivalent lateral stiffness of each hazard level can be obtained at the target displacement.

8.4.6.1 Actual equivalent lateral stiffness of two-story specimen at DBE

As shown in Figure 8.22, using the overall displacement of 0.57 in., an equivalent lateral stiffness of 291 kip/in. can be determined from the capacity curve.

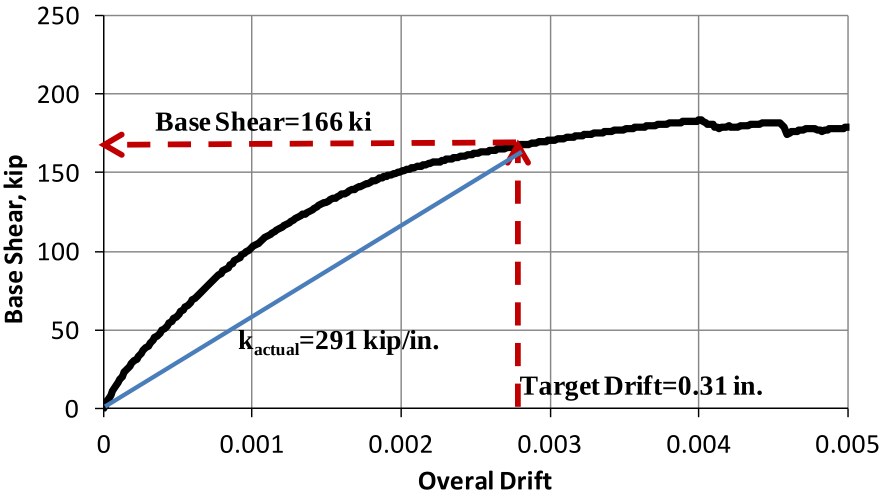

Figure 8.22 Calculation of the actual equivalent lateral stiffness of two-story specimen at DBE

$$\left(k_{eq}\right)_{actual} = \frac{166\ kip}{0.57\ in.} = 291\ \frac{kip}{in.}$$

$$(V_{base})_{actual} = 166\ kip$$

8.4.6.2 Actual equivalent lateral stiffness of two-story specimen at MCE

As shown in Figure 8.23, using the overall displacement of 1.16 in., an equivalent lateral stiffness of 151 kip/in. can be determined from the capacity curve.

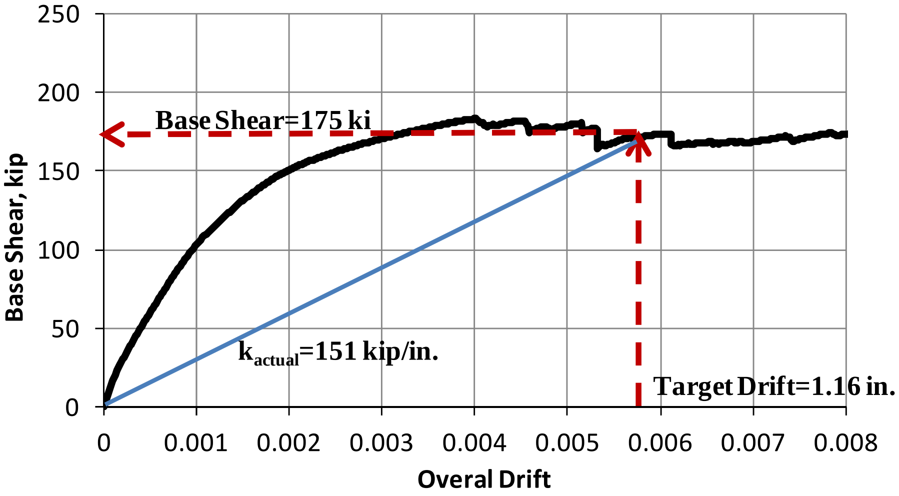

Figure 8.23 Calculation of the actual equivalent lateral stiffness of two-story specimen at MCE

$$(k_{eq})_{actual} = \frac{175\ kip}{1.16\ in.} = 151\ \frac{kip}{in.}$$

$$(V_{base})_{actual} = 175\ kip$$

8.4.7 Step 7: Verify Lateral Stiffness for Two-Story Specimen

In this step, the actual stiffness values are compared to the required equivalent lateral stiffness corresponding to each hazard level.

8.4.7.1 Comparison of actual and required lateral stiffness at DBE

These results indicate that the structural actual and required lateral stiffnesses at DBE level are close; however, the required stiffness is slightly greater than the actual lateral stiffness.

$$\left(k_{eq}\right)_r = 304\ \frac{kip}{in.}$$

$$\left(k_{eq}\right)_{actual} = 291\ \frac{kip}{in.}$$

8.4.7.2 Comparison of actual and required lateral stiffness at MCE

These results indicate that the required stiffness is greater than the actual stiffness.

$$\left(k_{eq}\right)_r = 187\ \frac{kip}{in.}$$

$$\left(k_{eq}\right)_{actual} = 151\ \frac{kip}{in.}$$

For this reason, the required lateral stiffness of the building can be modified by reducing the inertial mass factor of 1.7.

8.4.8 Step 8: Required Base Shear Capacity and Structural Detailing for Two-Story Specimen

Using pushover analysis results, base shear and local deformation demands for the wall segments of the two-story specimen can be calculated for each hazard level. Using capacity curves, the required base shear capacities at DBE and MCE hazard levels are 166 and 175 kips, respectively. In Figure 8.24 are shown the maximum deformation demands in ground-level Walls W-1, W-2, and W-3, under the DBE- and MCE-level shakings. Calculated maximum deformation demands are total relative lateral displacement between ends of each wall segment, divided by the height of that segment, and expressed in percent. The total lateral displacement demands and capacities of each wall segment are combinations of flexural and shearing deformations.

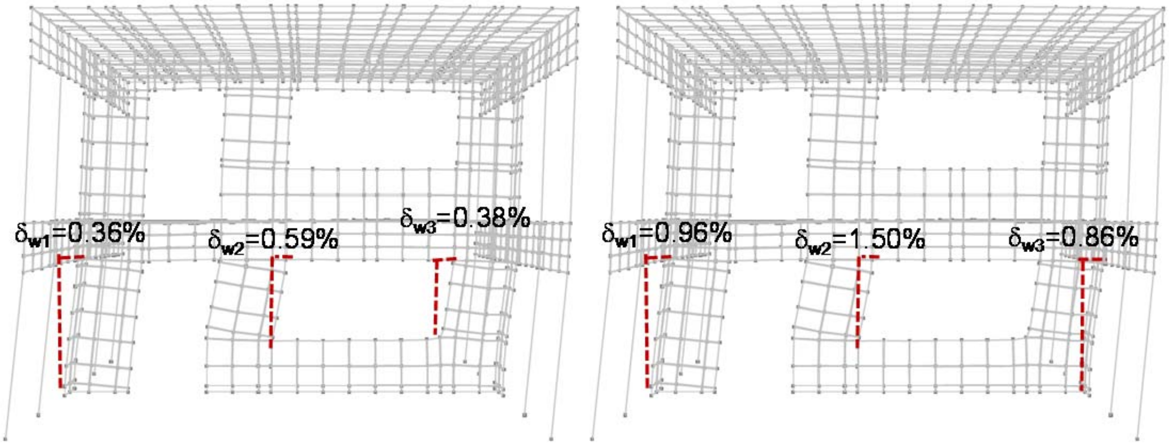

Local deformation demands at DBE *Local deformation demands at MCE*

Figure 8.24 Local deformation demands in wall segments of two-story specimen

Wall W-2 is critical, with the highest deformation demand at the ground level, and the lowest deformation capacity (because it is shear-controlled). As shown in Figure 8.24, the inelastic drift demand on Wall W-2 at the ground level is 0.59% at DBE, and

1.50% at MCE level. These local deformation demands exceed the expected deformation capacities discussed in Section 8.4.1 for shear-controlled wall elements.

In addition, these base shear and local deformation demands at both DBE and MCE levels are used for the following steps:

1. Control the elastic wall segments as force-controlled components, and reinforce each elastic wall segment for sufficient strength at the target displacement;
2. Control the axial load in shear- and flexure-controlled wall segments as force-controlled components, to confirm their structural stability; and
3. Reinforce each wall segment for sufficient inelastic shearing deformation capacity in shear hinging regions or for sufficient inelastic rotation capacity in flexural hinging regions.

8.4.9 Design Summary of Two-Story Specimen

As shown in Figure 8.25, the webs of Walls W-1 and W-3 require flexural reinforcement consisting of No. 4 bars at 16 in., and the 24-in. flanges require two No. 4 longitudinal bars. Transverse reinforcement consists of No. 4 horizontal bars at 16 in. in the webs and flanges. The 40-in. lineal Wall W-2 had longitudinal reinforcement consisting of No. 4 bars at 16 in., and transverse reinforcement consisting of No. 4 horizontal bars at 16 in. Drawings and details for the two-story specimen are provided in Appendix I.

Horizontal reinforcement in walls was placed starting in the lowest course. Control joints were introduced on each side of the lintel beams above door openings, and the flexural reinforcing bars in the lintels were de-bonded in regions beyond the control joints to reduce the coupling moments transmitted to the wall elements. Wall segments had vertical reinforcement spliced at the base, as permitted by the MSJC *Code*.

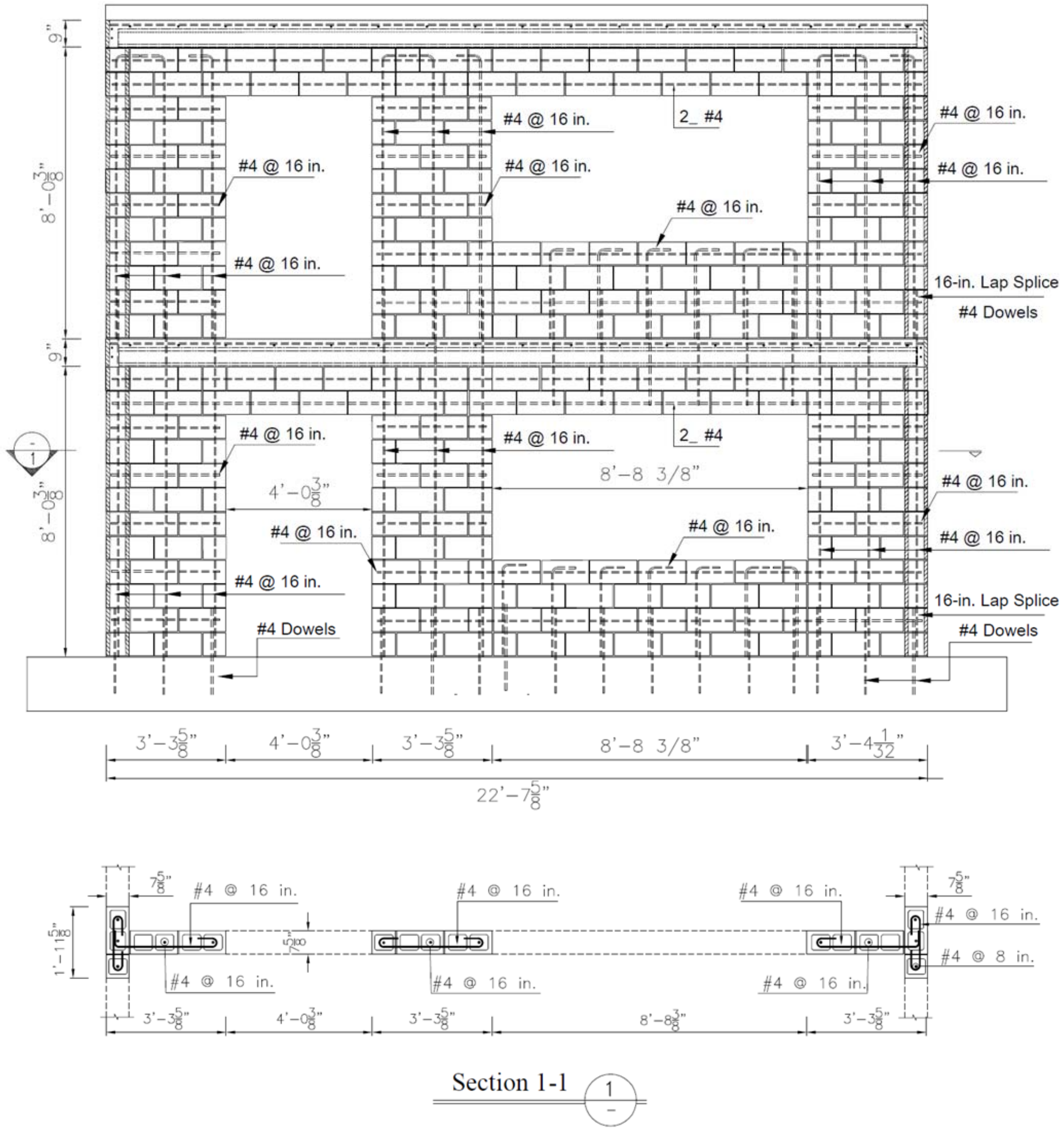

Figure 8.25 Detailing of reinforcement in web of two-story specimen

8.5 CONSTRUCTION OF 2-STORY SPECIMEN

The construction of the 2-story specimen lasted four weeks in the summer of 2012. The following pictures show the construction of the specimen, including the construction sequence and different components of the building specimen that might not have been clear in the specimen description in this chapter.

Figure 8.26 Footing formwork and reinforcement ready for casting, 2-story specimen

Figure 8.27 Casting of reinforced concrete footing, 2-story specimen

Figure 8.28 Laying hollow CMU

Figure 8.29 Placing horizontal reinforcement

Figure 8.30 Detail of horizontal reinforcement in T-walls

Figure 8.31 Laying lintels

Figure 8.32 Control joint detail

Figure 8.33 De-bonding of longitudinal reinforcement at control joints

Figure 8.34 Placing 90-degree hooks for floor-wall intersection

Figure 8.35 Grouting wall segments

Figure 8.36 Vibrating grout

Figure 8.37 Placing prestressed concrete planks on walls

Figure 8.38 Sealing gap between planks before placing topping

Figure 8.39 Bending 90-degree hooks for floor-wall intersection

Figure 8.40 Reinforcement for concrete topping

Figure 8.41 Casting concrete topping

Figure 8.42 Constructing second story

Figure 8.43 Casting roof topping

8.6 INSTRUMENTATION OF TWO-STORY SPECIMEN

An array of about 400 sensors (strain gauges, displacement transducers, and accelerometers) was deployed on the specimen to measure accelerations, displacements, and strains at various locations of the specimen. Displacement transducers were used to monitor the wall segment deformations and floor displacements with respect to the table. The interstory lateral deformations were measured with the use of aluminum reference frames which had very small mass and high stiffness so that their deformations were negligible as compared to displacements they would measure (Stavridis 2009). In addition the specimen was instrumented with a variety of strain gauges, linear potentiometers, string potentiometers, linear variable differential transformers (LVDT). The reinforcement of the specimen was instrumented with strain gauges at critical locations. Emphasis was given at the lap-splice regions and at the locations where yielding was anticipated. Linear potentiometers were located on the specimen to monitor local shear and flexural deformations, incremental vertical deformations at the ends of the wall segments, axial deformations, sliding between foundation and shear wall panels, control joints, and any potential sliding between floors and shear wall panels. The instrumentation scheme for the 2-story CMU building specimen is shown in Appendix H. Figure 8.44 shows some examples of the instrumentation scheme for the specimen in the first story. To determine whether the displacement data are reliable, consistency with other displacement data was checked using structural symmetry or the location of the measuring device on the reference frame system.

Figure 8.44 First-story instrumentation of two-story specimen

8.7 PREDICTED RESPONSE OF TWO-STORY SPECIMEN

Using PERFORM 3D, the response of the 2-story specimen is predicted under the input motions as shown in Figure 8.45, sequenced as shown in Table 8-2. The structure is assigned a gravitational and inertial mass M; the inertial mass is increased to 1.70M in time-history analyses.

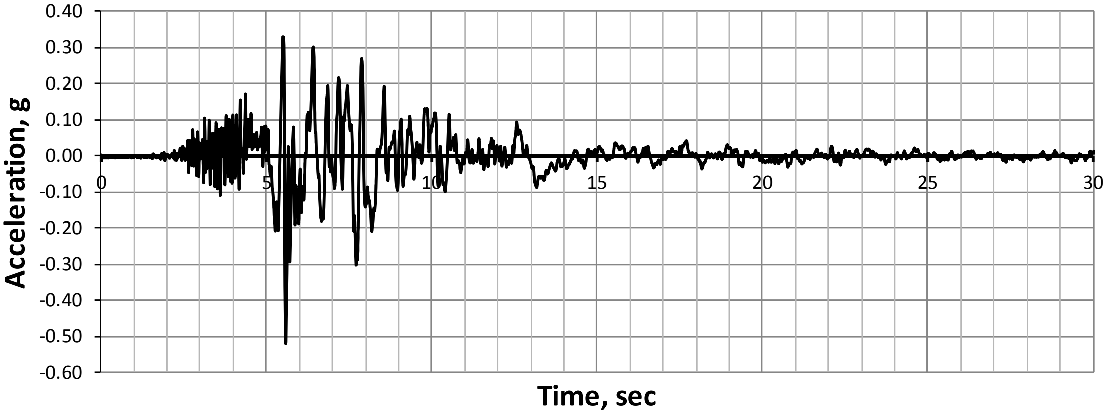

Figure 8.45 Unscaled El Centro 1979 ground motion used for time-history analyses

Table 8-2 Input motions and scale factors used for time-history analyses

order	ground motion	hazard level
1	**30% El Centro 1979**	
2	**43% El Centro 1979**	0.50 DBE
3	**86% El Centro 1979**	0.80 DBE
4	**108% El Centro 1979**	Slightly above DBE
5	**145 % El Centro 1979**	Slightly below MCE
6	**160% El Centro 1979**	above MCE

8.7.1 Results of Time-History Analyses

Results of the time-history analyses, summarized in Table 8-3, include the maximum predicted deformation demands in ground-level Walls W-1, W-2, and W-3. Shown in Figure 8.46 are the maximum local deformation ratios in each ground-level segment. Presented maximum deformation demands are total relative lateral displacement between ends of each wall segment, divided by the height of that segment, and expressed in percent. The total lateral displacement of each wall segment includes flexural deformation and shear deformations.

Table 8-3 Overview of results of time-history analyses, 2-story specimen

order	ground motion	PGA, g	inter-story drift, %		base shear, kips	maximum local deformation, %		
			positive direction	negative direction		W-1	W-2	W-3
1	**30% El Centro**	-0.263	0.07	0.05	73	0.09	0.13	0.12
2	**43% El Centro**	-0.385	0.103	0.062	104	0.14	0.19	0.18
3	**86% El Centro**	-0.656	0.23	0.10	158	0.28	0.44	0.44
4	**108% El Centro**	-0.747	0.28	0.17	175	0.41	0.62	0.64
5	**145% El Centro**	-1.025	0.42	0.28	195	0.59	0.95	0.98
6	**160% El Centro**	-0.919	0.50	0.36	198	0.72	1.10	1.12

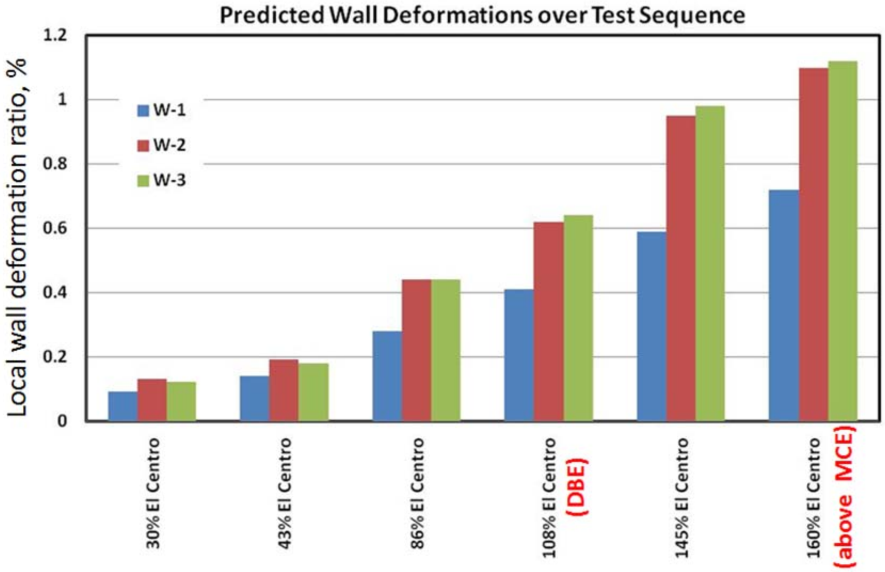

Figure 8.46 Maximum local deformation ratios for each ground-floor wall segment

In Figure 8.47 are shown the maximum predicted local deformation ratios in ground-level wall segments W-1, W-2, and W-3, under the scaled 108% El Centro ground motion (slightly above DBE).

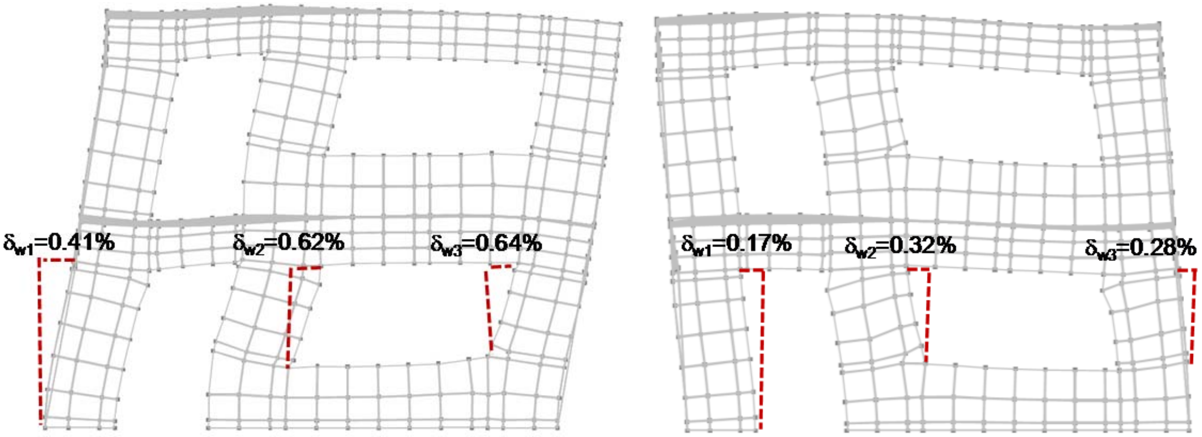

Figure 8.47 Maximum predicted local deformation ratios under 108% El Centro

In Figure 8.48 are shown the maximum predicted local deformation ratios in ground-level wall segments W-1, W-2, and W-3, under the scaled 160% El Centro ground motion (above MCE).

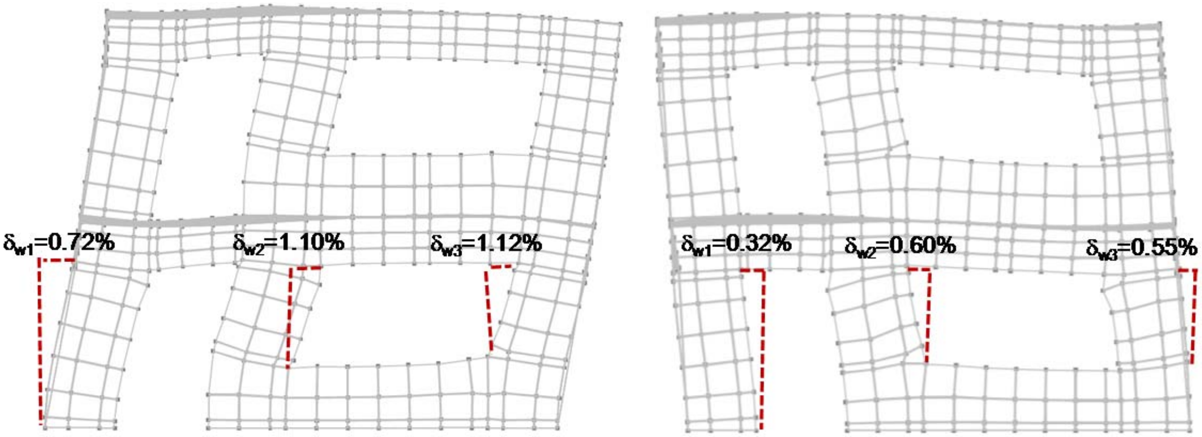

Figure 8.48 Maximum local deformation ratios under 160% El Centro

8.7.2 Predicted Behavior of 2-Story Specimen

In Figure 8.49 are shown local deformation ratios versus expected deformation capacities for each ground-level wall segment over the test sequence. Walls W-2 and W-3 are critical, with the highest predicted local deformation ratios at the ground level, and the lowest deformation capacities, because these segments are shear-controlled. Based on cyclic test results, flexure-controlled wall segments (such as Wall W-1) can withstand a local deformation ratio of 1.5% at MCE level, while shear-controlled wall segments (such as Segments W-2 and W-3) can withstand a local deformation ratio of 1.0% at MCE level.

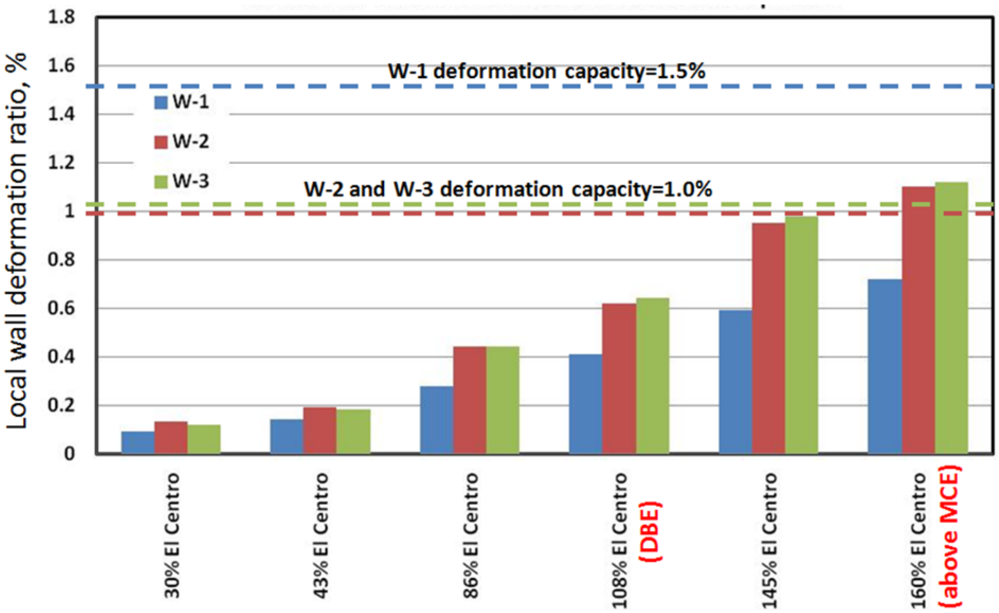

Figure 8.49 Deformation demand versus capacity for each ground-level wall segment over test sequence

Comparing local drift-ratio demands with capacities for each ground-level wall segment, the 2-story specimen can be expected to safely withstand 145% El Centro (slightly below MCE) and 160% El Centro ground motions (above MCE). However, under 160% El Centro ground motion (above MCE), local deformation demands on wall segments W-2 and W-3 slightly exceed the expected deformation capacities, and the specimen could collapse after 160% El Centro (above MCE). The input sequence was proposed for use through 160% El Centro, and was suggested for use with caution beyond that level.

8.8 SUMMARY OF SHAKE-TABLE TESTS AND TEST RESULTS FOR 2-STORY SPECIMEN

Between September 5 and September 12, 2012, the 2-story specimen was subjected to an extended series of ground motions. In this section, the test history and specimen response are first summarized, and the significance of that response is then discussed. Figure 8.50 shows the completed structure on the shaking table on the testing day. The shake-table testing and the test results will be described in detail in the PhD dissertation now being prepared by Marios Mavros at the University of California at San Diego (UCSD).

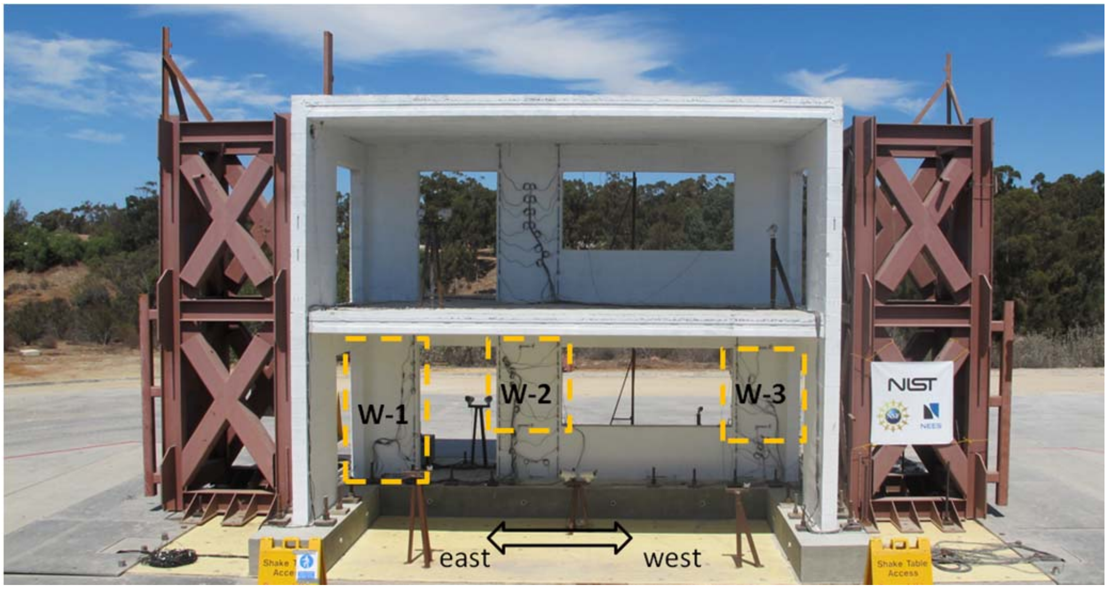

Figure 8.50 Two-story specimen on UCSD shake-table

8.8.1 Sequence of Ground Motions used in Shake-table Tests of 2-Story Specimen

The shake-table tests used a series of El Centro ground-motions of Imperial Valley 1979 earthquake factored (scaled) as discussed below. The record was obtained from the Center for Engineering Strong Motion Data (www.strongmotioncenter.org); its characteristics are summarized in Table 8-4 and it is shown (before scaling) in Figure 8.45. This ground motion was later modified during the test, based on the shake-table performance at each shaking level.

Table 8-4 Characteristics of ground motion (El Centro 1979) used for testing of 2-story specimen

Earthquake	Year	Magnitude	Motion	PGA (g)	PGV (cm/s)	Duration (s)	Time-step (s)
Imperial Valley	1979	7.0	El Centro	0.519	46.9	39.2 s	0.005

8.8.1.1 Scaling of inertial mass in testing 2-story specimen

When the 2-story specimen was tested, its inertial mass was increased by a factor of 1.7 to ensure that sufficient lateral force could be applied to the structure to reach its calculated base shear capacity. This increase was also a convenient way to impose increased inertial mass without increasing gravitational mass (which could have increased the shear capacity of the in-plane walls). This increase in inertial mass was simulated by scaling the ordinates and time scale of the ground motion, as explained in Table 8-5. Suppose that an undamped single-degree-of-freedom (SDOF) system with mass αM and stiffness K is shaken by sinusoidal ground motion with frequency p. The maximum response of that system is identical to the maximum response of an undamped SDOF system with mass M and stiffness K, shaken by sinusoidal ground motion with frequency$\sqrt{\alpha}\,p$, and maximum ordinates equal to α times those of the original ground motion. By implication (verified analytically), the same relationships hold for a nonlinear multi-degree-of-freedom system subjected to general earthquake ground motion. If we wish to increase the inertial mass of our specimen by a factor α, we can achieve exactly the same result by increasing frequency of the ground motion by a factor $\sqrt{\alpha}$, and scaling that accelerations by a factor α. In these series of tests, the inertial mass is increased to 1.70M by scaling the ordinates of the acceleration of ground motion by a factor of 1.70, and by scaling the time values of the ground motion by a factor of $1/\sqrt{1.70}$.

Table 8-5 Inertial mass scaling for SDOF systems

Original Mass, Original Ground Motion 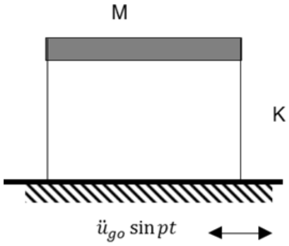 	This original SDOF system has a circular frequency $\omega = \sqrt{\frac{K}{M}}$ and a corresponding period $T = 2\pi\sqrt{\frac{M}{K}}$. Its maximum response to the original sinusoidal ground motion at frequency *p* is $u_{max} = \frac{-M\,\ddot{u}_{go}}{1-\frac{p^2\,M}{K}}$
Increased Mass, Original Ground Motion 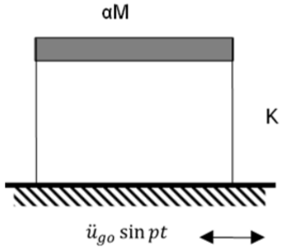 	This SDOF system with increased mass has a circular frequency $\omega = \sqrt{\frac{K}{\alpha M}} = \frac{1}{\sqrt{\alpha}}\sqrt{\frac{K}{M}}$ and a corresponding period $T = 2\pi\sqrt{\alpha}\sqrt{\frac{M}{K}}$. Its maximum response to the original sinusoidal ground motion at frequency p is $u_{max} = \frac{-(\alpha M)\,\ddot{u}_{go}}{1-\frac{p^2\,(\alpha M)}{K}}$
Original Mass, Modified Ground Motion 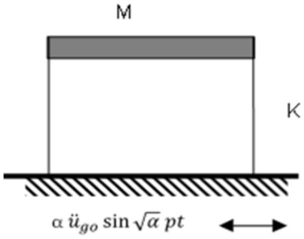 	This SDOF system has a circular frequency $\omega = \sqrt{\frac{K}{M}}$ and a corresponding period $T = 2\pi\sqrt{\frac{M}{K}}$. Because this original SDOF system has a lower mass and the same stiffness as the second SDOF system, its circular frequency is greater than that of the second SDOF system by a factor $\sqrt{\alpha}$.. To preserve the same relationship between the frequency of the structure and the frequency of the ground motion, the frequency of the input motion must be increased by the same factor $\sqrt{\alpha}$. The ordinates of the original ground motion are also scaled by α. The maximum response of this system to the modified sinusoidal ground motion at frequency $\sqrt{\alpha}\,p$ is $u_{max} = \frac{-M\alpha\,\ddot{u}_{go}}{1-\frac{(\sqrt{\alpha}p)^2\,M}{K}}$ This is identical to the response of the system with increased mass, under the original ground motion.

In Figure 8.51, the response spectra for the El Centro 1979 ground motions (scaled to DBE and MCE levels and factored by 1.70) are compared with design response spectra at the DBE and MCE levels (also factored by 1.70). The initial fundamental period of the structure was 0.07 sec, and at the beginning of very last shaking it was 0.21 sec. As shown in Figure 8.51, 160% El Centro is about MCE for structural period of 0.21 sec. One concern is the spike in the spectrum at a period of 0.27 sec., corresponding to a strong pulse in the ground motion.

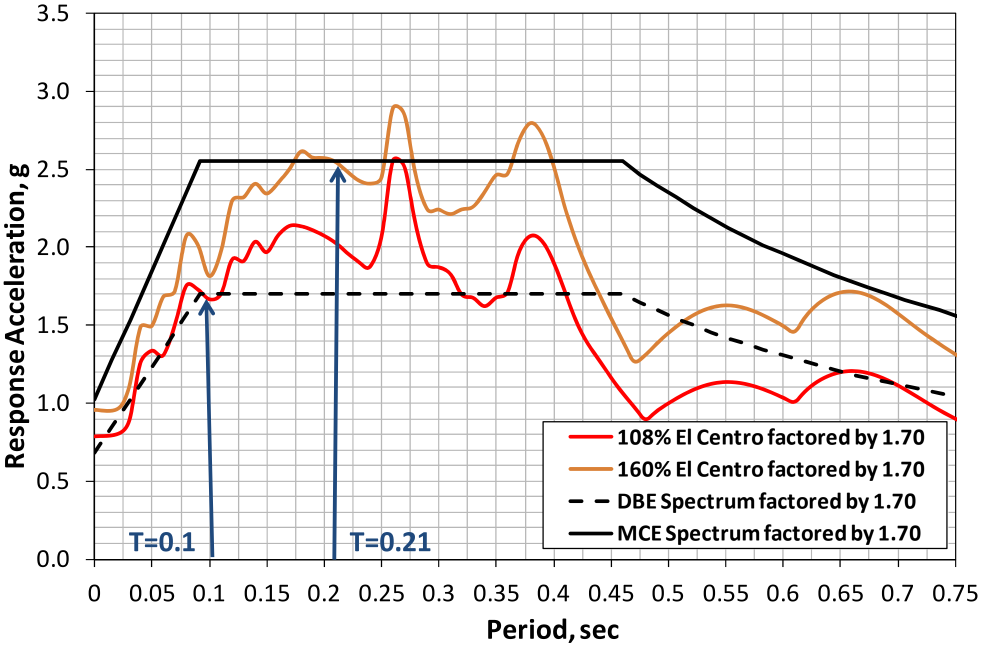

Figure 8.51 Response spectra (El Centro 1979 with inertial mass factor of 1.70) after scaling to DBE and MCE levels

8.8.1.2 Test sequence for 2-story specimen

In Table 8-6, the sequence of ground motions used to test the 2-story specimen is summarized, along with the Peak Ground Acceleration (PGA) measured from the table for each ground motion. Ground motions were interspersed with white-noise excitation to assess the increase in periods of the specimen from the start to the end of the testing. The white noise had a root-mean-squared acceleration of 0.03 g, and swept a frequency range of 1 – 33 Hz.

Table 8-6 Test sequence for 2-story specimen

Date	Test	Measured PGA
Thursday, 6 September 2012	10 minutes ambient vibration	
	5 minutes white noise	
	15% of El Centro 1979	**0.24 g**
	5 minutes white noise	
	25% of El Centro 1979	**0.36 g**
	5 minutes white noise	
	10 minutes ambient vibration	
Friday, 7 September 2012	10 minutes ambient vibration	
	5 minutes white noise	
	30% of El Centro 1979	**0.27 g**
	5 minutes white noise	
	43% of El Centro 1979	**0.39 g**
	5 minutes white noise	
	86% of El Centro 1979	**0.66 g**
	5 minutes white noise	
	10 minutes ambient vibration	
Monday, 10 September 2012	10 minutes ambient vibration	
	5 minutes white noise	
	108% of El Centro 1979	**0.75 g**
	5 minutes white noise	
	145% of El Centro 1979	**1.02 g**
	5 minutes white noise	
	10 minutes ambient vibration	
Tuesday, 11 September 2012	10 minutes ambient vibration	
	5 minutes white noise	
	160% of El Centro 1979	**0.92 g**

8.8.2 Overall Behavior of 2-story Specimen

Key behaviors of the 2-story specimen are listed in Table 8-7. Most of the visible damage took place during the run to El Centro 145% (slightly below MCE). During that run, the specimen experienced top sliding of Wall W-2; distributed diagonal shear cracks in Wall W-3; and flexural cracks at the base and splice ends, combined with minor diagonal shear cracks, in Wall W-1.

During the run to El Centro 160% (above MCE), severe damage occurred in the first floor, as shown in Figure 8.52. Wall W-1 experienced flexural hinging at the base; Wall W-2 experienced severe shearing degradation; and Wall W-3 experienced flexural hinging in one direction, and shear hinging in the other direction.

Figure 8.52 Severe damage in first floor of 2-story specimen, 160% El Centro 1979 (above MCE)

Table 8-7 Summary of test history and specimen response

Ground Motion	Level of Excitation	Observations
15% El Centro 1979		No visible damage was observed. Structural period T before and after test was about 0.067 sec.
25% El Centro 1979		No visible damage was observed.
30% El Centro 1979		No visible damage was observed.
43% El Centro 1979	0.50 DBE	Hairline cracking was observed at the bases of the W-1 Wall segment and out-of-plane walls max. 1st story drift = 0.03%.
86% El Centro 1979	0.80 DBE	Hairline cracking was observed at the bases of the W-1 wall segment and out-of-plane walls, indicating flexural cracking of the W-1 in-plane wall and the out-of-plane walls; flexural cracks developed at ends of lintel beam near control joints and the window opening corners at the first floor; a diagonal crack observed below W-3 wall segment; max. 1st story drift = 0.12%; structural period after test was about 0.09 sec.
108% El Centro 1979	DBE	More cracking was observed at the bases of the W-1 wall segment and out-of-plane walls, indicating flexural cracking of the W-1 in-plane wall and the out-of-plane walls; more cracks developed at ends of lintel beam near control joints and the window opening corners at the first floor; W-2 wall (middle wall) had very minor top sliding; diagonal crack extended below W-3 wall segment; max. 1st story drift = 0.21%; structural period T after test was about 0.10 sec.
145 % El Centro 1979	Slightly below MCE	Flexural cracks developed at wall base of Wall W-1 (west T-wall); a diagonal shear cracks developed in Wall W-1; horizontal crack extended at the top of W-2 wall (middle wall) segment, followed with shear sliding at that line; flexural-shear cracks developed below W-2 wall segment; distributed web-shear cracks formed in Wall W-3 (east T-wall) in both directions; vertical cracks developed in the intersection between web and flange in in both 1st story T-walls; minor cracks observed in 2nd story wall segments in the edges of openings and control joints; horizontal flexural cracks develop near top and base of out of plane walls and flanges; max. 1st story drift = 0.40%; structural period T after test was about 0.21 sec.
160% El Centro 1979	above MCE	Structure was severely damaged; wide diagonal cracks formed in the 1st story W-2 and W-3 wall segments; the opened shear crack in wall segment W-2 extended through the flange; diagonals crushed; significant spalling of the diagonal strut face shells; residual opening of the web-shear crack of 2.0 in. ; wall W-2 (middle wall) slid on the top about 0.25 in.; opened flexural cracks at the base and top of out-of-plane walls in the 1st and 2nd stories; max. 1st story drift = 1.9%, period T after test was 0.84s.

8.8.3 Detailed Behavior of 2-Story Specimen

Initial response of the 2-story specimen was marked by vertical and horizontal cracks at the dog-leg control joints at both ends of the lintel connecting Walls W-1 and W-2. At DBE-level ground motion (108% El Centro 1970), cracks formed at the edges of the ground-floor window opening (Figure 8.53). Although the longitudinal reinforcement passing through the lintel had been de-bonded on one side of each control joint, the strong connection between the precast planks and the wall segments caused the lintels to move with the planks rather than the walls, and caused some lintel cracking. In addition, flexural cracks formed at the base of Wall W-1, and a diagonal crack formed below Wall W-3.

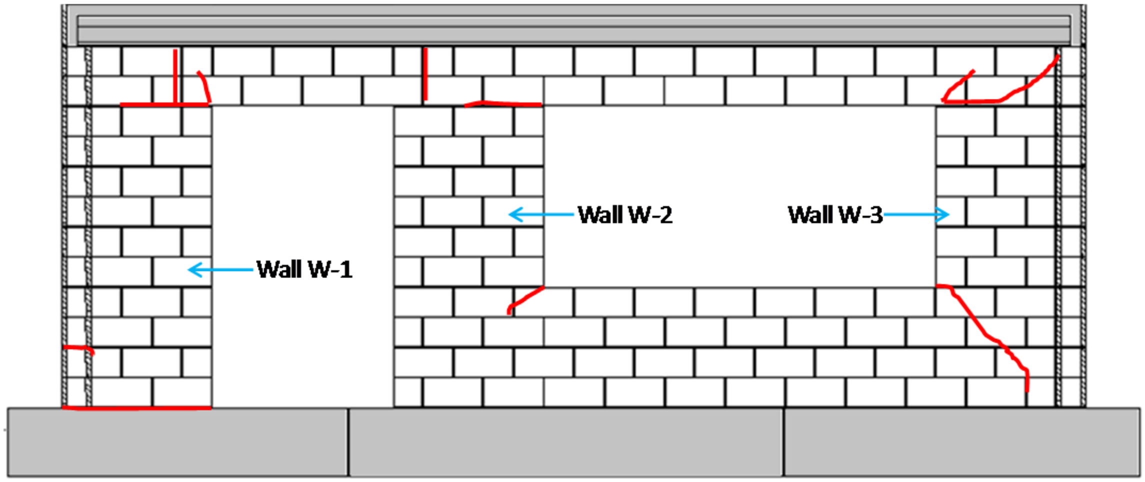

Figure 8.53 Observed cracks in first story of 2-story specimen, 108% El Centro 1979 (above DBE)

As shown in Figure 8.54, Figure 8.55, and Figure 8.56, shaking between DBE and MCE (145% El Centro 1979) caused diagonal shear cracking in Wall W-1 (Figure 8.55), minor top sliding of Wall W-2, and distributed shear cracks in Wall W-3 (Figure 8.56). This ground motion also produced additional flexural cracking at the base and top of Wall W-1, horizontal and diagonal shear cracking at the wall segment below Wall W-2, , and out-of-plane flexural cracking at the bases and tops of the out-of plane walls.

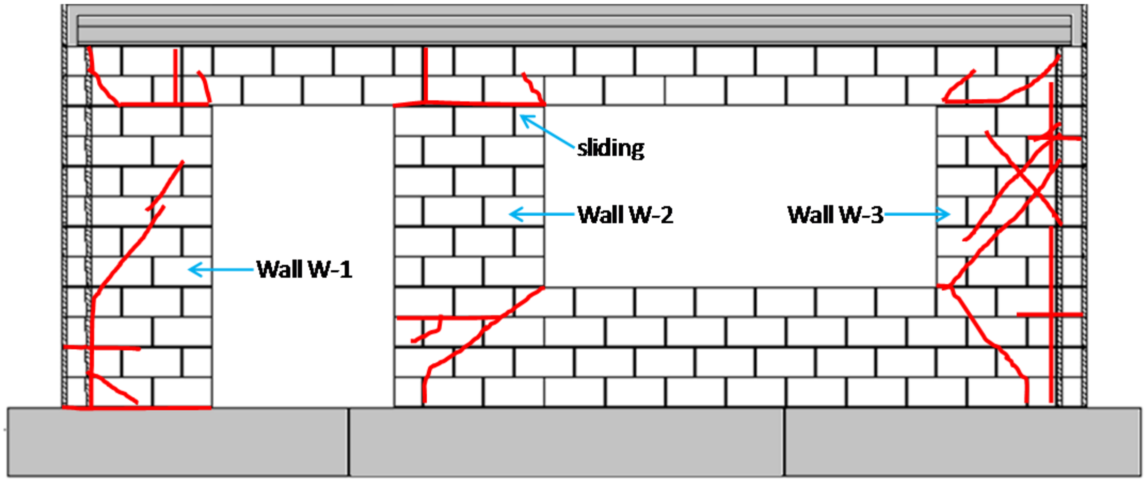

Figure 8.54 Observed crack in first story of 2-story specimen, 145% El Centro 1979 (below MCE)

Figure 8.55 Diagonal shear cracking of Wall W-1 after 145% El Centro 1979

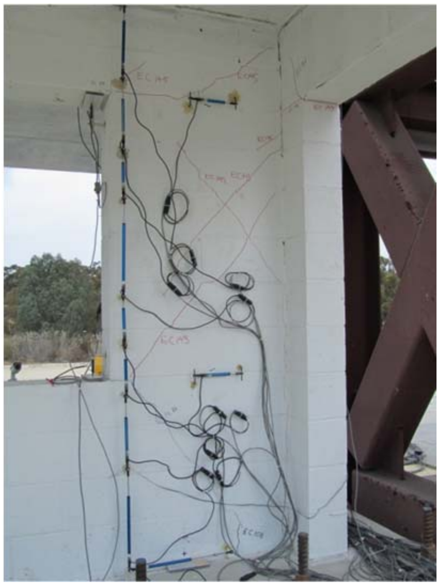

Figure 8.56 Shear cracking of Wall W-3 after 145% El Centro 1979

As shown in Figure 8.57, continued shaking with 160% El Centro 1979 (above MCE) caused distributed flexural and shear cracks in Wall W-1 (Figure 8.58 and Figure 8.59); significant sliding at the top of Wall W-2 at the beginning of shaking; followed by extensive diagonal cracks and shear failure of Wall W-2 (Figure 8.60 through Figure 8.64); the widening of shear cracks in Wall W-3 (Figure 8.65 through Figure 8.67); the crushing of the diagonal struts and face-shell spalling in Walls W-2 and W-3; and out-of-plane flexural cracking at the bases and tops of the out-of plane walls (Figure 8.68). In addition, this ground motion produced vertical cracks along the length of Walls W-1 and W-3 (T-walls) between flanges and webs (Figure 8.69).

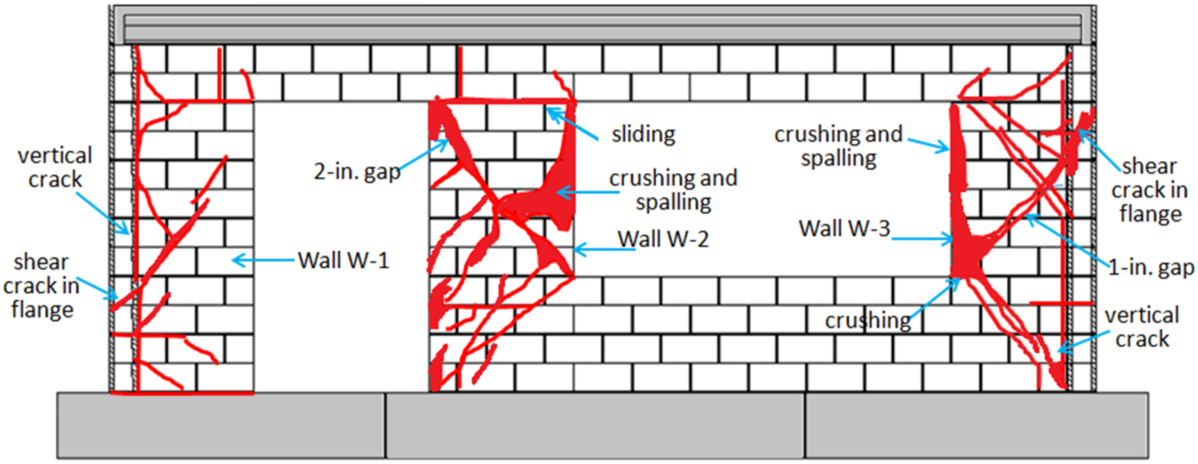

Figure 8.57 Observed damage in first story of 2-story specimen, 160% El Centro 1979 (above MCE)

Figure 8.58 Flexural and shear cracking in Wall W-1 (160% El Centro 1979)

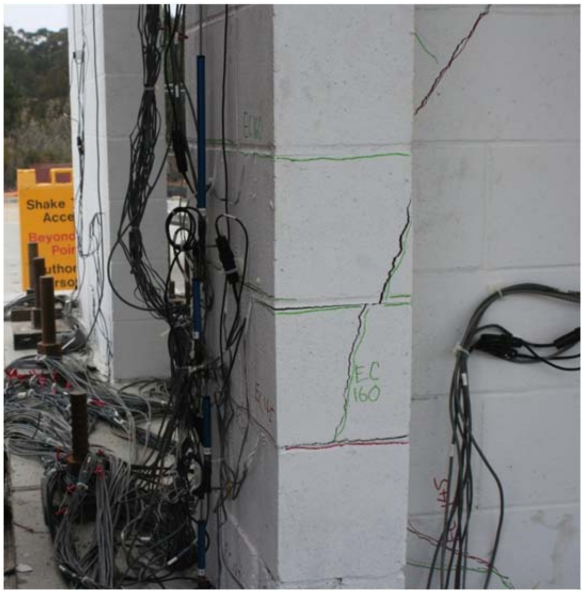

Figure 8.59 Extended shear crack in web of Wall W-1 (160% El Centro 1979)

Figure 8.60 Wall W-2 after 160% El Centro

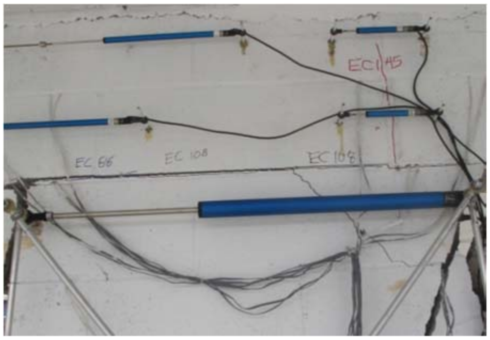

Figure 8.61 Sliding of Wall W-2 (160% El Centro)

Figure 8.62 Crushing of diagonal strut in Wall W-2 (160% El Centro)

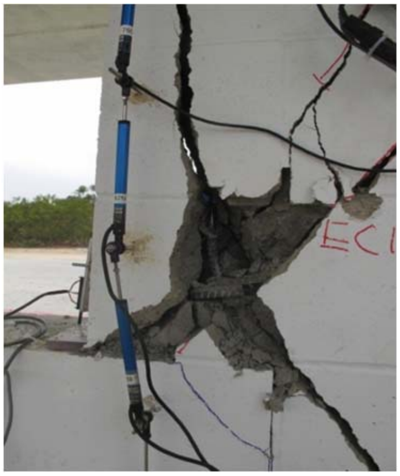

Figure 8.63 Damage to corner of Wall W-2 (160% El Centro)

Figure 8.64 Extensive crushing and spalling of Wall W-2 (160% El Centro)

Figure 8.65 Wall W-3 after 160% El Centro

Figure 8.66 Extended shear crack in flange of Wall W-3 (160% El Centro)

Figure 8.67 Damage to flange of Wall W-3 (160% El Centro)

Figure 8.68 West out-of-plane wall after 160% El Centro 1979

Figure 8.69 Vertical cracks over height of Wall W-1 between flange and webs after 160% El Centro 1979

8.8.4 Displacement and Deformation Demands on 2-Story Specimen

Because the diaphragms of the 2-story specimen were essentially rigid in their own planes, overall behavior of the specimen was governed by the in-plane responses of Walls W-2 and W-3. Table 8-8 includes the maximum shear deformation ratios in ground-level Walls W-2 and W-3 for each ground motion, in the positive direction (to the east in Figure 8.50) and to the negative direction (to the west in Figure 8.50). Calculated maximum shear deformation ratios in ground-level segments are the shear deformations between the ends of each wall segment, divided by the height of that segment, and expressed in percent. Responses to ground motions before El Centro 43% are not shown in Table 8-8 because they were too small to be useful.

Table 8-8 Overview of structural response, 2-story specimen

No.	ground motion	level of excitation	measured PGA (g)	inter-story drift, %		base shear, kips	maximum shear deformation ratio, %	
				neg	pos		W-2	W-3
1	El Centro 43%	0.50 DBE	0.39	0.016	0.028	84	0.006	0.006
2	El Centro 86%	0.80 DBE	0.66	0.058	0.121	152	0.007	0.008
3	El Centro 108%	slightly above DBE	0.75	0.092	0.202	185	0.007	0.010
4	El Centro 145%	between DBE and MCE	1.02	0.407	0.370	217	0.020	0.177
5	El Centro 160%	above MCE	0.92	1.825	1.062	221	2.470	1.524

Structural responses of the 2-story specimen at El Centro 160% are shown in Figure 8.70 through Figure 8.72.

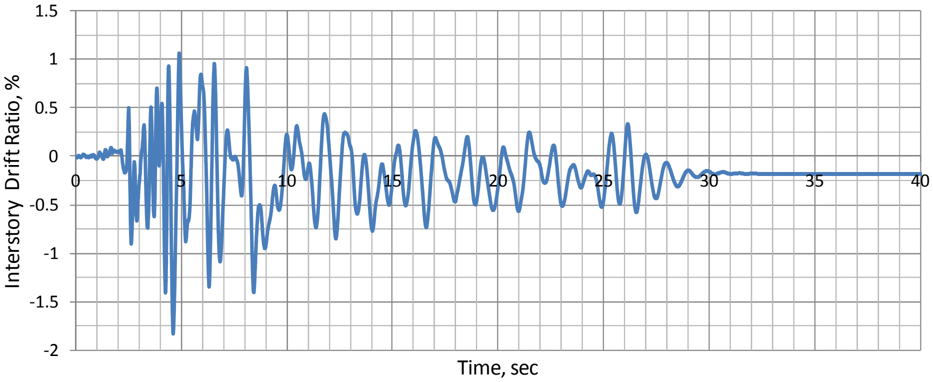

Figure 8.70 Interstory drift ratio of 2-story specimen, 160% El Centro

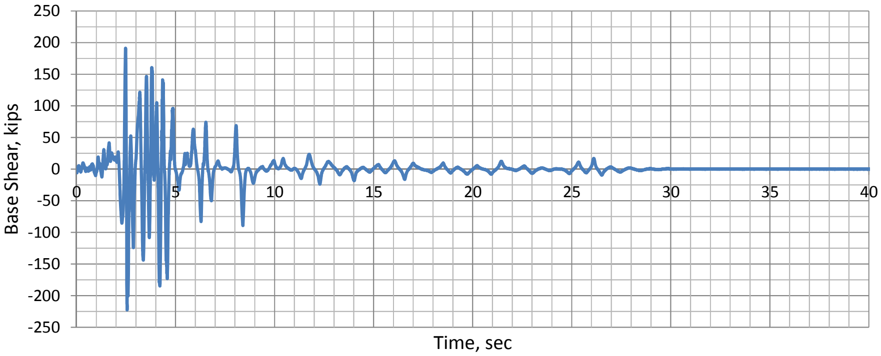

Figure 8.71 Base shear in 2-story specimen, 160% El Centro

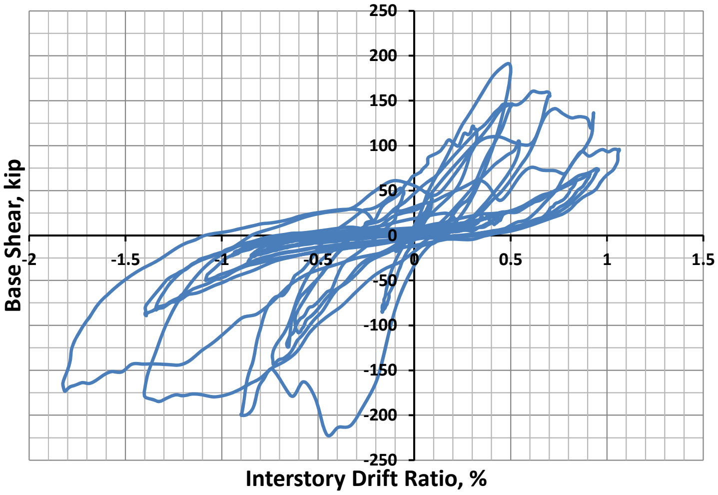

Figure 8.72 Load-displacement curve for ground story of 2-story specimen, 160% El Centro

The total in-plane relative displacements between ends of each wall segment were the result of combined flexural, sliding, and shearing deformations. In these tests, linear potentiometers recorded the average sliding displacements at the interface between the wall base and top and the adjacent masonry for each wall segment in the ground floor. Shearing deformations were measured with two diagonally oriented linear potentiometers and were calculated as proposed by Massone and Wallace (2004).

For 160% El Centro, sliding displacement, shearing deformation, and shear deformation ratio are given for Wall W-2 in Figure 8.73 through Figure 8.75, and for Wall W-3 in Figure 8.76 and Figure 8.77. No sliding displacements were recorded for Wall W-3.

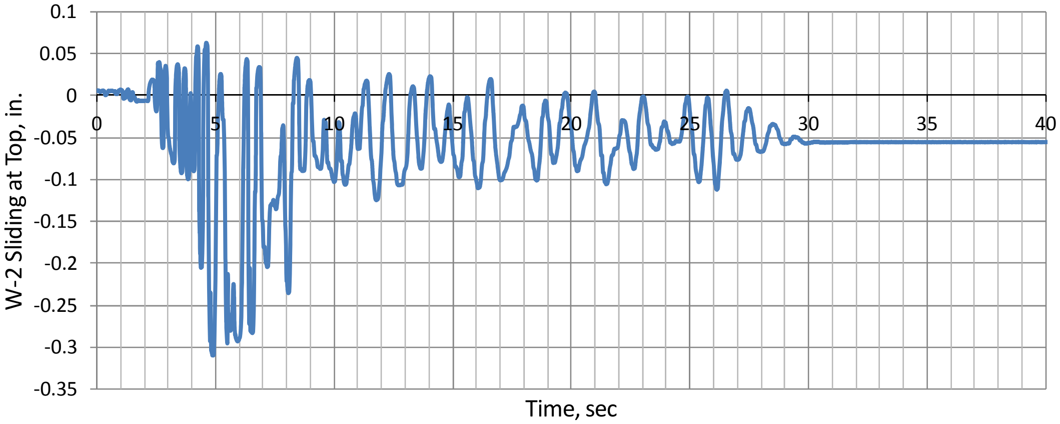

Figure 8.73 Sliding displacement at top of Wall W-2, 160% El Centro (2-story specimen)

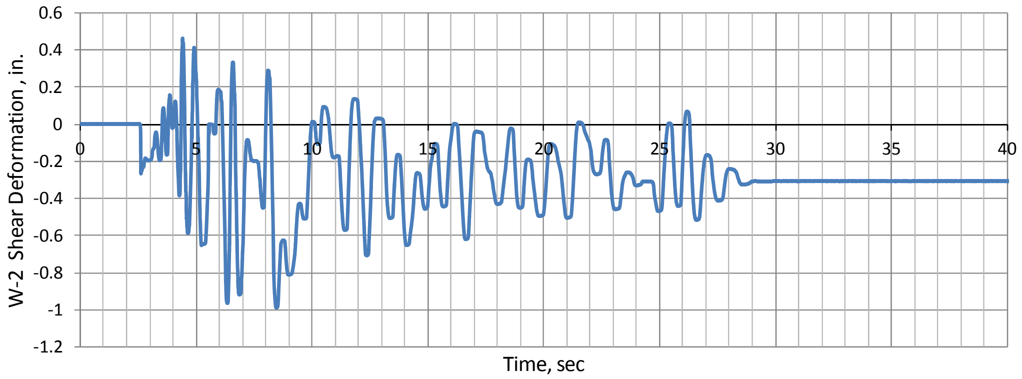

Figure 8.74 Shearing deformation in Wall W-2, 160% El Centro (2-story specimen)

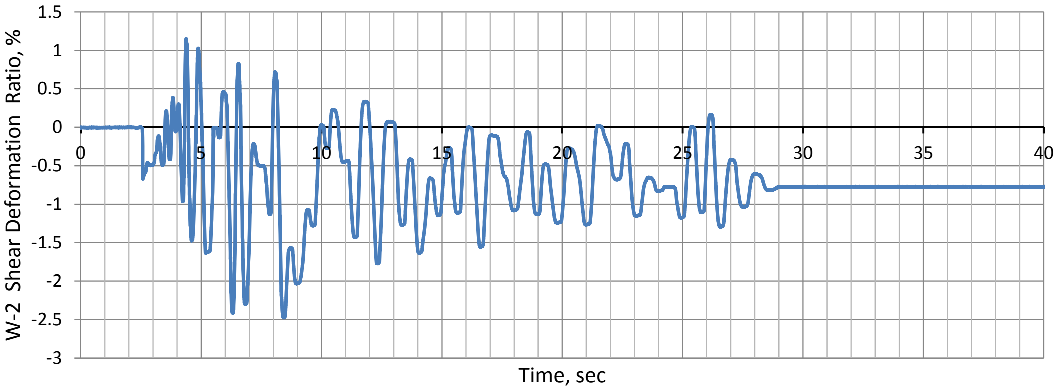

Figure 8.75 Shearing deformation ratio in Wall W-2, 160% El Centro (2-story specimen)

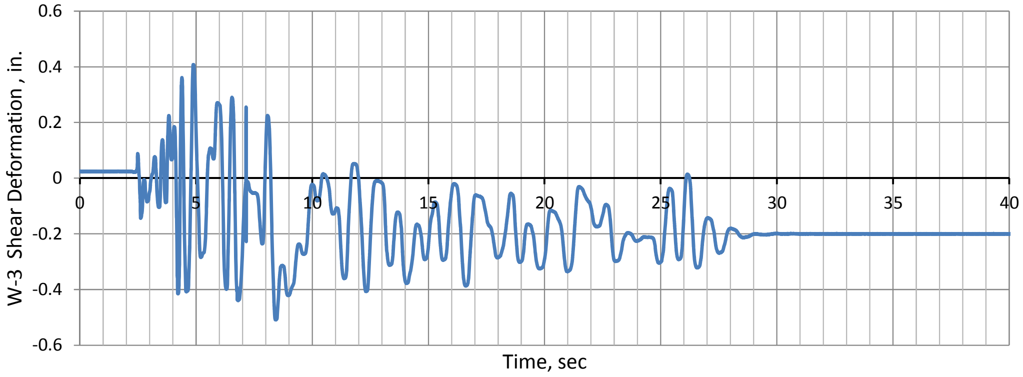

Figure 8.76 Shearing deformation in Wall W-3, 160% El Centro (2-story specimen)

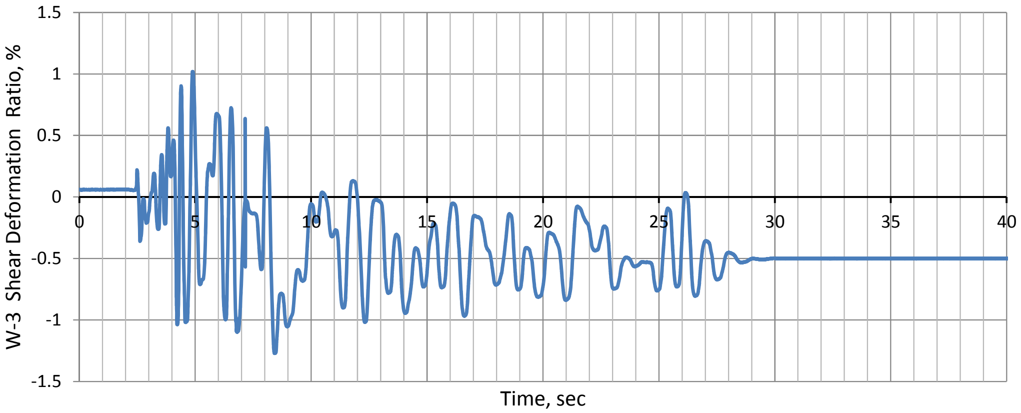

Figure 8.77 Shearing deformation ratio in Wall W-3, 160% El Centro (2-story specimen)

The structural period of 2-story specimen after 160% El Centro was estimated using free-vibration response at the roof as shown in Figure 8.78. A common way of finding the dominant period of time-dependent signals is to use the corresponding period of peak of the Fourier amplitudes. As shown in Figure 8.79, for the roof accelerations of the 2-story specimen, that peak occurs at about 0.84 sec, indicating that the fundamental period of the 2-story specimen had increased to that value by the end of the test. As shown in Figure 8.51, the response spectrum for 160% El Centro has two strong pulses between 0.21 sec and 0.84 sec, indicating that the shaking was stronger than anticipated and exceeded the MCE level during the last run to 160% El Centro 1979.

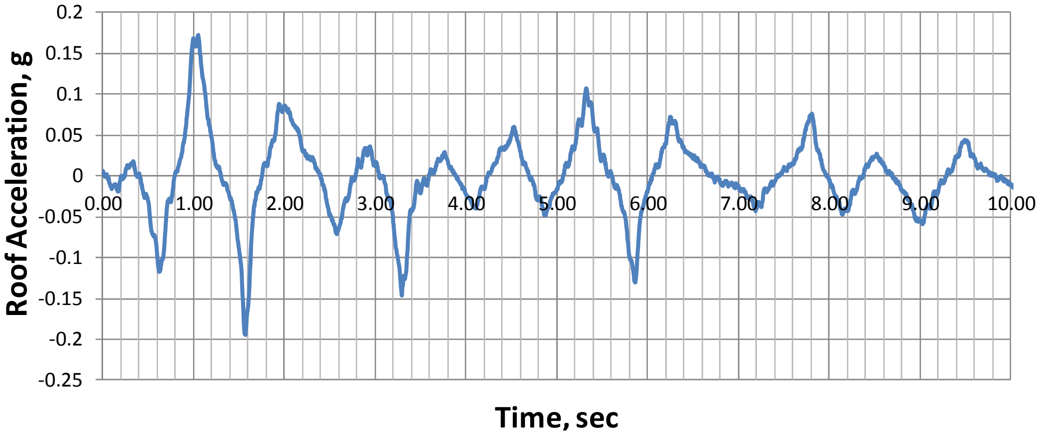

Figure 8.78 Free-vibration acceleration at roof level after 160% El Centro

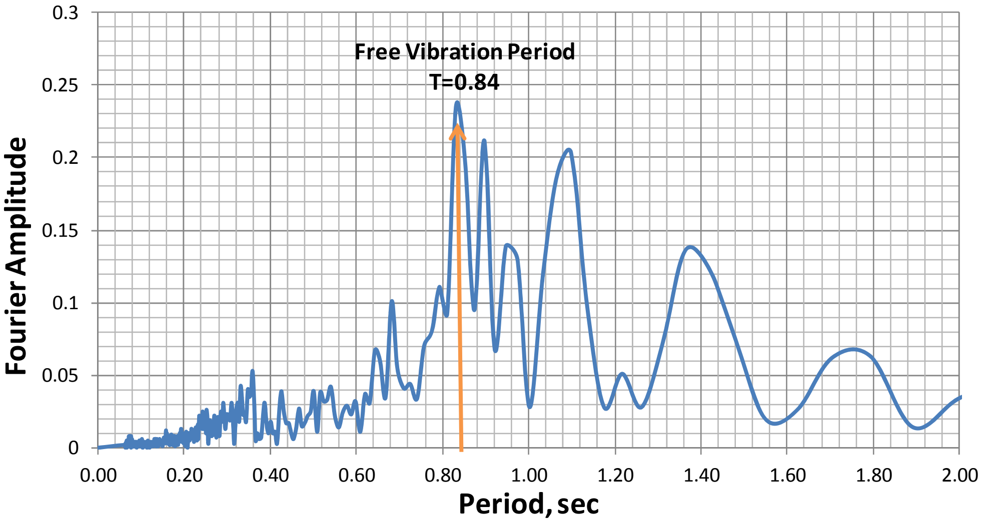

Figure 8.79 Fourier amplitude of free-vibration acceleration at roof level after 160% El Centro

8.9 COMPARISON BETWEEN PREDICTED BEHAVIOR AND TEST RESULTS OF 2-STORY SPECIMEN

In this section, responses predicted using nonlinear time-history analyses are compared with experimental results for the 2-story specimen in terms of three key parameters: first-story displacement versus time; base shear versus time; and load-displacement hysteresis loops. So that cumulative degradation could be modeled, the same sequence of table motions used in the test was used in the analyses. Motions were input in sequence, separated by segments of zero input to allow the analytical model to come to rest. In the interest of space, those comparisons are discussed here for only the last 2 of the 8 input motions:

- 145% El Centro 1979 (between DBE and MCE); and
- 160% El Centro 1979 (slightly above MCE).

8.9.1 Predicted versus Measured Responses to 145% El Centro 1979

The input motion of 145% El Centro 1979 corresponds to shaking between DBE and MCE, based on recorded table accelerations.

8.9.1.1 First-floor Displacements versus Time (145% El Centro 1979)

Under 145% El Centro 1979, the predicted and measured first-floor displacement time-histories are shown in Figure 8.80. Response of the specimen was well captured. Peak displacements were predicted within 10%. In general, agreement between predictions and experiment is quite good.

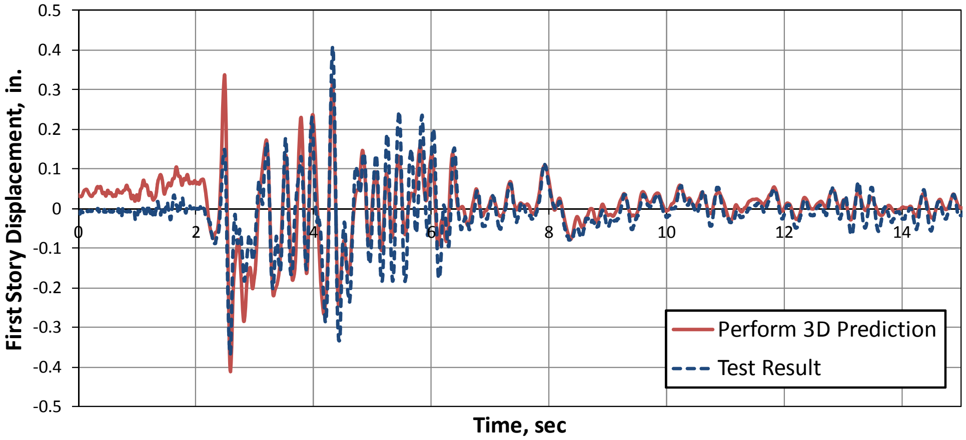

Figure 8.80 First-floor displacement time-history for 2-story specimen (145% El Centro 1979)

8.9.1.1.1 Base Shear versus Time (145% El Centro 1979)

The predicted and measured base shears are shown in Figure 8.81. As with displacements, response was well captured. Peak values are within 5% of the measured values. In general, agreement between prediction and experiment is quite good for a complex structure with significant degradation.

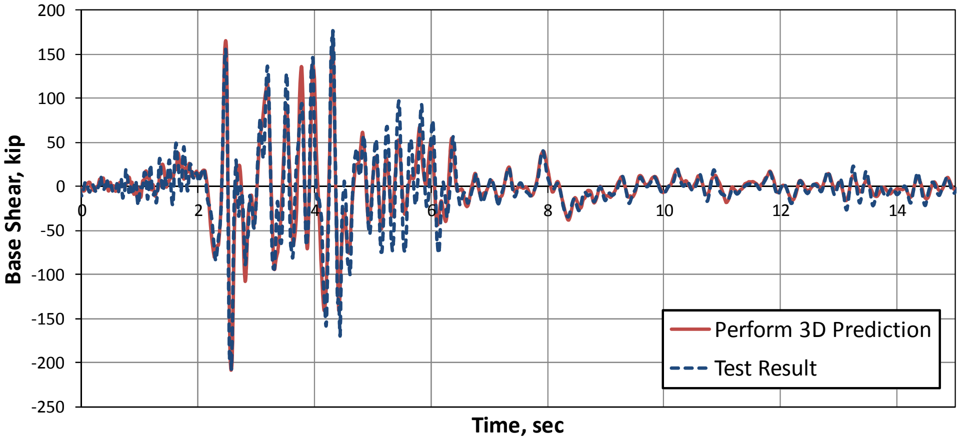

Figure 8.81 Base shear time-history for 2-story specimen (145% El Centro 1979)

8.9.1.1.2 Load-displacement Hysteresis Loops (145% El Centro 1979)

Hysteresis loops of base shear versus first-floor displacement are shown in Figure 8.82. Because the histories of first-floor displacements and base shears were accurately predicted, it is not surprising that the hysteresis loops also compare well. However, the analytical model shows slightly less degradation and nonlinearity than the experimental response.

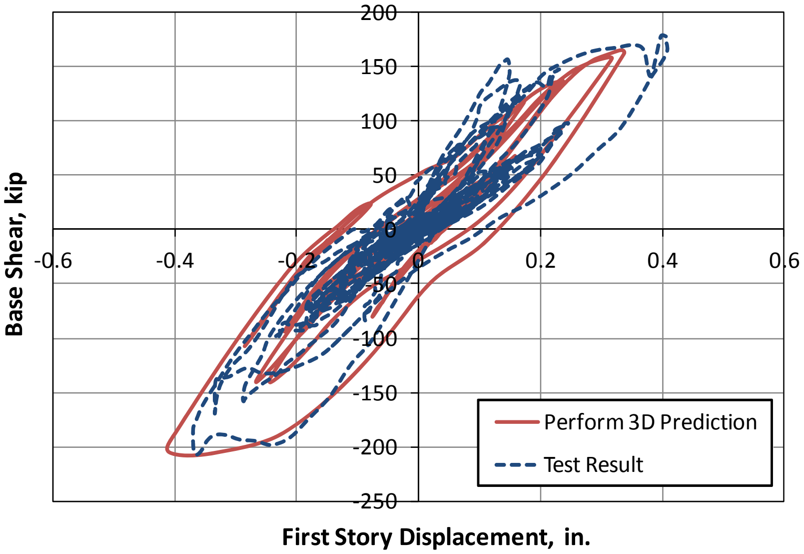

Figure 8.82 Load-displacement hysteresis loops for 2-story specimen (145% El Centro 1979)

8.9.2 Predicted versus Measured Responses to 160% El Centro 1979

An input motion of 160% El Centro 1979 corresponds to shaking at MCE level, based on recorded table accelerations.

8.9.2.1 First-Floor Displacements versus Time (160% El Centro 1979)

Under 160% El Centro 1979, the predicted and measured first-floor displacement time-histories are shown in Figure 8.83. Due to the extensive damage to the specimen, its response was not well predicted.

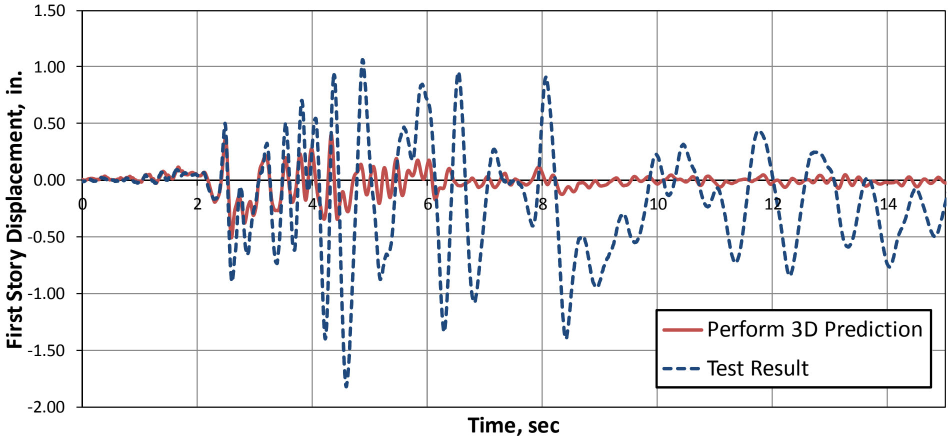

Figure 8.83 Time history of first-floor displacement history for 2-story specimen (160% El Centro 1979)

8.9.2.1.1 Base Shear versus Time (160% El Centro 1979)

The predicted and measured base shears are shown in Figure 8.84. The response was well captured, even as the structure degraded extensively. Peak values are within 10% of the measured values. In general, agreement between prediction and experiment is quite good for a complex structure with significant degradation.

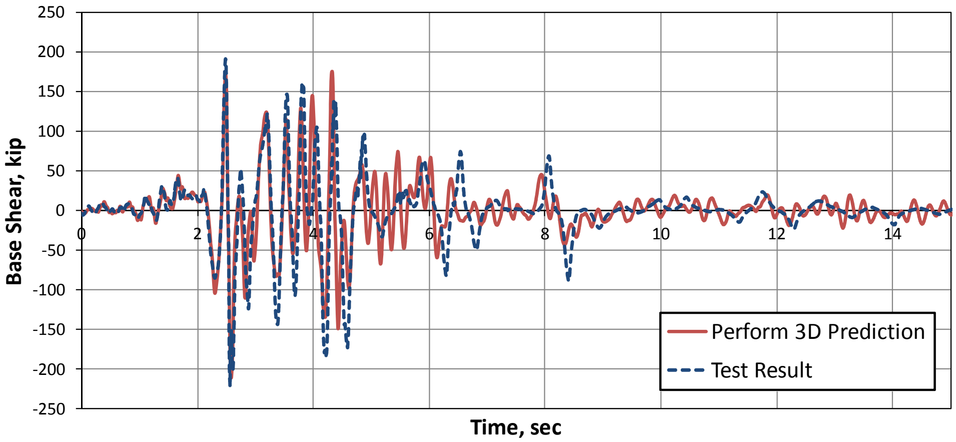

Figure 8.84 Time history of base shear for 2-story specimen (160% El Centro 1979)

8.9.2.1.2 Load-displacement Hysteresis Loops (160% El Centro 1979)

Hysteresis loops of base shear versus first-floor displacement are shown in Figure 8.85. Because the history of first-floor displacements was not accurately predicted, it is not surprising that the hysteresis loops also were different. However, in this ground motion the analytical model shows much less deformation, displacement, and nonlinearity than the experimental response. This was due to gross in-plane deformations and degradation of wall segments.

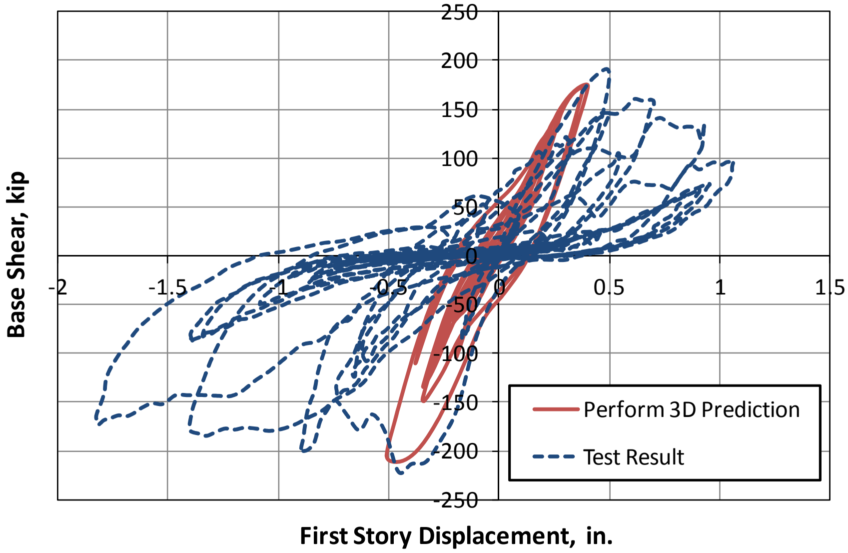

Figure 8.85 Load-displacement hysteresis loops for 2-story specimen (160% El Centro 1979)

During the run to 145% El Centro, significant sliding was observed at the top of Wall W-2. In an effort to improve the accuracy of analytical predictions, an attempt was made to model the possibility of extreme sliding by modifying the PERFORM 3D model of the 2-story specimen. In the row of General Wall elements at the top of Wall W-2, the strength of the shear layer was set equal to the sliding capacity calculated in Chapter 5, including the effects of axial load. However, the attempt was not successful. The modified model had almost the same deformation, displacement, and base shear as the original model, and was not able to capture the extreme sliding behavior exhibited by Wall W-2 in the run to 160% El Centro.

8.9.3 Comparison between Measured and Predicted Inter-story Drifts

In this section, the measured inter-story drift in the ground floor is compared with the predicted inter-story drift from the displacement-based design (push-over analysis), and from the time history analysis for 160% El Centro ground motion (above MCE). As shown in Figure 8.86, the assumed MCE inter-story drift limit for displacement-based design was 0.70%, corresponding to a local deformation demand in Wall W-2 of about twice that value. Under 160% El Centro, the measured inter-story drift ratio (the blue curve reaches maximum values of about +1.1% and about -1.7%, considerably greater than the drifts predicted using time-history analysis, and also greater than the MCE drift limits assumed in the displacement-based design of the 2-story specimen.

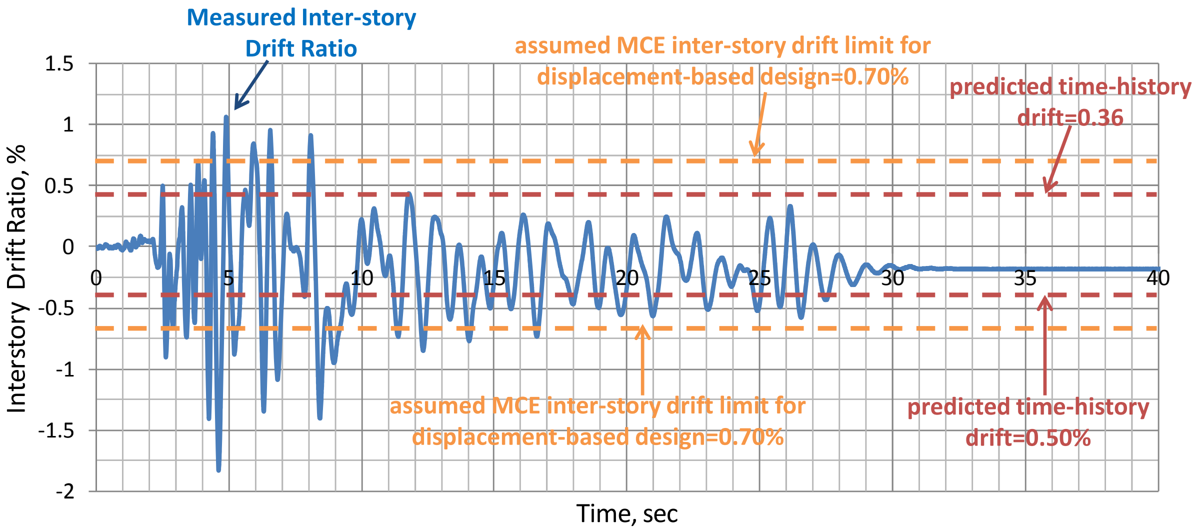

Figure 8.86 Comparison between measured and predicted inter-story drift ratios for two-story specimen (160% El Centro 1979)

8.9.4 Comparison between Measured Deformation Demands and Predicted Deformation Capacities for Two-story Specimen

The total lateral deformation ratio of each wall segment is roughly the difference in displacement between the two ends of the segment, divided by the distance between the two ends. It represents the summation of flexural, shearing, and sliding deformations. In the shake-table tests of the 2-story specimen, differences in end displacements were not measured, so total lateral deformation ratios were not available. Shearing deformations in ground-level walls were measured, however, using data from two diagonally oriented and two vertically oriented potentiometers in each segment, and the calculation procedure of Massone and Wallace (2004). In this section, the measured shearing deformations (less than or equal to the total lateral deformations) in Walls W-2 and W-3 at ground level can be used to estimate the total lateral deformations of those walls, which can then be compared with the expected total lateral deformation capacities of those wall segments based on reversed cyclic load tests.

For 160% El Centro, shear deformation ratios are given for Wall W-2 in Figure 8.75, and for Wall W-3 in Figure 8.77. Based on the results from reversed cyclic load tests of fixed-fixed specimens with an aspect ratio of 1.0 (similar to that of Wall W-2 and Wall W-3), the average ratio of displacement from shearing deformations to total displacement at the end of the tests was 0.64. Therefore, dividing the measured shearing deformation ratios in Walls W-2 and W-3 by 0.64 gives an estimate of the total lateral deformation ratios of those wall segments. These estimated total lateral deformation ratios can then be compared with the expected total deformation capacities for shear-controlled wall segments.

In Figure 8.87 and Figure 8.88, estimated total lateral deformation ratios are compared with expected total deformation capacities for ground-level Walls W-2 and W-3. For Wall W-2 (Figure 8.87), estimated total lateral deformation ratios reached almost 2% in the positive direction and almost 4% in the negative direction, much higher than the expected total deformation capacity ratio of 1% at the MCE level. This was probably due to the high sliding deformations observed in Wall W-2. Those are not included in the ratio of 0.64 that was used to estimate total lateral deformations using measured shearing deformations. For Wall W-3 (Figure 8.88), estimated total lateral deformation ratios reached almost 2% in the positive direction and almost 2.5% in the negative direction, considerably higher than the expected total lateral deformation capacity ratio of 1% at the MCE level. This was probably due to the increase in effective length of Wall W-3 due to the diagonal cracking at the base of that wall. Based on the successful performance of the specimen at these local deformation ratios, the proposed total lateral deformation limits of 1% for shear-dominated walls with closely spaced orthogonal reinforcement seems reasonable and perhaps even conservative.

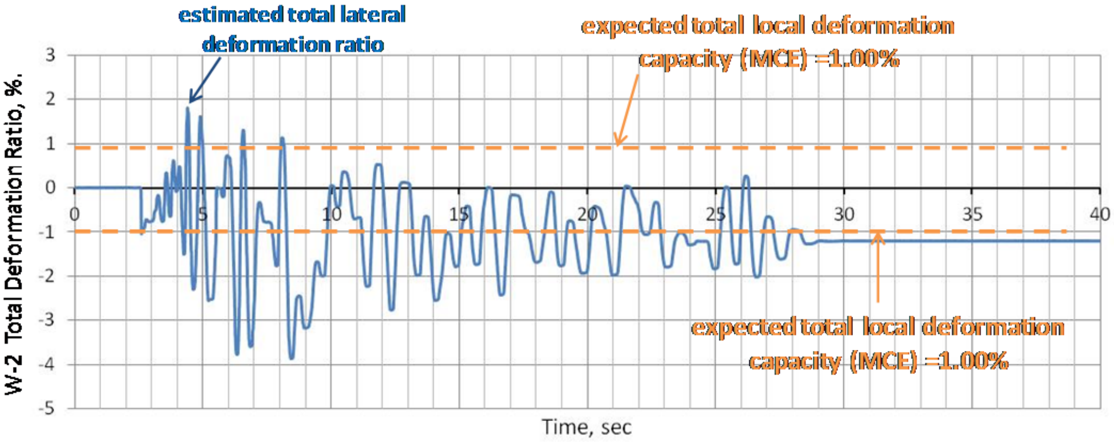

Figure 8.87 **Comparison between estimated total lateral deformation ratios and expected total deformation capacity for Wall W-2 (160% El Centro 1979)**

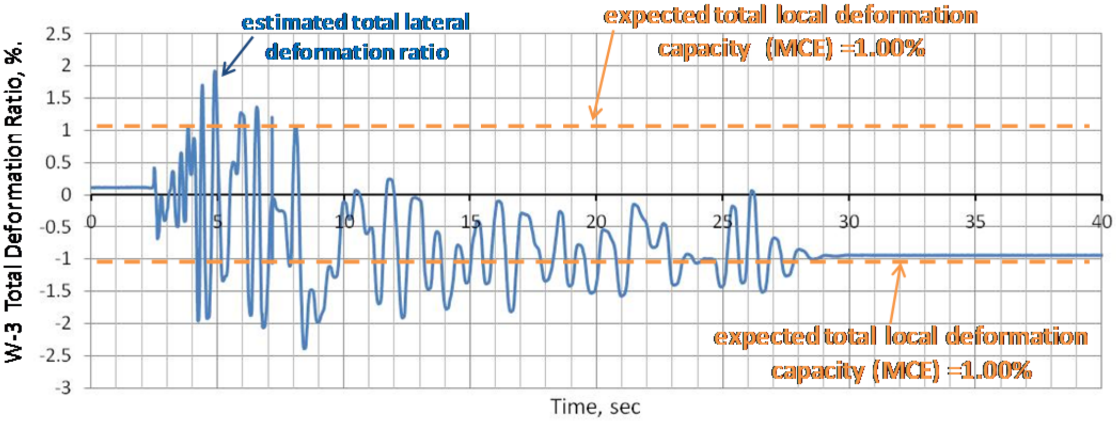

Figure 8.88 Comparison between estimated total lateral deformation ratios and expected total local deformation capacity for Wall W-3 (160% El Centro 1979)

8.10 SUMMARY FROM SHAKE-TABLE TESTING OF 2-STORY SPECIMEN

8.10.1 Summary of Experimental Work

In summer 2012, a 2-story, full-scale, reinforced masonry shear-wall specimen was tested on the large outdoor shake-table at the University of California at San Diego. The specimen was designed with using a displacement-based design procedure that anticipates the formation of a plastic mechanism, calculates the deformation demands associated with that mechanism, and ensures that those deformation demands remain below realistic deformation limits for flexure-dominated and shear-dominated segments.

The 2-story specimen successfully resisted repeated ground motions with intensities up to the Maximum Considered Earthquake (MCE). The specimen suffered extensive damage when subjected to ground motions with intensities exceeding MCE level, and severe diagonal cracks developed in shear-dominated wall segments. In critical regions of this specimen, elements detailed in accordance with limit-design requirements showed more inelastic deformation capacity than the deformation limits imposed by the limit-design provisions of the draft 2013 MSJC *Code* (Section 8.4), and by the displacement-based design provisions proposed in this dissertation.

8.10.2 Summary of Analytical Predictions versus Observed Responses

Using PERFORM 3D (CSI 2007), nonlinear analytical models were developed, and were calibrated using the results of reversed cyclic load tests. The models provided a reasonable compromise between ease of modeling, quality of results, and computational effort. They require about a day to develop; about 30 minutes to run a pushover analysis; and about 18 hours to run the sequence of 8 ground motions used in the shake-table testing. The models accurately predicted the hysteretic response of the 2-story specimen up to MCE.

CHAPTER 9

Summary, Conclusions and Recommendations

9.1 SUMMARY

This dissertation describes part of the work performed on a NIST-sponsored project entitled “Performance-based Seismic Design Methods and Tools for Reinforced Masonry Shear-Wall Structures.” In this study, an innovative and practical displacement-based seismic design procedure was developed for masonry shear-wall structures, and was validated using reversed cyclic load tests on 21 reinforced masonry shear walls and shake-table tests on two full-scale, multi-story reinforced masonry structures. The project used shaking-table facilities at the University of California at San Diego, provided by the US National Science Foundation’s Network for Earthquake Engineering Simulation (NSF NEES). In addition to direct funding and equipment support from the NIST and NSF NEES program, this project received financial and in-kind support from many segments of the masonry industry.

9.1.1 Summary of Experimental Work

Twenty-one reinforced concrete masonry shear-wall specimens were designed, constructed and tested under reversed cyclic lateral loading at The University of Texas at

Austin. The specimens included fifteen cantilever walls and six fixed-fixed walls. The first eight cantilever specimens were detailed according to the requirements of the 2011 MSJC *Code*. The remaining seven cantilever specimens were tested to investigate the response of masonry shear walls with the wider range of reinforcement contents and layouts that are possible for displacement-based design. The six fixed-fixed specimens were intended to provide experimental data to develop analytical models for shear-dominated wall segments.

Two full-scale, multi-story masonry building specimens were also designed and tested on the shake-table at UCSD. The first of these, a full-scale, 3-story reinforced concrete masonry shear-wall system with a regular configuration of openings, was designed using the force-based procedures of ASCE7-05 for Seismic Design Category D, and was detailed in accordance with 2011 MSJC *Code* requirements. The 3-story specimen was subjected to an extended series of ground motions. It was very strong and stiff, and suffered little damage when subjected to ground motions at the DBE (design basis earthquake) and MCE (maximum considered earthquake) levels. Its performance validates the requirements of the 2011 MSJC *Code* for design and detailing of special reinforced masonry shear wall structures. The second of these, a full-scale, 2-story reinforced concrete masonry shear-wall system with an irregular configuration of openings, was designed using a displacement-based design procedure that anticipates the formation of a plastic mechanism, calculates the deformation demands associated with that mechanism, and ensures that those deformation demands remain below realistic deformation limits for flexure-dominated and shear-dominated segments. The 2-story specimen was subjected to an extended series of ground motions. It successfully resisted repeated ground motions with intensities up to and beyond the MCE level. It experienced extensive damage when subjected to ground motions with intensities exceeding MCE level, and severe diagonal cracks developed in shear-dominated wall segments. In critical regions of this specimen, elements detailed in accordance with limit-design requirements showed more inelastic deformation capacity than the deformation limits imposed by the limit-design provisions of the draft 2013 MSJC *Code*, and by the displacement-based design provisions proposed in this dissertation.

9.1.2 Summary of Analytical Work

Using PERFORM 3D, nonlinear analytical models for masonry shear-wall structures were developed and calibrated using the results of cyclic tests of CMU wall specimens at UT Austin and elsewhere. Those calibrated models were then used to predict the response of the full-scale, 3-story specimen tested at the UCSD shake-table in early 2011. The nonlinear analytical models provided a reasonable compromise between ease of modeling, quality of results, and computational effort. They require about a day to develop; about 30 minutes to run a pushover analysis; and about 18 hours to run a sequence of ground motions like those used in this shake-table testing. The predicted responses are quite close to the envelopes of the measured reversed cyclic test responses. The analytical model captures the measured response quite well, including capacities, stiffnesses, stiffness degradation, hysteretic shape, residual displacements, and pinching. The same approach was used to predict the response of the full-scale, 2-story specimen tested on the UCSD shake table in August and September 2012, with similarly good results. Responses were predicted quite accurately up to MCE level, and less accurately above that level.

9.1.3 Summary of Work on Displacement-based Design

Starting with general frameworks that have been previously proposed, a specific displacement-based design procedure was developed that anticipates the formation of a plastic mechanism, calculates the deformation demands associated with that mechanism, and ensures that those deformation demands remain below realistic deformation limits for flexure-dominated and shear-dominated wall segments. The procedure was used to for the successful design of the full-scale, 2-story specimen.

9.2 CONCLUSIONS

9.2.1 Primary Conclusions

The research described here provides a comprehensive validation of a specific displacement-based seismic design procedure for reinforced masonry structures. The procedure produces structures that behave reliably in strong earthquakes. It is more consistent and transparent than current force-based seismic design procedures. It can be used for structures with configurations of openings that are difficult or practically impossible for force-based design, and that are commonly encountered in practice. It is suitable for experienced design offices. The research described here also provides additional validation for the concepts underlying limit design, recently approved for the draft 2013 MSJC *Code*.

9.2.2 Secondary Conclusions

1) The cantilever wall specimens tested in this research exhibited predominantly flexural behavior, as expected. Specimen behavior was in good agreement with that reported in previous research work. The provisions of the 2011 MSJC *Code* give conservative (low) predictions of flexural capacity, and the response of these specimens is generally consistent with performance expectations.

2) Some fixed-fixed specimens tested here were governed by shear. Capacities of those specimens that also met the requirements of the 2011 MSJC *Code* for special reinforced masonry shear walls were safely predicted by the provisions of the 2011 MSJC *Code*, because the additional requirements for capacity design in effect impose an additional factor of safety of at least 1.56 for such walls. For shear-governed walls not meeting the requirements for special reinforced masonry

shear walls, the provisions of the 2011 MSJC *Code* were slightly unconservative, giving nominal capacities about 12% above the lower 5% fractile of test data that is normally associated with nominal capacities. Based on results of tests conducted at UT Austin for this research and tests conducted previously by other researchers, nominal shear resistance is given by the summation of summation of ($A_s f_y + P_n$), multiplied by a coefficient of friction of 0.68. This coefficient of friction is valid whether or not the interface is intentionally roughened.

3) The full-scale, 3-story specimen was designed and constructed using current MSJC requirements for reinforced masonry. Its performance on the shake-table validates the requirements of the 2011 MSJC *Code* for design, detailing, and construction of special reinforced masonry shear walls. The shake-table tests demonstrate that reinforced masonry shear-wall structures can resist earthquakes above MCE without collapse. They validate MSJC *Code* requirements for the capacity design for shear of special reinforced masonry shear walls, for requirements for transverse reinforcement, and for the inclusion of lap splices in longitudinal reinforcement in potential plastic hinge zones.

4) The full-scale, 2-story specimen was designed using displacement-based procedures and detailing. Its performance on the shake-table demonstrates that a reinforced masonry structure designed, detailed, and constructed using the proposed displacement-based design procedure can resist MCE earthquakes without collapse. In critical regions of this specimen, elements detailed in accordance with limit-design requirements showed more inelastic deformation capacity than the deformation limits imposed by the limit-design provisions of the draft 2013 MSJC *Code*, and also by the displacement-based design provisions proposed here.

9.3 RECOMMENDATIONS FOR DESIGN

1) Provisions permitting displacement-based seismic design procedures should be incorporated into ASCE 7. Such procedures produce more predictable and consistent seismic performance than do current force-based design procedures, particularly for short-period shear-wall structures. They permit the design of perforated-wall configurations that are difficult or impossible to design by current force-based procedures.
2) Corresponding provisions permitting displacement-based design should be included in future editions of the MSJC *Code*.
3) Modern computer-based tools (such as PERFORM 3D) can be used as part of specific procedures for displacement-based design.
4) Provisions for sliding-shear capacity should be included in the MSJC *Code,* and should be applied to prevent bed-joint sliding.

9.4 RECOMMENDATIONS FOR FUTURE RESEARCH

1) Extend the displacement-based design method to one-story masonry structures with low aspect ratios and deformable roof or floor diaphragms.
2) Refine the proposed equation for sliding shear capacity of shear walls by conducting more tests.
3) Extend the displacement-based seismic design procedure developed here, to other materials and structural systems.

APPENDIX A Design of Cantilever Wall Specimens

A.1 DESIGN OF CANTILEVER WALL SPECIMEN UT-W-14

Specimen UT-W-14 has a height of 12 ft and a plan length of 4.0 ft (aspect ratio 3.0), special reinforcement, and a normalized axial load ratio P / ($f_m{}'A_g$) = 0.10.

A.1.1 Preliminary Check of Prescriptive Reinforcement Requirements for Wall Specimen UT-W-14

Specimen UT-W-14 must meet prescriptive reinforcement requirements. In accordance with the 2008 MSJC *Code*, Section 1.17.3.2.6, the total reinforcement percentage (horizontal and vertical) shall be at least 0.002, with at least one-third of this placed in each direction. The corresponding steel area per foot is 0.002 x 8 in. x 12 in. = 0.2 in.^{2} per foot. These requirements will be re-checked as the design proceeds.

A.1.2 Compute ρ_{max} based on Axial Load

Now check ρ_{max} , considering the wall as a special reinforced masonry shear wall (R = 5, α = 4).

$$\rho_{\max} = \frac{0.64\, f_m^{'} \left(\dfrac{\varepsilon_{mu}}{\alpha\, \varepsilon_y + \varepsilon_{mu}} \right) - \dfrac{N_{critical}}{bd}}{f_y \left(\dfrac{\alpha\, \varepsilon_y - \varepsilon_{mu}}{\alpha\, \varepsilon_y + \varepsilon_{mu}} \right)}$$

$$N_{critical} = 0.10\, f_m^{'}\, A_g = 0.05 \times 2.5\, ksi \times 48\, in. \times 7.625\, in. = 91.5\,\text{kips}$$

$$\rho_{\max} = \frac{0.64 \times 2500\, psi \left(\dfrac{0.0025}{4 \times 0.00207 + 0.0025} \right) - \dfrac{91500\, lb}{7.625\, in. \times 48\, in.}}{60000\, psi \left(\dfrac{4 \times 0.00207 - 0.0025}{4 \times 0.00207 + 0.0025} \right)}$$

$$\rho_{\max} = \frac{1600\, psi\, (0.231) - 250}{60000\, psi\, (0.536)} = \frac{369.6 - 250}{32160}$$

$$\rho_{\max} = 0.0037$$

This maximum reinforcement is greater than the minimum vertical reinforcement (0.0007), so a design solution is possible.

A.1.3 Flexural Capacity of Wall Specimen UT-W-14

Specimen UT-W-14 has a plan length of 4.0 ft, and an axial load of 91.5 kips. Using a spreadsheet, the nominal interaction diagram for Wall Specimen UT-W-14 is shown in Figure A.1.

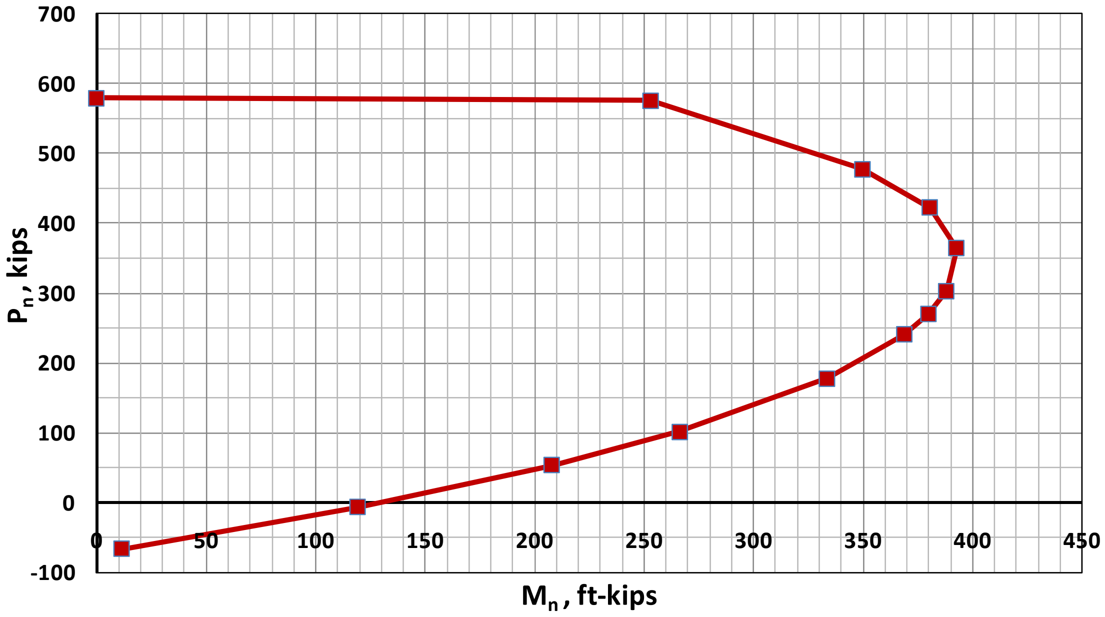

Figure A.1 Strength moment-axial force interaction diagram for Specimen UT-W-14

At an axial load of 91.5 kips, the nominal moment capacity of the wall is 255 kip-ft.

Spreadsheet for calculating strength moment-axial force interaction diagram for concrete masonry shear wall W-14

depth	47.63
emu	0.0025
f'm	2.5
fy	60
Es	29000
d	43.63
(c/d)balanced	0.54717
width	7.63
phi	1

steel layers are counted from the extreme compression fiber to the extreme tension fiber
distances are measured from the extreme compression fiber
compression in masonry and reinforcement is taken as positive
stress in compressive reinforcement is set to zero, because the reinforcement is not laterally supported

Row of Reinforcement	distance	Area
1	4.00	0.20
2	12.00	0.20
3	20.00	0.20
4	28.00	0.20
5	36.00	0.20
6	44.00	0.20
7	52.00	0.00
8	60.00	0.00
9	68.00	0.00
10	76.00	0.00

	c/d	c	Cmas	fs(1)	fs(2)	fs(3)	fs(4)	fs(5)	fs(6)	fs(7)	fs(8)	fs(9)	fs(10)	Moment	Axial Force
pure axial load														0	580
Points controlled by mas	1.08	47.12	575	0.00	0.00	0.00	0.00	0.00	0.00	-7.51	-19.82	-32.13	-44.43	253	575
	0.9	39.27	479	0.00	0.00	0.00	0.00	0.00	-8.74	-23.51	-38.28	-53.05	-60.00	350	478
	0.8	34.90	426	0.00	0.00	0.00	0.00	-2.28	-18.89	-35.51	-52.13	-60.00	-60.00	381	422
	0.7	30.54	373	0.00	0.00	0.00	0.00	-12.96	-31.95	-50.94	-60.00	-60.00	-60.00	393	364
	0.6	26.18	320	0.00	0.00	0.00	-5.05	-27.20	-49.36	-60.00	-60.00	-60.00	-60.00	388	303
Points controlled by stee	0.54717	23.87	291	0.00	0.00	0.00	-12.53	-36.83	-60.00	-60.00	-60.00	-60.00	-60.00	380	270
	0.5	21.82	266	0.00	0.00	0.00	-20.56	-47.14	-60.00	-60.00	-60.00	-60.00	-60.00	369	241
	0.4	17.45	213	0.00	0.00	-10.59	-43.82	-60.00	-60.00	-60.00	-60.00	-60.00	-60.00	334	178
	0.26	11.34	138	0.00	-4.19	-55.32	-60.00	-60.00	-60.00	-60.00	-60.00	-60.00	-60.00	255	91
	0.2	8.73	107	0.00	-27.20	-60.00	-60.00	-60.00	-60.00	-60.00	-60.00	-60.00	-60.00	208	53
	0.1	4.36	53	0.00	-60.00	-60.00	-60.00	-60.00	-60.00	-60.00	-60.00	-60.00	-60.00	119	-7
	0.01	0.44	5	-60.00	-60.00	-60.00	-60.00	-60.00	-60.00	-60.00	-60.00	-60.00	-60.00	12	-67

A.1.4 Capacity Design for Shear, Wall Specimen UT-W-14

Now check Code Section 3.1.3 (capacity design for shear) for Wall Specimen UT-W-14. The wall is a special reinforced masonry shear wall, so the capacity design requirements of Code Section 1.17.3.2.6.1.1 apply. At an axial load of 91.5 kips, the nominal flexural capacity of this wall is 255 kip-ft. That corresponds to an applied shear of 255 kip-ft divided by the height of the wall (12 ft), or 21.25 kips. Including the additional factor of 1.25, the required nominal shear capacity is,

$$\phi V_n \geq 1.25\, V_u$$
$$V_n \geq \frac{1.25}{\phi} V_u = \frac{1.25}{0.8} V_u = 1.56\, V_u = 1.56 \times 21.25\, kips = 33.1\, kips$$

Now check shear capacity. From the 2008 MSJC *Code*, Section 3.3.4.1.2.1,

$$V_n = V_{nm} = \left[4.0 - 1.75 \left(\frac{M_u}{V_u\, d_v} \right) \right] A_n \sqrt{f_m'} + 0.25 P_u$$

Because the wall is a cantilever,

$$\frac{M_u}{V_u\, d_v} = \frac{H}{d_v} = \frac{12\ ft}{4\, ft} = 3.0$$

However, this quotient need not be taken greater than 1.0, so set it equal to that value:

$$V_n = V_{nm} = \left[4.0 - 1.75\,(1.0) \right] A_n \sqrt{f_m'} + 0.25 P_u$$
$$V_n = V_{nm} = 2.25 \times 7.63\, in. \times 47.63\, in. \sqrt{2500} psi + 0.25 \times 91{,}500\, lb$$
$$V_n = V_{nm} = 63.7\, kips$$

The shear capacity of the wall is sufficient without shear reinforcement. Nominal reinforcement is sufficient. Prescriptive reinforcement requirements must be met. We need horizontal shear reinforcement of at least 0.0007. Use No. 4 bars at 16 in. horizontally.

$$\rho_{horizontal} = \frac{A_s}{bt} = \frac{0.2\ in.^2}{7.625 \times 16\ in.^2} = 0.0016$$

From the 2008 MSJC *Code*, Section 3.3.4.1.2.2,

$$V_{ns} = 0.5\left(\frac{A_v}{s}\right) f_y d_v$$

$$V_{ns} = 0.5\left(\frac{0.2\ in.^2}{16\ in.}\right) 60\ kips / in.^2 \times 43.63\ in.$$

$$V_{ns} = 16.3\ kips$$

$$V_n = V_{nm} + V_{ns} = 63.7\ kips + 16.3\ kips = 80.0\ kips$$

This exceeds the required nominal shear capacity of 33.1 kips, and the design is satisfactory for shear.

A.1.5 Summary of Design for Wall Specimen UT-W-14

Use No. 4 vertical bars at 8 in. (6 bars total), and No. 4 horizontal bars at 16 in.

A.1.6 Details of Wall Specimen UT-W-14

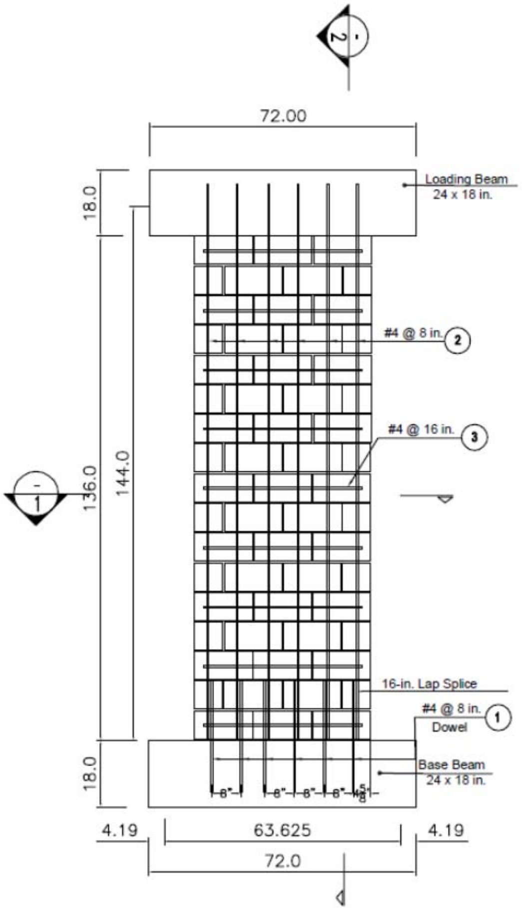

Specimen Wall # 14

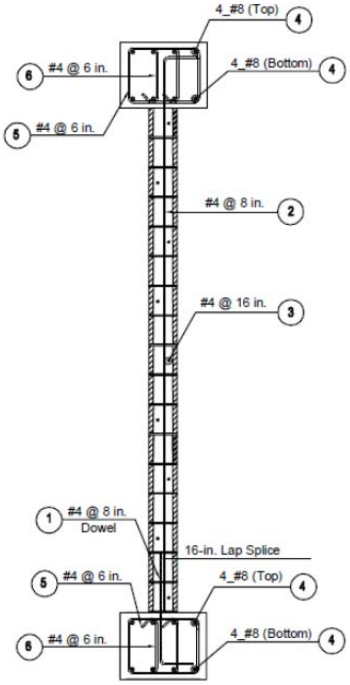

Section 2-2

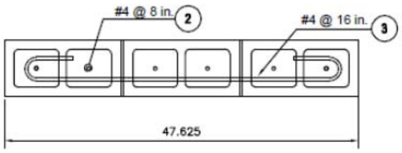

Section 1-1

A.2 DESIGN OF CANTILEVER SHEAR WALL SPECIMEN UT-W-15

Specimen UT-W-15 has a height of 12 ft and a plan length of 4 ft (aspect ratio 3.0), intermediate reinforcement, and a normalized axial load ratio P / ($f_m{}'A_g$) = 0.10.

A.2.1 Preliminary Check of Prescriptive Reinforcement Requirements for Wall Specimen UT-W-15

Specimen UT-W-15 must meet prescriptive reinforcement requirements. In accordance with the 2008 MSJC *Code*, Section 1.17.3.2.6, the total reinforcement percentage (horizontal and vertical) shall be at least 0.002, with at least one-third of this placed in each direction. The corresponding steel area per foot is 0.002 x 8 in. x 12 in. = 0.2 in.^{2} per foot. These requirements will be re-checked as the design proceeds.

A.2.2 Compute ρ_{max} based on Axial Load

Now check ρ_{max} , considering the wall as a intermediate reinforced masonry shear wall (α = 3).

$$\rho_{\max} = \frac{0.64\, f_m^{'} \left(\dfrac{\varepsilon_{mu}}{\alpha\, \varepsilon_y + \varepsilon_{mu}} \right) - \dfrac{N_{critical}}{bd}}{f_y \left(\dfrac{\alpha\, \varepsilon_y - \varepsilon_{mu}}{\alpha\, \varepsilon_y + \varepsilon_{mu}} \right)}$$

$$N_{critical} = 0.10 f_m^{'}\ A_g = 0.10 \times 2.5\ ksi \times 48\ in. \times 7.625\ in. = 91.5\ \text{kips}$$

$$\rho_{\max} = \frac{0.64 \times 2500\ psi \left(\dfrac{0.0025}{3 \times 0.00207 + 0.0025} \right) - \dfrac{91500\ lb}{7.625\ in. \times 48\ in.}}{60000\ psi \left(\dfrac{3 \times 0.00207 - 0.0025}{3 \times 0.00207 + 0.0025} \right)}$$

$$\rho_{\max} = \frac{1600\ psi\ (0.287) - 250}{60000\ psi\ (0.426)} = \frac{459.2 - 250}{25560}$$

$$\rho_{\max} = 0.0082$$

This maximum reinforcement is greater than the minimum vertical reinforcement (0.0007), so a design solution is possible.

A.2.3 Flexural Capacity of Wall Specimen UT-W-15

Specimen UT-W-15 has a plan length of 4.0 ft and an axial load of 91.5 kips. Using a spreadsheet, the nominal interaction diagram for Wall Specimen 15 is shown in Figure A.2. At an axial load of 91.5 kips, the nominal moment capacity of the wall is 347 kip-ft.

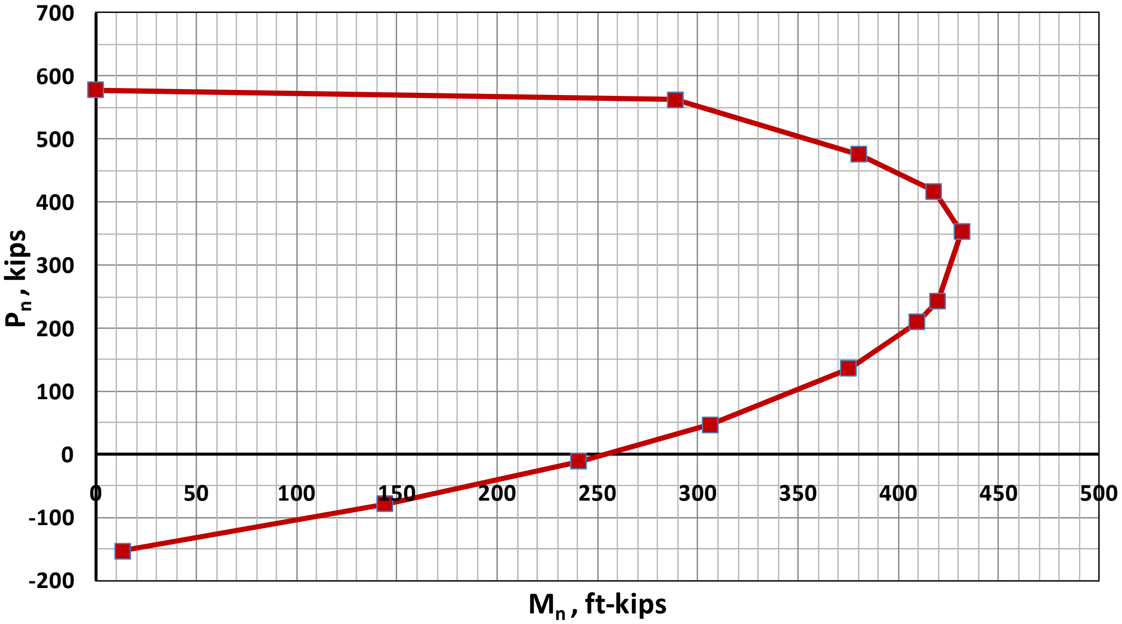

Figure A.2 Strength moment-axial force interaction diagram for Specimen UT-W-15

Spreadsheet for calculating strength moment-axial force interaction diagram for concrete masonry shear wall W-15

depth	47.63
emu	0.0025
f'm	2.5
fy	60
Es	29000
d	43.63
(c/d)balanced	0.54717
width	7.63
phi	1

steel layers are counted from the extreme compression fiber to the extreme tension fiber
distances are measured from the extreme compression fiber
compression in masonry and reinforcement is taken as positive
stress in compressive reinforcement is set to zero, because the reinforcement is not laterally supported

Row of Reinforcement	distance	Area
1	4.00	0.44
2	12.00	0.44
3	20.00	0.44
4	28.00	0.44
5	36.00	0.44
6	44.00	0.44
7	52.00	0.00
8	60.00	0.00
9	68.00	0.00
10	76.00	0.00

	c/d	c	Cmas	fs(1)	fs(2)	fs(3)	fs(4)	fs(5)	fs(6)	fs(7)	fs(8)	fs(9)	fs(10)	Moment	Axial Force
pure axial load														0	577
Points controlled by mas	1.055	46.03	562	0.00	0.00	0.00	0.00	0.00	0.00	-9.40	-22.00	-34.60	-47.21	288	562
	0.9	39.27	479	0.00	0.00	0.00	0.00	0.00	-8.74	-23.51	-38.28	-53.05	-60.00	380	476
	0.8	34.90	426	0.00	0.00	0.00	0.00	-2.28	-18.89	-35.51	-52.13	-60.00	-60.00	418	417
	0.7	30.54	373	0.00	0.00	0.00	0.00	-12.96	-31.95	-50.94	-60.00	-60.00	-60.00	432	353
	0.54717	23.87	291	0.00	0.00	0.00	-12.53	-36.83	-60.00	-60.00	-60.00	-60.00	-60.00	420	243
Points controlled by stee	0.54717	23.87	291	0.00	0.00	0.00	-12.53	-36.83	-60.00	-60.00	-60.00	-60.00	-60.00	420	243
	0.5	21.82	266	0.00	0.00	0.00	-20.56	-47.14	-60.00	-60.00	-60.00	-60.00	-60.00	409	210
	0.4	17.45	213	0.00	0.00	-10.59	-43.82	-60.00	-60.00	-60.00	-60.00	-60.00	-60.00	375	136
	0.275	12.00	146	0.00	-0.01	-48.35	-60.00	-60.00	-60.00	-60.00	-60.00	-60.00	-60.00	306	46
	0.2	8.73	107	0.00	-27.20	-60.00	-60.00	-60.00	-60.00	-60.00	-60.00	-60.00	-60.00	241	-11
	0.1	4.36	53	0.00	-60.00	-60.00	-60.00	-60.00	-60.00	-60.00	-60.00	-60.00	-60.00	144	-79
	0.01	0.44	5	-60.00	-60.00	-60.00	-60.00	-60.00	-60.00	-60.00	-60.00	-60.00	-60.00	13	-153

A.2.4 Capacity Design for Shear, Wall Specimen UT-W-15

Now check Code Section 3.1.3 (capacity design for shear) for Wall Specimen UT-W-15. The wall is a intermediate reinforced masonry shear wall, so the capacity design requirements of Code Section 1.17.3.2.6.1.1 apply. At an axial load of 91.5 kips, the nominal flexural capacity of this wall is 306 kip-ft. That corresponds to an applied shear of 306 kip-ft divided by the height of the wall (12 ft), or 28.90 kips. Including the additional factor of 1.25, , the required nominal shear capacity is,

$$\phi V_n \geq 1.25\, V_u$$
$$V_n \geq \frac{1.25}{\phi} V_u = \frac{1.25}{0.8} V_u = 1.56\, V_u = 1.56 \times 28.90\, kips = 45.1\, kips$$

Now check shear capacity. From the 2008 MSJC *Code*, Section 3.3.4.1.2.1,

$$V_n = V_{nm} = \left[4.0 - 1.75 \left(\frac{M_u}{V_u\, d_v} \right) \right] A_n \sqrt{f_m^{'}} + 0.25 P_u$$

Because the wall is a cantilever,

$$\frac{M_u}{V_u\, d_v} = \frac{H}{d_v} = \frac{12\ ft}{4 ft} = 3.0$$

However, this quotient need not be taken greater than 1.0, so set it equal to that value:

$$V_n = V_{nm} = \left[4.0 - 1.75\,(1.0)\right] A_n \sqrt{f_m^{'}} + 0.25 P_u$$
$$V_n = V_{nm} = 2.25 \times 7.63\, in. \times 47.63\, in. \sqrt{2500} psi + 0.25 \times 91{,}500\ lb$$
$$V_n = V_{nm} = 63.7\ kips$$

The shear capacity of the wall is sufficient without shear reinforcement. Nominal reinforcement is sufficient.

Prescriptive reinforcement requirements must be met. We need horizontal shear reinforcement of at least 0.0007. Use No. 4 bars at 16 in. horizontally.

$$\rho_{horizontal} = \frac{A_s}{bt} = \frac{0.2\ in.^2}{7.625 \times 16\ in.^2} = 0.0016$$

From the 2008 MSJC *Code*, Section 3.3.4.1.2.2,

$$V_{ns} = 0.5\left(\frac{A_v}{s}\right) f_y d_v$$

$$V_{ns} = 0.5\left(\frac{0.2\ in.^2}{16\ in.}\right) 60\ kips / in.^2 \times 43.63\ in.$$

$$V_{ns} = 16.3\ kips$$

$$V_n = V_{nm} + V_{ns} = 63.7\ kips + 16.3\ kips = 80.0\ kips$$

This exceeds the required nominal shear capacity of 45.1 kips, and the design is satisfactory for shear.

A.2.5 Summary of Design for Wall Specimen UT-W-15

Use No. 6 vertical bars at 8 in. (6 bars total), and No. 4 horizontal bars at 16 in.

A.2.6 Details of Wall Specimen UT-W-15

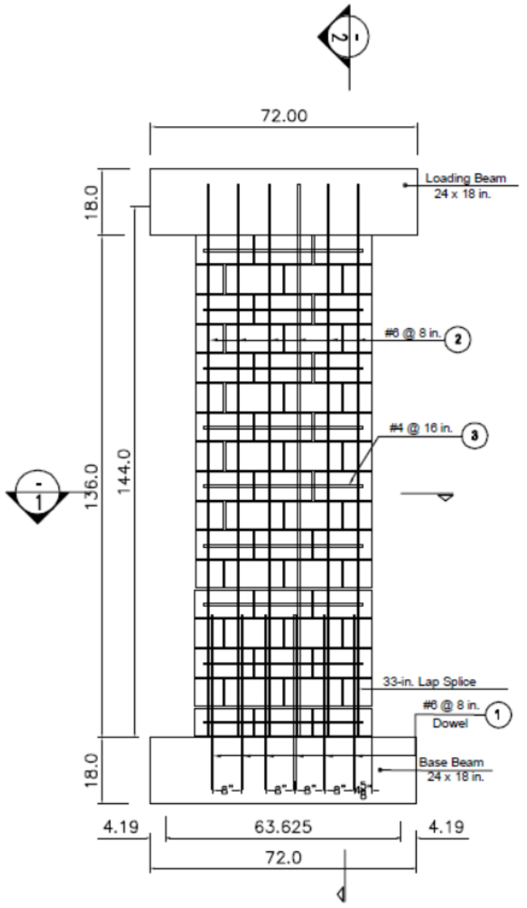

Specimen Wall # 15

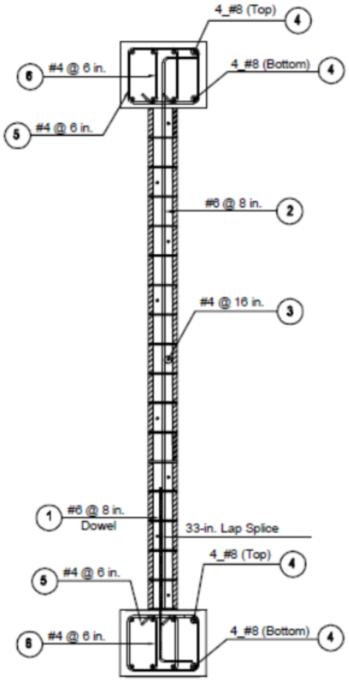

Section 2-2

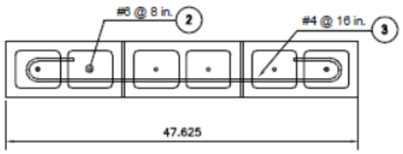

Section 1-1

A.3 DESIGN OF CANTILEVER WALL SPECIMEN UT-W-16

Specimen UT-W-16 has a height of 12 ft and a plan length of 4 ft (aspect ratio 3.0), intermediate reinforcement, and a normalized axial load ratio P / ($f_m{}' A_g$) = 0.15.

A.3.1 Preliminary Check of Prescriptive Reinforcement Requirements for Wall Specimen UT-W-16

Specimen UT-W-16 must meet prescriptive reinforcement requirements. In accordance with the 2008 MSJC *Code*, Section 1.17.3.2.6, the total reinforcement percentage (horizontal and vertical) shall be at least 0.002, with at least one-third of this placed in each direction. The corresponding steel area per foot is 0.002 x 8 in. x 12 in. = 0.2 in.^{2} per foot. These requirements will be re-checked as the design proceeds.

A.3.2 Compute ρ_{max} based on Axial Load

Now check ρ_{max} , considering the wall as a special reinforced masonry shear wall (α = 3).

$$\rho_{\max} = \frac{0.64\, f_m^{'} \left(\dfrac{\varepsilon_{mu}}{\alpha\, \varepsilon_y + \varepsilon_{mu}} \right) - \dfrac{N_{critical}}{bd}}{f_y \left(\dfrac{\alpha\, \varepsilon_y - \varepsilon_{mu}}{\alpha\, \varepsilon_y + \varepsilon_{mu}} \right)}$$

$$N_{critical} = 0.15\, f_m^{'}\, A_g = 0.15 \times 2.5\, ksi \times 48\, in. \times 7.625\, in. = 137.25 \text{ kips}$$

$$\rho_{\max} = \frac{0.64 \times 2500\, psi \left(\dfrac{0.0025}{3 \times 0.00207 + 0.0025} \right) - \dfrac{137250\, lb}{7.625\, in. \times 48\, in.}}{60000\, psi \left(\dfrac{3 \times 0.00207 - 0.0025}{3 \times 0.00207 + 0.0025} \right)}$$

$$\rho_{\max} = \frac{1600\, psi\, (0.287) - 375}{60000\, psi\, (0.426)} = \frac{459.2 - 375}{25560}$$

$$\rho_{\max} = 0.0040$$

This maximum reinforcement is greater than the minimum vertical reinforcement (0.0007), so a design solution is possible.

A.3.3 Flexural Capacity of Wall Specimen UT-W-16

Specimen UT-W-16 has a plan length of 4 ft and an axial load (see above) of 137.25 kips. Using a spreadsheet, the nominal interaction diagram for Wall Specimen 16 is shown in Figure A.3.

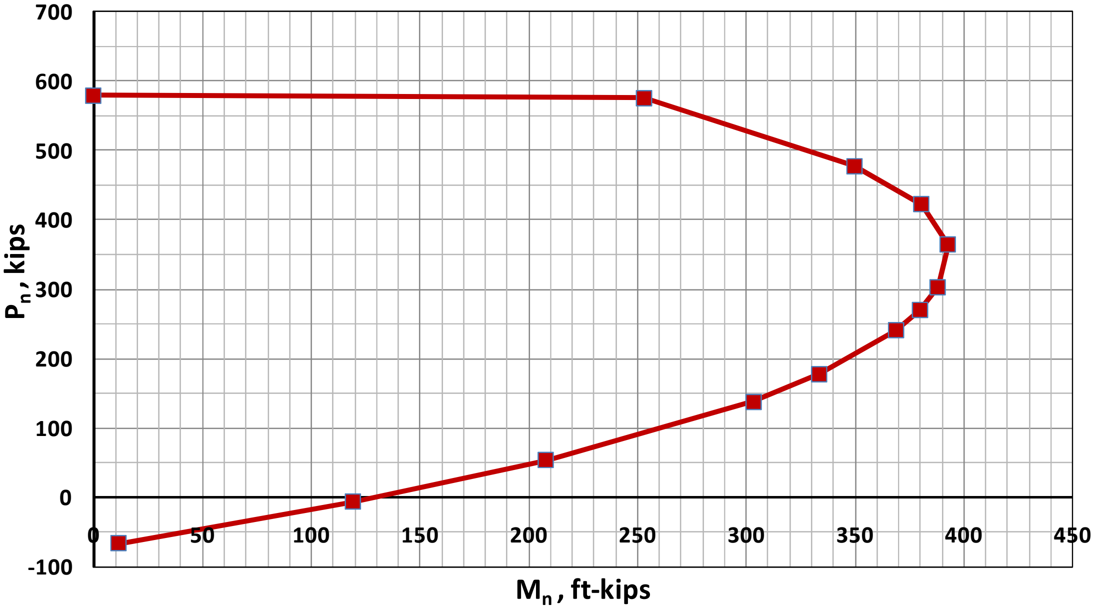

Figure A.3 Strength moment-axial force interaction diagram for Specimen UT-W-16

At an axial load of 137.25 kips, the nominal moment capacity of the wall is 303 kip-ft.

Spreadsheet for calculating strength moment-axial force interaction diagram for concrete masonry shear wall W-16

depth	47.63
emu	0.0025
f'm	2.5
fy	60
Es	29000
d	43.63
(c/d)balanced	0.54717
width	7.63
phi	1

steel layers are counted from the extreme compression fiber to the extreme tension fiber
distances are measured from the extreme compression fiber
compression in masonry and reinforcement is taken as positive
stress in compressive reinforcement is set to zero, because the reinforcement is not laterally supported

Row of Reinforcement	distance	Area
1	4.00	0.20
2	12.00	0.20
3	20.00	0.20
4	28.00	0.20
5	36.00	0.20
6	44.00	0.20
7	52.00	0.00
8	60.00	0.00
9	68.00	0.00
10	76.00	0.00

	c/d	c	Cmas	fs(1)	fs(2)	fs(3)	fs(4)	fs(5)	fs(6)	fs(7)	fs(8)	fs(9)	fs(10)	Moment	Axial Force
pure axial load														0	580
Points controlled by mas	1.08	47.12	575	0.00	0.00	0.00	0.00	0.00	0.00	-7.51	-19.82	-32.13	-44.43	253	575
	0.9	39.27	479	0.00	0.00	0.00	0.00	0.00	-8.74	-23.51	-38.28	-53.05	-60.00	350	478
	0.8	34.90	426	0.00	0.00	0.00	0.00	-2.28	-18.89	-35.51	-52.13	-60.00	-60.00	381	422
	0.7	30.54	373	0.00	0.00	0.00	0.00	-12.96	-31.95	-50.94	-60.00	-60.00	-60.00	393	364
	0.6	26.18	320	0.00	0.00	0.00	-5.05	-27.20	-49.36	-60.00	-60.00	-60.00	-60.00	388	303
Points controlled by stee	0.54717	23.87	291	0.00	0.00	0.00	-12.53	-36.83	-60.00	-60.00	-60.00	-60.00	-60.00	380	270
	0.5	21.82	266	0.00	0.00	0.00	-20.56	-47.14	-60.00	-60.00	-60.00	-60.00	-60.00	369	241
	0.4	17.45	213	0.00	0.00	-10.59	-43.82	-60.00	-60.00	-60.00	-60.00	-60.00	-60.00	334	178
	0.337	14.70	179	0.00	0.00	-26.12	-60.00	-60.00	-60.00	-60.00	-60.00	-60.00	-60.00	303	138
	0.2	8.73	107	0.00	-27.20	-60.00	-60.00	-60.00	-60.00	-60.00	-60.00	-60.00	-60.00	208	53
	0.1	4.36	53	0.00	-60.00	-60.00	-60.00	-60.00	-60.00	-60.00	-60.00	-60.00	-60.00	119	-7
	0.01	0.44	5	-60.00	-60.00	-60.00	-60.00	-60.00	-60.00	-60.00	-60.00	-60.00	-60.00	12	-67

A.3.4 Capacity Design for Shear, Wall Specimen UT-W-16

Now check Code Section 3.1.3 (capacity design for shear) for Wall Specimen UT-W-16. The wall is a special reinforced masonry shear wall, so the capacity design requirements of Code Section 1.17.3.2.6.1.1 apply. At an axial load of 137.25 kips, the nominal flexural capacity of this wall is 303 kip-ft. That corresponds to an applied shear of 303 kip-ft divided by the height of the wall (12 ft), or 25.25 kips. Including the additional factor of 1.25, the required nominal shear capacity is,

$$\phi V_n \geq 1.25\, V_u$$
$$V_n \geq \frac{1.25}{\phi} V_u = \frac{1.25}{0.8} V_u = 1.56\, V_u = 1.56 \times 25.25\ kips = 39.4\ kips$$

Now check shear capacity. From the 2008 MSJC *Code*, Section 3.3.4.1.2.1,

$$V_n = V_{nm} = \left[4.0 - 1.75\left(\frac{M_u}{V_u\ d_v}\right)\right] A_n \sqrt{f_m'} + 0.25 P_u$$

Because the wall is a cantilever,

$$\frac{M_u}{V_u\ d_v} = \frac{H}{d_v} = \frac{12\ ft}{4\,ft} = 3.0$$

However, this quotient need not be taken greater than 1.0, so set it equal to that value:

$$V_n = V_{nm} = [4.0 - 1.75\,(1.0)] A_n \sqrt{f_m'} + 0.25 P_u$$
$$V_n = V_{nm} = 2.25 \times 7.63\ in. \times 47.63\ in. \sqrt{2500} psi + 0.25 \times 137{,}250\ lb$$
$$V_n = V_{nm} = 75.1\ kips$$

The shear capacity of the wall is sufficient without shear reinforcement. Nominal reinforcement is sufficient.

Prescriptive reinforcement requirements must be met. We need horizontal shear reinforcement of at least 0.0007. Use No. 4 bars at 16 in. horizontally.

$$\rho_{horizontal} = \frac{A_s}{bt} = \frac{0.2\ in.^2}{7.625 \times 16\ in.^2} = 0.0016$$

From the 2008 MSJC *Code*, Section 3.3.4.1.2.2,

$$V_{ns} = 0.5\left(\frac{A_v}{s}\right) f_y d_v$$

$$V_{ns} = 0.5\left(\frac{0.2\ in.^2}{16\ in.}\right) 60\ kips/in.^2 \times 43.63\ in.$$

$$V_{ns} = 16.3\ kips$$

$$V_n = V_{nm} + V_{ns} = 75.1\ kips + 16.3\ kips = 91.4\ kips$$

This exceeds the required nominal shear capacity of 39.4 kips, and the design is satisfactory for shear.

A.3.5 Summary of Design for Wall Specimen UT-W-16

Use No. 4 vertical bars at 8 in. (6 bars total), and No. 4 horizontal bars at 16 in.

A.3.6 Details of Wall Specimen UT-W-16

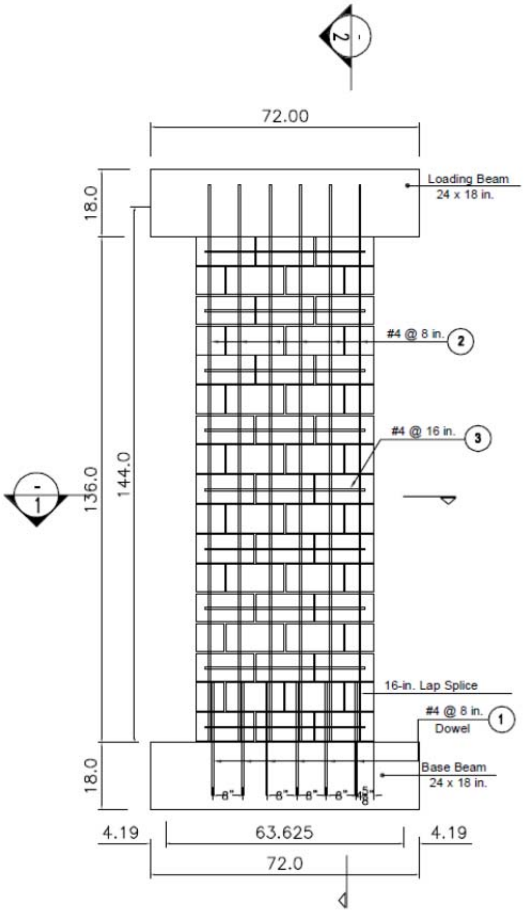

Specimen Wall # 16

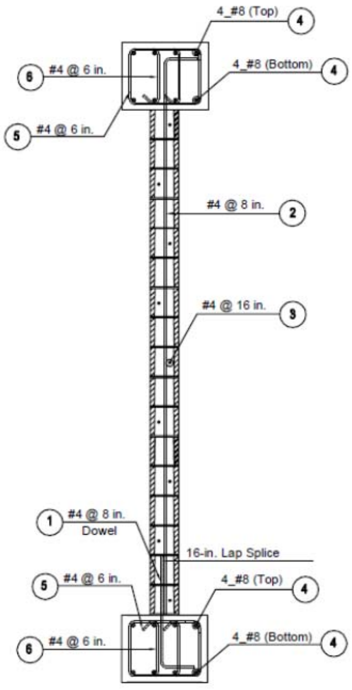

Section 2-2 2

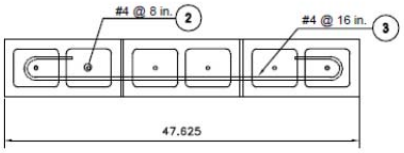

Section 1-1 1

A.4 DESIGN OF CANTILEVER WALL SPECIMEN UT-W-17

Specimen UT-W-17 has a height of 12 ft and a plan length of 2.67 ft (aspect ratio 4.5), special reinforcement, and a normalized axial load ratio P / ($f_m' A_g$) = 0.05.

A.4.1 Preliminary Check of Prescriptive Reinforcement Requirements for Wall Specimen UT-W-17

Specimen UT-W-17 must meet prescriptive reinforcement requirements. In accordance with the 2008 MSJC *Code*, Section 1.17.3.2.6, the total reinforcement percentage (horizontal and vertical) shall be at least 0.002, with at least one-third of this placed in each direction. The corresponding steel area per foot is 0.002 x 8 in. x 12 in. = 0.2 in.^{2} per foot. These requirements will be re-checked as the design proceeds.

A.4.2 Compute ρ_{max} based on Axial Load

Now check ρ_{max}, considering the wall as a special reinforced masonry shear wall (R = 5, α = 4).

$$\rho_{\max} = \frac{0.64\, f_m' \left(\dfrac{\varepsilon_{mu}}{\alpha\, \varepsilon_y + \varepsilon_{mu}} \right) - \dfrac{N_{critical}}{bd}}{f_y \left(\dfrac{\alpha\, \varepsilon_y - \varepsilon_{mu}}{\alpha\, \varepsilon_y + \varepsilon_{mu}} \right)}$$

$$N_{critical} = 0.05\, f_m'\, A_g = 0.05 \times 2.5\, ksi \times 32\, in. \times 7.625\, in. = 30.5 \text{ kips}$$

$$\rho_{\max} = \frac{0.64 \times 2500\, psi \left(\dfrac{0.0025}{4 \times 0.00207 + 0.0025} \right) - \dfrac{30500 lb}{7.625\, in. \times 32\, in.}}{60000\, psi \left(\dfrac{4 \times 0.00207 - 0.0025}{4 \times 0.00207 + 0.0025} \right)}$$

$$\rho_{\max} = \frac{1600\, psi\,(0.231) - 125}{60000\, psi\,(0.536)} = \frac{369.6 - 125}{32160}$$

$$\rho_{\max} = 0.0076$$

This maximum reinforcement is greater than the minimum vertical reinforcement (0.0007), so a design solution is possible..

A.4.3 Flexural Capacity of Wall Specimen UT-W-17

Specimen UT-W-17 has a plan length of 2.67 ft and an axial load (see above) of 30.5 kips. Using a spreadsheet, the nominal interaction diagram for Wall Specimen UT-W-17 is shown in Figure A.4.

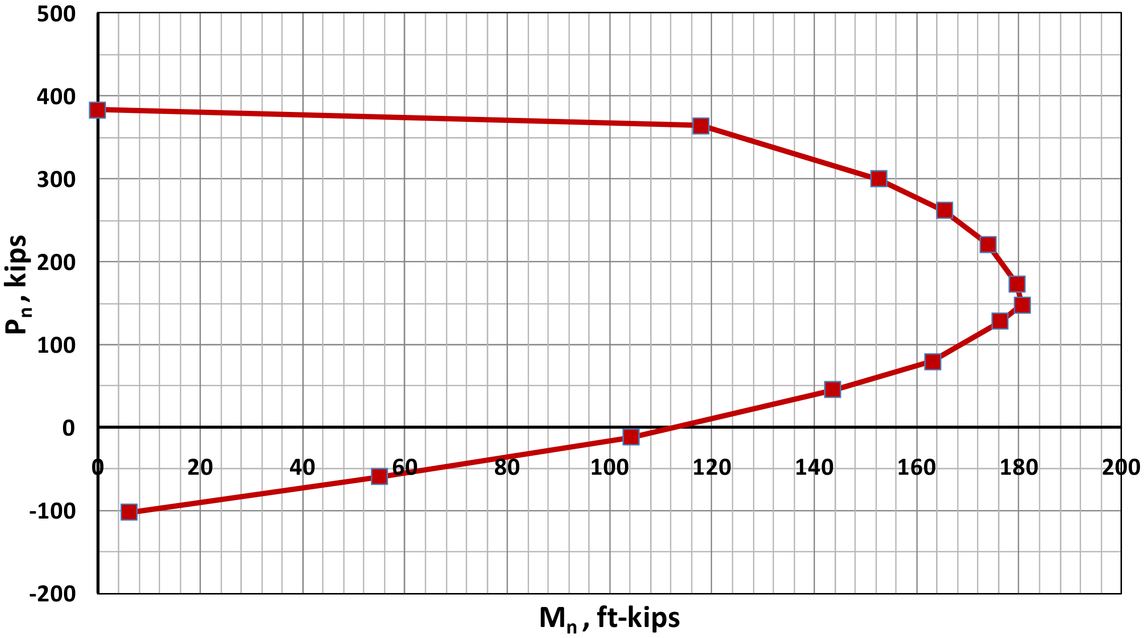

Figure A.4 Strength moment-axial force interaction diagram for Specimen UT-W-17

At an axial load of 30.5 kips, the nominal moment capacity of the wall is 135 kip-ft.

Spreadsheet for calculating strength moment-axial force interaction diagram for concrete masonry shear wall W-17

depth	31.63
emu	0.0025
f'm	2.5
fy	60
Es	29000
d	27.63
(c/d)balanced	0.54717
width	7.63
phi	1

steel layers are counted from the extreme compression fiber to the extreme tension fiber

distances are measured from the extreme compression fiber

compression in masonry and reinforcement is taken as positive

stress in compressive reinforcement is set to zero, because the reinforcement is not laterally supported

Row of Reinforcement	distance	Area
1	4.00	0.44
2	12.00	0.44
3	20.00	0.44
4	28.00	0.44
5	36.00	0.00
6	44.00	0.00
7	52.00	0.00
8	60.00	0.00
9	68.00	0.00
10	76.00	0.00

	c/d	c	Cmas	fs(1)	fs(2)	fs(3)	fs(4)	fs(5)	fs(6)	fs(7)	fs(8)	fs(9)	fs(10)	Moment	Axial Force
pure axial load														0	383
Points controlled by mas	1.08	29.84	364	0.00	0.00	0.00	0.00	-14.97	-34.40	-53.84	-60.00	-60.00	-60.00	118	364
	0.9	24.87	304	0.00	0.00	0.00	-9.13	-32.46	-55.78	-60.00	-60.00	-60.00	-60.00	153	300
	0.8	22.10	270	0.00	0.00	0.00	-19.34	-45.58	-60.00	-60.00	-60.00	-60.00	-60.00	165	261
	0.7	19.34	236	0.00	0.00	-2.47	-32.46	-60.00	-60.00	-60.00	-60.00	-60.00	-60.00	174	221
	0.6	16.58	202	0.00	0.00	-14.97	-49.95	-60.00	-60.00	-60.00	-60.00	-60.00	-60.00	180	174
Points controlled by stee	0.54717	15.12	185	0.00	0.00	-23.41	-60.00	-60.00	-60.00	-60.00	-60.00	-60.00	-60.00	181	148
	0.5	13.82	169	0.00	0.00	-32.46	-60.00	-60.00	-60.00	-60.00	-60.00	-60.00	-60.00	176	128
	0.4	11.05	135	0.00	-6.22	-58.70	-60.00	-60.00	-60.00	-60.00	-60.00	-60.00	-60.00	163	80
	0.293	8.10	99	0.00	-34.97	-60.00	-60.00	-60.00	-60.00	-60.00	-60.00	-60.00	-60.00	135	31
	0.2	5.53	67	0.00	-60.00	-60.00	-60.00	-60.00	-60.00	-60.00	-60.00	-60.00	-60.00	104	-12
	0.1	2.76	34	-32.46	-60.00	-60.00	-60.00	-60.00	-60.00	-60.00	-60.00	-60.00	-60.00	55	-60
	0.01	0.28	3	-60.00	-60.00	-60.00	-60.00	-60.00	-60.00	-60.00	-60.00	-60.00	-60.00	6	-102

A.4.4 Capacity Design for Shear, Wall Specimen UT-W-17

Now check Code Section 3.1.3 (capacity design for shear) for Wall Specimen UT-W-17. The wall is a special reinforced masonry shear wall, so the capacity design requirements of Code Section 1.17.3.2.6.1.1 apply. At an axial load of 30.5 kips, the nominal flexural capacity of this wall is 135 kip-ft. That corresponds to an applied shear of 135 kip-ft divided by the height of the wall (12 ft), or 11.55 kips. Including the additional factor of 1.25, the required nominal shear capacity is,

$$\phi V_n \geq 1.25\, V_u$$
$$V_n \geq \frac{1.25}{\phi} V_u = \frac{1.25}{0.8}\, V_u = 1.56\, V_u = 1.56 \times 11.55\ kips = 17.55\ kips$$

Now check shear capacity. From the 2008 MSJC *Code*, Section 3.3.4.1.2.1,

$$V_n = V_{nm} = \left[4.0 - 1.75\left(\frac{M_u}{V_u\, d_v}\right)\right] A_n \sqrt{f_m^{'}} + 0.25 P_u$$

Because the wall is a cantilever,

$$\frac{M_u}{V_u\, d_v} = \frac{H}{d_v} = \frac{12\ ft}{2.67\, ft} = 4.5$$

However, this quotient need not be taken greater than 1.0, so set it equal to that value:

$$V_n = V_{nm} = \left[4.0 - 1.75\,(1.0)\right] A_n \sqrt{f_m^{'}} + 0.25 P_u$$
$$V_n = V_{nm} = 2.25 \times 7.63\ in. \times 31.63\ in. \sqrt{2500} psi + 0.25 \times 40{,}500\ lb$$
$$V_n = V_{nm} = 34.7\ kips$$

The shear capacity of the wall is sufficient without shear reinforcement. Nominal reinforcement is sufficient. Prescriptive reinforcement requirements must be met. We need horizontal shear reinforcement of at least 0.0007. Use No. 4 bars at 16 in. horizontally.

$$\rho_{horizontal} = \frac{A_s}{bt} = \frac{0.2\ in.^2}{7.625 \times 8\ in.^2} = 0.0033$$

From the 2008 MSJC *Code*, Section 3.3.4.1.2.2,

$$V_{ns} = 0.5\left(\frac{A_v}{s}\right) f_y d_v$$

$$V_{ns} = 0.5\left(\frac{0.2\ in.^2}{8\ in.}\right) 60\ kips / in.^2 \times 27.63\ in.$$

$$V_{ns} = 20.\ 7 kips$$

$$V_n = V_{nm} + V_{ns} = 34.7\ kips + 20.7\ kips = 55.4\ kips$$

This exceeds the required nominal shear capacity of 17.55 kips, and the design is satisfactory for shear.

A.4.5 Summary of Design for Wall Specimen UT-W-17

Use No. 6 vertical bars at 8 in. (4 bars total), and No. 4 horizontal bars at 8 in.

A.4.6 Details of Wall Specimen UT-W-17

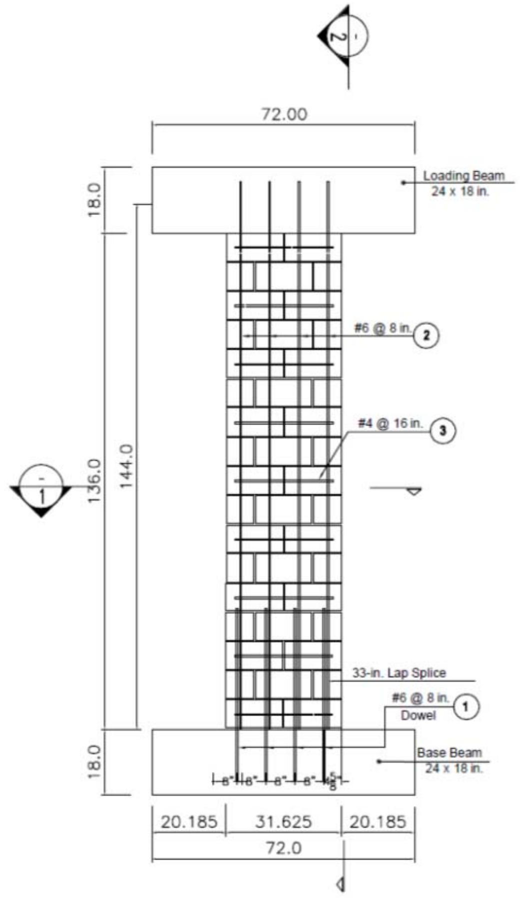

Specimen Wall # 17

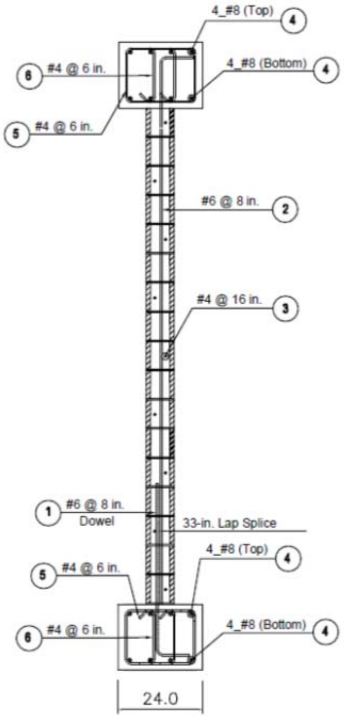

Section 2-2

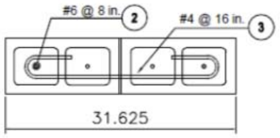

Section 1-1

A.5 DESIGN OF CANTILEVER WALL SPECIMEN UT-W-18

Specimen UT-W-18 has a height of 12 ft and a plan length of 2.67 ft (aspect ratio 4.5), special reinforcement, and a normalized axial load ratio P / ($f_m'A_g$) = 0.10.

A.5.1 Preliminary Check of Prescriptive Reinforcement Requirements for Wall Specimen UT-W-18

Specimen UT-W-18 must meet prescriptive reinforcement requirements. In accordance with the 2008 MSJC *Code*, Section 1.17.3.2.6, the total reinforcement percentage (horizontal and vertical) shall be at least 0.002, with at least one-third of this placed in each direction. The corresponding steel area per foot is 0.002 x 8 in. x 12 in. = 0.2 in.^{2} per foot. These requirements will be re-checked as the design proceeds.

A.5.2 Compute ρ_{max} based on Axial Load

Now check ρ_{max} , considering the wall as a special reinforced masonry shear wall (R = 5, α = 4).

$$\rho_{\max} = \frac{0.64\, f_m' \left(\dfrac{\varepsilon_{mu}}{\alpha\, \varepsilon_y + \varepsilon_{mu}} \right) - \dfrac{N_{critical}}{bd}}{f_y \left(\dfrac{\alpha\, \varepsilon_y - \varepsilon_{mu}}{\alpha\, \varepsilon_y + \varepsilon_{mu}} \right)}$$

$$N_{critical} = 0.10\, f_m'\, A_g = 0.05 \times 2.5\, ksi \times 32\, in. \times 7.625\, in. = 61.0\,\text{kips}$$

$$\rho_{\max} = \frac{0.64 \times 2500\, psi \left(\dfrac{0.0025}{4 \times 0.00207 + 0.0025} \right) - \dfrac{61000\, lb}{7.625\, in. \times 32\, in.}}{60000\, psi \left(\dfrac{4 \times 0.00207 - 0.0025}{4 \times 0.00207 + 0.0025} \right)}$$

$$\rho_{\max} = \frac{1600\, psi\,(0.231) - 250}{60000\, psi\,(0.536)} = \frac{369.6 - 250}{32160}$$

$$\rho_{\max} = 0.0037$$

This maximum reinforcement is greater than the minimum vertical reinforcement (0.0007), so a design solution is possible.

A.5.3 Flexural Capacity of Wall Specimen UT-W-18

Specimen UT-W-18 has a plan length of 2.67 ft and an axial load (see above) of 61.0 kips. Using a spreadsheet, the nominal interaction diagram for Wall UT-W-18 is shown in Figure A.5.

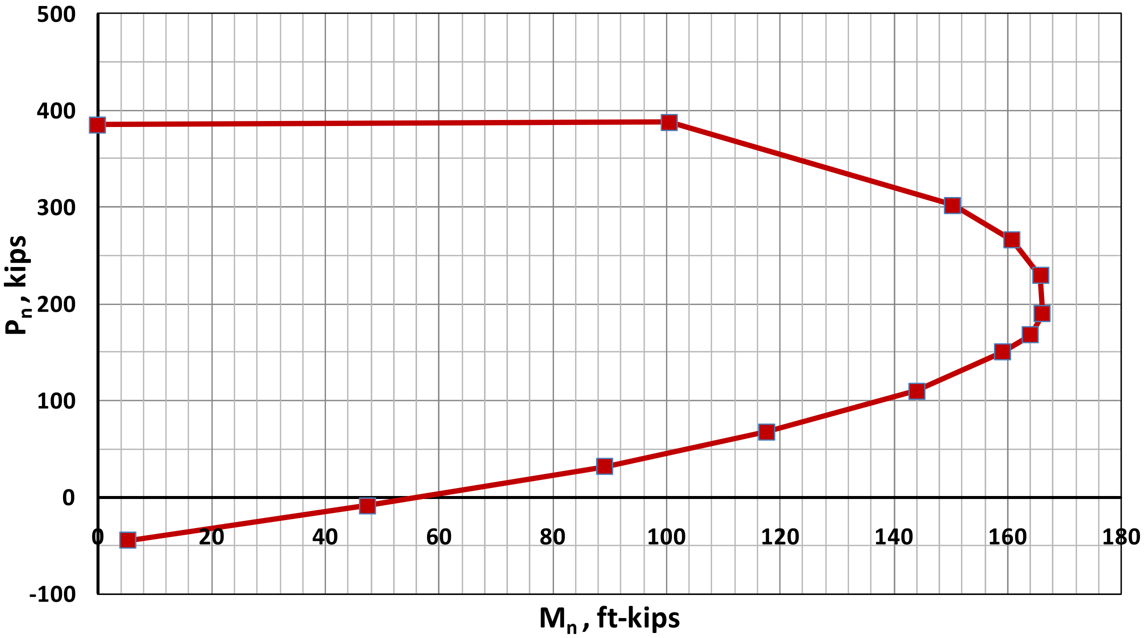

Figure A.5 Strength moment-axial force interaction diagram for Specimen UT-W-18

At an axial load of 61.0 kips, the nominal moment capacity of the wall is 110 kip-ft.

Spreadsheet for calculating strength moment-axial force interaction diagram for concrete masonry shear wall W-18

depth	31.63
emu	0.0025
f'm	2.5
fy	60
Es	29000
d	27.63
(c/d)balanced	0.54717
width	7.63
phi	1

steel layers are counted from the extreme compression fiber to the extreme tension fiber
distances are measured from the extreme compression fiber
compression in masonry and reinforcement is taken as positive
stress in compressive reinforcement is set to zero, because the reinforcement is not laterally supported

Row of Reinforcement	distance	Area
1	4.00	0.20
2	12.00	0.20
3	20.00	0.20
4	28.00	0.20
5	36.00	0.00
6	44.00	0.00
7	52.00	0.00
8	60.00	0.00
9	68.00	0.00
10	76.00	0.00

	c/d	c	Cmas	fs(1)	fs(2)	fs(3)	fs(4)	fs(5)	fs(6)	fs(7)	fs(8)	fs(9)	fs(10)	Moment	Axial Force
pure axial load														0	385
Points controlled by mas	1.15	31.77	388	0.00	0.00	0.00	0.00	-9.64	-27.89	-46.15	-60.00	-60.00	-60.00	100	388
	0.9	24.87	304	0.00	0.00	0.00	-9.13	-32.46	-55.78	-60.00	-60.00	-60.00	-60.00	150	302
	0.8	22.10	270	0.00	0.00	0.00	-19.34	-45.58	-60.00	-60.00	-60.00	-60.00	-60.00	161	266
	0.7	19.34	236	0.00	0.00	-2.47	-32.46	-60.00	-60.00	-60.00	-60.00	-60.00	-60.00	166	229
	0.6	16.58	202	0.00	0.00	-14.97	-49.95	-60.00	-60.00	-60.00	-60.00	-60.00	-60.00	166	189
Points controlled by stee	0.54717	15.12	185	0.00	0.00	-23.41	-60.00	-60.00	-60.00	-60.00	-60.00	-60.00	-60.00	164	168
	0.5	13.82	169	0.00	0.00	-32.46	-60.00	-60.00	-60.00	-60.00	-60.00	-60.00	-60.00	159	150
	0.4	11.05	135	0.00	-6.22	-58.70	-60.00	-60.00	-60.00	-60.00	-60.00	-60.00	-60.00	144	110
	0.28	7.74	94	0.00	-39.96	-60.00	-60.00	-60.00	-60.00	-60.00	-60.00	-60.00	-60.00	114	62
	0.2	5.53	67	0.00	-60.00	-60.00	-60.00	-60.00	-60.00	-60.00	-60.00	-60.00	-60.00	89	31
	0.1	2.76	34	-32.46	-60.00	-60.00	-60.00	-60.00	-60.00	-60.00	-60.00	-60.00	-60.00	48	-9
	0.01	0.28	3	-60.00	-60.00	-60.00	-60.00	-60.00	-60.00	-60.00	-60.00	-60.00	-60.00	5	-45

A.5.4 Capacity Design for Shear, Wall Specimen UT-W-18

Now check Code Section 3.1.3 (capacity design for shear) for Wall Specimen UT-W-18. The wall is a special reinforced masonry shear wall, so the capacity design requirements of Code Section 1.17.3.2.6.1.1 apply. At an axial load of 61.0 kips, the nominal flexural capacity of this wall is 110 kip-ft. That corresponds to an applied shear of 114 kip-ft divided by the height of the wall (12 ft), or 9.10 kips. Including the additional factor of 1.25, the required nominal shear capacity is,

$$\phi V_n \geq 1.25\, V_u$$
$$V_n \geq \frac{1.25}{\phi} V_u = \frac{1.25}{0.8} V_u = 1.56\, V_u = 1.56 \times 9.1\, kips = 14.8\, kips$$

Now check shear capacity. From the 2008 MSJC *Code*, Section 3.3.4.1.2.1,

$$V_n = V_{nm} = \left[4.0 - 1.75 \left(\frac{M_u}{V_u\, d_v} \right) \right] A_n \sqrt{f'_m} + 0.25 P_u$$

Because the wall is a cantilever,

$$\frac{M_u}{V_u\, d_v} = \frac{H}{d_v} = \frac{12\ ft}{2.67\, ft} = 4.0$$

However, this quotient need not be taken greater than 1.0, so set it equal to that value:

$$V_n = V_{nm} = [4.0 - 1.75\,(1.0)] A_n \sqrt{f'_m} + 0.25 P_u$$
$$V_n = V_{nm} = 2.25 \times 7.63\, in. \times 31.63\, in. \sqrt{2500} psi + 0.25 \times 61{,}000\ lb$$
$$V_n = V_{nm} = 42.4\ kips$$

The shear capacity of the wall is sufficient without shear reinforcement. Nominal reinforcement is sufficient. Prescriptive reinforcement requirements must be met. We need horizontal shear reinforcement of at least 0.0007. Use No. 4 bars at 8 in. horizontally.

$$\rho_{horizontal} = \frac{A_s}{bt} = \frac{0.2\ in.^2}{7.625 \times 8\ in.^2} = 0.0033$$

From the 2008 MSJC *Code*, Section 3.3.4.1.2.2,

$$V_{ns} = 0.5\left(\frac{A_v}{s}\right)f_y d_v$$

$$V_{ns} = 0.5\left(\frac{0.2\ in.^2}{8\ in.}\right)60\ kips/in.^2 \times 27.63\ in.$$

$$V_{ns} = 20.7\ kips$$

$$V_n = V_{nm} + V_{ns} = 42.4\ kips + 20.7\ kips = 54.1\ kips$$

This exceeds the required nominal shear capacity of 14.8 kips, and the design is satisfactory for shear.

A.5.5 Summary of Design for Wall Specimen UT-W-18

Use No. 4 vertical bars at 8 in. (4 bars total), and No. 4 horizontal bars at 8 in.

A.5.6 Details of Wall Specimen UT-W-18

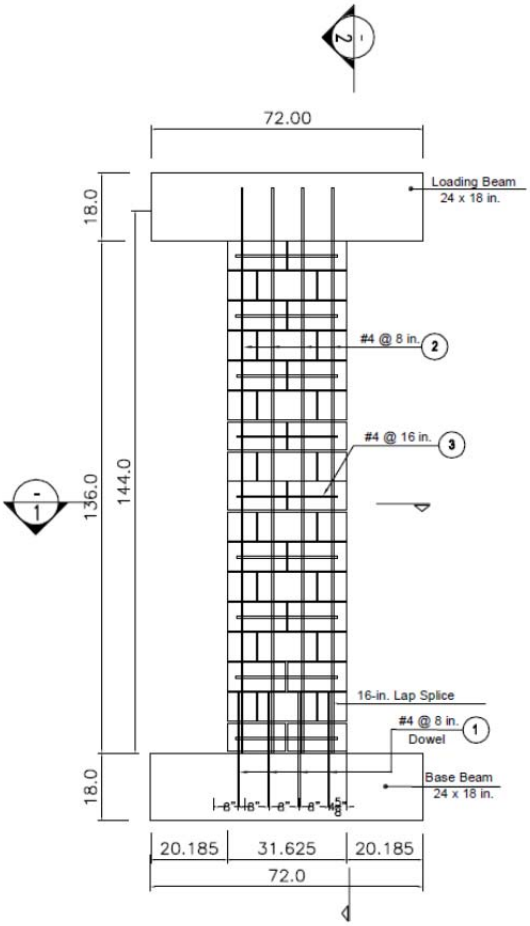

Specimen Wall # 18

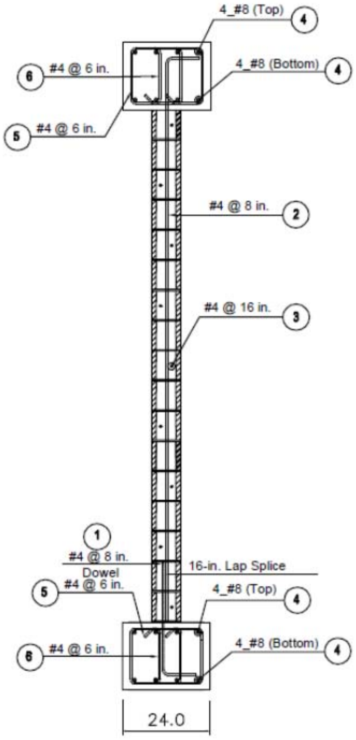

Section 2-2

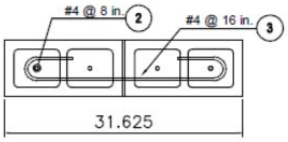

Section 1-1

A.6 DESIGN OF CANTILEVER WALL SPECIMEN UT-W-19

Specimen UT-W-19 has a height of 12 ft and a plan length of 2.67 ft (aspect ratio 4.5), intermediate reinforcement, and a normalized axial load ratio P / ($f_m{}'A_g$) = 0.10.

A.6.1 Preliminary Check of Prescriptive Reinforcement Requirements for Wall Specimen UT-W-19

Specimen UT-W-19 must meet prescriptive reinforcement requirements. In accordance with the 2008 MSJC *Code*, Section 1.17.3.2.6, the total reinforcement percentage (horizontal and vertical) shall be at least 0.002, with at least one-third of this placed in each direction. The corresponding steel area per foot is 0.002 x 8 in. x 12 in. = 0.2 in.^{2} per foot. These requirements will be re-checked as the design proceeds.

A.6.2 Compute ρ_{max} based on Axial Load

Now check ρ_{max} , considering the wall as a intermediate reinforced masonry shear wall (α = 3).

$$\rho_{\max} = \frac{0.64\, f_m^{'} \left(\dfrac{\varepsilon_{mu}}{\alpha\, \varepsilon_y + \varepsilon_{mu}} \right) - \dfrac{N_{critical}}{bd}}{f_y \left(\dfrac{\alpha\, \varepsilon_y - \varepsilon_{mu}}{\alpha\, \varepsilon_y + \varepsilon_{mu}} \right)}$$

$$N_{critical} = 0.10\, f_m^{'}\, A_g = 0.1 \times 2.5\, ksi \times 32\, in. \times 7.625\, in. = 61.0 \text{ kips}$$

$$\rho_{\max} = \frac{0.64 \times 2500\, psi \left(\dfrac{0.0025}{3 \times 0.00207 + 0.0025} \right) - \dfrac{61000\, lb}{7.625\, in. \times 32\, in.}}{60000\, psi \left(\dfrac{3 \times 0.00207 - 0.0025}{3 \times 0.00207 + 0.0025} \right)}$$

$$\rho_{\max} = \frac{1600\, psi\, (0.287) - 187.5}{60000\, psi\, (0.426)} = \frac{459.2 - 250}{25560}$$

$$\rho_{\max} = 0.0082$$

This maximum reinforcement is greater than the minimum vertical reinforcement (0.0007), so a design solution is possible.

A.6.3 Flexural Capacity of Wall Specimen UT-W-19

Specimen UT-W-19 has a plan length of 2.67 ft and an axial load (see above) of 61.0 kips. Using a spreadsheet, the nominal interaction diagram for Wall Specimen UT-W-19 is shown in Figure A.6.

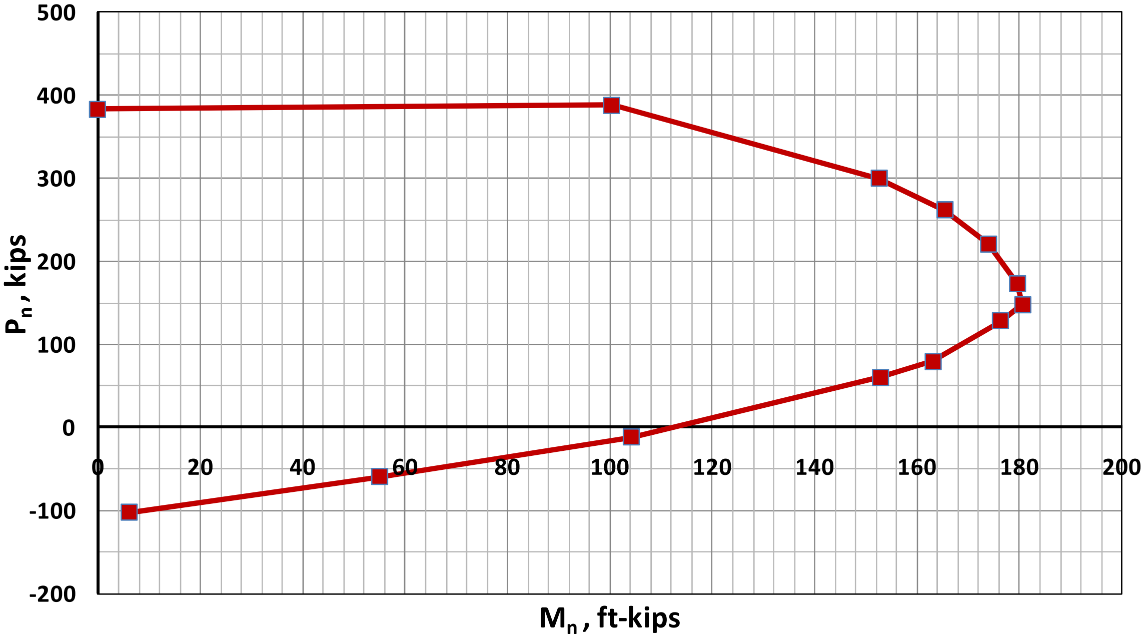

Figure A.6 Strength moment-axial force interaction diagram for Specimen UT-W-19

At an axial load of 61.0 kips, the nominal moment capacity of the wall is 153 kip-ft.

Spreadsheet for calculating strength moment-axial force interaction diagram for concrete masonry shear wall W-19

depth	31.63
emu	0.0025
f'm	2.5
fy	60
Es	29000
d	27.63
(c/d)balanced	0.54717
width	7.63
phi	1

steel layers are counted from the extreme compression fiber to the extreme tension fiber
distances are measured from the extreme compression fiber
compression in masonry and reinforcement is taken as positive
stress in compressive reinforcement is set to zero, because the reinforcement is not laterally supported

Row of Reinforcement	distance	Area
1	4.00	0.44
2	12.00	0.44
3	20.00	0.44
4	28.00	0.44
5	36.00	0.00
6	44.00	0.00
7	52.00	0.00
8	60.00	0.00
9	68.00	0.00
10	76.00	0.00

	c/d	c	Cmas	fs(1)	fs(2)	fs(3)	fs(4)	fs(5)	fs(6)	fs(7)	fs(8)	fs(9)	fs(10)	Moment	Axial Force
pure axial load														0	383
Points controlled by mas	1.15	31.77	388	0.00	0.00	0.00	0.00	-9.64	-27.89	-46.15	-60.00	-60.00	-60.00	100	388
	0.9	24.87	304	0.00	0.00	0.00	-9.13	-32.46	-55.78	-60.00	-60.00	-60.00	-60.00	153	300
	0.8	22.10	270	0.00	0.00	0.00	-19.34	-45.58	-60.00	-60.00	-60.00	-60.00	-60.00	165	261
	0.7	19.34	236	0.00	0.00	-2.47	-32.46	-60.00	-60.00	-60.00	-60.00	-60.00	-60.00	174	221
	0.6	16.58	202	0.00	0.00	-14.97	-49.95	-60.00	-60.00	-60.00	-60.00	-60.00	-60.00	180	174
Points controlled by stee	0.54717	15.12	185	0.00	0.00	-23.41	-60.00	-60.00	-60.00	-60.00	-60.00	-60.00	-60.00	181	148
	0.5	13.82	169	0.00	0.00	-32.46	-60.00	-60.00	-60.00	-60.00	-60.00	-60.00	-60.00	176	128
	0.4	11.05	135	0.00	-6.22	-58.70	-60.00	-60.00	-60.00	-60.00	-60.00	-60.00	-60.00	163	80
	0.357	9.86	120	0.00	-15.70	-60.00	-60.00	-60.00	-60.00	-60.00	-60.00	-60.00	-60.00	153	61
	0.2	5.53	67	0.00	-60.00	-60.00	-60.00	-60.00	-60.00	-60.00	-60.00	-60.00	-60.00	104	-12
	0.1	2.76	34	-32.46	-60.00	-60.00	-60.00	-60.00	-60.00	-60.00	-60.00	-60.00	-60.00	55	-60
	0.01	0.28	3	-60.00	-60.00	-60.00	-60.00	-60.00	-60.00	-60.00	-60.00	-60.00	-60.00	6	-102

A.6.4 Capacity Design for Shear, Wall Specimen UT-W-19

Now check Code Section 3.1.3 (capacity design for shear) for Wall Specimen UT-W-19. The wall is a intermediate reinforced masonry shear wall, so the capacity design requirements of Code Section 1.17.3.2.6.1.1 apply. At an axial load of 61.0 kips, the nominal flexural capacity of this wall is 153 kip-ft. That corresponds to an applied shear of 153 kip-ft divided by the height of the wall (12 ft), or 12.75 kips. Including the additional factor of 1.25, the required nominal shear capacity is,

$$\phi V_n \geq 1.25\, V_u$$
$$V_n \geq \frac{1.25}{\phi} V_u = \frac{1.25}{0.8} V_u = 1.56\, V_u = 1.56 \times 12.75\, kips = 19.9\, kips$$

Now check shear capacity. From the 2008 MSJC *Code*, Section 3.3.4.1.2.1,

$$V_n = V_{nm} = \left[4.0 - 1.75 \left(\frac{M_u}{V_u\, d_v} \right) \right] A_n \sqrt{f_m^{'}} + 0.25 P_u$$

Because the wall is a cantilever,

$$\frac{M_u}{V_u\, d_v} = \frac{H}{d_v} = \frac{12\ ft}{2.67\, ft} = 4.5$$

However, this quotient need not be taken greater than 1.0, so set it equal to that value:

$$V_n = V_{nm} = \left[4.0 - 1.75\,(1.0) \right] A_n \sqrt{f_m^{'}} + 0.25 P_u$$
$$V_n = V_{nm} = 2.25 \times 7.63\, in. \times 31.63\, in. \sqrt{2500} psi + 0.25 \times 61{,}000\, lb$$
$$V_n = V_{nm} = 42.4\, kips$$

The shear capacity of the wall is sufficient without shear reinforcement.

Prescriptive reinforcement requirements must be met. We need horizontal shear reinforcement of at least 0.0007. Use No. 4 bars at 16 in. horizontally.

$$\rho_{horizontal} = \frac{A_s}{bt} = \frac{0.2\ in.^2}{7.625 \times 16\ in.^2} = 0.0016$$

From the 2008 MSJC *Code*, Section 3.3.4.1.2.2,

$$V_{ns} = 0.5\left(\frac{A_v}{s}\right) f_y d_v$$

$$V_{ns} = 0.5\left(\frac{0.2\, in.^2}{16\, in.}\right) 60\, kips / in.^2 \times 27.63\, in.$$

$$V_{ns} = 10.36\, kips$$

$$V_n = V_{nm} + V_{ns} = 42.4\, kips + 10.36\, kips = 52.76\, kips$$

This exceeds the required nominal shear capacity of 19.9 kips, and the design is satisfactory for shear.

A.6.5 Summary of Design for Wall Specimen UT-W-19

Use No. 6 vertical bars at 8 in. (4 bars total), and No. 4 horizontal bars at 16 in.

A.6.6 Details of Wall Specimen UT-W-19

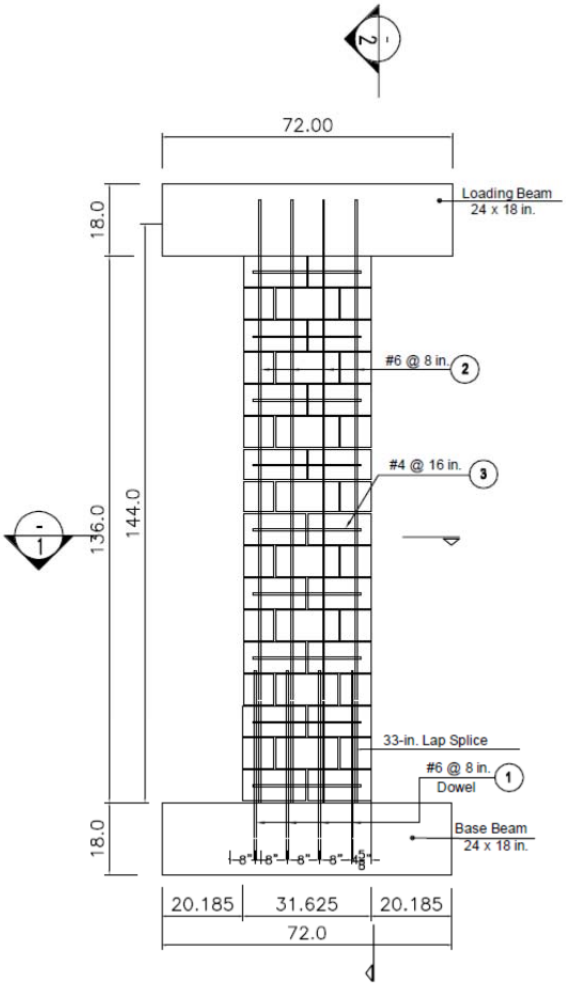

Specimen Wall # 19

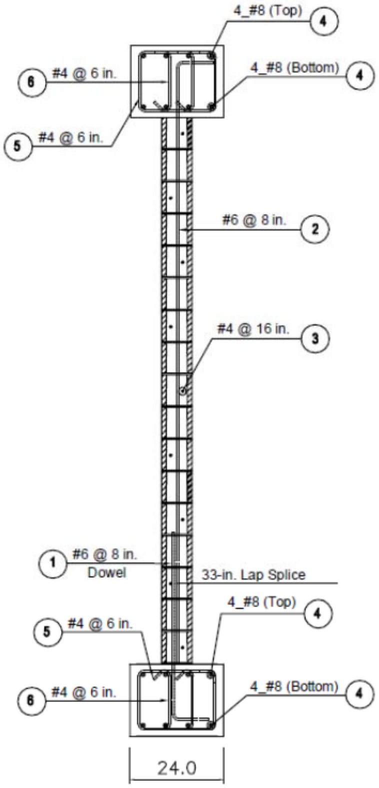

Section 2-2

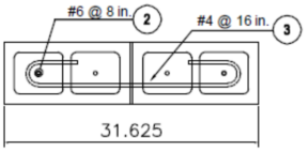

Section 1-1

A.7 DESIGN OF CANTILEVER WALL SPECIMEN UT-W-20

Specimen UT-W-20 has a height of 12 ft and a plan length of 2.67 ft (aspect ratio 4.5), intermediate reinforcement, and a normalized axial load ratio P / ($f_m{}'A_g$) = 0.15.

A.7.1 Preliminary Check of Prescriptive Reinforcement Requirements for Wall Specimen 20

Specimen UT-W-20 must meet prescriptive reinforcement requirements. In accordance with the 2008 MSJC *Code*, Section 1.17.3.2.6, the total reinforcement percentage (horizontal and vertical) shall be at least 0.002, with at least one-third of this placed in each direction. The corresponding steel area per foot is 0.002 x 8 in. x 12 in. = 0.2 in.^{2} per foot. These requirements will be re-checked as the design proceeds.

A.7.2 Compute ρ_{max} based on Axial Load

Now check ρ_{max} , considering the wall as a special reinforced masonry shear wall (α = 3).

$$\rho_{\max} = \frac{0.64\, f_m^{'} \left(\dfrac{\varepsilon_{mu}}{\alpha\,\varepsilon_y + \varepsilon_{mu}} \right) - \dfrac{N_{critical}}{bd}}{f_y \left(\dfrac{\alpha\,\varepsilon_y - \varepsilon_{mu}}{\alpha\,\varepsilon_y + \varepsilon_{mu}} \right)}$$

$$N_{critical} = 0.15\, f_m^{'}\, A_g = 0.15 \times 2.5\, ksi \times 32\, in. \times 7.625\, in. = 91.5 \text{ kips}$$

$$\rho_{\max} = \frac{0.64 \times 2500\, psi \left(\dfrac{0.0025}{3 \times 0.00207 + 0.0025} \right) - \dfrac{91500\, lb}{7.625\, in. \times 32\, in.}}{60000\, psi \left(\dfrac{3 \times 0.00207 - 0.0025}{3 \times 0.00207 + 0.0025} \right)}$$

$$\rho_{\max} = \frac{1600\, psi\,(0.287) - 375}{60000\, psi\,(0.426)} = \frac{459.2 - 375}{25560}$$

$$\rho_{\max} = 0.004$$

This maximum reinforcement is greater than the minimum vertical reinforcement (0.0007), so a design solution is possible.

A.7.3 Flexural Capacity of Wall Specimen UT-W-20

Specimen UT-W-20 has a plan length of 2.67 ft and an axial load (see above) of 91.5 kips. Using a spreadsheet, the nominal interaction diagram for Wall Specimen UT-W-20 is shown in Figure A.7.

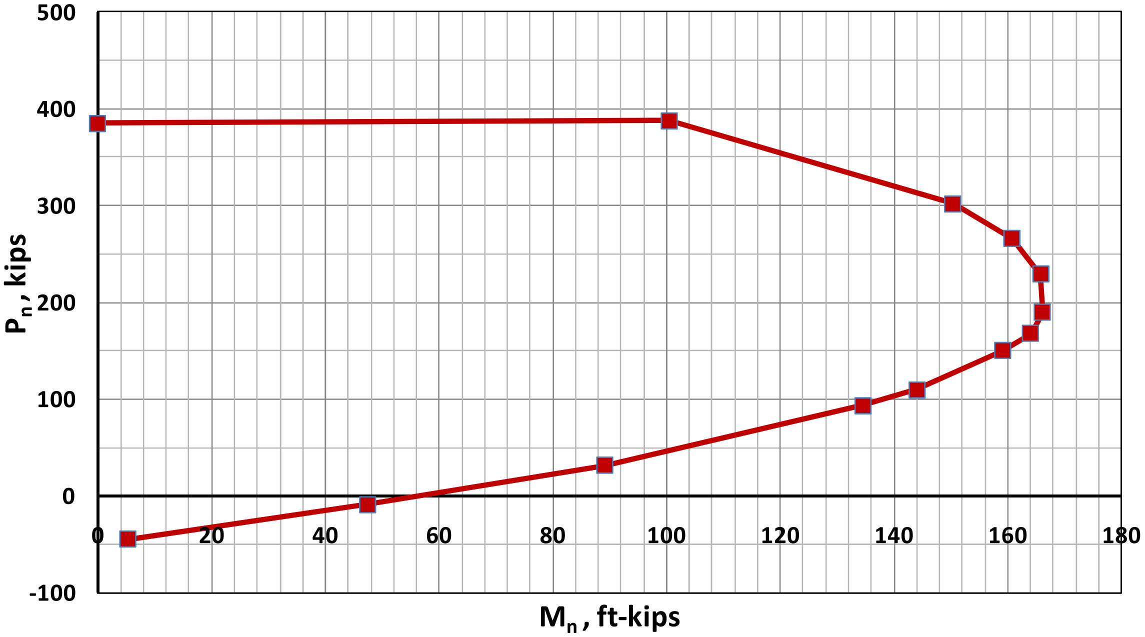

Figure A.7 Strength moment-axial force interaction diagram for Specimen UT-W-2At an axial load of 91.5 kips, the nominal moment capacity of the wall is 134 kip-ft.

Spreadsheet for calculating strength moment-axial force interaction diagram for concrete masonry shear wall W-20

depth	31.63
emu	0.0025
f'm	2.5
fy	60
Es	29000
d	27.63
(c/d)balanced	0.54717
width	7.63
phi	1

steel layers are counted from the extreme compression fiber to the extreme tension fiber

distances are measured from the extreme compression fiber

compression in masonry and reinforcement is taken as positive

stress in compressive reinforcement is set to zero, because the reinforcement is not laterally supported

Row of Reinforcement	distance	Area
1	4.00	0.20
2	12.00	0.20
3	20.00	0.20
4	28.00	0.20
5	36.00	0.00
6	44.00	0.00
7	52.00	0.00
8	60.00	0.00
9	68.00	0.00
10	76.00	0.00

	c/d	c	Cmas	fs(1)	fs(2)	fs(3)	fs(4)	fs(5)	fs(6)	fs(7)	fs(8)	fs(9)	fs(10)	Moment	Axial Force
pure axial load														0	385
Points controlled by mas	1.15	31.77	388	0.00	0.00	0.00	0.00	-9.64	-27.89	-46.15	-60.00	-60.00	-60.00	100	388
	0.9	24.87	304	0.00	0.00	0.00	-9.13	-32.46	-55.78	-60.00	-60.00	-60.00	-60.00	150	302
	0.8	22.10	270	0.00	0.00	0.00	-19.34	-45.58	-60.00	-60.00	-60.00	-60.00	-60.00	161	266
	0.7	19.34	236	0.00	0.00	-2.47	-32.46	-60.00	-60.00	-60.00	-60.00	-60.00	-60.00	166	229
	0.6	16.58	202	0.00	0.00	-14.97	-49.95	-60.00	-60.00	-60.00	-60.00	-60.00	-60.00	166	189
Points controlled by stee	0.54717	15.12	185	0.00	0.00	-23.41	-60.00	-60.00	-60.00	-60.00	-60.00	-60.00	-60.00	164	168
	0.5	13.82	169	0.00	0.00	-32.46	-60.00	-60.00	-60.00	-60.00	-60.00	-60.00	-60.00	159	150
	0.4	11.05	135	0.00	-6.22	-58.70	-60.00	-60.00	-60.00	-60.00	-60.00	-60.00	-60.00	144	110
	0.353	9.75	119	0.00	-16.70	-60.00	-60.00	-60.00	-60.00	-60.00	-60.00	-60.00	-60.00	134	92
	0.2	5.53	67	0.00	-60.00	-60.00	-60.00	-60.00	-60.00	-60.00	-60.00	-60.00	-60.00	89	31
	0.1	2.76	34	-32.46	-60.00	-60.00	-60.00	-60.00	-60.00	-60.00	-60.00	-60.00	-60.00	48	-9
	0.01	0.28	3	-60.00	-60.00	-60.00	-60.00	-60.00	-60.00	-60.00	-60.00	-60.00	-60.00	5	-45

A.7.4 Capacity Design for Shear, Wall Specimen UT-W-20

Now check Code Section 3.1.3 (capacity design for shear) for Wall Specimen UT-W-20. The wall is a special reinforced masonry shear wall, so the capacity design requirements of Code Section 1.17.3.2.6.1.1 apply. At an axial load of 91.5 kips, the nominal flexural capacity of this wall is 134 kip-ft. That corresponds to an applied shear of 134 kip-ft divided by the height of the wall (12 ft), or 11.1 kips. Including the additional factor of 1.25, the required nominal shear capacity is,

$$\phi V_n \geq 1.25\, V_u$$

$$V_n \geq \frac{1.25}{\phi} V_u = \frac{1.25}{0.8} V_u = 1.56\, V_u = 1.56 \times 11.1\, kips = 17.31\, kips$$

Now check shear capacity. From the 2008 MSJC *Code*, Section 3.3.4.1.2.1,

$$V_n = V_{nm} = \left[4.0 - 1.75 \left(\frac{M_u}{V_u\, d_v} \right) \right] A_n \sqrt{f_m'} + 0.25 P_u$$

Because the wall is a cantilever,

$$\frac{M_u}{V_u\, d_v} = \frac{H}{d_v} = \frac{12\ ft}{2.67\, ft} = 4.50$$

However, this quotient need not be taken greater than 1.0, so set it equal to that value:

$$V_n = V_{nm} = [4.0 - 1.75\, (1.0)] A_n \sqrt{f_m'} + 0.25 P_u$$

$$V_n = V_{nm} = 2.25 \times 7.63\, in. \times 31.63\, in. \sqrt{2500} psi + 0.25 \times 91{,}500\ lb$$

$$V_n = V_{nm} = 50.0\ kips$$

The shear capacity of the wall is sufficient without shear reinforcement. Nominal reinforcement is sufficient. Prescriptive reinforcement requirements must be met. We need horizontal shear reinforcement of at least 0.0007. Use No. 4 bars at 16 in. horizontally.

$$\rho_{horizontal} = \frac{A_s}{bt} = \frac{0.2\ in.^2}{7.625 \times 16\ in.^2} = 0.0016$$

From the 2008 MSJC *Code*, Section 3.3.4.1.2.2,

$$V_{ns} = 0.5\left(\frac{A_v}{s}\right) f_y d_v$$

$$V_{ns} = 0.5\left(\frac{0.2\,in.^2}{16\,in.}\right) 60\,kips/in.^2 \times 27.63\,in.$$

$$V_{ns} = 10.36\,kips$$

$$V_n = V_{nm} + V_{ns} = 50.0\,kips + 10.36\,kips = 60.36\,kips$$

This exceeds the required nominal shear capacity of 17.3 kips, and the design is satisfactory for shear.

A.7.5 Summary of Design for Wall Specimen UT-W-20

Use No. 4 vertical bars at 8 in. (4 bars total), and No. 4 horizontal bars at 16 in.

A.7.6 Details of Wall Specimen UT-W-20

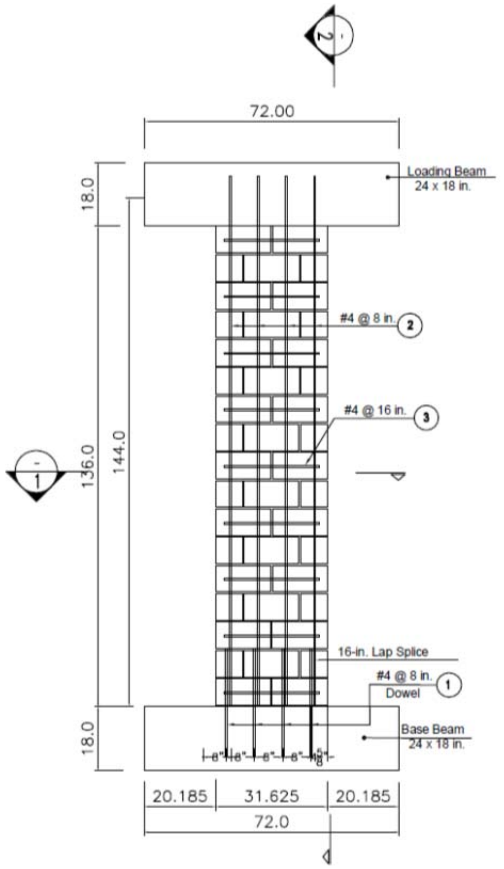

Specimen Wall # 20

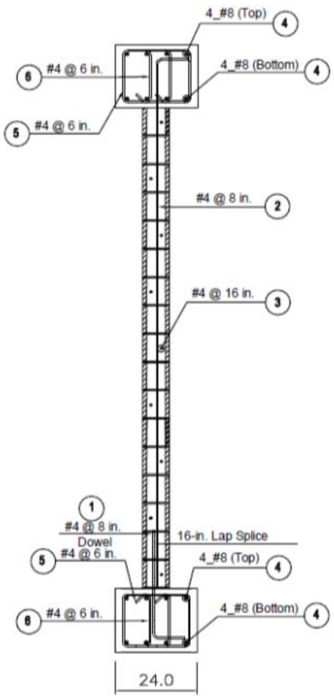

Section 2-2

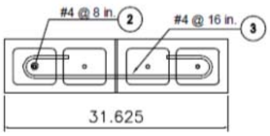

Section 1-1

APPENDIX B Test Results of Cantilever CMU Wall Specimens

B.1 TEST RESULTS FOR SPECIMEN UT-W-14

Specimen UT-W-14 was detailed according to the requirements of the 2008 MSJC *Code*. It has a height of 12 ft and a plan length of 4 ft (aspect ratio 3.0), required prescriptive reinforcement for a Special Reinforced Masonry Shear Wall (2008 MSJC *Code*), and a normalized axial load ratio P / ($f_m' A_g$) of 0.10. The vertical reinforcement ratio was 0.0033, with No. 4 reinforcing bars at 8 in. (every cell); and the horizontal reinforcement ratio was 0.0016, with No. 4 bars at 16 in. The specimen used cement-lime mortar conforming to the proportion specification for Type S of ASTM C270, and grout conforming to the strength specification of ASTM C476. A photo of the specimen before testing is shown in Figure B.1, and details for the specimen are shown in Figure B.2.

Figure B.1 Specimen UT-W-14 before testing

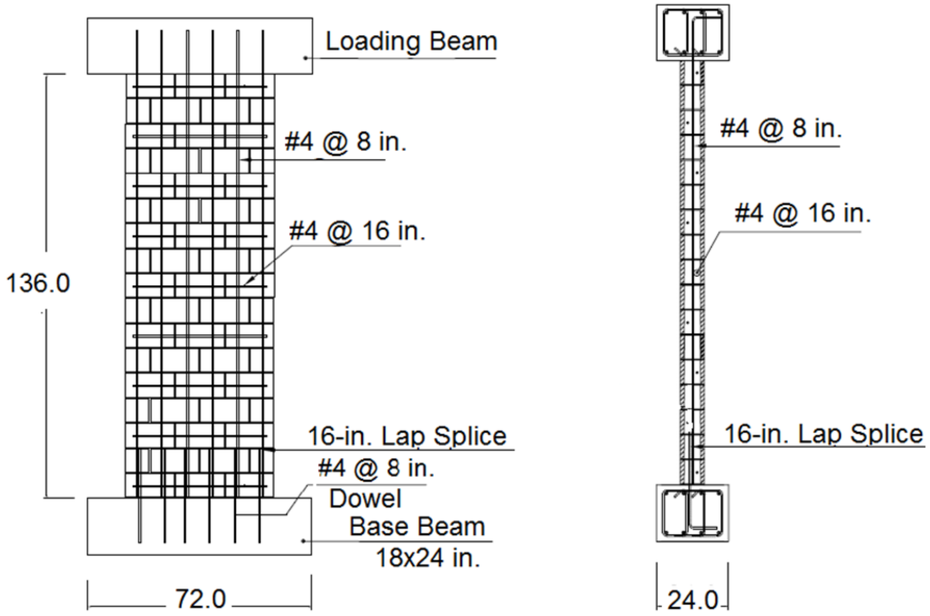

Figure B.2 Details for Specimen UT-W-14

B.1.1 Loading History for Specimen UT-W-14

Specimen UT-W-14 was first subjected to a preliminary test to estimate the yield displacement, Δ_y. The planned in-plane loading history for base shear in the specimen is shown in Figure B.3. On July 5, 2011, Specimen UT-W-14 was loaded at a rate of 0.3 in./min to two cycles of reversed displacements of ±1, 2, 3, 4, and 6 times that predicted yield displacement, as shown in Figure B.3. It was then loaded to a half-cycle to a displacement of 8 times that predicted yield displacement. The test was stopped when the peak capacity dropped to 20% or less of the experimentally observed maximum capacity (capping point). The testing took about 10 hours. In this test the specimen was loaded first to the north and then to the south.

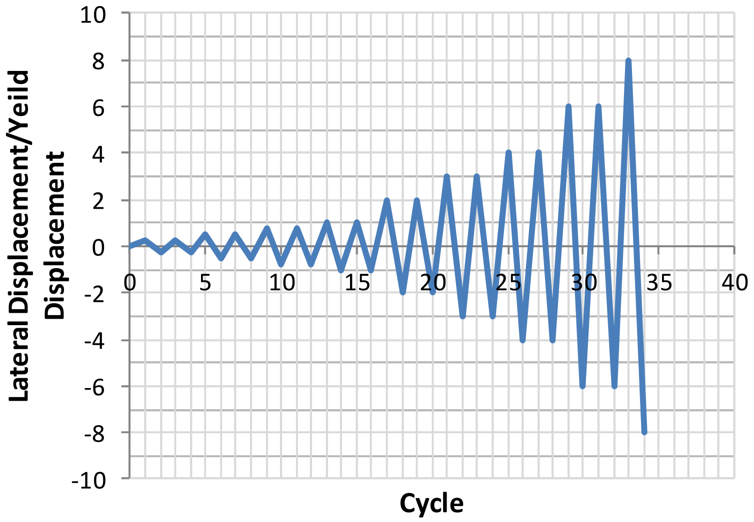

Figure B.3 Proposed loading history, Specimen UT-W-14

B.1.2 Major Test Observations, Specimen UT-W-14

The behavior of Specimen UT-W-14 was controlled by flexure. The value of Δ_y calculated in the preliminary phase of the test was 0.80 in., equivalent to a drift ratio of 0.56%. Flexural cracks (horizontal cracks in the bed joints) started early in the test before $1\Delta_y$, followed by shear cracks which propagated at $2\Delta_y$ (1.12% drift ratio) as presented in Figure B.4a. As shown in Figure B.5, evidence of toe crushing was found first at the south end at first cycle of $2\Delta_y$ (1.12% drift ratio) and then at the north end at second cycle of $2\Delta_y$ (1.12% drift). As shown in Figure B.4b, significant toe crushing and spalling at toes were observed, followed by buckling of extreme vertical bars at the second cycles to $6\Delta_y$ (3.36% drift ratio). There was no evidence of fracture of the vertical bars at the base.

(a) Cycle 2∆y *(a) Cycle 6∆y*

Figure B.4 Flexural and shear cracking, severe crushing and spalling, and buckling of longitudinal bars, Specimen UT-W-14

North toe ***South toe***

Figure B.5 Onset of toe crushing, Specimen UT-W-14

Figure B.6 shows the specimen upon completion of the test. As shown in Figure B.7, reversed cyclic loading caused toe crushing at the base of the specimen. The transverse reinforcing bars, even with extensive toe crushing and spalling, hooked around the longitudinal bar splices, kept the spliced bars from coming apart.

Figure B.6 Specimen UT-W-14 at end of test

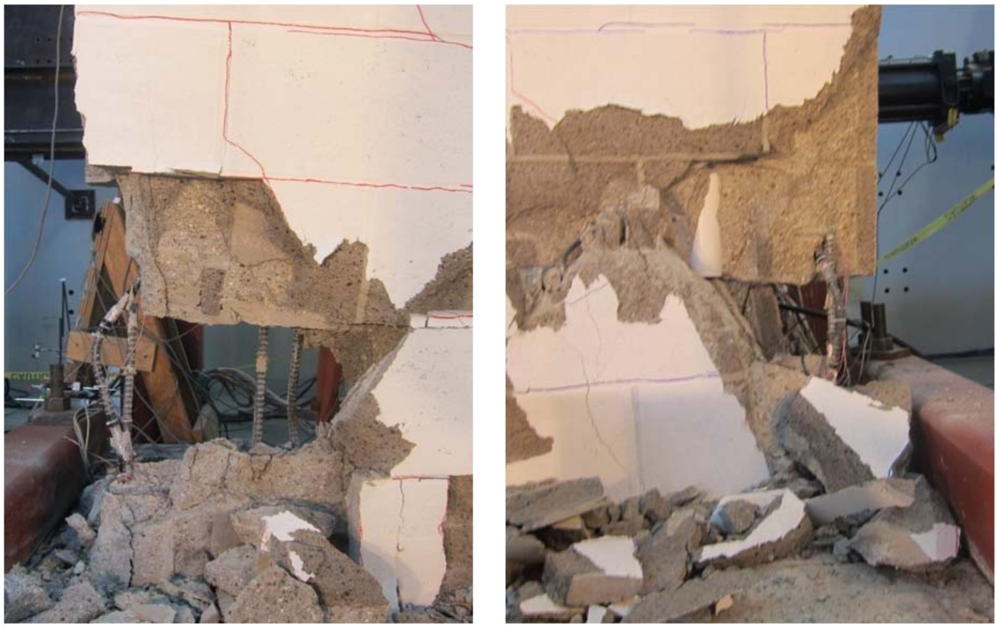

North toe ***South toe***

Figure B.7 Detail of toe splices at end of test, Specimen UT-W-14

B.1.3 Load-Displacement Behavior for Specimen UT-W-14

The load-displacement relationship of Specimen UT-W-14 is presented in Figure B.8 in terms of lateral displacement, which references five major events during testing:

1) first yield of the extreme vertical reinforcement ($\varepsilon_y = 0.0022$);
2) maximum useful strain in the masonry ($\varepsilon_{mu} = 0.0025$);
3) maximum capacity (capping point);
4) onset of toe crushing ; and
5) decrease in capacity to 50% of maximum capacity.

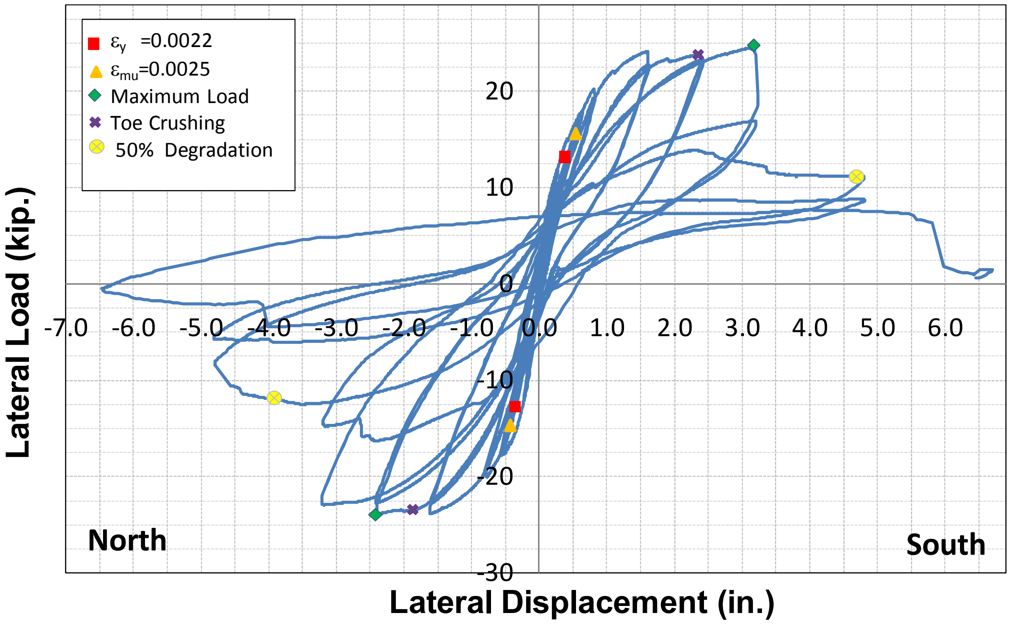

Figure B.8 Load versus top displacement, Specimen UT-W-14

Curvatures were determined over the wall height based on strain profiles, and are shown in Figure B.9. The strain profiles were calculated using five potentiometers along the inside edge of the wall (this was mirrored on the opposite side). The curvatures were determined for the first cycle to each displacement. Due to spalling of the face shells at the wall toes and detachment of the displacement potentiometer anchors, these displacement measurements were discontinued at later stages of testing. Therefore, strains and curvatures at larger displacements were not available.

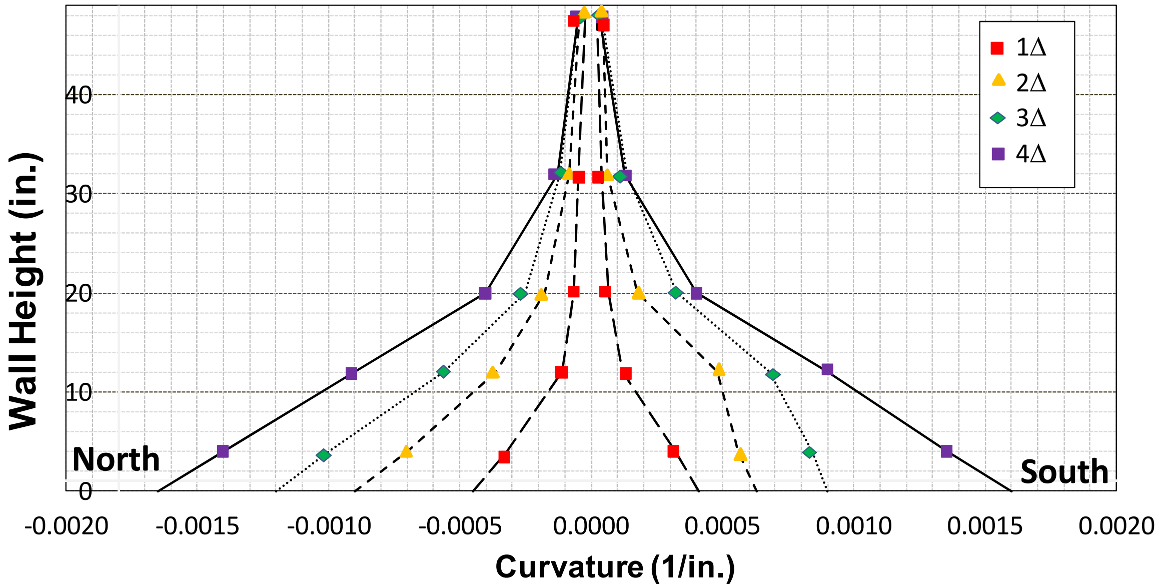

Figure B.9 Wall Curvature of Specimen UT-W-14

B.1.4 Displacement Ductility, Specimen UT-W-14

The values obtained for the displacement ductility are presented in Table B-1. The results are presented for both load directions (push to the North and pull to the South), and then averaged.

Table B-1 Calculated displacement ductilities for Specimen UT-W-14

Direction of Load	**Moment and Curvature Parameters**					
	P'_y (kips)	Δ'_y (in.)	Δ_u (in.)	P_y (kips)	Δ_y (in.)	μ_Δ
Push (North)	12.95	0.40	3.62	23.31	0.72	5.02
Pull (South)	13.45	0.38	3.15	22.45	0.63	4.96
					Average	4.99

The curvature ductility of Specimen UT-W-14 was also determined using a similar process as above. The values obtained for the curvature ductility are presented in

Table B-2. The results are presented for both load directions: push to the north and pull to the south, and then averaged.

Table B-2 Calculated curvature ductilities for Specimen UT-W-14

Direction of Load	**Moment and Curvature Parameters**					
	M'_y (kip-in.)	ϕ'_y (in.$^{-1}$)	ϕ_u (in.$^{-1}$)	M_y (kip-in.)	ϕ_y (in.$^{-1}$)	μ_ϕ
Push (North)	1865	0.00009	0.0017	3357	0.00016	10.5
Pull (South)	1937	0.00010	0.0016	3233	0.00017	9.6
					Average	10.0

B.1.5 Calculation of Plastic Hinge Lengths, Specimen UT-W-14

B.1.5.1 Method 1 (Bohl and Adebar 2011 and Shedid et al. 2010)

In Table B-3, the calculated yielded lengths are presented as a function of drift ratio for each load direction, and are then averaged between the two directions. In the last line of the table, the calculated yielded lengths are expressed in terms of L_w , the plan length of the wall.

Table B-3 Extent of Plasticity of Specimen UT Wall-14

Drift Ratio (Displacement)	**Yielded Lengths, $L_{yielded}$ (in.), for Different Drift Ratios**			
	0.56% (Δ_y)	**1.11% ($2\Delta_y$)**	**1.67% ($3\Delta_y$)**	**2.22% ($4\Delta_y$)**
Push North	10.25	23.5	29.5	31.5
Pull South	10.5	21.25	30.5	31.0
Average	10.37	22.37	30.0	31.25
$L_{yielded}/L_w$	21.6%	46.6%	62.5%	65.1%

If the plastic hinge length l_p is assumed equal to 0.5 $L_{yielded}$, then the resulting plastic hinge lengths are as shown in Table B-4 for each drift ratio.

Table B-4 Calculation of plastic hinge lengths of Specimen UT-W-14

	Plastic Hinge Lengths, l_p (in.), for Different Drift Ratios			
Drift Ratio (Displacement)	**0.56% (Δ_y)**	**1.11% ($2\Delta_y$)**	**1.67% ($3\Delta_y$)**	**2.22% ($4\Delta_y$)**
Yielded Length	10.37	22.37	30.0	31.25
Plastic Hinge Length (l_p)	5.18	11.19	15.0	15.63
l_p/L_w	10.8%	23.3%	31.25%	32.6%

B.1.5.2 Method 2 (Shedid et al. 2010 and Dazio 2009)

The equivalent plastic hinge lengths for both load directions at different drift ratios are calculated as shown in Table B-5.

Table B-5 Equivalent plastic hinge length of Specimen UT-W-14

Drift Ratio (Displacement)	Plastic Hinge Lengths, l_p (in.), for Different Drift Ratios			
	0.56% (Δ_y)	**1.11% ($2\Delta_y$)**	**1.67% ($3\Delta_y$)**	**2.22% ($4\Delta_y$)**
Push North	8.3	10.8	13.2	13.1
Pull South	9.3	16.7	18.5	13.6
Average	8.8	13.8	15.9	13.4
l_p/L_w	18.5%	28.9%	33.4%	28.1%

B.1.5.3 Method 3 (Bohl and Adebar 2011)

The calculated plastic hinge lengths were determined for both load direction: push to the north and pull to the south. The results are shown in Table B-6.

Table B-6 Predicted plastic hinge lengths for Specimen UT-W-14

Direction of Load	**Moment and Plastic Hinge Parameters**					
	M_y (kip-in.)	M_{max} (kip-in.)	z (in.)	$L_{yielded}$ (in.)	$l_p = 0.5L_{yielded}$ (in.)	l_p/L_w
Push (North)	1865	3525	144	67.8	33.9	0.71
Pull (South)	1937	3628	144	67.1	33.5	0.70
					Average	0.70

B.1.6 Components of Displacements for Specimen UT-W-14

Load-displacement curves for total sliding and shear component of total tip displacement are given in Figure B.10 and Figure B.11, and total displacement and shear deformation are compared in Figure B.12.

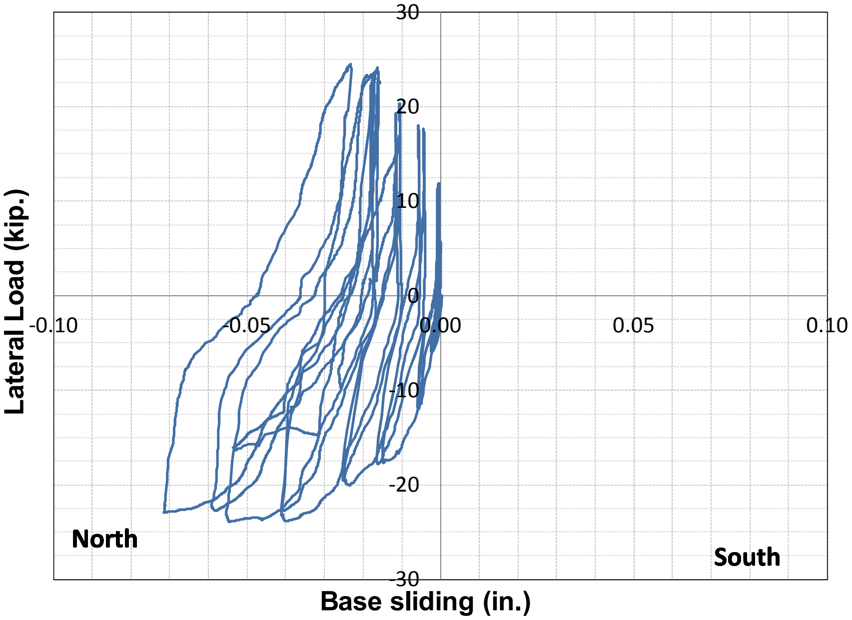

Figure B.10 Base sliding, Specimen UT-W-14

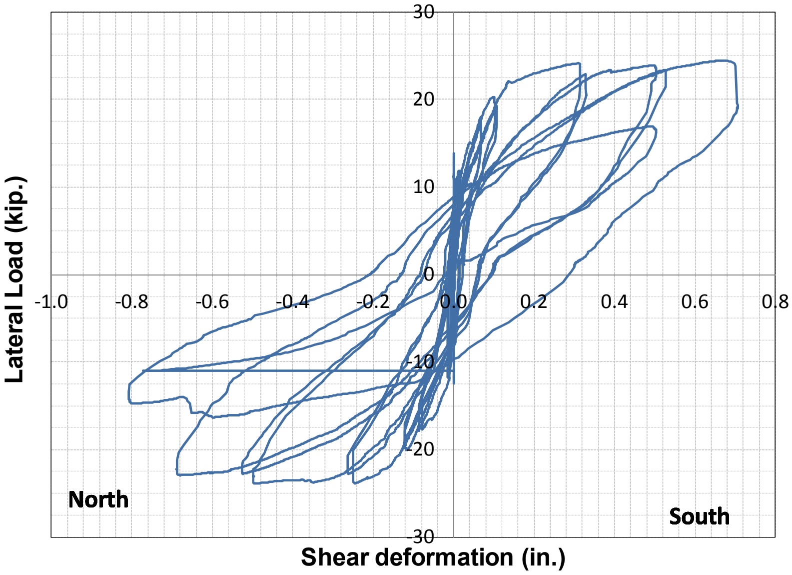

Figure B.11 Shear deformation, Specimen UT-W-14

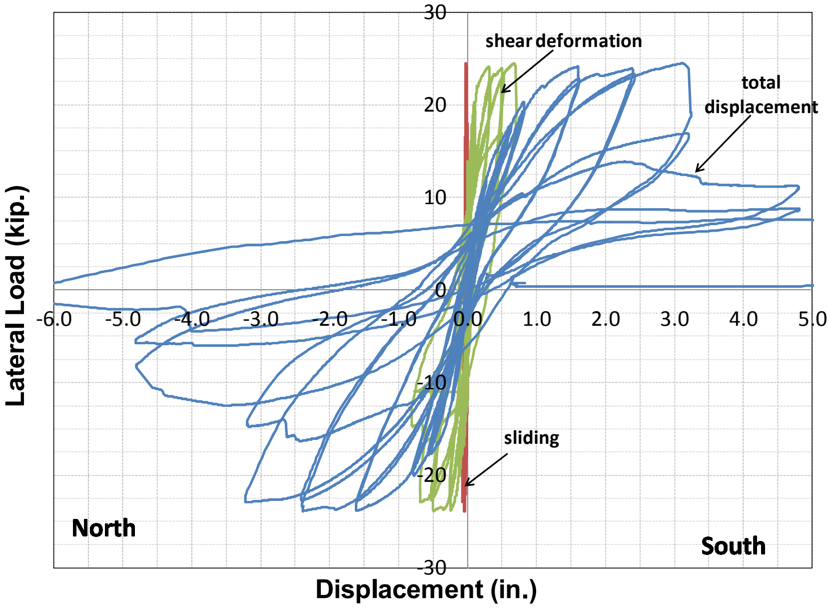

Figure B.12 Components of displacements for Specimen UT-W-14

B.2 TEST RESULTS FOR SPECIMEN UT-W-15

Specimen UT-W-15 was detailed according to the requirements of the 2008 MSJC *Code*. It has a height of 12 ft and a plan length of 4 ft (aspect ratio 3.0), required prescriptive reinforcement for an Intermediate Reinforced Masonry Shear Wall (2008 MSJC *Code*), and a normalized axial load ratio P / ($f_m{}' A_g$) of 0.10. The vertical reinforcement ratio was 0.0072, with No. 6 reinforcing bars at 8 in. (every cell); and the horizontal reinforcement ratio was 0.0016, with No. 4 bars at 16 in. The specimen used cement-lime mortar conforming to the proportion specification for Type S of ASTM C270, and grout conforming to the strength specification of ASTM C476. A photo of the specimen before testing is shown in Figure B.13, and details for the specimen are shown Figure B.14.

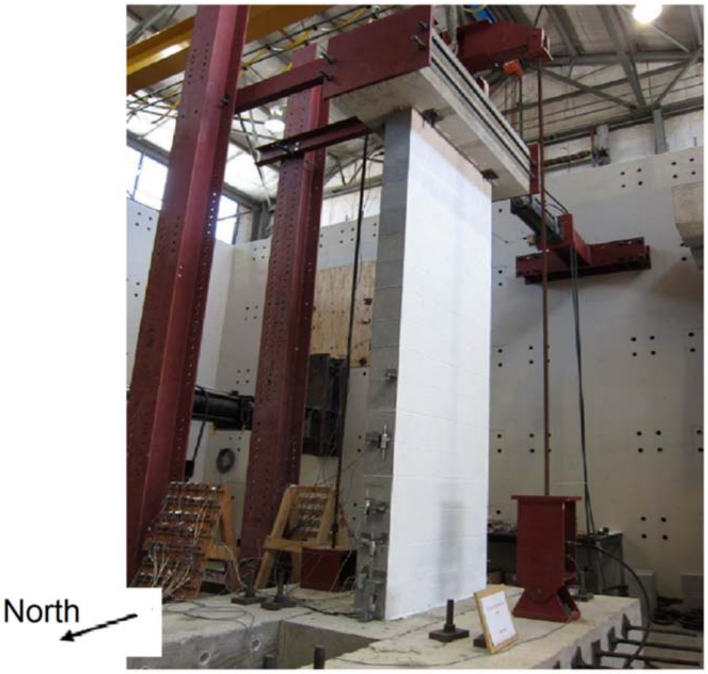

Figure B.13 Specimen UT-W-15 before testing

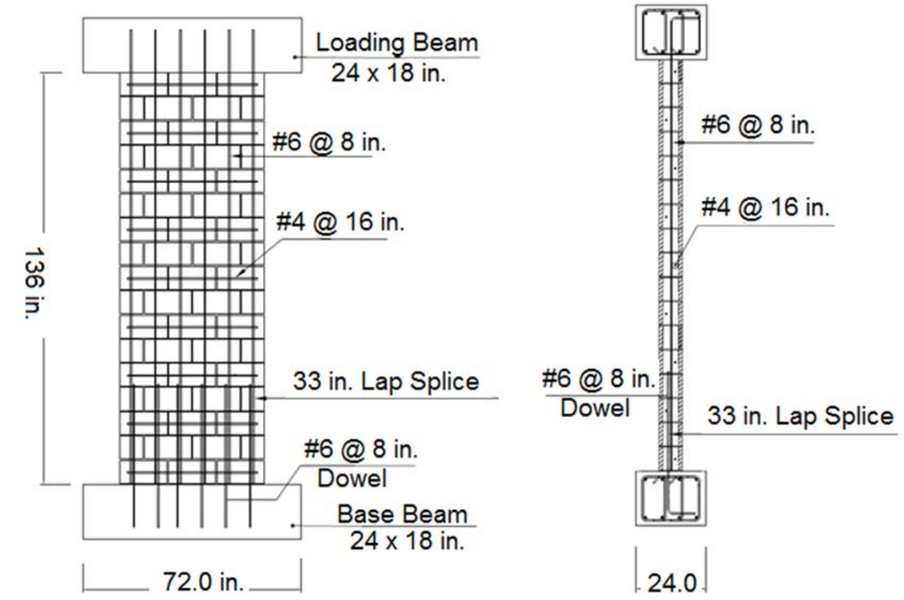

Figure B.14 Details for Specimen UT-W-15

B.2.1 Loading History for Specimen UT-W-15

Specimen UT-W-15 was first subjected to a preliminary test to estimate the yield displacement, Δ_y. The planned in-plane loading history for base shear in the specimen is shown in Figure B.15. On June 21, 2011, Specimen UT-W-15 was loaded at a rate of 0.3 in./min to two cycles of reversed displacements of ±1, 2, 3, and 4 times that predicted yield displacement. It was then loaded to a half-cycle to a displacement of 6 times that predicted yield displacement. The test was stopped when the maximum capacity dropped to 20% or less of the experimentally observed maximum capacity (capping point). The testing took about 6 hours.

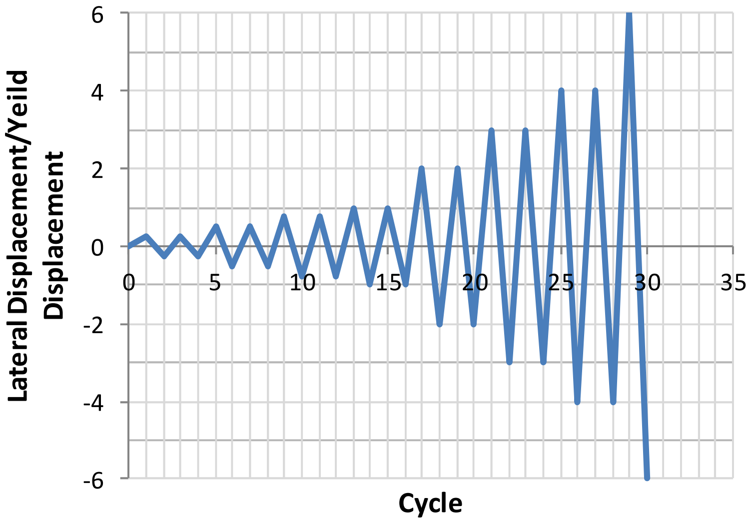

Figure B.15 Proposed loading history, Specimen UT-W-15

B.2.2 Major Test Observations, Specimen UT-W-15

The behavior of Specimen UT-W-15 was controlled by flexure. The value of Δ_y calculated in the preliminary phase of the test was 0.72 in., equivalent to a drift ratio of 0.50%. Flexural cracks (horizontal cracks in the bed joints) started early in the test before $1\Delta_y$, followed by shear cracks which propagated at $2\Delta_y$ (1.00% drift ratio) as shown in Figure B.16a. As shown in Figure B.17, evidence of toe crushing was found first at the south end at first cycle of $2\Delta_y$ (1.12% drift ratio) and then at the north end at second cycle of $2\Delta_y$ (1.12% drift). As shown in Figure B.16, extensive toe crushing and spalling at the base were observed, followed by buckling of north end vertical reinforcement at the second cycles to $4\Delta_y$ (2.00% drift ratio). There was no evidence of fracture of the vertical bars at the base.

(a) Cycle 2∆y ***(a) Cycle 4∆y***

Figure B.16 Flexural and shear cracking, severe crushing and spalling and buckling of longitudinal bars, Specimen UT-W-15

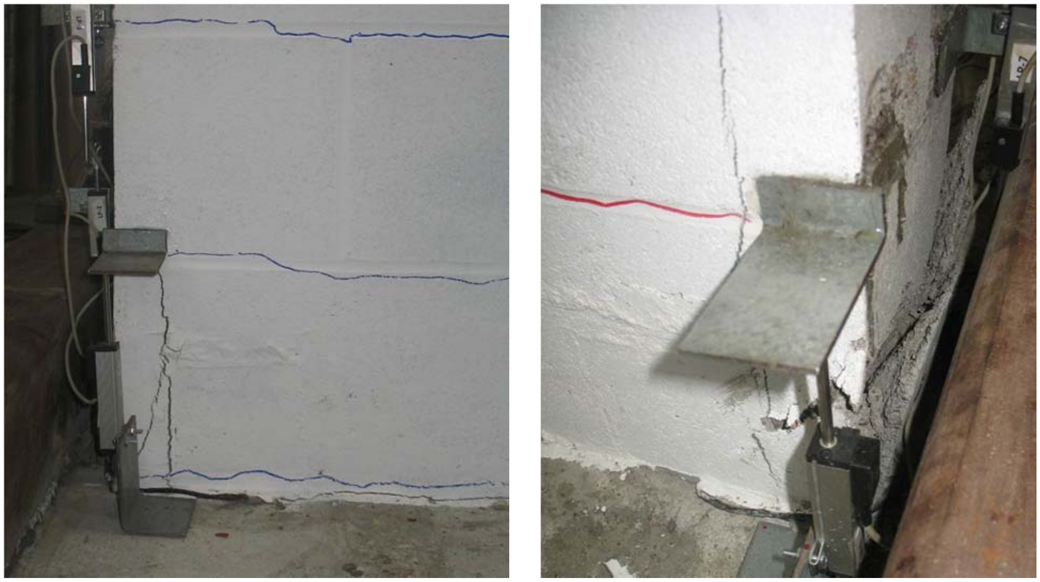

North toe ***South toe***

Figure B.17 Onset of toe crushing, Specimen UT-W-15

Figure B.18 shows the specimen upon completion of the test. As shown in Figure B.19, reversed cyclic loading caused toe crushing and severe spalling in the compression toes at the base of the specimen. The transverse reinforcing bars, hooked around the longitudinal bar splices, kept the spliced bars from coming apart.

Figure B.18 ***Specimen UT-W-15 at end of test***

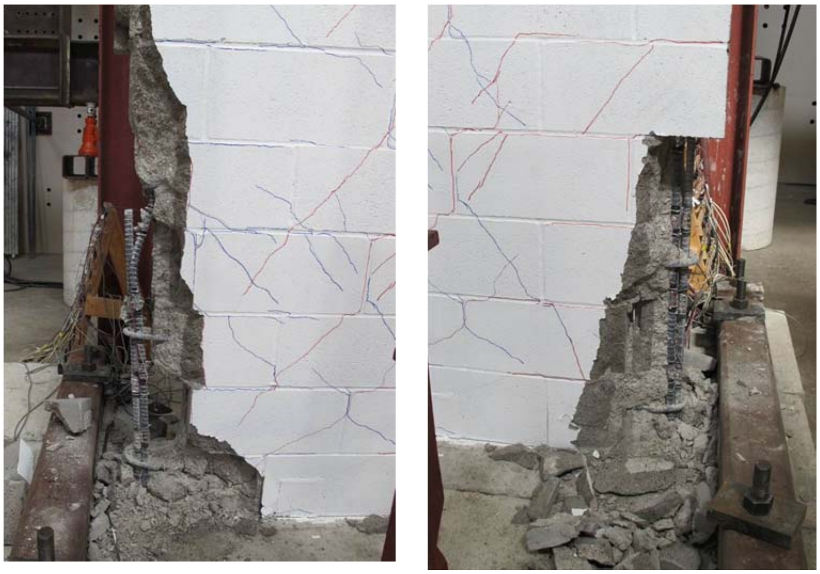

North toe ***South toe***

Figure B.19 Detail of toe splices at end of test, Specimen UT-W-15

B.2.3 Load-Displacement Behavior for Specimen UT-W-15

The load-displacement relationship of Specimen UT-W-15 is presented in Figure B.20 in terms of lateral displacement, which references five major events during testing:

1) first yield of the extreme vertical reinforcement ($\varepsilon_y = 0.0021$);
2) maximum useful strain in the masonry ($\varepsilon_{mu} = 0.0025$);
3) maximum capacity (capping point);
4) onset of toe crushing; and
5) decrease in capacity to 50% of maximum capacity.

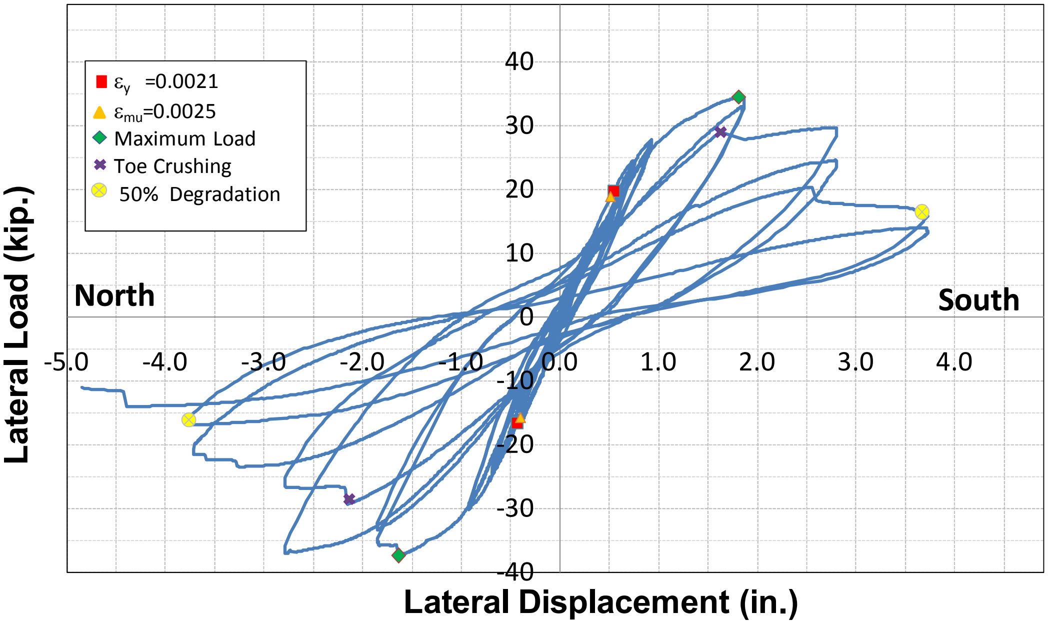

Figure B.20 Load versus top displacement, Specimen UT-W-15

Curvatures were determined over the wall height based on strain profiles, and are shown in Figure B.21. The strain profiles were calculated using five potentiometers along the inside edge of the wall (this was mirrored on the opposite side). The curvatures were determined for the first cycle to each displacement. Due to spalling of the face shells at the wall toes and detachment of the displacement potentiometer anchors, these displacement measurements were discontinued at later stages of testing. Therefore, strains and curvatures at larger displacements were not available.

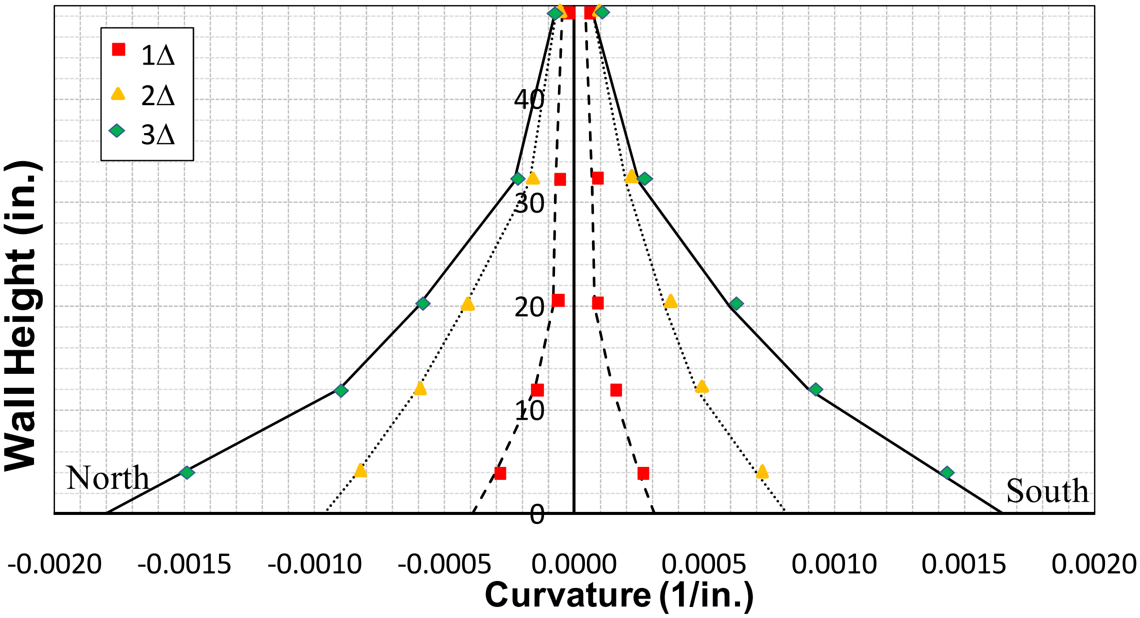

Figure B.21 Wall curvature of Specimen UT-W-15

B.2.4 Displacement Ductility, Specimen UT-W-15

The values obtained for the displacement ductility are presented in Table B-7. The results are presented for both load directions (push to the North and pull to the South), and then averaged.

Table B-7 Calculated displacement ductilities for Specimen UT-W-15

Direction of Load	**Load and Displacement Parameters**					
	P'$_y$ (kips)	Δ'$_y$ (in.)	Δ$_u$ (in.)	P$_y$ (kips)	Δ$_y$ (in.)	μ_Δ
Push (North)	16.60	0.43	3.20	32.75	0.84	3.80
Pull (South)	18.85	0.51	3.02	31.25	0.83	3.60
					Average	3.70

The curvature ductility of Specimen UT-W-15 was also determined using a similar process as above. The values obtained for the curvature ductility are presented in Table B-8. The results are presented for both load directions: push to the north and pull to the south, and then averaged.

Table B-8 Calculated curvature ductilities for Specimen UT-W-15

Direction of Load	Moment and Curvature Parameters					
	M'_y (kip-in.)	ϕ'_y (in.$^{-1}$)	ϕ_u (in.$^{-1}$)	M_y (kip-in.)	ϕ_y (in.$^{-1}$)	μ_ϕ
Push (North)	2390	0.00011	0.0015	4716	0.00021	7.14
Pull (South)	2714	0.00011	0.0016	4504	0.00018	8.89
					Average	8.01

B.2.5 Calculation of Plastic Hinge Lengths, Specimen UT-W-15

B.2.5.1 Method 1 (Bohl and Adebar 2011 and Shedid et al. 2010)

In Table B-9, the calculated yielded lengths are presented as a function of drift ratio for each load direction, and are then averaged between the two directions. In the last line of the table, the calculated yielded lengths are expressed in terms of L_w, the plan length of the wall.

Table B-9 Yielded lengths of Specimen UT-W-15

Drift Ratio (Displacement)	Yielded Lengths, $L_{yielded}$ (in.), for Different Drift Ratios		
	0.50% (Δ_y)	**1.00% ($2\Delta_y$)**	**1.50% ($3\Delta_y$)**
Push North	12.5	33.5	39.0
Pull South	10.5	37.0	41.5
Average	11.5	35.25	40.25
$L_{yielded}/L_w$	23.9%	73.4%	83.8%

If the plastic hinge length l_p is assumed equal to $0.5\,L_{yielded}$, then the resulting plastic hinge lengths are as shown in Table B-10 for each drift ratio.

Table B-10 Calculation of plastic hinge lengths of Specimen UT-W-15

Drift Ratio (Displacement)	Plastic Hinge Lengths, l_p (in.), for Different Drift Ratios		
	0.50% (Δ_y)	**1.00% ($2\Delta_y$)**	**1.50% ($3\Delta_y$)**
Yielded Length	11.5	35.25	40.25
Plastic Hinge Length (l_p)	5.75	17.63	20.12
l_p/L_w	11.9%	36.7%	41.9%

B.2.5.2 Method 2 (Shedid et al. 2010 and Dazio 2009)

The equivalent plastic hinge lengths for both load directions at different drift ratios are calculated as shown in Table B-11.

Table B-11 Equivalent plastic hinge length of Specimen UT-W-15

Drift Ratio (Displacement)	**Plastic Hinge Lengths, l_p (in.), for Different Drift Ratios**		
	0.50% (Δ_y)	**1.00% ($2\Delta_y$)**	**1.50% ($3\Delta_y$)**
Push North	8.29	9.05	7.34
Pull South	5.96	8.31	6.99
Average	7.13	8.68	7.16
l_p/L_w	14.8%	18.1%	14.9%

B.2.5.3 Method 3 (Bohl and Adebar 2011)

The calculated plastic hinge lengths were determined for both load direction: push to the north and pull to the south. The results are shown in Table B-12.

Table B-12 Predicted plastic hinge lengths for Specimen UT-W-15

Direction of Load	**Moment and Plastic Hinge Parameters**					
	M_y (kip-in.)	M_{max} (kip-in.)	z (in.)	$L_{yielded}$ (in.)	$l_p = 0.5L_{yielded}$ (in.)	l_p/L_w
Push (North)	2390	5184	144	77.7	38.8	0.80
Pull (South)	2714	4968	144	64.8	32.4	0.67
					Average	0.74

B.2.6 Components of Displacements for Specimen UT-W-15

Load-displacement curves for total sliding and shear component of total tip displacement are given in Figure B.22 and Figure B.23, and total displacement and shear deformation are compared in Figure B.24.

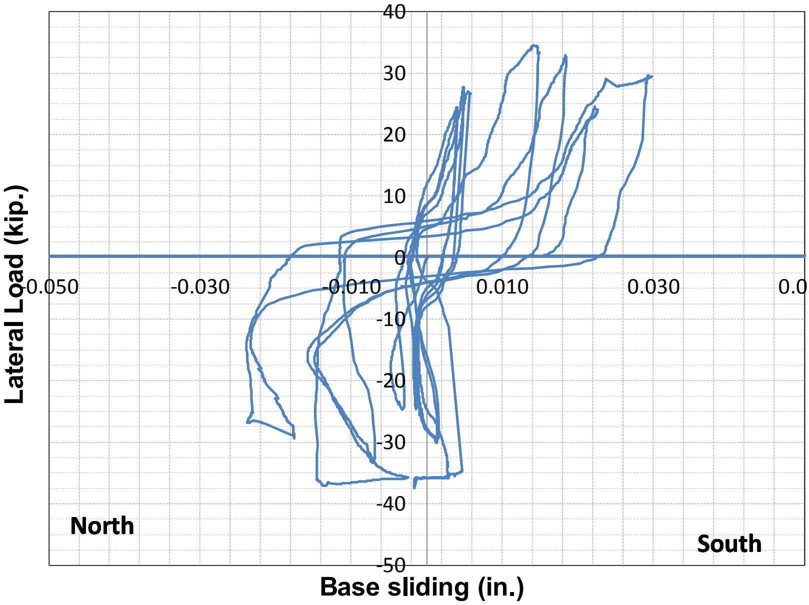

Figure B.22 Base sliding, Specimen UT-W-15

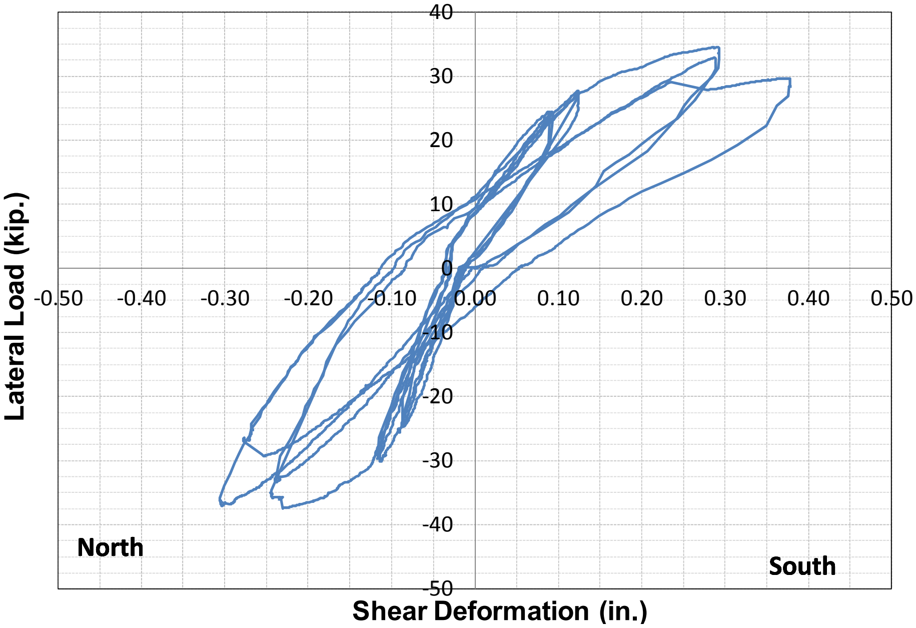

Figure B.23 Shear deformation, Specimen UT-W-15

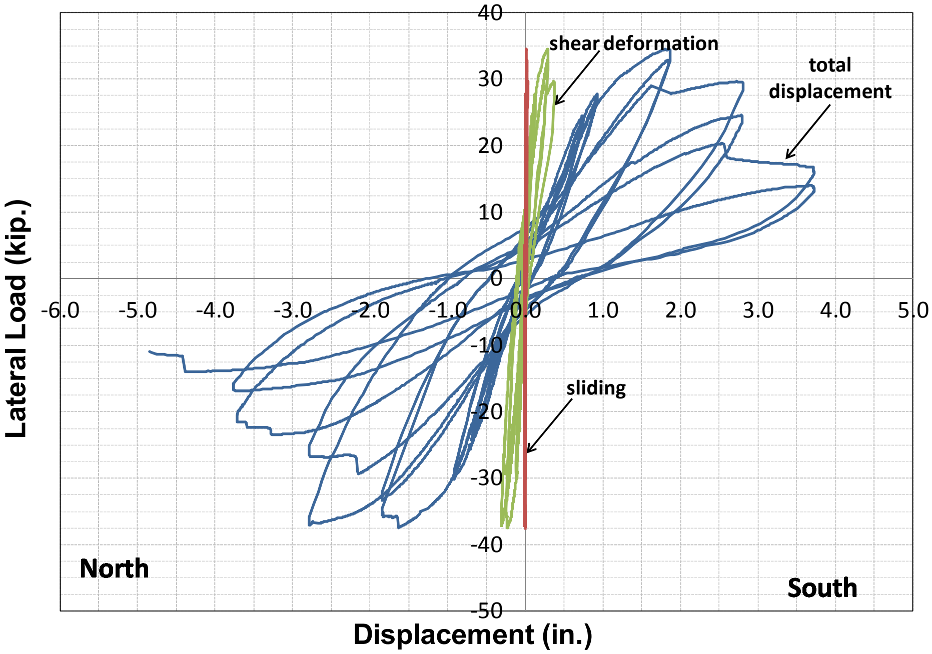

Figure B.24 Components of displacements for Specimen UT-W-15

B.3 TEST RESULTS FOR SPECIMEN UT-W-16

Specimen UT-W-16 was detailed according to the requirements of the 2008 MSJC *Code*. It has a height of 12 ft and a plan length of 4 ft (aspect ratio 3.0), required prescriptive reinforcement for a Intermediate Reinforced Masonry Shear Wall (2008 MSJC *Code*), and a normalized axial load ratio P / ($f_m' A_g$) of 0.15. The vertical reinforcement ratio was 0.0033, with No. 4 reinforcing bars at 8 in. (every cell); and the horizontal reinforcement ratio was 0.0016, with No. 4 bars at 16 in. The specimen used cement-lime mortar conforming to the proportion specification for Type S of ASTM C270, and grout conforming to the strength specification of ASTM C476. A photo of the specimen before testing is shown in Figure B.25, and details for the specimen are shown in Figure B.26.

Figure B.25 Specimen UT-W-16 before testing

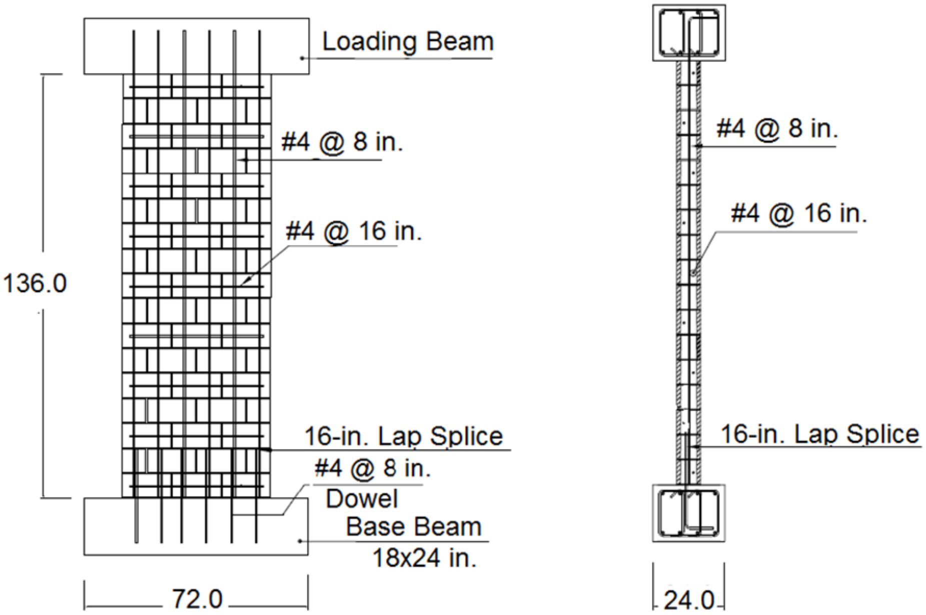

Figure B.26 Details for Specimen UT-W-16

B.3.1 Loading History for Specimen UT-W-16

Specimen UT-W-16 was first subjected to a preliminary test to estimate the yield displacement, Δ_y. Lateral yield displacement was determined as 0.73 in. The planned in-plane loading history for base shear in the specimen is shown in Figure B.27. On September 6, 2011, Specimen UT-W-16 was loaded at a rate of 0.3 in./min to two cycles of reversed displacements of ±1, 2, 3, 4, and 6 times that predicted yield displacement. It was then loaded to a half-cycle to a displacement of 8 times that predicted yield displacement. The test was stopped when the peak capacity dropped to 20% or less of the experimentally observed maximum capacity (capping point). The testing took about 8 hours.

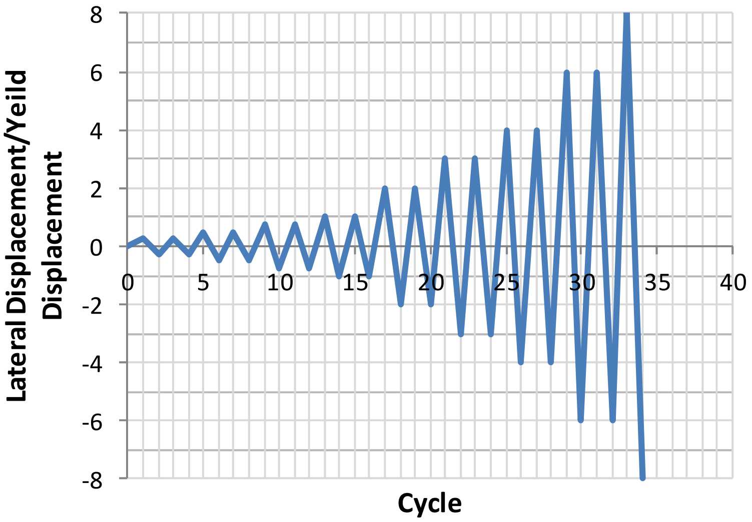

Figure B.27 Proposed loading history, Specimen UT-W-16

B.3.2 Test Major Observations, Specimen UT-W-16

The behavior of Specimen UT-W-16 was controlled by flexure. The value of Δ_y calculated in the preliminary phase of the test was 0.73 in., equivalent to a drift ratio of 0.51%. Flexural cracks (horizontal cracks in the bed joints) started early in the test before $1\Delta_y$, followed by opened flexural cracks which propagated at $2\Delta_y$ (1.01% drift ratio). As shown in Figure B.28, evidence of toe crushing and minor spalling were found first at both ends at first cycles of 3Δy displacement (1.52% drift ratio). As shown in Figure B.29a, extensive toe crushing and spalling at north end were observed, followed by buckling of vertical bar at the second cycle to 4Δy (2.03% drift ratio). As shown in Figure B.29b, similar damage occurred while loading to the south at the first cycle to $6\Delta_y$ (3.04% drift ratio). The test was ended when the specimen suddenly failed because of the lack of compression capacity at the toes. Figure B.30 and Figure B.31 show the specimen upon completion of the test.

South toe

North toe

Figure B.28 Onset of toe crushing, Specimen UT-W-16

(a) Cycle 4Δy *(b) Cycle 6Δy*

Figure B.29 Severe toe crushing and spalling followed by vertical reinforcement buckling, Specimen UT-W-16

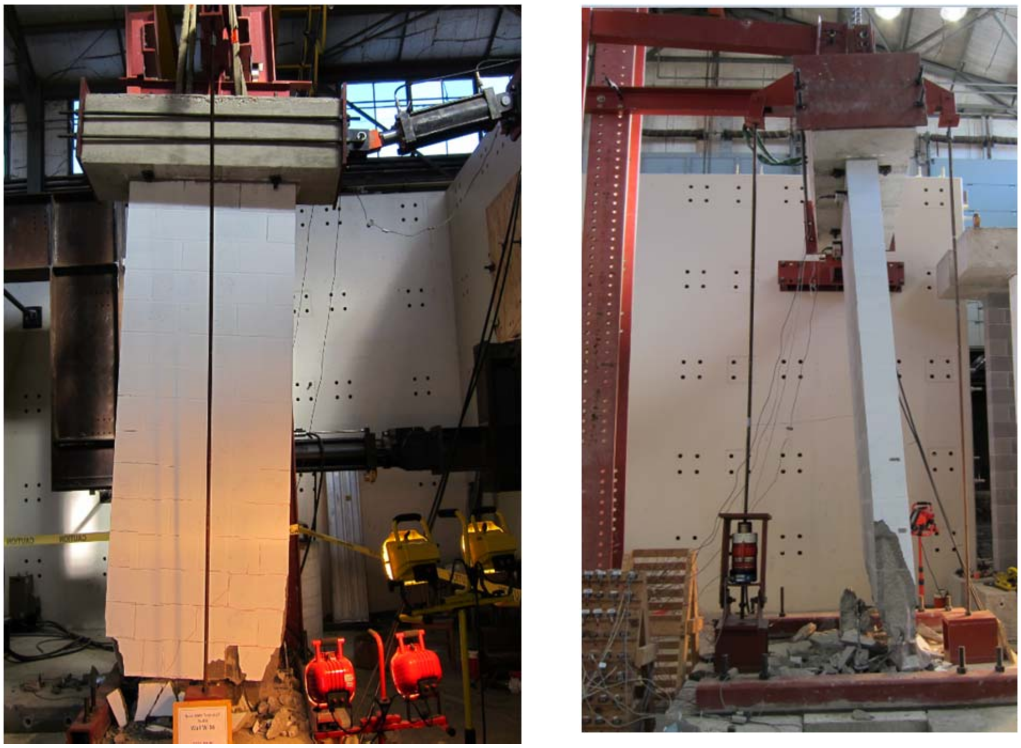

Figure B.30 Specimen UT-W-16 at end of test

North view ***South view***

Figure B.31 Detail of failure at end of test, Specimen UT-W-16

B.3.3 Load-Displacement Behavior for Specimen UT-W-16

The load-displacement relationship of Specimen UT-W-16 is presented in Figure B.32 in terms of the lateral displacement, which references five major events during testing:

1) first yield of the extreme vertical reinforcement ($\varepsilon_y = 0.0022$);
2) maximum useful strain in the masonry ($\varepsilon_{mu} = 0.0025$);
3) maximum capacity (capping point);
4) onset of toe crushing; and
5) decrease in capacity to 50% of maximum capacity.

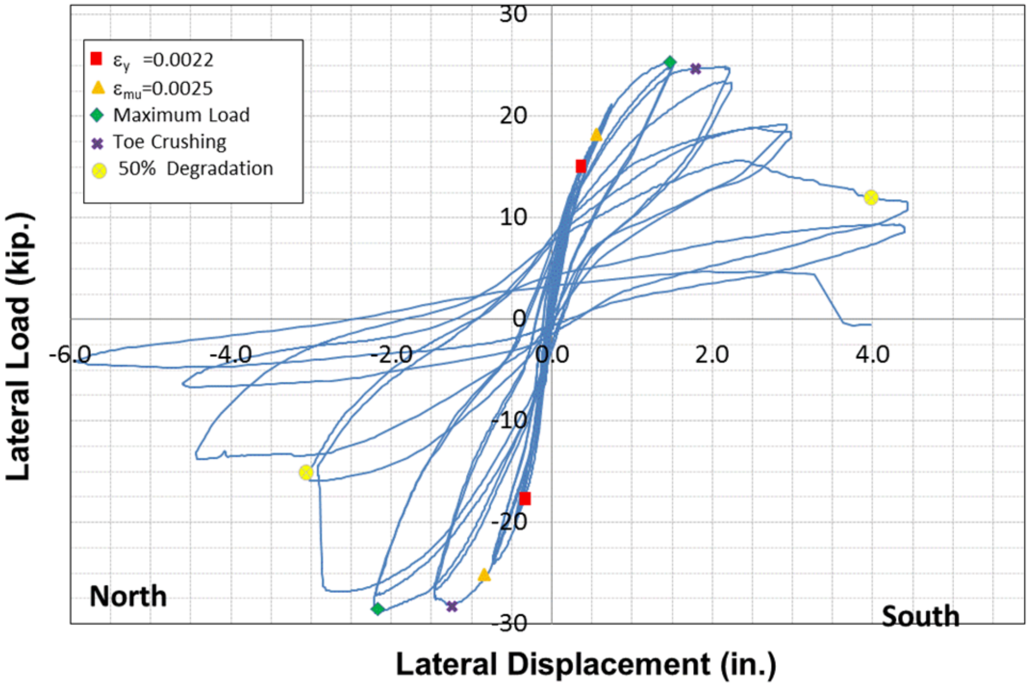

Figure B.32 Load versus top displacement, Specimen UT-W-16

Curvatures were determined over the wall height based on strain profiles, and are shown in Figure B.33. The strain profiles were calculated using five potentiometers along the inside edge of the wall (this was mirrored on the opposite side). The curvatures were determined for the first cycle to each displacement. Due to spalling of the face shells at the wall toes and detachment of the displacement potentiometer anchors, these displacement measurements were discontinued at later stages of testing. Therefore, strains and curvatures at larger displacements were not available.

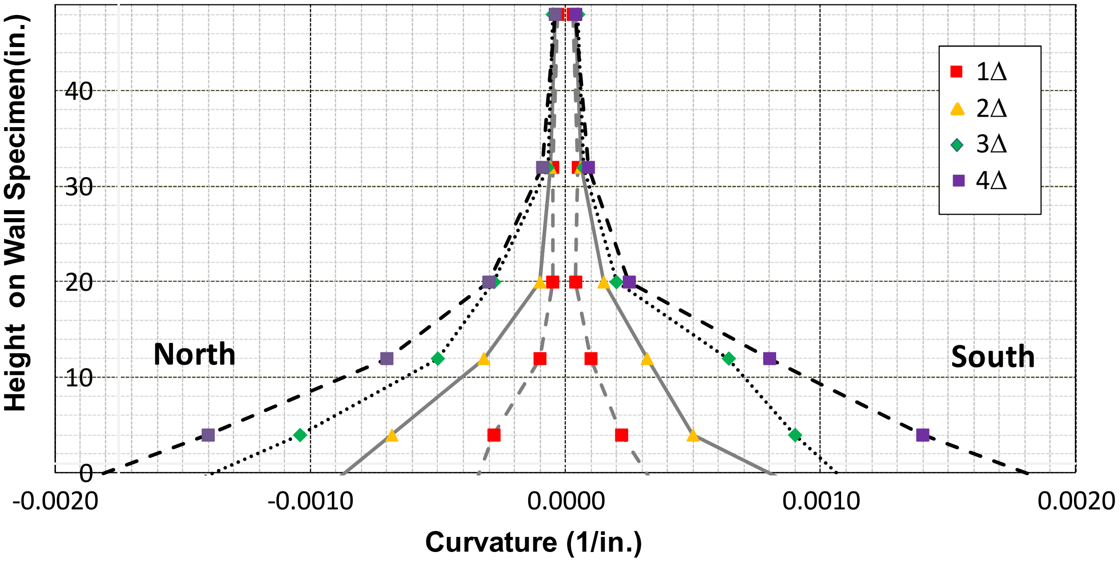

Figure B.33 Wall curvature of Specimen UT-W-16

B.3.4 Displacement Ductility, Specimen UT-W-16

The values obtained for the displacement ductility are presented in Table B-13. The results are presented for both load directions (push to the North and pull to the South), and then averaged.

Table B-13 Calculated displacement ductilities for Specimen UT-W-16

Direction of Load	**Load and Displacement Parameters**					
	P'_y (kips)	Δ'_y (in.)	Δ_u (in.)	P_y (kips)	Δ_y (in.)	μ_Δ
Push (North)	17.62	0.33	2.45	25.9	0.49	5.00
Pull (South)	15.05	0.36	2.72	23.5	0.54	5.03
					Average	5.02

The curvature ductility of Specimen UT-W-16 was also determined using a similar process as above. The values obtained for the curvature ductility are presented in Table B-14. The results are presented for both load directions: push to the north and pull to the south, and then averaged.

Table B-14 Calculated curvature ductilities for Specimen UT-W-16

Direction of Load	**Moment and Curvature Parameters**					
	M'_y (kip-in.)	ϕ'_y (in.$^{-1}$)	ϕ_u (in.$^{-1}$)	M_y (kip-in.)	ϕ_y (in.$^{-1}$)	μ_ϕ
Push (North)	2537	0.00008	0.0018	3729	0.00011	16.3
Pull (South)	2167	0.00009	0.0018	3384	0.00013	13.8
					Average	15.0

B.3.5 Calculation of Plastic Hinge Lengths, Specimen UT-W-16

B.3.5.1 Method 1 (Bohl and Adebar 2011 and Shedid et al. 2010)

In Table B-15, the calculated yielded lengths are presented as a function of drift ratio for each load direction, and are then averaged between the two directions. In the last line of the table, the calculated yielded lengths are expressed in terms of L_w, the plan length of the wall.

Table B-15 Yielded lengths of Specimen UT Wall-16

Drift Ratio (Displacement)	**Yielded Lengths, $L_{yielded}$ (in.), for Different Drift Ratios**			
	0.50% (Δ_y)	**1.01% ($2\Delta_y$)**	**1.52% ($3\Delta_y$)**	**2.02% ($4\Delta_y$)**
Push North	11.0	18.5	28.25	29.5
Pull South	12.5	25.5	28.5	30.25
Average	11.8	22.0	28.4	29.8
$L_{yielded}/L_w$	24.4%	45.8%	59.1%	62.2%

If the plastic hinge length l_p is assumed equal to 0.5 $L_{yielded}$, then the resulting plastic hinge lengths are as shown in Table B-16 for each drift ratio.

Table B-16 Calculation of plastic hinge lengths of Specimen UT Wall-16

Drift Ratio (Displacement)	**Plastic Hinge Lengths, l_p (in.), for Different Drift Ratios**			
	0.50% (Δ_y)	**1.01% ($2\Delta_y$)**	**1.52% ($3\Delta_y$)**	**2.02% ($4\Delta_y$)**
Yielded Length	11.8	22.0	28.4	29.8
Plastic Hinge Length (l_p)	5.9	11.0	14.2	14.9
l_p/L_w	12.2%	27.9%	29.5%	31.1%

B.3.5.2 Method 2 (Shedid et al. 2010 and Dazio 2009)

The equivalent plastic hinge lengths for both load directions at different drift ratios are calculated as shown in Table B-17.

Table B-17 Equivalent plastic hinge length of Specimen UT-W-16

Drift Ratio (Displacement)	Plastic Hinge Lengths, l_p (in.), for Different Drift Ratios			
	0.50% (Δ_y)	1.01% ($2\Delta_y$)	1.52% ($3\Delta_y$)	2.02% ($4\Delta_y$)
Push North	11.1	10.4	12.1	10.9
Pull South	10.2	14.3	13.1	10.8
Average	10.65	12.35	12.6	10.85
l_p/L_w	22.19%	25.73%	26.25%	22.60%

B.3.5.3 Method 3 (Bohl and Adebar 2011)

The calculated plastic hinge lengths were determined for both load direction: push to the north and pull to the south. The results are shown in Table B-18.

Table B-18 Predicted plastic hinge lengths for Specimen UT-W-16

Direction of Load	Moment and Plastic Hinge Parameters					
	M_y (kip-in.)	M_{max} (kip-in.)	z (in.)	$L_{yielded}$ (in.)	$l_p = 0.5L_{yielded}$ (in.)	l_p/L_w
Push (North)	2537	3960	144	51.7	25.8	0.53
Pull (South)	2167	3708	144	59.8	29.9	0.62
					Average	0.57

B.3.6 Components of Displacements for Specimen UT-W-16

Load-displacement curves for total sliding and shear component of total tip displacement are given in Figure B.34 and Figure B.23, and total displacement and shear deformation are compared in Figure B.24.

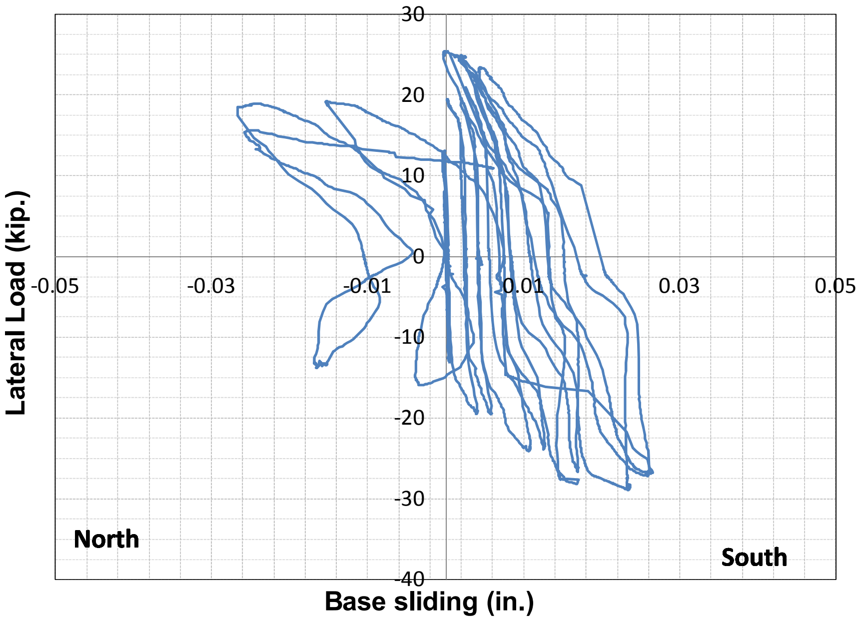

Figure B.34 Base sliding, Specimen UT-W-16

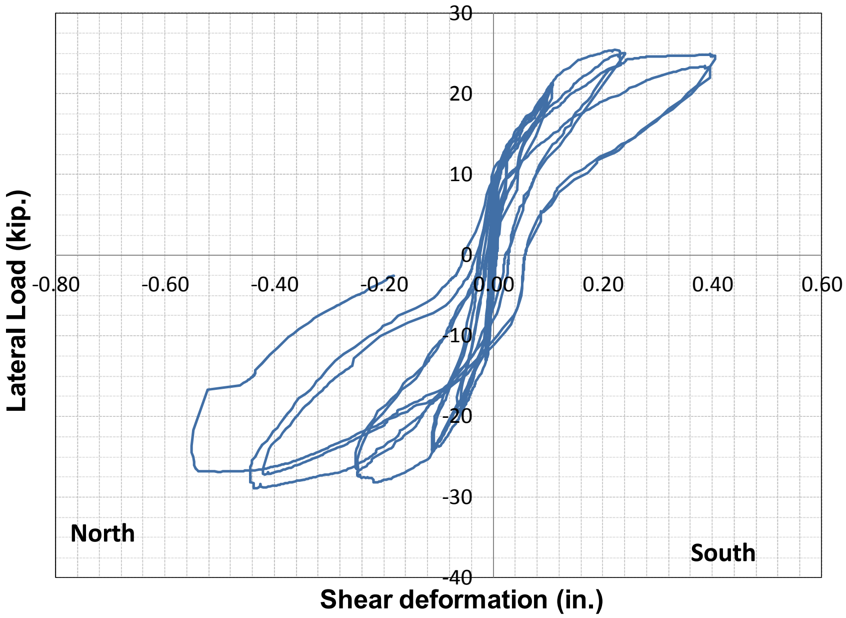

Figure B.35 Shear deformation, Specimen UT-W-16

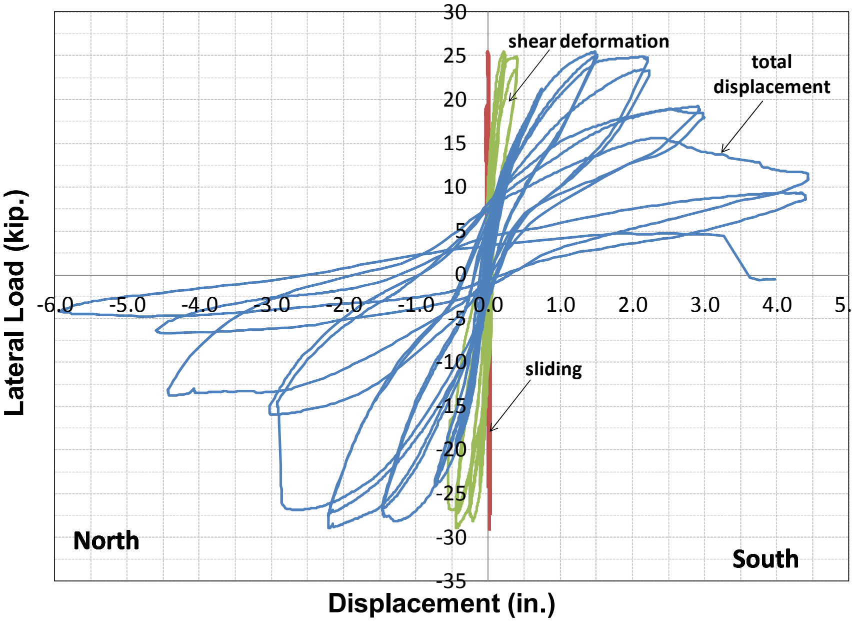

Figure B.36 Components of displacements for Specimen UT-W-16

B.4 TEST RESULTS FOR SPECIMEN UT-W-17

Specimen UT-W-17 was detailed according to the requirements of the 2008 MSJC *Code*. It has a height of 12 ft and a plan length of 2.67 ft (aspect ratio 4.5), required prescriptive reinforcement for a Special Reinforced Masonry Shear Wall (2008 MSJC *Code*), and a normalized axial load ratio P / ($f_m' A_g$) of 0.10. The vertical reinforcement ratio was 0.0072, with No. 6 reinforcing bars at 8 in. (every cell); and the horizontal reinforcement ratio was 0.0033, with No. 4 bars at 8 in. The specimen used cement-lime mortar conforming to the proportion specification for Type S of ASTM C270, and grout conforming to the strength specification of ASTM C476. A photo of the specimen before testing is shown in Figure B.37, and details for the specimen are shown in Figure B.38.

Figure B.37 Specimen UT-W-17 before testing

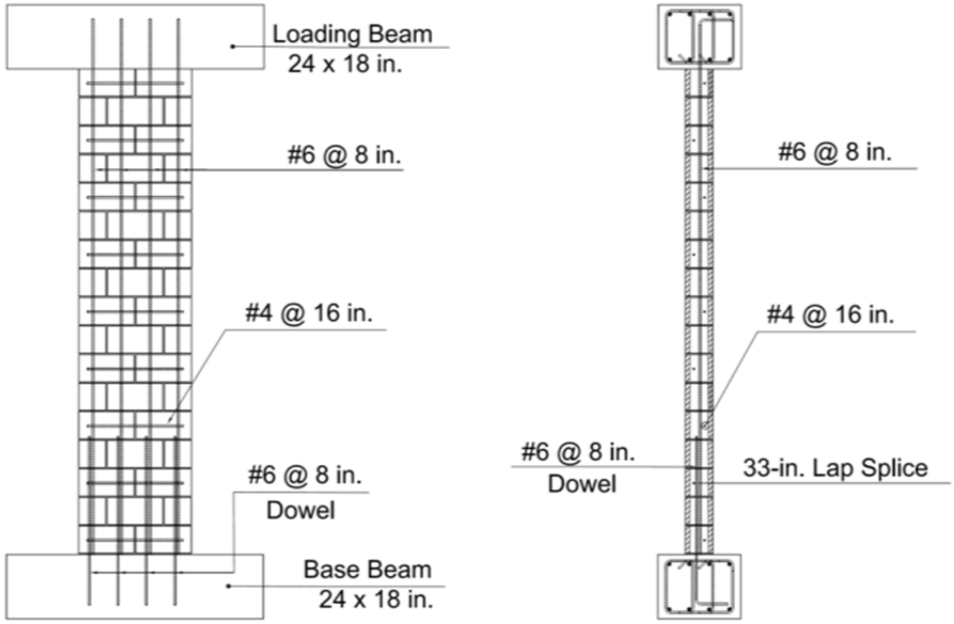

Figure B.38 Details for Specimen UT-W-17

B.4.1 Loading History for Specimen UT-W-17

Specimen UT-W-17 was first subjected to a preliminary test to estimate the yield displacement, Δ_y. The planned in-plane loading history for base shear in the specimen is shown in Figure B.39. Lateral loads were manually controlled using a hydraulic actuator. On September 13, 2011, Specimen UT-W-17 was loaded at a rate of 0.3 in./min to two cycles of reversed displacements of ±1, 2, 3, 4 and 6 times that predicted yield displacement. It was then loaded to a half-cycle to a displacement of 8 times that predicted yield displacement. The test was stopped when the peak capacity dropped to 20% or less of the experimentally observed maximum capacity (capping point). The testing took about 10 hours.

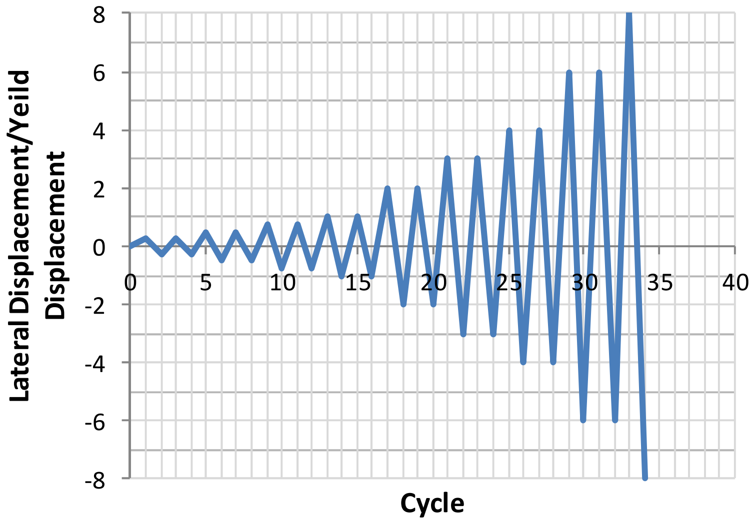

Figure B.39 Proposed loading history, Specimen UT-W-17

B.4.2 Major Test Observations, Specimen UT-W-17

The behavior of Specimen UT-W-17 was controlled by flexure. The value of Δ_y calculated in the preliminary phase of the test was 1.08 in., equivalent to a drift ratio of 0.75%. Flexural cracks (horizontal cracks in the bed joints) started early in the test before $1\Delta_y$, followed by opened flexural cracks which observed from $2\Delta_y$ displacement (1.50% drift ratio). As shown in Figure B.40, evidence of toe crushing was found first at both ends at first cycles of $3\Delta_y$ displacement (2.25% drift ratio). As shown in Figure B.41, extensive toe crushing and face shell spalling at both ends were observed at the second cycles to $4\Delta_y$ displacements (3.00% drift ratio). Extreme vertical bars at the both ends fractured at the first cycles to $6\Delta_y$ (4.50% drift ratio) as shown in Figure B.42. Figure B.43 shows the specimen upon completion of the test. As shown in Figure B.44, reversed cyclic loading caused toe crushing and vertical bars fracture at the base of the specimen.

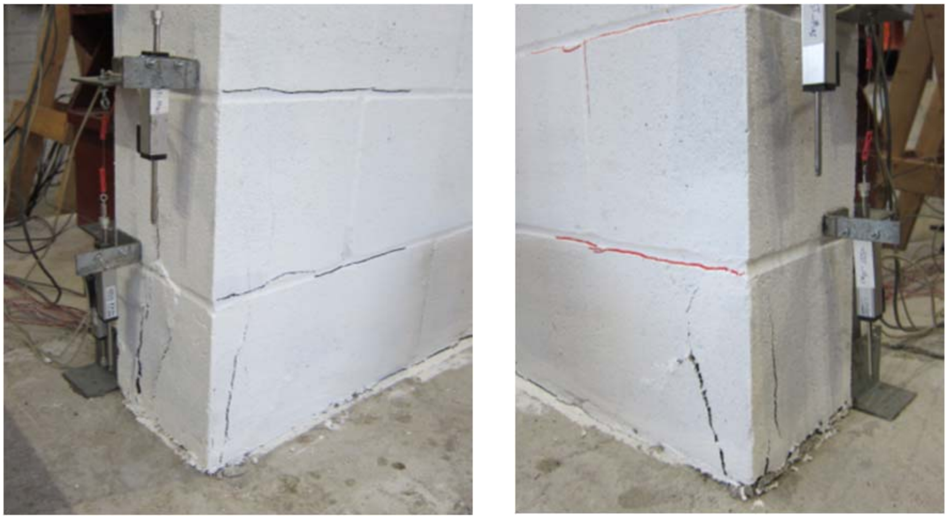

North toe ***South toe***

Figure B.40 Onset of toe crushing, Specimen UT-W-17

(a) Cycle 4Δy, loading north ***(b) Cycle 4Δy, loading south***

Figure B.41 Severe toe crushing and spalling, Specimen UT-W-17

(a) Cycle 6Δy, loading south *(b) Cycle 6Δy, loading north*

Figure B.42 Fracture of extreme vertical bars, Specimen UT-W-17

Figure B.43 Specimen UT-W-17 at end of test

North toe **South toe**

Figure B.44 Detail of toes at end of test, Specimen UT-W-17

B.4.3 Load-Displacement Behavior for Specimen UT-W-17

The load-displacement relationship of Specimen UT-W-17 is presented in Figure B.45 in terms of lateral displacement, which references five major events during testing:

1) first yield of the extreme vertical reinforcement (ε_y = 0.0021);
2) maximum useful strain in the masonry (ε_{mu} = 0.0025);
3) maximum capacity (capping point);
4) onset of toe crushing ; and
5) decrease in capacity to 50% of maximum capacity.

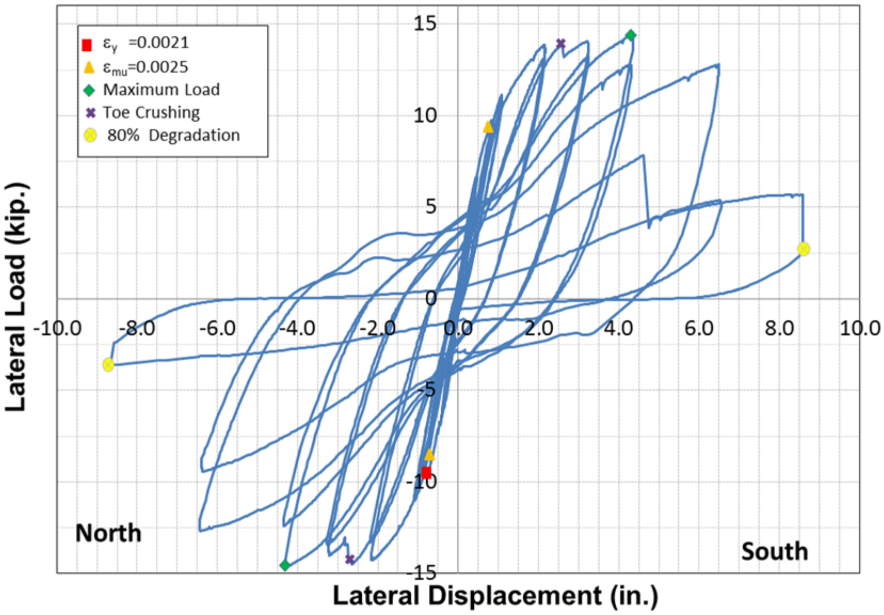

Figure B.45 Load versus top displacement, Specimen UT-W-17

Curvatures were determined over the wall height based on strain profiles, and are shown in Figure B.46. The strain profiles were calculated using five potentiometers along the inside edge of the wall (this was mirrored on the opposite side). The curvatures were determined for the first cycle to each displacement. Due to spalling of the face shells at the wall toes and detachment of the displacement potentiometer anchors, these displacement measurements were discontinued at later stages of testing. Therefore, strains and curvatures at larger displacements were not available.

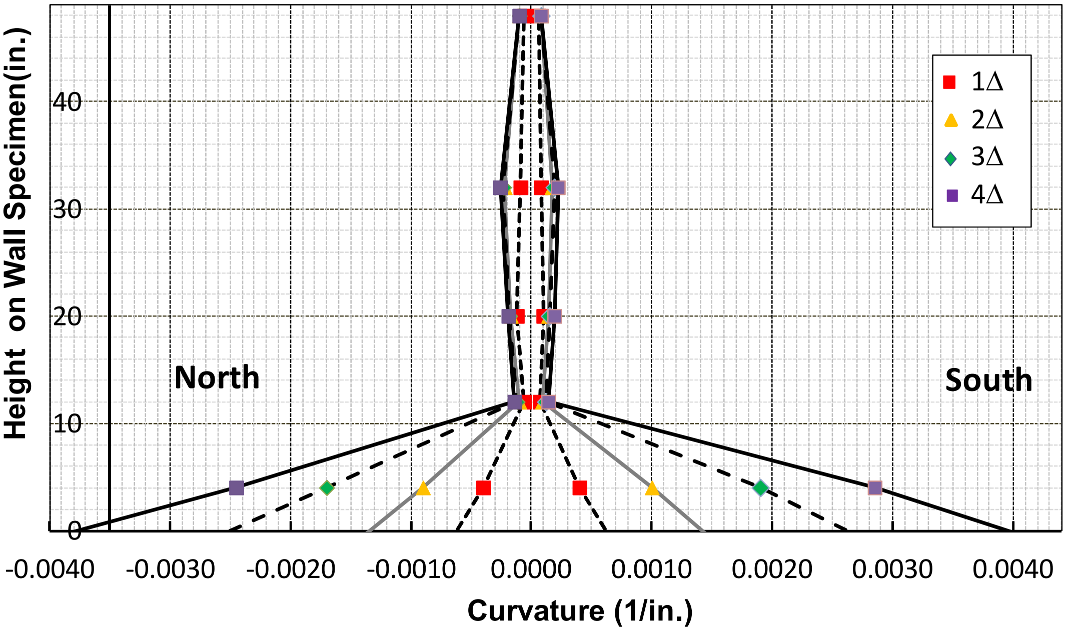

Figure B.46 Wall Curvature of Specimen UT-W-17

B.4.4 Displacement Ductility, Specimen UT-W-17

The values obtained for the displacement ductility are presented in Table B-19. The results are presented for both load directions (push to the North and pull to the South), and then averaged.

Table B-19 Calculated displacement ductilities for Specimen UT-W-17

Direction of Load	**Load and Displacement Parameters**					
	P'_y (kips)	Δ'_y (in.)	Δ_u (in.)	P_y (kips)	Δ_y (in.)	μ_Δ
Push (North)	9.36	0.74	6.62	13.52	1.06	6.20
Pull (South)	9.21	0.73	6.85	13.41	1.08	6.37
					Average	6.28

The curvature ductility of Specimen UT-W-17 was also determined using a similar process as above. The values obtained for the curvature ductility are presented in Table B-20. The results are presented for both load directions: push to the north and pull to the south, and then averaged.

Table B-20 Calculated curvature ductilities for Specimen UT-W-17

Direction of Load	**Moment and Curvature Parameters**					
	M'_y (kip-in.)	ϕ'_y (in.$^{-1}$)	ϕ_u (in.$^{-1}$)	M_y (kip-in.)	ϕ_y (in.$^{-1}$)	μ_ϕ
Push (North)	1326	0.00015	0.0041	1946	0.00022	19.07
Pull (South)	1347	0.00015	0.0042	1931	0.00021	19.07
					Average	19.07

B.4.5 Calculation of Plastic Hinge Lengths, Specimen UT-W-17

B.4.5.1 Method 1 (Bohl and Adebar 2011 and Shedid et al. 2010)

In Table B-21, the calculated yielded lengths are presented as a function of drift ratio for each load direction, and are then averaged between the two directions. In the last line of the table, the calculated yielded lengths are expressed in terms of L_w , the plan length of the wall.

Table B-21 Yielded lengths of Specimen UT-W-17

Drift Ratio (Displacement)	Yielded Lengths, $L_{yielded}$ (in.), for Different Drift Ratios			
	0.75% (Δ_y)	1.5% ($2\Delta_y$)	2.25% ($3\Delta_y$)	3.00% ($4\Delta_y$)
Push North	10.2	11.5	11.8	12.0
Pull South	10.0	11.5	11.9	12.0
Average	10.1	11.5	11.85	12.0
$L_{yielded}/L_w$	31.9%	36.3%	37.5%	37.9%

If the plastic hinge length l_p is assumed equal to 0.5 $L_{yielded}$, then the resulting plastic hinge lengths are as shown in Table B-22 for each drift ratio.

Table B-22 Calculation of plastic hinge lengths of Specimen UT-W-17

Drift Ratio (Displacement)	Plastic Hinge Lengths, l_p (in.), for Different Drift Ratios			
	0.75% (Δ_y)	1.5% ($2\Delta_y$)	2.25% ($3\Delta_y$)	3.00% ($4\Delta_y$)
Yielded Length	10.1	11.5	11.85	12.0
Plastic Hinge Length (l_p)	5.05	6.25	6.92	6.00
l_p/L_w	15.95%	18.3%	18.75%	18.95%

B.4.5.2 Method 2 (Shedid et al. 2010 and Dazio 2009)

The equivalent plastic hinge lengths for both load directions at different drift ratios are calculated as shown in Table B-23.

Table B-23 Equivalent plastic hinge length of Specimen UT-W-17

Drift Ratio (Displacement)	Plastic Hinge Lengths, l_p (in.), for Different Drift Ratios			
	0.75% (Δ_y)	1.5% ($2\Delta_y$)	2.25% ($3\Delta_y$)	3.00% ($4\Delta_y$)
Push North	4.7	7.8	7.0	6.5
Pull South	4.8	7.5	6.8	6.3
Average	4.7	7.7	6.9	6.4
l_p/L_w	15.0%	24.3%	21.8%	20.2%

B.4.5.3 Method 3 (Bohl and Adebar 2011)

The calculated plastic hinge lengths were determined for both load direction: push to the north and pull to the south. The results are shown in Table B-24.

Table B-24 Predicted plastic hinge lengths for Specimen UT-W-17

Direction of Load	Moment and Plastic Hinge Parameters					
	M_y (kip-in.)	M_{max} (kip-in.)	z (in.)	$L_{yielded}$ (in.)	$l_p = 0.5L_{yielded}$ (in.)	l_p/L_w
Push (North)	1326	2109	144	53.5	26.75	0.84
Pull (South)	1347	2072	144	50.4	25.2	0.79
					Average	0.82

B.4.6 Components of Displacements for Specimen UT-W-17

Load-displacement curves for total sliding and shear component of total tip displacement are given in Figure B.47 and Figure B.48, and total displacement and shear deformation are compared in Figure B.49.

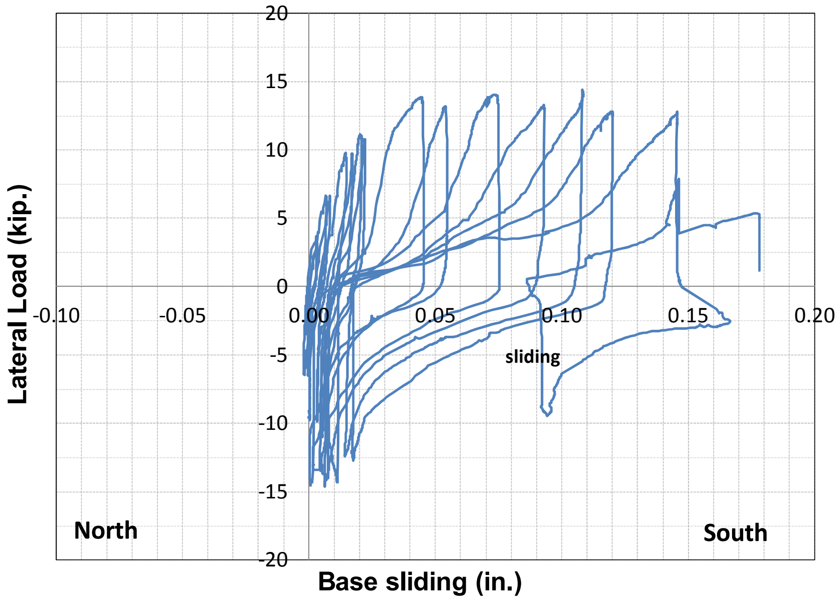

Figure B.47 Base sliding, Specimen UT-W-17

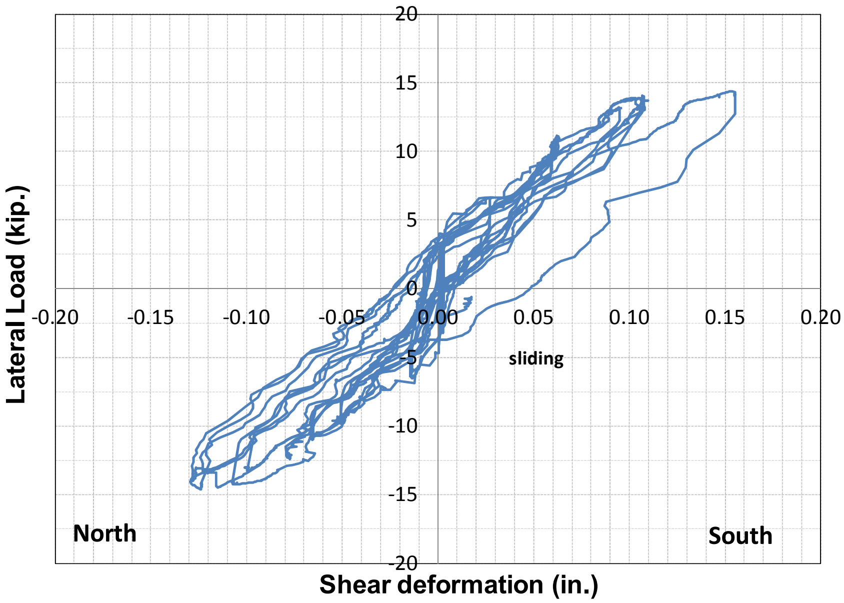

Figure B.48 Shear deformation, Specimen UT-W-17

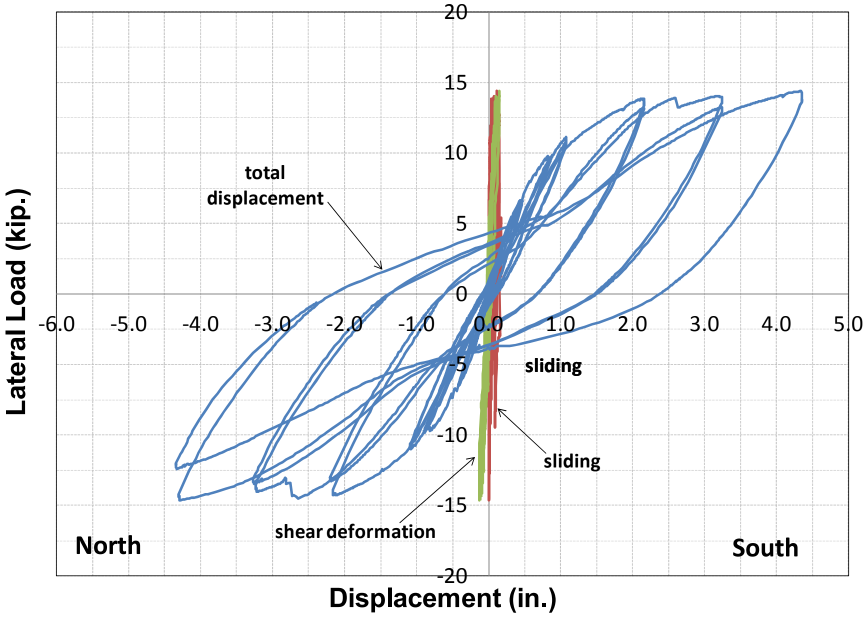

Figure B.49 Components of displacements for Specimen UT-W-17

B.5 TEST RESULTS FOR SPECIMEN UT-W-18

Specimen UT-W-18 was detailed according to the requirements of the 2008 MSJC *Code*. It has a height of 12 ft and a plan length of 2.67 ft (aspect ratio 4.5), required prescriptive reinforcement for a Special Reinforced Masonry Shear Wall (2008 MSJC *Code*), and a normalized axial load ratio P / ($f_m' A_g$) of 0.10. The vertical reinforcement ratio was 0.0033, with No. 4 reinforcing bars at 8 in. (every cell); and the horizontal reinforcement ratio was 0.0033, with No. 4 bars at 8 in. The specimen used cement-lime mortar conforming to the proportion specification for Type S of ASTM C270, and grout conforming to the strength specification of ASTM C476. A photo of the specimen before testing is shown in Figure B.50, and details for the specimen are shown in Figure B.51.

Figure B.50 Specimen UT-W-18 before testing

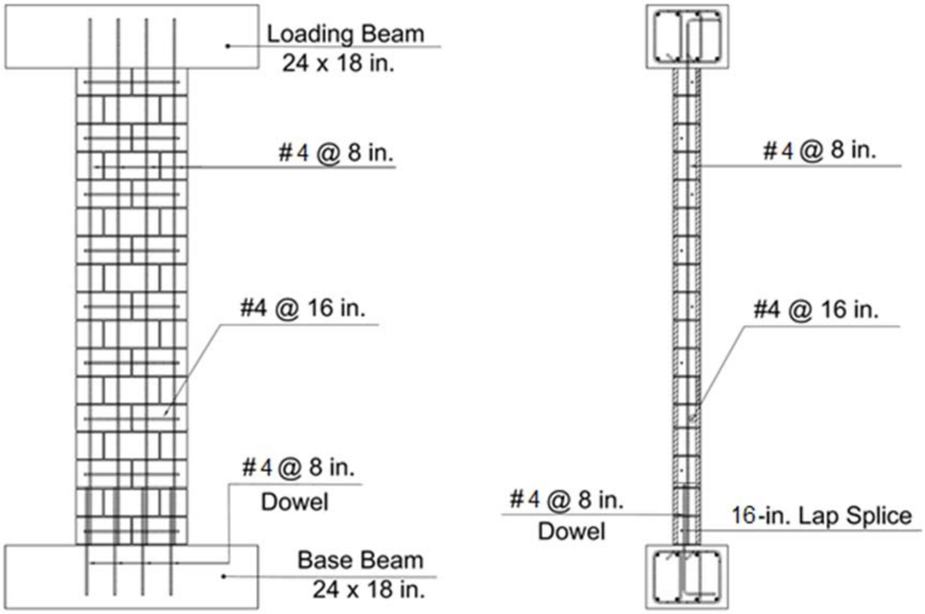

Figure B.51 Details for Specimen UT-W-18

B.5.1 Loading History for Specimen UT-W-18

Specimen UT-W-18 was first subjected to a preliminary test phase to estimate the yield displacement, Δ_y. On September 20, 2011, Specimen UT-W-18 was loaded at a maximum rate of 0.3 in./min. to two cycles of reversed displacements of ±1, 2, 3, 4, 6, and 8 times that predicted yield displacement, as shown in Figure B.52. It was then loaded to a half-cycle to a displacement of 10 times that predicted yield displacement. The test was stopped when the peak capacity dropped to 20% or less of the experimentally observed maximum capacity (capping point). The testing took about 8 hours. In this test the specimen was loaded first to the north and then to the south.

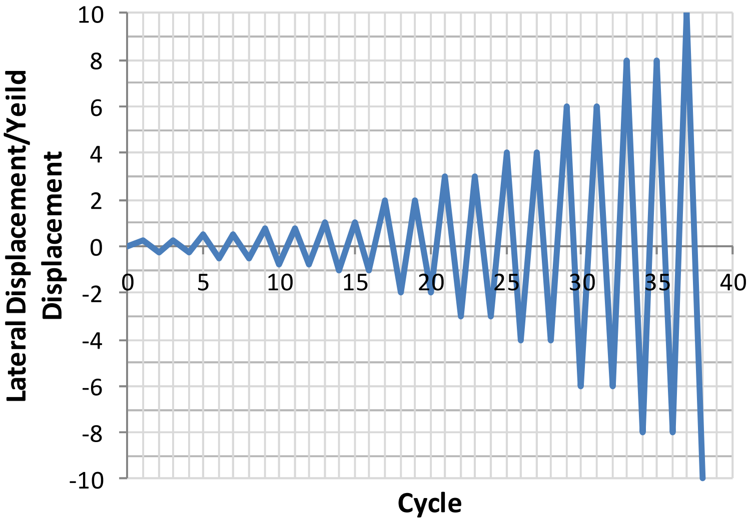

Figure B.52 Proposed loading history, Specimen UT-W-18

B.5.2 Major Test Observations, Specimen UT-W-18

The behavior of Specimen UT-W-18 was controlled by flexure. The value of Δ_y calculated in the preliminary phase of the test was 0.75 in., equivalent to a drift ratio of 0.52%. Flexural cracks (horizontal cracks in the bed joints) started early in the test before $1\Delta_y$, followed by opened flexural cracks which observed from $2\Delta_y$ displacement (1.50% drift ratio). As shown in Figure B.53, evidence of toe crushing and were found first at both ends at first cycles of $3\Delta_y$ displacement (2.25% drift ratio). As shown in Figure B.54, severe toe crushing and face shell spalling at both ends were observed at the second cycles to $4\Delta_y$ displacements (3.00% drift ratio). Extreme vertical bars at the both ends fractured at the end of displacements of $8\Delta_y$ (4.16% drift ratio) as shown in Figure B.55. Figure B.56 shows the specimen upon completion of the test. As shown in Figure B.57, reversed cyclic loading caused toe crushing and spalling, and vertical bars fracture at the base of the specimen.

North toe ***South toe***

Figure B.53 Onset of toe crushing, Specimen UT-W-18

(a) Cycle 4∆y, loading north ***(b) Cycle 4∆y, loading south***

Figure B.54 Severe toe crushing and face shell spalling, Specimen UT-W-18

(a) Cycle 8Δy, loading south *(b) Cycle 8Δy, loading north*

Figure B.55 Fracture of extreme vertical bars, Specimen UT-W-18

Figure B.56 Specimen UT-W-18 at end of test

North toe ***South toe***

Figure B.57 Detail of toe crushing at end of test, Specimen UT-W-18

B.5.3 Load-Displacement Behavior for Specimen UT-W-18

The load-displacement relationship of Specimen UT-W-18 is presented in Figure B.58 in terms of the lateral displacemnet, which references five major events during testing:

1) first yield of the extreme vertical reinforcement ($\varepsilon_y = 0.0021$);
2) maximum useful strain in the masonry ($\varepsilon_{mu} = 0.0025$);
3) maximum capacity (capping point);
4) onset of toe crushing; and
5) decrease in capacity to 50% of maximum capacity.

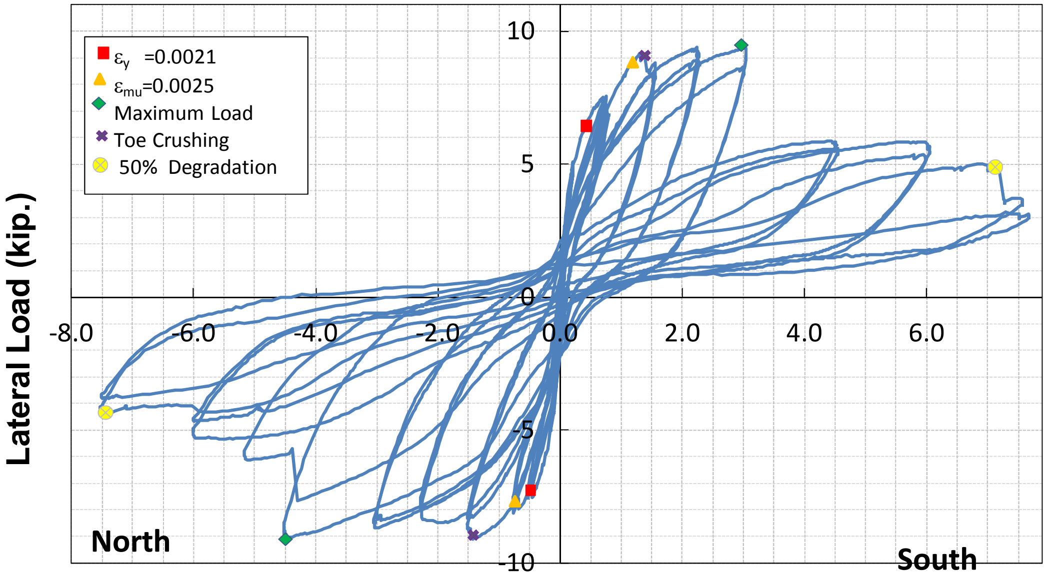

Figure B.58 Load versus top displacement, Specimen UT-W-18

Curvatures were determined over the wall height based on strain profiles, and are shown in Figure B.59. The strain profiles were calculated using five potentiometers along the inside edge of the wall (this was mirrored on the opposite side). The curvatures were determined for the first cycle to each displacement. Due to spalling of the face shells at the wall toes and detachment of the displacement potentiometer anchors, these displacement measurements were discontinued at later stages of testing. Therefore, strains and curvatures at larger displacements were not available.

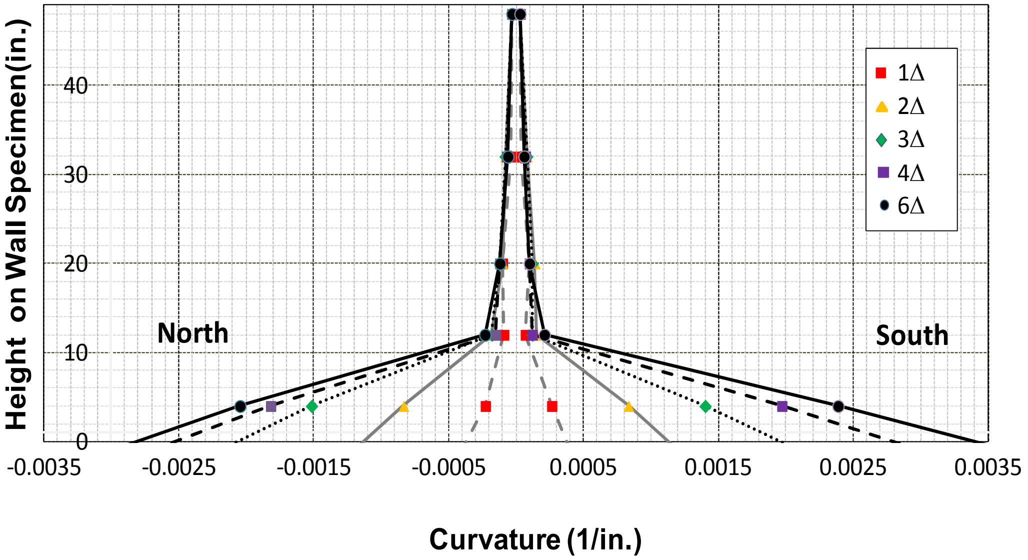

Figure B.59 Wall curvature of Specimen UT-W-18

B.5.4 Displacement Ductility, Specimen UT-W-18

The values obtained for the displacement ductility are presented in Table B-25. The results are presented for both load directions (push to the North and pull to the South), and then averaged.

Table B-25 Calculated displacement ductilities for Specimen UT-W-18

Direction of Load	**Load and Displacement Parameters**					
	P'_y (kips)	Δ'_y (in.)	Δ_u (in.)	P_y (kips)	Δ_y (in.)	μ_Δ
Push (North)	7.16	0.39	5.21	8.34	0.45	11.57
Pull (South)	6.40	0.41	3.80	8.37	0.53	7.16
					Average	9.36

The curvature ductility of Specimen UT-W-18 was also determined using a similar process as above. The values obtained for the curvature ductility are presented in

Table B-26. The results are presented for both load directions: push to the north and pull to the south, and then averaged.

Table B-26 Calculated curvature ductilities for Specimen UT-W-18

Direction of Load	**Moment and Curvature Parameters**					
	M'_y (kip-in.)	ϕ'_y (in.$^{-1}$)	ϕ_u (in.$^{-1}$)	M_y (kip-in.)	ϕ_y (in.$^{-1}$)	μ_ϕ
Push (North)	1031	0.00018	0.0030	1200	0.00021	14.3
Pull (South)	924	0.00018	0.0034	1205	0.00023	14.5
					Average	14.4

B.5.5 Calculation of Plastic Hinge Lengths, Specimen UT-W-18

B.5.5.1 Method 1 (Bohl and Adebar 2011 and Shedid et al. 2010)

In Table B-27, the calculated yielded lengths are presented as a function of drift ratio for each load direction, and are then averaged between the two directions. In the last line of the table, the calculated yielded lengths are expressed in terms of L_w , the plan length of the wall.

Table B-27 Yielded lengths of Specimen UT-W-18

Drift Ratio (Displacement)	**Yielded Lengths, $L_{yielded}$ (in.), for Different Drift Ratios**				
	0.52% (Δ_y)	**1.04% ($2\Delta_y$)**	**1.56% ($3\Delta_y$)**	**2.08% ($4\Delta_y$)**	**3.12% ($6\Delta_y$)**
Push North	4.5	12.0	12.0	12.0	14.0
Pull South	6.3	11.5	11.5	11.5	12.5
Average	5.4	11.75	11.75	11.75	13.25
$L_{yielded}/L_w$	17.0%	37.1%	37.1%	37.1%	41.8%

If the plastic hinge length l_p is assumed equal to 0.5 $L_{yielded}$, then the resulting plastic hinge lengths are as shown in Table B-28 for each drift ratio.

Table B-28 Calculation of plastic hinge lengths of Specimen UT-W-18

Drift Ratio (Displacement)	**Plastic Hinge Lengths, l_p (in.), for Different Drift Ratios**				
	0.52% (Δ_y)	**1.04% ($2\Delta_y$)**	**1.56% ($3\Delta_y$)**	**2.08% ($4\Delta_y$)**	**3.12% ($6\Delta_y$)**
Yielded Length	5.4	11.75	11.75	11.75	13.25
Plastic Hinge Length (l_p)	2.7	5.88	5.88	5.88	6.63
l_p/L_w	8.5%	18.5%	18.5%	18.5%	20.9%

B.5.5.2 Method 2 (Shedid et al. 2010 and Dazio 2009)

The equivalent plastic hinge lengths for both load directions at different drift ratios are calculated as shown in Table B-29.

Table B-29 Equivalent plastic hinge length of Specimen UT-W-18

Drift Ratio (Displacement)	**Plastic Hinge Lengths, l_p (in.), for Different Drift Ratios**				
	0.52% (Δ_y)	**1.04% ($2\Delta_y$)**	**1.56% ($3\Delta_y$)**	**2.08% ($4\Delta_y$)**	**3.12% ($6\Delta_y$)**
Push North	11.8	7.8	6.6	7.4	10.5
Pull South	11.2	7.7	6.8	6.6	9.1
Average	11.5	7.7	6.7	7.0	9.8
I_p/L_w	36.3%	24.3%	21.2%	22.1%	30.9%

B.5.5.3 Method 3 (Bohl and Adebar 2011)

The calculated plastic hinge lengths were determined for both load direction: push to the north and pull to the south. The results are shown in Table B-30.

Table B-30 Predicted plastic hinge lengths for Specimen UT-W-18

Direction of Load	Moment and Plastic Hinge Parameters					
	M_y (kip-in.)	M_{max} (kip-in.)	z (in.)	$L_{yielded}$ (in.)	$l_p = 0.5L_{yielded}$ (in.)	l_p/L_w
Push (North)	1031	1288	144	28.7	14.4	0.45
Pull (South)	924	1285	144	40.6	20.3	0.64
					Average	0.54

B.5.6 Components of Displacements for Specimen UT-W-18

Load-displacement curves for total sliding and shear component of total tip displacement are given in Figure B.60 and Figure B.61, and total displacement and shear deformation are compared in Figure B.62.

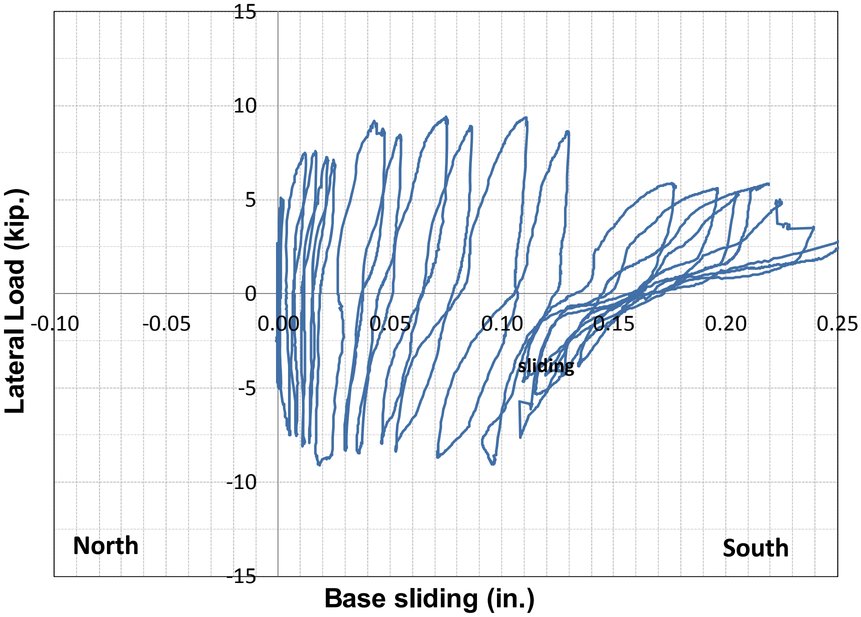

Figure B.60 Base sliding, Specimen UT-W-18

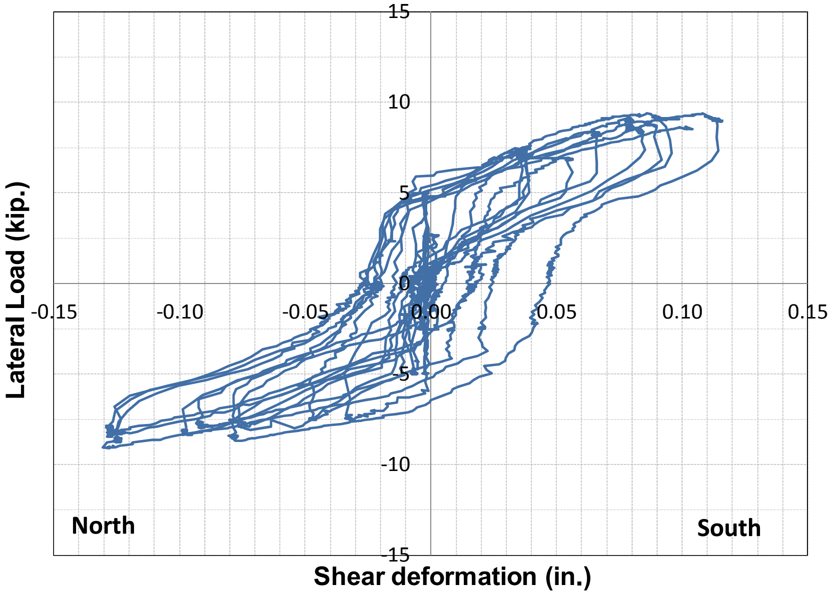

Figure B.61 Shear deformation, Specimen UT-W-18

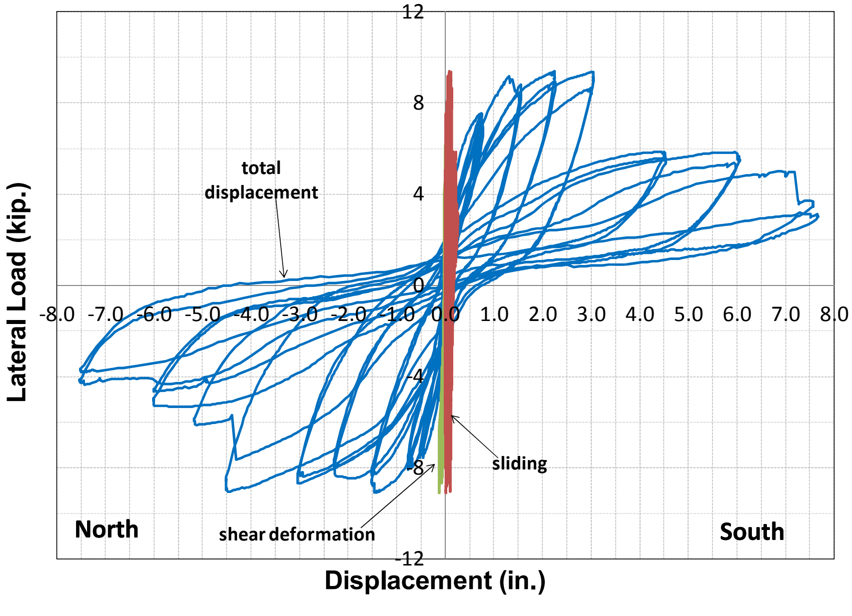

Figure B.62 Components of displacement for Specimen UT-W-18

B.6 TEST RESULTS FOR SPECIMEN UT-W-19

Specimen UT-W-19 was detailed according to the requirements of the 2008 MSJC *Code*. It has a height of 12 ft and a plan length of 2.67 ft (aspect ratio 4.5), required prescriptive reinforcement for a Intermediate Reinforced Masonry Shear Wall (2008 MSJC *Code*), and a normalized axial load ratio P / ($f_m' A_g$) of 0.10. The vertical reinforcement ratio was 0.0072, with No. 6 reinforcing bars at 8 in. (every cell); and the horizontal reinforcement ratio was 0.0016, with No. 4 bars at 16 in. The specimen used cement-lime mortar conforming to the proportion specification for Type S of ASTM C270, and grout conforming to the strength specification of ASTM C476. A photo of the specimen before testing is shown in Figure B.63, and details for the specimen are shown in Figure B.64.

Figure B.63 Specimen UT-W-19 before testing

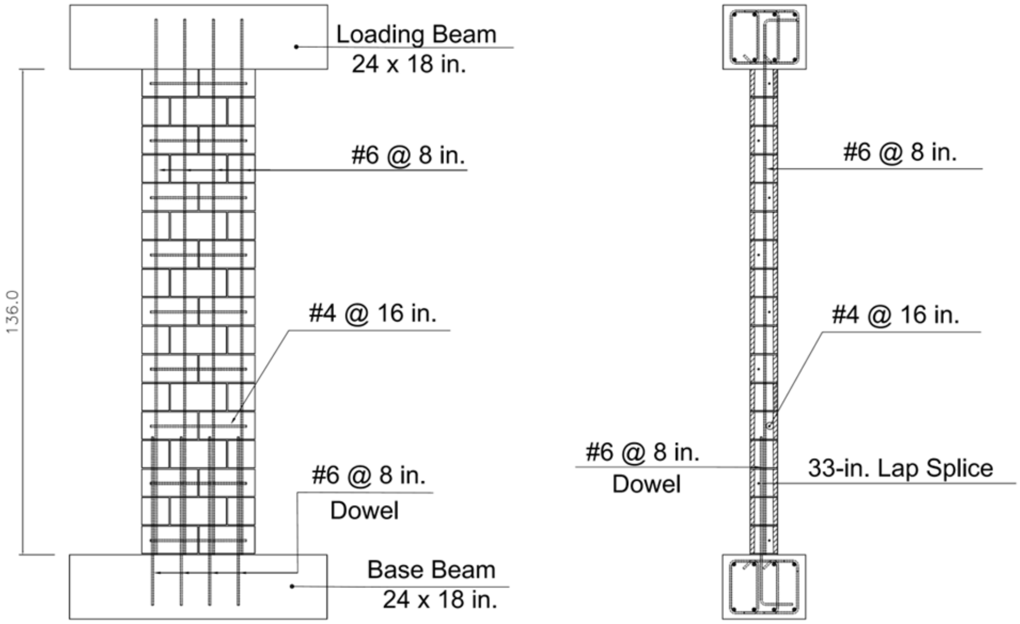

Figure B.64 Details for Specimen UT-W-19

B.6.1 Loading History for Specimen UT-W-19

Specimen UT-W-19 was first subjected to a preliminary test to estimate the yield displacement, Δ_y. On July 15, 2011, Specimen UT-W-19 was loaded at a rate of 0.3 in./min to two cycles of reversed displacements of ±1, 2, 3, and 4 times that predicted yield displacement, as shown in Figure B.65 . It was then loaded to a half-cycle to a displacement of 6 times that predicted yield displacement. The test was stopped when the peak capacity dropped to 20% or less of the experimentally observed maximum capacity (capping point). The testing took about 10 hours.

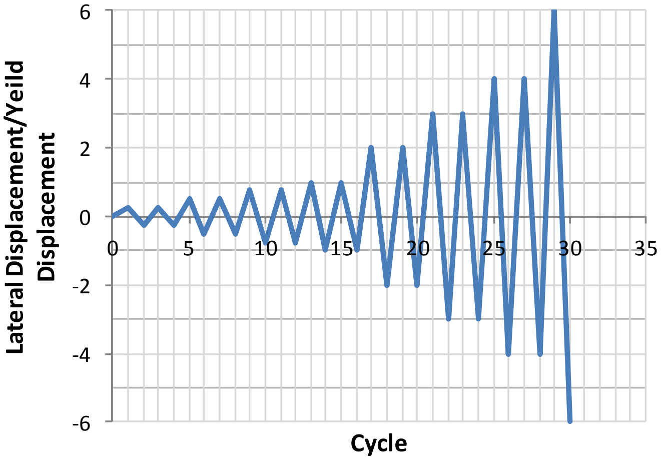

Figure B.65 Proposed loading history, Specimen UT-W-19

B.6.2 Major Test Observations, Specimen UT-W-19

The behavior of Specimen UT-W-19 was controlled by flexure. The value of Δ_y calculated in the preliminary phase of the test was 1.34 in., equivalent to a drift ratio of 0.93%. Flexural cracks (horizontal cracks in the bed joints) started early in the test before $1\Delta_y$. As shown in Figure B.66, evidence of toe crushing and were found first at both ends at first cycle of $2\Delta_y$ displacements (1.86% drift ratio). As shown in Figure B.67, extensive toe crushing and spalling, and vertical cracks at north end were observed at the second cycle to $4\Delta_y$ displacement (3.72% drift ratio), followed by buckling of north end vertical reinforcement at the first cycle to $6\Delta_y$ (5.58% drift ratio). Similar damage occurred while loading to the south at the first cycle to $6\Delta_y$ (5.58% drift ratio) as shown in Figure B.67c. The test was ended when the specimen suddenly failed because of vertical bars buckling and lack of compression capacity at the toes. Figure B.68 and Figure B.69 show the specimen upon completion of the test. As shown in Figure B.69, reversed cyclic loading caused toe crushing at the base of the specimen. The transverse reinforcing bars, hooked around the longitudinal bar splices, kept the spliced bars from coming apart.

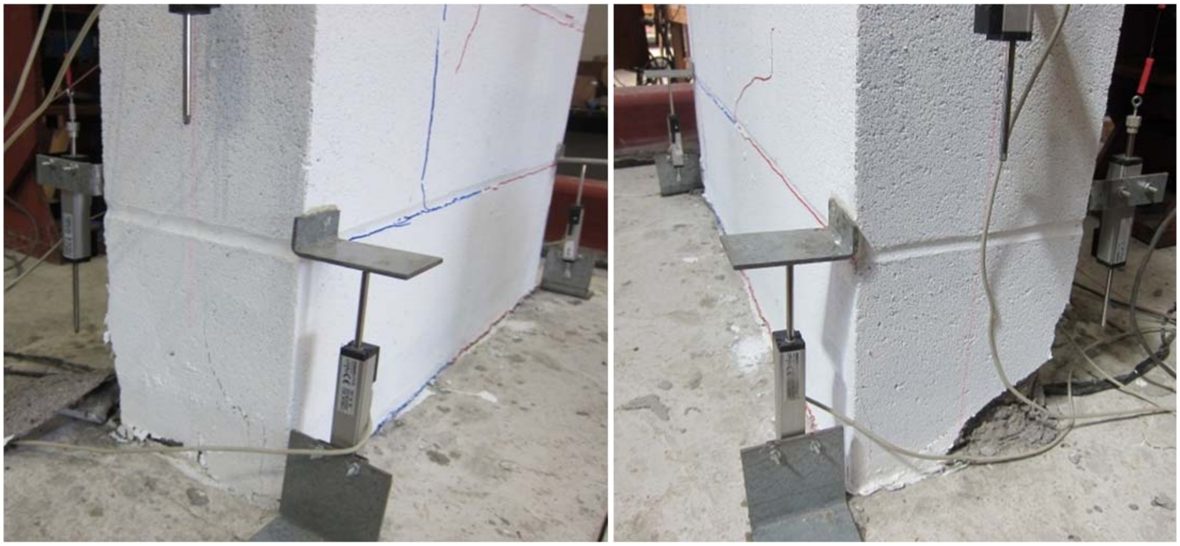

North toe *South toe*

Figure B.66 Onset of toe crushing, Specimen UT-W-19

(a) Cycle 4Δy, loading north *(b) Cycle 6Δy, loading north* *(c) Cycle 6Δy, loading south*

Figure B.67 Severe toe crushing and spalling, followed by buckling of longitudinal bars, Specimen UT-W-19

Figure B.68 Specimen UT-W-19 at end of test

North toe **South toe**

Figure B.69 Detail of toe splices at end of test, Specimen UT-W-19

B.6.3 Load-Displacement Behavior for Specimen UT-W-19

The load-displacement relationship of Specimen UT-W-19 is presented in Figure B.70 in terms of the lateral displacement, which references five major events during testing:

1) first yield of the extreme vertical reinforcement ($\varepsilon_y = 0.0021$);
2) maximum useful strain in the masonry ($\varepsilon_{mu} = 0.0025$);
3) maximum capacity (capping point);
4) onset of toe crushing; and
5) decrease in capacity to 50% of maximum capacity.

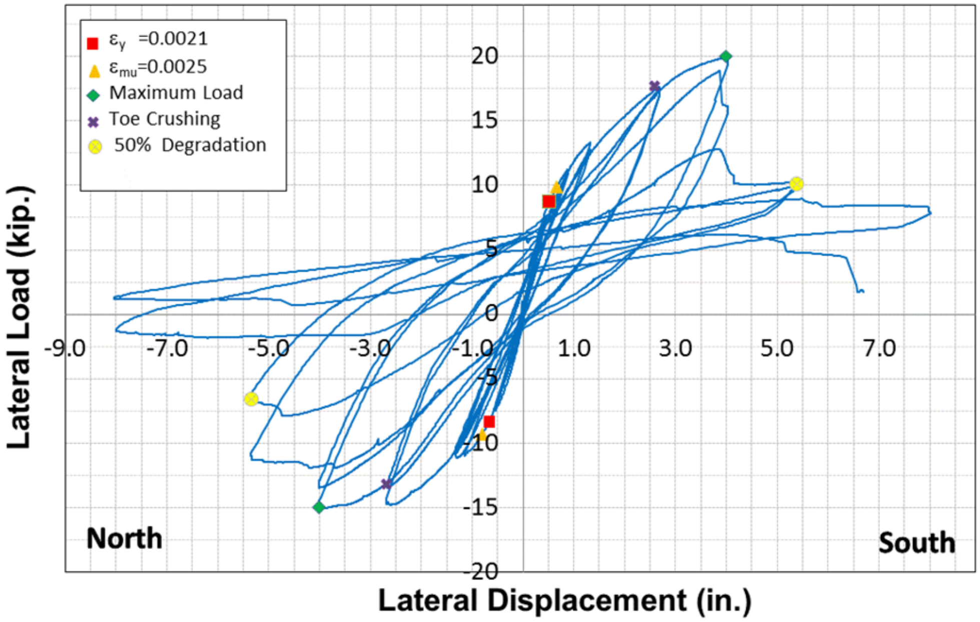

Figure B.70 Load versus top displacement, Specimen UT-W-19

Curvatures were determined over the wall height based on strain profiles, and are shown in Figure B.71. The strain profiles were calculated using five potentiometers along the inside edge of the wall (this was mirrored on the opposite side). The curvatures were determined for the first cycle to each displacement. Due to spalling of the face shells at the wall toes and detachment of the displacement potentiometer anchors, these displacement measurements were discontinued at later stages of testing. Therefore, strains and curvatures at larger displacements were not available.

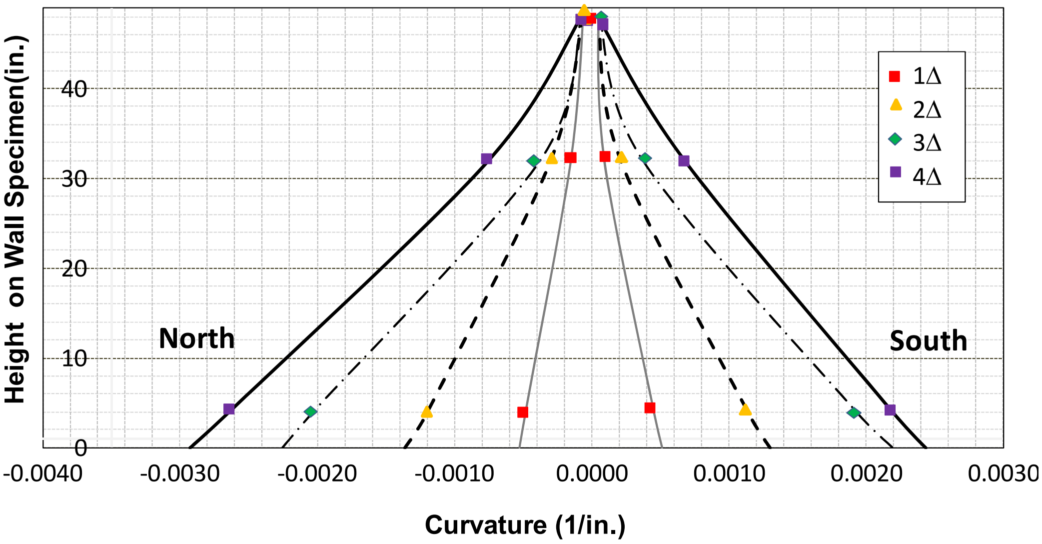

Figure B.71 Wall Curvature of Specimen UT-W-19

B.6.4 Displacement Ductility, Specimen UT-W-19

The values obtained for the displacement ductility are presented in Table B-31. The results are presented for both load directions (push to the North and pull to the South), and then averaged.

Table B-31 Calculated displacement ductilities for Specimen UT-W-19

Direction of Load	Load and Displacement Parameters					
	P'_y (kips)	Δ'_y (in.)	Δ_u (in.)	P_y (kips)	Δ_y (in.)	μ_Δ
Push (North)	8.71	0.53	4.56	13.45	0.82	5.57
Pull (South)	8.34	0.66	5.02	15.52	1.22	4.08
					Average	4.96

The curvature ductility of Specimen UT-W-19 was also determined using a similar process as above. The values obtained for the curvature ductility are presented in Table B-32. The results are presented for both load directions: push to the north and pull to the south, and then averaged.

Table B-32 Calculated curvature ductilities for Specimen UT-W-19

Direction of Load	Moment and Curvature Parameters					
	M'_y (kip-in.)	ϕ'_y (in.$^{-1}$)	ϕ_u (in.$^{-1}$)	M_y (kip-in.)	ϕ_y (in.$^{-1}$)	μ_ϕ
Push (North)	1254	0.00017	0.0029	1936	0.00026	11.2
Pull (South)	1200	0.00017	0.0024	2234	0.00031	7.8
					Average	9.5

B.6.5 Calculation of Plastic Hinge Lengths, Specimen UT-W-19

B.6.5.1 Method 1 (Bohl and Adebar 2011 and Shedid et al. 2010)

In Table B-33, the calculated yielded lengths are presented as a function of drift ratio for each load direction, and are then averaged between the two directions. In the last line of the table, the calculated yielded lengths are expressed in terms of L_w, the plan length of the wall.

Table B-33 Yielded lengths of Specimen UT Wall-19

Drift Ratio (Displacement)	**Yielded Lengths, $L_{yielded}$ (in.), for Different Drift Ratios**			
	0.93% (Δ_y)	**1.86% ($2\Delta_y$)**	**2.79% ($3\Delta_y$)**	**3.72% ($4\Delta_y$)**
Push North	17.5	31.0	33.5	41.0
Pull South	15.0	28.5	34.0	40.5
Average	16.25	29.75	33.75	40.75
$L_{yielded}/L_w$	50.8%	92.9%	105.5%	127.3%

If the plastic hinge length l_p is assumed equal to 0.5 $L_{yielded}$, then the resulting plastic hinge lengths are as shown in Table B-34 for each drift ratio.

Table B-34 Calculation of plastic hinge lengths of Specimen UT Wall-19

Drift Ratio (Displacement)	**Plastic Hinge Lengths, l_p (in.), for Different Drift Ratios**			
	0.93% (Δ_y)	**1.86% ($2\Delta_y$)**	**2.79% ($3\Delta_y$)**	**3.72% ($4\Delta_y$)**
Yielded Length	16.25	29.75	33.75	40.75
Plastic Hinge Length (l_p)	8.12	14.87	16.871	20.38
l_p/L_w	25.4%	46.5%	52.7%	63.7%

B.6.5.2 Method 2 (Shedid et al. 2010 and Dazio 2009)

The equivalent plastic hinge lengths for both load directions at different drift ratios are calculated as shown in Table B-35.

Table B-35 Equivalent plastic hinge length of Specimen UT-W-19

Drift Ratio (Displacement)	Plastic Hinge Lengths, l_p (in.), for Different Drift Ratios			
	0.93% (Δ_y)	1.86% ($2\Delta_y$)	2.79% ($3\Delta_y$)	3.72% ($4\Delta_y$)
Push North	16.8	13.1	12.2	12.7
Pull South	14.0	12.3	11.7	12.4
Average	15.4	12.7	11.95	12.55
l_p/L_w	48.1%	39.7%	37.3%	39.2%

B.6.5.3 Method 3 (Bohl and Adebar 2011)

The calculated plastic hinge lengths were determined for both load direction: push to the north and pull to the south. The results are shown in Table B-36.

Table B-36 Predicted plastic hinge lengths for Specimen UT-W-19

Direction of Load	Moment and Plastic Hinge Parameters					
	M_y (kip-in.)	M_{max} (kip-in.)	z (in.)	$L_{yielded}$ (in.)	$l_p = 0.5L_{yielded}$ (in.)	l_p/L_w
Push (North)	1254	2160	144	60.4	30.2	0.94
Pull (South)	1200	2880	144	84.0	42.0	1.31
					Average	1.15

B.6.6 Components of Displacements for Specimen UT-W-19

Load-displacement curves for total sliding and shear component of total tip displacement are given in Figure B.72 and Figure B.73, and total displacement and shear deformation are compared in Figure B.74.

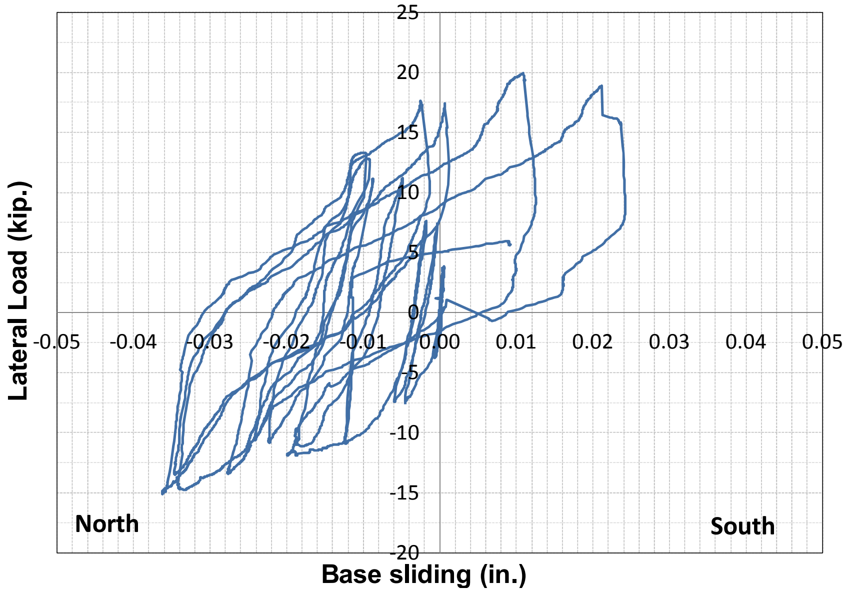

Figure B.72 Base sliding, Specimen UT-W-19

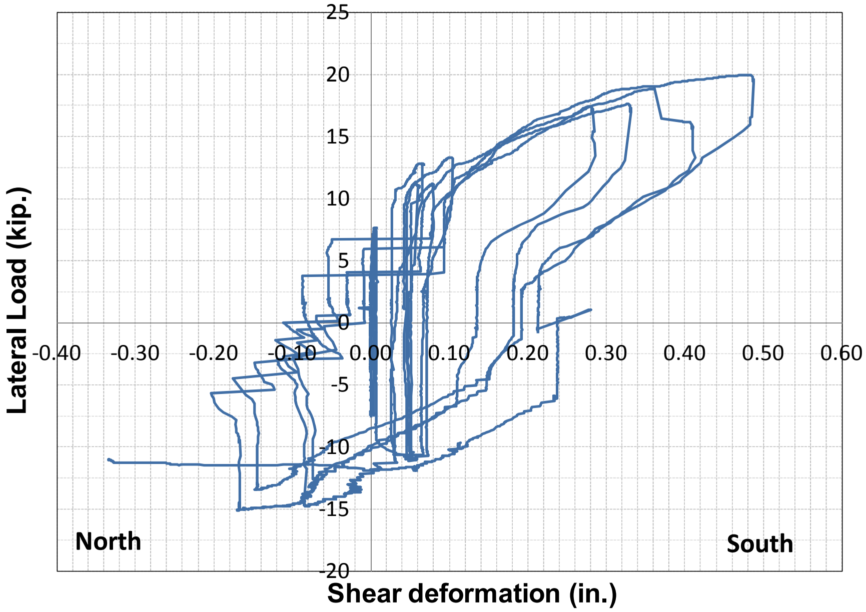

Figure B.73 Shear deformation, Specimen UT-W-19

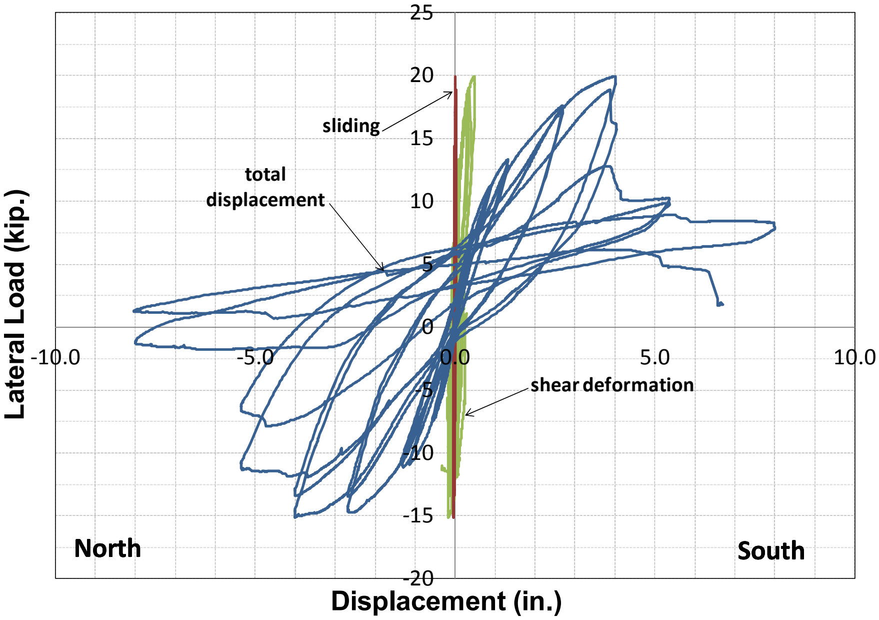

Figure B.74 Components of displacement for Specimen UT-W-19

B.7 TEST RESULTS FOR SPECIMEN UT-W-20

Specimen UT-W-20 was detailed according to the requirements of the 2008 MSJC *Code*. It has a height of 12 ft and a plan length of 2.67 ft (aspect ratio 4.5), required prescriptive reinforcement for a Intermediate Reinforced Masonry Shear Wall (2008 MSJC *Code*), and a normalized axial load ratio P / ($f_m' A_g$) of 0.15. The vertical reinforcement ratio was 0.0033, with No. 4 reinforcing bars at 8 in. (every cell); and the horizontal reinforcement ratio was 0.0016, with No. 4 bars at 16 in. The specimen used cement-lime mortar conforming to the proportion specification for Type S of ASTM C270, and grout conforming to the strength specification of ASTM C476. A photo of the specimen before testing is shown in Figure B.75, and details for the specimen are shown in Figure B.76.

Figure B.75 Specimen UT-W-20 before testing

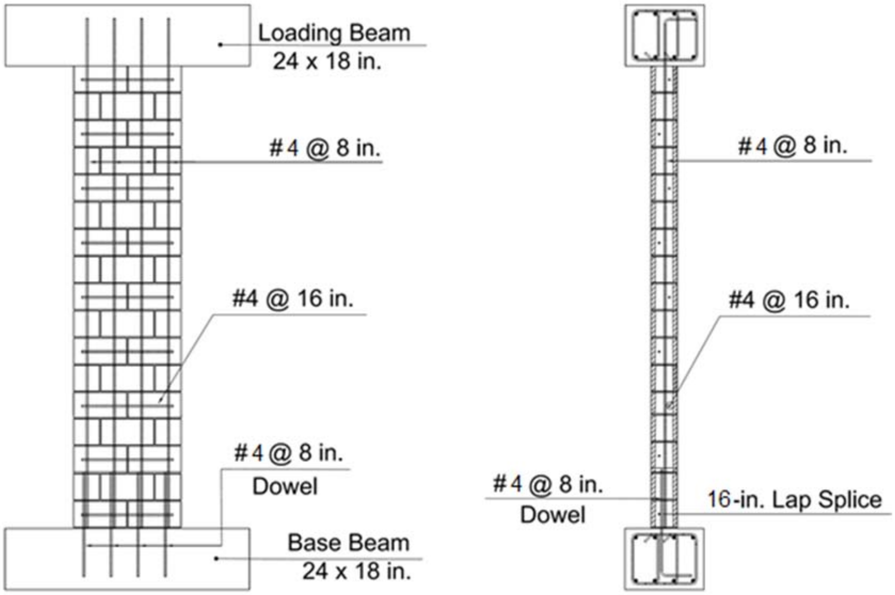

Figure B.76 Details for Specimen UT-W-20

B.7.1 Loading History for Specimen UT-W-20

Specimen UT-W-20 was first subjected to a preliminary test to estimate the yield displacement, Δ_y. On July 25, 2011, Specimen UT-W-20 was loaded at a rate of 0.3 in./min to two cycles of reversed displacements of ±1, 2, 3, 4, 6, 8 and 10 times that predicted yield displacement, as shown in Figure B.77. It was then loaded to a half-cycle to a displacement of 12 times that predicted yield displacement. The test was stopped when the peak capacity dropped to 20% or less of the experimentally observed maximum capacity (capping point). . The testing took about 8 hours.

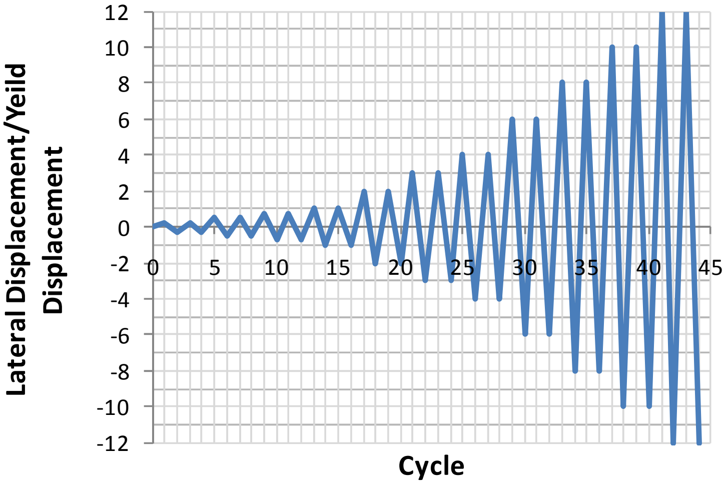

Figure B.77 Proposed loading history, Specimen UT-W-20

B.7.2 Test Major Observations, Specimen UT-W-20

The behavior of Specimen UT-W-20 was controlled by flexure. The value of Δ_y calculated in the preliminary phase of the test was 0.68 in., equivalent to a drift ratio of 0.47%. Flexural cracks (horizontal cracks in the bed joints) started early in the test before 1Δ_y, followed by opened flexural cracks which observed from 2Δ_y displacement (0.94% drift ratio). As shown in Figure B.78, evidence of toe crushing was found first at both ends at first cycles of 3Δ_y displacement (1.41% drift ratio). As shown in Figure B.54, severe toe crushing and face shell spalling at north end were observed at the second cycle to 6Δ_y displacement (2.82% drift ratio). Similar damage occurred while loading to the south at the first cycle to 8Δ_y (3.76% drift ratio) as shown in Figure B.78. Extreme vertical bars at the north end fractured at the end of displacement of 10Δ_y (4.70% drift ratio). Figure B.80 shows the specimen upon completion of the test. As shown in Figure B.81, reversed cyclic loading caused toe crushing at the base of the specimen. The transverse reinforcing bars, hooked around the longitudinal bar splices, kept the spliced bars from coming apart.

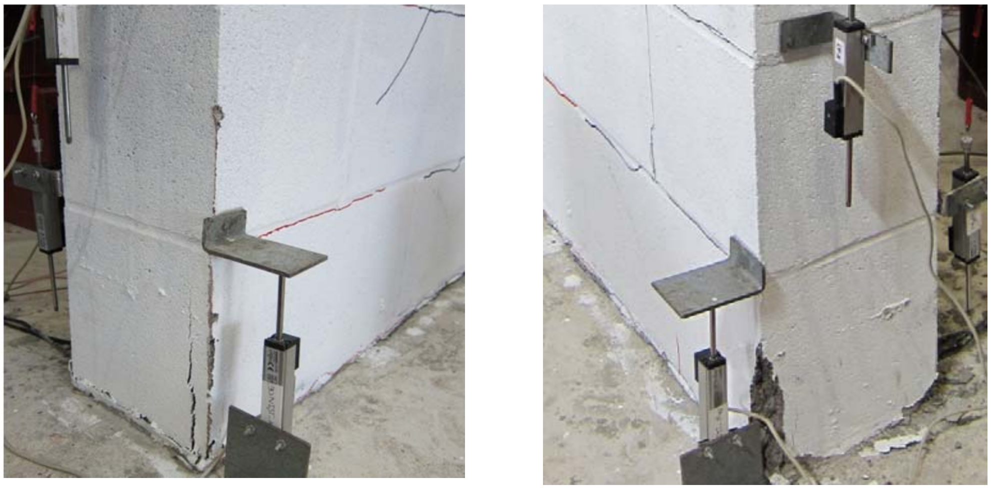

North toe ***South toe***

Figure B.78 Onset of toe crushing, Specimen UT-W-20

(a) Cycle 6∆y, loading north ***(b) Cycle 8∆y, loading south***

Figure B.79 Severe toe crushing and face shell spalling, Specimen UT-W-20

Figure B.80 Specimen UT-W-20 at end of test

North toe *South toe*

Figure B.81 Detail of toe splices at end of test, Specimen UT-W-20

B.7.3 Load-Displacement Behavior for Specimen UT-W-20

The load-displacement relationship of Specimen UT-W-20 is presented in Figure B.82 in terms of the lateral displacement, which references five major events during testing:

1) first yield of the extreme vertical reinforcement ($\varepsilon_y = 0.0022$);
2) maximum useful strain in the masonry ($\varepsilon_{mu} = 0.0025$);
3) maximum capacity (capping point);
4) onset of toe crushing; and
5) decrease in capacity to 50% of maximum capacity.

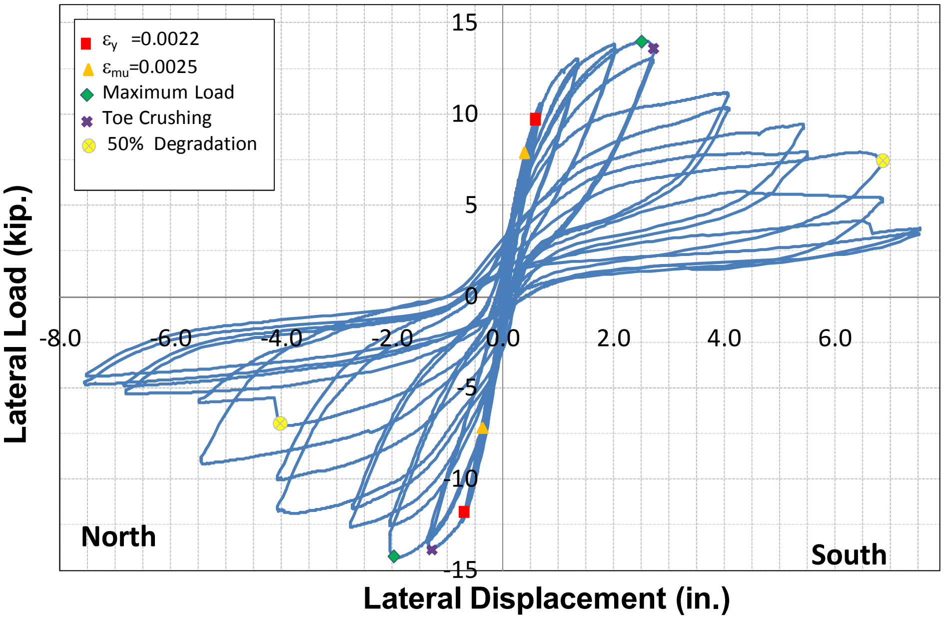

Figure B.82 Load versus top displacement, Specimen UT-W-20

Curvatures were determined over the wall height based on strain profiles, and are shown in Figure B.83. The strain profiles were calculated using five potentiometers along the inside edge of the wall (this was mirrored on the opposite side). The curvatures were determined for the first cycle to each displacement. Due to spalling of the face shells at the wall toes and detachment of the displacement potentiometer anchors, these displacement measurements were discontinued at later stages of testing. Therefore, strains and curvatures at larger displacements were not available.

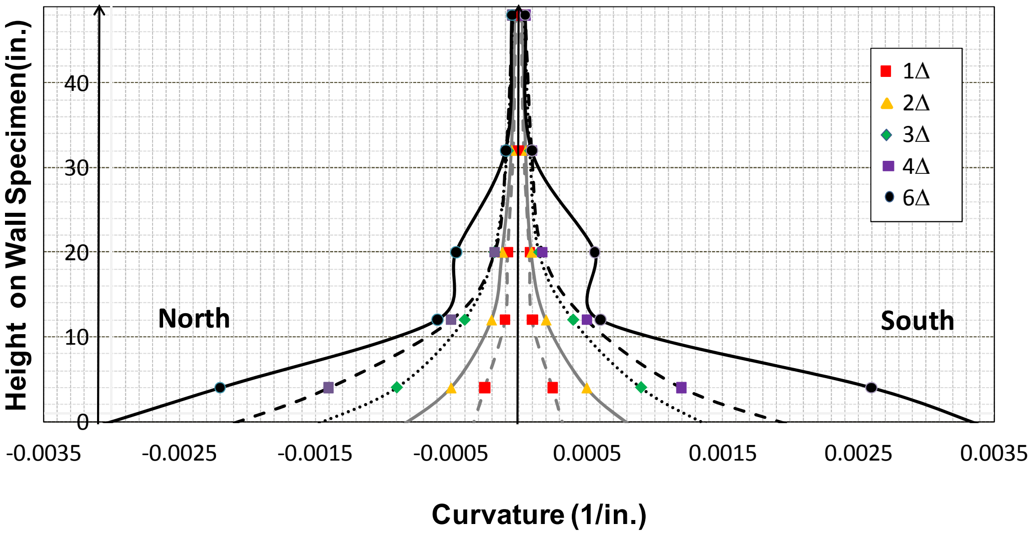

Figure B.83 Wall Curvature of Specimen UT-W-20

B.7.4 Displacement Ductility, Specimen UT-W-20

The values obtained for the displacement ductility are presented in Table B-37. The results are presented for both load directions (push to the North and pull to the South), and then averaged.

Table B-37 Calculated displacement ductilities for Specimen UT-W-20

Direction of Load	Load and Displacement Parameters					
	P'_y (kips)	Δ'_y (in.)	Δ_u (in.)	P_y (kips)	Δ_y (in.)	μ_Δ
Push (North)	12.14	0.69	4.21	13.15	0.74	5.64
Pull (South)	9.75	0.58	4.20	12.67	0.75	5.57
					Average	5.60

The curvature ductility of Specimen UT-W-20 was also determined using a similar process as above. The values obtained for the curvature ductility are presented in Table B-38. The results are presented for both load directions: push to the north and pull to the south, and then averaged.

Table B-38 Calculated curvature ductilities for Specimen UT-W-20

Direction of Load	Moment and Curvature Parameters					
	M'_y (kip-in.)	ϕ'_y (in.$^{-1}$)	ϕ_u (in.$^{-1}$)	M_y (kip-in.)	ϕ_y (in.$^{-1}$)	μ_ϕ
Push (North)	1748	0.00013	0.0030	1894	0.00014	21.4
Pull (South)	1404	0.00011	0.0032	1824	0.00014	22.8
					Average	22.1

B.7.5 Calculation of plastic hinge lengths

B.7.5.1 Method 1 (Bohl and Adebar 2011 and Shedid et al. 2010)

In Table B-39, the calculated yielded lengths are presented as a function of drift ratio for each load direction, and are then averaged between the two directions. In the last line of the table, the calculated yielded lengths are expressed in terms of L_w, the plan length of the wall.

Table B-39 Yielded lengths of Specimen UT Wall-20

Drift Ratio (Displacement)	Yielded Lengths, $L_{yielded}$ (in.), for Different Drift Ratios				
	0.47% (Δ_y)	0.94% ($2\Delta_y$)	1.42% ($3\Delta_y$)	1.88% ($4\Delta_y$)	1.88% ($6\Delta_y$)
Push North	10.5	16.5	21.5	22.0	30.5
Pull South	11.5	18.0	24.0	25.5	32.0
Average	11.0	17.25	22.75	23.75	31.25
$L_{yielded}/L_w$	34.3%	53.9%	71.0%	75.2%	97.6%

If the plastic hinge length l_p is assumed equal to 0.5 $L_{yielded}$, then the resulting plastic hinge lengths are as shown in Table B-40 for each drift ratio.

Table B-40 Calculation of plastic hinge lengths of Specimen UT Wall-20

Drift Ratio (Displacement)	Plastic Hinge Lengths, l_p (in.), for Different Drift Ratios				
	0.47% (Δ_y)	0.94% ($2\Delta_y$)	1.42% ($3\Delta_y$)	1.88% ($4\Delta_y$)	1.88% ($6\Delta_y$)
Yielded Length	11.0	17.25	22.75	23.75	31.25
Plastic Hinge Length (l_p)	5.5	8.62	11.37	11.87	11.87
l_p/L_w	17.1%	26.9%	35.5%	37.6%	48.8%

B.7.5.2 Method 2 (Shedid et al. 2010 and Dazio 2009)

The equivalent plastic hinge lengths for both load directions at different drift ratios are calculated as shown in Table B-41.

Table B-41 Equivalent plastic hinge length of Specimen UT-W-20

Drift Ratio (Displacement)	Plastic Hinge Lengths, l_p (in.), for Different Drift Ratios			
	0.94% ($2\Delta_y$)	1.42% ($3\Delta_y$)	1.88% ($4\Delta_y$)	1.88% ($6\Delta_y$)
Push North	7.1	7.1	7.4	8.5
Pull South	8.3	8.9	8.7	7.9
Average	7.7	8.0	8.05	8.2
l_p/L_w	24.0%	25.0%	25.1%	25.6%

B.7.5.3 Method 3 (Bohl and Adebar 2011)

The calculated plastic hinge lengths were determined for both load direction: push to the north and pull to the south. The results are shown in Table B-42.

Table B-42 Predicted plastic hinge lengths for Specimen UT-W-20

Direction of Load	Moment and Plastic Hinge Parameters					
	M_y (kip-in.)	M_{max} (kip-in.)	z (in.)	$L_{yielded}$ (in.)	$l_p = 0.5L_{yielded}$ (in.)	l_p/L_w
Push (North)	1748	2088	144	23.4	11.7	0.37
Pull (South)	1404	1973	144	41.5	20.8	0.65
					Average	0.50

B.7.6 Components of Displacements for Specimen UT-W-20

Load-displacement curves for total sliding and shear component of total tip displacement are given in Figure B.84 and Figure B.85, and total displacement and shear deformation are compared in Figure B.86.

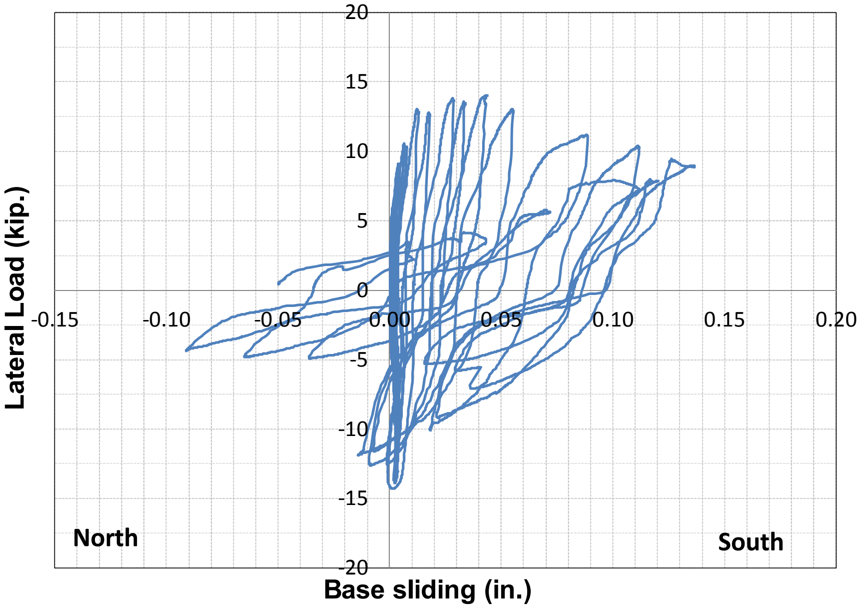

Figure B.84 Base sliding, Specimen UT-W-20

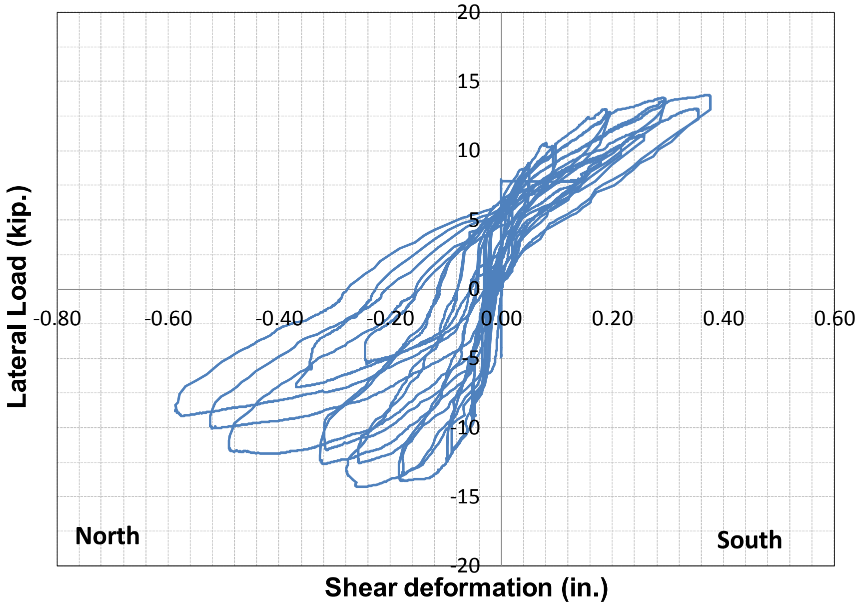

Figure B.85 Shear deformation, Specimen UT-W-20

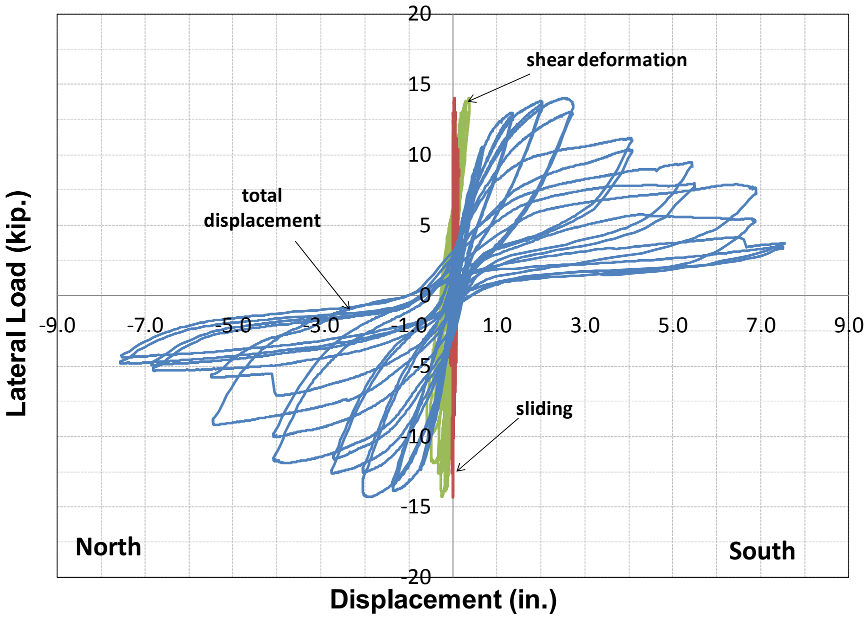

Figure B.86 Components of displacement for Specimen UT-W-20

B.8 TEST RESULTS FOR SPECIMEN UT-PBF-05

Specimen UT-PBF-05 has a height of 12 ft and a plan length of 2.67 ft (aspect ratio 4.5), required a normalized axial load ratio P / ($f_m{}' \, A_g$) of 0.00. The vertical reinforcement ratio was 0.0129, with No. 8 reinforcing bars at 8 in. (every cell); and the horizontal reinforcement ratio was 0.0033, with No. 4 bars at 8 in. The specimen used cement-lime mortar conforming to the proportion specification for Type S of ASTM C270, and grout conforming to the strength specification of ASTM C476. A photo of the specimen before testing is shown in Figure B.87, and details for the specimen are shown in Figure B.88.

Figure B.87 Specimen UT-PBF-05 before testing

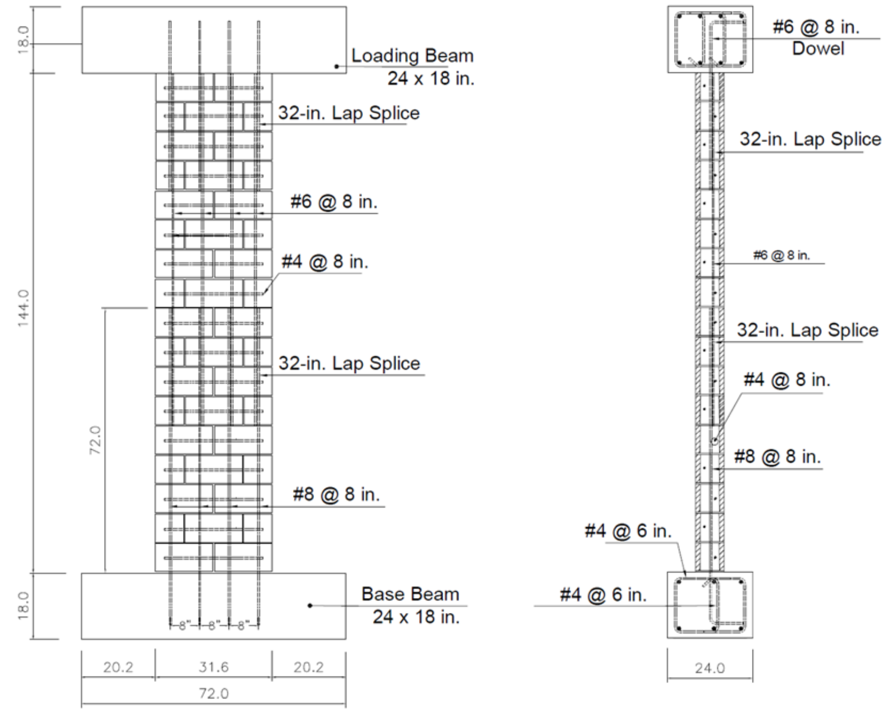

Figure B.88 Details for Specimen UT-W-18

B.8.1 Loading History for Specimen UT-PBF-05

Specimen UT-PBF-05 was first subjected to a preliminary test phase to estimate the yield displacement, Δ_y. On September 20, 2011, Specimen UT-PBF-05 was loaded at a maximum rate of 0.3 in./min. to two cycles of reversed displacements of ±1, 2, 3, and 4 times that predicted yield displacement, as shown in Figure B.89. It was then loaded to a half-cycle to a displacement of 6 times that predicted yield displacement. The test was stopped when the peak capacity dropped to 20% or less of the experimentally observed maximum capacity (capping point). The testing took about 6 hours. In this test the specimen was loaded first to the north and then to the south.

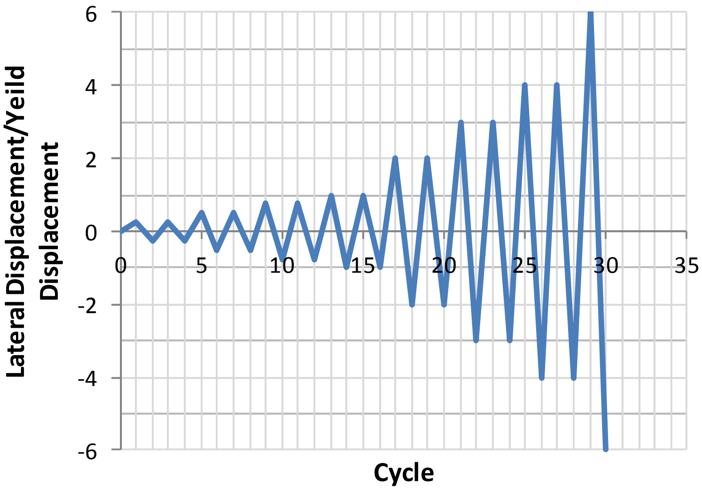

Figure B.89 Proposed loading history, Specimen UT-PBF-05

B.8.2 Major Test Observations, Specimen UT-PBF-05

The behavior of Specimen UT-PBF-05 was controlled by flexure. The value of Δ_y calculated in the preliminary phase of the test was 1.40 in., equivalent to a drift ratio of 0.97%. Flexural cracks (horizontal cracks in the bed joints) started early in the test before $1\Delta_y$, followed by shear cracks which observed at $2\Delta_y$ displacement (1.94% drift ratio). As shown in Figure B.90, evidence of toe crushing was found first at both ends at second cycles of $2\Delta_y$ displacement (1.94% drift ratio). Figure B.91 shows distributed shear cracks observed at displacement of $3\Delta_y$ (2.91% drift ratio), followed by crushing and spalling of compression toes at $4\Delta_y$ (3.88% drift ratio). As shown in Figure B.92, while loading to north vertical bar at the north end buckled at the end of displacement of $6\Delta_y$ (5.82% drift ratio). Similar damage occurred while loading to the south at the same displacement and drift ratio. Figure B.93 shows the specimen upon completion of the test. As shown in Figure B.94, reversed cyclic loading caused crushing and spalling at the base of the specimen.

North toe ***South toe***

Figure B.90 Onset of toe crushing, Specimen UT-PBF-05

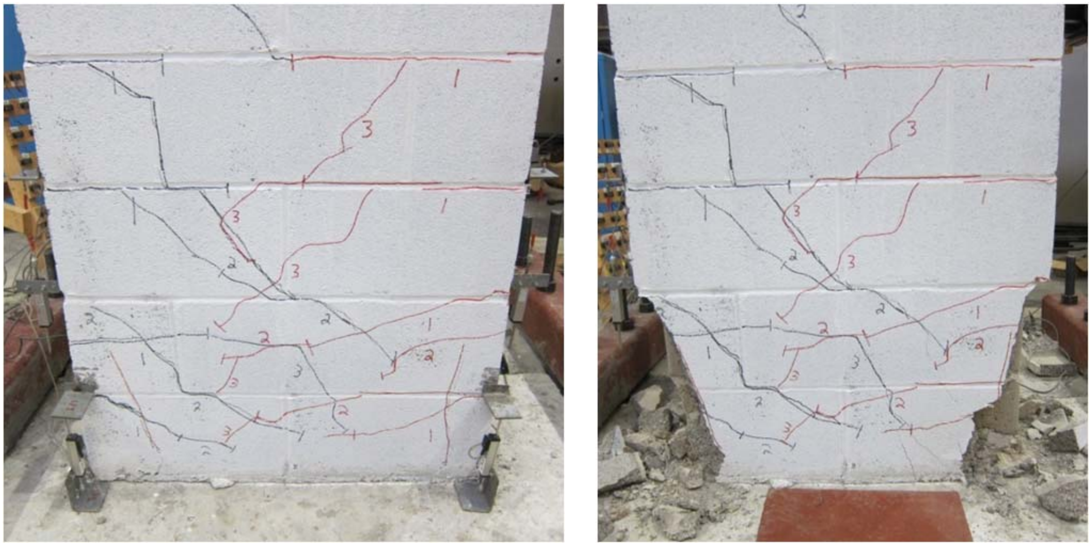

(a) Cycle 3Δy ***(b) Cycle 4Δy***

Figure B.91 Distributed shear cracks and toe crushing and spalling, Specimen UT-PBF-05

(a) Cycle 6∆y, loading north ***(b) Cycle 6∆y, loading south***

Figure B.92 Buckling of longitudinal bars, Specimen UT-PBF-05

Figure B.93 Specimen UT-PBF-05at end of test

North toe ***South toe***

Figure B.94 Detail of toe splices at end of test, Specimen UT-PBF-05

B.8.3 Load-Displacement Behavior for Specimen UT-PBF-05

The load-displacement relationship of Specimen UT-PBF-05 is presented in Figure B.95 in terms of lateral displacement, which references five major events during testing:

1) first yield of the extreme vertical reinforcement ($\varepsilon_y = 0.0021$);
2) maximum useful strain in the masonry ($\varepsilon_{mu} = 0.0025$);
3) maximum capacity (capping point);
4) onset of toe crushing; and
5) decrease in capacity to 50% of maximum capacity.

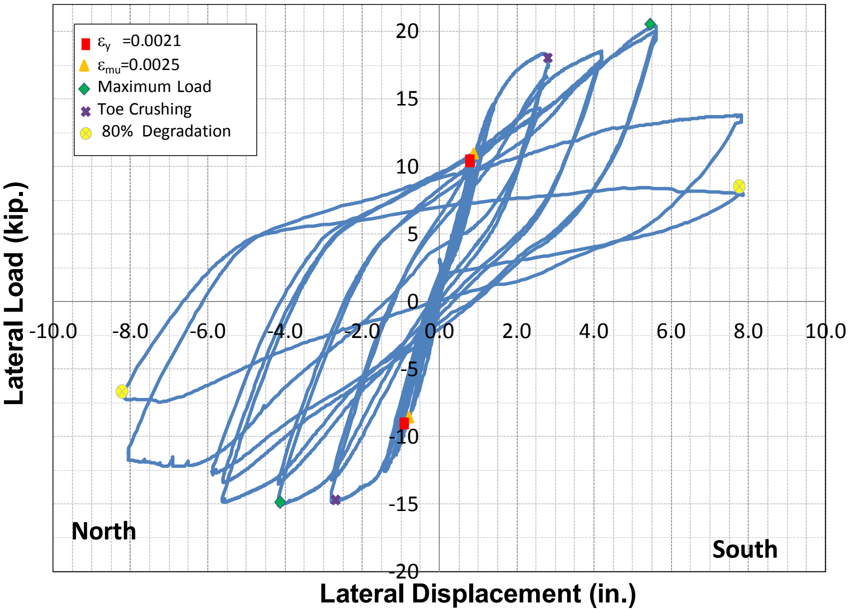

Figure B.95 Load versus top displacement, Specimen UT-PBF-05

Curvatures were determined over the wall height based on strain profiles, and are shown in Figure B.96. The strain profiles were calculated using five potentiometers along the inside edge of the wall (this was mirrored on the opposite side). The curvatures were determined for the first cycle to each displacement. Due to spalling of the face shells at the wall toes and detachment of the displacement potentiometer anchors, these displacement measurements were discontinued at later stages of testing. Therefore, strains and curvatures at larger displacements were not available.

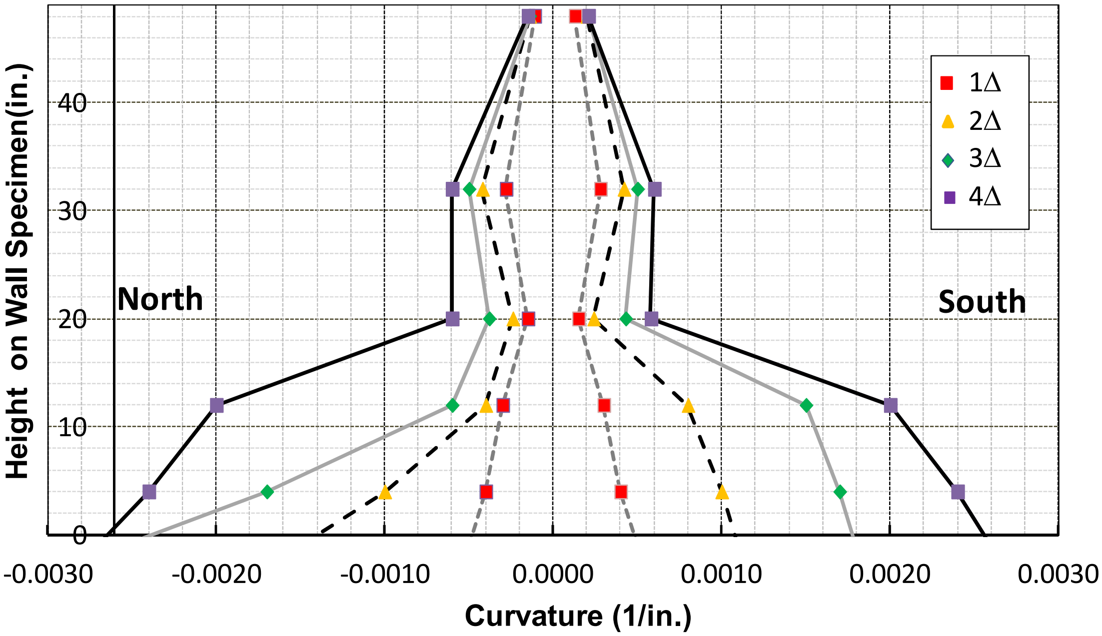

Figure B.96 Wall curvature of Specimen UT-PBF-05

B.8.4 Displacement Ductility, Specimen UT-PBF-05

The values obtained for the displacement ductility are presented in Table B-43. The results are presented for both load directions (push to the North and pull to the South), and then averaged.

Table B-43 Calculated displacement ductilities for Specimen UT-PBF-05

Direction of Load	**Load and Displacement Parameters**					
	P'_y (kips)	Δ'_y (in.)	Δ_u (in.)	P_y (kips)	Δ_y (in.)	μ_Δ
Push (North)	9.75	0.91	8.25	14.05	1.31	6.3
Pull (South)	10.63	0.89	7.05	18.18	1.49	4.7
					Average	5.5

The curvature ductility of Specimen UT-PBF-05 was also determined using a similar process as above. The values obtained for the curvature ductility are presented in Table B-44. The results are presented for both load directions: push to the North and pull to the South, and then averaged.

Table B-44 Calculated curvature ductilities for Specimen UT-PBF-05

Direction of Load	**Moment and Curvature Parameters**					
	M'_y (kip-in.)	ϕ'_y (in.$^{-1}$)	ϕ_u (in.$^{-1}$)	M_y (kip-in.)	ϕ_y (in.$^{-1}$)	μ_ϕ
Push (North)	1404	0.00012	0.0027	2023	0.00017	15.6
Pull (South)	1530	0.00016	0.0028	2617	0.00027	10.2
					Average	12.9

B.8.5 Calculation of Plastic Hinge Lengths, Specimen UT-PBF-05

B.8.5.1 Method 1 (Bohl and Adebar 2011 and Shedid et al. 2010)

In Table B-45, the calculated yielded lengths are presented as a function of drift ratio for each load direction, and are then averaged between the two directions. In the last line of the table, the calculated yielded lengths are expressed in terms of L_w , the plan length of the wall.

Table B-45 Yielded lengths of Specimen UT-PBF-05

Drift Ratio (Displacement)	**Yielded Lengths, $L_{yielded}$ (in.), for Different Drift Ratios**			
	0.97% (Δ_y)	**1.94% ($2\Delta_y$)**	**2.91% ($3\Delta_y$)**	**3.88% ($4\Delta_y$)**
Push North	18.5	42.5	45.0	45.5
Pull South	11.5	18.5	40.0	43.5
Average	15	30.25	42.5	43.5
$L_{yielded}/L_w$	46.8%	94.5%	132.8%	135.9%

If the plastic hinge length l_p is assumed equal to $0.5\,L_{yielded}$, then the resulting plastic hinge lengths are as shown in Table B-46 for each drift ratio.

Table B-46 Calculation of plastic hinge lengths of Specimen UT-PBF-05

Drift Ratio (Displacement)	**Plastic Hinge Lengths, l_p (in.), for Different Drift Ratios**			
	0.97% (Δ_y)	**1.94% ($2\Delta_y$)**	**2.91% ($3\Delta_y$)**	**3.88% ($4\Delta_y$)**
Yielded Length	15	30.25	42.5	43.5
Plastic Hinge Length (l_p)	7.5	15.125	21.25	21.75
l_p/L_w	23.4%	47.2%	66.4%	67.9%

B.8.5.2 Method 2 (Shedid et al. 2010 and Dazio 2009)

The equivalent plastic hinge lengths for both load directions at different drift ratios are calculated as shown in Table B-47.

Table B-47 Equivalent plastic hinge length of Specimen UT-PBF-05

Drift Ratio (Displacement)	Plastic Hinge Lengths, l_p (in.), for Different Drift Ratios			
	0.97% (Δ_y)	**1.94% ($2\Delta_y$)**	**2.91% ($3\Delta_y$)**	**3.88% ($4\Delta_y$)**
Push North	9.3	9.8	9.7	13.2
Pull South	11.3	15.0	14.9	14.2
Average	10.3	12.4	12.3	13.7
l_p/L_w	32.1%	38.9%	38.4%	42.8%

B.8.5.3 Method 3 (Bohl and Adebar 2011)

The calculated plastic hinge lengths were determined for both load direction: push to the north and pull to the south. The results are shown in Table B-48.

Table B-48 Predicted plastic hinge lengths for Specimen UT-PBF-05

Direction of Load	Moment and Plastic Hinge Parameters					
	M_y (kip-in.)	M_{max} (kip-in.)	z (in.)	$L_{yielded}$ (in.)	$l_p = 0.5L_{yielded}$ (in.)	l_p/L_w
Push (North)	1404.0	2152.8	144.0	50.1	25.0	0.78
Pull (South)	1530.0	2952.0	144.0	69.4	34.7	1.08
					Average	0.95

B.8.6 Components of Displacements for Specimen UT-PBF-05

Load-displacement curves for total sliding and shear component of total tip displacement are given in Figure B.97 and Figure B.98, and total displacement and shear deformation are compared in Figure B.99.

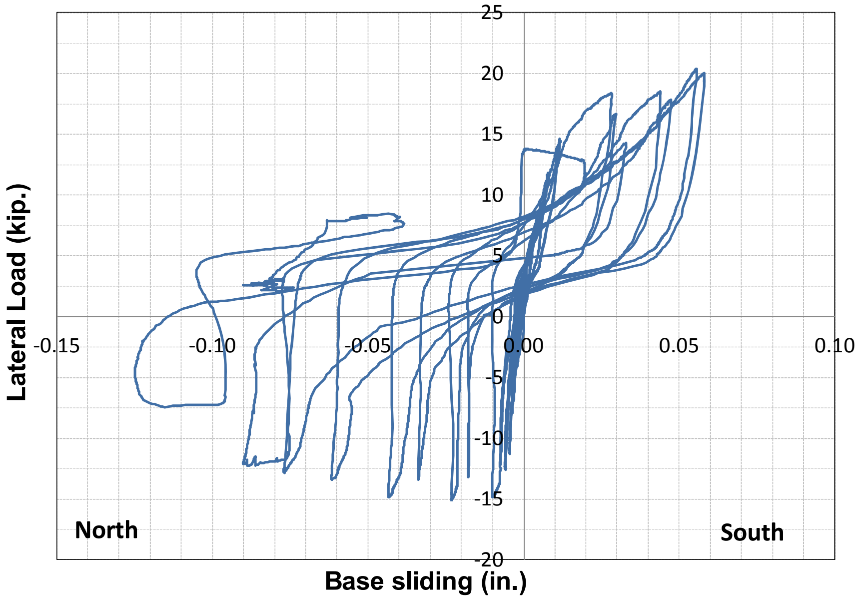

Figure B.97 Base sliding, Specimen UT-PBF-05

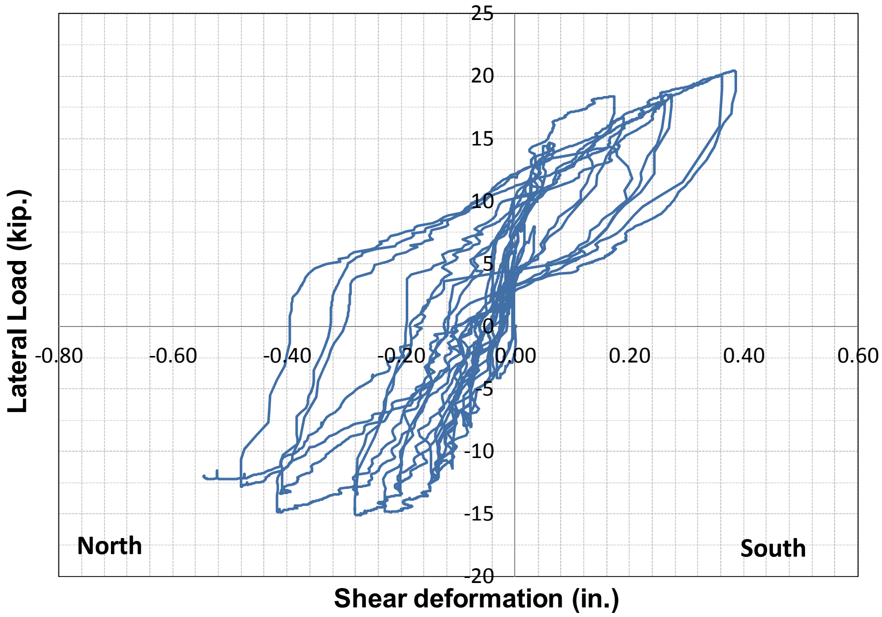

Figure B.98 Shear deformation, Specimen UT-PBF-05

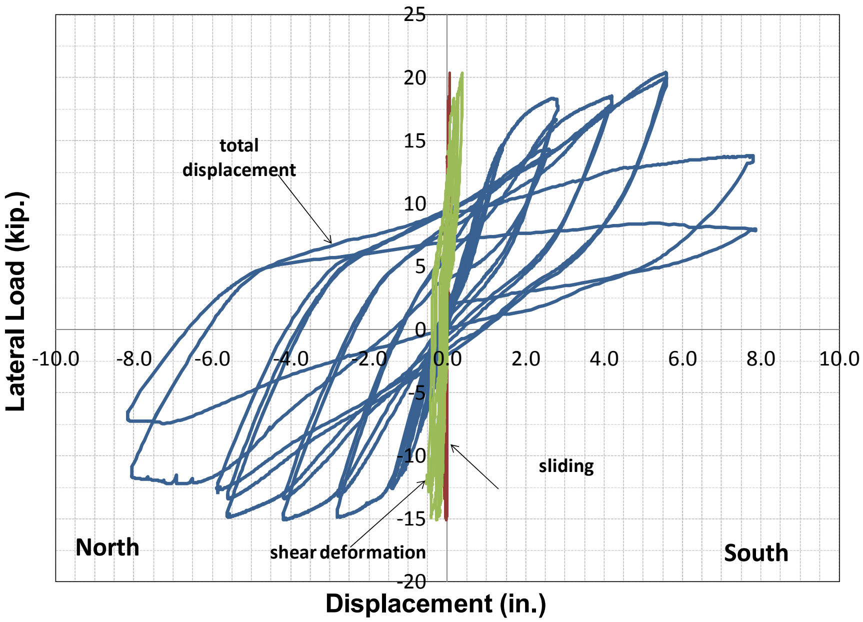

Figure B.99 Components of displacement for Specimen UT-PBF-05

APPENDIX C Test Results of Cantilever CMU Wall Specimens with Aspect Ratio of 1.0

In this appendix, the behavior under reversed in-plane cyclic load of the cantilever masonry shear-wall segments with aspect ratio of 1.0, is described. The information in this appendix is taken verbatim from the MS thesis of Jaime Hernandez (2012). It is included here for completeness.

C.1 SPECIMEN UT-PBS-03

Specimen UT-PBS-03 was 96-in. wide and 96-in. high (aspect ratio equal to 1.0) with No. 4 bars every 8 in. vertically and horizontally and an axial load equal to zero. The dowels were extended 16 in. (two courses) from the base of the wall segment. The expected moment capacity of Specimen UT-PBS-03 was 526 ft-kips, equivalent to a lateral load of 60.11 kips as calculated in Section 3.2. Specimen UT-PBS-03 before the test is shown in Figure C.1.

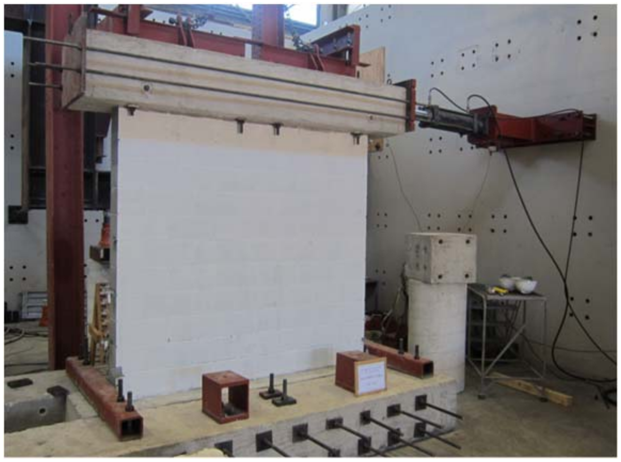

Figure C.1 Specimen UT-PBS-03 before testing

C.1.1 Test Observations, Specimen UT-PBS-03

The behavior of Specimen UT-PBS-03 was controlled by flexure. The value of Δ_y calculated in the preliminary phase of the test was 0.10 in., equivalent to a drift ratio of 0.10%. Flexural cracks (horizontal cracks in the bed joints) started early in the test before $1\Delta_y$, followed by shear cracks (diagonal cracks) which propagated at $2\Delta_y$ (0.21% drift ratio) as shown in Figure C.2a. A major concentration of shear cracks at mid-height of the wall segment was noticed at $6\Delta_y$ (0.63% drift ratio), coinciding with yield of the horizontal reinforcement in the fifth course (Figure C.2b). Minor sliding at the base was observed at $8\Delta_y$ (0.83% drift ratio). Evidence of toe crushing was found first at the south end at $14\Delta_y$ (1.46% drift ratio) and then at the north end at $16\Delta_y$ (1.67% drift). Four vertical bars at the north end fractured: two at the first cycle to $16\Delta_y$ (1.67% drift ratio), one at the first cycle to $20\Delta_y$ (2.08% drift ratio), and one more at the second cycle to $20\Delta_y$ (2.08% drift ratio), when the test ended. There was no evidence of fracture of the vertical bars at the south end. The specimen at the end of the test is shown in Figure C.3 and Figure C.4.

(a) Cycle 2∆y *(b) Cycle 6∆y*

Figure C.2 Specimen UT-PBS-03, flexural and shear cracking

Figure C.3 Specimen UT-PBS-03 at end of test

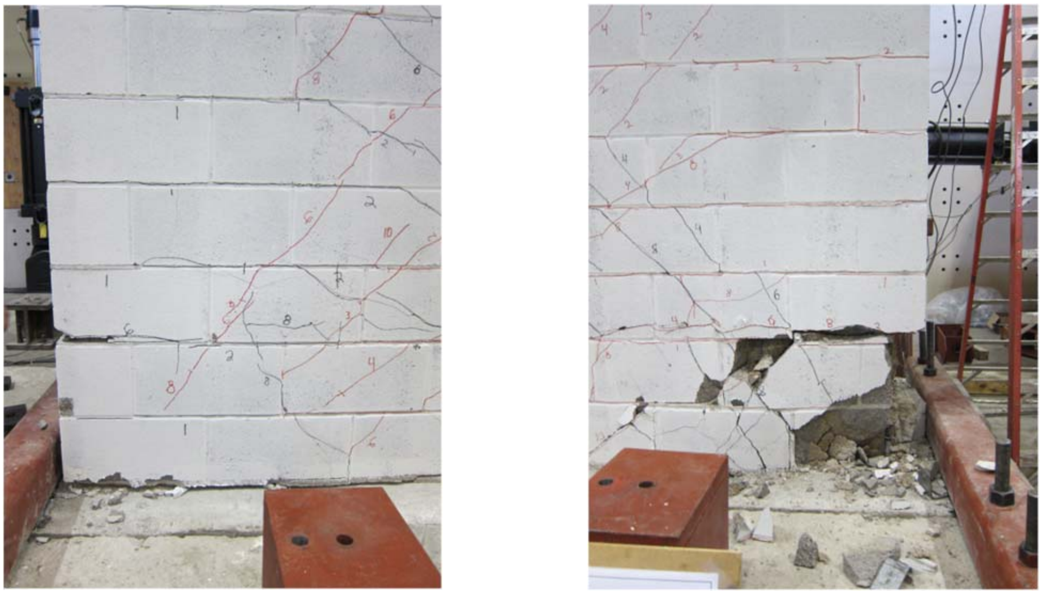

(a) North end *(b) South end*

Figure C.4 Toe crushing in Specimen UT-PBS-03

C.1.2 Load-Displacement Curve, Specimen UT-PBS-03

The load-displacement curve (hysteretic curve) for Specimen UT-PBS-03 is shown in Figure C.5. That plot and others like it in this appendix use the displacement sign convention originally reported by Hernandez (2012), which is opposite to that used consistently for all wall specimens in the body of this dissertation. The plot references five major events during testing: first yield of the extreme vertical reinforcement (ε_s=0.0021); maximum useful strain in the masonry (ε_{mu}=0.0025); maximum capacity of the specimen; onset of toe crushing; and 80% of the maximum capacity. First yield of the extreme bars was determined based on the average of the strains in the strain gauges located in the dowels at the base of the wall segment. The value of the maximum useful strain in the masonry was calculated using the displacement of the first two linear potentiometers of each side of the specimen (LP-1 and LP-2 for the north and LP-5 and LP-6 for the south). The displacements from LP-1 and LP-5 were divided by 8.375 in. and those from LP-2 and LP-6 by 8 in., to obtain the average strain at 4 and 12 in. above the base of the wall segment, respectively. The average strain at the base of the wall segment was obtained by extrapolating the average strains of the linear potentiometers mentioned above. The onset of toe crushing was determined visually during testing after each cycle, and the maximum capacity and the ultimate capacity (80% of the maximum capacity) were determined from the hysteretic curve.

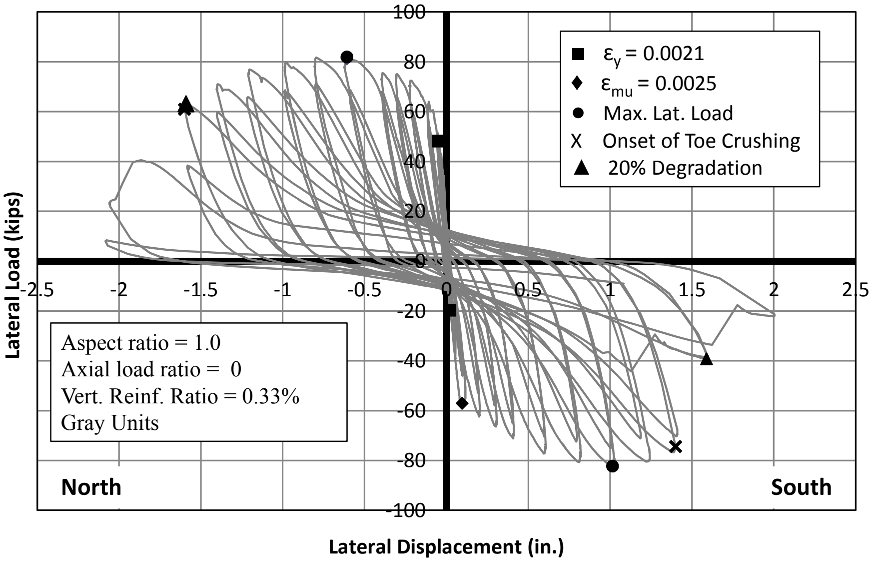

Figure C.5 Load-displacement curve for Specimen UT-PBS-03

The extreme vertical reinforcement in both ends yielded in the preliminary phase of the test. The maximum useful strain in the masonry at the south toe occurred before 1Δy (0.1% drift ratio); however, the maximum useful strain in the masonry at the north toe occurred at 6Δy (0.6% drift ratio). The maximum lateral load in the north direction was 81.85 kips at 6Δy (0.6% drift ratio) and 82.26 kips at 10Δy (1.0% drift ratio) in the south direction. Maximum useful strain and maximum load in the north direction occurred almost simultaneously. Toe crushing began in the south direction at 14Δy (1.4% drift ratio) and in the north direction at 16Δy (1.6% drift ratio). The ultimate capacity in both directions occurred at 16Δy (1.6% drift ratio) after the first bar fractured.

C.1.3 Displacement Components

The sliding deformation at the top and base of the wall segment was calculated directly from linear potentiometers attached to the specimen. The remaining deformation was considered as flexural deformation. The relative contributions of flexural, shearing, and sliding deformation at maximum load and at ultimate (80% of the maximum capacity) are summarized in Table C-1.

Table C-1 Relative flexural, shearing, and sliding deformation contributions for Specimen UT-PBS-03

Direction	**Maximum Load**			**80% of Maximum capacity**		
	Flexure	**Shear**	**Sliding**	**Flexure**	**Shear**	**Sliding**
North-Push	68%	15%	17%	51%	19%	30%
South- Pull	59%	11%	30%	69%	9%	22%

C.1.4 Backbone and Idealized Elasto-plastic Curve

The backbone curve for each direction (north-pushing and south-pulling) was calculated by connecting the points of maximum lateral force for each first cycle in the hysteresis curve. The principal elements of backbone and elasto-plastic curve for Specimen UT-PBS-03 are summarized in Table C-2.

Table C-2 Elasto-plastic and backbone curve main values for Specimen UT-PBS-03

Direction	Elasto-plastic curve					Backbone	
	Δ'_y (in.)	P'_y (kips)	Δ_y (in.)	P_y (kips)	Δ_u (in.)	Δ_{Pmax} (in.)	P_{max} (kips)
North-Push	0.0468	46.76	0.0761	76.00	1.4992	0.6071	81.85
South- Pull	0.0798	54.43	0.1107	75.50	1.4248	1.0052	82.10

The values of the maximum lateral load of the elasto-plastic and backbone curve were higher than the nominal capacity for Specimen UT-PBS-03 (60.11 kips) by factors of 1.26 and 1.36, respectively.

C.1.5 Displacement Ductility

Table C-3 shows the values of ultimate and yield displacement, and the corresponding displacement ductility for Specimen UT-PBS-03 in both directions.

Table C-3 Displacement ductility for Specimen UT-PBS-03

Direction	Δ_y (in.)	Δ_u (in.)	μ_Δ
North-Push	0.0761	1.4992	19.71
South- Pull	0.1107	1.4248	12.88
Average	**0.09336**	**1.4620**	**16.29**

C.1.6 Wall Segment Curvatures

Assuming plane sections, the curvature at each height was calculated as the sum of the average strains at both ends divided by the distance between their corresponding linear potentiometers. The curvature at the base was calculated by extrapolating the curvature values from the linear potentiometers at 4 and 12 in. from the base. The curvatures of the last cycles of the test were not calculated because the instrumentation detached as a result of the block spalling. Figure C.6 shows the curvature profile for Specimen UT-PBS-03 at different cycles.

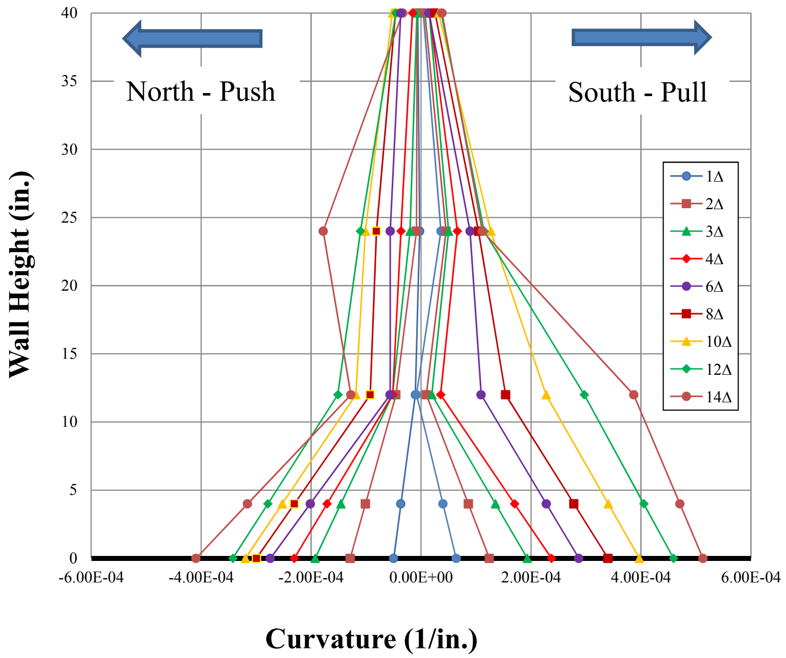

Figure C.6 Curvature profile for Specimen UT-PBS-03

C.1.7 Curvature Ductility

Table C-4 shows the values of ultimate and yield curvatures and the corresponding curvature ductility for Specimen UT-PBS-03 in both directions.

Table C-4 Curvature ductility for Specimen UT-PBS-03

Direction	ϕ_y ($x10^{-05}$ in.$^{-1}$)	ϕ_u ($x10^{-05}$ in.$^{-1}$)	μ_ϕ
North-Push	4.92	40.95	8.33
South- Pull	6.19	51.27	8.29
Average	**5.55**	**46.11**	**8.31**

C.1.8 Height of Plasticity and Plastic Hinge Length

The height of plasticity, L_p , was calculated at ultimate curvature (at 80% of the maximum capacity) or using data from the last cycle available from the instrumentation. Table C-5 shows the height of plasticity and its ratio with the total plan length of the wall segment for both directions of loading.

Table C-5 Height of plasticity for Specimen UT-PBS-03

Direction	**L_p (in.)**	**L_p/L_w**
North-Push	40.33	42%
South- Pull	38.63	40%
Average	**39.48**	**41%**

Table C-6 shows the plastic hinge length and its portion of the total plan length of the wall segment for Specimen UT-PBS-03 in both directions of loading.

Table C-6 Plastic hinge length for Specimen UT-PBS-03

Direction	**l_p (in.)**	**l_p/L_w**
North-Push	48.22	50%
South- Pull	33.93	35%
Average	**41.07**	**43%**

C.1.9 Energy Dissipation and Equivalent Hysteretic Damping

Energy dissipation and equivalent hysteretic damping were calculated for the hysteretic loops whose drifts were close or equal to 0.6% and 1.5%. The energy dissipation, $E_{D\Delta t}$, was calculated as the area of the hysteretic loop using the trapezoidal rule. The equivalent hysteretic damping, ξ_{eq} , was determined as proposed by Clough and Penzien (2003), where the nominal damping ratio, ξ_o , was taken as 0.05 as recommended by Priestley (2007).

$$\xi_{eq} = \frac{E_{D\Delta t}}{2\pi\, k_{eq}\, \Delta_t^2} + \xi_o$$

Figure C.7 shows the hysteretic loops of 0.65% and 1.46% drift ratios for Specimen UT-PBS-03, and Table C-7 presents the value of energy dissipation and equivalent hysteretic damping for both curves.

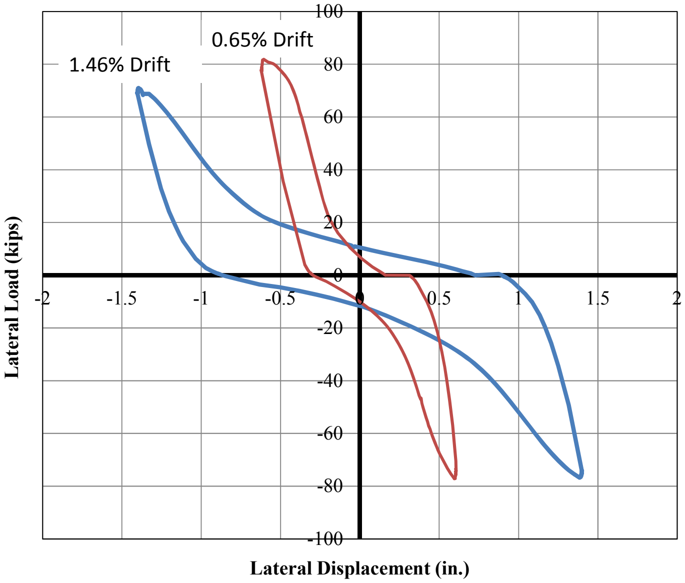

Figure C.7 Hysteretic loops at 0.65% and 1.46% drift ratios for Specimen UT-PBS-03

Table C-7 Energy dissipation and equivalent hysteretic damping for UT-PBS-03 wall

Drift Ratio	Drift	$E_{D\Delta t}$ (kip-in)	ξ_{eq}
0.60%	0.65%	37.15	17.3%
1.50%	1.46%	84.44	18.9%

C.2 SPECIMEN UT-PBS-04

Specimen UT-PBS-04 was 96-in. wide and 96-in. high (aspect ratio equal to 1.0) with #4 bars every 16 in. vertically and horizontally and an axial load equal to zero. The dowels were extended 16 in. (two courses) from the base of the wall. The expected moment capacity of Specimen UT-PBS-04 was 275 ft-kips, equivalent to a lateral load of 31.43 kips as shown in Section 3.2. Specimen UT-PBS-04 before testing is shown in Figure C.8.

Figure C.8 Specimen UT-PBS-04 before testing

C.2.1 Test Observations, Specimen UT-PBS-04

The value of Δ_y calculated in the preliminary test was equal to 0.28 in., equivalent to a drift ratio of 0.29%. Asymmetrical flexural and shear cracking started at $2\Delta_y$ (0.54% drift ratio) as shown in Figure C.9. The asymmetry could have been produced by slip of the extreme vertical bar at the south end. At $3\Delta_y$ (0.81% drift ratio), widening of the 2nd bed joint from the base (extension of dowels) and sliding at the base were observed. Toe crushing at the north end was identified at $4\Delta_y$ (1.08% drift ratio). Spalling at ends, buckling and fracture occurred during the two cycles to $6\Delta_y$ (1.61% drift ratio), as shown in Figure C.10. The test was ended at $10\Delta_y$ (2.69% drift ratio) when the lateral capacity was 80% of the maximum capacity. Specimen UT-PBS-04 at the end of the test is shown in Figure C.11.

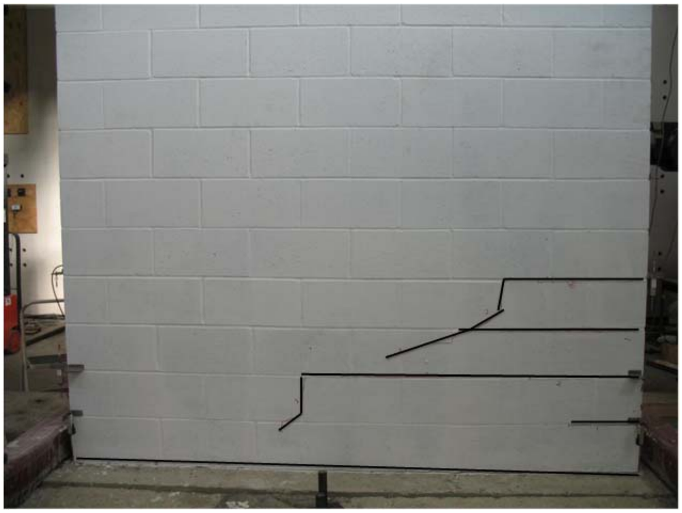

Figure C.9 Specimen UT-PBS-04 at 2Δy

(a) Spalling at north end

(b) Spalling at south end

(c) Fracture at north end

(d) Fracture at south end

Figure C.10 Specimen UT-PBS-04 at 6Δy

Figure C.11 Specimen UT-PBS-04 at end of test

C.2.2 Load-Displacement Curve, Specimen UT-PBS-04

The load-displacement curve (hysteretic curve) for Specimen UT-PBS-04 is shown in Figure C.12.

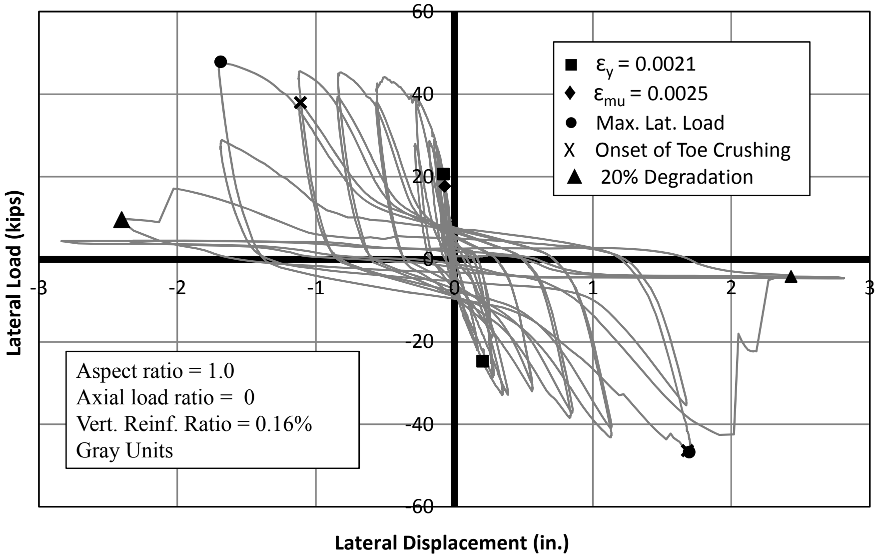

Figure C.12 Load-displacement curve for Specimen UT-PBS-04

The maximum useful strain in the masonry at the north end occurred before the yielding of the extreme bar at the south end, in the preliminary phase of the test. The extreme bar at the north end also yielded during the preliminary phase of the test. The maximum lateral load in both directions, 47.85 kips (pushing to the north) and 46.77 kips (pulling to the south), occurred at $6\Delta_y$ (1.61% drift ratio). The lateral capacity in both directions dropped suddenly to much lower values than 80% of the maximum capacity at the cycle of $8\Delta_y$ (2.15% drift ratio), at which point the test was ended.

C.2.3 Displacement Components

The relative contributions of flexural, shearing, and sliding deformation at maximum load and at ultimate load (80% of the maximum capacity) for Specimen UT-PBS-04 are summarized in Table C-8.

Table C-8 Relative flexural, shearing, and sliding deformation contributions for Specimen UT-PBS-04

Direction	Maximum Load			80% of Maximum capacity		
	Flexure	Shear	Sliding	Flexure	Shear	Sliding
North-Push	55%	15%	30%	68%	4%	28%
South- Pull	52%	6%	42%	63%	4%	33%

C.2.4 Backbone and Idealized Elasto-Plastic Curve

The principal elements of backbone and elasto-plastic curve for Specimen UT-PBS-04 are summarized in Table C-9.

Table C-9 Elasto-plastic and backbone curve for Specimen UT-PBS-04

Direction	Elasto-plastic curve					Backbone	
	Δ'_y (in.)	P'_y (kips)	Δ_y (in.)	P_y (kips)	Δ_u (in.)	Δ_{Pmax} (in.)	P_{max} (kips)
North-Push	0.0787	20.62	0.1661	43.50	1.8651	1.6868	47.85
South- Pull	0.2098	25.14	0.3338	40.00	1.8474	1.6825	46.38

The values of the maximum lateral load of the elasto-plastic and backbone curve were higher than the nominal capacity for Specimen UT-PBS-04 (31.43 kips) by factors of 1.32 and 1.50, respectively.

C.2.5 Displacement Ductility

The displacement ductility for Specimen UT-PBS-04 was calculated from the elasto-plastic curve of each direction. Table C-10 presents the values for both directions and their corresponding averages.

Table C-10 Displacement ductility for Specimen UT-PBS-04

Direction	Δ_y (in.)	Δ_u (in.)	μ_Δ
North-Push	0.1661	1.8651	11.23
South- Pull	0.3338	1.8474	5.53
Average	**0.24998**	**1.8563**	**8.38**

C.2.6 Wall Segment Curvatures

The curvatures along the height of the Specimen UT-PBS-04 could not be calculated because of the problems in two linear potentiometers (LP-4 and LP-6). Several unsuccessful attempts were made to estimate what would have been the data from those instruments. Because of the missing data, it was not possible to compute curvature ductility, height of plasticity, or plastic hinge length for this specimen.

C.2.7 Energy Dissipation and Equivalent Hysteretic Damping

Energy dissipation, $E_{D\Delta t}$, and equivalent hysteretic damping, ξ_{eq}, for Specimen UT-PBS-04 were calculated for the hysteretic loops of 0.59% and 1.77% drift ratios, as shown in Figure C.13. Table C-11 presents the value of energy dissipation and equivalent hysteretic damping for both curves.

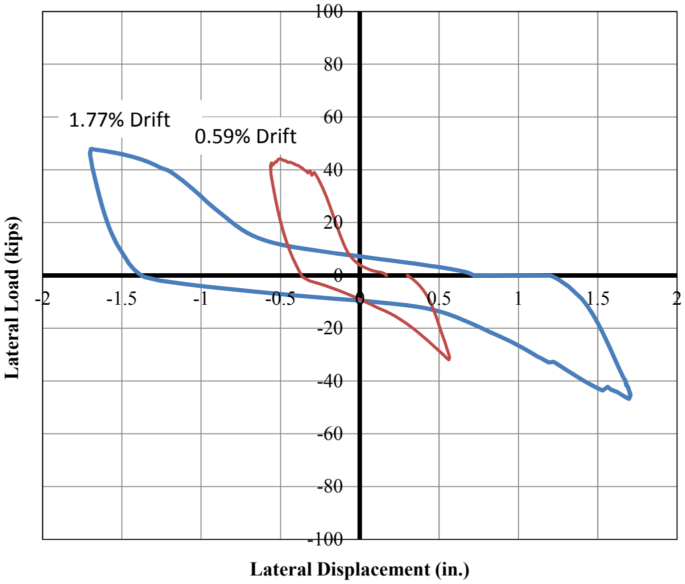

Figure C.13 Hysteretic loops at 0.59% and 1.77% drift ratios for Specimen UT-PBS-04

Table C-11 Energy dissipation and equivalent hysteretic damping for Specimen UT-PBS-04

Drift Ratio	Drift	$E_{D\Delta t}$ (kip-in)	ξ_{eq}
0.60%	**0.59%**	23.86	21.5%
1.50%	**1.77%**	82.40	21.8%

C.3 SPECIMEN UT-PBS-04G

Specimen UT-PBS-04G was 96-in. wide and 96-in. high (aspect ratio equal to 1.0) with No. 4 bars every 16 in. vertically and horizontally and an axial load equal to zero. The dowels were extended 16 in. (two courses) from the base of the wall. The expected moment capacity of Specimen UT-PBS-04G was 275 ft-kips, equivalent to a lateral load of 31.43 kips as shown in Section 3.2. Specimen UT-PBS-04G before testing is shown in Figure C.14.

Figure C.14 Specimen UT-PBS-04G before testing

C.3.1 Test Observations, Specimen UT-PBS-04G

The value of Δ_y calculated in the preliminary test was equal to 0.29 in., equivalent to a drift ratio of 0.30%. A few flexural cracks (horizontal cracks) were observed at $1\Delta_y$ (0.30% drift ratio), followed rapidly for shear cracks (diagonal cracks) at $2\Delta_y$ (0.60% drift ratio). At $3\Delta_y$ (0.91% drift ratio), flexural and shear cracks concentrated at four courses from the base and started to widen. During the next cycle, to $4\Delta_y$ (1.21% drift ratio), a 0.40-in. gap was measured at the base of the wall segment. Several new flexural and shear cracks appeared at higher courses, and toe crushing was observed at both ends of the wall at $6\Delta_y$ (1.81% drift ratio). A large gap opened at the north side along the 2nd bed joint from the bottom (Figure C.15a), suggesting that splices slipped at $8\Delta_y$ (2.42% drift ratio). Similarly, a large gap opened at the south side at the base of the wall segment, suggesting fracture in the vertical reinforcement as shown in Figure C.15b. After this point, the specimen degraded by fracture of the longitudinal bars and crushing of the toes. The test was ended when the lateral capacity dropped to 20% of the maximum capacity at the first cycle to 12Δ_y (3.63% drift ratio). Figure C.16 and Figure C.17 show Specimen UT-PBS-04G at the end of the test.

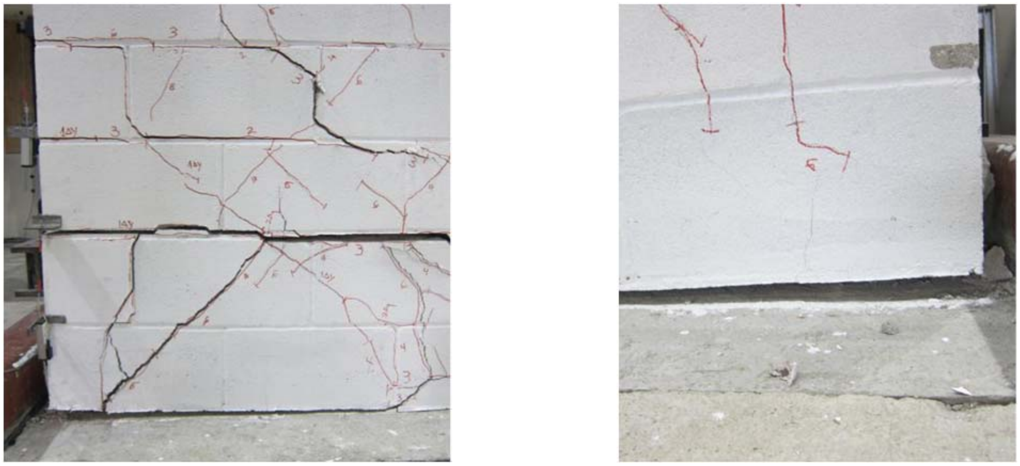

(a) North end ***(b) South end***

Figure C.15 Specimen UT-PBS-04G at 8Δy

Figure C.16 Specimen UT-PBS-04G at end of test

(a) North end ***(b) South end***

Figure C.17 Toes of Specimen UT-PBS-04G at end of test

C.3.2 Load-Displacement Curve, Specimen UT-PBS-04G

A load-displacement curve (hysteretic curve) was obtained from the test of Specimen UT-PBS-04G, as shown in Figure C.18.

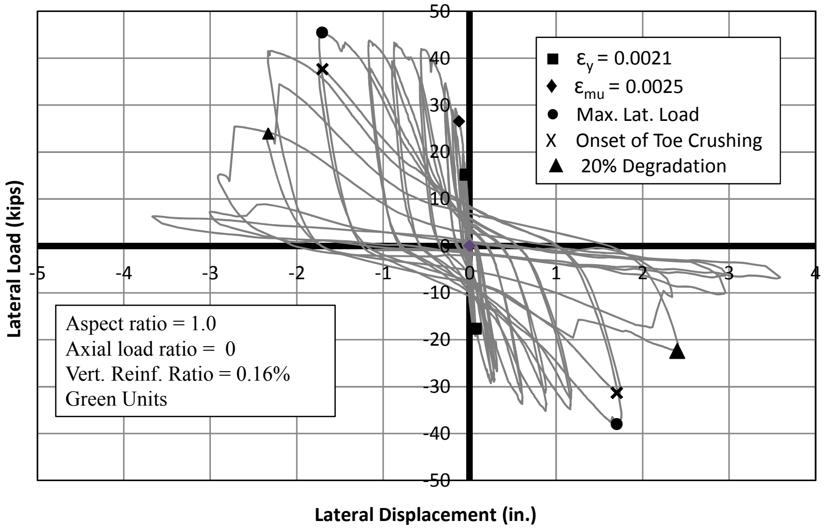

Figure C.18 Load-displacement curve for Specimen UT-PBS-04G

In the preliminary phase of the test, the extreme vertical reinforcement yielded at both ends and the masonry reached its maximum useful strain at the north end. The maximum lateral load occurred at $6\Delta_y$ (1.70% drift ratio): 45.47 kips in the north direction and 38.00 kips in the south direction. Toe crushing was observed at the second cycle in both directions at $6\Delta_y$ (1.70% drift ratio).The ultimate capacity (80% of the maximum capacity) occurred at the first cycle in the south direction to $8\Delta_y$ (2.32% drift ratio) and at the second cycle in the north direction to $8\Delta_y$ (2.32% drift ratio).

C.3.3 Displacement Components

The relative contributions of flexural, shearing, and sliding deformation at maximum load and at ultimate (80% of the maximum capacity) for Specimen UT-PBS-04G are summarized in Table C-12. Values at 80% of the maximum capacity could not be calculated for the north-pushing direction because of the above-mentioned problems with instrumentation at the last stages of the test.

Table C-12 Relative flexural, shearing, and sliding deformation contributions for Specimen UT-PBS-04G

Direction	**Maximum Load**			**80% of Maximum capacity**		
	Flexure	**Shear**	**Sliding**	**Flexure**	**Shear**	**Sliding**
North-Push	58%	22%	19%	-	-	-
South- Pull	50%	22%	27%	57%	20%	23%

C.3.4 Backbone and Idealized Elasto-plastic Curve

The principal elements of backbone and elasto-plastic curve for Specimen UT-PBS-04G are summarized in Table C-13.

Table C-13 Elasto-plastic and backbone curve for Specimen UT-PBS-04G

Direction	**Elasto-plastic curve**					**Backbone**	
	Δ'_y (in.)	**P'_y (kips)**	**Δ_y (in.)**	**P_y (kips)**	**Δ_u (in.)**	**Δ_{Pmax} (in.)**	**P_{max} (kips)**
North-Push	0.0460	15.15	0.1259	41.50	2.4311	1.7061	45.47
South- Pull	0.0720	17.68	0.1384	34.00	2.0425	1.7012	38.00

The average values of the maximum lateral load of the elasto-plastic and backbone curve were higher than the nominal capacity for Specimen UT-PBS-04G (31.43 kips) by 20% and 33%, respectively.

C.3.5 Displacement Ductility

The displacement ductility for Specimen UT-PBS-04G was calculated from the elasto-plastic curve of each direction. Table C-14 presents the values for both directions and their average.

Table C-14 Displacement ductility for Specimen UT-PBS-04G

Direction	**Δ_y (in.)**	**Δ_u (in.)**	**μ_Δ**
North-Push	0.1259	2.4311	19.31
South- Pull	0.1384	2.0425	14.76
Average	**0.13214**	**2.2368**	**17.04**

C.3.6 Wall Segment Curvatures

The curvatures along the height of the Specimen UT-PBS-04G were calculated for different cycles, as shown in

Figure C.19. The curvatures after the first cycle to 8 Δy are not presented because the instrumentation detached as a consequence of masonry spalling.

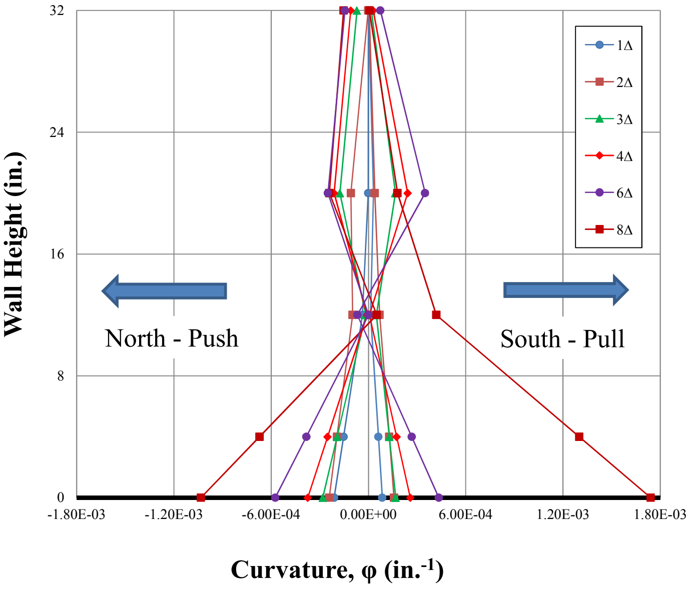

Figure C.19 Curvature profile for Specimen UT-PBS-04G

C.3.7 Curvature Ductility

Curvature ductility for Specimen UT-PBS-04G was calculated as the ratio of ultimate curvature and yield curvature. Table C-15 shows the value of yield curvature, ultimate curvature, and curvature ductility for both directions.

Table C-15 Curvature ductility for Specimen UT-PBS-04G

Direction	**ϕ_y (x10^{-05} in.$^{-1}$)**	**ϕ_u (x10^{-05} in.$^{-1}$)**	**μ_ϕ**
North-Push	8.77	103.34	11.78
South- Pull	6.92	174.08	25.15
Average	**7.85**	**138.71**	**18.47**

C.3.8 Height of Plasticity and Plastic Hinge Length

The height of plasticity, L_p, was calculated at ultimate curvature (80% of the maximum capacity) or using data from the last cycle available from the instrumentation. Table C-16 shows the height of plasticity and its portion of the total plan length of the wall segment for both directions of loading.

Table C-16 Height of plasticity for Specimen UT-PBS-04G

Direction	**L_p (in.)**	**L_p/L_w**
North-Push	48.55	51%
South- Pull	29.94	31%
Average	**39.25**	**41%**

Table C-17 shows the plastic hinge length and its portion of the total plan length of the wall segment for both directions of loading.

Table C-17 Plastic hinge length for Specimen UT-PBS-04G

Direction	**l_p (in.)**	**l_p/L_w**
North-Push	26.24	27%
South- Pull	14.81	15%
Average	**20.52**	**21%**

C.3.9 Energy Dissipation and Equivalent Hysteretic Damping

Energy dissipation, $E_{D\Delta t}$, and equivalent hysteretic damping, ξ_{eq}, of Specimen UT-PBS-04G were calculated for the hysteretic loops of 0.59% and 1.81% drift ratios, as shown in Figure C.20 and Table C-18 presents the value of energy dissipation and equivalent hysteretic damping for both curves.

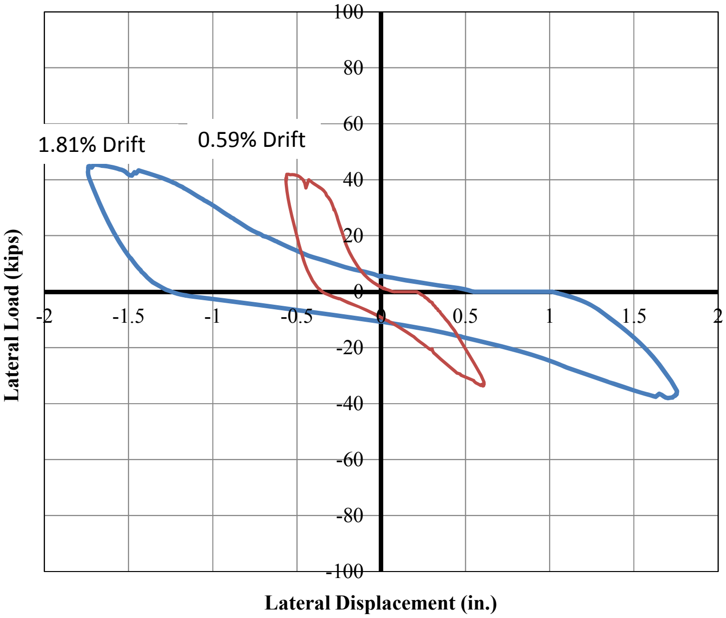

Figure C.20 Hysteretic loops at 0.59% and 1.81% drift ratios for Specimen UT-PBS-04G

Table C-18 Energy dissipation and equivalent hysteretic damping for Specimen UT-PBS-04G

Drift Ratio	Drift	$E_{D\Delta t}$ (kip-in)	ξ_{eq}
0.60%	0.59%	20.68	19.6%
1.50%	1.81%	78.71	21.8%

C.4 SPECIMEN UT-PBS-11

Specimen UT-PBS-11 was 96-in. wide and 96-in. high (aspect ratio equal to 1.0) with No. 4 bars every 8 in. vertically and horizontally and axial load ratio, $P\ /\ (f_m{}'A_g)$, equal to 0.10. The dowels were extended 16 in. (two courses) from the base of the wall segment. The expected moment capacity of Specimen UT-PBS-11 was 1049 ft-kips, equivalent to a lateral load of 119.89 kips as shown in Section 3.2. Specimen UT-PBS-11 before the test is shown in Figure C.21.

Figure C.21 Specimen UT-PBS-11 before testing

C.4.1 Test Observations, Specimen UT-PBS-11

The value of Δ_y calculated in the preliminary phase of the test was equal to 0.12 in., equivalent to a drift ratio of 0.125%, and no cracks were observed. Minor flexural and shear cracks were present at $2\Delta_y$ (0.25% drift ratio); a major flexural crack at the base of the wall segment was observed at the south end (Figure C.22a), along with crushing at the north end. At $4\Delta y$ (0.50% drift ratio) flexural cracks reached the ninth course from the base and shear cracks extended from that point to the north toe; toe crushing at the south end was identified (Figure C.22b), and the crack at the base widened. From this point, significant shear degradation and spalling at toes were observed; the spalling showed that several vertical bars buckled (Figure C.23) at the second cycle to $8\Delta_y$ (1.00% drift ratio). Crushing extended two courses high which permitted vertical bars to slide at $12\Delta_y$ (1.50% drift ratio). The test was ended when the lateral capacity dropped to 20% of the maximum capacity at the first cycles of $16\Delta_y$ (2.00% drift ratio). The specimen at the end of the test is shown in Figure C.24 and Figure C.25.

(a) North end ($2\Delta_y$) ***(b) South end ($4\Delta_y$)***

Figure C.22 Toe crushing in Specimen UT-PBS-11

Figure C.23 Buckling of longitudinal bars at south end of Specimen UT-PBS-11 ($8\Delta y$)

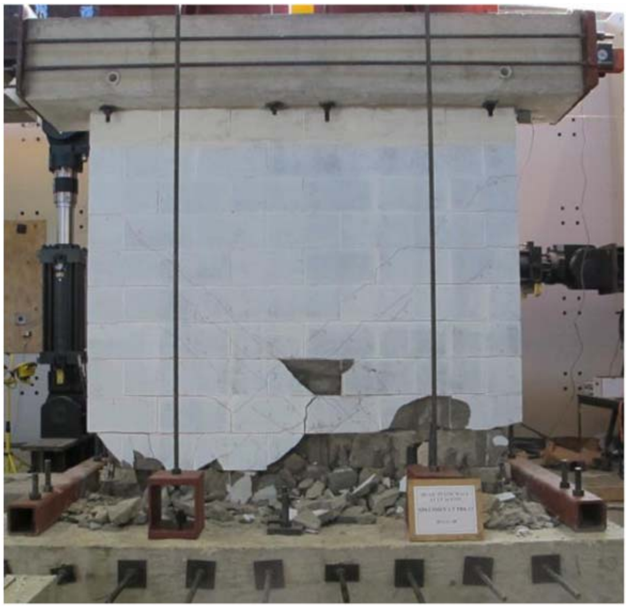

Figure C.24 Specimen UT-PBS-11 at end of test

(a) North end *(b) South end*

Figure C.25 Toes of Specimen UT-PBS-11 at end of test

C.4.2 Load-Displacement Curve, Specimen UT-PBS-11

The load-displacement curve (hysteretic curve) of Specimen UT-PBS-11 is shown in Figure C.26.

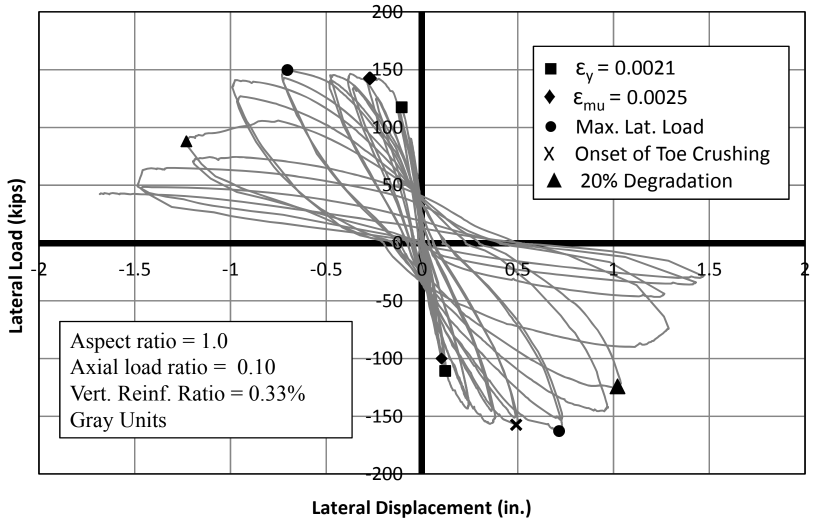

Figure C.26 Load-displacement curve for Specimen UT-PBS-11

The extreme vertical reinforcement at the south end yielded in the preliminary phase of the test while the one at the north end yielded at $1\Delta_y$ (0.125% drift ratio). The maximum useful strain in the masonry at the south toe occurred before $1\Delta_y$ (0.125% drift ratio); the maximum useful strain in the masonry at the north toe occurred at $2\Delta_y$ (0.25% drift ratio). Crushing was observed in the north toe at $2\Delta_y$ (0.25% drift ratio) and in the south toe at $4\Delta_y$ (0.50% drift ratio). The maximum lateral load in both directions occurred at $6\Delta_y$ (0.75% drift ratio): 142.46 kips in the north direction and 157.26 kips in the south direction. The ultimate capacity (80% of the maximum capacity) occurred at the first cycle in the south direction to $8\Delta_y$ (1.00% drift ratio) and at the second cycle in the north direction to $10\Delta_y$ (1.25% drift ratio).

C.4.3 Displacement Components

The relative contributions of flexural, shearing, and sliding deformation at maximum load and at ultimate (80% of the maximum capacity) for Specimen UT-PBS-11 were not included because the data of the string potentiometers showed inconsistencies.

C.4.4 Backbone and idealized elasto-plastic curve

The principal elements of backbone and elasto-plastic curve for Specimen UT-PBS-11 are summarized in Table C-19.

Table C-19 Elasto-plastic and backbone curve for Specimen UT-PBS-11

Direction	**Elasto-plastic curve**					**Backbone**	
	Δ'_y (in.)	**P'_y (kips)**	**Δ_y (in.)**	**P_y (kips)**	**Δ_u (in.)**	**Δ_{Pmax} (in.)**	**P_{max} (kips)**
North-Push	0.1052	117.30	0.1283	143.00	1.0272	0.7280	146.95
South- Pull	0.1222	110.82	0.1643	149.00	1.0836	0.7324	159.60

The values of the maximum lateral load of the elasto-plastic and backbone curve were higher than the nominal capacity for Specimen UT-PBS-11 (119.89 kips) by 21% and 28%, respectively.

C.4.5 Displacement Ductility

The displacement ductility for Specimen UT-PBS-11 was calculated from the elasto-plastic curve of each direction. Table C-20 presents the values for both directions and their average.

Table C-20 Displacement ductility for Specimen UT-PBS-11

Direction	Δ_y (in.)	Δ_u (in.)	μ_Δ
North-Push	0.1283	1.0272	8.01
South- Pull	0.1643	1.0836	6.59
Average	**0.1463**	**1.0554**	**7.30**

C.4.6 Wall Segment Curvatures

The curvatures along the height of the Specimen UT-PBS-11 were calculated for different cycles, as shown in Figure C.27. The curvatures after the first cycle to 8 Δy are not presented because the instrumentation detached as a consequence of masonry spalling.

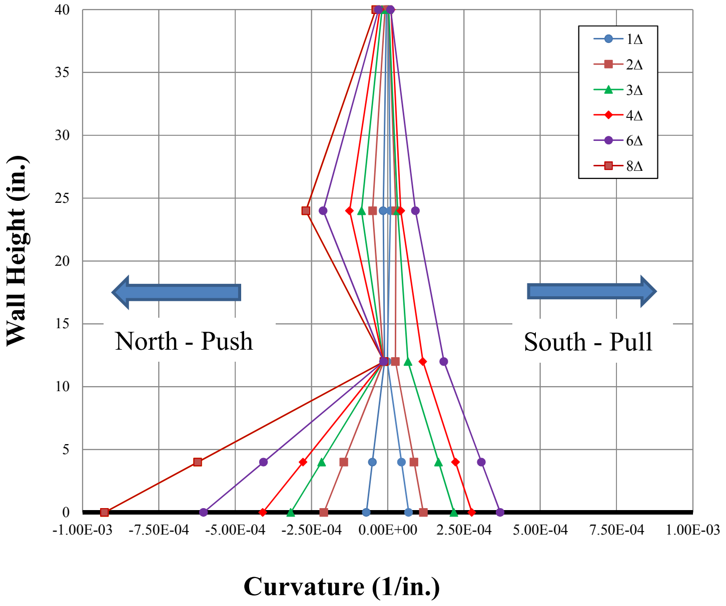

Figure C.27 Curvature profile for Specimen UT-PBS-11

C.4.7 Curvature Ductility

Curvature ductility for Specimen UT-PBS-11 was calculated as the ratio of ultimate curvature and yield curvature. Table C-21 shows the value of yield curvature, ultimate curvature, and curvature ductility for both directions.

Table C-21 Curvature ductility for Specimen UT-PBS-11

Direction	ϕ_y (x10^{-05} in.$^{-1}$)	ϕ_u (x10^{-05} in.$^{-1}$)	μ_ϕ
North-Push	7.36	36.87	5.01
South- Pull	9.61	92.80	9.66
Average	**8.48**	**64.84**	**7.33**

C.4.8 Height of Plasticity and Plastic Hinge Length

The height of plasticity, L_p, was calculated at ultimate curvature, 80% of the maximum capacity or using data from the last cycle available from the instrumentation. Table C-22 shows the height of plasticity and its portion of the total plan length of the wall segment for both directions of loading.

Table C-22 Height of plasticity for Specimen UT-PBS-11

Direction	L_p (in.)	L_p/L_w
North-Push	29.96	31%
South- Pull	37.72	39%
Average	**33.84**	**35%**

Table C-23 shows the plastic hinge length and its portion of the total plan length of the wall segment for both directions of loading.

Table C-23 Plastic hinge length for Specimen UT-PBS-11

Direction	**l_p (in.)**	**l_p/L_w**
North-Push	32.35	34%
South- Pull	5.64	6%
Average	**19.00**	**20%**

C.4.9 Energy Dissipation and Equivalent Hysteretic Damping

Energy dissipation, $E_{D\Delta t}$, and equivalent hysteretic damping, ξ_{eq} , for Specimen UT-PBS-11 were calculated for the hysteretic loop of 0.73% and 1.73% drift ratios, as shown in Figure C.28. Table C-24 presents the value of energy dissipation and equivalent hysteretic damping for both curves. It can be seen that the energy dissipated at 1.73% drift was smaller than the one at 0.73%, which resulted in a lower equivalent hysteretic damping at the end of the test.

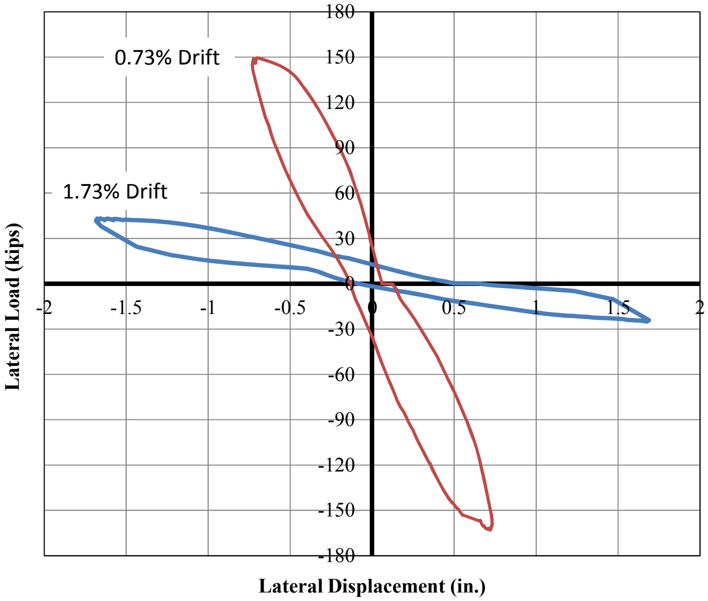

Figure C.28 Hysteretic loops at 0.73% and 1.73% drift ratios for Specimen UT-PBS-11

Table C-24 Energy dissipation and equivalent hysteretic damping for Specimen UT-PBS-11

Drift Ratio	Drift	$E_{D\Delta t}$ (kip-in)	ξ_{eq}
0.60%	**0.76%**	95.50	19.4%
1.50%	**1.75%**	50.14	16.4%

C.5 SPECIMEN UT-PBS-12

Specimen UT-PBS-12 was 96-in. wide and 96-in. high (aspect ratio equal to 1.0) with #4 bars every 16 in. vertically and horizontally and axial load ratio, P / ($f_m' A_g$), equal to 0.10. The dowels extended 16 in. (two courses) from the base of the wall segment. The expected moment capacity of Specimen UT-PBS-12 was 858 ft-kips, equivalent to a lateral load of 98.06 kips. Specimen UT-PBS-12 before the test is shown in Figure C.29.

Figure C.29 Specimen UT-PBS-12 before testing

C.5.1 Test Observations, Specimen UT-PBS-12

The value of Δ_y calculated in the preliminary phase of the test was 0.13 in., equivalent to a drift ratio of 0.14%; no cracks were observed at this stage. Early in the test, $1\Delta_y$ (0.14% drift ratio), a diagonal crack at the north toe (Figure C.30a) and a major crack at the base in the south end (Figure C.30b) were observed. Damage was concentrated at those points in the next cycles and flexural and shear cracking were slight elsewhere. Crushing was observed in the south toe at $4\Delta_y$ (0.54% drift ratio) and in the north toe at $6\Delta_y$ (0.81% drift ratio). At $8\Delta_y$ (1.08% drift ratio), spalling at the south toe suggested bar buckling; in addition, a wide crack at the north end indicated a possible sliding of the dowel. After this point, the degradation of the wall segment was based on crushing of the toes and sliding of the vertical bars, as shown in Figure C.31. The test was ended when the lateral capacity dropped to 20% of the maximum capacity at the first cycle to $20\Delta_y$ (2.71% drift ratio). The specimen at the end of the test is shown in Figure C.32 and Figure C.33.

(a) North end ***(b) South end***

Figure C.30 Specimen UT-PBS-12 at 1Δy

Figure C.31 Specimen UT-PBS-12 at 10∆y

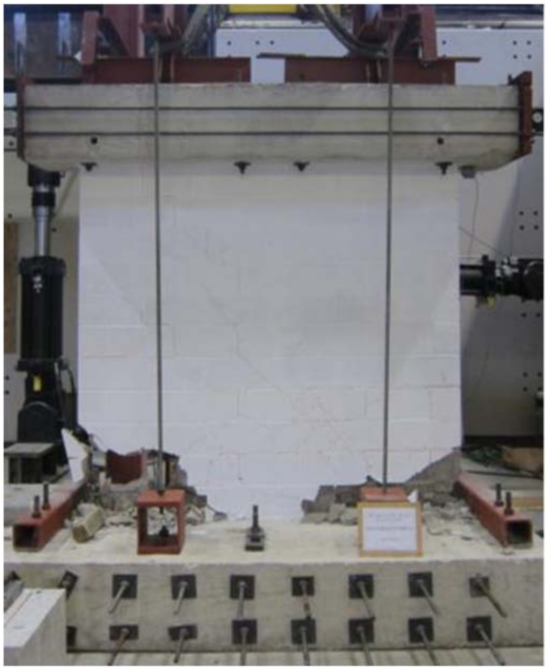

Figure C.32 Specimen UT-PBS-12 at end of test

(a) North end *(b) South end*

Figure C.33 Toes of Specimen UT-PBS-12 at end of test

C.5.2 Load-Displacement Curve, Specimen UT-PBS-12

The load-displacement curve (hysteretic curve) of Specimen UT-PBS-12 is shown in Figure C.34.

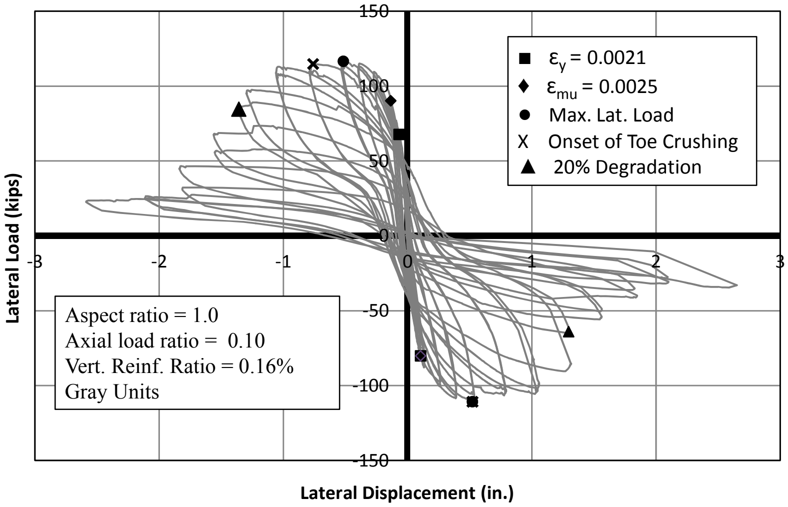

Figure C.34 Load-displacement curve for Specimen UT-PBS-12

In the preliminary phase of the test, the extreme vertical bars yielded at both ends at $1\Delta_y$ (0.14% drift ratio). The maximum useful strain in the masonry toe in both directions was found at $1\Delta_y$ (0.14% drift ratio); for loading to the south, yielding in extreme bars and maximum useful strain in masonry occurred simultaneously. The maximum lateral load occurred at $4\Delta_y$ (0.54% drift ratio) for both directions: 116.53 kips in the north direction and 110.85 kips in the south direction. Crushing was observed first in the south toe at $4\Delta_y$ (0.54% drift ratio), and then in the north toe at $6\Delta_y$ (0.81% drift ratio). The ultimate capacity (80% of the maximum capacity) occurred at $12\Delta_y$ (1.63% drift ratio) in both directions.

C.5.3 Displacement Components

The relative contributions of flexural, shearing, and sliding deformation at maximum load and at ultimate (80% of the maximum capacity) for Specimen UT-PBS-12 are summarized in Table C-25. Values at ultimate could not be calculated for the south-pulling direction because of problems in instrumentation at the last stages of the test.

Table C-25 Relative flexural, shearing, and sliding deformation contributions for Specimen UT-PBS-12

Direction	**Maximum Load**			**80% of Maximum capacity**		
	Flexure	**Shear**	**Sliding**	**Flexure**	**Shear**	**Sliding**
North-Push	73%	15%	12%	77%	13%	10%
South- Pull	89%	10%	2%	-	-	-

C.5.4 Backbone and Idealized Elasto-plastic Curve

The principal elements of backbone and elasto-plastic curve for Specimen UT-PBS-12 are summarized in Table C-26.

Table C-26 Elasto-plastic and backbone curve for Specimen UT-PBS-12

Direction	Elasto-plastic curve					Backbone	
	Δ'_y (in.)	P'_y (kips)	Δ_y (in.)	P_y (kips)	Δ_u (in.)	Δ_{Pmax} (in.)	P_{max} (kips)
North-Push	0.0620	66.10	0.1031	110.00	1.3143	0.5152	116.53
South- Pull	0.1050	80.24	0.1348	103.00	1.2655	0.5226	110.85

The values of the maximum lateral load of the elasto-plastic and backbone curve were higher than the nominal capacity for Specimen UT-PBS-12 (98.06 kips) by 9% and 16%, respectively.

C.5.5 Displacement Ductility

The displacement ductility for Specimen UT-PBS-12 was calculated from the elasto-plastic curve of each direction. Table C-27 presents the values for both directions and their average.

Table C-27 Displacement ductility for Specimen UT-PBS-12

Direction	Δ_y (in.)	Δ_u (in.)	μ_Δ
North-Push	0.1031	1.3143	12.75
South- Pull	0.1348	1.2655	9.39
Average	**0.11896**	**1.2899**	**11.07**

C.5.6 Wall Segment Curvatures

The curvatures along the height of the Specimen UT-PBS-12 were calculated for different cycles, as shown in Figure C.35. The curvatures after the cycle of 8 Δy are not presented because the instrumentation detached as a consequence of masonry spalling.

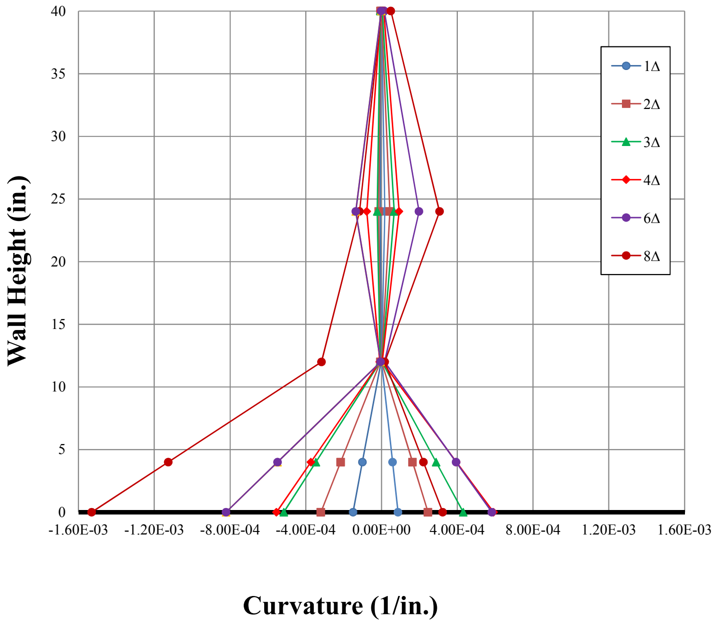

Figure C.35 Curvature profile for Specimen UT-PBS-12

C.5.7 Curvature Ductility

Curvature ductility for Specimen UT-PBS-12 was calculated as the ratio of ultimate curvature and yield curvature. Table C-28 shows the value of yield curvature, ultimate curvature, and curvature ductility for both directions.

Table C-28 Curvature ductility for Specimen UT-PBS-12

Direction	ϕ_y ($x10^{-05}$ in.$^{-1}$)	ϕ_u ($x10^{-05}$ in.$^{-1}$)	μ_ϕ
North-Push	8.56	153.10	17.89
South- Pull	6.45	32.28	5.00
Average	**7.50**	**92.69**	**11.45**

C.5.8 Height of Plasticity and Plastic Hinge Length

The height of plasticity, L_p, was calculated at ultimate (80% of the maximum capacity) or using data from the last cycle available from the instrumentation. Table C-29 shows the height of plasticity and its portion of the total plan length of the wall segment for both directions of loading.

Table C-29 Height of plasticity for Specimen UT-PBS-12

Direction	L_p (in.)	L_p/L_w
North-Push	45.75	48%
South- Pull	47.00	49%
Average	**46.38**	**48%**

Table C-30 shows the plastic hinge length and its portion of the total plan length of the wall segment for both directions of loading.

Table C-30 Plastic hinge length for Specimen UT-PBS-12

Direction	l_p (in.)	l_p/L_w
North-Push	5.89	6%
South- Pull	44.24	46%
Average	**25.06**	**26%**

C.5.9 Energy Dissipation and Equivalent Hysteretic Damping

Energy dissipation, $E_{D\Delta t}$, and equivalent hysteretic damping, ξ_{eq} , were calculated for the hysteretic loops whose drifts were close or equal to 0.6 and 1.5%. Figure C.36 shows the hysteretic loops of 0.55% and 1.63% drift ratios for Specimen UT-PBS-12, and Table C-31 presents the value of energy dissipation and equivalent hysteretic damping for both curves.

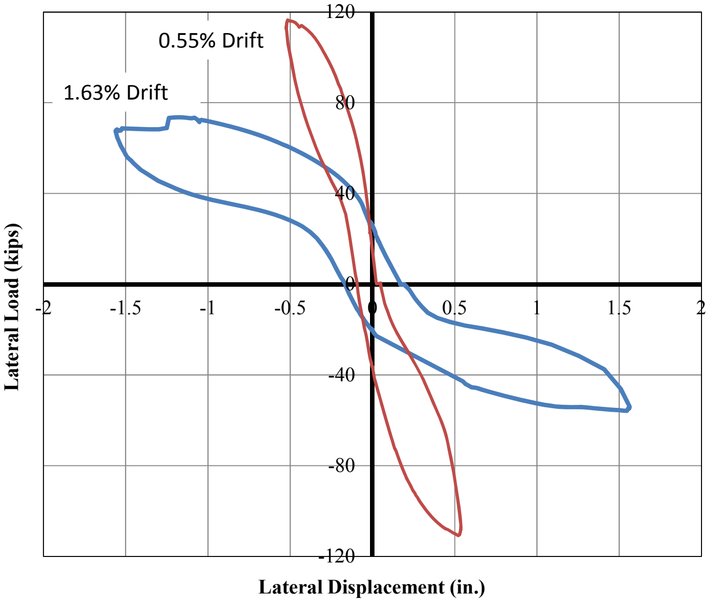

Figure C.36 Hysteretic loops at 0.55% and 1.63% drift ratios for Specimen UT-PBS-12

Table C-31 Energy dissipation and equivalent hysteretic damping for Specimen UT-PBS-12

Drift Ratio	Drift	$E_{D\Delta t}$ (kip-in)	ξ_{eq}
0.60%	**0.55%**	49.96	18.4%
1.50%	**1.63%**	89.12	18.5%

C.6 SPECIMEN UT-PBS-12G

Specimen UT-PBS-12G was 96-in. wide and 96-in. high (aspect ratio equal to 1.0) with No. 4 bars every 16 in. vertically and horizontally and axial load ratio, $P / (f_m' A_g)$, equal to 0.10. The dowels were extended 16 in. (two courses) from the base of the wall segment. This specimen was built with "Green Blocks," which are hollow concrete masonry units containing recycled material. The expected moment capacity of Specimen UT-PBS-12G was 858 ft-kips, equivalent to a lateral load of 98.06 kips as shown in Section 3.2. Specimen UT-PBS-12G before the test is shown in Figure C.37.

Figure C.37 Specimen UT-PBS-12G before testing

C.6.1 Test Observations, Specimen UT-PBS-12G

The value of Δy calculated in the preliminary phase of the test was equal to 0.20 in., equivalent to a drift ratio of 0.21%, and no cracks were observed. Within the test, rapid transition from flexural to shear cracks was observed at the first cycles, concentrated in the lowest four courses. The base joint cracked early in the test, at

$1\Delta_y$ (0.21% drift ratio), and the crack progressively widened in each cycle. Crushing of the north toe (Figure C.38a) was identified at the second cycle to $3\Delta_y$ (0.63% drift ratio), and in the south toe (Figure C.38b) at the second cycle to $4\Delta_y$ (0.83% drift ratio). The toes started to spall at $8\Delta_y$ (1.67% drift ratio), accompanied by buckling of the extreme longitudinal bars. During this cycle, the degradation concentrated in the toes, producing more spalling, buckling in the longitudinal bars there, and slip of the dowels there, as shown in Figure C.39. The test was ended when the specimen suddenly failed because of the lack of compression capacity at the toes. The specimen at the end of the test is shown in Figure C.40.

(a) North end ***(b) South end***

Figure C.38 Toe crushing of Specimen UT-PBS-12G at end of test

(a) North end *(b) South end*

Figure C.39 Specimen UT-PBS-12G at 8∆y

Figure C.40 Specimen UT-PBS-12G at end of test

C.6.2 Load-Displacement Curve, Specimen UT-PBS-12G

The load-displacement curve (hysteretic curve) of Specimen UT-PBS-12G is shown in Figure C.41.

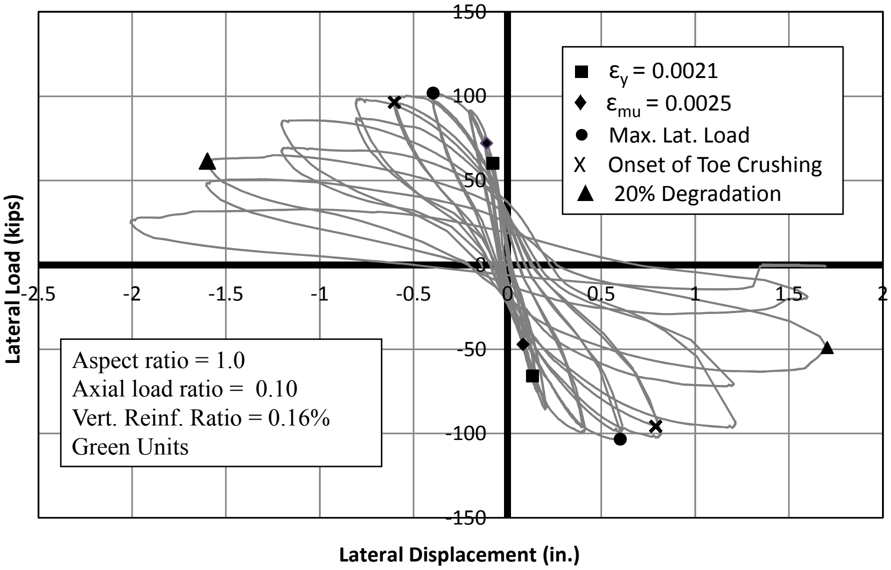

Figure C.41 Load-displacement curve for Specimen UT-PBS-12G

In the preliminary phase of the test, the extreme vertical bar yielded at the south end, and the maximum useful masonry strain was reached at both ends. The extreme bar at the north end yielded at 1Δ_y (0.21% drift ratio). Toes crushed in both directions after the maximum load. When loading to the north, the maximum load and the toe crushing appeared at 2Δ_y and 3Δ_y (0.42 and 0.63% drift ratio), respectively. When loading to the south, the maximum load and the toe crushing appeared at 3Δ_y and 4Δ_y (0.63 and 0.83% drift ratio), respectively.

C.6.3 Displacement Components

The relative contributions of flexural, shearing, and sliding deformation at maximum load and at ultimate load (80% of the maximum capacity) for Specimen UT-PBS-12G are summarized in Table C-32. Values at ultimate could not be calculated for the north-pushing direction because of problems in instrumentation at the last stages of the test.

Table C-32 Relative flexural, shearing, and sliding deformation contributions for Specimen UT-PBS-12G

Direction	Maximum Load			80% of Maximum capacity		
	Flexure	Shear	Sliding	Flexure	Shear	Sliding
North-Push	82%	11%	6%	-	-	-
South- Pull	79%	15%	6%	93%	5%	2%

C.6.4 Backbone and idealized elasto-plastic curve

The principal elements of backbone and elasto-plastic curve for Specimen UT-PBS-12G are summarized in Table C-33.

Table C-33 Elasto-plastic and backbone curve for Specimen UT-PBS-12G

Direction	Elasto-plastic curve					Backbone	
	Δ'_y (in.)	P'_y (kips)	Δ_y (in.)	P_y (kips)	Δ_u (in.)	Δ_{Pmax} (in.)	P_{max} (kips)
North-Push	0.0766	60.20	0.1196	94.00	1.2578	0.3972	101.07
South- Pull	0.1335	66.03	0.1982	98.00	1.3490	0.6026	103.14

The values of the maximum lateral load of the elasto-plastic and backbone curve were 3% lower and 4% higher, respectively, than the nominal capacity for Specimen UT-PBS-12G (98.06 kips).

C.6.5 Displacement Ductility

The displacement ductility for Specimen UT-PBS-12G was calculated from the elasto-plastic curve of each direction. Table C-34 presents the values for both directions and their average.

Table C-34 Displacement ductility for Specimen UT-PBS-12G

Direction	Δ_y **(in.)**	Δ_u **(in.)**	μ_Δ
North-Push	0.1196	1.2578	10.52
South- Pull	0.1982	1.3490	6.81
Average	**0.15887**	**1.3034**	**8.66**

C.6.6 Wall Segment Curvatures

The curvatures along the height of the Specimen UT-PBS-12G were calculated for different cycles, as shown in Figure C.42. The curvatures after the first cycle to $4\Delta_y$ are not presented because the instrumentation detached as a consequence of masonry spalling.

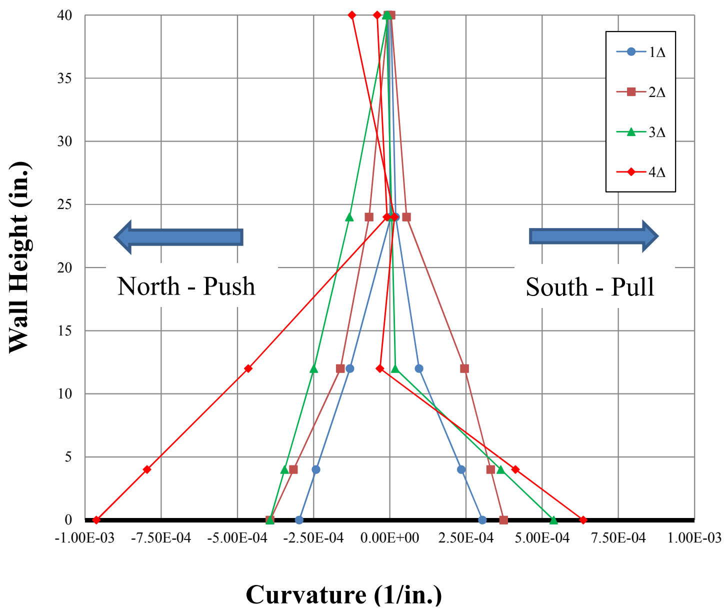

Figure C.42 Curvature profile for Specimen UT-PBS-12G

C.6.7 Curvature Ductility

Curvature ductility for Specimen UT-PBS-12G was calculated as the ratio of ultimate curvature and yield curvature. Table C-35 shows the value of yield curvature, ultimate curvature, and curvature ductility for both directions.

Table C-35 Curvature ductility for Specimen UT-PBS-12G

Direction	**ϕ_y (x10^{-05} in.$^{-1}$)**	**ϕ_u (x10^{-05} in.$^{-1}$)**	**μ_ϕ**
North-Push	11.27	96.23	8.54
South- Pull	6.39	63.49	9.93
Average	**8.83**	**79.86**	**9.23**

C.6.8 Height of Plasticity and Plastic Hinge Length

The height of plasticity, L_p, was calculated at ultimate curvature (80% of the maximum capacity) or using data from the last cycle available from the instrumentation. Table C-36 shows the height of plasticity and its portion of the total plan length of the wall segment for both directions of loading.

Table C-36 Height of plasticity for Specimen UT-PBS-12G

Direction	**L_p (in.)**	**L_p/L_w**
North-Push	55.41	58%
South- Pull	20.84	22%
Average	**38.12**	**40%**

Table C-37 shows the plastic hinge length and its portion of the total plan length of the wall segment for both directions of loading.

Table C-37 Plastic hinge length for Specimen UT-PBS-12G

Direction	**l_p (in.)**	**l_p/L_w**
North-Push	11.15	12%
South- Pull	20.46	21%
Average	**15.81**	**16%**

C.6.9 Energy Dissipation and Equivalent Hysteretic Damping

Energy dissipation, $E_{D\Delta t}$, and equivalent hysteretic damping, ξ_{eq}, were calculated for the hysteretic loops whose drifts were close or equal to 0.6 and 1.5%. Figure C.43 shows the hysteretic loops of 0.62% and 1.67% drift ratios for Specimen UT-PBS-12G, and Table C-38 presents the value of energy dissipation and equivalent hysteretic damping for both curves.

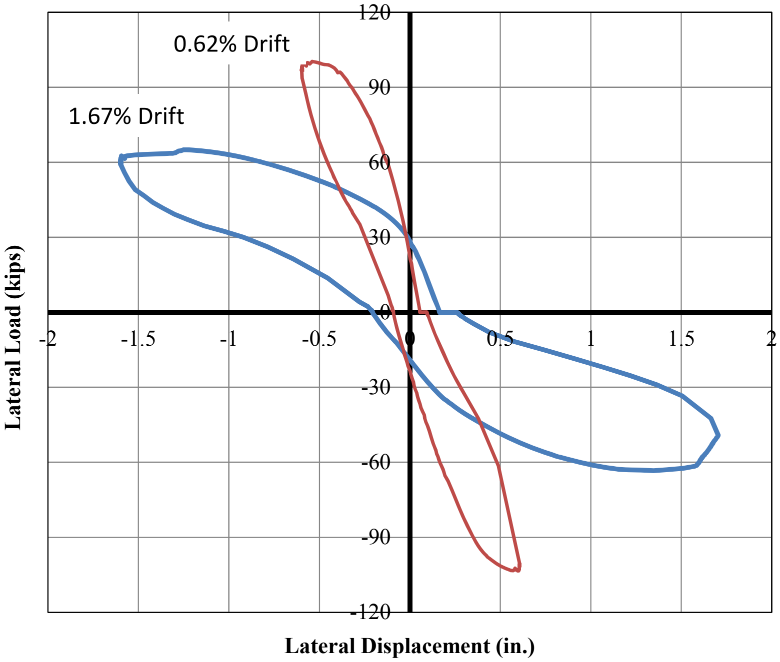

Figure C.43 Hysteretic loops at 0.62% and 1.67% drift ratios for UT-PBS-12G wall

Table C-38 Energy dissipation and equivalent hysteretic damping for Specimen UT-PBS-12G

Drift Ratio	**Drift**	**$E_{D\Delta t}$ (kip-in)**	**ξ_{eq}**
0.60%	**0.62%**	51.24	19.1%
1.50%	**1.67%**	113.57	23.8%

APPENDIX D
Cyclic Tests of Fixed-fixed CMU Wall Specimens

D.1 SHEAR WALL SPECIMEN UT-PBS-02

An interaction diagram for base shear capacity as a function of axial load for Specimen UT-PBS-02 is presented in Figure D.1. The axial load applied to Specimen UT-PBS-02 was 103 kips, as shown by a dashed horizontal line in Figure D.1. At this level of axial load the following major events are predicted in order of occurrence: web-shear cracking; shear yielding; shear sliding (based on shear dowel action); and flexural yielding. Specimen UT PBS-02 before testing is shown in Figure D.2.

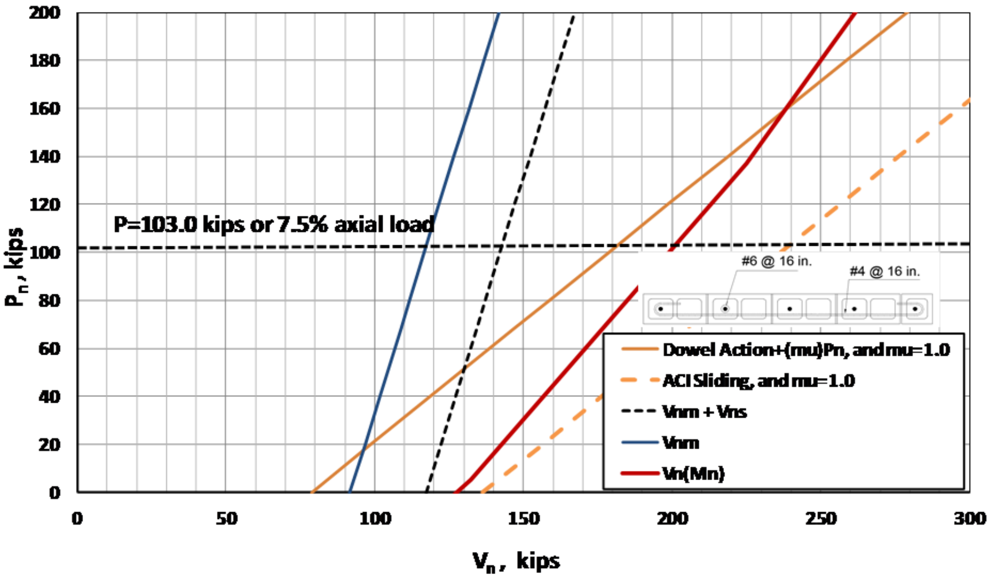

Figure D.1 Strength interaction diagrams for Specimen UT-PBS-02

Figure D.2 Specimen UT-PBS-02 before testing

D.1.1 Loading History and Major Events for Specimen UT-PBS-02

Specimen UT-PBS-02 was first subjected to a preliminary test phase to estimate the yield displacement, Δ_y. A moment-curvature analysis of the specimen was used to estimate the maximum moment capacity, which was then converted to a peak horizontal load capacity. The specimen was subjected to two reversed cycles of load of ±25%, ±50%, and ±75% of that peak horizontal load capacity. The displacement from the first cycle to 75% of that peak horizontal load capacity was used to establish the probable Δ_{y}, by extrapolating the displacement at 75% of the maximum load to the displacement at 100% of the maximum load (displacement at 100% maximum load equal to 4/3 times displacement at 75% maximum load. Lateral yield displacement was determined as 0.12

in. On May 12, 2012, Specimen UT-PBS-02 was loaded two cycles of reversed displacements of ±1, 2, 3, 4, and 6 times that predicted yield displacement. It was then loaded to a half-cycle to a displacement of 8 times that predicted yield displacement. The test was stopped when the peak capacity dropped to 20% or less of the experimentally observed maximum capacity (capping point). The testing took about 8 hours. The actual lateral loading, lateral displacement, and axial load histories for Specimen UT-PBS-02 are presented in Figure D.3 through Figure D.5. Loading to the north is considered positive; loading to the south, negative. In this test the specimen was loaded first to the north and then to the south.

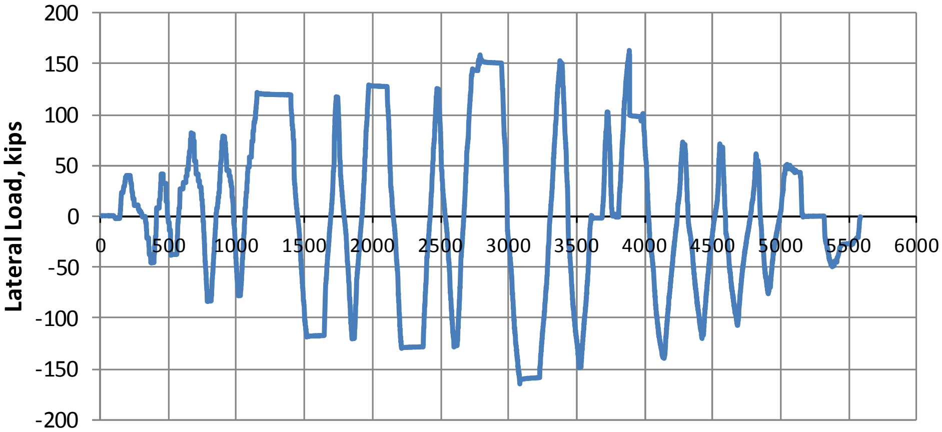

Figure D.3 Actual lateral loading history for Specimen UT-PBS-02

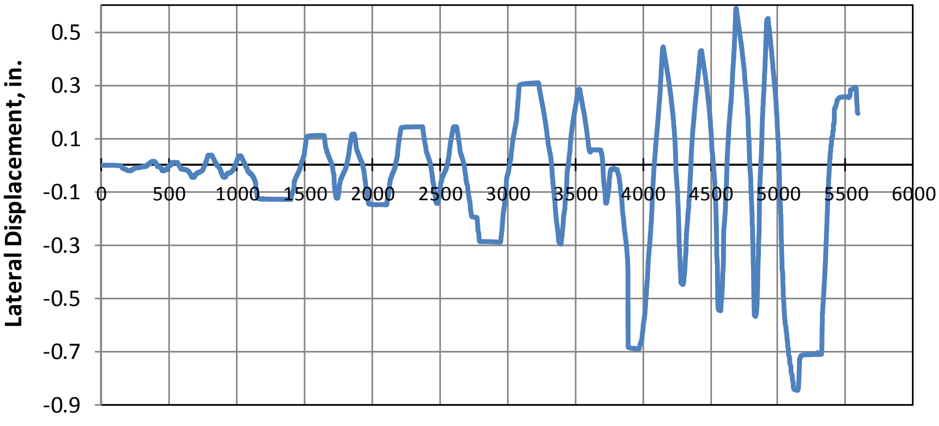

Figure D.4 Actual lateral displacement history for Specimen UT-PBS-02

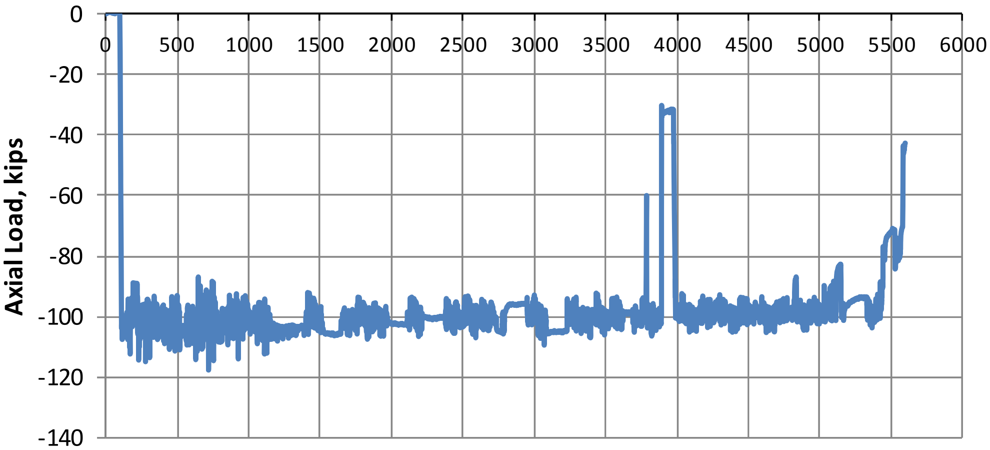

Figure D.5 Actual axial load history for Specimen UT-PBS-02

D.1.2 Sequence of Crack Formation for Specimen UT-PBS-02

The sequence of crack formation in Specimen UT-PBS-02 is described in terms of major events: drift ratios during the test when the condition of the specimen changed (for example, flexural cracking or shear cracking). Table D-1 lists the major events and the drift ratio at which they occurred. In the following figures, where crack maps are presented for some of the major events, cracks that formed on loading to the north are shown in black, and cracks that formed on loading to the south are shown in red.

D.1.2.1 Flexural and web-shear cracking in Specimen UT-PBS-02

Major Events 1 and 2, as shown in Figure D.6, correspond to flexural cracking and web-shear cracking. At the drift ratio of 0.17%, flexural cracks and web-shear cracks formed while loading to the north and south at a load of 120 kips. A web-shear crack formed along the entire height of the wall while loading to the north at a base shear and drift ratio of 120 kips and 0.17%. In addition, while loading to the south, parallel smaller web-shear cracks formed along the wall at the same base shear and drift ratio. The predicted nominal capacity in web-shear cracking based on MSJC 2011 *Code* at the corresponding axial load is 117 kips. The ratio of observed to predicted web-shear cracking capacity is 1.02.

Table D-1 Description of major events for Specimen UT-PBS-02

major event	lateral drift ratio	physical description
1	0.17%	flexural cracking and web-shear cracking, loading north
2	0.17%	flexural cracking and web-shear cracking, loading south
3	0.39%	additional web-shear cracking, loading north
4	0.39%	additional web-shear cracking, loading south
5	0.58%	opened diagonal cracks, and minor crushing of diagonal struts
6	0.58%	opened diagonal cracks, and minor crushing of diagonal struts
7	0.78%	minor crushing of diagonal struts
8	1.16%	crushing and spalling of diagonal struts, spalling at toes
9	1.16%	crushing and spalling of diagonal struts, spalling at toes
10	end of test	shear failure and axial collapse

D.1.2.1 Additional web-shear cracking in Specimen UT-PBS-02

Major Events 3 and 4 correspond to the development of additional web-shear cracks in the specimen. The base shears were 155 kips and 161 kips for loading north and loading south and the drift ratio was 0.39% for both loading directions. Damage in the specimen at the end of Major Event 4 is shown in Figure D.7.

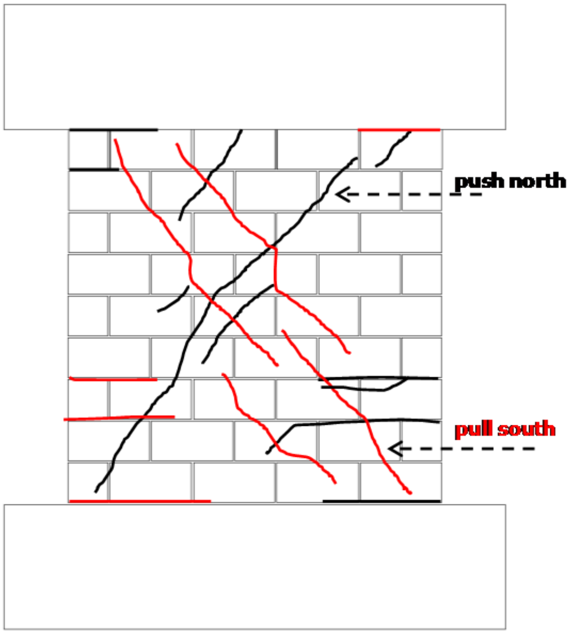

Figure D.6 Flexural cracking and web-shear cracking at 0.17% drift ratio (UT-PBS-02)

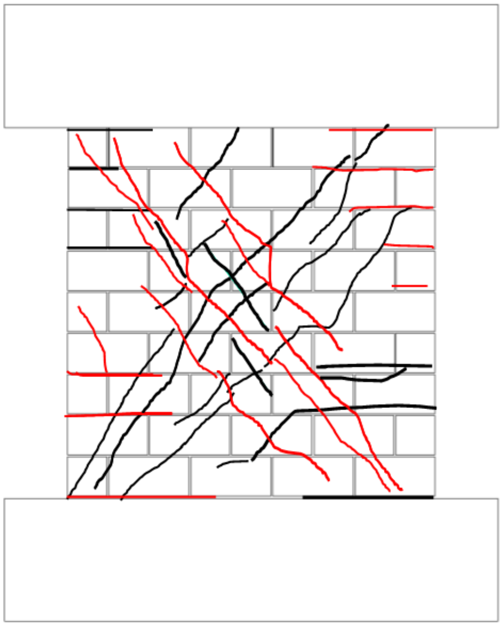

Figure D.7 Additional web-shear cracking at 0.39% drift ratio (UT-PBS-02)

D.1.2.2 Distributed open web-shear cracking in Specimen UT-PBS-02

Figure D.8 shows how wide shear cracks had opened in wall segment in Major Events 5 and 6, at a drift ratio of 0.58%. Major Events 5 through 7 were distributed web-shear cracks combined with minor spalling in the compression toe. As the load continued to increase to the north, a web-shear crack formed, and spalling occurred at the north toe at a drift ratio of 0.58%. Similar damage occurred while loading to the south at a drift ratio of 0.58%. This damage was also combined with a 0.25-in. gap in the web-shear cracks along the entire height of the wall that formed in both diagonal directions, as shown in Figure D.8. In Major Event 7, minor crushing of diagonal struts was observed while loading to the north at drift ratio of 0.78%.

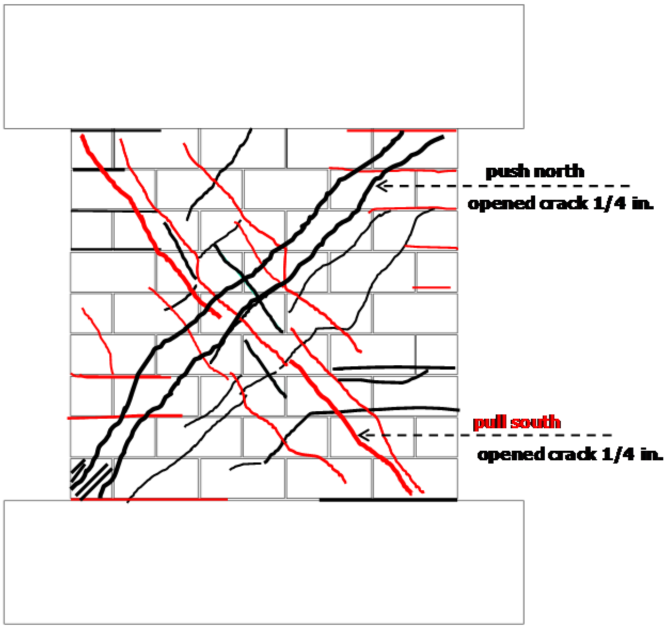

Figure D.8 Distributed open web-shear cracks at 0.58% drift ratio (UT-PBS-02)

D.1.2.3 Crushing and spalling of the compression toe and diagonal struts in Specimen UT-PBS-02

In the last two cycles of the test, in Major Events 8 and 9, severe spalling at the compression toes and crushing of diagonal were observed at a drift ratio of 1.16% for northward loading. In Major Event 9 vertical cracks were observed at the lower north corner and upper south end while loading to the south, which indicated that load was being transferred through a diagonal strut. The test was unloaded and discontinued after Major Event 9 due to crushing of the south and north compression toes, significant spalling of the diagonal strut face shells, and opening of the web-shear crack of 0.75 in. This damage at the end of test is shown in Figure D.9 and Figure D.10. As shown in Figure D.10, reversed cyclic loading caused diagonal strut crushing, toe crushing, and spalling of the specimen.

Figure D.9 Crushing and spalling of the compression toe and diagonal struts at 1.16% drift ratio (UT-PBS-02)

Figure D.10 Crushing and spalling of compression toe and diagonal struts at end of test (UT-PBS-02)

D.1.3 Load-Displacement Behavior for Specimen UT-PBS-02

The load-displacement relationship of Specimen UT-PBS-02 is presented in Figure D.11 in terms of the non-dimensional drift ratio, which references seven major events during testing:

1) first web-shear cracking
2) first yield of the extreme vertical reinforcement ($\varepsilon_y = 0.0021$);
3) first yield of the horizontal reinforcement ($\varepsilon_y = 0.0021$);
4) maximum useful strain in the masonry ($\varepsilon_{mu} = 0.0025$);
5) maximum capacity (capping point);
6) onset of crushing of toes or diagonal struts; and
7) decrease in capacity to 50% of maximum capacity.

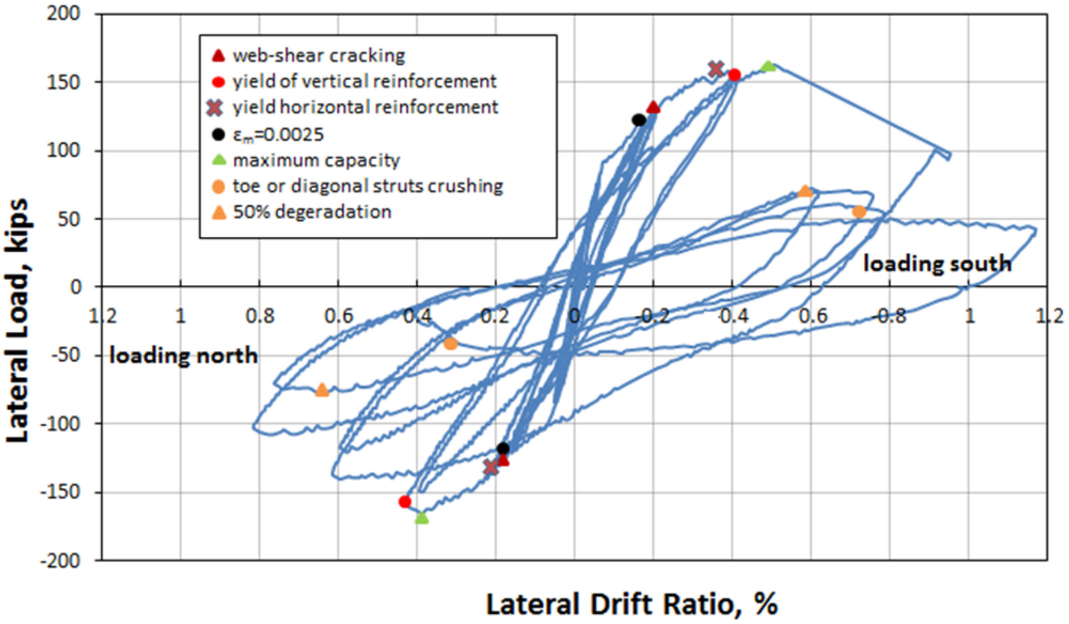

Figure D.11 Lateral load versus top drift ratio (UT-PBS-02)

D.1.4 Components of Displacements and Drifts

Sliding was measured between the base and top of the wall and the concrete loading and base beams. These load-sliding curves for the top and the base of wall are shown in Figure D.12. Load-displacement curves for total sliding and shear component of total tip displacement are given in Figure D.13 and Figure D.14, and comparison between total displacement and shear deformation is shown Figure D.15.

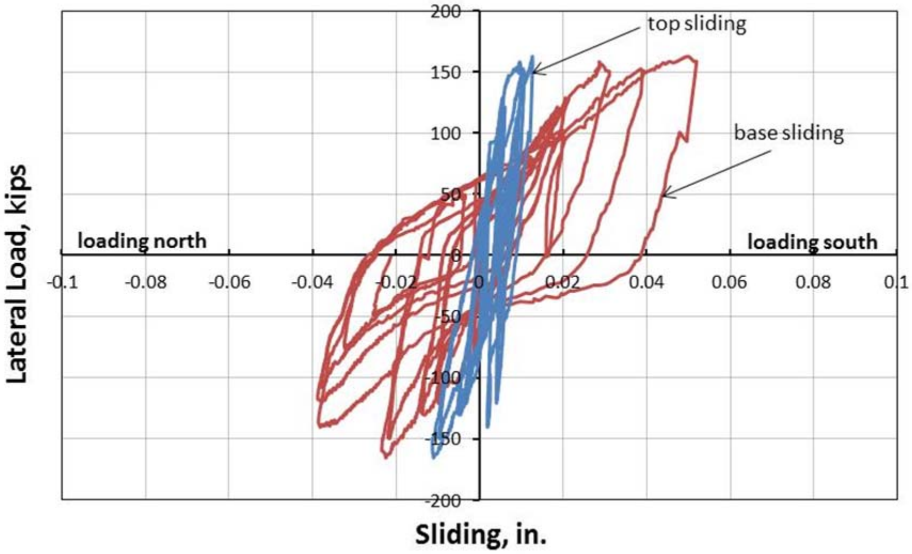

Figure D.12 Curves of load versus sliding at top and base (UT-PBS-02)

Figure D.13 Total sliding versus lateral load (UT-PBS-02)

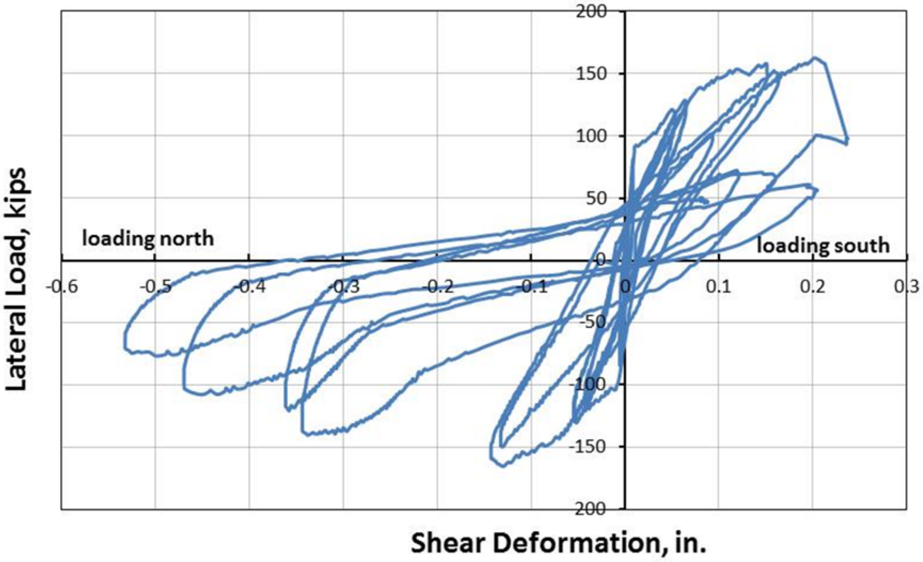

Figure D.14 Shear deformation versus lateral load (UT-PBS-02)

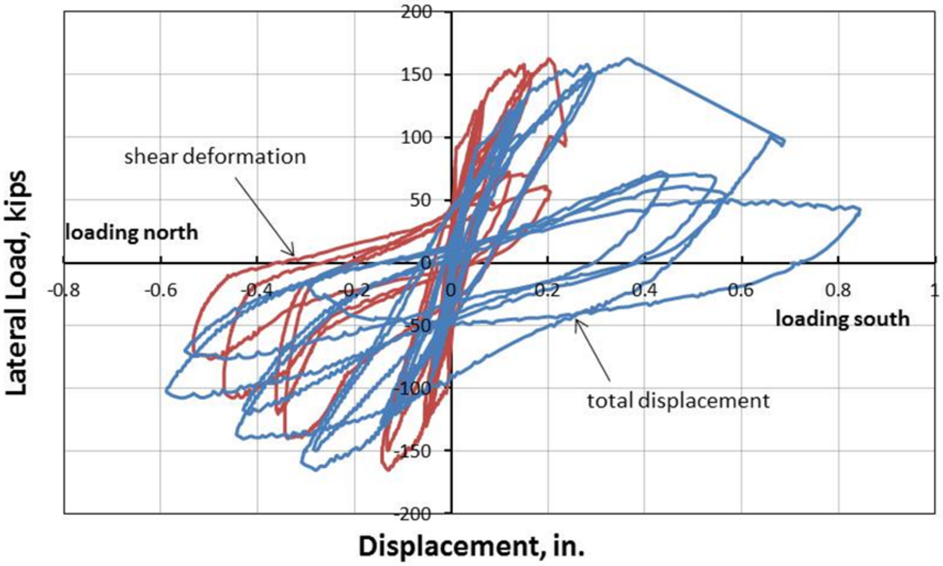

Figure D.15 Comparison of total top displacement and shear deformation (UT-PBS-02)

D.2 SHEAR WALL SPECIMEN UT-PBS-05

An interaction diagram for base shear capacity as a function of axial load for Specimen UT-PBS-05 is presented in Figure D.16. The axial load applied to Specimen UT-PBS-05 was 81.3 kips, as shown by a dashed horizontal line in Figure D.16. At this level of axial load the following major events are predicted in order of occurrence: web-shear cracking; shear sliding (based on shear dowel action); shear yielding; and flexural yielding.

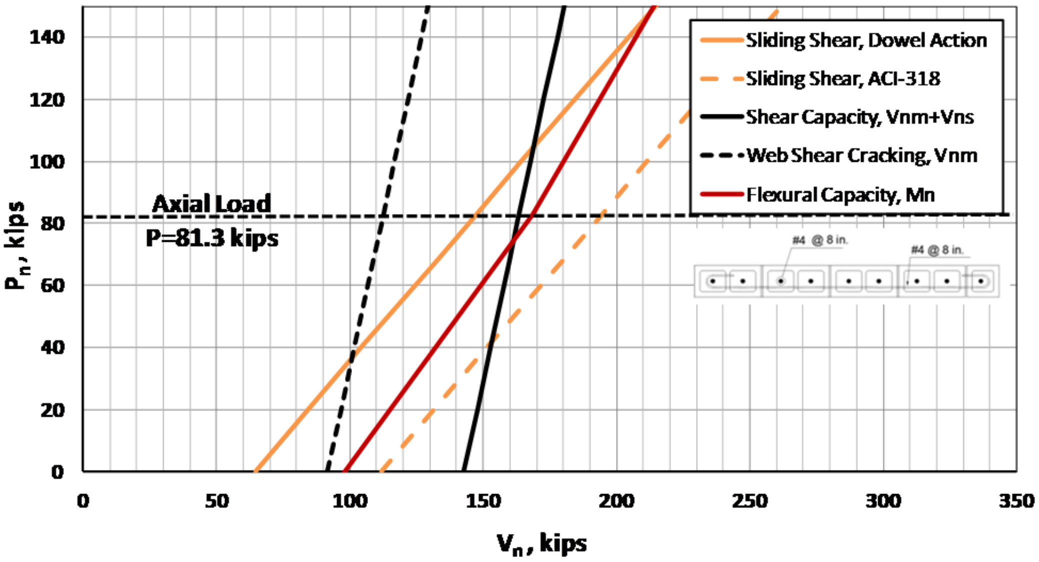

Figure D.16 Strength interaction diagrams for Specimen UT-PBS-05

Specimen UT-PBS-05 before testing is shown in ***Figure D.17***.

Figure D.17 Specimen UT-PBS-05 before testing

D.2.1 Loading History and Major Events for Specimen UT-PBS-05

Specimen UT-PBS-05 was first subjected to a preliminary test to estimate the yield displacement, Δ_y. A moment-curvature analysis of the specimen was used to estimate the maximum moment capacity, which was then converted to a peak horizontal load capacity. The specimen was subjected to two reversed cycles of load of ±25%, ±50%, and ±75% of that peak horizontal load capacity. The displacement from the first cycle to 75% of that peak horizontal load capacity was used to establish the probable Δ_{y}, by extrapolating the displacement at 75% of the maximum load to the displacement at 100% of the maximum load (displacement at 100% maximum load equal to 4/3 times displacement at 75% maximum load. Lateral yield displacement was determined as 0.11 in.

On May 12, 2012, Specimen UT-PBS-05 was loaded two cycles of reversed displacements of ±1, 2, 3, 4, 6, 8, 10, and 12 times that predicted yield displacement. It was then loaded to a half-cycle to a displacement of 14 times that predicted yield displacement. The test was stopped when the peak capacity dropped to 20% or less of the experimentally observed maximum capacity (capping point). The testing took about 8 hours. The actual lateral loading, lateral displacement, and axial load histories for Specimen UT-PBS-05 are presented in Figure D.18 through Figure D.20. Loading to the north is considered positive; loading to the south, negative. Negative axial loads denote compression. In this test the wall was loaded first to the north and then to the south.

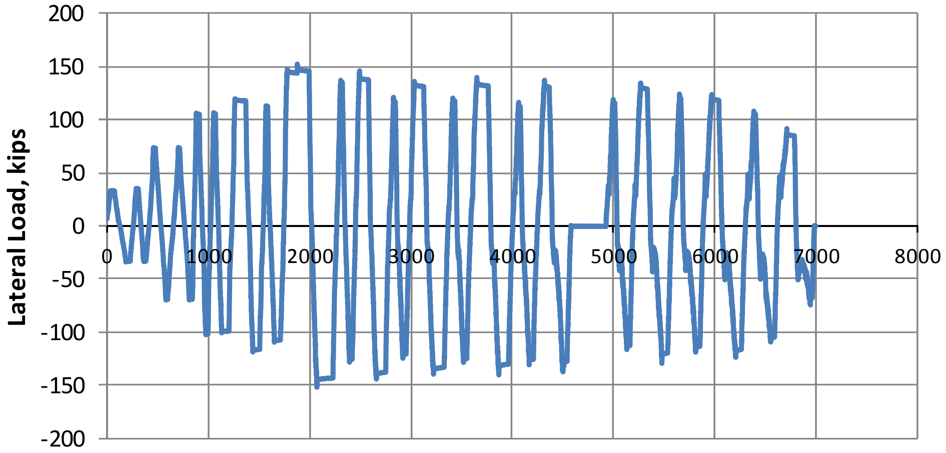

Figure D.18 Actual lateral loading history for Specimen UT-PBS-05

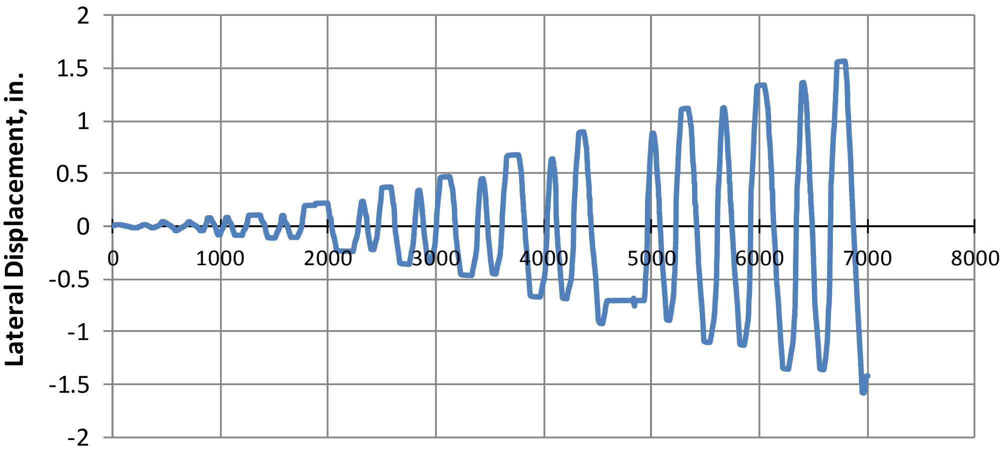

Figure D.19 Actual lateral displacement history for Specimen UT-PBS-05

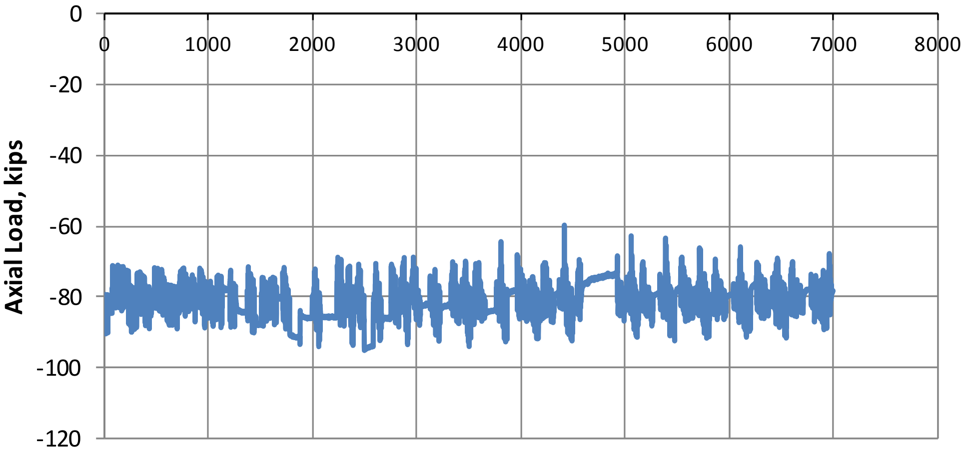

Figure D.20 Actual axial load history for Specimen UT-PBS-05

D.2.2 Sequence of Crack Formation for Specimen UT-PBS-05

The sequence of crack formation in Specimen UT-PBS-05 is described in terms of major events: drift ratios during the test when the condition of the specimen changed (for example, flexural cracking, sliding or shear cracking). Table D-2 lists the major events and the load point at which they occurred. In the following figures, where crack maps are presented for some of the major events, cracks that formed on loading to the north are shown in black, and cracks that formed on loading to the south are shown in red.

D.2.2.1 Flexural and web-shear cracking in Specimen UT-PBS-05

Major Events 1 and 2, as shown in Figure D.21, correspond to flexural cracking and web-shear cracking. At the drift ratio of 0.16%, flexural cracks formed while loading to the north and south at a load of 120.0 kips. Also, in these major events correspond to the formation of web-shear cracking while loading to the north and south respectively. Web-shear crack formed along the height of the wall while loading to the south at a base shear and drift ratio of 120.0 kips and 0.16%, respectively. In addition to while loading to the north, smaller web-shear cracks formed along the wall at the same base shear and drift ratio. The prediction for web-shear cracking based on MSJC 2011 *Code* at the corresponding axial load is 112 kips. The ratio of observed to predicted web-shear cracking capacity is 1.07.

Table D-2 Description of major events for Specimen UT-PBS-05

major event	lateral drift ratio	physical description
1	0.16%	flexural cracking and web-shear cracking, loading north
2	0.16%	flexural cracking and web-shear cracking, loading south
3	0.62%	additional web-shear cracking and observed sliding, loading north
4	0.62%	additional web-shear cracking and observed sliding, loading south
5	1.53%	severe sliding and crushing and spalling of diagonal struts, loading north
6	1.53%	Severe sliding and crushing and spalling of diagonal struts, loading south
7	2.13%	crushing and spalling of diagonal struts, spalling at toes loading north
8	end of test	crushing and spalling of diagonal struts, spalling at toes, and axial collapse, loading south

D.2.2.2 Additional web-shear cracking and sliding observed in Specimen UT-PBS-05

Major Events 3 and 4 correspond to the development of additional web-shear cracks and sliding in the specimen. The base shears were 136 kips and 138 kips for loading north and loading south respectively and the drift ratio was 0.62% for both. Damage in the specimen at the end of Major Event 4 is shown in Figure D.22. In these major events web-shear cracks combined with sliding at both directions, as shown in Figure D.22. During cyclic loading north at drift ratio of 0.62%, it was clear the wall had slid at the base at a load of 136 kips. Similar damage occurred while loading to the south at a drift ratio of 0.62%, and as the wall was loaded to the south sliding was also observed at a load of 138 kips.

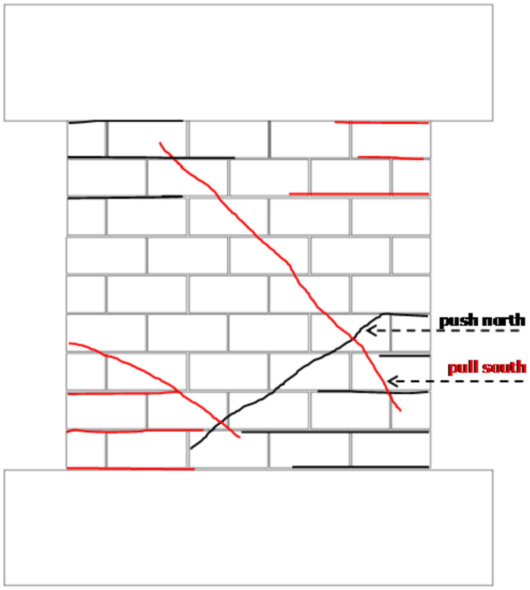

Figure D.21 Flexural cracking and web-shear cracking at 0.16% drift (UT-PBS-05)

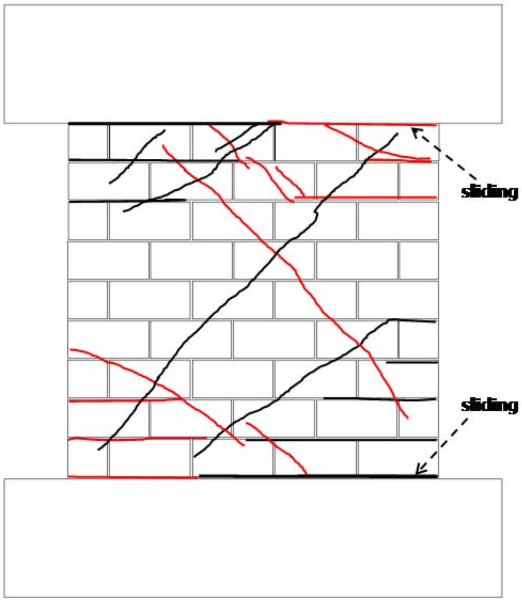

Figure D.22 Additional web-shear cracking and sliding at 0.62% drift (UT-PBS-05)

D.2.2.3 Severe sliding and crushing and spalling of diagonal struts in Specimen UT-PBS-05

In Major Events 5 and 6, because of reversed sliding at the top of the specimen, vertical cracks propagated from the horizontal crack at the toes caused crushing and spalling of diagonal struts and toes. While loading to the north, at the total drift ratio of 1.53%, significant sliding at the top of the wall combined with extensive spalling occurred on both faces of the wall as shown in Figure D.23. Similar damage occurred while loading to the south at a total drift ratio of 1.53%.

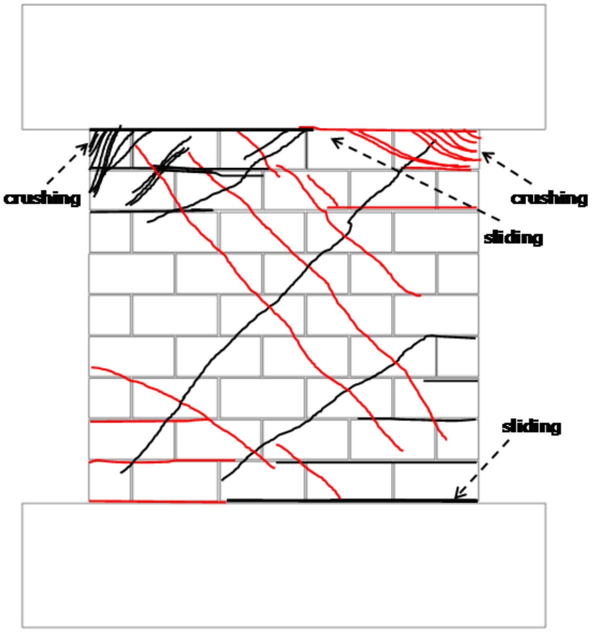

Figure D.23 Crushing and spalling of diagonal struts and observed sliding at drift ratio of 1.53% (UT-PBS-05)

D.2.2.4 Crushing and spalling of compression diagonal struts at top of Specimen UT-PBS-05

Finally, in the last two cycles of the test (Major Events 7 and 8), severe spalling at the compression toes and extensive crushing of diagonal were observed at drift ratio of 2.13% at the top while loading to the north. This damage combined with significant 1.01-in. sliding at the top of the wall segment. In Major Event 8, similar damage occurred while loading to the south at a total drift ratio of 2.13%, and the loading beam moved downward about 0.5 in. The test was unloaded after Major Event 8 due to potential instability of the test setup and axial load system. The extent of severe crushing at the top of the specimen is shown in Figure D.24. As shown in Figure D.25 reversed cyclic loading caused extensive crushing and spalling at the top of the specimen at the end of the test.

Figure D.24 Specimen UT-PBS-05 at end of test

Figure D.25 Detail of severe spalling and crushing of top compression toes (Specimen UT-PBS-05)

D.2.3 Load-Displacement Behavior for Specimen UT-PBS-05

The load-displacement relationship of Specimen UT-PBS-05 is presented in Figure D.26 in terms of the non-dimensional drift ratio, which references seven major events during testing:

1) first web-shear cracking
2) first yield of the extreme vertical reinforcement (ε_y = 0.0021);
3) first yield of the horizontal reinforcement (ε_y = 0.0021);
4) maximum useful strain in the masonry (ε_{mu} = 0.0025);
5) maximum capacity (capping point);
6) onset of crushing of toes or diagonal struts; and
7) decrease in capacity to 50% of maximum capacity.

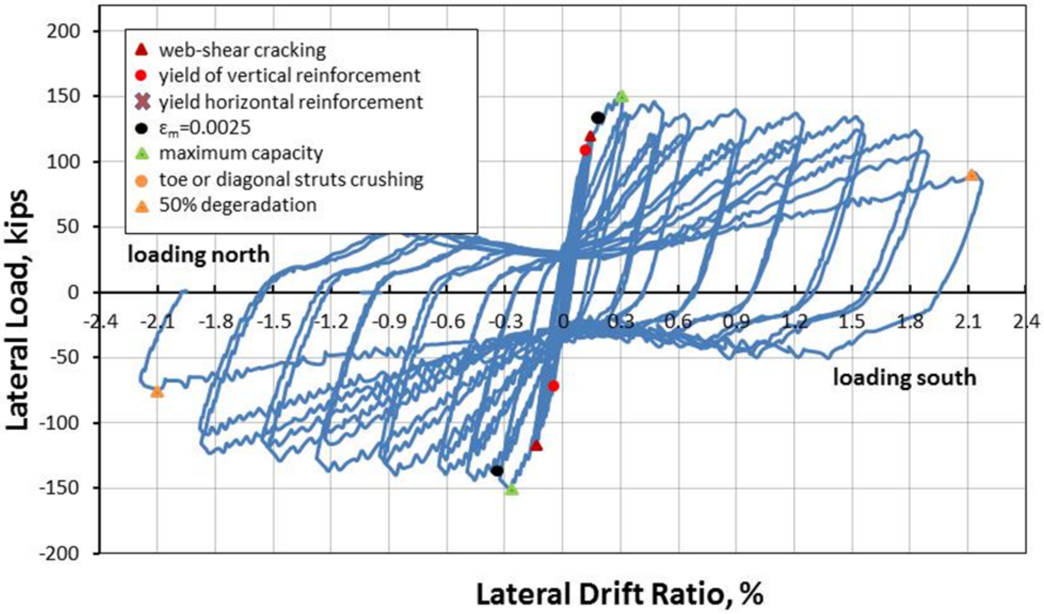

Figure D.26 Load versus top drift ratio (UT-PBS-05)

D.2.4 Components of Displacements and Drifts

Linear potentiometers recorded the average sliding displacements between the wall base and the base beam. Sliding was also measured between the top of the wall and the top concrete beam. These load-sliding curves for the top and the base of wall are shown in Figure D.27. Load-displacement curves for sliding component of displacement is given in Figure D.28, and comparison between total displacement and sliding deformation is shown Figure D.29.

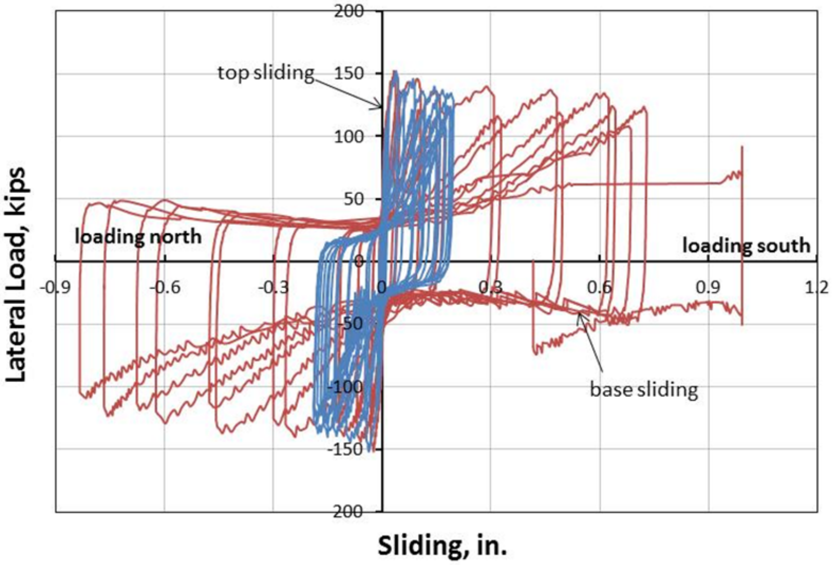

Figure D.27 Curves of load versus sliding at top and base (UT-PBS-05)

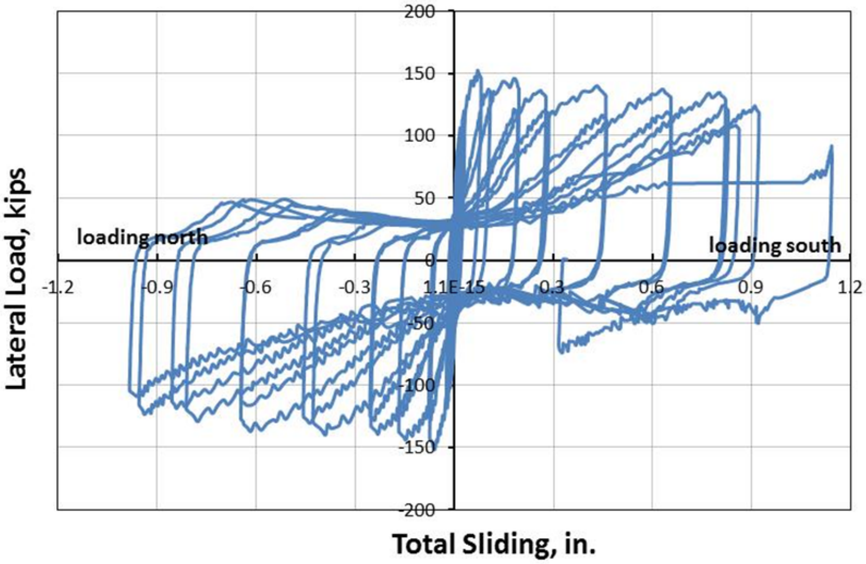

Figure D.28 Total sliding versus lateral load (UT-PBS-05)

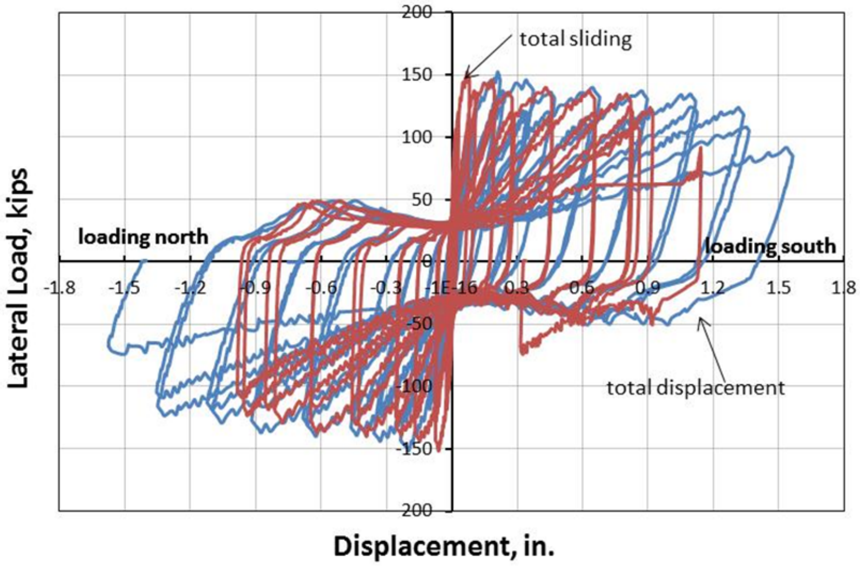

Figure D.29 Comparison of total top displacement and sliding deformation (UT-PBS-05)

D.3 SHEAR WALL SPECIMEN UT-PBS-06

An interaction diagram for base shear capacity as a function of axial load for Specimen UT-PBS-06 is presented in Figure D.30. The axial load applied to Specimen UT-PBS-06 was 68.3 kips, as shown by a dashed horizontal line in Figure D.30. At this level of axial load the following major events are predicted in order of occurrence: shear sliding (based on shear dowel action); web-shear cracking; and flexural yielding; and shear yielding.

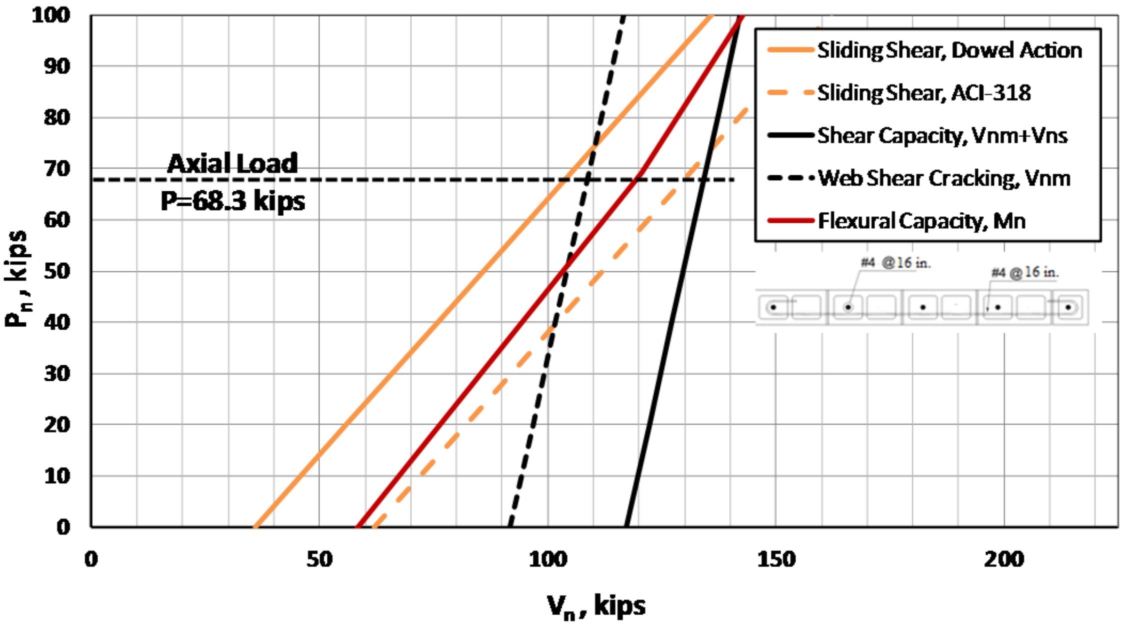

Figure D.30 Strength interaction diagrams for Specimen UT-PBS-06

Specimen UT-PBS-06 before testing is shown in ***Figure D.31***.

Figure D.31 Specimen UT-PBS-06 before testing

D.3.1 Loading History and Major Events for Specimen UT-PBS-06

Specimen UT-PBS-06 was first subjected to a preliminary test to estimate the yield displacement, Δ_y. A moment-curvature analysis of the specimen was used to estimate the maximum moment capacity, which was then converted to a peak horizontal load capacity. The specimen was subjected to two reversed cycles of load of ±25%, ±50%, and ±75% of that peak horizontal load capacity. The displacement from the first cycle to 75% of that peak horizontal load capacity was used to establish the probable Δ_{y}, by extrapolating the displacement at 75% of the maximum load to the displacement at 100% of the maximum load (displacement at 100% maximum load equal to 4/3 times displacement at 75% maximum load. Lateral yield displacement was determined as 0.075 in.

On March 19, 2012, Specimen UT-PBS-06 was loaded two cycles of reversed displacements of ±1, 2, 3, 4, 6, 8, and 10 times that predicted yield displacement. It was then loaded to a half-cycle to a displacement of 12 times that predicted yield displacement. The test was stopped when the peak capacity dropped to 20% or less of the experimentally observed maximum capacity (capping point). The testing took about 8 hours. The actual lateral loading, lateral displacement, and axial load histories for Specimen UT-PBS-06 are presented in Figure D.32 through Figure D.34. Loading to the north is considered positive; loading to the south, negative. Compressive axial load is considered negative. In this test the wall was loaded first to the north and then to the south.

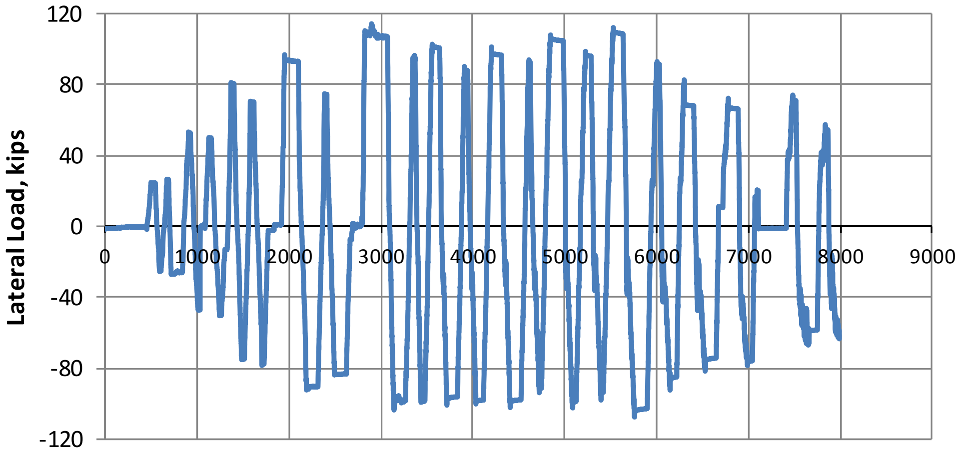

Figure D.32 Actual lateral loading history for Specimen UT-PBS-06

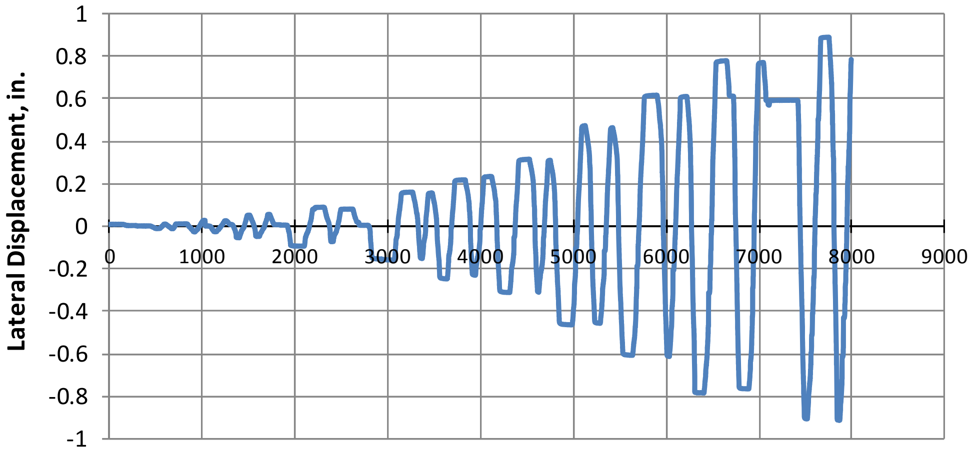

Figure D.33 Actual lateral displacement history for Specimen UT-PBS-06

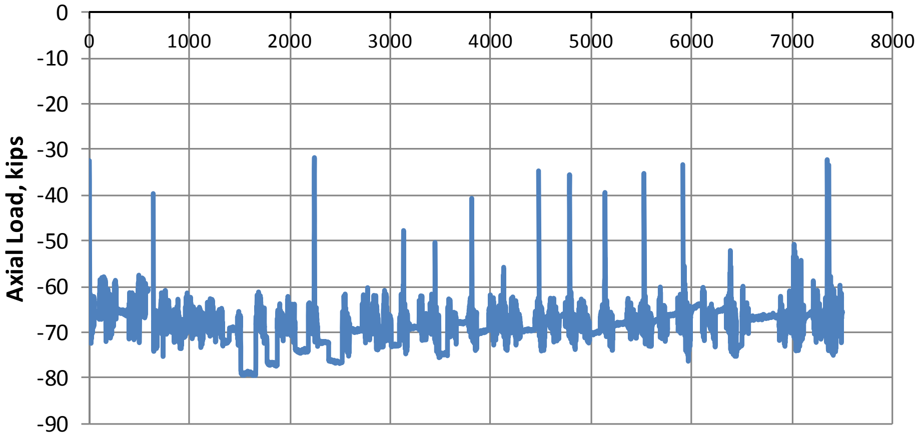

Figure D.34 Actual axial load history for Specimen UT-PBS-06

D.3.2 Sequence of Crack Formation for Specimen UT-PBS-06

The sequence of crack formation in Specimen UT-PBS-06 is described in terms of major events: drift ratios during the test when the condition of the specimen changed (for example, flexural cracking or shear cracking). Table D-3 lists the major events and the load point at which they occurred. In the following figures, where crack maps are presented for some of the major events, cracks that formed on loading to the north are shown in black, and cracks that formed on loading to the south are shown in red.

D.3.2.1 Flexural and web-shear cracking in Specimen UT-PBS-06

Major Events 1 and 2, shown in Figure D.35, correspond to flexural cracking and web-shear cracking. At a drift ratio of 0.21%, flexural cracks formed while loading to the north and south at a load of 107 and 101 kips. Also, in these major events correspond to the formation of web-shear cracking while loading to the north and south respectively. A web-shear crack formed along the entire height of the wall while loading to the north at a base shear and drift ratio of 107 kips and 0.21%, respectively. In addition to while loading to the south, smaller web-shear cracks formed along the wall at a base shear of 101 kip and the same drift ratio. The prediction for web-shear cracking based on MSJC 2011 Code at the corresponding axial load is 109 kips. The ratios of observed to predicted web-shear cracking capacity are 0.98 and 0.93.

Table D-3 Description of major events for Specimen UT-PBS-06

major event	lateral drift ratio	physical description
1	0.21%	flexural cracking and web-shear cracking, loading north
2	0.21%	flexural cracking and web-shear cracking, loading south
3	0.41%	observed sliding, loading north
4	0.41%	observed sliding, loading south
5	0.83%	additional web-shear cracking, minor toe crushing, and observed sliding, loading north
6	0.83%	additional web-shear cracking, minor toe crushing, and observed sliding, loading south
7	1.25%	severe sliding and reinforcement rupture at the base, loading north
8	1.25%	severe sliding and reinforcement rupture at the base, loading south

D.3.2.2 Observed sliding at the base, Specimen UT-PBS-06

Major Events 3 and 4 were sliding at the base of the wall for both directions, as shown in Figure D.36. During cyclic loading north at drift ratio of 0.41%, it was clear the wall had slid at the base at a load of 98.0 kips. Similar damage occurred while loading to the south at a drift ratio of 0.41%, and as the wall was loaded to the south sliding was observed at a load of 101 kips.

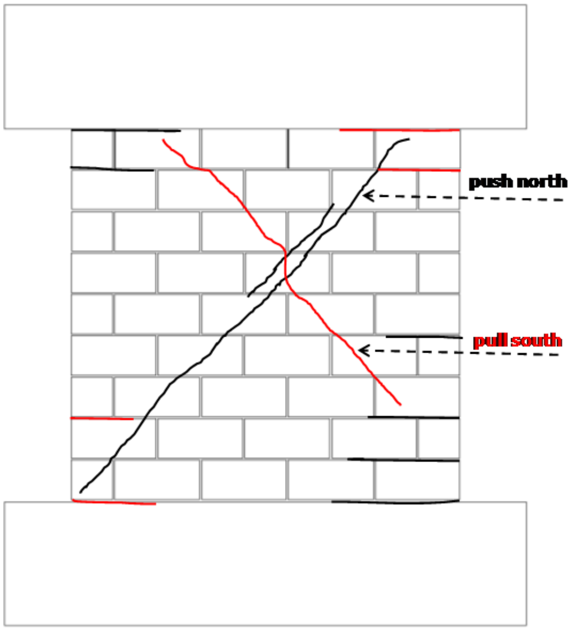

Figure D.35 Flexural cracking and web-shear cracking at 0.21% drift ratio (UT-PBS-06)

Figure D.36 Observed sliding at the base at 0.41% drift ratio (UT-PBS-06)

D.3.2.3 Additional web-shear cracking and observed significant sliding in Specimen UT-PBS-06

Major Events 5 and 6 were additional web-shear cracks combined with significant sliding at both directions, and minor crushing in the lower compression toe, as shown in Figure D.37. As the load continued to increase to the north, more web-shear cracks occurred in the specimen. In addition, during cyclic loading north at drift ratio of 0.83%, it was clear the wall had slid at the base at a load of 112 kip. Similar damage occurred while loading to the south at a drift ratio of 0.83%, and as the wall was loaded to the south, base sliding was observed at a load of 105 kip, combined with minor crushing of the compression lower toes.

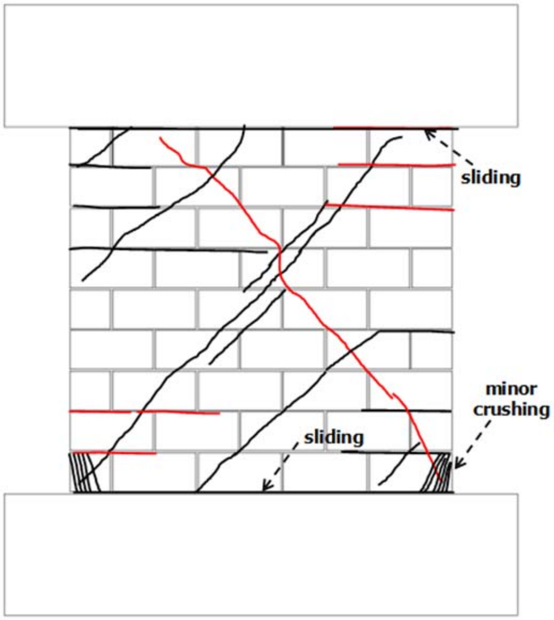

Figure D.37 Additional web-shear cracking and observed sliding at drift ratio of 0.83% (UT-PBS-06)

D.3.2.4 Severe base sliding, Specimen UT-PBS-06

Finally, in the last two cycles of the test (Major Event 7), severe base sliding was observed at a drift ratio of 1.25% while loading to the north. This damage combined with vertical reinforcement rupture at the base. In Major Event 8, similar damage occurred while loading to the south at a total drift ratio of 1.25%, and vertical cracks were observed at the lower toes while loading south. The test was unloaded after Major Event 8 due to potential lateral instability of the wall segment because of rupture of vertical reinforcement at the base (Figure D.39). As shown in Figure D.39, reversed cyclic loading caused crushing and spalling at the base toes of the specimen.

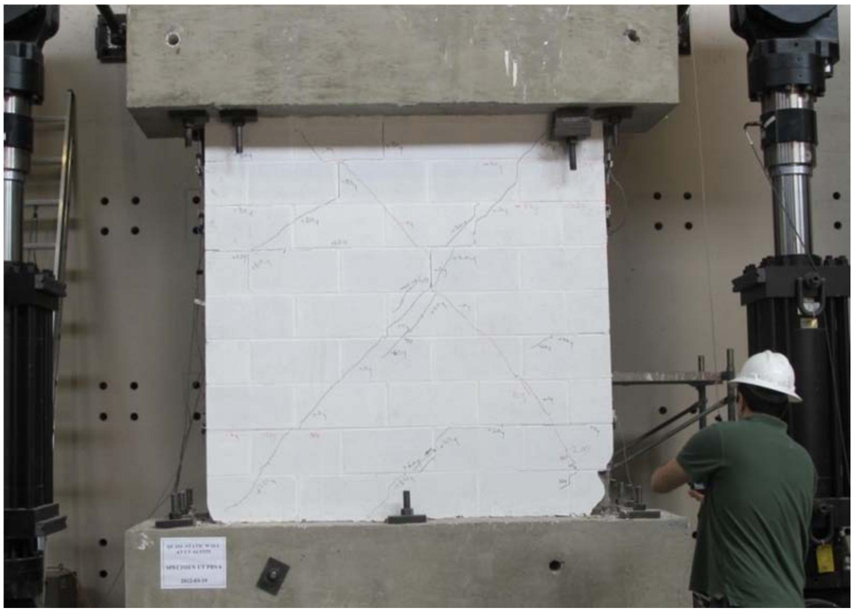

Figure D.38 Specimen UT-PBS-09 at end of test

Figure D.39 Detail of reinforcement rupture, and spalling and crushing at the compression toes

D.3.3 Load-Displacement Behavior for Specimen UT-PBS-06

The load-displacement relationship of Specimen UT-PBS-06 is presented in Figure D.40 in terms of the non-dimensional drift ratio, which references seven major events during testing:

1) first web-shear cracking
2) first yield of the extreme vertical reinforcement ($\varepsilon_y = 0.0021$);
3) first yield of the horizontal reinforcement ($\varepsilon_y = 0.0021$);
4) maximum useful strain in the masonry ($\varepsilon_{mu} = 0.0025$);
5) maximum capacity (capping point);
6) onset of crushing of toes or diagonal struts; and
7) decrease in capacity to 50% of maximum capacity.

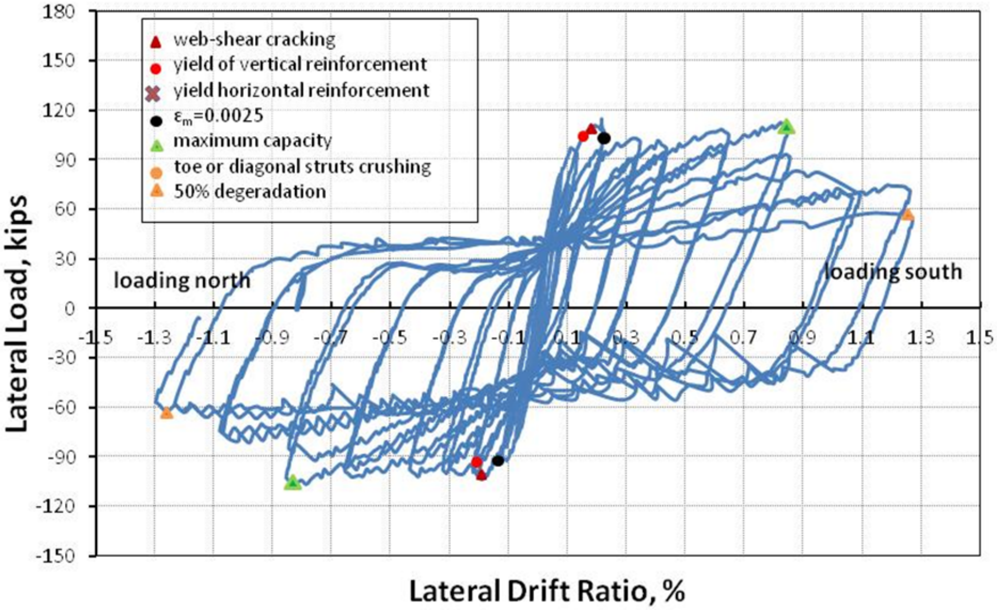

Figure D.40 Load versus top drift ratio (UT-PBS-06)

D.3.4 Components of Displacements and Drifts

Linear potentiometers recorded the average sliding displacements between the wall base and the base beam. Sliding was also measured between the top of the wall and the top concrete beam. These load-sliding curves for the top and the base of wall are shown in Figure D.41. Load-displacement curves for total sliding and shear component of displacement are given in Figure D.42 and Figure D.43, and comparison among total displacement, total sliding, and shear deformation is shown Figure D.44.

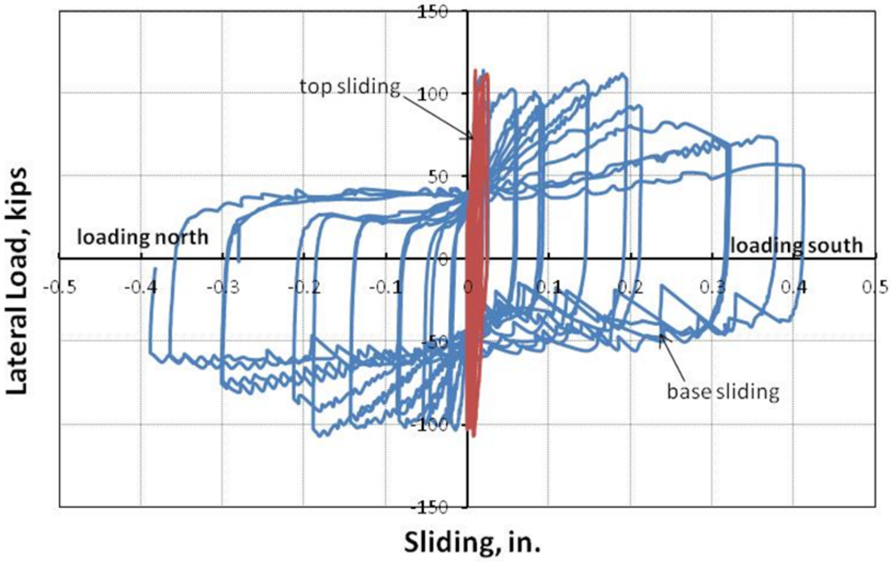

Figure D.41 Curves of load versus sliding at top and base (UT-PBS-06)

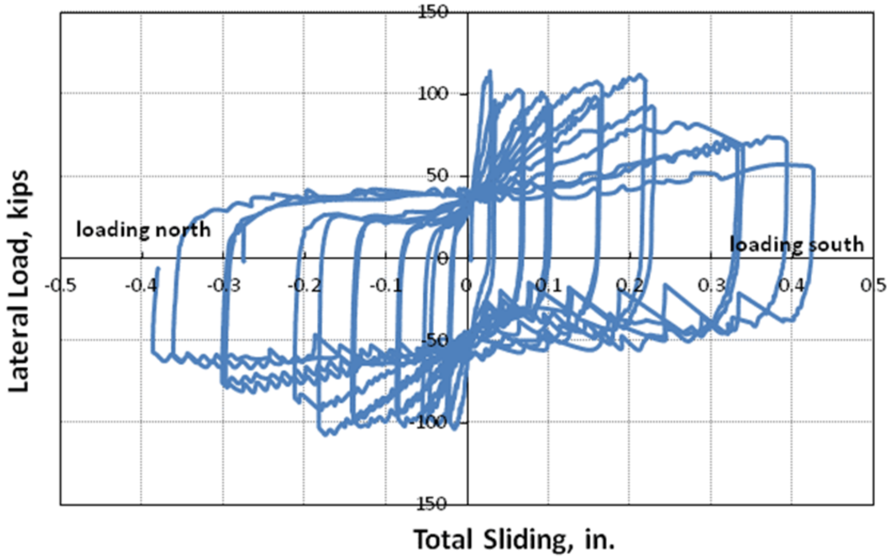

Figure D.42 Total sliding versus lateral load (UT-PBS-06)

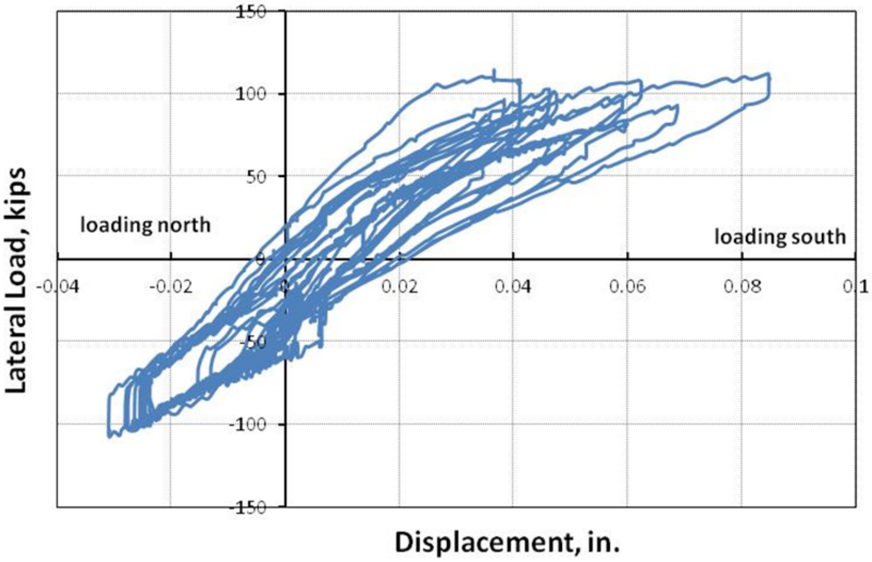

Figure D.43 Shear deformation versus lateral load (UT-PBS-06)

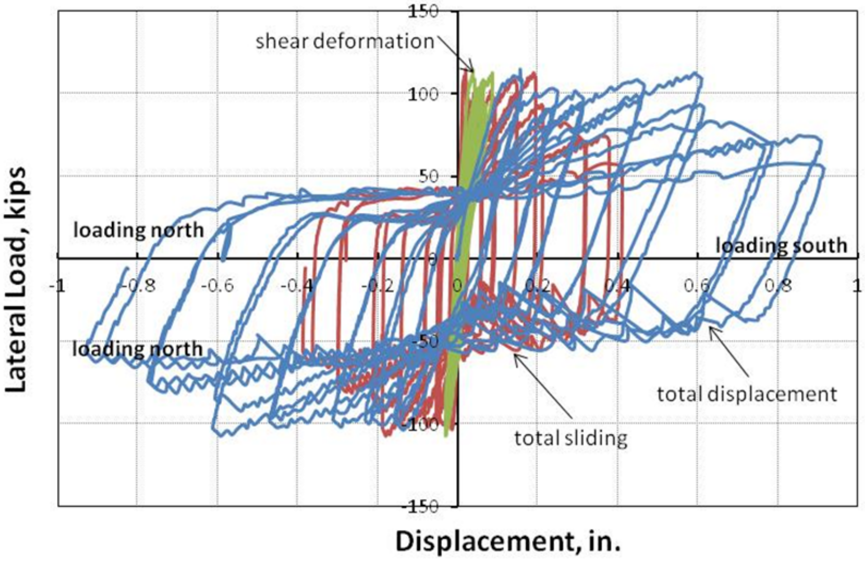

Figure D.44 Comparison of total top displacement, sliding, and shear deformation (UT-PBS-06)

D.4 SHEAR WALL SPECIMEN UT-PBS-09

An interaction diagram for base shear capacity as a function of axial load for Specimen UT-PBS-09 is presented in Figure D.45. The axial load applied to Specimen UT-PBS-09 was 136.6 kips, as shown by a dashed horizontal line in Figure D.45. At this level of axial load the following major events are predicted in order of occurrence: web-shear cracking; shear yielding; shear sliding (based on shear dowel action); and flexural yielding.

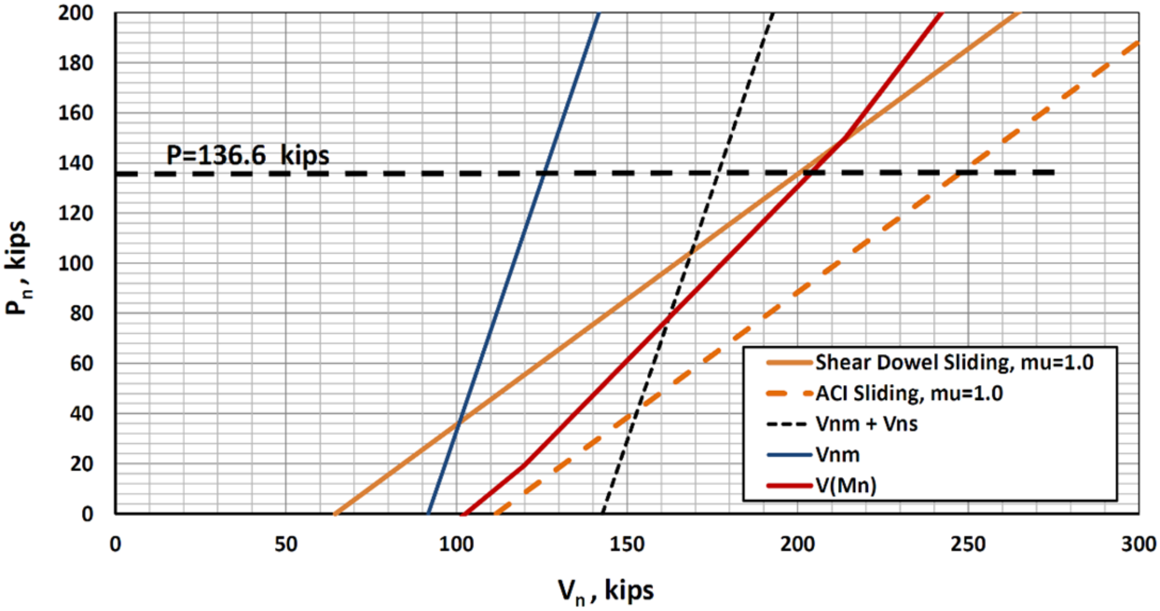

Figure D.45 Strength interaction diagram for Specimen UT-PBS-09

Specimen UT PBS-09 before testing is shown in Figure D.46.

Figure D.46 Specimen UT-PBS-09 before testing

D.4.1 Loading History and Major Events for Specimen UT-PBS-09

Specimen UT-PBS-09 was first subjected to a preliminary test to estimate the yield displacement, Δ_y. A moment-curvature analysis of the specimen was used to estimate the maximum moment capacity, which was then converted to a peak horizontal load capacity. The specimen was subjected to two reversed cycles of load of ±25%, ±50%, and ±75% of that peak horizontal load capacity. The displacement from the first cycle to 75% of that peak horizontal load capacity was used to establish the probable Δ_y, by extrapolating the displacement at 75% of the maximum load to the displacement at

100% of the maximum load (displacement at 100% maximum load equal to 4/3 times displacement at 75% maximum load. Lateral yield displacement was determined as 0.12 in. On May 12, 2012, Specimen UT-PBS-09 was loaded two cycles of reversed displacements of ±1, 2, 3, 4, 6, 8, and 10 times that predicted yield displacement. It was then loaded to a half-cycle to a displacement of 12 times that predicted yield displacement. The test was stopped when the peak capacity dropped to 20% or less of the experimentally observed maximum capacity (capping point). The testing took about 8 hours. The actual lateral loading, lateral displacement, and axial load histories for Specimen UT-PBS-09 are presented in Figure D.47 through Figure D.49. Loading to the north is considered positive; loading to the south, negative. Compressive axial load is considered negative. In this test the wall was loaded first to the north and then to the south.

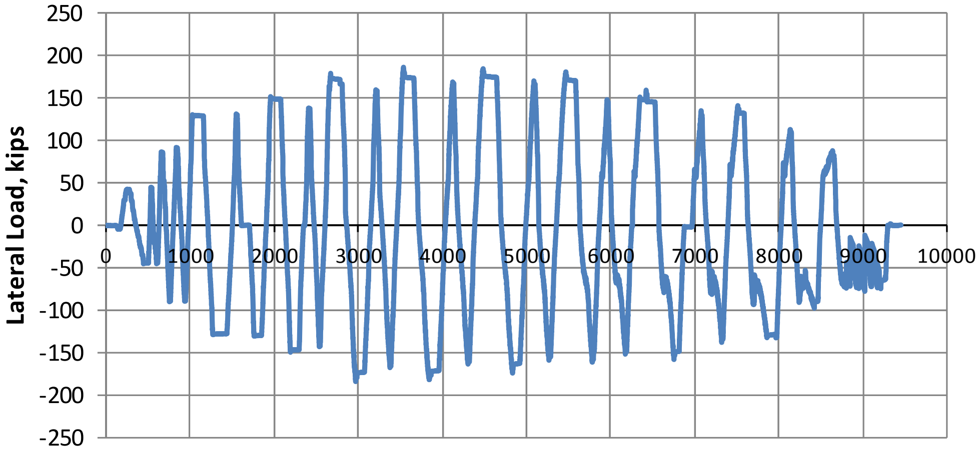

Figure D.47 Actual lateral loading history for Specimen UT-PBS-09

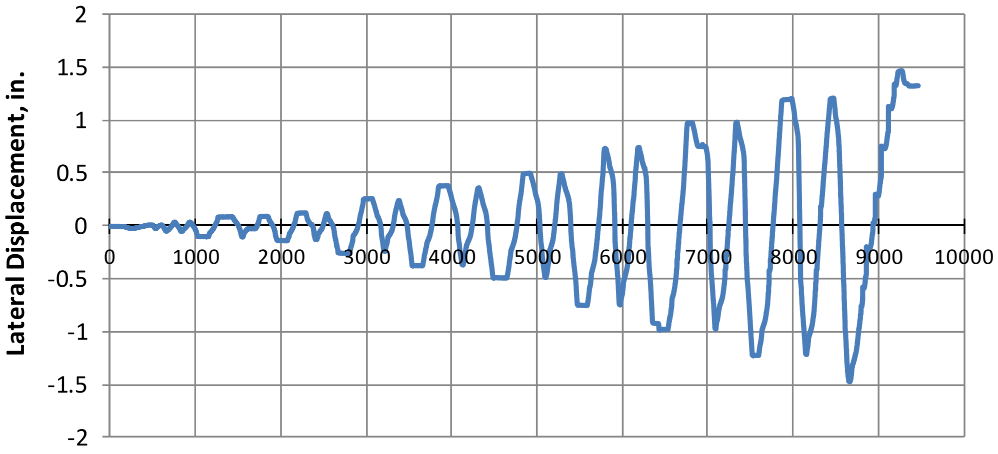

Figure D.48 Actual lateral displacement history for Specimen UT-PBS-09

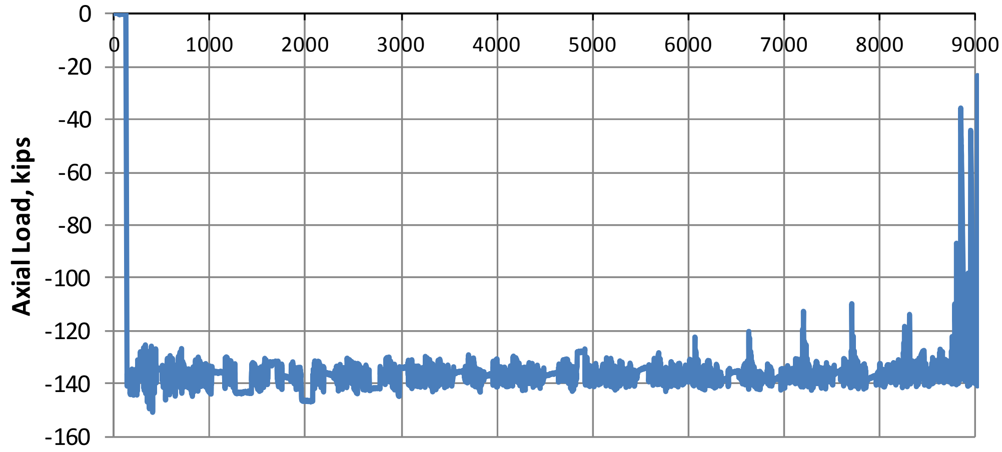

Figure D.49 Actual axial load history for Specimen UT-PBS-09

D.4.2 Sequence of Crack Formation for Specimen UT-PBS-09

The sequence of crack formation in Specimen UT-PBS-09 is described in terms of major events: drift ratios during the test when the condition of the specimen changed (for example, flexural cracking or shear cracking). Table D-4 lists the major events and the load point at which they occurred. In the following figures, where crack maps are presented for some of the major events, cracks that formed on loading to the north are shown in black, and cracks that formed on loading to the south are shown in red.

D.4.2.1 Flexural and web-shear cracking in Specimen UT-PBS-09

Major Events 1 and 2, as shown in Figure D.50, correspond to flexural cracking and web-shear cracking. At the drift ratio of 0.13%, flexural cracks formed while loading to the north and south at a load of 130.5 kips. Also, in these major events correspond to the formation of web-shear cracking while loading to the north and south respectively. A web-shear crack formed along the entire height of the wall while loading to the south at a base shear and drift ratio of 130.5 kips and 0.13%, respectively. In addition to while loading to the north, smaller web-shear cracks formed along the wall at the same base shear and drift ratio. The prediction for web-shear cracking based on MSJC 2011 *Code* at the corresponding axial load is 123 kips. The ratio of observed to predicted web-shear cracking capacity is 1.07.

Table D-4 Description of major events for Specimen UT-PBS-09

major event	**lateral drift ratio**	**physical description**
1	0.13%	flexural cracking and web-shear cracking, loading north
2	0.13%	flexural cracking and web-shear cracking, loading south
3	0.33%	additional web-shear cracking, loading north
4	0.33%	additional web-shear cracking, loading south
5	0.67%	distributed web-shear cracking, and observed sliding, loading north
6	0.67%	distributed web-shear cracking, minor toe crushing, and observed sliding, loading south
7	1.33%	additional web-shear cracking, and observed sliding, loading north
8	1.33%	crushing and spalling of diagonal struts, spalling at toes, and observed sliding, loading south
9	2.00%	crushing and spalling of diagonal struts, spalling at toes loading north
10	end of test, 2.00%	crushing and spalling of diagonal struts, spalling at toes, and axial collapse, loading south

D.4.2.2 Additional web-shear cracking in Specimen UT-PBS-09

Major Events 3 and 4correspond to the development of additional web-shear cracks in the specimen. The base shears were 175 kips and 179 kips for loading north and loading south respectively and the drift ratio was 0.33% for both. Damage in the specimen at the end of Major Event 4 is shown in Figure D.51.

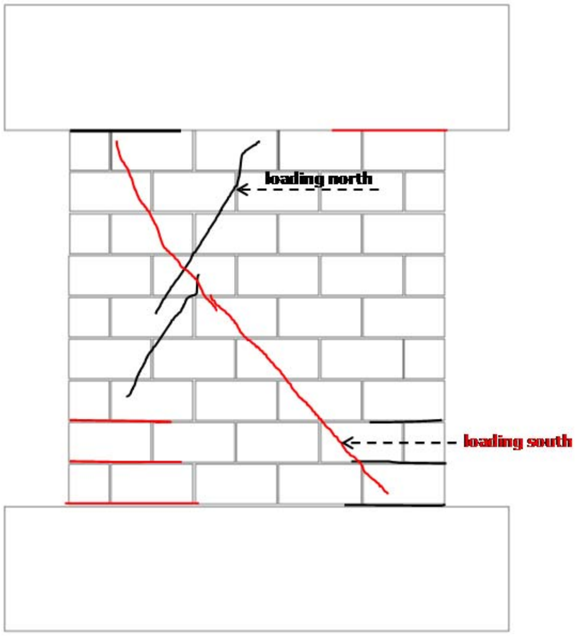

Figure D.50 Flexural cracking and web-shear cracking at 0.13% drift ratio (UT-PBS-09)

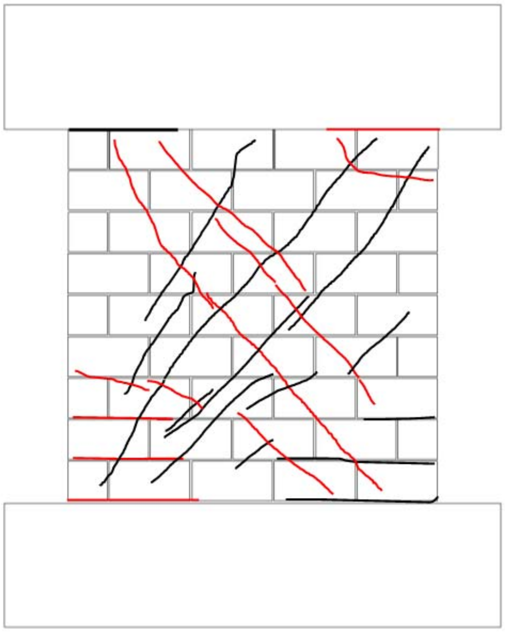

Figure D.51 Additional web-shear cracking at 0.33% drift ratio (UT-PBS-09)

D.4.2.3 Distributed web-shear cracking and observed sliding in Specimen UT-PBS-09

Major Events 5 and 6 corresponded to distributed web-shear cracks combined with sliding at both directions and minor crushing in the south compression toe, as shown in Figure D.52. As the load continued to increase to the north, more web-shear cracks occurred in the specimen. In addition to during cyclic loading north at drift ratio of 0.67%, it was clear the wall had slid at the base at a load of 186 kips. Similar damage occurred while loading to the south at a drift ratio of 0.67%, and as the wall was loaded to the south sliding was also observed at a load of 163 kips. Crushing of the lower south end toe also occurred at this drift ratio. In both loading directions this damage was also combined with a 0.10-in. opening of the web-shear cracks over the wall height.

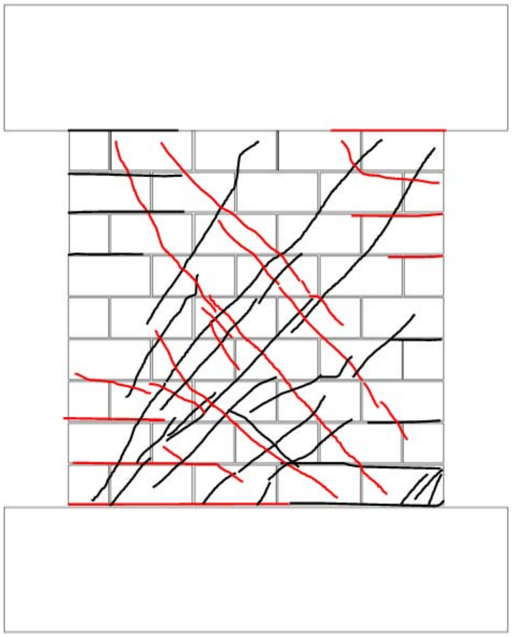

Figure D.52 Distributed web-shear cracking and observed sliding at drift ratio of 0.67% (UT-PBS-09)

D.4.2.4 Crushing and spalling of diagonal struts and observed sliding, in Specimen UT-PBS-09

In the Major Events 7 and 8, vertical cracks propagated from the horizontal crack at the south toe caused crushing and spalling of diagonal struts and toes combined with significant sliding at both directions. While loading to the north, at the total drift ratio of 1.33% distributed web-shear cracks combined with significant sliding at the base of the wall. Similar damage occurred while loading to the south at a total drift ratio of 1.33%, in addition to extensive spalling occurred on both faces of the wall at the lower south end as shown in Figure D.53.

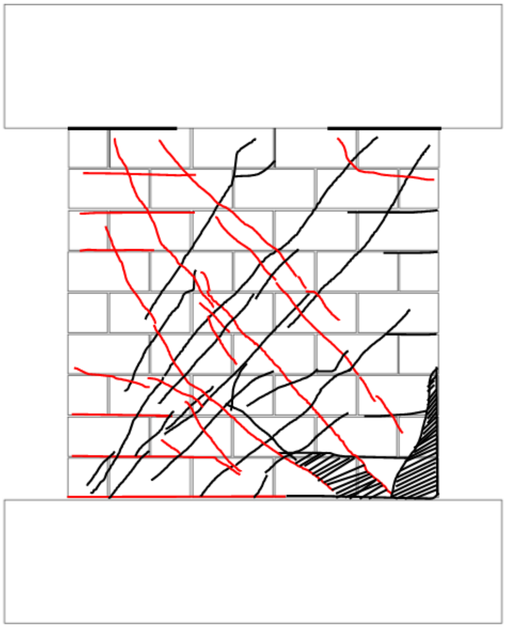

Figure D.53 Crushing and spalling of diagonal struts and observed sliding at drift ratio of 1.33% (UT-PBS-09)

D.4.2.5 Crushing and spalling of the compression diagonal struts at the base in Specimen UT-PBS-09

Finally, in the last two cycles of the test (Major Events 9 and 10), severe spalling at the compression toes and extensive crushing of diagonal were observed at drift ratio of 2.00% at the base while loading to the north. This damage combined with significant 0.75-in. sliding at the base. In Major Event 10, similar damage occurred while loading to the south at a total drift ratio of 2.00%, and vertical cracks were observed at the south end while loading to the south. In the middle of loading south the specimen collapsed axially, and the loading beam moved downward about 1.0 in. The test was unloaded after Major Event 10 due to instability of test setup and axial load system. The extent of severe crushing at the base is shown in Figure D.54. As shown in Figure D.55, reversed cyclic loading caused extensive crushing and spalling at the base of the specimen.

Figure D.54 Specimen UT-PBS-09 at end of test

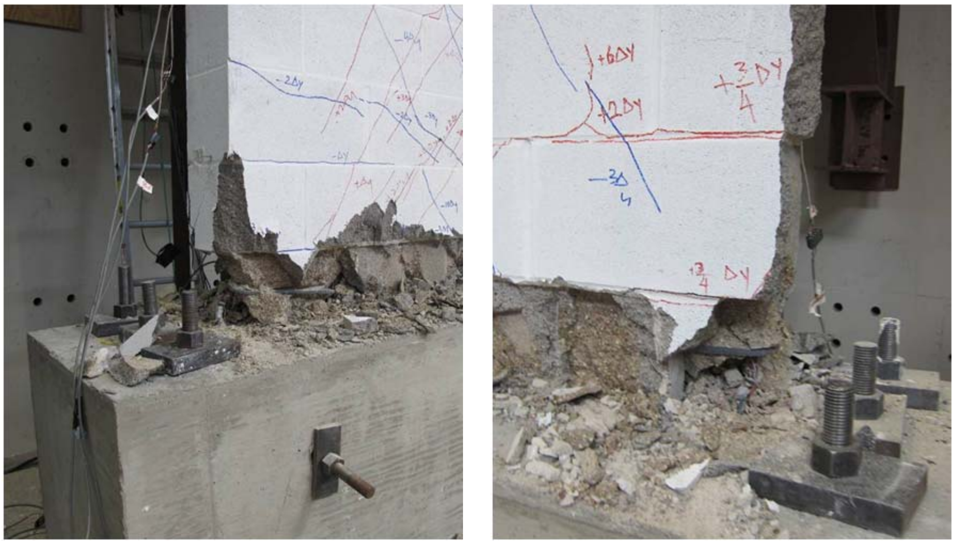

Figure D.55 Detail of severe spalling and crushing at the compression toes (UT-PBS-09)

D.4.3 Load-Displacement Behavior for Specimen UT-PBS-09

The load-displacement relationship of Specimen UT-PBS-09 is presented in Figure D.56 in terms of the non-dimensional drift ratio, which references seven major events during testing:

1) first web-shear cracking
2) first yield of the extreme vertical reinforcement ($\varepsilon_y = 0.0021$);
3) first yield of the horizontal reinforcement ($\varepsilon_y = 0.0021$);
4) maximum useful strain in the masonry ($\varepsilon_{mu} = 0.0025$);
5) maximum capacity (capping point);
6) onset of crushing of toes or diagonal struts; and
7) decrease in capacity to 50% of maximum capacity.

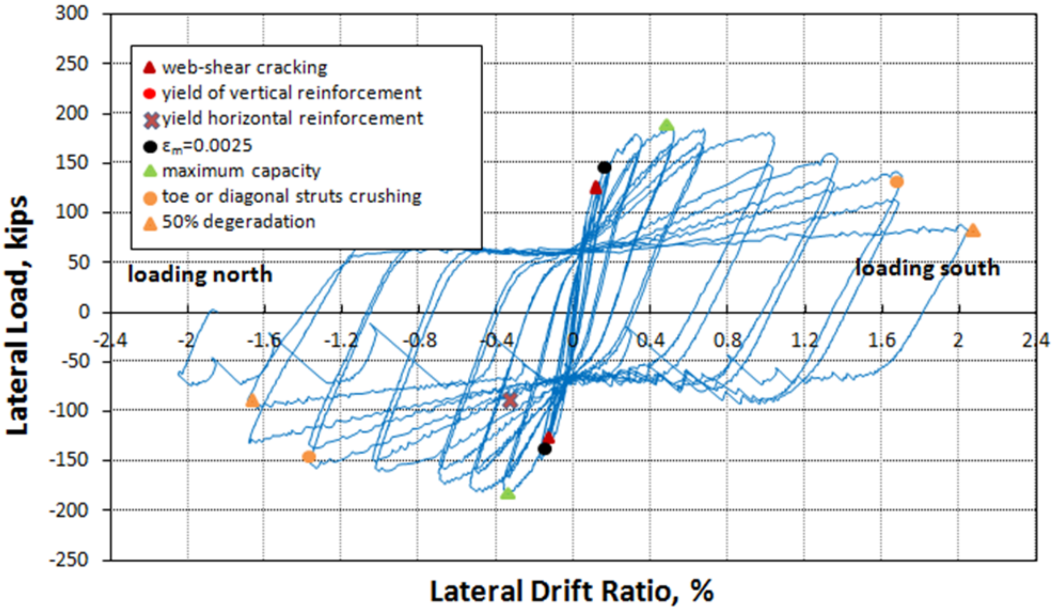

Figure D.56 Load versus top drift ratio (UT-PBS-09)

D.4.4 Components of Displacements and Drifts

Linear potentiometers recorded the average sliding displacements between the wall base and the base beam. Sliding was also measured between the top of the wall and the top concrete beam. These load-sliding curves for the top and the base of wall are shown in Figure D.57.

Shear displacements were measured with two diagonally- and two vertically-oriented linear potentiometers and were calculated based on a previous study by Massone (2004). Load-displacement curves for sliding and shear component of displacement are given in Figure D.58 and Figure D.59, and total displacement and shear deformation are compared in Figure D.60.

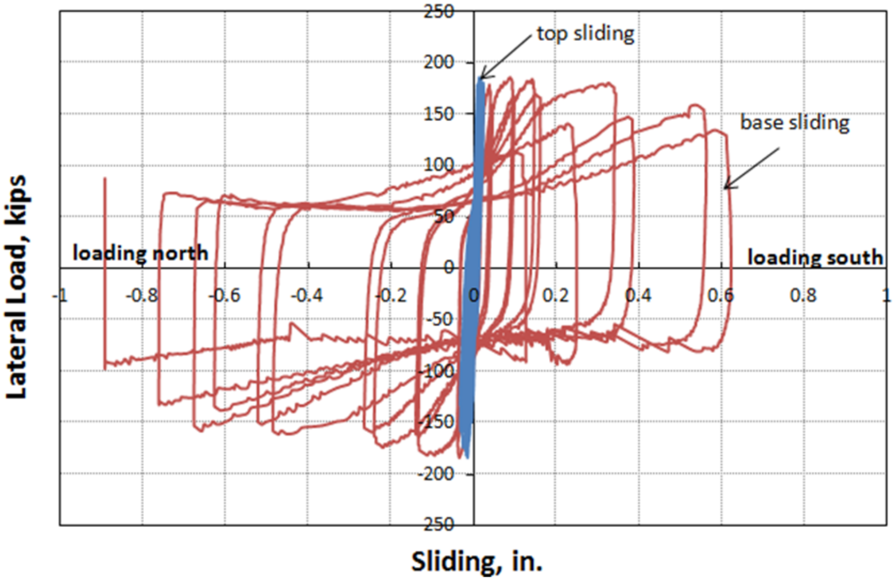

Figure D.57 Curves of load versus sliding at top and base (UT-PBS-09)

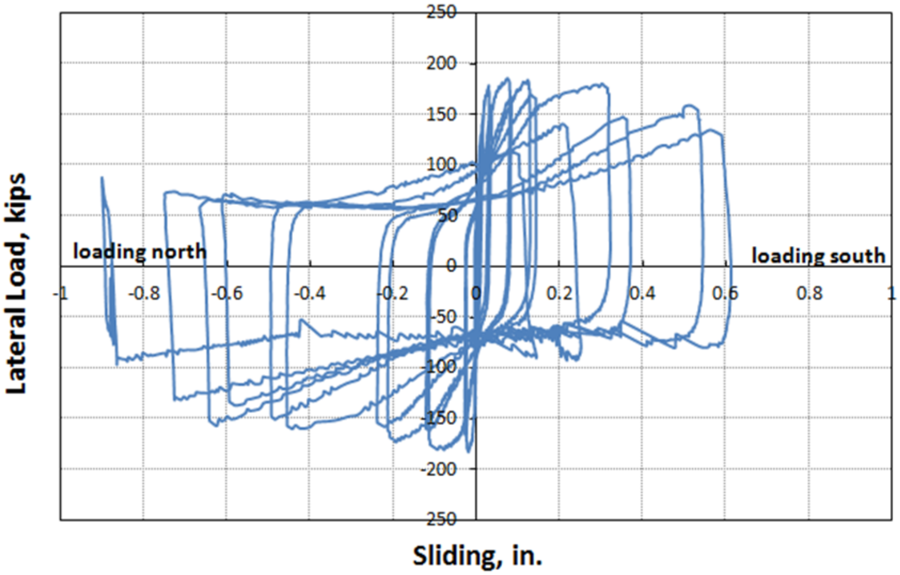

Figure D.58 Total sliding versus lateral load (UT-PBS-09)

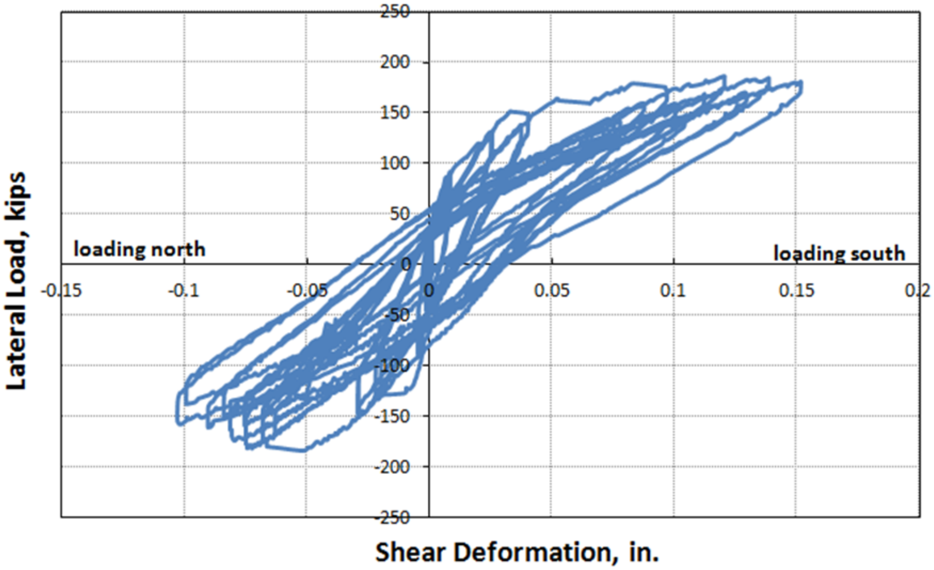

Figure D.59 Shear deformation versus lateral load (UT-PBS-09)

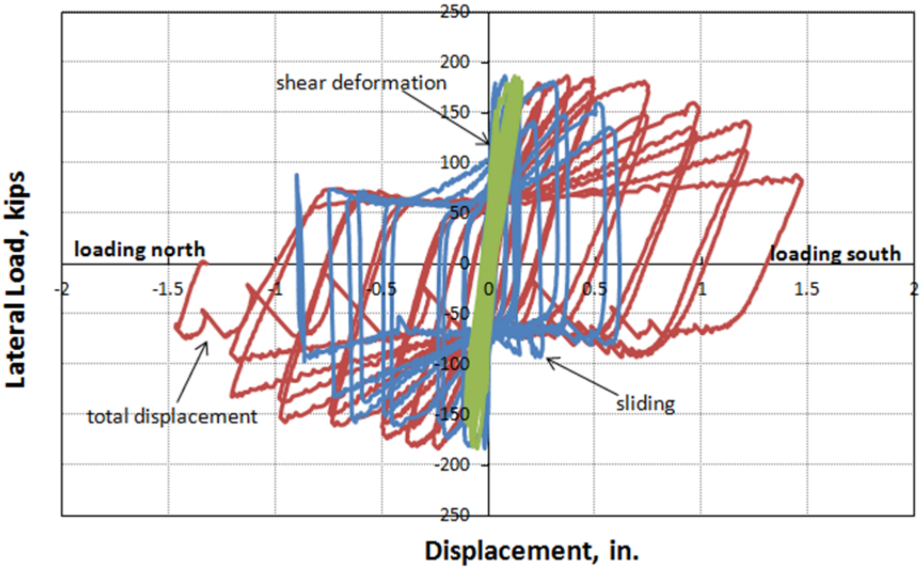

Figure D.60 Comparison of total top displacement and shear deformation (UT-PBS-09)

D.5 SHEAR WALL SPECIMEN UT-PBS-10

An interaction diagram for base shear capacity as a function of axial load for Specimen UT-PBS-10 is presented in Figure D.61. The axial load applied to Specimen UT-PBS-10 was 136.6 kips, as shown by a dashed horizontal line in Figure D.61. At this level of axial load the following major events are predicted in order of occurrence: web-shear cracking; shear yielding; shear sliding (based on shear dowel action); and flexural yielding.

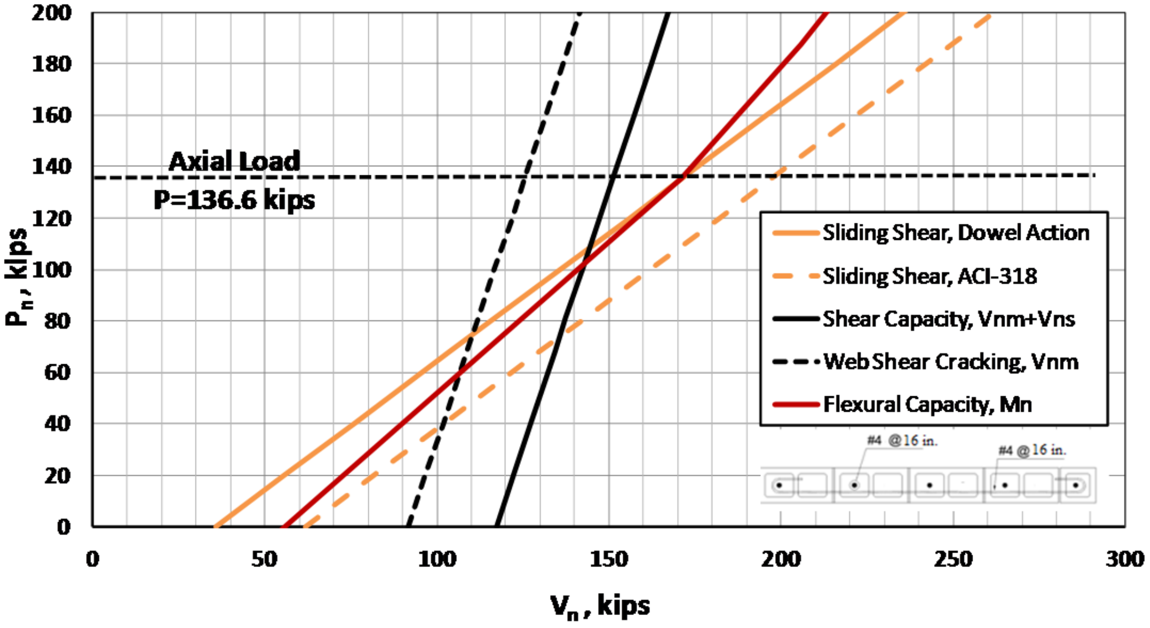

Figure D.61 Strength interaction diagram for Specimen UT-PBS-10

Specimen UT-PBS-10 before testing is shown in Figure D.62.

Figure D.62 Specimen UT-PBS-10 before testing

D.5.1 Loading History and Major Events for Specimen UT-PBS-10

Specimen UT-PBS-10 was first subjected to a preliminary test phase to estimate the yield displacement, Δ_y. A moment-curvature analysis of the specimen was used to estimate the maximum moment capacity, which was then converted to a peak horizontal load capacity. The specimen was subjected to two reversed cycles of load of ±25%, ±50%, and ±75% of that peak horizontal load capacity. The displacement from the first cycle to 75% of that peak horizontal load capacity was used to establish the probable Δ_y, by extrapolating the displacement at 75% of the maximum load to the displacement at 100% of the maximum load (displacement at 100% maximum load equal to 4/3 times displacement at 75% maximum load. Lateral yield displacement was determined as 0.12

in. On May 4, 2012, Specimen UT-PBS-10 was loaded two cycles of reversed displacements of ±1, 2, 3, 4, 6, 8, 10 and 12 times that predicted yield displacement. It was then loaded to a half-cycle to a displacement of 14 times that predicted yield displacement. The test was stopped when the peak capacity dropped to 20% or less of the experimentally observed maximum capacity (capping point). The testing took about 8 hours. The actual lateral loading, lateral displacement, and axial load histories for Specimen UT-PBS-10 are presented in Figure D.63 through Figure D.65. Loading to the north is considered positive; loading to the south, negative. Compressive axial loads are considered negative. In this test the specimen was loaded first to the north and then to the south.

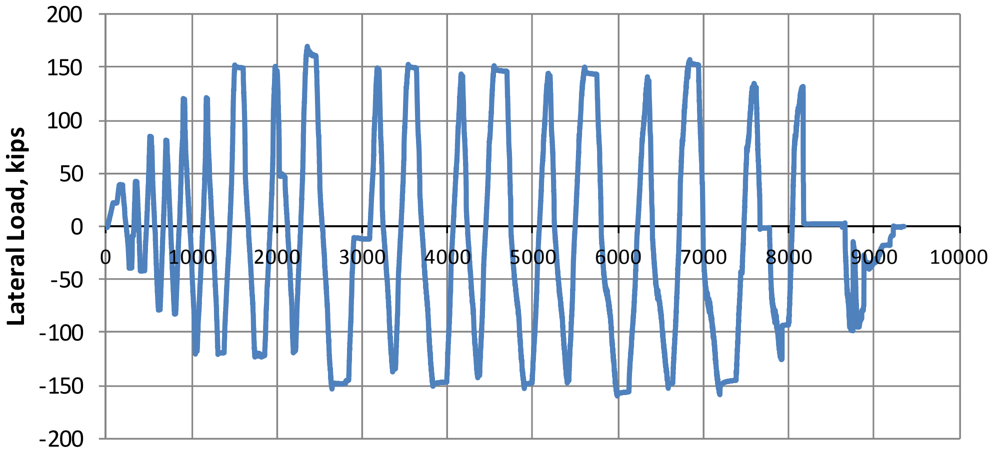

Figure D.63 Actual lateral loading history for Specimen UT-PBS-10

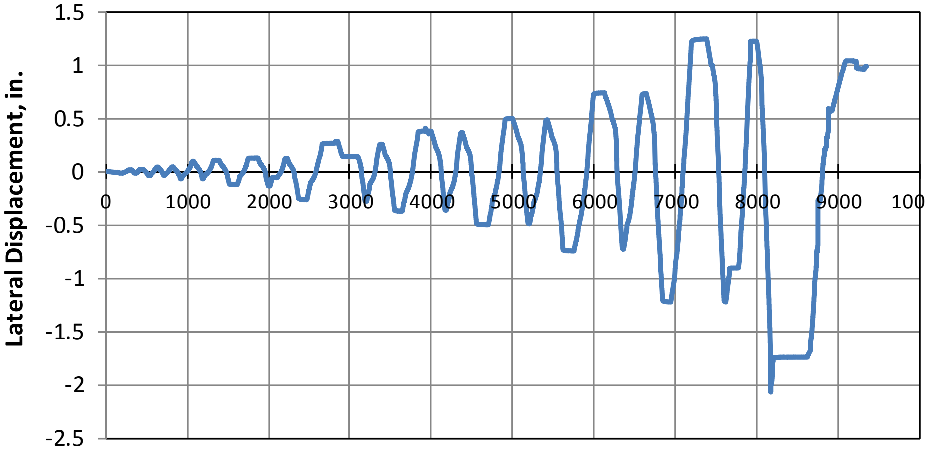

Figure D.64 Actual lateral displacement history for Specimen UT-PBS-10

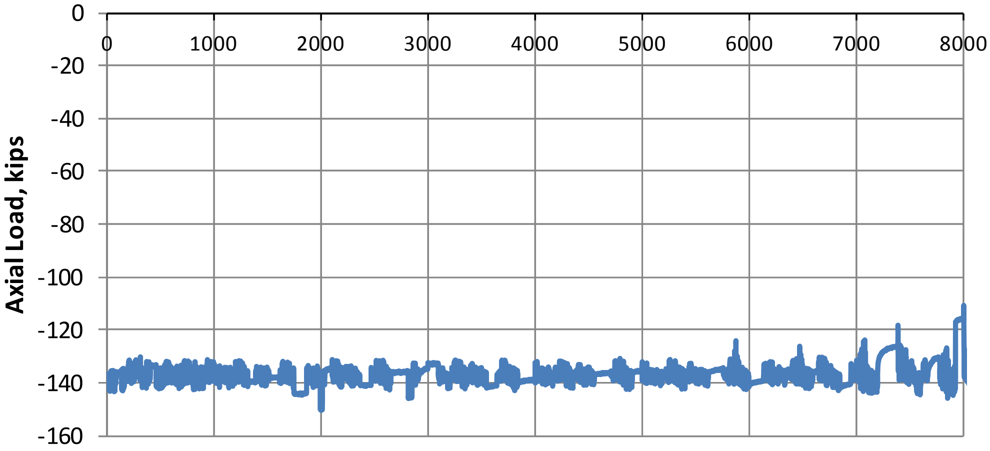

Figure D.65 Actual axial load history for Specimen UT-PBS-10

D.5.2 Sequence of Crack Formation for Specimen UT-PBS-10

The sequence of crack formation in Specimen UT-PBS-10 is described in terms of major events: drift ratios during the test when the condition of the specimen changed (for example, flexural cracking or shear cracking). Table D-5 lists the major events and the drift ratio at which they occurred. In the following figures, where crack maps are presented for some of the major events, cracks that formed on loading to the north are shown in black, and cracks that formed on loading to the south are shown in red.

D.5.2.1 Flexural and web-shear cracking in Specimen UT-PBS-10

Major Events 1 and 2, as shown in Figure D.66, correspond to flexural cracking and web-shear cracking. At the drift ratio of 0.17%, flexural cracks and web-shear cracks formed while loading to the north and south directions at a load of 151 and 135 kips. A web-shear crack formed along the entire height of the wall while loading to the north at a base shear and drift ratio of 151 kips and 0.17%, respectively. In addition, while loading to the south, q smaller web-shear cracks formed along the wall at a base shear and drift ratio of 135 kips and 0.17%. The predicted nominal capacity in web-shear cracking based on MSJC 2011 *Code* at the corresponding axial load is 126 kips. The ratios of observed to predicted web-shear cracking capacity are 1.19 and 1.07 for loading in north and south directions, respectively.

Table D-5 Description of major events for Specimen UT-PBS-10

major event	lateral drift ratio	physical description
1	0.17%	flexural cracking and web-shear cracking, loading north
2	0.17%	flexural cracking and web-shear cracking, loading south
3	0.50%	additional web-shear cracking and observed sliding,, loading north
4	0.50%	additional web-shear cracking and observed sliding,, loading south
5	1.00%	severe sliding and minor crushing of diagonal struts, loading north
6	1.00%	severe sliding and minor crushing of diagonal struts, loading south
7	2.00%	severe sliding and minor crushing of diagonal struts and spalling at toes, loading north
8	2.00%	crushing and spalling of diagonal struts, spalling at toes, and wide opened wide diagonal shear crack, loading south
9	end of test	shear failure and axial collapse

D.5.2.2 Additional web-shear cracking and observed sliding in Specimen UT-PBS-05

Major Events 3 and 4 correspond to the development of additional web-shear cracks and sliding in the specimen. The base shears were 175 kips and 151 kips for loading north and loading south respectively and the drift ratio was 0.50% for both. Damage in the specimen at the end of Major Event 4 is shown in Figure D.67. In these major events web-shear cracks combined with sliding at both directions. During cyclic loading north at drift ratio of 0.50%, it was clear the wall had slid at the base at a load of 175 kips. Similar damage occurred while loading to the south at a drift ratio of 0.50%, and as the wall was loaded to the south sliding was also observed at a load of 151 kips. In addition, a web-shear crack formed along the entire height of the wall while loading to the south at this drift ratio as shown in Figure D.67.

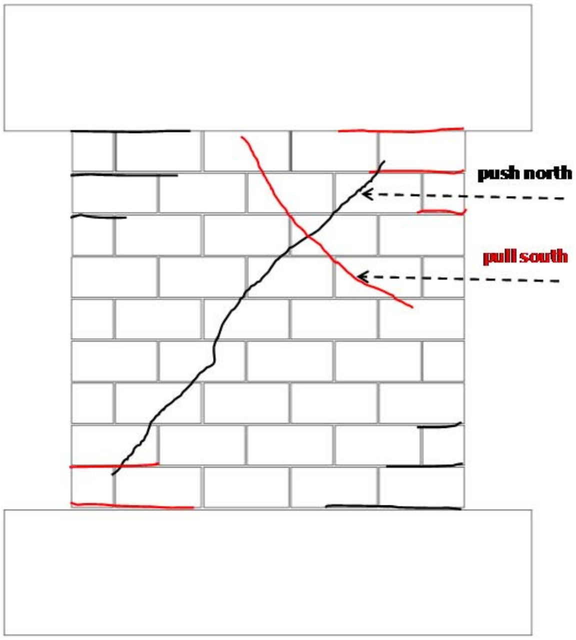

Figure D.66 Flexural cracking and web-shear cracking at 0.17% drift ratio (UT-PBS-10)

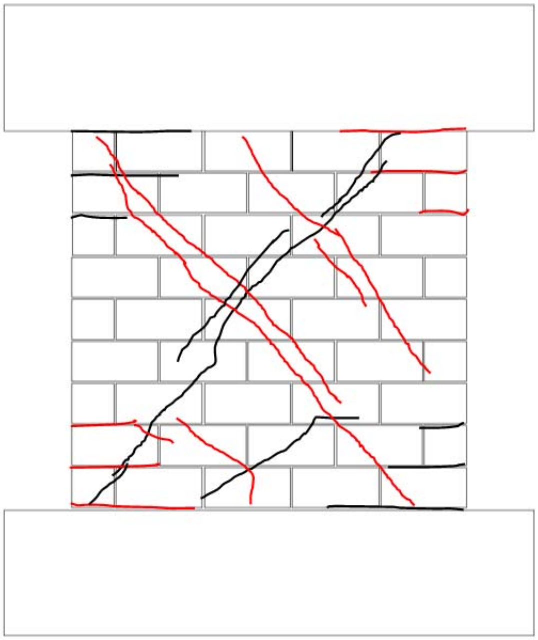

Figure D.67 Additional web-shear cracking and sliding at 0.50% drift ratio (UT-PBS-10)

D.5.2.3 Severe sliding and minor crushing of diagonal struts, loading north in Specimen UT-PBS-10

In the Major Events 5 and 6, because of reversed sliding at the base of the specimen, vertical cracks propagated from the horizontal crack at the toes, causing crushing and spalling at the toes. Major Event 5 was observed sliding at top and base of the wall, combined with minor spalling in the compression toe. While loading to the north, at a total drift ratio of 1.00% and a base shear of 148 kips, significant sliding occurred at the base and top of the wall, combined with minor crushing of diagonal struts and toes at the base (Figure D.68). Similar damage occurred while loading to the south at a total drift ratio of 1.00%, and as the wall was loaded to the north, significant sliding was also observed at a load of 160 kips.

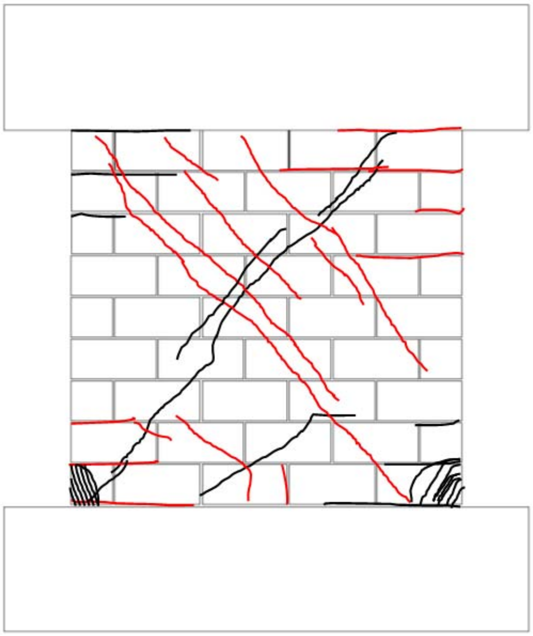

Figure D.68 Distributed open web-shear cracks at 0.58% drift ratio(UT-PBS-10)

D.5.2.4 *Crushing and spalling of compression toe and diagonal struts in Specimen UT-PBS-10*

In the last two cycles of the test, in Major Events 7 and 8, severe spalling at the compression toes and crushing of diagonal were observed at a drift ratio of 2.00% for southward loading. In Major Event 7, vertical cracks were observed at the lower north corner and lower south end while loading to the north, combined with shear sliding at top and base of the wall segment. As the load continued to increase to the south, a 0.25-in. gap formed in the web-shear crack along the entire height of the wall, and spalling occurred at the toes and diagonal struts at a drift ratio of 2.00%, as shown in Figure D.69.

The test was unloaded and discontinued after Major Event 8 due to crushing of the diagonal struts and compression toes, significant spalling of the diagonal strut face shells, and opening of the web-shear crack of 1.25 in. This damage at the end of test is shown in Figure D.69 and Figure D.70. As shown in Figure D.70, reversed cyclic loading caused diagonal strut crushing, toe crushing, and spalling of the specimen.

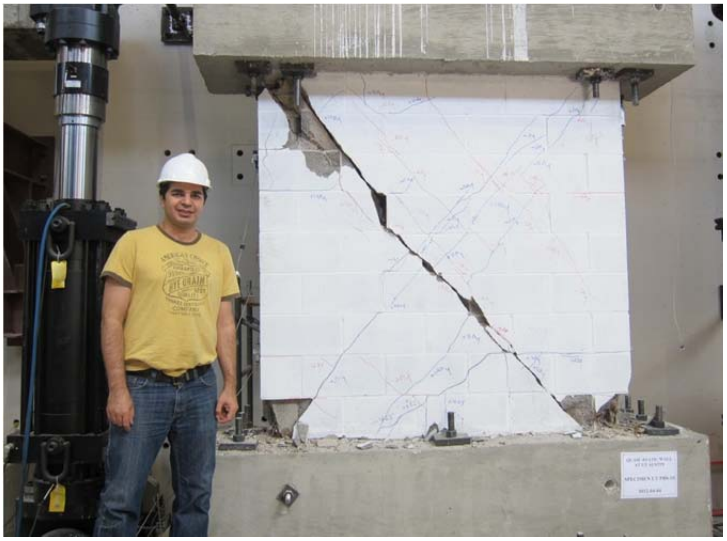

Figure D.69 Crushing and spalling of compression toe and diagonal struts at 2.00% drift ratio (UT-PBS-10)

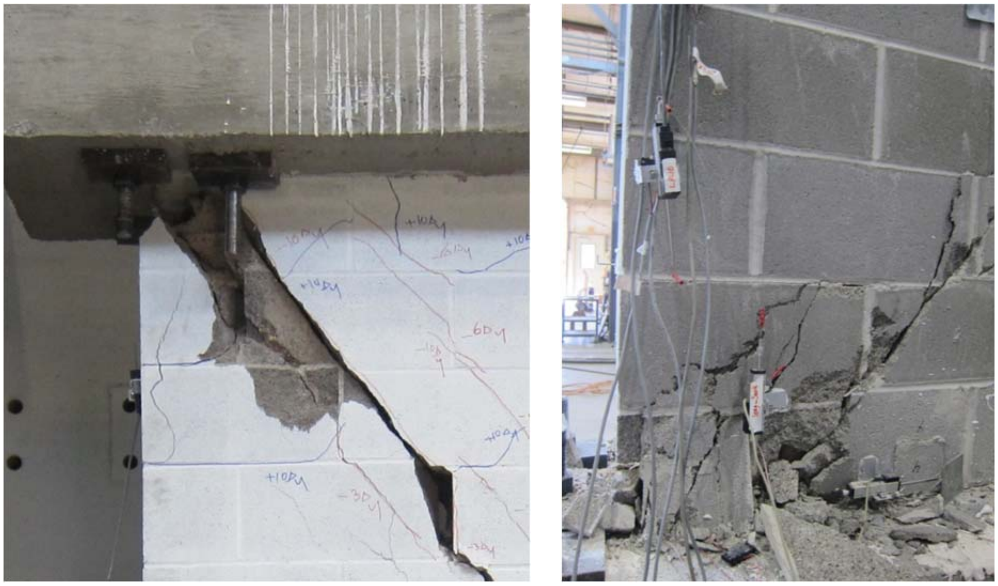

Figure D.70 Crushing and spalling of compression toe and diagonal struts at end of test (UT-PBS-10)

D.5.3 Load-Displacement Behavior for Specimen UT-PBS-10

The load-displacement relationship of Specimen UT-PBS-10 is presented in Figure D.71 in terms of the non-dimensional drift ratio, which references seven major events during testing:

1) first web-shear cracking
2) first yield of the extreme vertical reinforcement ($\varepsilon_y = 0.0021$);
3) first yield of the horizontal reinforcement ($\varepsilon_y = 0.0021$);
4) maximum useful strain in the masonry ($\varepsilon_{mu} = 0.0025$);
5) maximum capacity (capping point);
6) onset of crushing of toes or diagonal struts; and
7) decrease in capacity to 50% of maximum capacity.

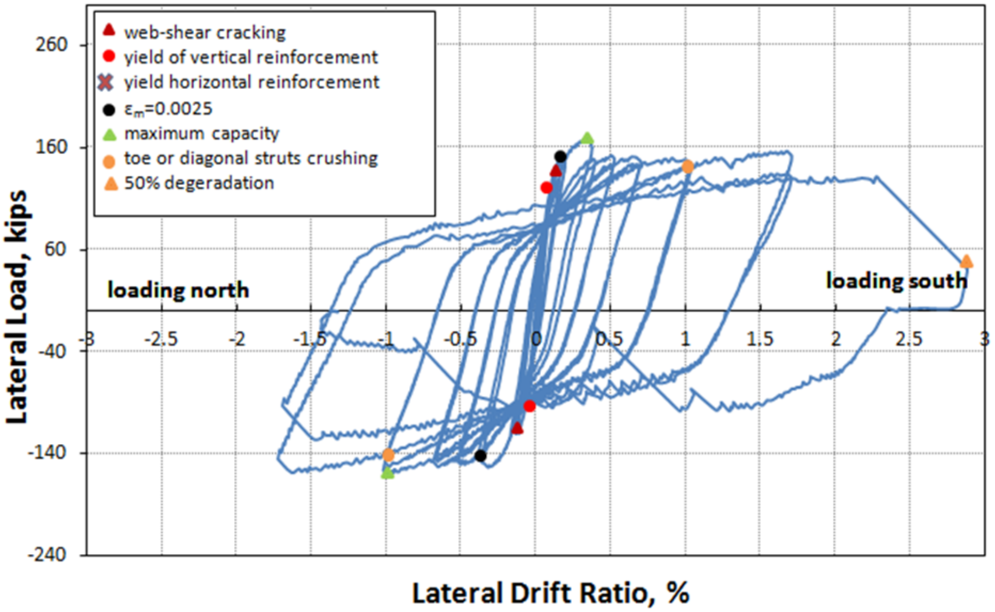

Figure D.71 Lateral load versus top drift ratio (UT-PBS-10)

D.5.4 Components of Displacements and Drifts

Linear potentiometers recorded the average sliding displacements between the wall base and the base beam. Sliding was also measured between the top of the wall and the top concrete beam. These load-sliding curves for the top and the base of wall are shown in Figure D.72. Load-displacement curves for total sliding component of total tip displacement are given in Figure D.73, and comparison between total displacement and total sliding is shown in Figure D.74.

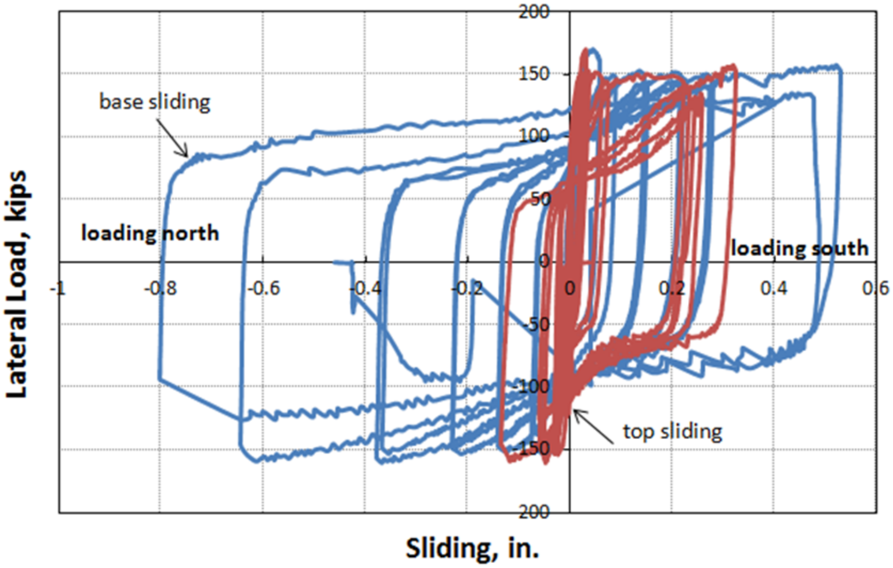

Figure D.72 Curves of load versus sliding at top and base (UT-PBS-10)

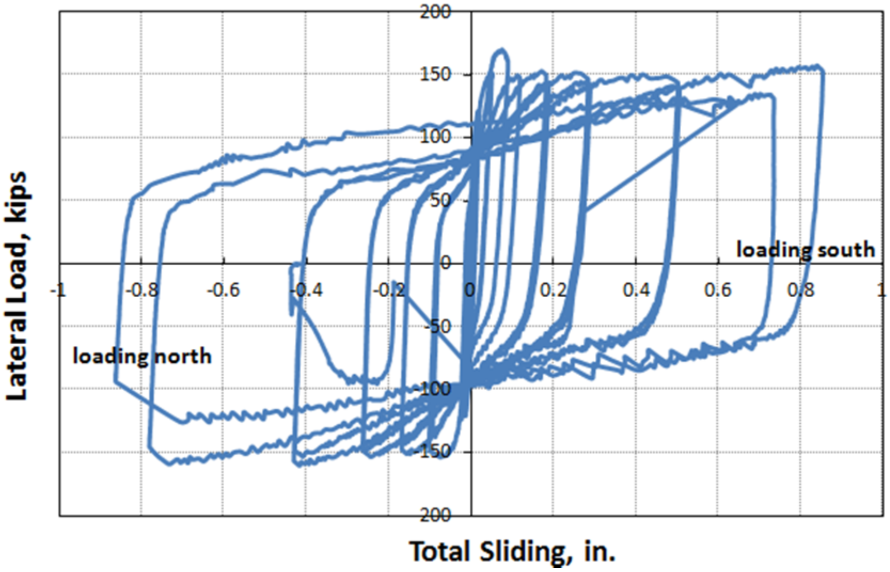

Figure D.73 Total sliding versus lateral load (UT-PBS-10)

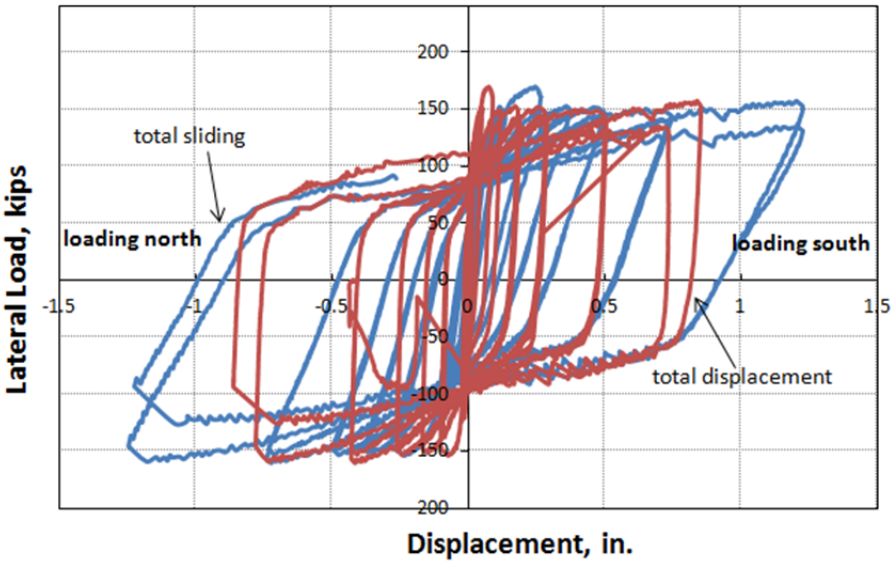

Figure D.74 Comparison of total top displacement and sliding (UT-PBS-10)

APPENDIX E

PRELIMINARY STRENGTH DESIGN OF FULL-SCALE, THREE-STORY SPECIMEN

E.1 Plan and Elevation of Prototype Building

The typical plan and elevation of the prototype building are shown in Figure E.1 and Figure E.2.

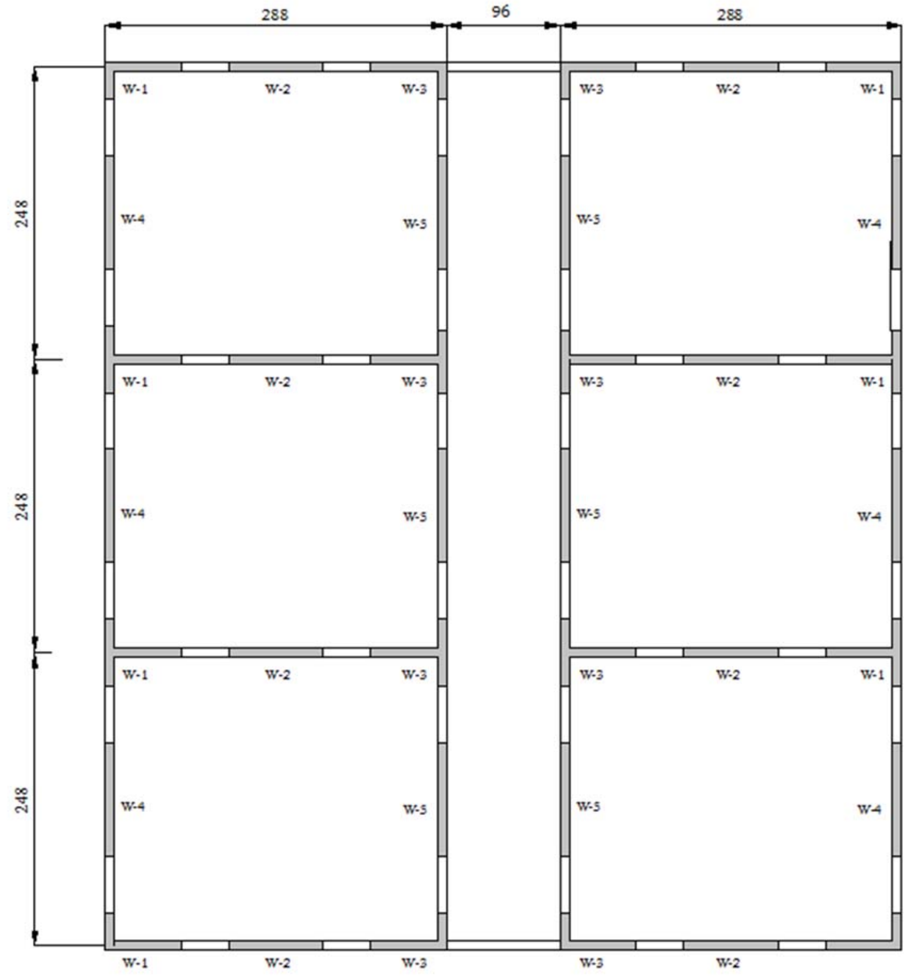

Figure E.1 Plan view of typical floor of three-story prototype building

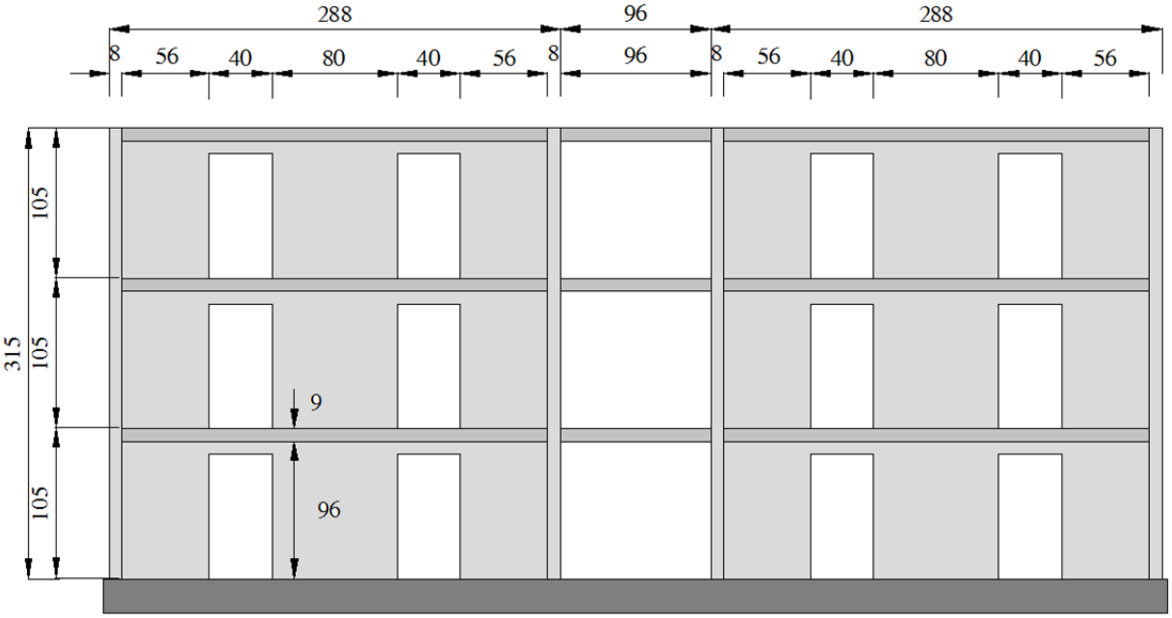

Figure E.2 Elevation of three-story prototype building (dimensions in inches)

E.2 PLAN AND ELEVATION OF SPECIMEN

On the plan view shown in Figure E.3 the dashed rectangle shows the plan area occupied by the specimen. In the specimen, the walls parallel to the direction of shaking are two symmetrical T-walls and one lineal wall. The walls perpendicular to the direction of shaking are two lineal half-walls. For consistency in describing the specimen, the walls parallel to the direction of shaking are described as "longitudinal" walls, and the walls perpendicular to the direction of shaking are described as "transverse" walls. This admittedly could be a little confusing, because those descriptions are actually opposite to the sense of those walls in the complete prototype building. Nevertheless, the descriptions are very clear for the specimen itself, and we shall be discussing the specimen much more than the complete prototype building.

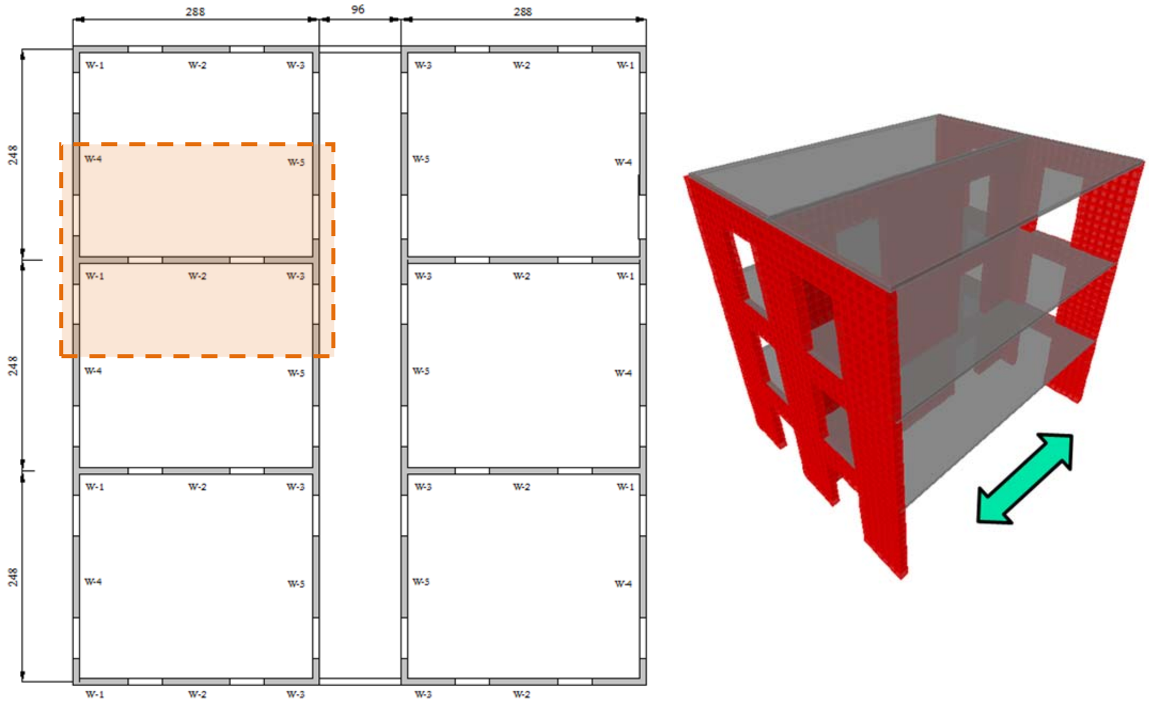

Figure E.3 Plan area and 3D view of the specimen

E.3 DESIGN GRAVITY LOADS

E.3.1 Design Roof Load due to Gravity

Design roof load due to gravity is calculated below.

Dead Load	9-in. slab (6-in. hollow-core slab + 3-in.topping)	80 lb/ft^2
	HVAC, Electrical and Plumbing	15 lb/ft^2
		95 lb/ft^2 total
Live Load	Live load	20 lb/ft^2

E.3.2 Design Floor Load due to Gravity

Design floor load due to gravity is calculated below:

Dead Load	9-in. slab (6-in. hollow-core slab + 3-in. topping)	80 lb/ft^2
	Partitions	15 lb/ft^2
	HVAC, Electrical and Plumbing	15 lb/ft^2
		110 lb/ft^2 total
Live Load	Live load	40 lb/ft^2

E.3.3 Design Lateral Load from Earthquake

Design earthquake loads are calculated according to Section 1613 of the 2009 IBC. That section essentially references *ASCE 7-05 (Supplement)*. Seismic design criteria are given in Chapter 11. The seismic design provisions of ASCE 7-05 (Supplement) begin in Chapter 12 of ASCE7-05, which prescribes basic requirements (including the requirement for continuous load paths) (Section 12.1); selection of structural systems (Section 12.2); diaphragm characteristics and other possible irregularities (Section 12.3); seismic load effects and combinations (Section 12.4); direction of loading (Section 12.5); analysis procedures (Section 12.6); modeling procedures (Section 12.7); and specific design approaches. Four procedures are prescribed: an equivalent lateral force procedure (Section 12.8); a modal response-spectrum analysis (Section 12.9); a simplified alternative procedure (Section 12.14); and a seismic response history procedure (Chapter 16 of ASCE7-05). The equivalent lateral-force procedure is described here, because it is relatively simple, and is permitted in most situations. The simplified alternative procedure is permitted in only a few situations. The other procedures are permitted in all situations, and are required in only a few situations.

Step 1: Determine S_S, the mapped MCE (maximum considered earthquake), 5-percent damped, spectral response acceleration parameter at short periods as defined in Section 11.4.1 of ASCE7-05.

Step 2: Determine S_1, the mapped MCE, 5-percent damped, spectral response acceleration parameter at a period of 1 second as defined in Section 11.4.1 of ASCE7-05.

Determine the parameters S_s and S_1 from the 0.2-second and 1-second spectral response maps shown in Figures 22-1 through 22-7 of ASCE7-05.

For San Diego, California, $S_S = 1.50$ g, and $S_1 = 0.60$ g.

Step 3: Determine the *site class (A* through *F*, a measure of soil response characteristics and soil stability) in accordance with Section 20.3 and Table 20.3-1 of ASCE7-05.

Assume Site Class D (stiff soil).

Step 4: Determine the MCE spectral response acceleration for short periods (S_{MS}) and at 1 second (S_{M1}), adjusted for Site Class effects, using Equations 11.4-1 and 11.4-2 (ASCE7-05), respectively.

The acceleration-dependent site coefficient, F_a, is 1.0 (Table 11.4-1).

The velocity-dependent site coefficient, F_v, is 1.5 (Table 11.4-2).

Then the maximum considered short-period response acceleration is:

$$S_{MS} = F_a \cdot S_s = 1.0 \cdot 1.50g = 1.5g$$

And the maximum considered 1-second response acceleration is:

$$S_{M1} = F_v \cdot S_1 = 1.5 \cdot 0.60g = 0.9g$$

Step 5: Determine the design response acceleration parameter for short periods, S_{DS}, and for a 1-second period, S_{D1}, using Equations 11.4-3 and 11.4-4 (ASCE7-05), respectively.

The design response acceleration is two-thirds of the maximum considered acceleration. For San Diego, California, the design response acceleration for short periods is:

$$S_{DS} = \frac{2}{3} \cdot S_{MS} = \frac{2}{3} \cdot 1.5g = 1.0g$$

and the design response acceleration for a 1-second period is:

$$S_{D1} = \frac{2}{3} \cdot S_{M1} = \frac{2}{3} \cdot 0.9g = 0.60g$$

Step 6: If required, determine the design response spectrum curve as prescribed by Section 11.4.5.

Because the equivalent lateral force procedure is being used, the response spectrum curve is not required. Nevertheless, it for completeness, it is shown here.

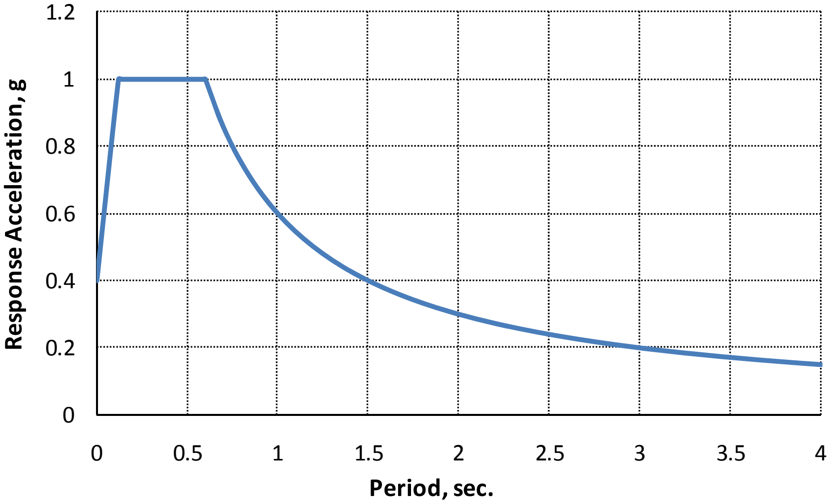

Figure E.4 Design response spectrum for San Diego, CA

Step 7: Determine the structure's importance factor, *I*, and occupancy category using Section 11.5.

Assume that the structure is assigned an Occupancy Category II. This corresponds to an Importance Factor of 1.0.

TABLE 11.5-1 IMPORTANCE FACTORS

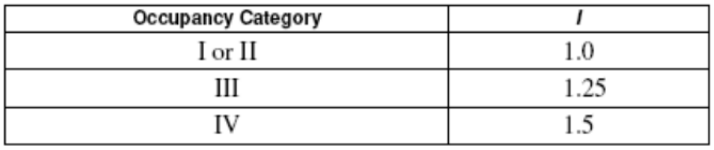

Occupancy Category	*I*
I or II	1.0
III	1.25
IV	1.5

Step 8: Determine the structure's Seismic Design Category using Section 11.6.

Because S_{D1} exceeds 0.20, the structure is assigned to Seismic Design Category D.

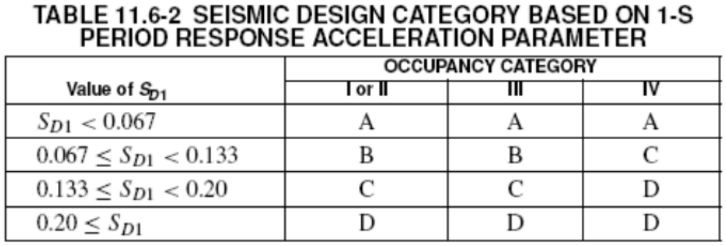

TABLE 11.6-2 SEISMIC DESIGN CATEGORY BASED ON 1-S PERIOD RESPONSE ACCELERATION PARAMETER

Value of S_{D1}	OCCUPANCY CATEGORY		
	I or II	III	IV
$S_{D1} < 0.067$	A	A	A
$0.067 \leq S_{D1} < 0.133$	B	B	C
$0.133 \leq S_{D1} < 0.20$	C	C	D
$0.20 \leq S_{D1}$	D	D	D

Step 9: Calculate the structure's seismic base shear using Sections 12.8.1 and 12.8.2.

In accordance with ASCE7-05 (Supplement), Section 12.8.1.1,

$$C_s = \frac{S_{DS}}{\left(\frac{R}{I}\right)}$$

Equation 12.8-2

In our case,

S_{DS} = 1.00 g

R = 5 (special reinforced masonry shear wall)

I = 1.00 (ASCE7-05, Table 11.5-1)

$$C_s = \frac{S_{DS}}{\left(\frac{R}{I}\right)} = \frac{1.00}{\left(\frac{5}{1}\right)} = 0.20$$

The value of C_s computed in accordance with Equation 12.8-2 need not exceed the following:

$$C_s = \frac{S_{D1}}{T\left(\frac{R}{I}\right)} \quad for \quad T \leq T_L$$

Equation 12.8-3

The corresponding equation for $T > T_L$ does not apply. In addition, C_s shall not be less than 0.01. In our case, the value of C_s given by Equation 12.8-3 is

$$C_s = \frac{S_{D1}}{T\left(\frac{R}{I}\right)} = \frac{0.60}{T\left(\frac{R}{I}\right)} = \frac{0.6}{5\,T} = \frac{0.12}{T}$$

And in our case, from Section 12.8.1.1 of ASCE7-05 (Supplement 2),

$$C_s = \frac{S_{D1}}{T\left(\frac{R}{I}\right)} \quad for \quad T \leq T_L$$

$$C_s = \frac{S_{D1}\,T_L}{T^2\left(\frac{R}{I}\right)} \quad for \quad T > T_L$$

On the left end of the plateau in the design response spectrum, at a period $T = T_0 =$ 0.12 sec, $C_s = 1.0$, and Equation 12.8-3 doesn't govern. Near the right end of the plateau, at $T = 0.60$ sec, $C_s = 0.20$, and Equation 12.8-3 might barely govern. Conservatively assume that the structure is stiff enough that Equation 12.8-3 doesn't govern.

Because the structure is assigned to SDC D, the redundancy factor, ρ, is assigned according to Section 12.3.4. The structure meets the required conditions for a redundancy factor, ρ, equal to 1.0.

Finally, in accordance with ASCE7-05, Section 12.4.2, the design horizontal seismic load effect E_h is

$$E_h = \rho Q_E \qquad \textbf{\textit{Equation 12.4-1}}$$

Now compute the seismic base shear. In accordance with ASCE 7-05, Section 12.8.1, the effects of horizontal seismic forces Q_E come from V. The design seismic base shear is given by:

$$\begin{aligned}
&V = C_s\, W \\
&\mathrm{T_a} = \mathrm{C_t}\ \mathrm{h_n^x} \\
&C_t = 0.02, x = 0.75 \\
&T_a = 0.02 \times 26.25^{0.75} = 0.23 \\
&C_s = \frac{1.00}{5/1} = 0.20 \\
&V = 0.20\, W
\end{aligned}$$

This is multiplied by the redundancy factor of 1.0, giving a product of 0.20. In other words, the building must be designed for 20% of its weight, applied as a lateral force.

Step 10: Distribute seismic base shear vertically using Section 12.8.3.

Beginning at this point, the design refers to the specimen, rather than the prototype building. The typical plan of the specimen, shown in Figure E.5 has a plan length of 24 ft and a plan width of 20.67 ft.

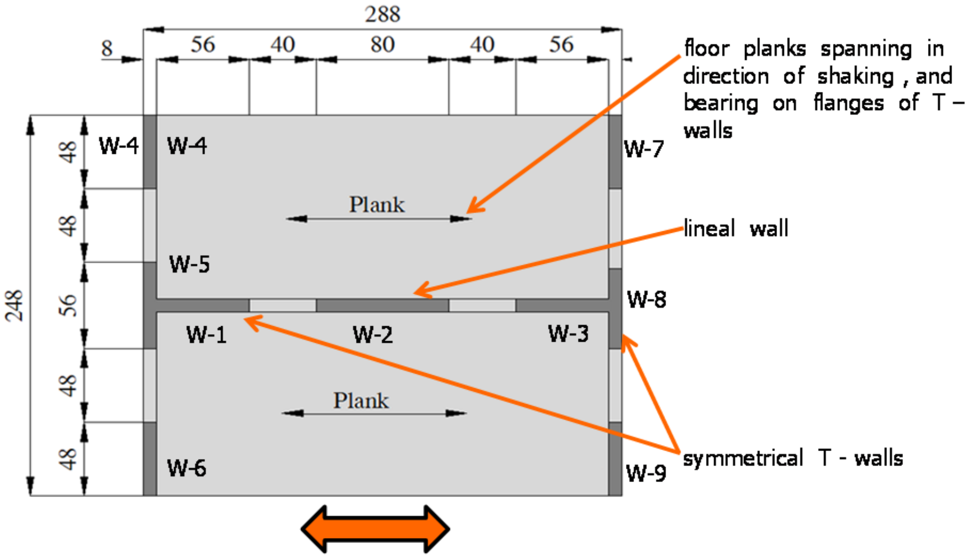

Figure E.5 Plan view of typical floor of three-story specimen

The weight of a typical floor is its area, times the dead load per square foot, plus the interior wall weight, plus the weight of the exterior walls. For the roof, the weight of floor is its area, times the dead load per square foot, plus half the longitudinal wall (interior wall weight), plus half the transverse walls (exterior walls) weight. Between story levels, half the wall weight goes to the story above, and half goes to the story below. Wall weights are computed as the weights without openings, and the weights of the openings are then subtracted.

Roof level:

Floor	95 lb/ft^2 x 20.67 x 24 ft^2	= 47.2kips
Longitudinal wall weight	1/2 x (22.67 x 8 – 2 x 6.67 x 3.33) ft^2 x 80 lb/ft^2	= 5.5 kips
Transverse wall weight	1/2x2 x (20.67 x 8 - 2 x 6.67 x 4) ft^2 x 80 lb/ft^2	= 9.0 kips

Total weight of the roof level is 61.7 kips.

First and second floor:

Floor	110 lb/ft^2 x 20.67 x 24 ft^2	= 54.6 kips
Longitudinal wall weight	(22.67 x 8 – 2 x 6.67 x 3.33) ft^2 x 80 lb/ft^2	= 10.9 kips
Transverse wall weight	2 x (20.67 x 8 - 2 x 6.67 x 4) ft^2 x 80 lb/ft^2	= 17.9 kips

Total weight of a typical floor is 83.4 kips.

The design base shear is calculated assuming a linear distribution of forces over the height of the structure. In our case the structural period is less than 0.5 sec, and k = 1.0.

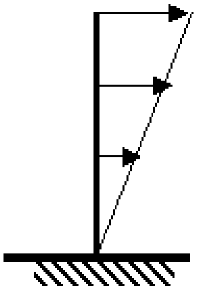

Level	W(kips)	H (ft)	WH	WH/SUM
R	61.7	26.25	1622	0.43
3	83.4	17.5	1464	0.38
2	83.4	8.75	732	0.19
Σ	228.5		3819	1.00

Total design base shear is 228.5 kips x 0.20 = 45.7 kips.

At the roof level, the factored design lateral force is the design base shear (45.7 kips), multiplied by 0.43 (the quotient of *WH/SUM*) for the triangular distribution, or 19.7 kips. At the next level down, the factored design lateral force is 45.7 kips, multiplied by 0.38, and so forth.

At each level, the design moment is the summation of the products of the design lateral forces above that level, each multiplied by its respective height above that level. Design shear and moment diagrams for the building are shown in Table E-1 and Figure E.6.

Table E-1 Seismic design lateral forces for three-story concrete masonry specimen

Level	F , k	H, ft	V, k	M , k-ft
R	19.7	26.25	19.7	0
3	17.3	17.5	37.0	172
2	8.7	8.75	45.7	498
Σ	45.7			896

Figure E.6 Seismic design shears and moments for three-story concrete masonry specimen

E.4 DESIGN TRANSVERSE SHEAR WALLS FOR GRAVITY PLUS EARTHQUAKE LOADS

The seismic design story shear in any story (V_x) is determined from the following equation:

$$V_x = \sum_{i=x}^{n} F_i$$

where F_i = the portion of the seismic base shear (V) induced at Level i. The seismic design story shear (V_x) is distributed to the various vertical elements of the seismic force resisting system in the story under consideration based on the relative lateral stiffness of the vertical resisting elements and the diaphragm. In this case there are three vertical elements, W-1, W-2, and W-3. The three walls are conservatively assumed to be uncoupled, so that each functions as an independent cantilever.

As shown in Figure E.7, design each wall as a beam-column. Walls W-1 and W-3 are T-shaped flanged wall, whose web is 64-in. long in plan parallel to the direction of loading, and whose flange has the effective width (plan length) that is prescribed by the 2008 MSJC Code, and is different in tension and compression (MSJC 2008a). The axial load of each wall due to self-weight is assumed to act through the plan centroid of the wall, which is essentially the same as the plastic centroid, because the cross-sectional area of reinforcement is small. The axial load due to the reaction from the floor planks is assumed to act at the center of the flange of each T-wall. The moment-axial force interaction diagrams for each wall are based on the plastic centroid for that wall.

The plan layout of the walls comprising the specimen is shown in Figure E.7. In determining effective flange widths for the flexural strength, the nominal flange thickness and the floor-to-floor wall height are taken as 8 in. and 8 ft, respectively. The effective flange widths on each side of the web are therefore 8 in. multiplied by 6 when the flange is in compression, and 8 ft multiplied by 0.75 when the flange is in tension (MSJC

2008a). Assume that the flange of Wall W-1 is in compression and the flange of Wall W-3 is in tension.

In this case, flange width is governed by ρ_{max} of the T-shaped walls, with the flange in tension. Because the earthquake could act in either direction, we need equal flange widths for the T-shaped walls, and an effective flange width of 56 in. works. This width is also less than the maximum effective width permitted by the 2008 MSJC *Code* in either tension or compression. The design shown below is the result of an iterative process.

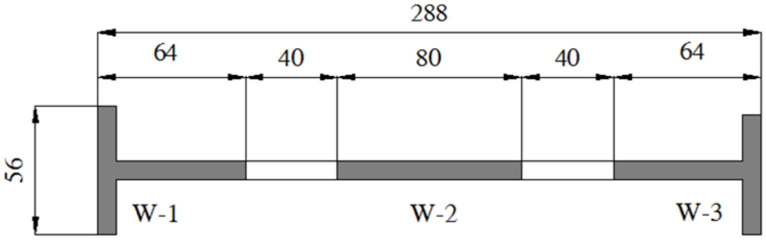

Figure E.7 Wall layout of masonry specimen (nominal dimensions in inches)

Sections 1.1.3 and 1.7.1 of the MSJC *Code* require global analysis of buildings, including calculation of building drift and the distribution of lateral loads to shear walls. To do this, the in-plane lateral stiffnesses of masonry shear walls must be determined. Those stiffnesses depend on the wall aspect ratio (h / l_w), boundary conditions, openings, and extent of cracking. Although cracking significantly reduces the stiffnesses of masonry walls, the 2008 MSJC *Code* permits stiffnesses to be computed on the basis of uncracked sections for many calculations. The justification for this assumption is that the distribution of lateral loads depends only on relative stiffnesses, which are the same whether or not cracking is included, provided that all walls are assumed to be cracked.

For calculations of lateral drift, however, Section 3.1.5.3 of the 2008 MSJC *Code* explicitly requires the use of cracked sections.

For a solid cantilever shear wall, the in-plane lateral stiffness is:

$$k_w = \frac{1}{\frac{(h')^3}{3E_m I} + \frac{1.2h'}{E_v A}}$$

where h' is the height of the wall and E_v is the shear modulus.

The effect of openings on wall stiffness depends on the size, shape, and distribution of those openings. While finite element methods are more accurate, approximate methods can be used to estimate the stiffnesses of walls with openings. For buildings with rigid diaphragms, it is simplest and usually accurate enough to distribute lateral load in each principal plan direction to the shear walls oriented in that direction, in proportion to their in-plane stiffnesses (Figure E.8).

For a system of walls in parallel, such as this one, the total stiffness is:

$$(k_w)_{lateral} = k_{w-1} + k_{w-2} + k_{w-3}$$

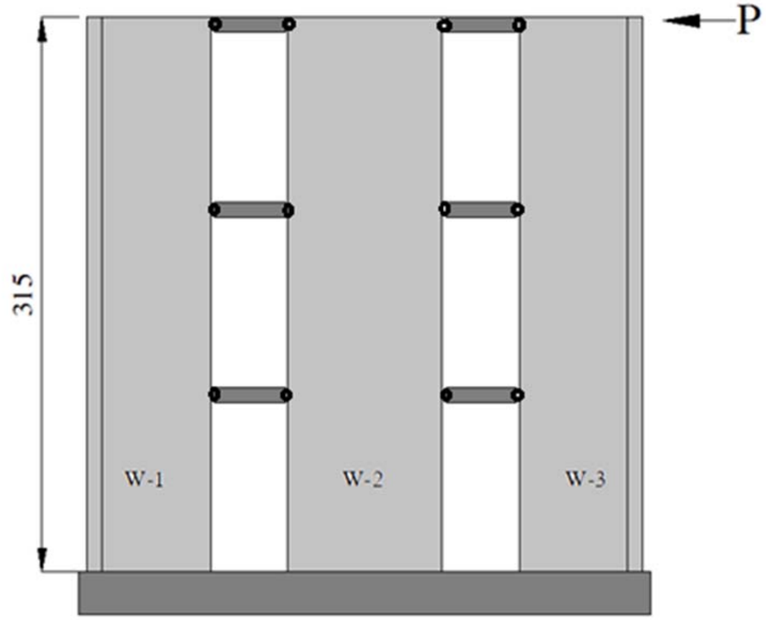

Figure E.8 Idealization used in computing stiffness of shear walls in parallel

The in-plane stiffness of each wall is calculated based on elastic theory, considering the flexural stiffness only, and including the effective flange width prescribed by the 2008 MSJC *Code*. That effective flange width depends on whether the flange is in tension or compression. The calculations for the in-plane stiffness (moment of inertia) of each wall segment are described below. All dimensions in the equations are in units of inches. For simplicity, effective stiffnesses are calculated using nominal wall lengths. Walls are assumed to be fully grouted.

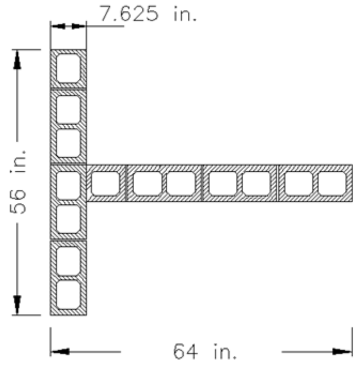

Wall W-1

$$\bar{y} = \frac{\left[56.375 \times 7.625 \times \frac{56.375}{2} + 56 \times 7.625 \times \left(64 - \frac{7.625}{2}\right)\right]}{56.375 \times 7.625 + 56 \times 7.625}$$

$$= 44.1\ in.$$

$$I = \frac{1}{12} \times 56.375^3 \times 7.625 + (56.375 \times 7.625)(\frac{56.375}{2} - 44.1)^2$$
$$+ \frac{1}{12} \times 7.625^3 \times 56 + 56 \times 7.625 \times (60.18 - 44.1)^2$$
$$= 3.35 \times 10^5\ in.^4$$

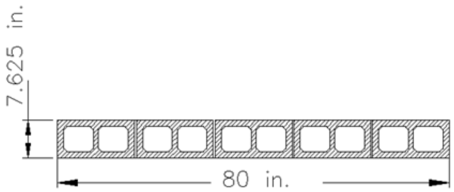

Wall W-2

$$I = \frac{1}{12} \times 80^3 \times 7.625$$
$$= 3.25 \times 10^5\ in.^4$$

Wall W-3

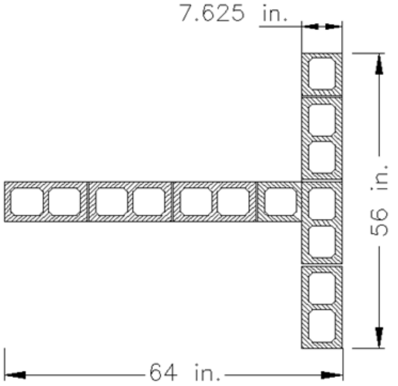

$$\bar{y} = 44.1\ in.$$

$$I = 3.35 \times 10^5\ in.^4$$

E.5 DESIGN OF SHEAR WALL W-1

Because the floor planks span parallel to the central axis of the specimen, and are debonded from the webs of Walls W-1, W-2, and W-3, design earthquake forces induce no axial loads from overturning in Walls W-1 and W-3.

E.5.1 Shear Design of Wall W-1

From the 2008 MSJC *Code*, Section 3.3.4.1.2.1,

$$V_n = V_{nm} = \left[4.0 - 1.75\left(\frac{M_u}{V_u\ d_v}\right)\right] A_n \sqrt{f'_m} + 0.25 P_u$$

Include the effects of axial load, assuming that each wall carries its self-weight plus the distributed floor weight on a tributary width. The shear and moment is distributed among the walls based on the lateral stiffness of each wall. The critical load case is (0.9 - 0.2 S_{DS}) D + 1.0 E.

E.5.1.1 Axial Load

Self-weight of wall (all dimensions are in units of feet):

Wall W-1 has a height of 26.25 ft, flange length of 4.67 ft, and web length of 5.33 ft. The self-weight of each wall is its weight, plus the weight of the lintels. The lintel weight is divided equally between the wall segments on each side of the lintel. Each story has three lintels, whose depth is (8 - 6.67) ft and whose length is 4 ft for exterior walls and 3.33 ft for interior wall.

$$\left[(26.25) \times 4.67 + 26.25 \times \left(5.33 - \frac{7.63}{12}\right) + 2 \times 3 \times 4/2 \times (8 - 6.67) + 1 \times 3 \times 3.33/2 \times (8 - 6.66)\right] \mathrm{ft}^2 \times 80\ \mathrm{lb/ft}^2 = 21.4\ \mathrm{kip}$$

Floor weight:

The floor system is composed of precast planks spanning parallel to the walls of the specimen, and bearing on the flanges of Walls W-1 and W-3, and on Walls W-4. The planks and topping are detailed so that they do not transfer gravity load to the webs of Walls W-1, W-2, or W-3. As a result, the planks within a transverse distance of 4 ft on either side of the central grid line of the specimen are supported equally on Walls W-1 and W-3 only. The planks outside of that distance are supported equally on the half-walls W-4 only. The tributary floor area supported by Wall W-1 is shown in Figure E.9.

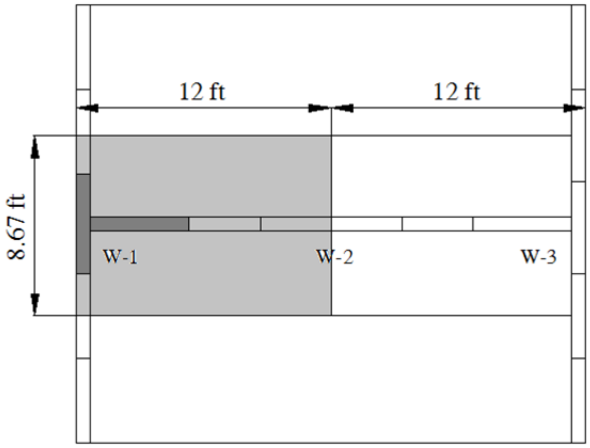

Figure E.9 Tributary floor area supported by Wall W-1

$$12 \times 8.67\ \text{ft}^2 \times (95 + 2 \times 110)\ \text{lb/ft}^2 = 32.8\ \text{kips}$$

The total unfactored axial dead load at the base is the sum of 21.4 kips and 32.8 kips, or 54.2 kips.

E.5.1.2 Moment

Based on the relative lateral stiffnesses of the shear walls,

$$M_{W-1} = \frac{k_{w-1}}{\sum k_{wi}} M_{base} = \frac{I_{w-1}}{\sum I_{wi}} M_{base} = \frac{3.35}{3.35 + 3.25 + 3.35} \times 896\ kip - ft$$

$$M_{W-1} = 0.33\ \times 896\ \text{kip} - \text{ft} = 298\ \text{kip} - \text{ft.}$$

Then the unfactored base moment for Wall W-1 is 298 kip-ft. This is slightly modified by the effects of eccentric axial load, and is included in the flexural design of the wall.

E.5.1.3 Shear:

$$V_{W-1} = \frac{k_{w-1}}{\sum k_{wi}} V_{base} = \frac{I_{w-1}}{\sum I_{wi}} V_{base} = \frac{3.35}{3.35 + 3.25 + 3.35} \times 45.7 \text{ kips}$$

$$V_{W-1} = 0.33 \times 45.7 \text{ kips} = 15.2 \text{ kips}$$

Then,

$$V_n = V_{nm} = \left[4.0 - 1.75 \left(\frac{M_u}{V_u \ d_v} \right) \right] A_n \sqrt{f_m^{'}} + 0.25 P_u$$

$$P_u = (0.9 - 0.2 \times 1) \cdot 54.2 kips = 37.9 kips$$

$$\left(\frac{M_u}{V_u \ d_v} \right) = \frac{298 \cdot 12 \ kip - in.}{15.2 \cdot 5.33 \cdot 12 \ kip - in.} = 3.67$$

However, the ratio ($M_u / V_u \ d_v$) need not be taken greater than 1.0. Take it equal to that value.

$$V_n = [4.0 - 1.75\,(1)] \cdot (64 \cdot 7.625\, in.^2) \sqrt{2500\, lb/in.^2} + 0.25 \cdot 37900\, lb$$

$$V_n = [4.0 - 1.75\ (1.0)] \cdot 488 in.^2 \cdot 50\ lb/in.^2 + 9{,}475\ lb$$

$$V_n = 2.25 \cdot 488\ in.^2 \cdot 50\ lb/in.^2 + 9{,}475\ lb$$

$$V_n = 54{,}900 + 9{,}475 = 64{,}375\ lb = 64.4\ kips$$

The ϕ-factor for shear is 0.80 (*Code* Section 3.1.4.3).

$$\phi V_n = 0.80 \times 64.4\, kips = 51.5\, kips$$

This considerably exceeds the factored design base shear (1 x 15.2 kips = 15.2 kips). No shear reinforcement is needed for strength. Capacity design for shear is checked later.

E.5.2 Preliminary Check of Prescriptive Reinforcement Requirements for Wall W-1

Wall W-1 must also meet the prescriptive reinforcement requirements for a special reinforced shear wall. In accordance with the 2008 MSJC *Code*, Section 1.17.3.2.6, the total reinforcement percentage (horizontal and vertical) must be at least 0.002, with at least one-third of this placed in each direction. The maximum spacing is one-third of the smaller of the story height or the plan length.

The corresponding steel area per foot is 0.002 x 8 in. x 12 in. = 0.2 in.^{2} per foot. If we put two-thirds of this vertically, that is equivalent to No. 4 bars at 18 in. If we put one-third of it horizontally, that is equivalent to No. 4 bars at 36 in.

Meet minimum reinforcement requirements using No. 4 bars at 16 in. vertically, and No. 4 bars at 16 in. horizontally. These requirements will be re-checked as the design proceeds.

E.5.3 Flexural Design of Wall W-1:

Wall W-1 has a plan length of 64 in. The factored base moment per wall is 298 ft-kips. The critical load case is (0.9 - 0.2 S_{DS}) D + 1.0 E. The factored axial load (see above) is 0.7 x 54.2 kips, or 37.9 kips. The moment-axial force interaction diagrams for each wall are based on the plastic centroid for that wall. For consistency, the factored design moments must be calculated using that same reference.

Because the location of the plastic centroid depends on the flexural reinforcement, it is not known in advance. For this reason, the plan centroid of the wall is used instead. This is very close to the plastic centroid, because the cross-sectional area of reinforcement is small. Because the axial load on the wall due to self-weight acts through the plan centroid of the wall, it produces no moment with respect to that reference. Because the dead-load reaction from the planks is applied near the middle of the flange of Wall W-1, the factored design moment M_u is increased by the product of the factored plank reaction and the eccentricity of that reaction from the plastic centroid. Therefore,

$$(M_{W-1})_u = 298\ \text{kip} - \text{ft} + 0.7 \times 32.8\ \text{kips}\ \times \frac{60.18 - 44.1}{12}\ \text{ft} = 328\ \text{kip} - \text{ft}$$

Using a spreadsheet, the interaction diagram for the wall is shown in Figure E.10. The spreadsheet is valid only for axial loads low enough to keep the neutral axis within the compression flange.

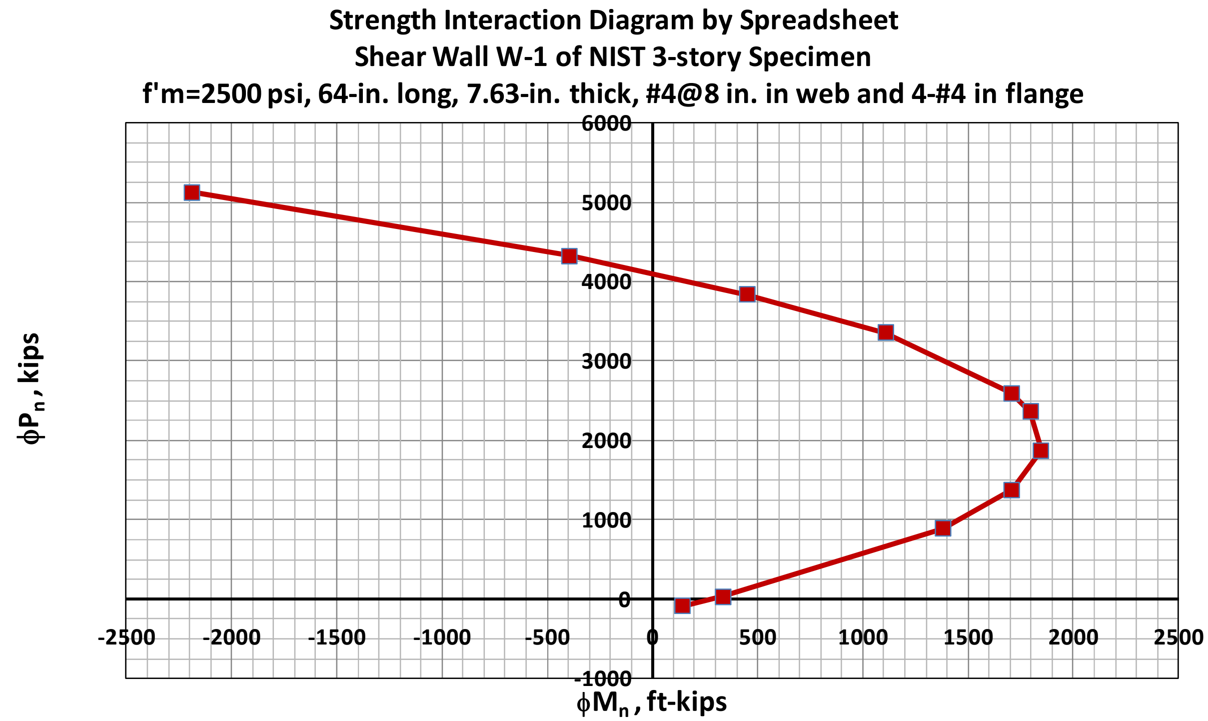

Figure E.10 Strength moment-axial force interaction diagram for Wall W-1

Examination of the values in the spreadsheet (with vertical reinforcement consisting of No. 4 bars spaced at 8 in. and one additional No. 4 at the end in the web, and five No. 4 bars in the flange) shows that at a factored axial load of 37.9 kips, the design capacity of 350 kip-ft exceeds the design moment in the wall (328 kip-ft), so the flexural design is satisfactory. The position of the neutral axis is 2.21 in. from the extreme compression fiber, so the interaction diagram is still valid. The plastic centroid of the section (y_p = 20.21 in.) is essentially the same as the plan centroid of the wall (19.9 in.).

The web requires flexural reinforcement consisting of No. 4 bars at 8 in. (7 bars), plus one additional No. 4 bar in the end cell of the web. The 56-in. flange has five No. 4 bars. The total area of reinforcement is 2.6 in.^{2}.

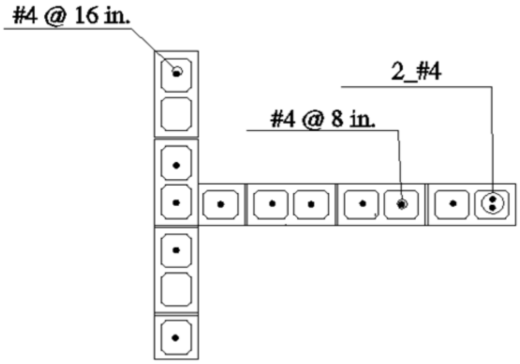

In the web, this is equivalent to a steel percentage of

$$\rho_{vertical} = \frac{A_s}{bt} = \frac{0.2\,in.^2}{7.625 \times 8\,in.^2} = 0.0032$$

This exceeds the required minimum of 0.0007 each way, and is satisfactory so far.

Spreadsheet for calculating strength moment-axial force interaction diagram for concrete masonry shear wall W-1

web depth	63.63
web thickness	7.63
flange width	56
flange thickness	7.63
emu	0.0025
f'm	2.5
fy	60
Es	29000
d	59.63
(c/d)balanced	0.54717
width	56
phi	0.9
plastic centroid	20.21

steel layers are counted from the extreme compression fiber to the extreme tension fiber

distances are measured from the extreme compression fiber

compression in masonry and reinforcement is taken as positive

stress in compressive reinforcement is set to zero, because the reinforcement is not laterally supported

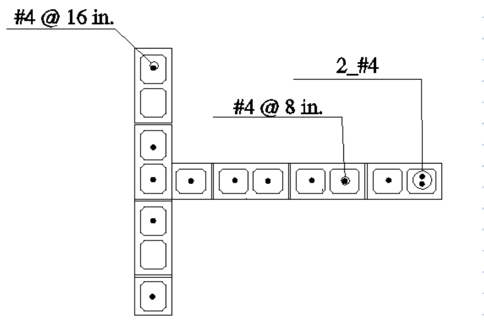

Row of Reinforcement	distance	Area
1	4.00	1.00
2	12.00	0.20
3	20.00	0.20
4	28.00	0.20
5	36.00	0.20
6	44.00	0.20
7	52.00	0.20
8	60.00	0.40

	c/d	c	Cmas	fs(1)	fs(2)	fs(3)	fs(4)	fs(5)	fs(6)	fs(7)	fs(8)	fs(9)	fs(10)	Moment	Axial Force
pure axial load															
Points controlled by mas	1.065	63.51	5690	0.00	0.00	0.00	0.00	0.00	0.00	0.00	0.00	-5.13	-14.26	-2191	5121
	0.9	53.67	4809	0.00	0.00	0.00	0.00	0.00	0.00	0.00	-8.56	-19.36	-30.17	-394	4325
	0.8	47.70	4274	0.00	0.00	0.00	0.00	0.00	0.00	-6.53	-18.69	-30.85	-43.00	449	3839
	0.7	41.74	3740	0.00	0.00	0.00	0.00	0.00	-3.92	-17.82	-31.71	-45.61	-59.50	1108	3351
	0.54717	32.63	2923	0.00	0.00	0.00	0.00	-7.49	-25.27	-43.05	-60.00	-60.00	-60.00	1705	2596
Points controlled by stee	0.54717	32.63	2923	0.00	0.00	0.00	0.00	-7.49	-25.27	-43.05	-60.00	-60.00	-60.00	1705	2596
	0.5	29.82	2671	0.00	0.00	0.00	0.00	-15.04	-34.49	-53.95	-60.00	-60.00	-60.00	1795	2364
	0.4	23.85	2137	0.00	0.00	0.00	-12.61	-36.92	-60.00	-60.00	-60.00	-60.00	-60.00	1847	1871
	0.3	17.89	1603	0.00	0.00	-8.56	-40.98	-60.00	-60.00	-60.00	-60.00	-60.00	-60.00	1710	1380
	0.2	11.93	1069	0.00	-0.45	-49.08	-60.00	-60.00	-60.00	-60.00	-60.00	-60.00	-60.00	1380	888
	0.037	2.21	198	-58.94	-60.00	-60.00	-60.00	-60.00	-60.00	-60.00	-60.00	-60.00	-60.00	350	38
	0.01	0.60	53	-60.00	-60.00	-60.00	-60.00	-60.00	-60.00	-60.00	-60.00	-60.00	-60.00	142	-92

Now check ρ_{max} , continuing to consider the wall as a special reinforced masonry shear wall ($R = 5$, $\alpha = 4$). As before, the flange of Wall W-1 is considered to be in compression.

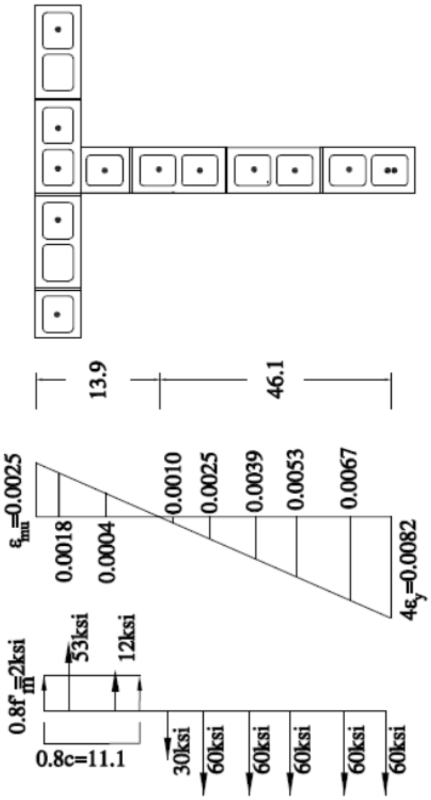

$$c = \frac{0.0025}{4 \times 0.00207 + 0.0025} \times 60 = 0.232 \times 60 \text{ in.} = 13.9 \text{ in.}$$

$$d - c = 60 - 13.9\ in. = 46.1 \text{ in.}$$

$$T_{reinforcement} = 6 \times 0.2 \text{ in.}^2 \times 60 \text{ ksi} + 0.2 \text{ in.}^2 \times 30 \text{ ksi} = 78.0 \text{ kips}$$

$C_{reinforcement} = 5 \times 0.2\ in.^2 \times 53\ ksi + 0.2\ in.^2 \times 12\ ksi = 55.4\ kips$

$$C_{masonry} = 0.8 \times 2.5\ \text{ksi} \times (7.625 \times 56 + (0.8 \times 13.9 - 7.625) \times 7.625)\ \text{in.}^2$$
$$= 907.0\ \text{kips}$$

$N_{\ crushing} = C_{masonry} + C_{reinforcement} - T_{reinforcement} = 884.4$ kips

(axial load corresponding to toe crushing)

$N_{critical} = N_{DL} + 0.75N_{LL} + 0.525Q_E$

$N_{DL} = 63.2$ kips (Unfactored axial dead load)

$N_{LL} = (0.25 + \frac{15}{\sqrt{K_{LL}A_T}})N_{LL_0}$

(Unfactored axial live load, reduced by reduction factor corresponding to the tributary area of three elevated floors)

$K_{LL} = 4$ (Table 4 – 2 ASCE7 – 05)
$A_T = 3 \times (8.67 \times 12)\ \text{ft}^2 = 312\ \text{ft}^2$ (Tributary area)
$N_{LL0} = (8.67 \times 12)\ \text{ft}^2 \times (20 + 40 + 40)\frac{\text{lb}}{\text{ft}^2} = 10400\ \text{lb} = 10.4$ kips
$N_{LL} = \left(0.25 + \frac{15}{\sqrt{4 \times 312}}\right) 10.4\ \text{kips} = 0.67 \times 10.4\ \text{kips} = 6.97$ kips
$Q_E = 0$

$N_{critical} = 54.2\ \text{kip} + 0.75 \times 6.97\ \text{kips} + 0 = 59.4$ kips

$$N_{crushing} = 884.4 \text{ kips} > N_{critical} = 59.4 \text{ kips}$$

The critical axial load is considerably less than the axial load corresponding to toe crushing, and maximum reinforcement limitations are satisfied.

E.5.4 Capacity Design for Shear, Wall W-1

Now check *Code* Section 3.1.3 (capacity design for shear) for Wall W-1. The wall is a special reinforced masonry shear wall, so the capacity design requirements of *Code* Section 1.17.3.2.6.1.1 apply.

At an axial load of 37.9 kips, the nominal flexural capacity of this wall is the design capacity of 350 kip-ft, divided by the strength reduction factor of 0.9, or 388 kip-ft. The ratio of this nominal flexural capacity to the factored design moment is 388 divided by 328, or 1.18. Including the additional factor of 1.25, gives a ratio of 1.47.

$$\phi V_n \geq 1.47\ V_u$$
$$V_n \geq \frac{1.47}{\phi} V_u = \frac{1.47}{0.8} V_u = 1.83\ V_u = 1.83 \times 15.2 = 27.8\ kips$$

Because $V_n = 64.4$ kips, the wall requires no shear reinforcement for strength.

Now re-check prescriptive reinforcement requirements. We need a total steel percentage of 0.002 (summation of required horizontal and vertical reinforcement), with at least 0.0007 horizontally and vertically. Vertical reinforcement is 0.0032, greater than the required sum, so horizontal reinforcement must meet only the minimum of 0.0007.

Use No. 4 bars at 16 in. horizontally.

$$\rho_{horizontal} = \frac{A_s}{bt} = \frac{0.2\,in.^2}{7.625 \times 16\,in.^2} = 0.0016$$

From the 2008 MSJC *Code*, Section 3.3.4.1.2.2,

$$\begin{aligned}
V_{ns} &= 0.5\left(\frac{A_v}{s}\right) f_y d_v \\
V_{ns} &= 0.5\left(\frac{0.2\,in.^2}{16\,in.}\right) 60\,kips/in.^2 \times 60\,in. \\
V_{ns} &= 22.5\,kips \\
V_n &= V_{nm} + V_{ns} = 64.4\,kips + 22.5\,kips = 86.9\,kips
\end{aligned}$$

This exceeds the required nominal shear capacity of 27.8 kips, and the design is satisfactory for shear.

E.5.5 Summary of Design for Wall W-1

Use No. 4 vertical bars at 8 in. in the web (7 bars), plus one additional No. 4 bar in the end cell, and five No. 4 vertical bars in the flange. Use No. 4 horizontal bars at 16 in. in the web and flange.

E.6 DESIGN OF SHEAR WALL W-2

Because the floor planks span parallel to the central axis of the specimen, and are debonded from the webs of Walls W-1, W-2, and W-3, design earthquake forces induce no axial loads from overturning in Walls W-1 and W-3.

E.6.1 Shear Design of Wall W-2

From the 2008 MSJC *Code*, Section 3.3.4.1.2.1,

$$V_n = V_{nm} = \left[4.0 - 1.75 \left(\frac{M_u}{V_u \, d_v} \right) \right] A_n \sqrt{f_m^{'}} + 0.25 P_u$$

Include the effects of axial load, assuming that each wall carries its self-weight plus the distributed floor weight on a tributary width. The shear and moment among the walls will be distributed based on the lateral stiffness of each wall. The critical load case is (0.9 - 0.2 S_{DS}) D + 1.0 E.

E.6.1.1 Axial Load

Self-weight of wall:

Wall W-2 has a height of 26.25 ft and a length of 6.67 ft .The self-weight of the wall is its weight, plus the weight of the lintels. The lintel weight is divided equally between the wall segments on each side of the lintel. At each story, there are two lintels, whose height is (8-6.67) ft and whose length is 3.33 ft.

$$[26.25 \times 6.67 \text{ ft}^2 + 3 \times 2 \times 3.33/2 \times (8 - 6.67) \text{ ft}^2] \times 80 \text{ lb/ft}^2 = 15.1 \text{ kip}$$

Floor weight:

The tributary floor weight carried by Wall W-2 is zero, so the total unfactored axial dead load at the base is 15.1 kips.

E.6.1.2 Moment

Based on the relative lateral stiffnesses of the shear walls:

$$M_{W-2} = \frac{k_{w-2}}{\sum k_{wi}} M_{base} = \frac{3.25}{3.35 + 3.25 + 3.35} \times 896 \text{ kip} - \text{ft} = 0.33 \ \times 896 \text{ kip} - \text{ft}$$

$$M_{W-2} = 298 \text{ kip} - \text{ft}$$

Then the unfactored base moment for W-2 is 298 kip-ft.

E.6.1.3 Shear

$$V_{W-2} = \frac{k_{w-2}}{\sum k_{wi}} V_{base} = \frac{3.25}{3.35 + 3.25 + 3.35} \times 45.7 \text{ kips} = 0.33 \ \times 45.7 \text{ kips}$$
$$= 15.2 \text{ kips}$$

Then,

$$V_n = V_{nm} = \left[4.0 - 1.75 \left(\frac{M_u}{V_u \ d_v} \right) \right] A_n \sqrt{f_m^{'}} + 0.25 P_u$$
$$P_u = (0.9 - 0.2 \times 1) \cdot 15.1 = 10.57 kips$$
$$\frac{M_u}{V_u \ d_v} = \frac{298 \cdot 12 \ kip - in.}{15.2 \cdot 6.67 \cdot 12 \ kip - in.} = 2.93$$

However, the ratio ($M_u / V_u \ d_v$) need not be taken greater than 1.0. Take it equal to that value.

$$V_{nm} = [4.0 - 1.75\,(1)] \cdot (76 \times 7.625\, in.^2)\sqrt{2500\, lb / in.^2} + 0.25 \cdot 10{,}570\, lb$$

$$V_n = [4.0 - 1.75\,(1.0)] \times 580\ in.^2 \times 50\ lb / in.^2 + 2{,}642 lb$$
$$V_n = 2.25 \times 580\ in.^2 \times 50\ lb / in.^2 + 2{,}642\ lb$$
$$V_n = 65{,}250 + 2{,}642 = 67{,}892\ lb = 67.9\ kips$$

The ϕ-factor for shear is 0.80 (*Code* Section 3.1.4.3).

$$\phi V_n = 0.80 \cdot 67.9\, kips = 54.3\, kips$$

This exceeds the factored design base shear (1 x 15.2 kips = 15.2 kips). No horizontal reinforcement is required for shear. Prescriptive requirements are checked later.

E.6.2 Preliminary Check of Prescriptive Reinforcement Requirements for Wall W-2

Wall W-2 must also meet prescriptive reinforcement requirements. In accordance with the 2008 MSJC *Code*, Section 1.17.3.2.6, the total reinforcement percentage (horizontal and vertical) shall be at least 0.002, with at least one-third of this placed in each direction.

The corresponding steel area per foot is 0.002 x 8 in. x 12 in. = 0.2 in.^{2} per foot. If we put two-thirds of this vertically, that is equivalent to No. 4 bars at 18 in. The maximum spacing is one-third of the smaller of the story height or the plan length. If we put one-third of it horizontally, that is equivalent to No. 4 bars at 36 in. Use No. 4 bars at 16 in. for modularity and consistency with the other walls.Meet minimum reinforcement requirements using No. 4 bars at 16 in. vertically, and No. 4 bars at 16 in. horizontally. These requirements will be re-checked as the design proceeds.

E.6.3 Flexural Design of Wall W-2:

Wall W-2 has a plan length of 6.67 ft. The factored base moment per wall is 385 ft-kips. The critical load case is (0.9 - 0.2 SDS) D + 1.0 E. The factored axial load (see above) is 0.7 x 15.1 kips, or 10.6 kips. Using a spreadsheet, the interaction diagram for Wall W-2 is shown in Figure E.11.

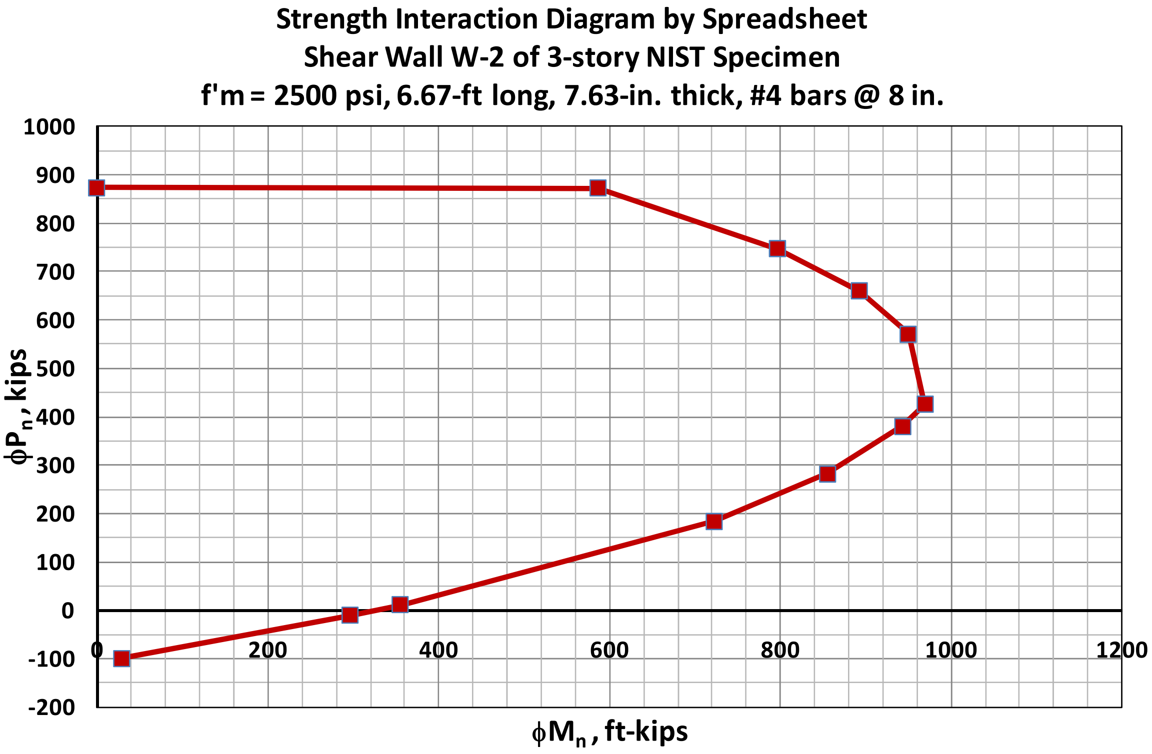

Figure E.11 Strength moment-axial force interaction diagram for Wall W-2

Examination of the values in the spreadsheet, with vertical reinforcement consisting of No. 4 bars at 8 in., shows that at a factored axial load of 10.6 kips, the design moment capacity of the wall is 355 kip-ft. This exceeds the design moment of 298 kip-ft, and flexural reinforcement is satisfactory.

Flexural reinforcement consisting of No. 4 bars at 8 in. is required. The total area of reinforcement is 0.2 in.^{2} (10) = 2.00 in.^{2}.

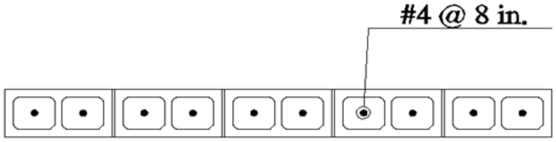

In the section, this is equivalent to a steel percentage of

$$\rho_{vertical} = \frac{A_s}{bt} = \frac{0.2\,in.^2}{7.625 \times 8\,in.^2} = 0.0032$$

This exceeds the required minimum of 0.0007 each way, and is satisfactory so far.

Now check ρ_{max} , continuing to consider the wall as a special reinforced masonry shear wall ($R = 5$, $\alpha = 4$).

$$\rho_{\max} = \frac{0.64\, f'_m \left(\dfrac{\varepsilon_{mu}}{\alpha\, \varepsilon_y + \varepsilon_{mu}} \right) - \dfrac{N_{critical}}{bd}}{f_y \left(\dfrac{\alpha\, \varepsilon_y - \varepsilon_{mu}}{\alpha\, \varepsilon_y + \varepsilon_{mu}} \right)}$$

$$N_{critical} = N_{DL} + 0.75 N_{LL} + 0.525 Q_E = 15.1 \text{ kips}$$

$$N_{DL} = 18.1 \text{ kips}$$

$$N_{LL} = 0$$

$$Q_E = 0$$

$$\rho_{\max} = \frac{0.64 \times 2500\ psi \left(\dfrac{0.0025}{4 \times 0.00207 + 0.0025} \right) - \dfrac{15100\ lb}{7.625\ in. \times 76\ in.}}{60000\ psi \left(\dfrac{4 \times 0.00207 - 0.0025}{4 \times 0.00207 + 0.0025} \right)}$$

$$\rho_{\max} = \frac{1600\ psi\,(0.231) - 24.7}{60000\ psi\,(0.536)} = \frac{369.6 - 24.7}{32160}$$

$$\rho_{\max} = 0.0106$$

Check the maximum permitted area of flexural reinforcement. We have $\rho_{\max} > \rho_{vertical}$ so the design is satisfactory.

Spreadsheet for calculating strength moment-axial force interaction diagram for concrete masonry shear wall W-2

depth	79.63
emu	0.0025
f'm	2.5
fy	60
Es	29000
d	75.63
(c/d)balanced	0.54717
width	7.63
phi	0.9

steel layers are counted from the extreme compression fiber to the extreme tension fiber

distances are measured from the extreme compression fiber

compression in masonry and reinforcement is taken as positive

stress in compressive reinforcement is set to zero, because the reinforcement is not laterally supported

Row of Reinforcement	distance	Area
1	4.00	0.20
2	12.00	0.20
3	20.00	0.20
4	28.00	0.20
5	36.00	0.20
6	44.00	0.20
7	52.00	0.20
8	60.00	0.20
9	68.00	0.20
10	76.00	0.20

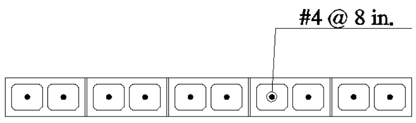

W-2

	c/d	c	Cmas	fs(1)	fs(2)	fs(3)	fs(4)	fs(5)	fs(6)	fs(7)	fs(8)	fs(9)	fs(10)	Moment	Axial Force
pure axial load														0	873
Points controlled by mas	1.049	79.34	969	0.00	0.00	0.00	0.00	0.00	0.00	0.00	0.00	0.00	0.00	587	872
	0.9	68.07	831	0.00	0.00	0.00	0.00	0.00	0.00	0.00	0.00	0.00	-8.45	797	746
	0.8	60.50	739	0.00	0.00	0.00	0.00	0.00	0.00	0.00	0.00	-8.98	-18.57	892	660
	0.7	52.94	646	0.00	0.00	0.00	0.00	0.00	0.00	0.00	-9.67	-20.62	-31.58	950	571
	0.54717	41.38	505	0.00	0.00	0.00	0.00	0.00	-4.59	-18.60	-32.62	-46.63	-60.00	970	425
Points controlled by stee	0.54717	41.38	505	0.00	0.00	0.00	0.00	0.00	-4.59	-18.60	-32.62	-46.63	-60.00	970	425
	0.5	37.82	462	0.00	0.00	0.00	0.00	0.00	-11.86	-27.20	-42.53	-57.87	-60.00	943	380
	0.4	30.25	369	0.00	0.00	0.00	0.00	-13.78	-32.95	-52.12	-60.00	-60.00	-60.00	855	282
	0.3	22.69	277	0.00	0.00	0.00	-16.97	-42.53	-60.00	-60.00	-60.00	-60.00	-60.00	723	185
	0.122	9.23	113	0.00	-21.79	-60.00	-60.00	-60.00	-60.00	-60.00	-60.00	-60.00	-60.00	355	11
	0.1	7.56	92	0.00	-42.53	-60.00	-60.00	-60.00	-60.00	-60.00	-60.00	-60.00	-60.00	296	-11
	0.01	0.76	9	-60.00	-60.00	-60.00	-60.00	-60.00	-60.00	-60.00	-60.00	-60.00	-60.00	29	-100

E.6.4 Capacity Design for Shear, Wall W-2

Now check *Code* Section 3.1.3 (capacity design for shear) for Wall W-2. The wall is a special reinforced masonry shear wall, so the capacity design requirements of *Code* Section 1.17.3.2.6.1.1 apply.

At an axial load of 10.6 kips, the nominal flexural capacity of this wall is the design capacity of 355 ft-kips, divided by the strength reduction factor of 0.9, or 394 ft-kips. The ratio of this nominal flexural capacity to the factored design moment is 394 divided by 298, or 1.32. Including the additional factor of 1.25, gives a ratio of 1.65.

$$\phi V_n \geq 1.65\, V_u$$

$$V_n \geq \frac{1.65}{\phi} V_u = \frac{1.65}{0.8} V_u = 2.06\, V_u = 2.06 \times 15.2\, kips = 31.3\, kips$$

Because V_n = 67.9 kips, the wall requires shear reinforcement for strength.

Prescriptive reinforcement requirements must also be met. We need a total steel percentage of 0.002 (summation of required horizontal and vertical reinforcement), with at least 0.0007 horizontally and vertically. Vertical reinforcement is 0.0032, greater than the required sum, so horizontal reinforcement must meet only the minimum of 0.0007.

Use No. 4 bars at 16 in. horizontally.

$$\rho_{horizontal} = \frac{A_s}{bt} = \frac{0.2\, in.^2}{7.625 \times 16\, in.^2} = 0.0016$$

From the 2008 MSJC *Code*, Section 3.3.4.1.2.2,

$$V_{ns} = 0.5\left(\frac{A_v}{s}\right) f_y d_v$$

$$V_{ns} = 0.5\left(\frac{0.2\ in.^2}{16\ in.}\right) 60\ kips / in.^2 \times 76\ in.$$

$$V_{ns} = 28.5\ kips$$

$$V_n = V_{nm} + V_{ns} = 67.9\ kips + 28.5\ kips = 96.4\ kips$$

This exceeds the required nominal shear capacity of 31.3 kips, and the design is satisfactory for shear.

E.6.5 Summary of Design for Wall W-2

Use No. 4 vertical bars at 8 in. (10 bars total), and No. 4 horizontal bars at 16 in.

E.7 DESIGN OF SHEAR WALL W-3

Because the floor planks span parallel to the central axis of the specimen, and are debonded from the webs of Walls W-1, W-2, and W-3, design earthquake forces induce no axial loads from overturning in Walls W-1 and W-3.

E.7.1 Shear Design of Wall W-3

From the 2008 MSJC *Code*, Section 3.3.4.1.2.1,

$$V_n = V_{nm} = \left[4.0 - 1.75\left(\frac{M_u}{V_u\ d_v}\right)\right] A_n \sqrt{f_m^{'}} + 0.25 P_u$$

Include the effects of axial load, assuming that each wall carries its self-weight plus the distributed floor weight on a tributary width. The shear and moment are distributed among the walls based on the lateral stiffness of each wall. The critical load case is (0.9 - 0.2 S_{DS}) D + 1.0 E.

E.7.1.1 Axial Load

Self-weight of wall (all dimensions are in units of feet):

Wall W-3 has a height of 26.25 ft, flange length of 4.67 ft, and web length of 5.33 ft. The self-weight of each wall is its weight, plus the weight of the lintels. The lintel weight is divided equally between the wall segments on each side of the lintel. At each story, there are three lintels, whose depth is (8 - 6.67) ft and whose length is 4 ft for exterior walls and 3.33 ft for interior wall.

$$\left[(26.25)\times 4.67+26.25\times\left(5.33-\frac{7.63}{12}\right)+2\times 3\times 4/2\times(8-6.67)+1\times 3\times 3.33/2\times(8-6.66)\right]\mathrm{ft}^2\times 80\ \mathrm{lb/ft}^2=21.4\ \mathrm{kip}$$

Floor weight:

The floor system is assumed to be composed of precast planks spanning parallel to the walls of the specimen, and bearing on the flanges of Walls W-1 and W-3, and on Walls W-4. The planks and topping will be detailed so that they do not transfer gravity load to the webs of Walls W-1, W-2, or W-3. As a result, the planks within a transverse distance of 4 ft on either side of the central grid line of the specimen are supported equally on Walls W-1 and W-3 only. The planks outside of that distance are supported equally on the half-walls W-4 only.

The tributary floor area supported by Wall W-3 is shown in Figure E.12.

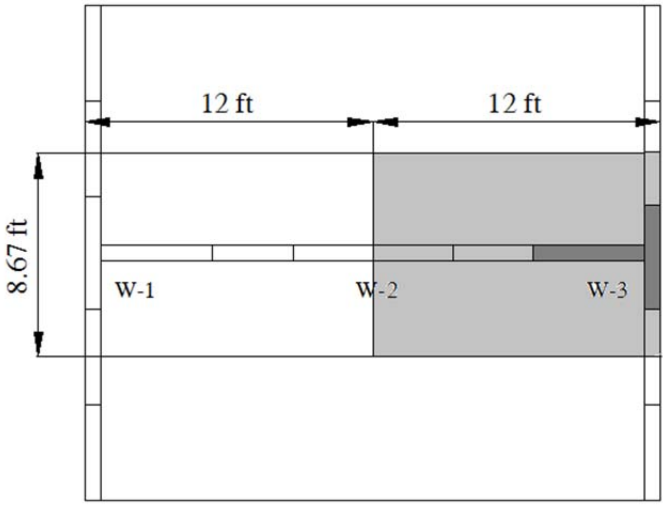

Figure E.12 Tributary floor area supported by Wall W-3

$$\frac{1}{2} \times 24 \times 8.67\ \text{ft}^2 \times (95 + 2 \times 110)\ \text{lb/ft}^2 = 32.8\ \text{kips}$$

The total unfactored axial dead load at the base is the sum of 21.4 kips and 32.8 kips, or 54.2 kips.

E.7.1.2 Moment

Based on the relative lateral stiffnesses of the shear walls,

$$M_{W-3} = \frac{k_{w-3}}{\sum\ k_{wi}} M_{base} = \frac{I_{w-3}}{\sum\ I_{wi}} M_{base} = \frac{3.35}{3.35 + 3.25 + 3.35} \times 896\ \text{kip} - \text{ft}$$

$$M_{W-3} = 0.33\ \times 896\ \text{kip} - \text{ft} = 298\ \text{kip} - \text{ft}$$

Then the unfactored base moment for Wall W-3 is 298 kip-ft. This is slightly modified by the effects of eccentric axial load, and is included in the flexural design of the wall.

Shear:

$$V_{W-3} = \frac{k_{w-3}}{\sum k_{wi}} V_{base} = \frac{I_{w-3}}{\sum I_{wi}} V_{base} = \frac{3.35}{3.35 + 3.25 + 3.35} \times 45.7 \text{ kips}$$

$$V_{W-3} = 0.33 \times 45.7 \text{ kips} = 15.2 \text{ kip}$$

Then,

$$V_n = V_{nm} = \left[4.0 - 1.75 \left(\frac{M_u}{V_u \; d_v} \right) \right] A_n \sqrt{f'_m} + 0.25 P_u$$

$$P_u = (0.9 - 0.2 \times 1) \cdot 54.2 kips = 37.9 kips$$

$$\left(\frac{M_u}{V_u \; d_v} \right) = \frac{297 \cdot 12 \; kip - in.}{15.2 \cdot 5.33 \cdot 12 \; kip - in.} = 3.67$$

However, the ratio ($M_u / V_u \; d_v$) need not be taken greater than 1.0. Take it equal to that value.

$$V_n = [4.0 - 1.75 \; (1)] \cdot (64 \cdot 7.625 \; in.^2) \sqrt{2500 \; lb / in.^2} + 0.25 \cdot 37{,}900 \; lb$$

$$V_n = [4.0 - 1.75 \; (1.0)] \cdot 488 in.^2 \cdot 50 \; lb / in.^2 + 9{,}475 \; lb$$

$$V_n = 2.25 \cdot 488 \; in.^2 \cdot 50 \; lb / in.^2 + 9{,}475 \; lb$$

$$V_n = 54{,}900 + 9{,}475 lb = 64.4 \; kips$$

The ϕ factor for shear is 0.80 (*Code* Section 3.1.4.3).

$$\phi V_n = 0.80 \times 64.4\, kips = 51.5\, kips$$

This considerably exceeds the factored design base shear (1 x 15.2 kips = 15.2 kips). No shear reinforcement is needed for strength. Capacity design for shear is checked later.

E.7.2 Preliminary Check of Prescriptive Reinforcement Requirements for Wall W-3

Wall W-3 must also meet prescriptive reinforcement requirements. In accordance with the 2008 MSJC *Code*, Section 1.17.3.2.6, the total reinforcement percentage (horizontal and vertical) shall be at least 0.002, with at least one-third of this placed in each direction.

The corresponding steel area per foot is 0.002 x 8 in. x 12 in. = 0.2 in.^{2} per foot. If we put two-thirds of this vertically, that is equivalent to No. 4 bars at 18 in. The maximum spacing is one-third of the smaller of the story height or the plan length. If we put one-third of it horizontally, that is equivalent to No. 4 bars at 36 in. Use 16 in. for modularity and consistency.

Meet minimum reinforcement requirements using No. 4 bars at 16 in. vertically, and No. 4 bars at 16 in. horizontally. These requirements will be re-checked as the design proceeds.

E.7.3 Flexural Design of Wall W-3:

Wall W-3 has a plan length of 64 in. The factored base moment per wall is 298 ft-kips. The critical load case is (0.9 - 0.2 S_{DS}) D + 1.0 E. The factored axial load (see above) is 0.7 x 54.2 kips, or 37.9 kips. The moment-axial force interaction diagrams for each wall are based on the plastic centroid for that wall. For consistency, the factored design moments must be calculated using that same reference.

Because the location of the plastic centroid depends on the flexural reinforcement, it is not known in advance. For this reason, the plan centroid of the wall is used instead. This is very close to the plastic centroid, because the cross-sectional area of reinforcement is small. Because the axial load on the wall due to self-weight acts through the plan centroid of the wall, it produces no moment with respect to that reference. Because the dead-load reaction from the planks is applied near the middle of the flange of Wall W-3, the factored design moment M_u is decreased by the product of the factored plank reaction and the eccentricity of that reaction from the plastic centroid. Therefore,

$$(M_{W-3})_u = 298 \text{ kip} - \text{ft} - 0.7 \times 32.8 \text{ kips } \times \frac{60.18 - 44.1}{12} \text{ ft} = 267 \text{ kip} - \text{ft}$$

Using a spreadsheet, the interaction diagram for the wall is shown in

Figure E.13. The spreadsheet is valid only for axial loads that are low enough to keep the neutral axis within the compression web.

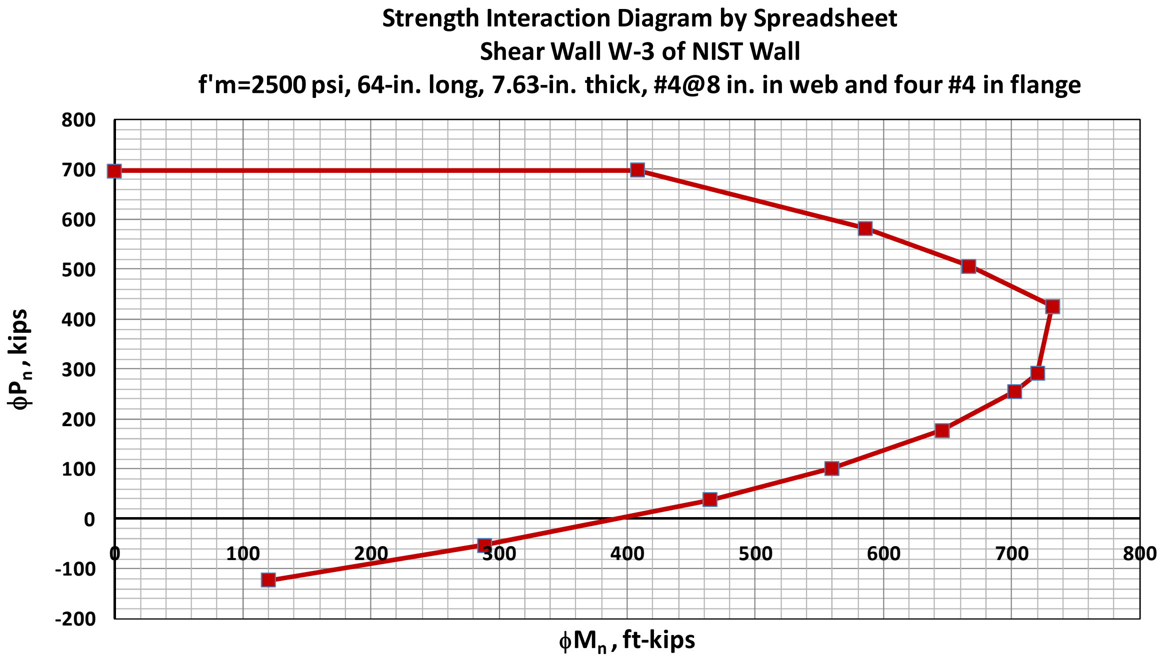

Figure E.13 Strength moment-axial force interaction diagram for Wall W-3

Examination of the values in the spreadsheet (with vertical reinforcement consisting of seven No. 4 bars spaced at 8 in. and one additional No. 4 bar in the end cell of the web, and five No. 4 bars in the flange) shows that at a factored axial load of 37.9 kips, the design moment of the wall (267 kip-ft) is less than the design capacity of 505 kip-ft, and the flexural design is satisfactory. The position of the neutral axis is 13.0 in. from the extreme compression fiber, so the interaction diagram is still valid. The plastic centroid of the section (y_p = 43.4 in.) is essentially the same as the plan centroid of the wall (44.1 in.).

The web requires flexural reinforcement consisting of No. 4 bars at 8 in. plus one additional No. 4 bar in the end cell. The 56-in. flange has five No. 4 bars. The total area of reinforcement is 2.6 in.^{2}.

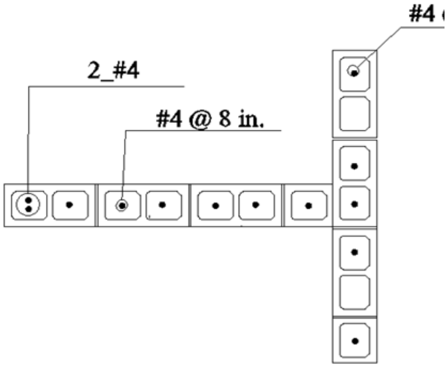

In the web, this is equivalent to a steel percentage of

$$\rho_{vertical} = \frac{A_s}{bt} = \frac{0.2\, in.^2}{7.625 \times 8\, in.^2} = 0.0032$$

This exceeds the required minimum of 0.0007 each way, and is satisfactory so far.

Spreadsheet for calculating strength moment-axial force interaction diagram for concrete masonry shear wall W-3

web depth	63.63
web thickness	7.63
flange width	56
flange thickness	7.63
emu	0.0025
f'm	2.5
fy	60
Es	29000
d	59.63
(c/d)balanced	0.54717
width	7.63
phi	0.9
plastic centroid	43.45

steel layers are counted from the extreme compression fiber to the extreme tension fiber

distances are measured from the extreme compression fiber

compression in masonry and reinforcement is taken as positive

stress in compressive reinforcement is set to zero, because the reinforcement is not laterally supported

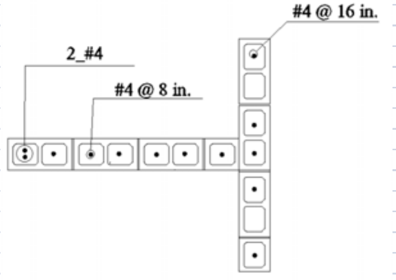

Row of Reinforcement	distance	Area
1	4.00	0.40
2	12.00	0.20
3	20.00	0.20
4	28.00	0.20
5	36.00	0.20
6	44.00	0.20
7	52.00	0.20
8	60.00	1.00

	c/d	c	Cmas	fs(1)	fs(2)	fs(3)	fs(4)	fs(5)	fs(6)	fs(7)	fs(8)	fs(9)	fs(10)	Moment	Axial Force
pure axial load														0	695
Points controlled by mas	1.065	63.51	775	0.00	0.00	0.00	0.00	0.00	0.00	0.00	0.00	-5.13	-14.26	1069	698
	0.9	53.67	655	0.00	0.00	0.00	0.00	0.00	0.00	0.00	-8.56	-19.36	-30.17	1121	582
	0.8	47.70	582	0.00	0.00	0.00	0.00	0.00	0.00	-6.53	-18.69	-30.85	-43.00	1121	506
	0.7	41.74	510	0.00	0.00	0.00	0.00	0.00	-3.92	-17.82	-31.71	-45.61	-59.50	1101	426
	0.54717	32.63	398	0.00	0.00	0.00	0.00	-7.49	-25.27	-43.05	-60.00	-60.00	-60.00	984	291
Points controlled by stee	0.54717	32.63	398	0.00	0.00	0.00	0.00	-7.49	-25.27	-43.05	-60.00	-60.00	-60.00	984	291
	0.5	29.82	364	0.00	0.00	0.00	0.00	-15.04	-34.49	-53.95	-60.00	-60.00	-60.00	937	255
	0.4	23.85	291	0.00	0.00	0.00	-12.61	-36.92	-60.00	-60.00	-60.00	-60.00	-60.00	814	178
	0.3	17.89	218	0.00	0.00	-8.56	-40.98	-60.00	-60.00	-60.00	-60.00	-60.00	-60.00	658	101
	0.218	13.00	159	0.00	0.00	-39.04	-60.00	-60.00	-60.00	-60.00	-60.00	-60.00	-60.00	504	39
	0.1	5.96	73	0.00	-60.00	-60.00	-60.00	-60.00	-60.00	-60.00	-60.00	-60.00	-60.00	237	-53
	0.01	0.60	7	-60.00	-60.00	-60.00	-60.00	-60.00	-60.00	-60.00	-60.00	-60.00	-60.00	-35	-134

Now check ρ_{max} , continuing to consider the wall as a special reinforced masonry shear wall ($R = 5,\ \alpha = 4$). Check the maximum permitted area of flexural reinforcement in the flange:

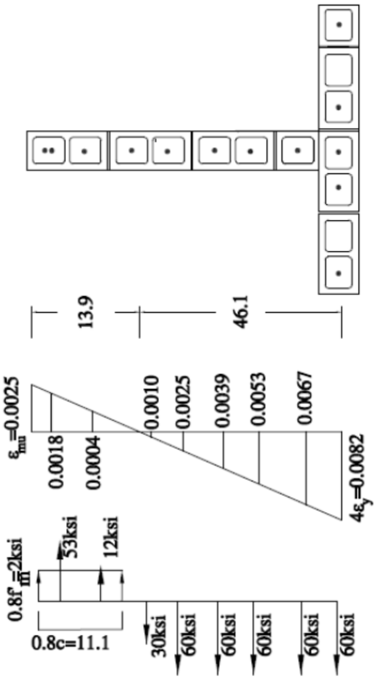

$$c = \frac{0.0025}{4 \times 0.00207 + 0.0025} \times 60 = 0.232 \times 60 = 13.9\ in.$$

$$d - c = 60 - 13.9 = 46.1\ in.$$

$$\begin{aligned} T_{reinforcement} &= 5 \times 0.2\text{ in.}^2 \times 60\text{ ksi} + 4 \times 0.2\text{ in.}^2 \times 60\text{ ksi} + 0.2\text{ in.}^2 \times 30\text{ ksi} \\ &= 114.0\text{ kips} \end{aligned}$$

$$C_{reinforcement} = 2 \times 0.2\text{ in.}^2 \times 53\text{ksi} + 0.2\text{ in.}^2 \times 12\text{ksi} = 23.6\text{ kips}$$

$C_{masonry} = 0.8 \times 2.5\ ksi \times (7.625 \times 0.8 \times 13.9)\text{in.}^2 = 169.6\ kips$

$N_{crushing} = C_{masonry} + C_{reinforcement} - T_{reinforcement} = 79.2\ kips$

(axial load corresponding to toe crushing)

$N_{critical} = N_{DL} + 0.75N_{LL} + 0.525Q_E$

$N_{DL} = 63.2$ kips (Unfactored axial dead load)

$N_{LL} = (0.25 + \frac{15}{\sqrt{K_{LL}A_T}})N_{LL_0}$

(Unfactored axial live load, reduced by a reduction factor corresponding to three elevated floors)

$K_{LL} = 4$ (Table $4 - 2$ ASCE$7 - 05$)

$A_T = 3 \times (8.67 \times 12)\ \text{ft}^2 = 312\ \text{ft}^2$ (Tributary area)

$$N_{LL0} = (8.67 \times 12)\ \text{ft}^2\ \times (20 + 40 + 40)\frac{\text{lb}}{\text{ft}^2} = 10400\ \text{lb} = 10.4\ \text{kips}$$

$$N_{LL} = \left(0.25 + \frac{15}{\sqrt{4 \times 312}}\right) 10.4\ \text{kips} = 0.67 \times 10.4\ \text{kips} = 6.97\ \text{kips}$$

$Q_E = 0$

$N_{critical} = 54.2\ \text{kip}\ + 0.75 \times 6.97\ \text{kips} + 0 = 59.4\ \text{kips}$

$$N_{crushing} = 79.2\ kips > N_{critical} = 59.4\ kips$$

The critical axial load is less than the axial load corresponding to toe crushing, and maximum reinforcement limitations are satisfied.

E.7.4 Capacity Design for Shear, Wall W-3

Now check *Code* Section 3.1.3 (capacity design for shear) for Wall W-3. The wall is a special reinforced masonry shear wall, so the capacity design requirements of *Code* Section 1.17.3.2.6.1.1 apply.

At an axial load of 37.9 kips, the nominal flexural capacity of this wall is the design capacity of 505 ft-kips, divided by the strength reduction factor of 0.9, or 561 ft-kips. The ratio of this nominal flexural capacity to the factored design moment is 561 divided by 267, or 2.10. Including the additional factor of 1.25, gives a ratio of 2.62.

$$\phi V_n \geq 2.62\, V_u$$

$$V_n \geq \frac{2.62}{\phi} V_u = \frac{2.62}{0.8} V_u = 3.27\, V_u = 3.27 \times 15.2 kips = 49.7\ kips$$

Because V_n = 64.4 kips, the wall requires no shear reinforcement for strength.

Re-check the effects of prescriptive seismic requirements. We need a total steel percentage of 0.002 (summation of required horizontal and vertical reinforcement), with at least 0.0007 horizontally and vertically. Vertical reinforcement is 0.0032 in the web, greater than the required sum, so horizontal reinforcement must meet only the minimum of 0.0007.

Use No. 3 bars at 16 in. horizontally.

$$\rho_{horizontal} = \frac{A_s}{bt} = \frac{0.2\,in.^2}{7.625 \times 16\,in.^2} = 0.0016$$

From the 2008 MSJC *Code*, Section 3.3.4.1.2.2,

$$V_{ns} = 0.5\left(\frac{A_v}{s}\right) f_y d_v$$

$$V_{ns} = 0.5\left(\frac{0.2\,in.^2}{16\,in.}\right) 60\,kips/in.^2 \times 60\,in.$$

$$V_{ns} = 22.5\,kips$$

$$V_n = V_{nm} + V_{ns} = 64.4\,kips + 22.5\,kips = 86.9\,kips$$

This exceeds the required nominal shear capacity of 49.7 kips, and the design is satisfactory for shear.

E.7.5 Summary of Design for Wall W-3

Use seven No. 4 vertical bars at 8 in. in the web, plus one additional No. 4 bar in the end cell of the web (8 bars total). Use five No. 4 vertical bars in the flange. Use No. 4 horizontal bars at 16 in. in the web and the flange.

APPENDIX F
Construction Drawings of Full-scale, 3-Story Specimen

In this appendix are shown the construction drawings for the full-scale, 3-story specimen tested at UCSD.

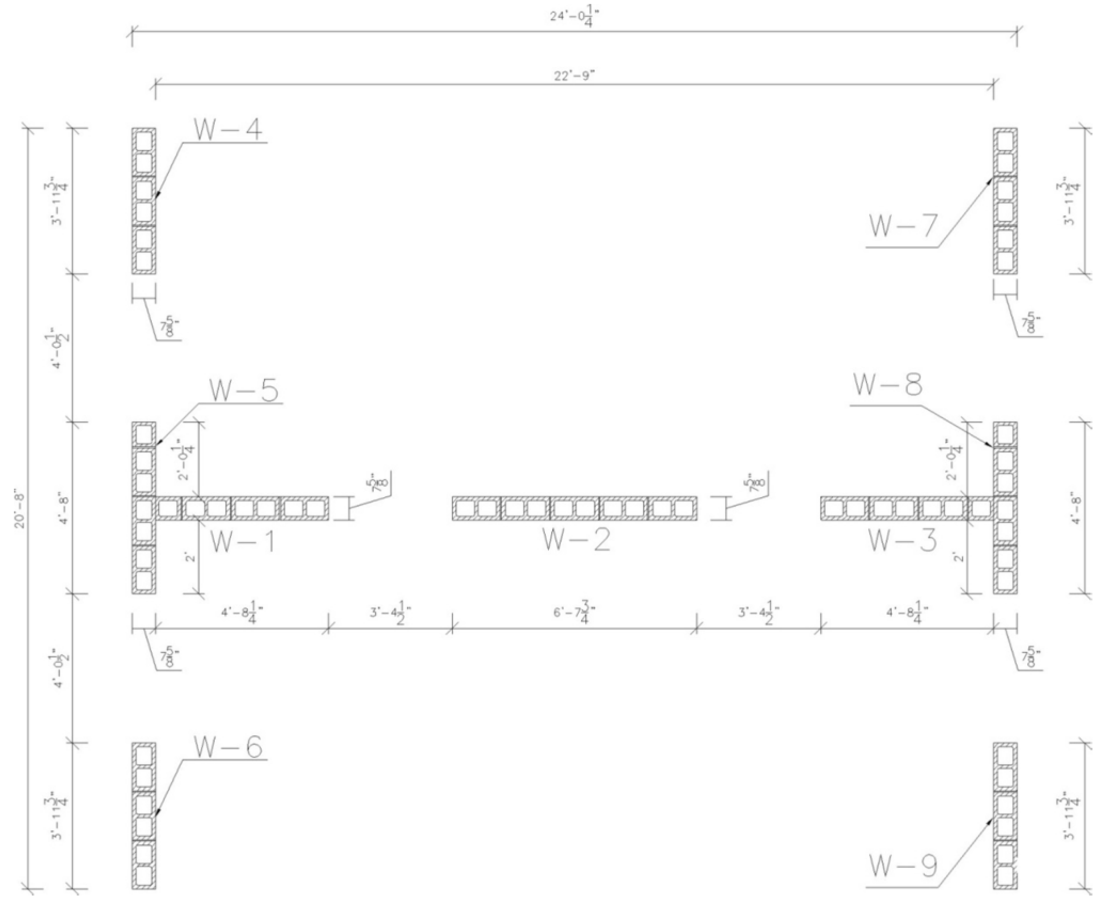

Figure F.1 Wall layout, dimensions, and naming convention

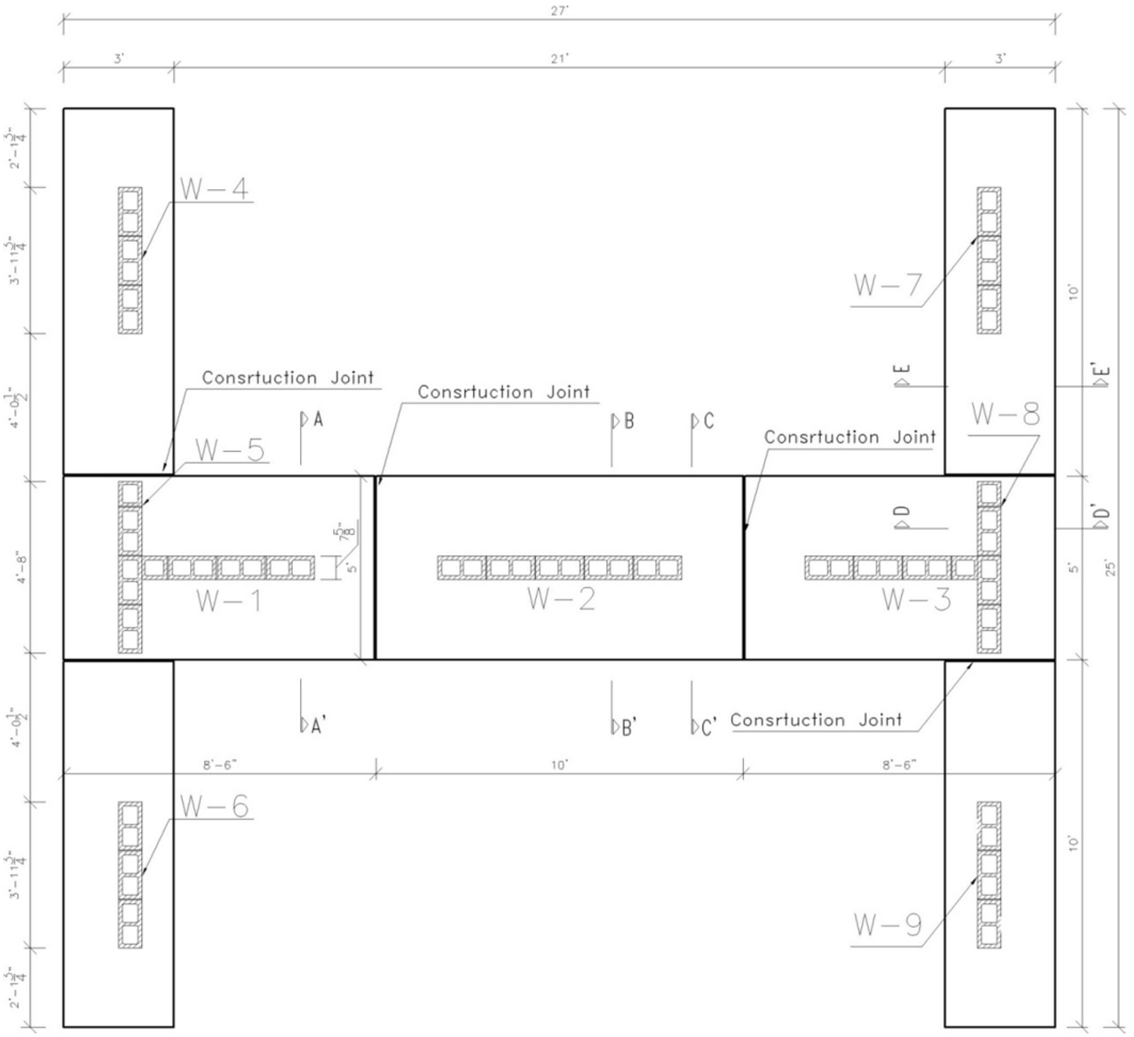

Figure F.2 Dimensions and construction details of foundation beams

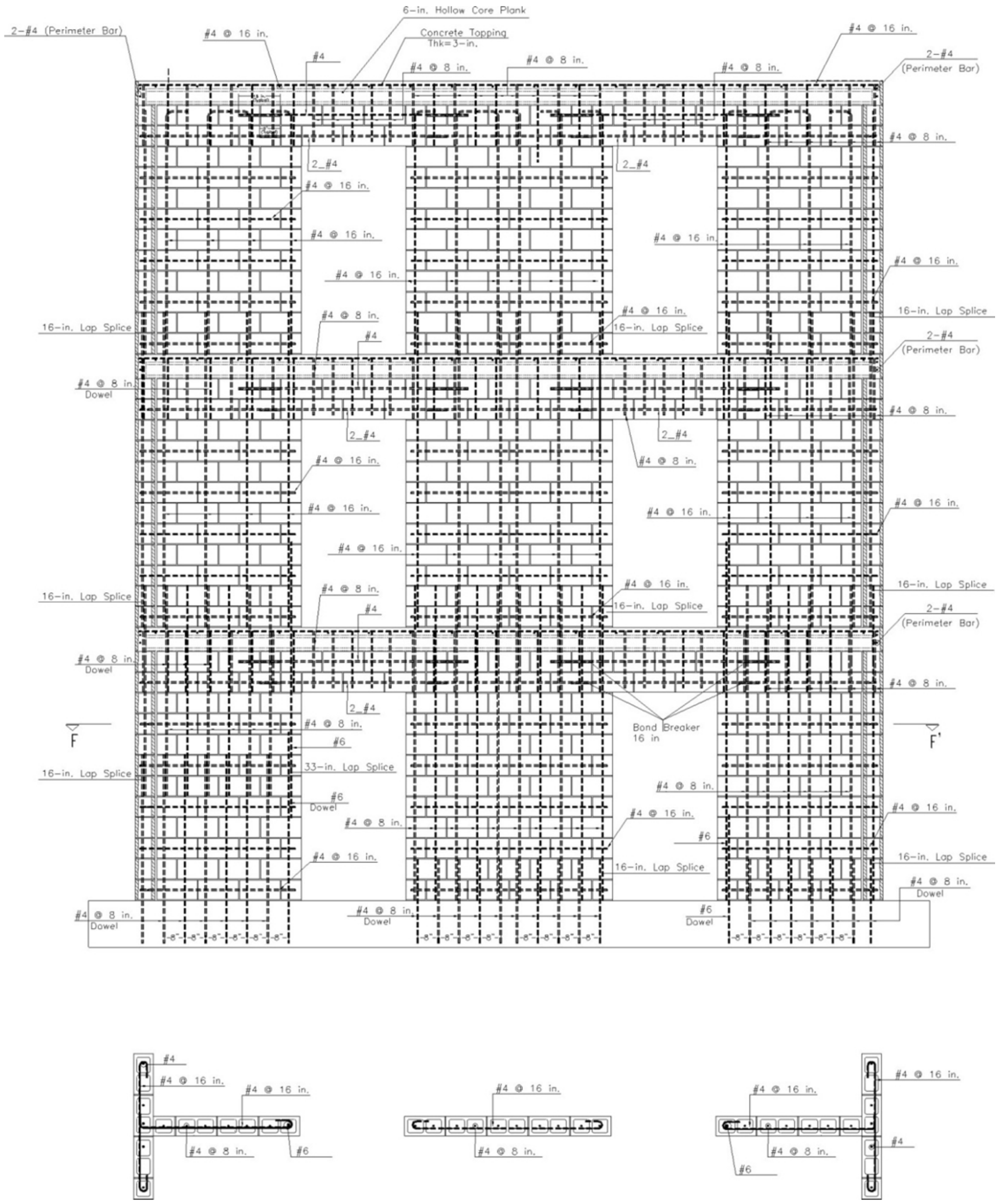

Figure F.3 Design and reinforcement details of Walls W-1, W-2, and W-3

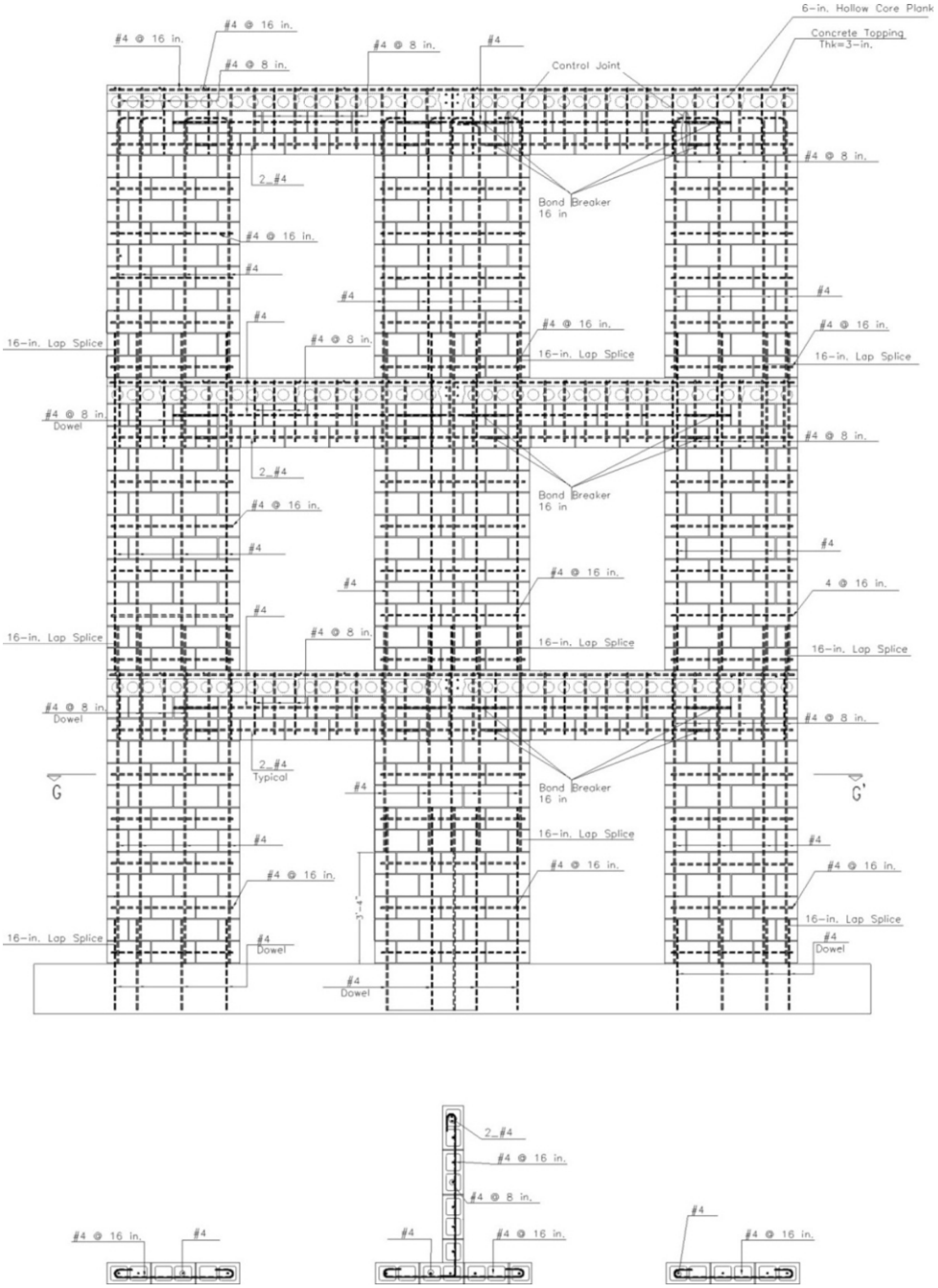

Figure F.4 Design and reinforcement details of Walls W-4, W-5, and W-6

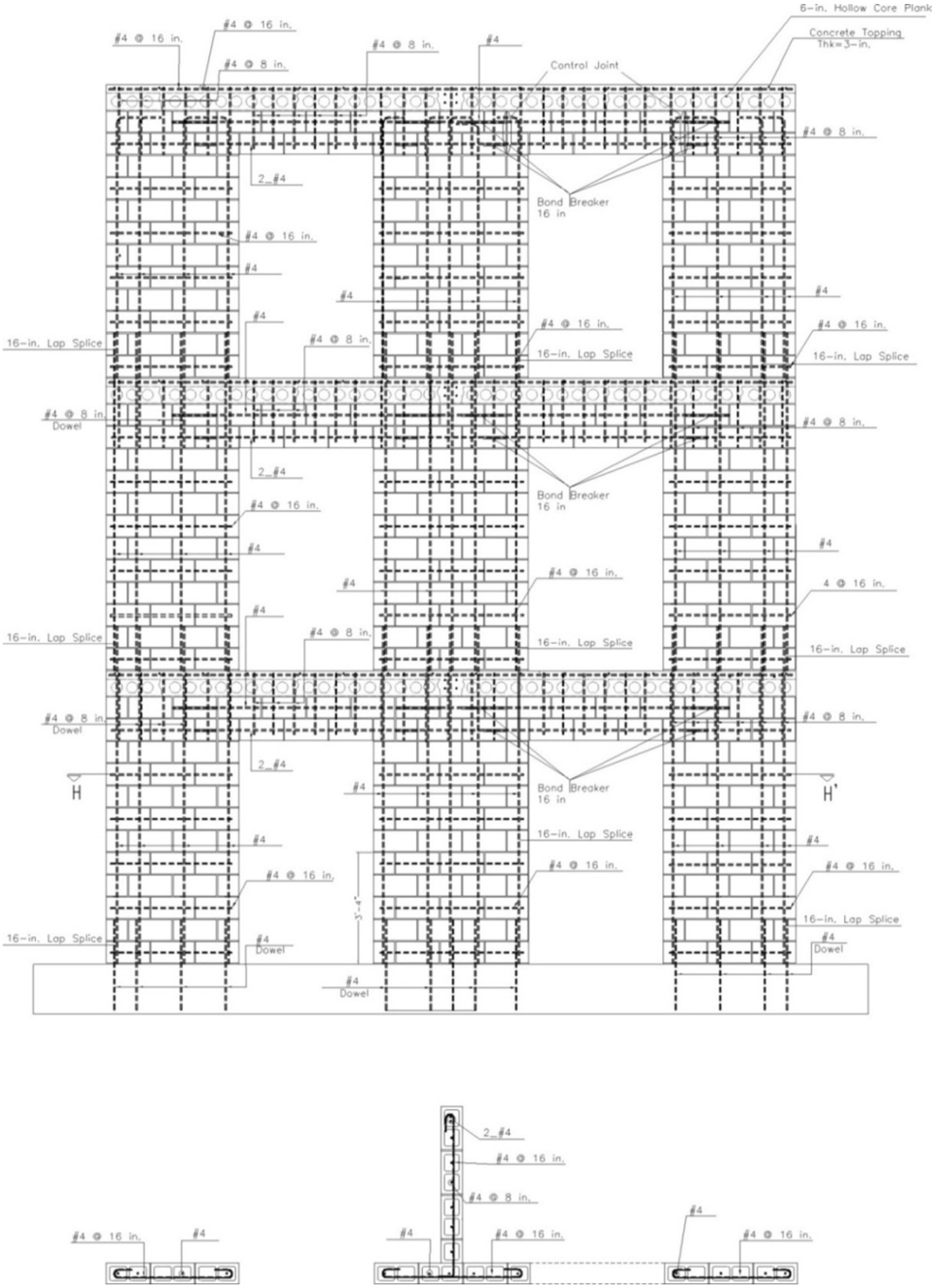

Figure F.5 Design and reinforcement details of Walls W-7, W-8, and W-9

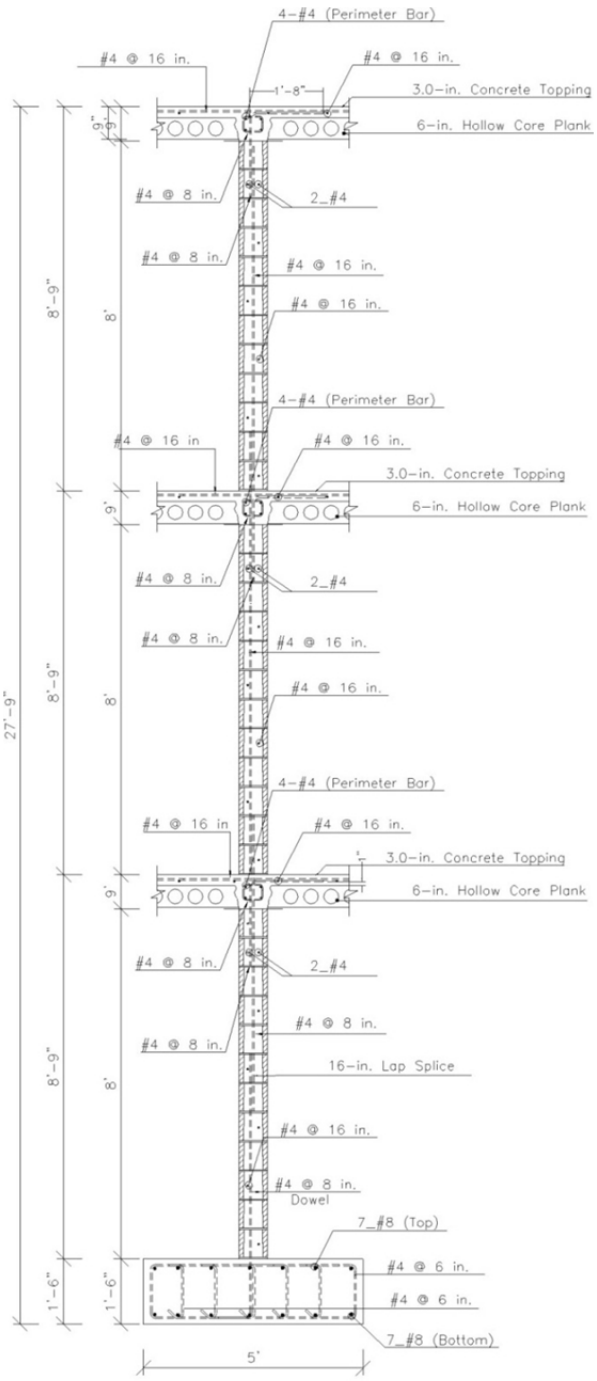

(a) Section A-A

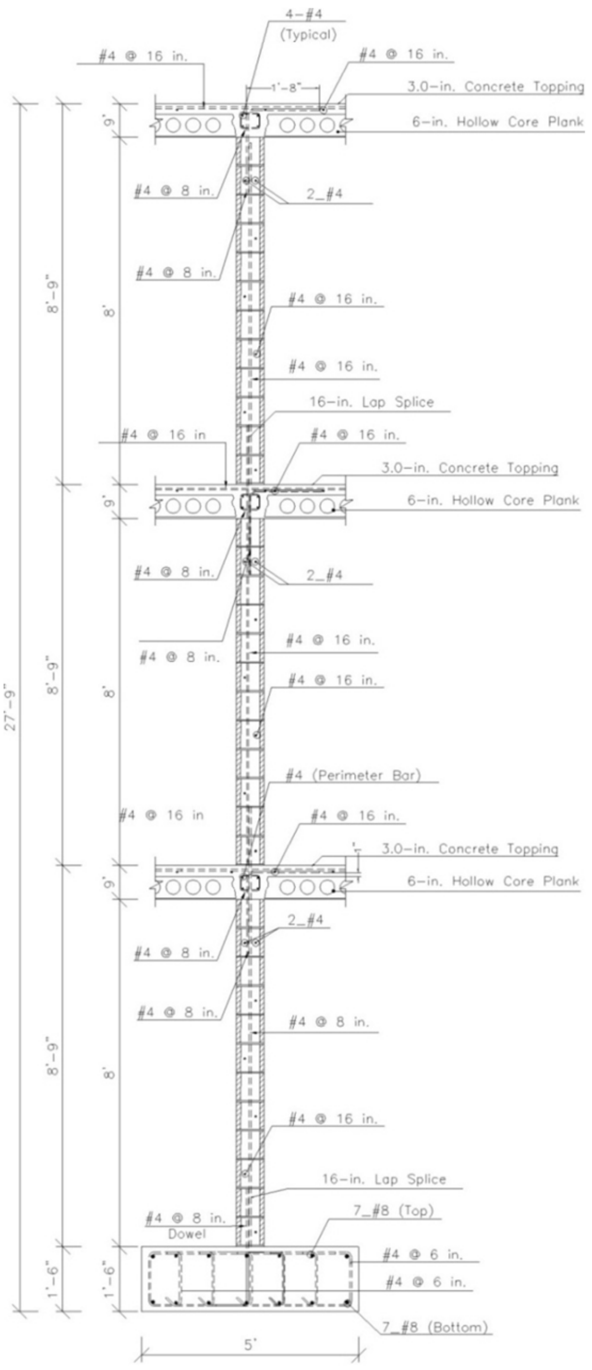

b) Section B-B

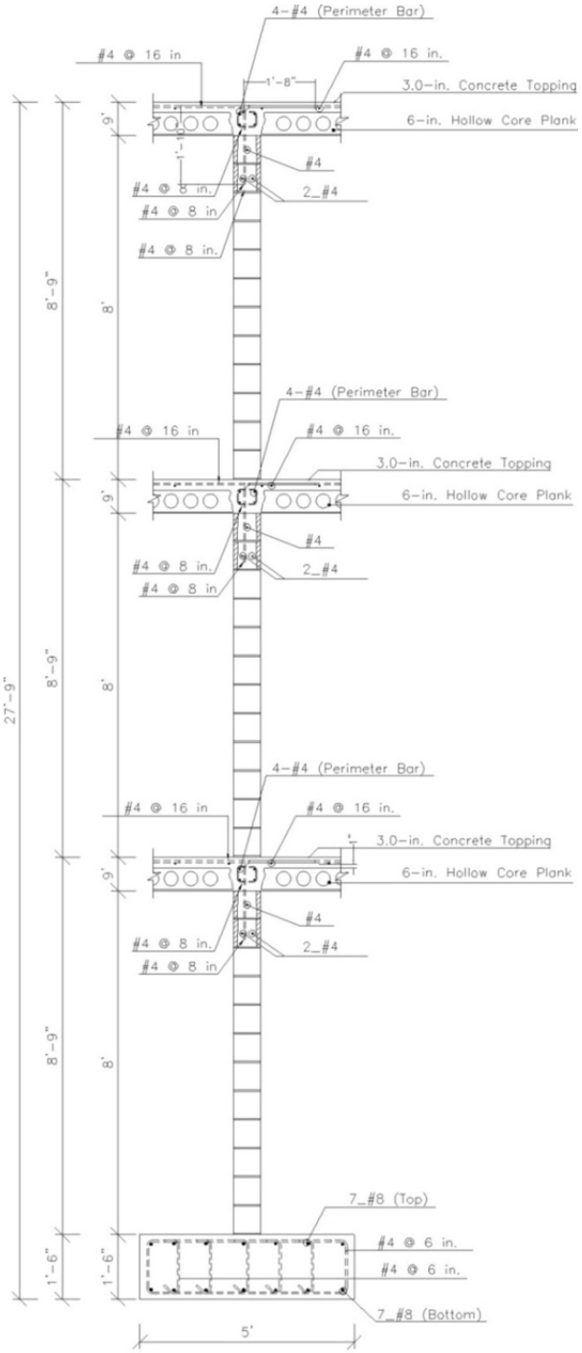

(c) section C-C

Figure F.6 Sections A-A, B-B, and C-C along Walls W-1, W-2, and W-3

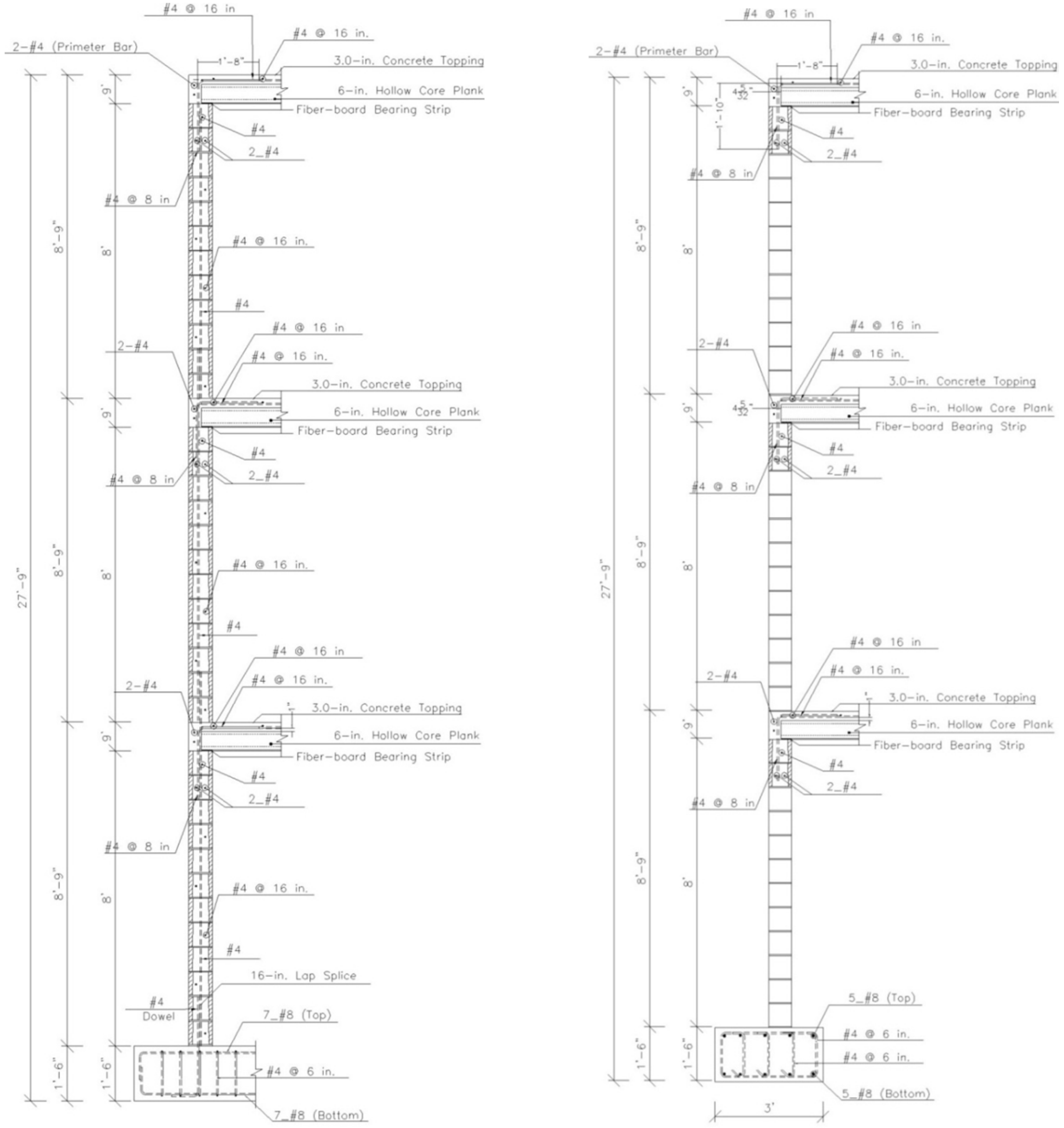

(a) Section D-D

(b) Section E-E

Figure F.7 Sections D-D and E-E along Walls W-7, W-8, and W-

APPENDIX G

Instrumentation Plan of Full-scale, 3-Story Specimen

The instrumentation plans shown here for the full-scale, 3-story specimen tested at UCSD were prepared by Marios Mavros, doctoral candidate at UCSD. They are repeated here for completeness.

Table G-1 Legend for the instrumentation drawings presented in this section

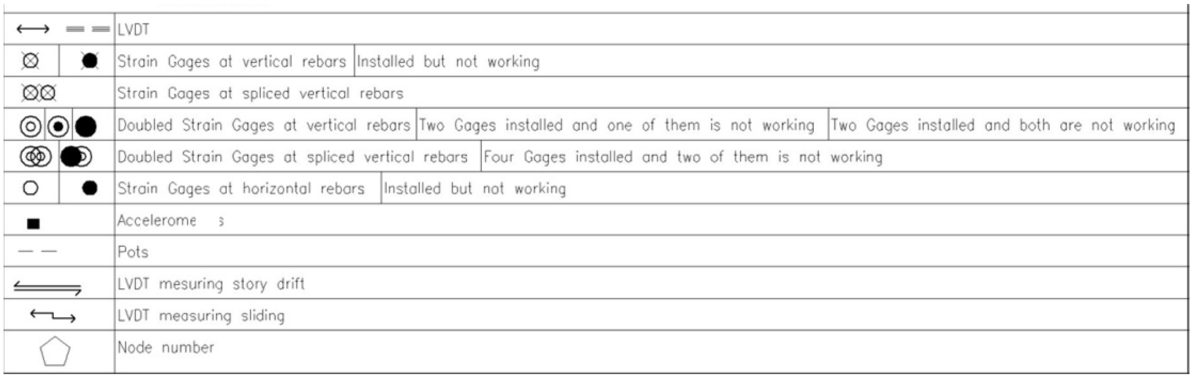

⟷	══	LVDT		
⊗	●	Strain Gages at vertical rebars	Installed but not working	
⊗⊗		Strain Gages at spliced vertical rebars		
◎	⊙ ●	Doubled Strain Gages at vertical rebars	Two Gages installed and one of them is not working	Two Gages installed and both are not working
◎◎	●◎	Doubled Strain Gages at spliced vertical rebars	Four Gages installed and two of them is not working	
○	●	Strain Gages at horizontal rebars	Installed but not working	
■		Accelerome s		
— —		Pots		
⇌		LVDT mesuring story drift		
⟷		LVDT measuring sliding		
⬠		Node number		

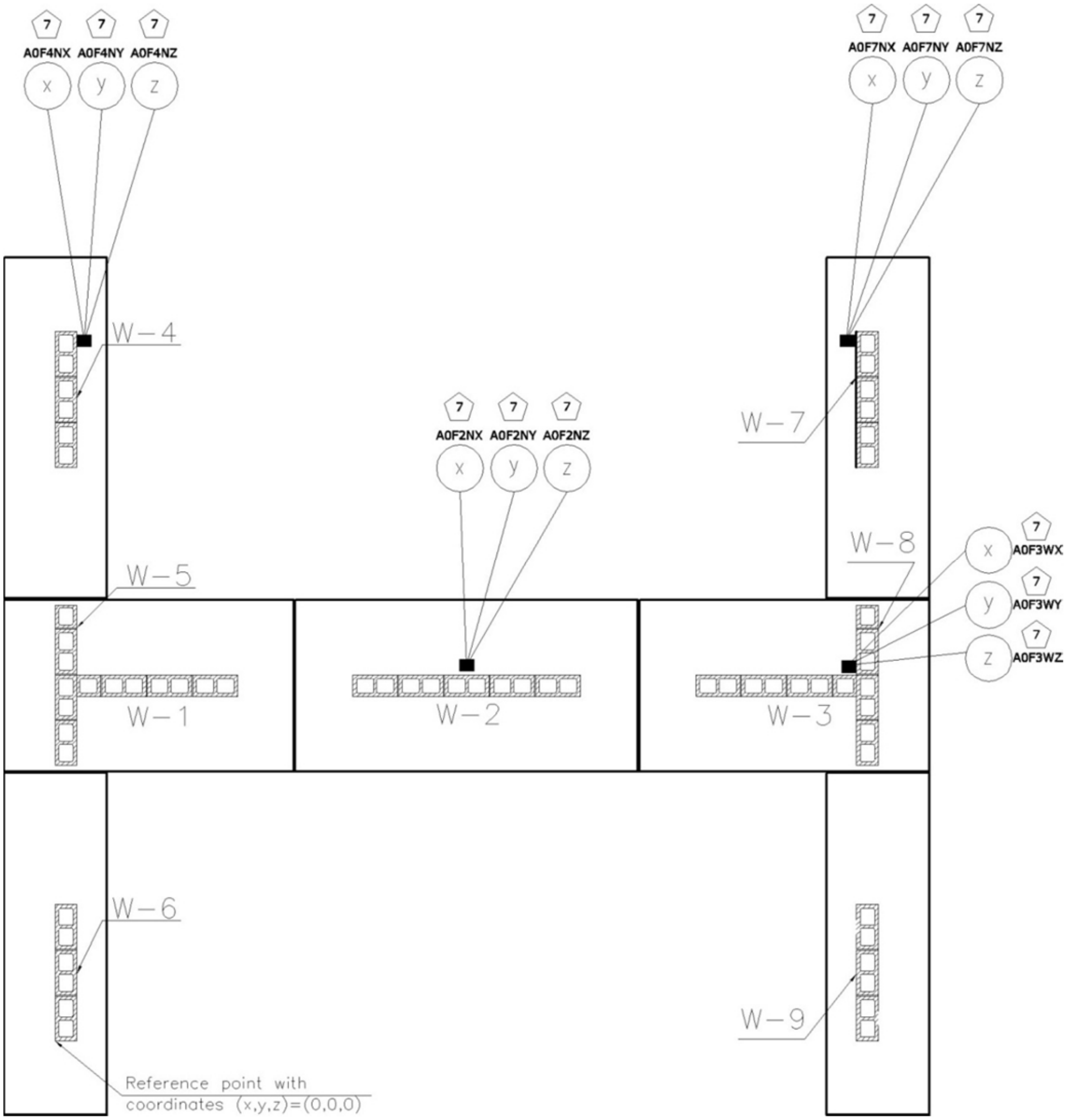

Figure G.1 Locations of accelerometers on foundation beams

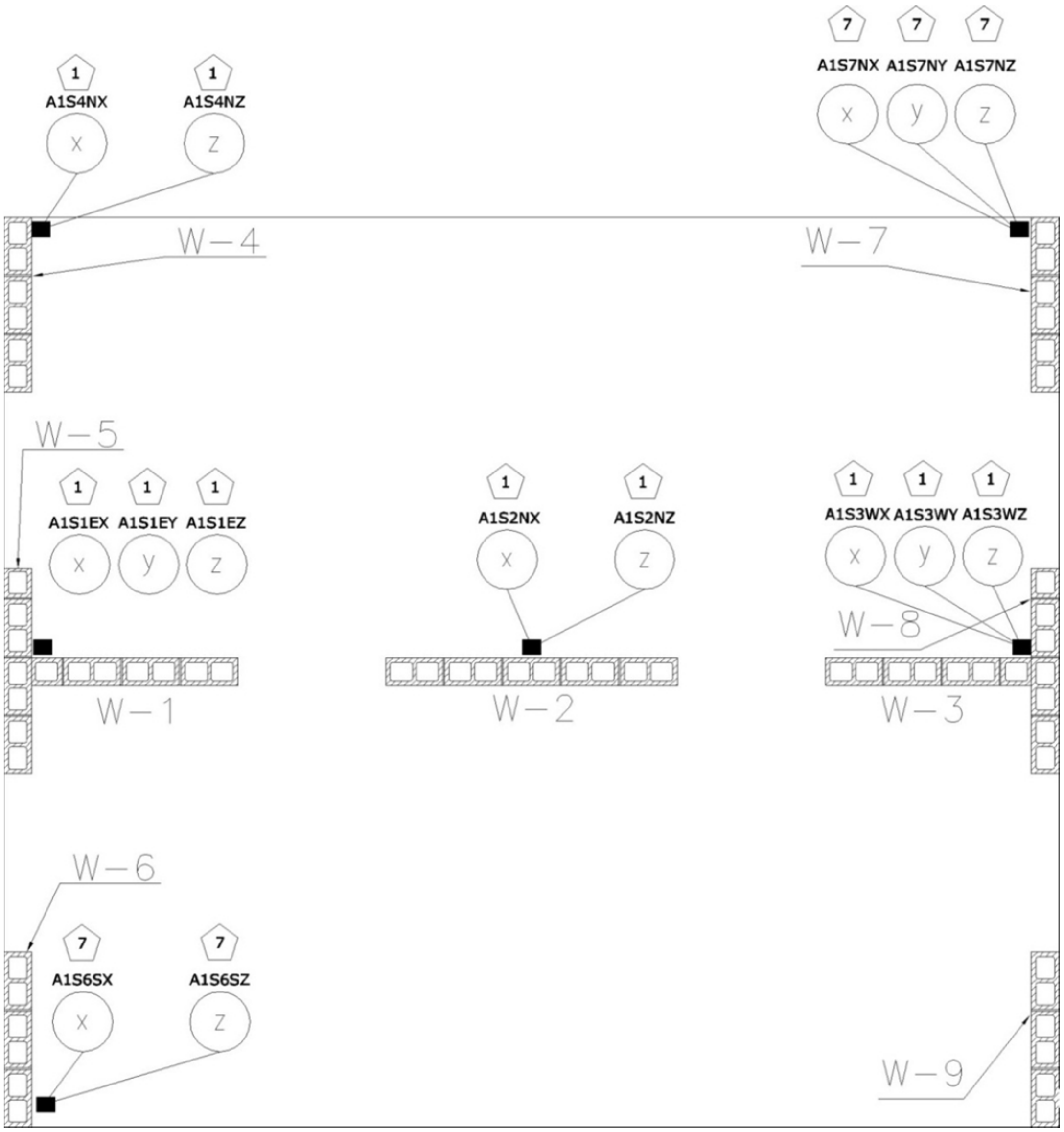

Figure G.2 Locations of accelerometers on second-story slab

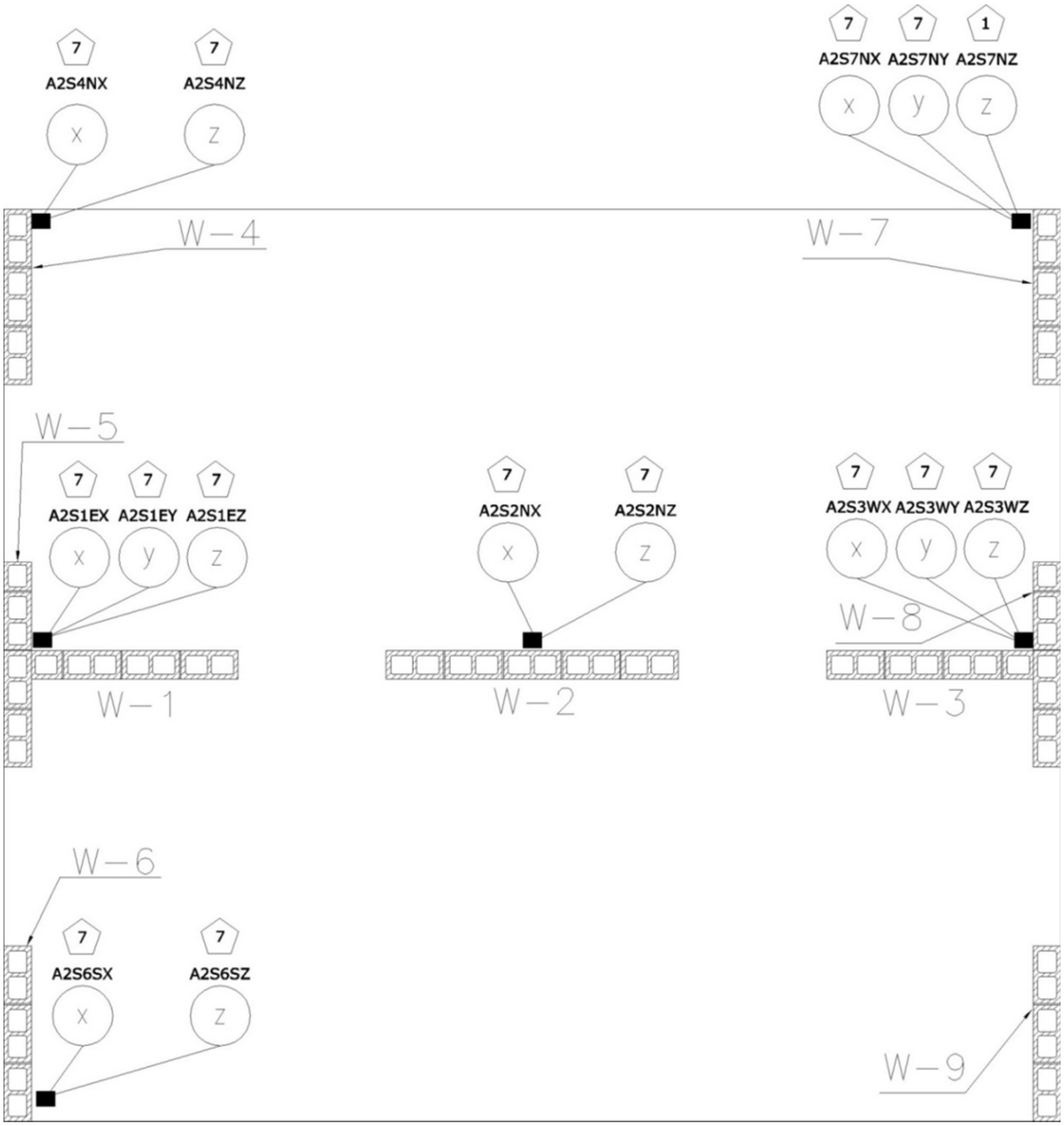

Figure G.3 Locations of accelerometers on third-story slab

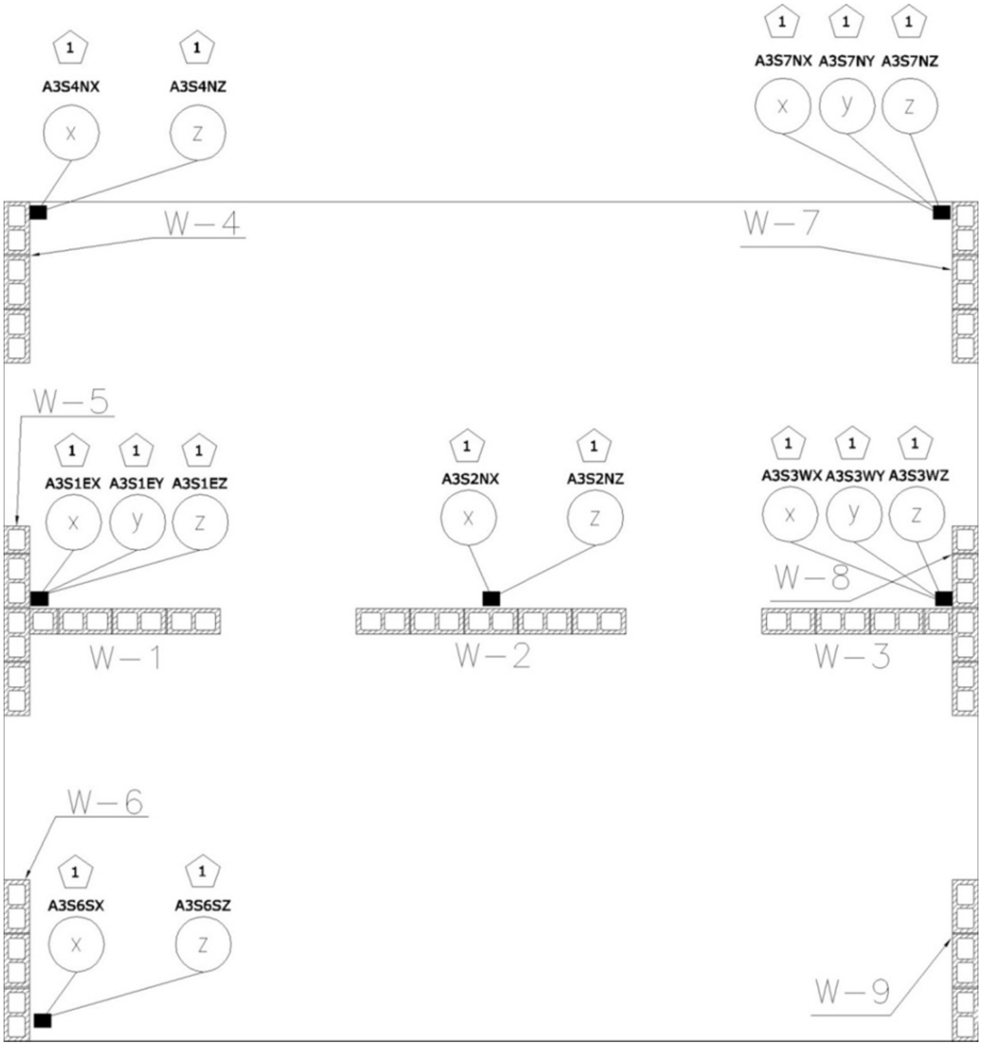

Figure G.4 Locations of accelerometers on roof slab

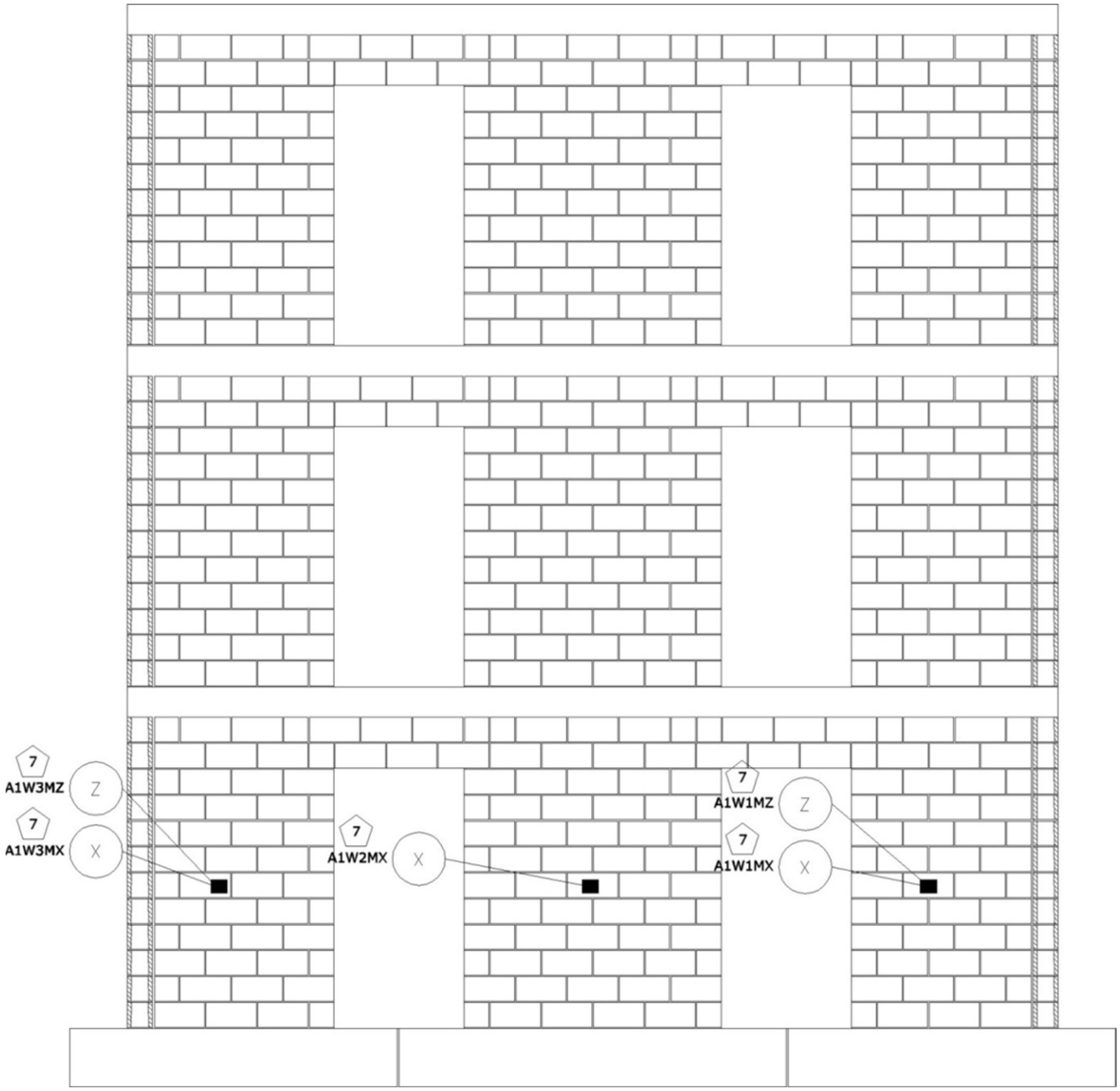

Figure G.5 Locations of accelerometers on Walls W-1, W-2, and W-3

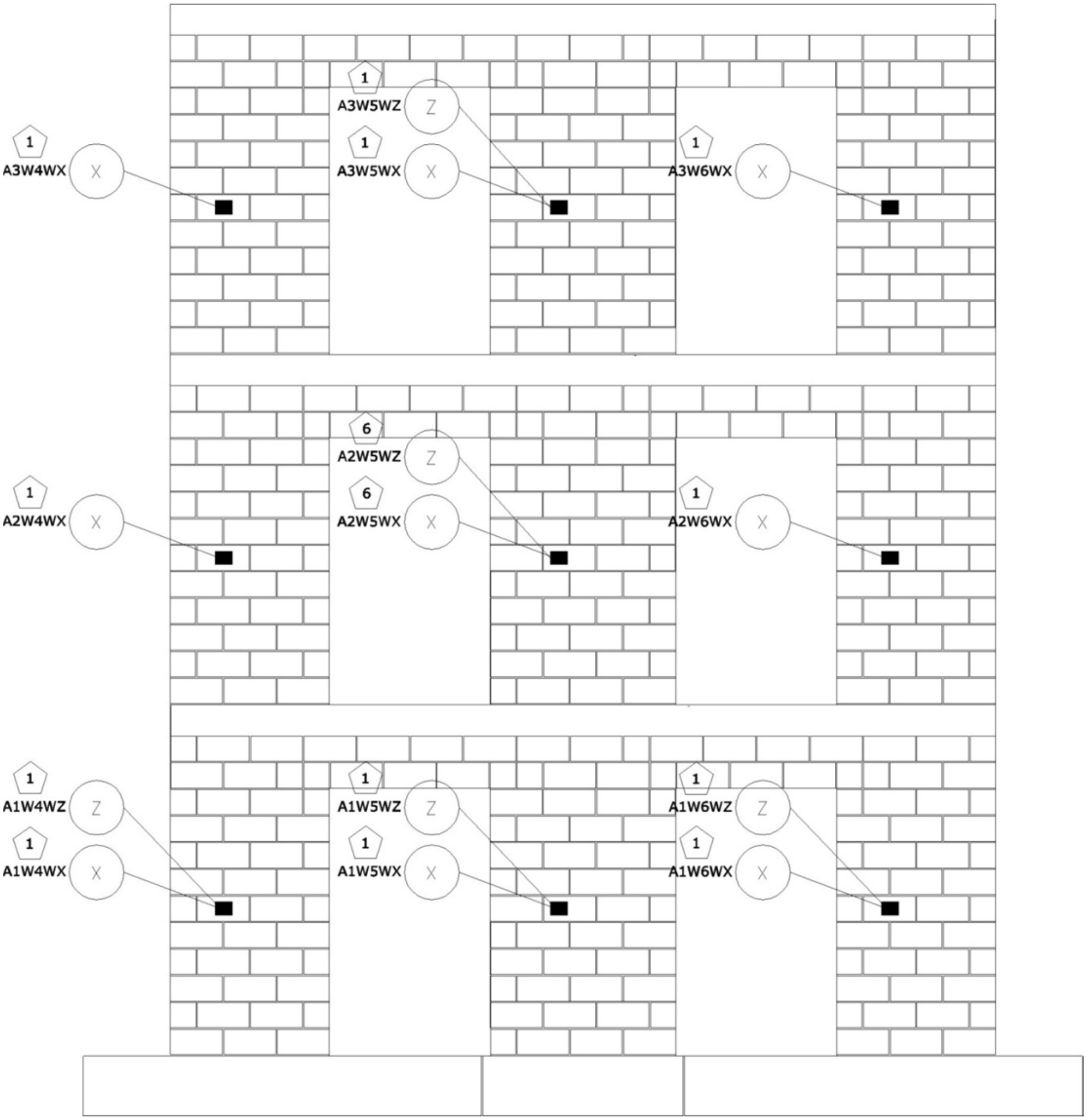

Figure G.6 Locations of accelerometers on Walls W-4, W-5, and W-6

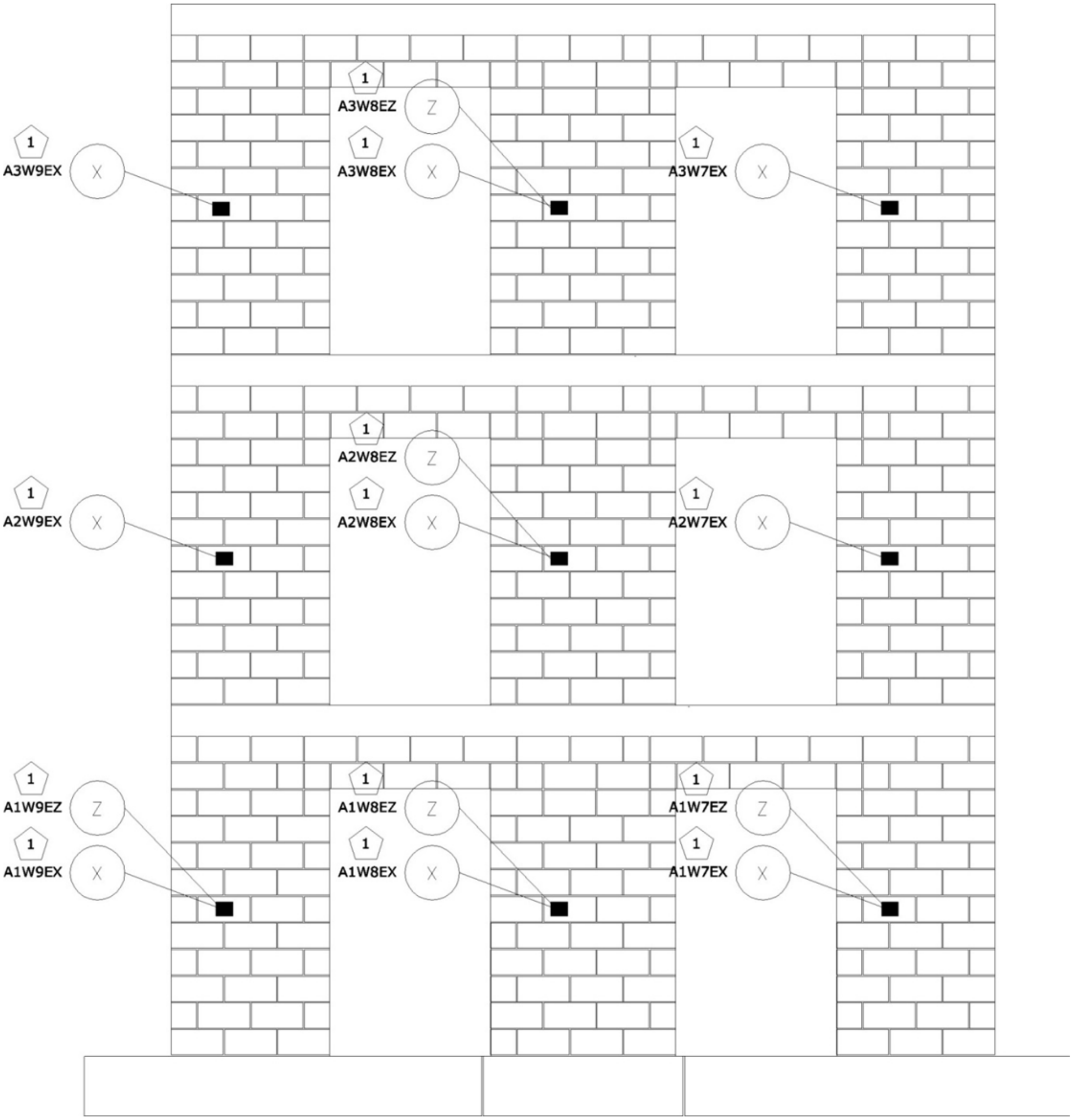

Figure G.7 Locations of accelerometers on Walls W-7, W-8, and W-9

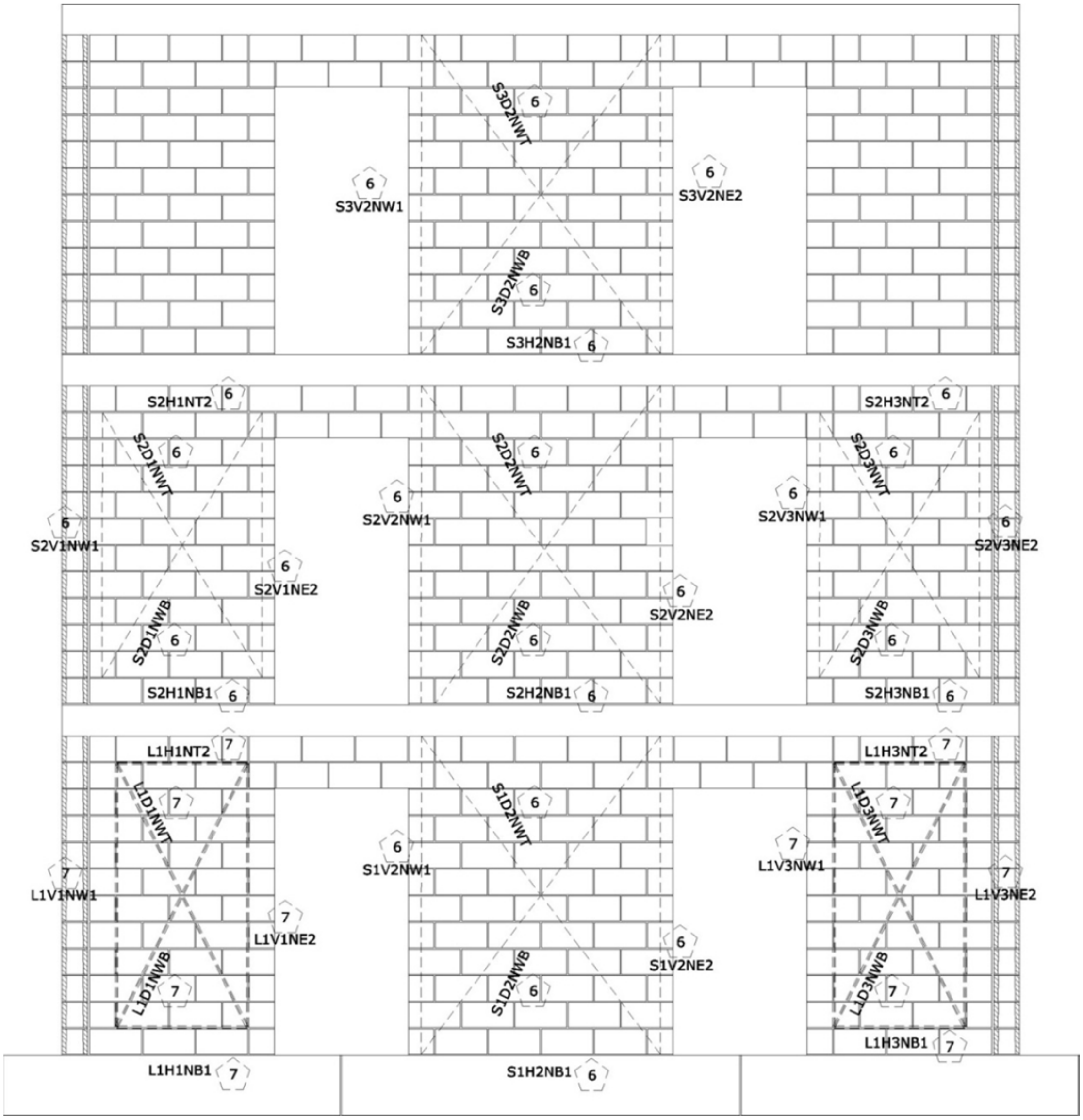

Figure G.8 Locations of displacement transducers on Walls W-1, W-2, and W-3

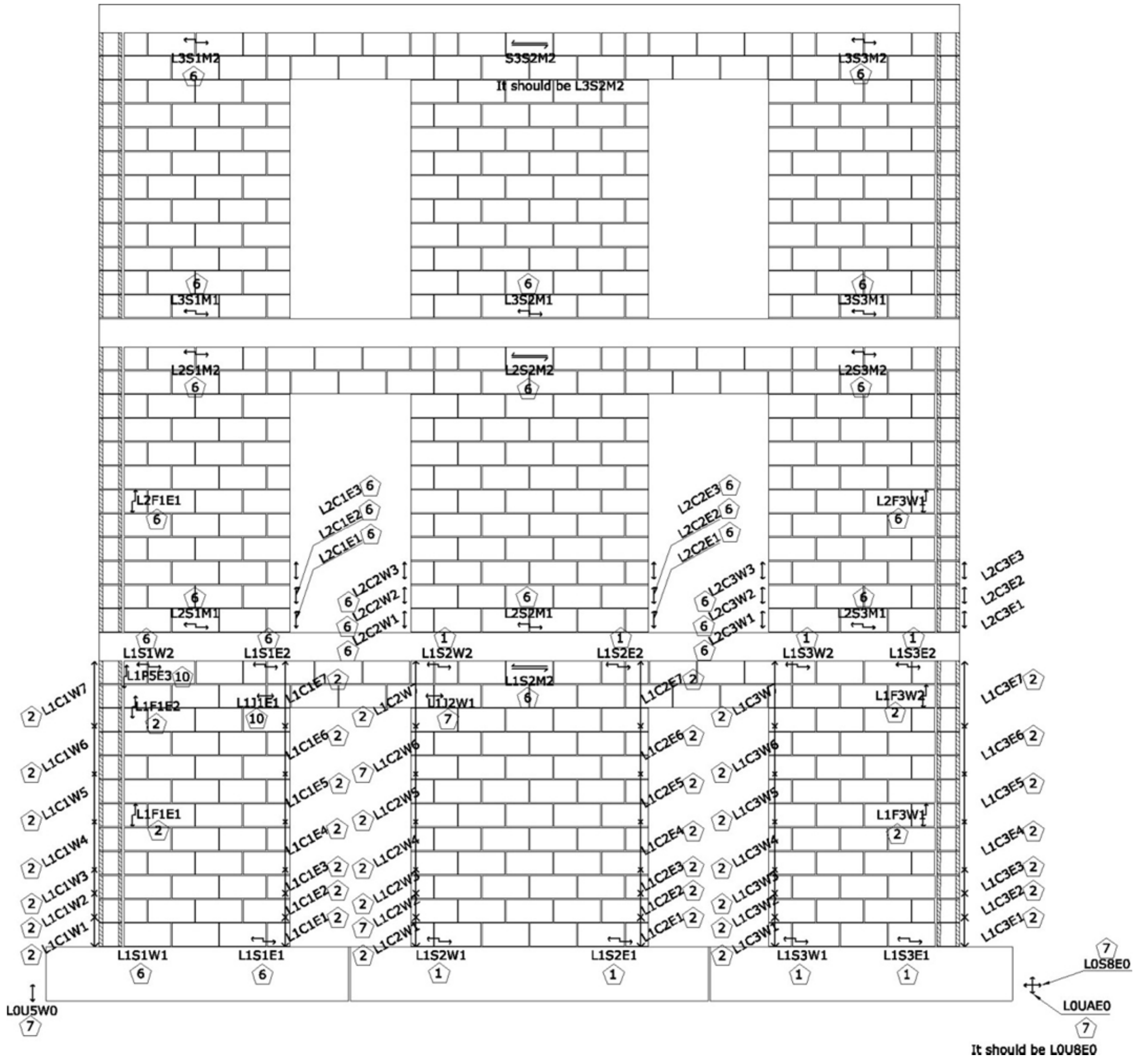

Figure G.9 Locations of displacement transducers on Walls W-1, W-2, and W-3

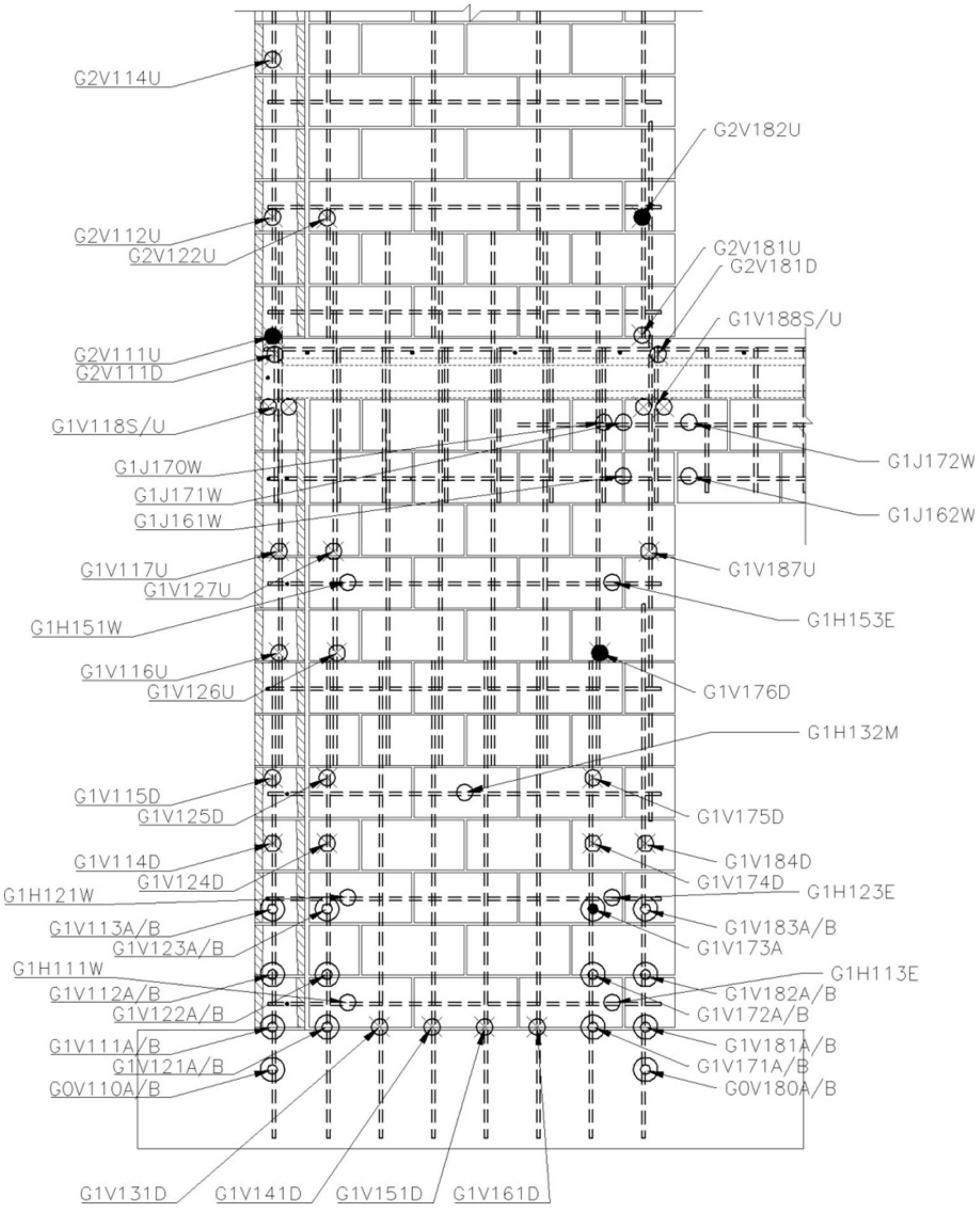

Figure G.10 Locations of strain gages on Wall W-1

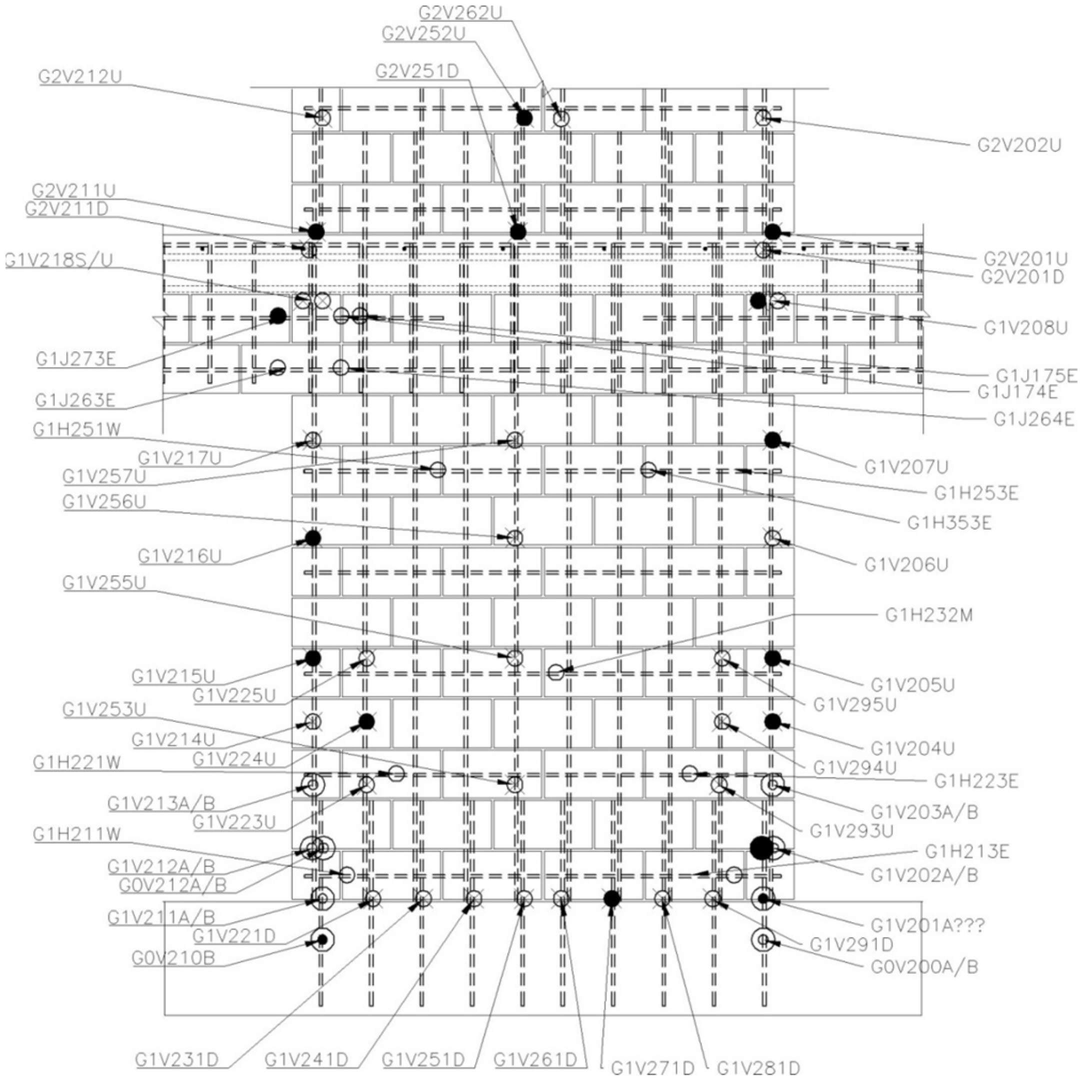

Figure G.11 Locations of strain gages on Wall W-2

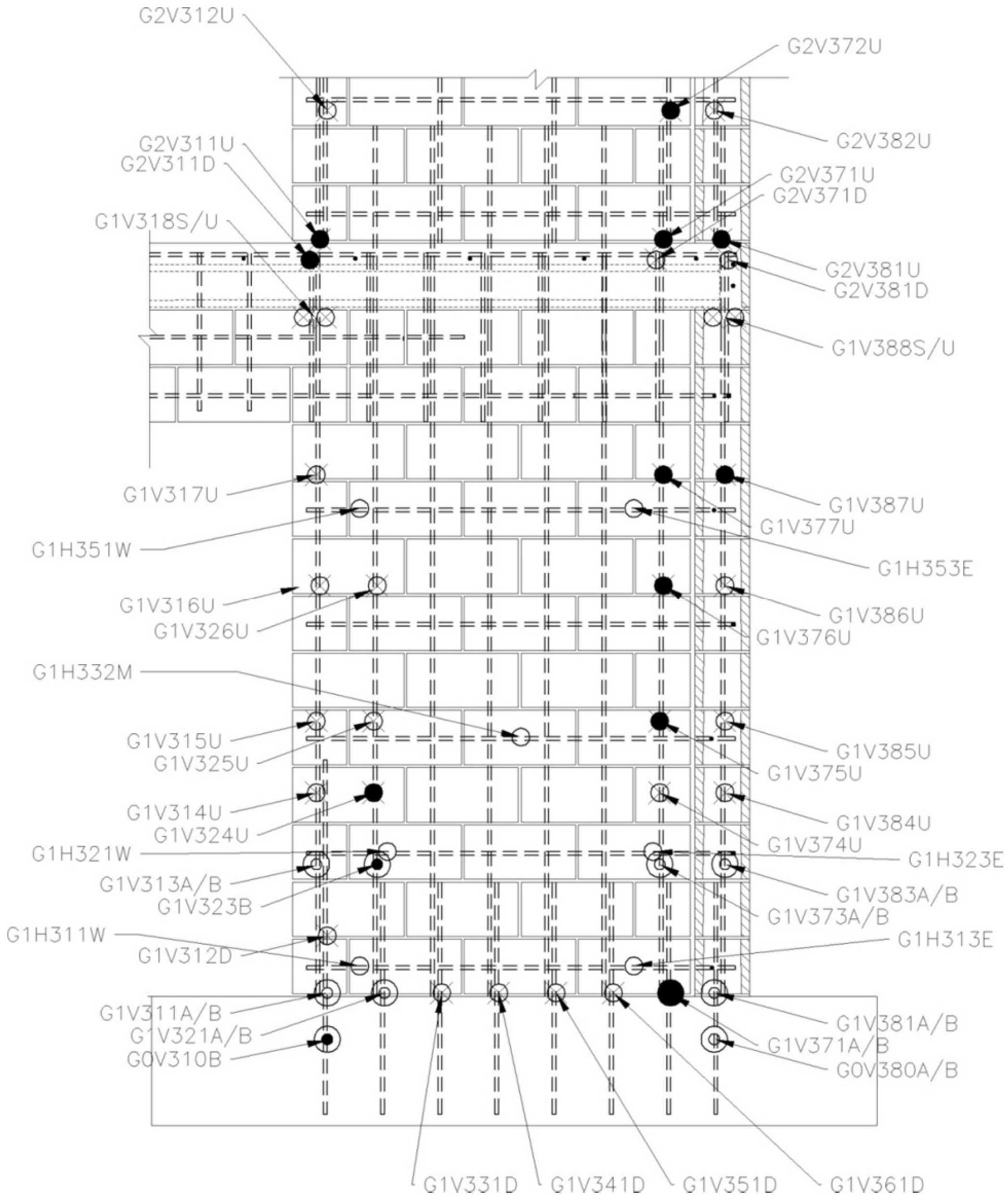

Figure G.12 Locations of strain gages on Wall W-3

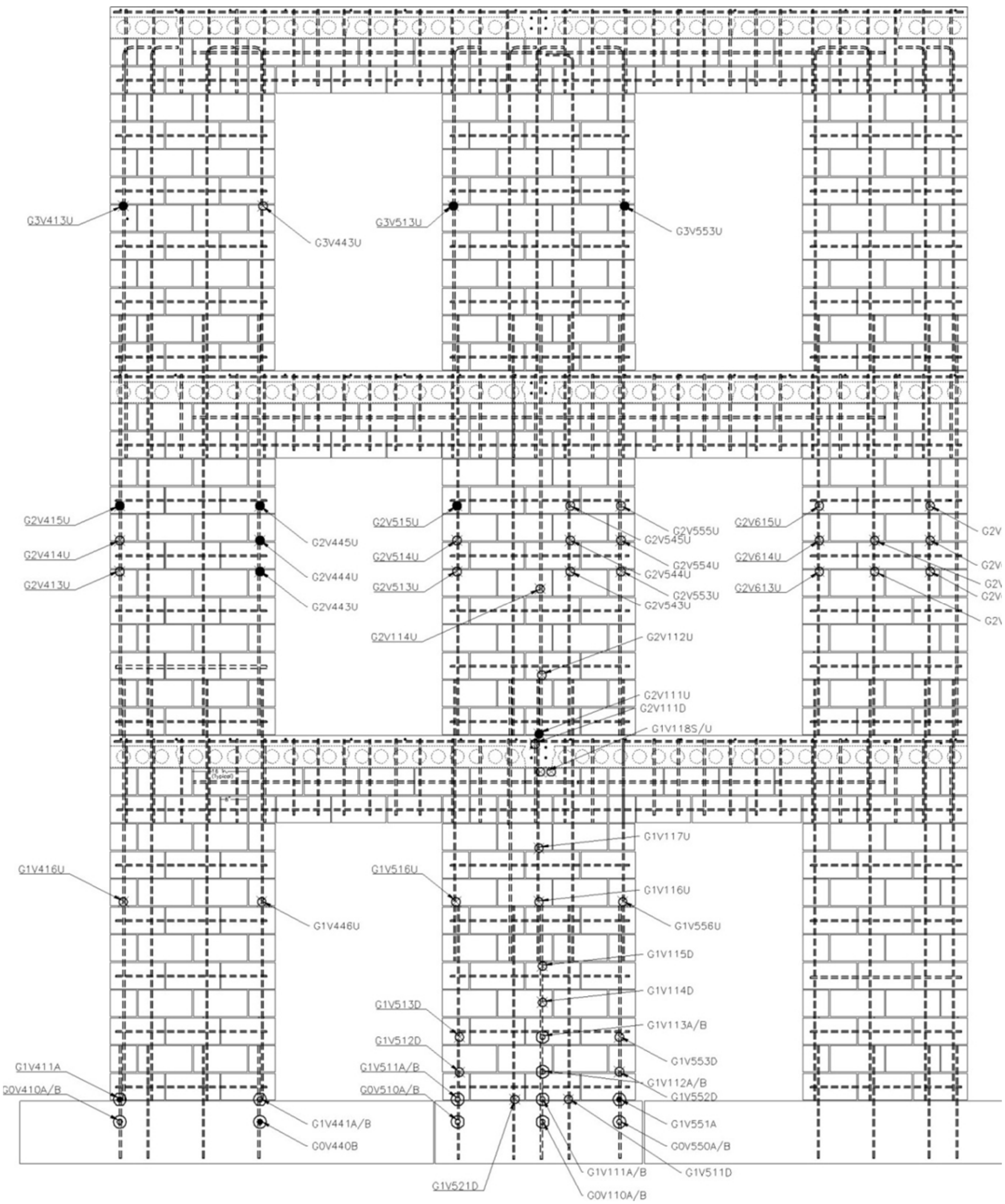

Figure G.13 Locations of strain gages on Walls W-4, W-5, and W-6

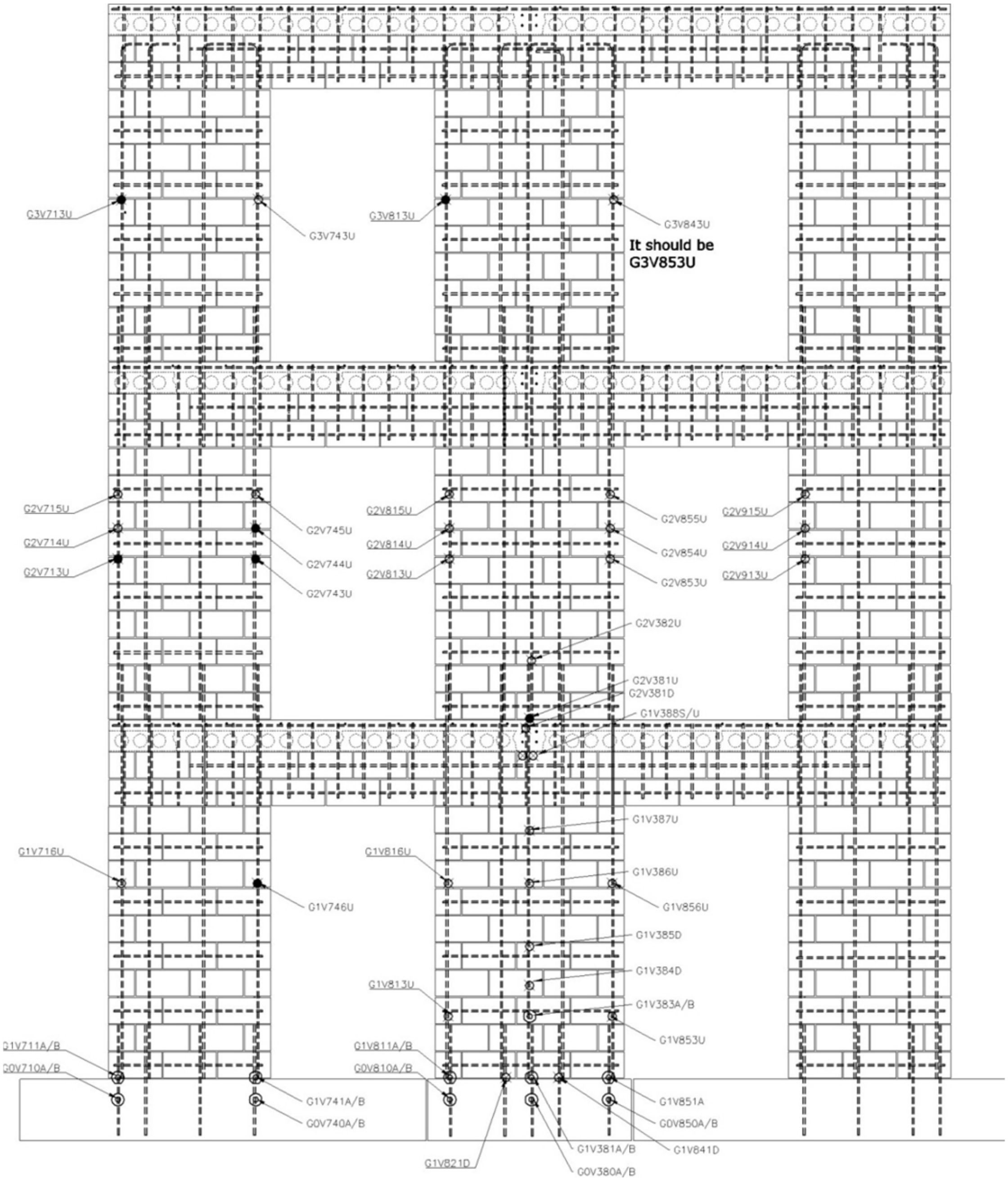

It should be G3V853U

Figure G.14 Locations of strain gages on Walls W-7, W-8, and W-9

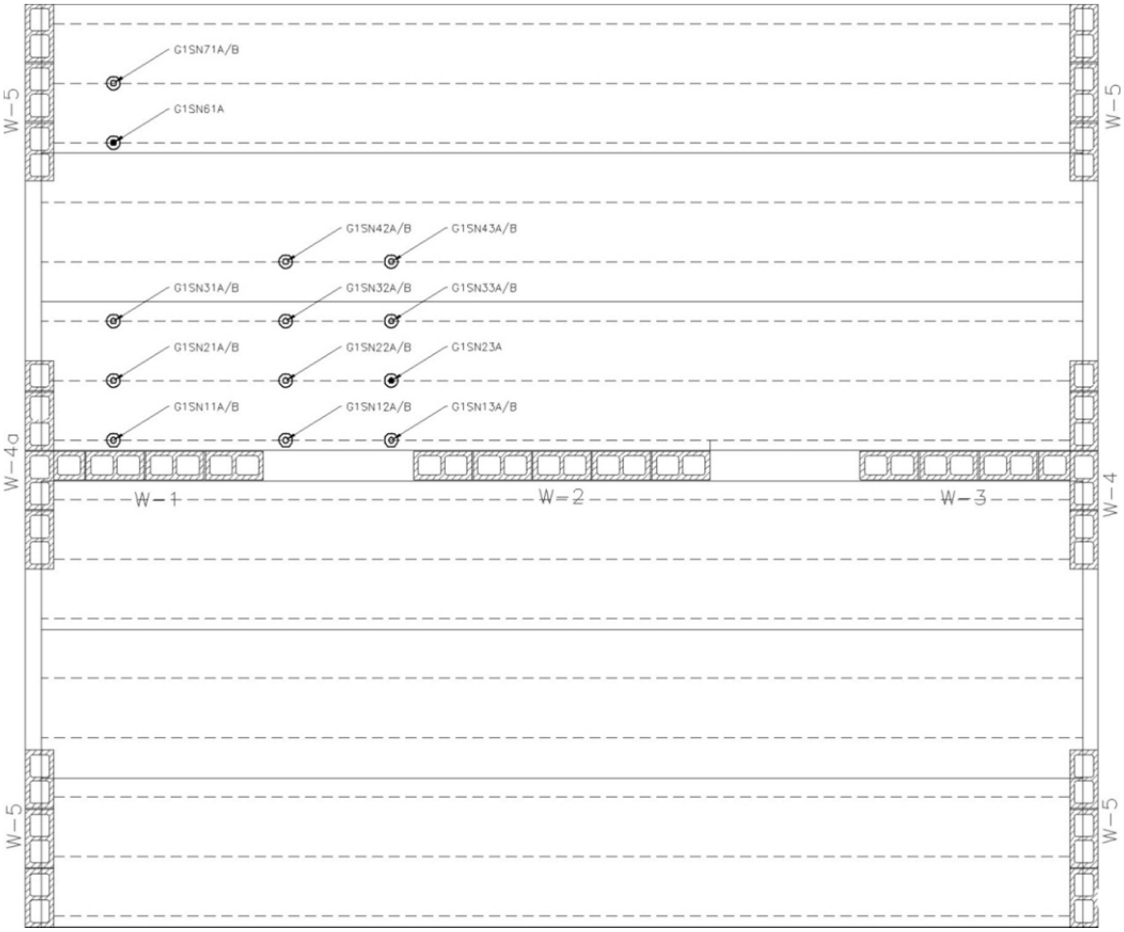

Figure G.15 Locations of strain gages on second-story slab

APPENDIX H Gravity Loads for Full-scale, Two-Story Specimen

In this appendix, gravity loads for the full-scale, two-story specimen tested at UCSD are calculated in accordance with ASCE-SEI 7-2010.

Design Roof Load due to Gravity: Design roof load due to gravity is calculated below.

Dead Load	11-in. slab (8-in. hollow-core slab + 3-in. topping)	102 lb/ft^2
Live Load	Live load	20 lb/ft^2

Design Floor Load due to Gravity: Design floor load due to gravity is calculated below:

Dead Load	11-in. slab (8-in. hollow-core slab + 3-in. topping)	102 lb/ft^2
Live Load	Live load	40 lb/ft^2

The typical plan of the specimen, shown here, has a plan length of 22.67 ft and a plan width of 20.67 ft.

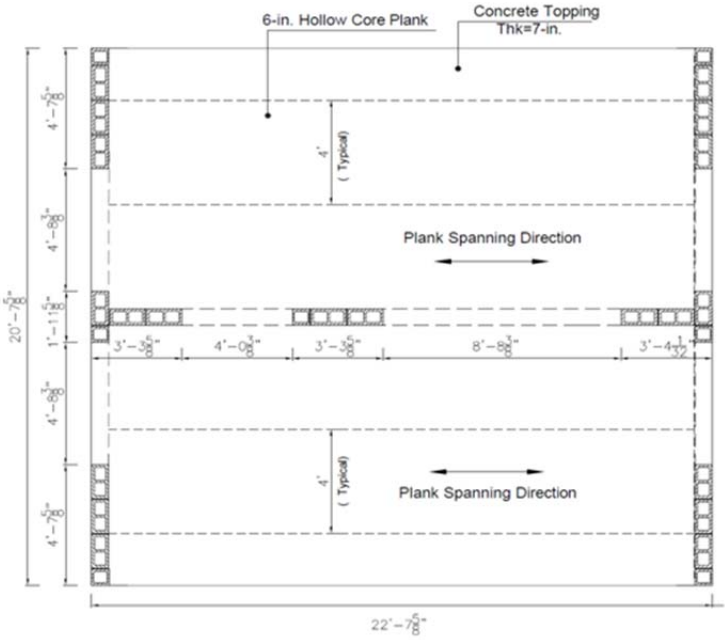

Figure H.1 Plan view of typical floor of two-story specimen

The weight of a typical floor is its area, times the dead load per square foot, plus the interior wall weight, plus the weight of the exterior walls. For the roof, the weight of floor is its area, times the dead load per square foot, plus half the longitudinal wall (interior wall) weight, plus half the transverse wall (exterior wall) weight. Between story levels, half the wall weight goes to the story above, and half goes to the story below. Wall weights are computed as the weights without openings, and the weights of the openings are then subtracted.

Roof level:

Floor	102 lb/ft^2 x 20.67 x 22.67 ft^2	= 47.8kips
Longitudinal wall	1/2 x (22.67 x 8 –8.0 x 3.33–4 x 6) x 126 lb/ft^2	= 5.3 kips

weight		
Transverse wall weight	1/2x2x (20.67 x 8 – 2 x 6.67 x 4) x 126 lb/ft^2	= 9.0 kips

Total weight of the roof level is 62.1 kips.

First floor:

Floor	102 lb/ft^2 x 20.67 x 22.67 ft^2	= 47.8 kips
Longitudinal wall weight	(22.67 x 8 –8.0 x 3.33–4 x 4) ft^2 x 80 lb/ft^2	= 11.1 kips
Transverse wall weight	2 x (20.67 x 8 – 2 x 6.67 x 4.0) ft^2 x 80	= 17.9 kips

Total weight of a typical floor is 76.8 kips.

APPENDIX I

Construction Drawings of Full-scale, 2-Story Specimen

This appendix provides construction drawings for the full-scale, 2-story specimen tested at UCSD.

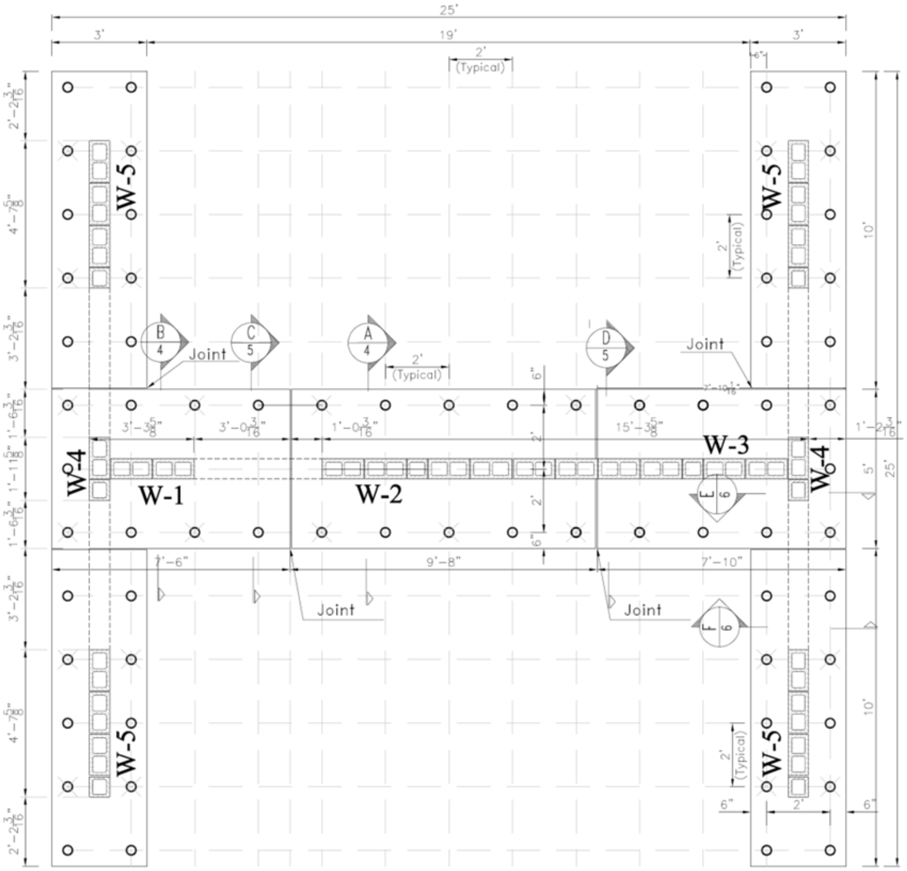

Figure I.1 Dimensions and construction details of foundation beams and wall layout

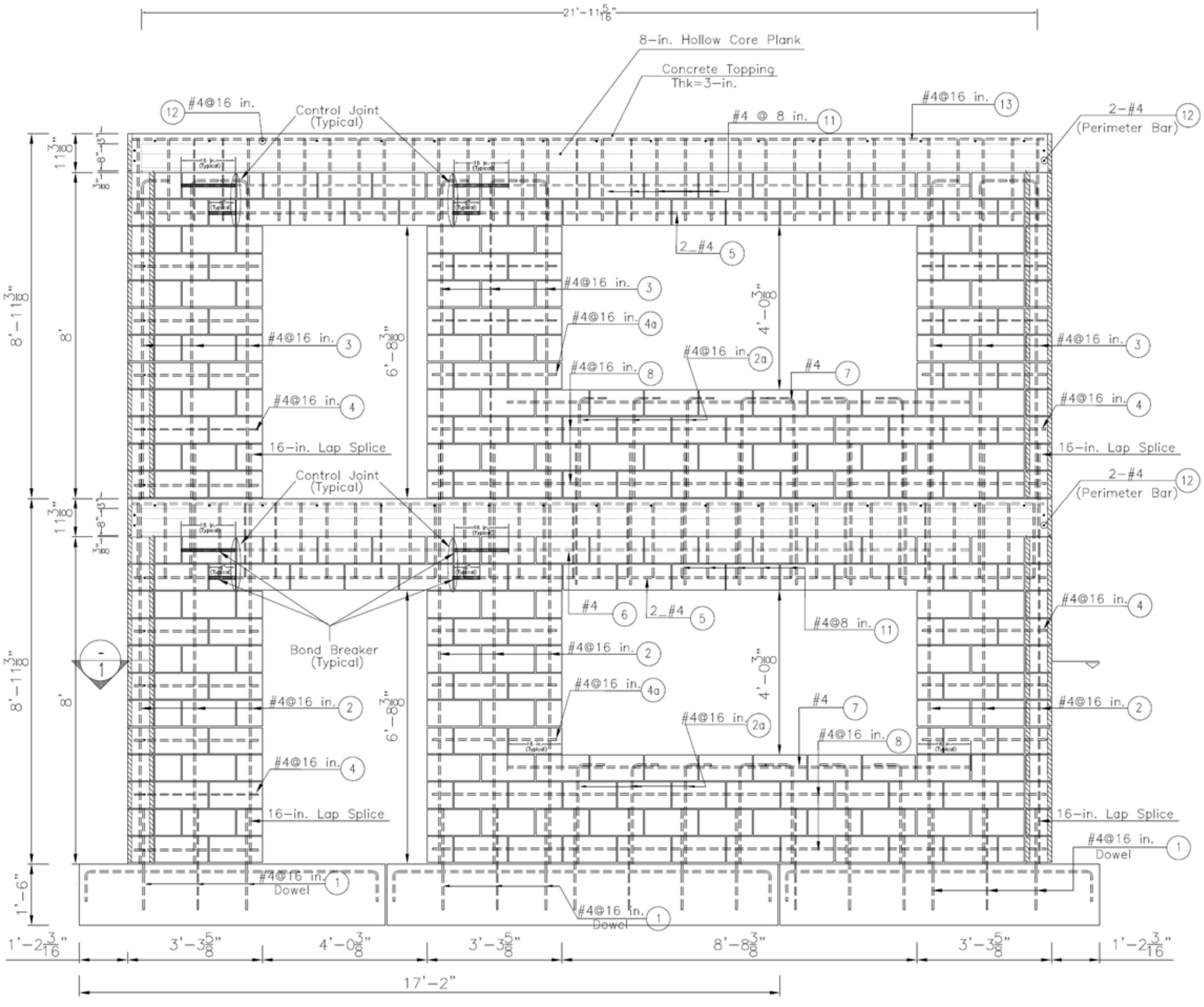

Figure I.2 Design and reinforcement details of Walls W-1, W-2, and W-3

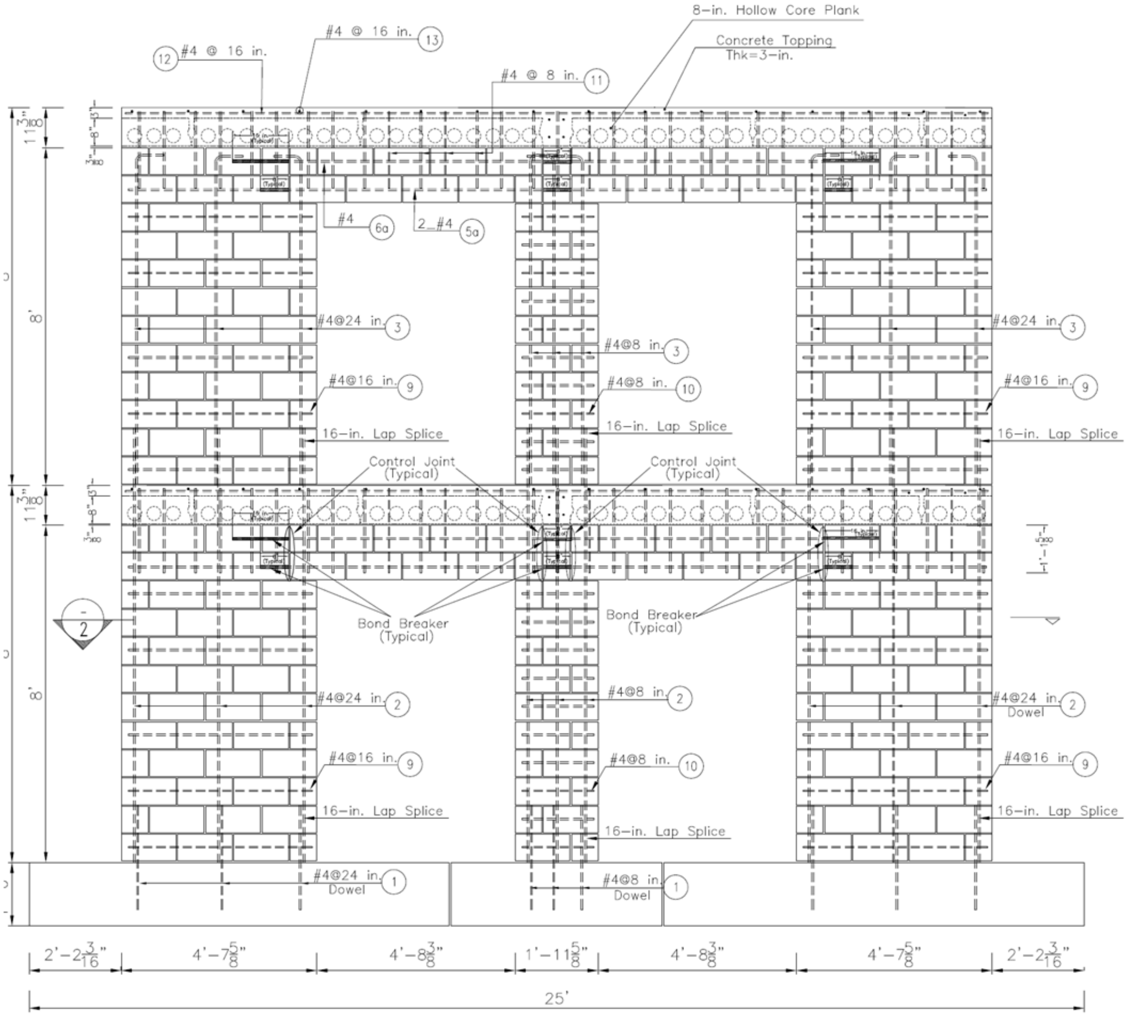

Figure I.3 Design and reinforcement details of Walls W-4 and W-5

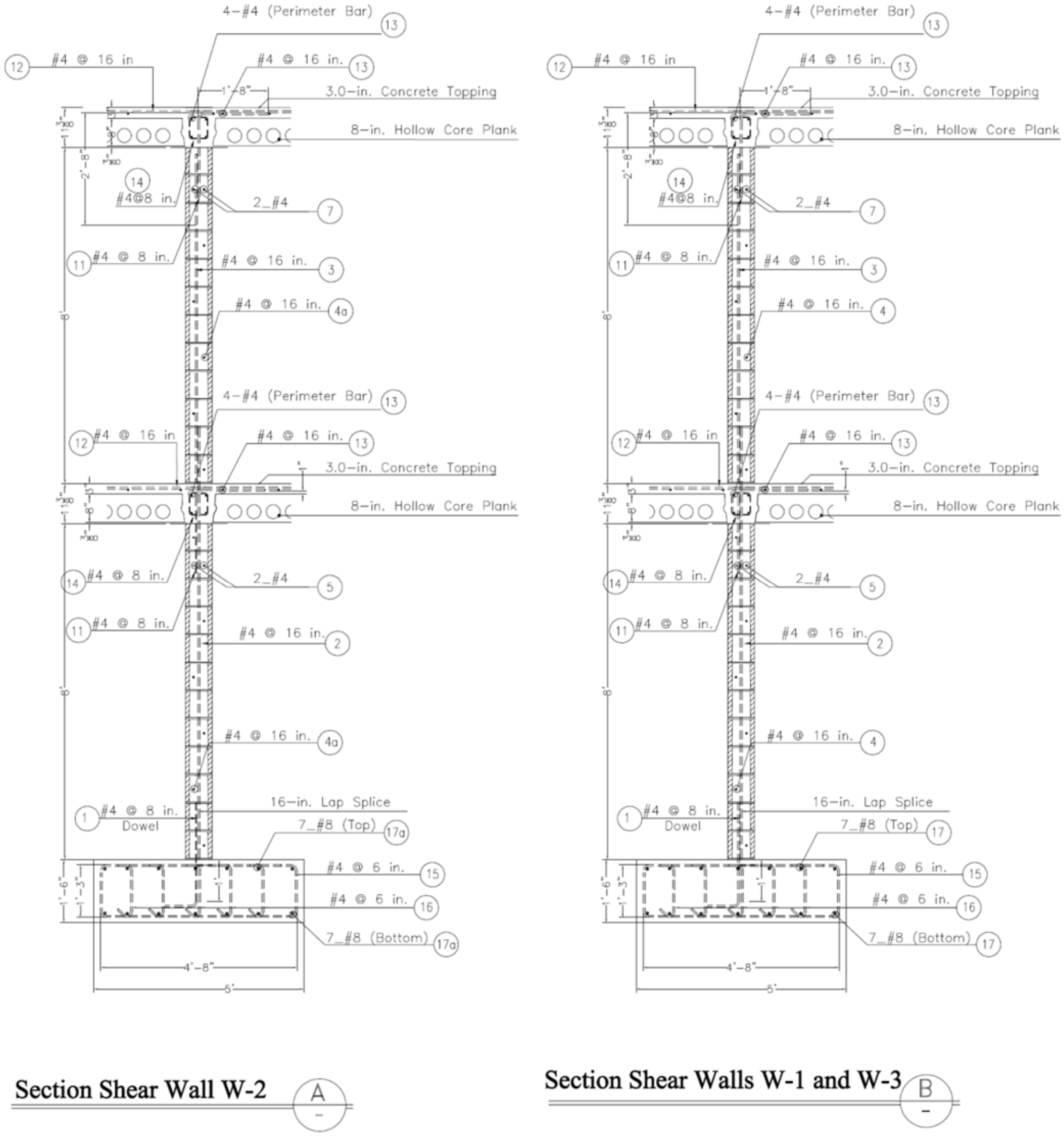

Section Shear Wall W-2

Section Shear Walls W-1 and W-3

Figure I.4 Sections A-A and B-B along Walls W-1, W-2, and W-3

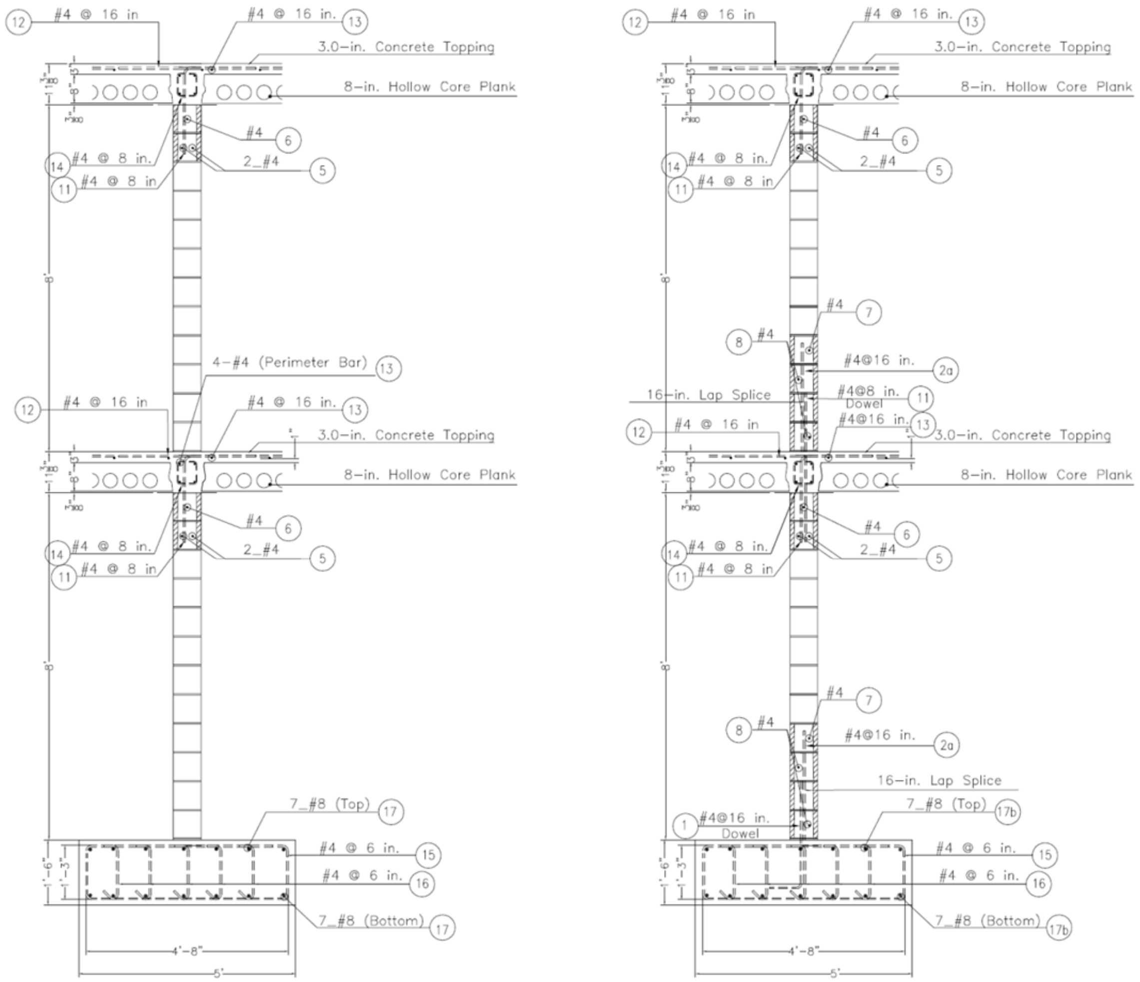

Section Lintel C

Section Lintel D

Figure I.5 Sections C-C and D-D along Walls W-1, W-2, and W-3

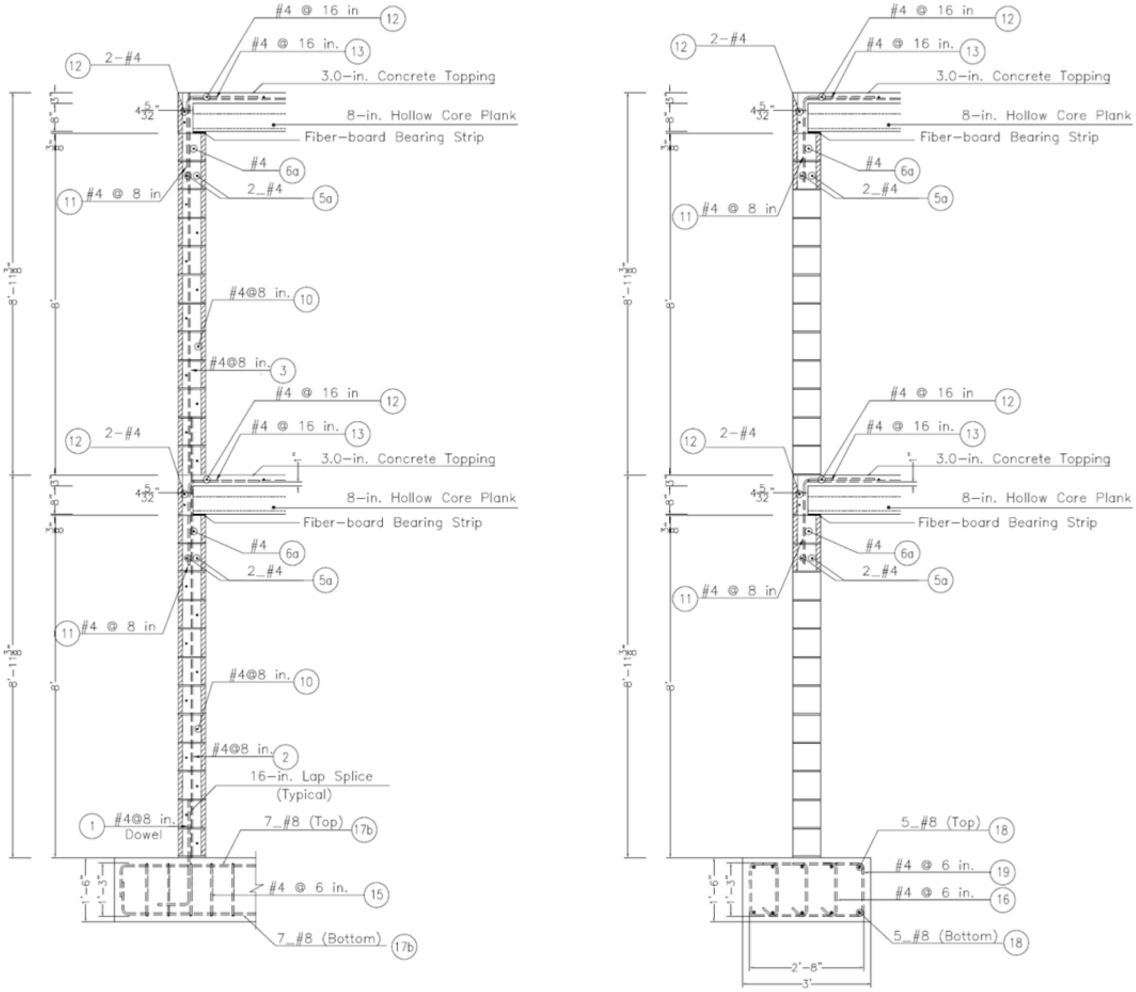

Section Shear Wall W-4 E

Section E F

Figure I.6 Sections C-C and D-D along Walls W-1, W-2, and W-3

APPENDIX J
Instrumentation Plan of Full-scale, 2-Story Specimen

This appendix provides the instrumentation plan for the full-scale, 2-story specimen tested at UCSD. It was prepared by Marios Mavros, doctoral candidate at UCSD. It is included here for completeness.

Table J-1 Legend for the instrumentation drawings presented in this appendix

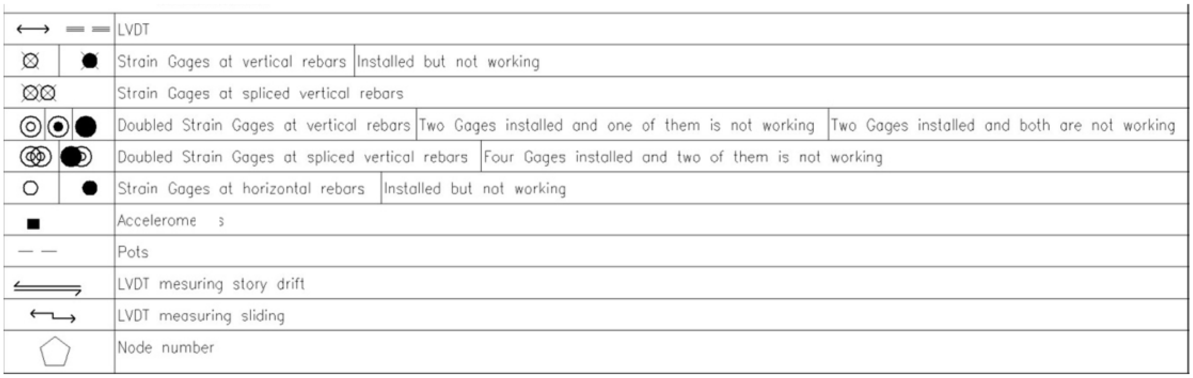

⟷ ═ ═	LVDT		
⊗ ●	Strain Gages at vertical rebars	Installed but not working	
⊗⊗	Strain Gages at spliced vertical rebars		
◎ ⊙ ●	Doubled Strain Gages at vertical rebars	Two Gages installed and one of them is not working	Two Gages installed and both are not working
◎◎ ●◎	Doubled Strain Gages at spliced vertical rebars	Four Gages installed and two of them is not working	
○ ●	Strain Gages at horizontal rebars	Installed but not working	
■	Accelerome s		
— —	Pots		
⇌	LVDT mesuring story drift		
↤↦	LVDT measuring sliding		
⬠	Node number		

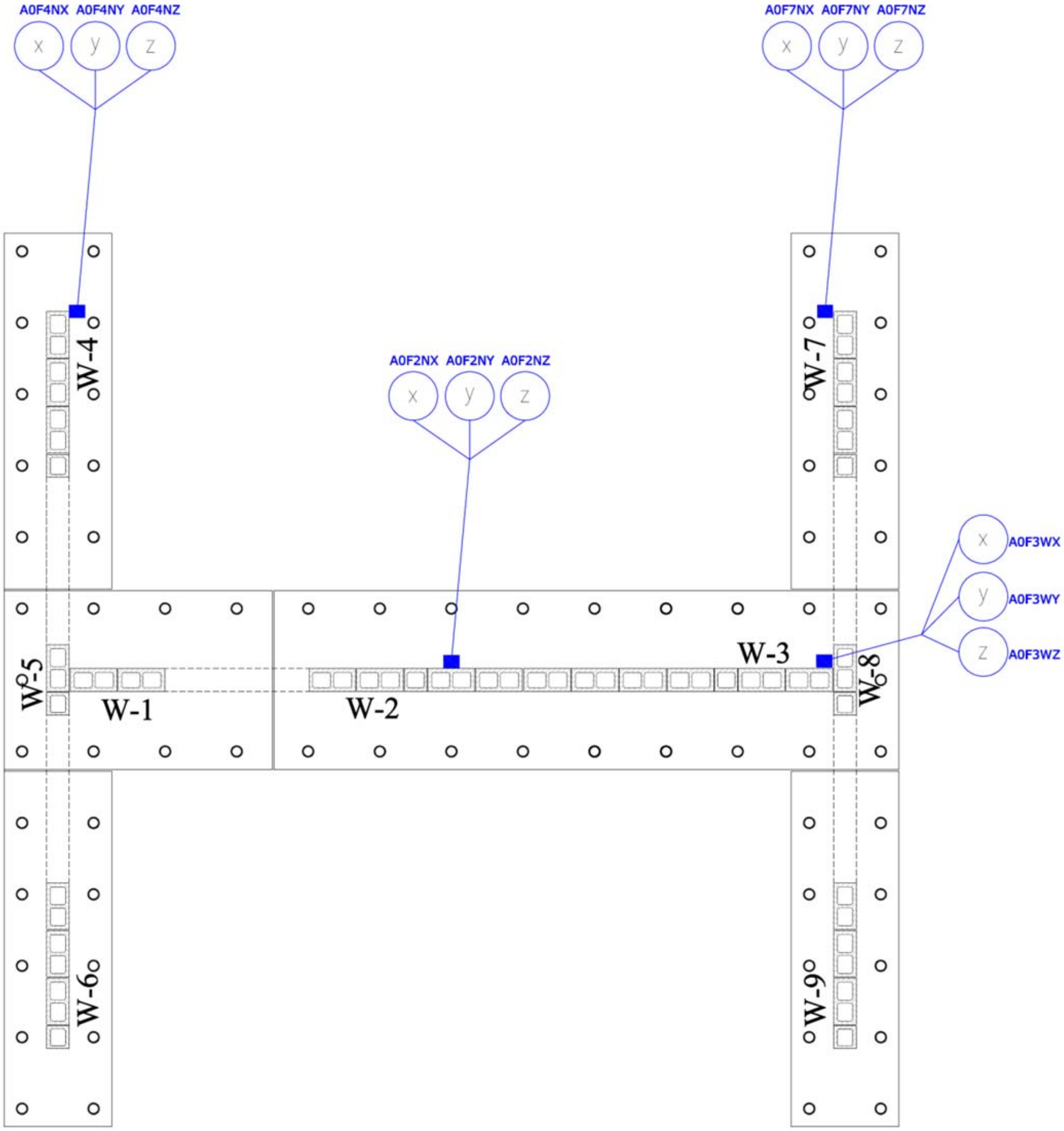

Figure J.1 Locations of accelerometers on foundation beams

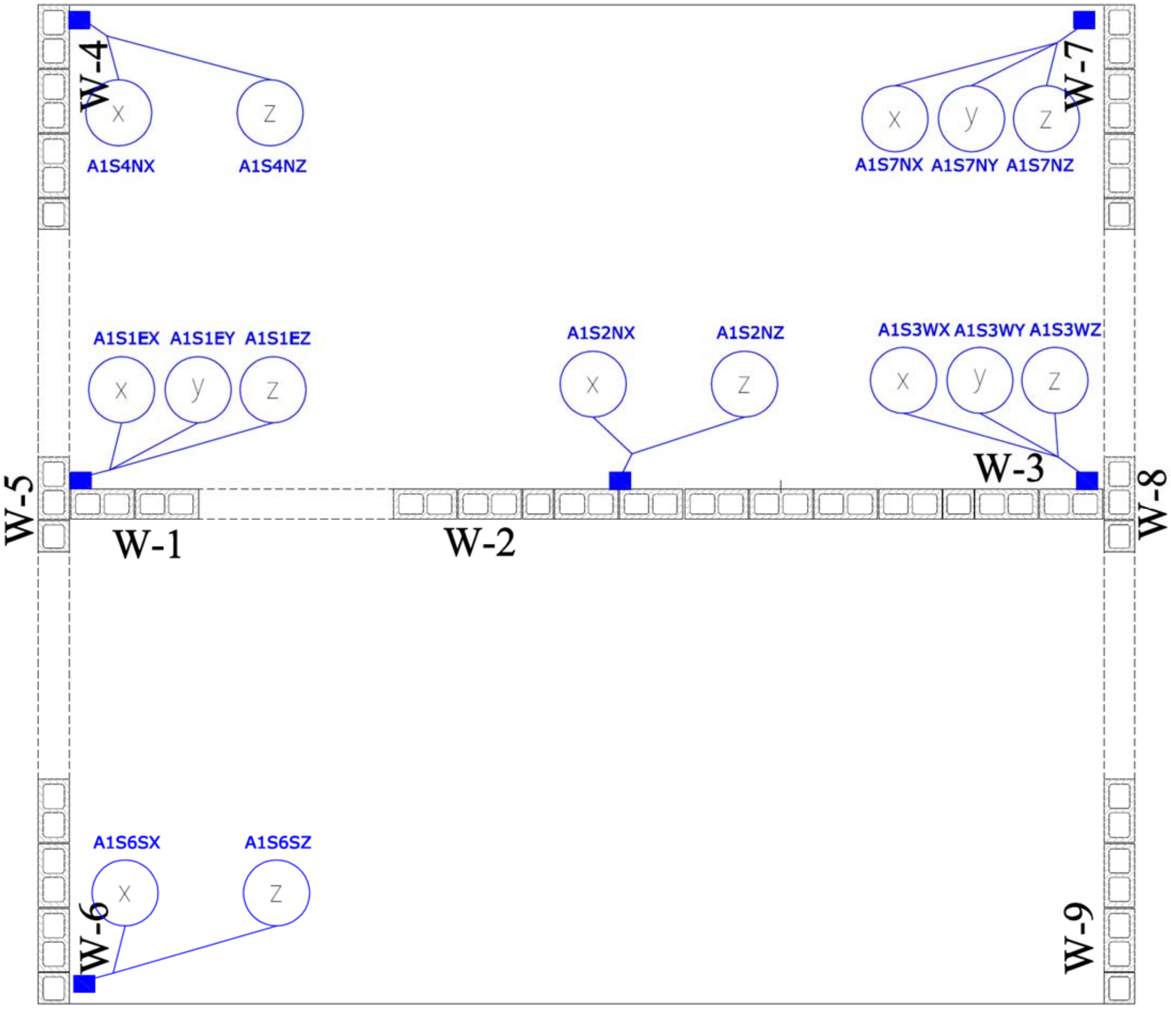

Figure J.2 Locations of accelerometers on second-story slab

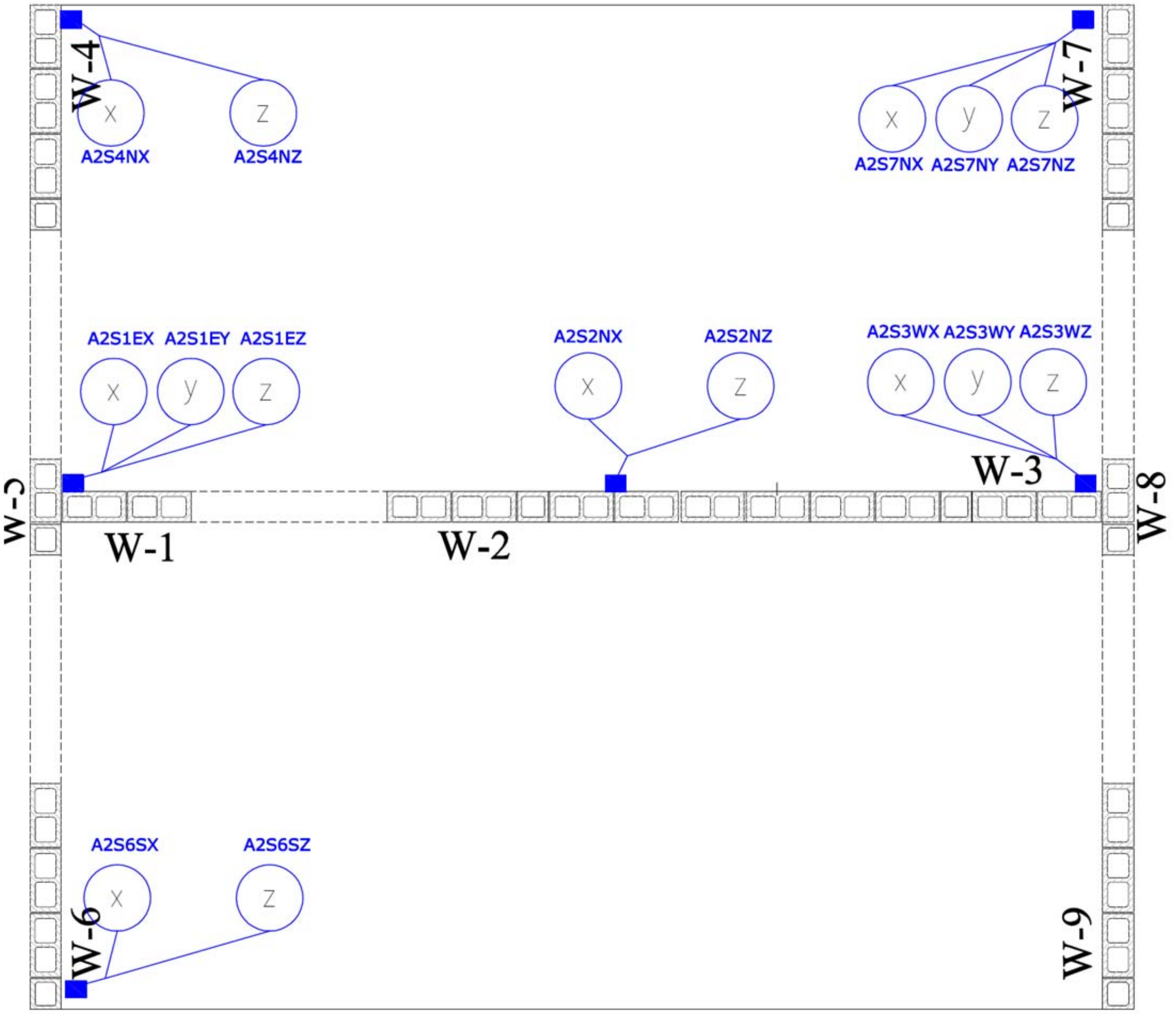

Figure J.3 Locations of accelerometers on roof slab

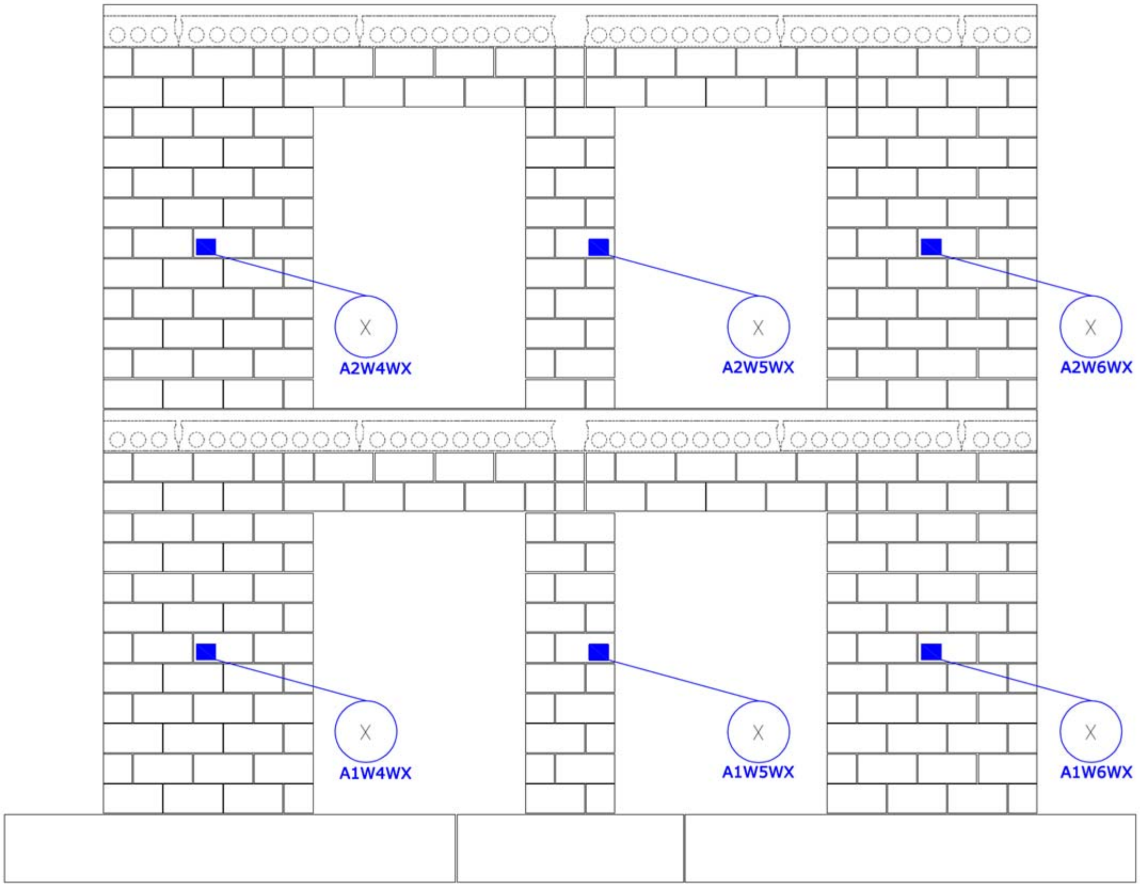

Figure J.4 Locations of accelerometers on west Walls W-4 and W-5

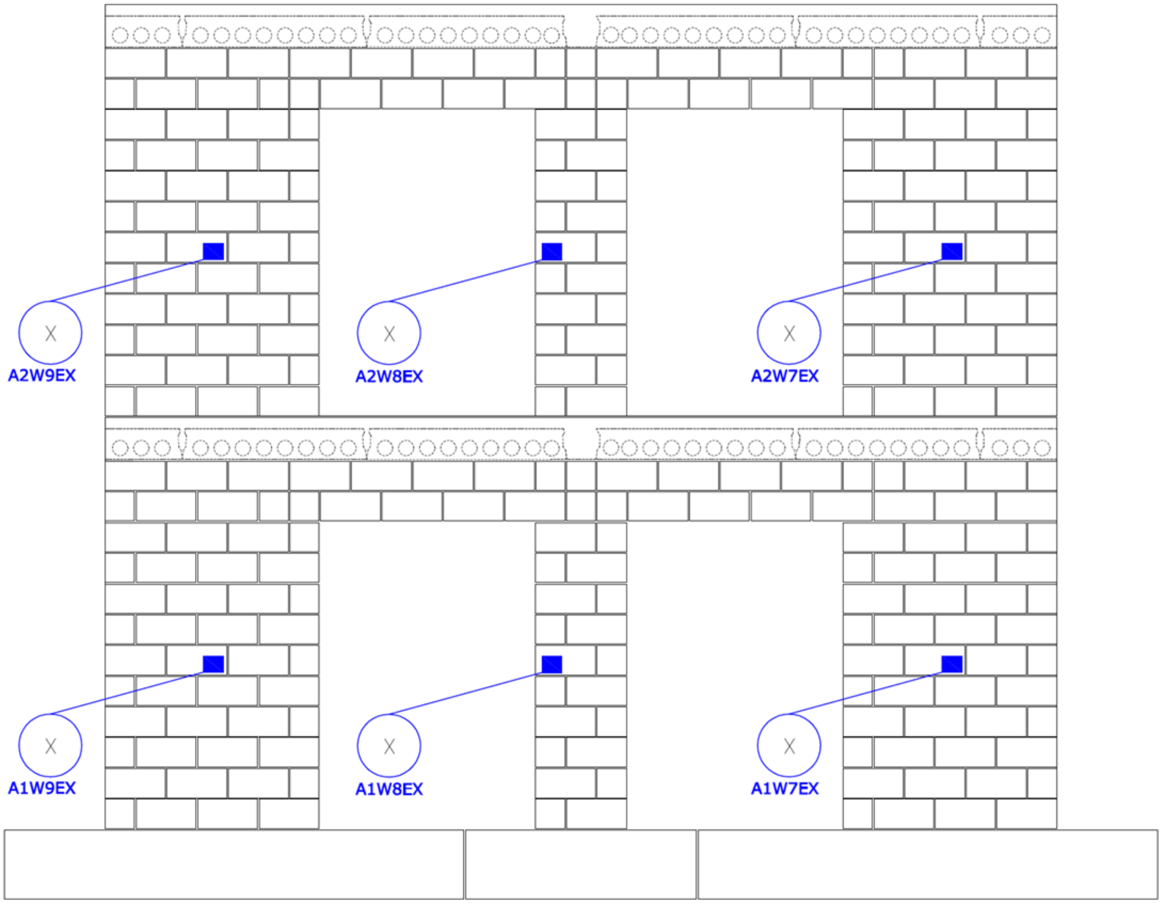

Figure J.5 Locations of accelerometers on east Walls W-4 and W-5

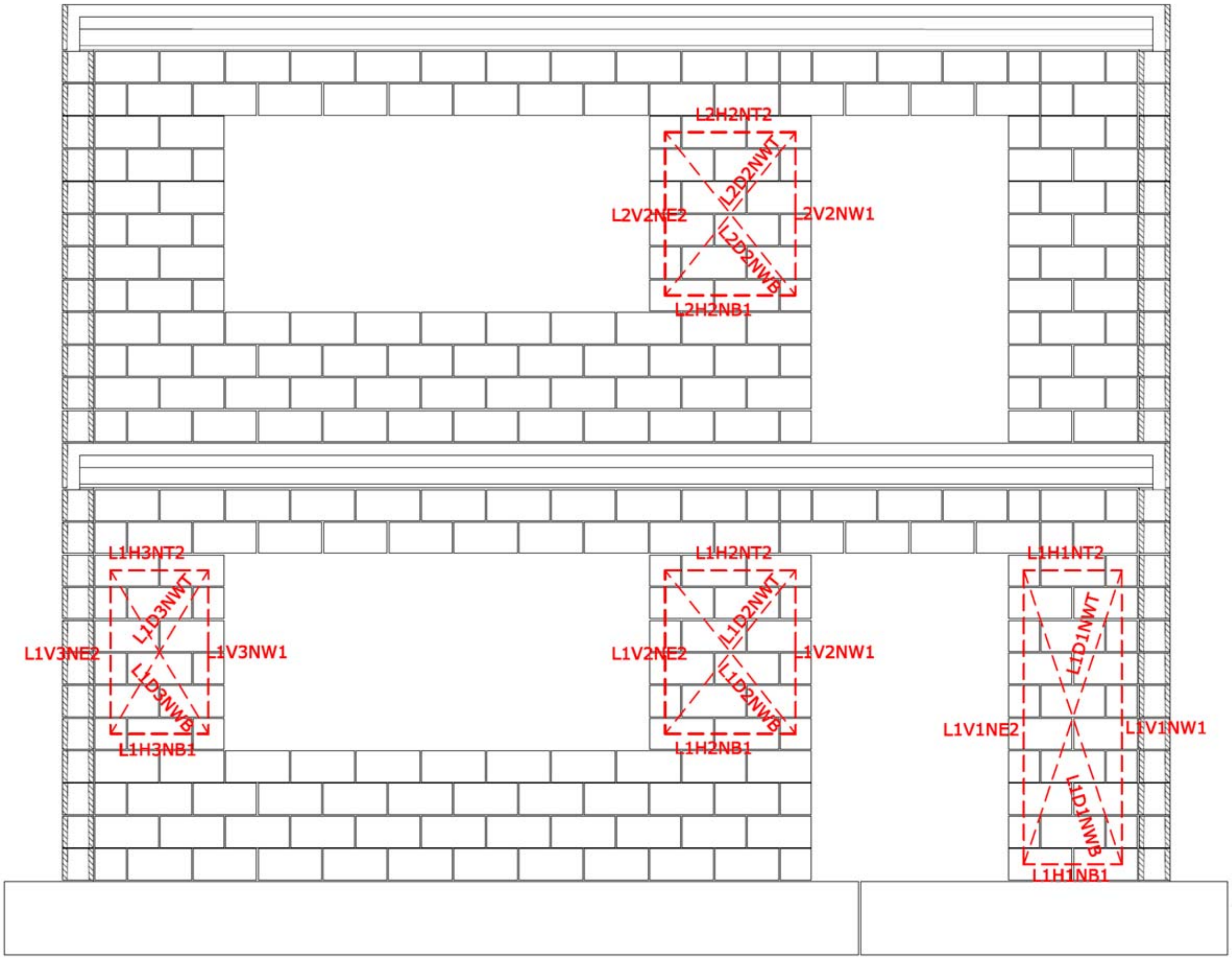

Figure J.6 Locations of displacement transducers on Walls W-1, W-2, and W-3

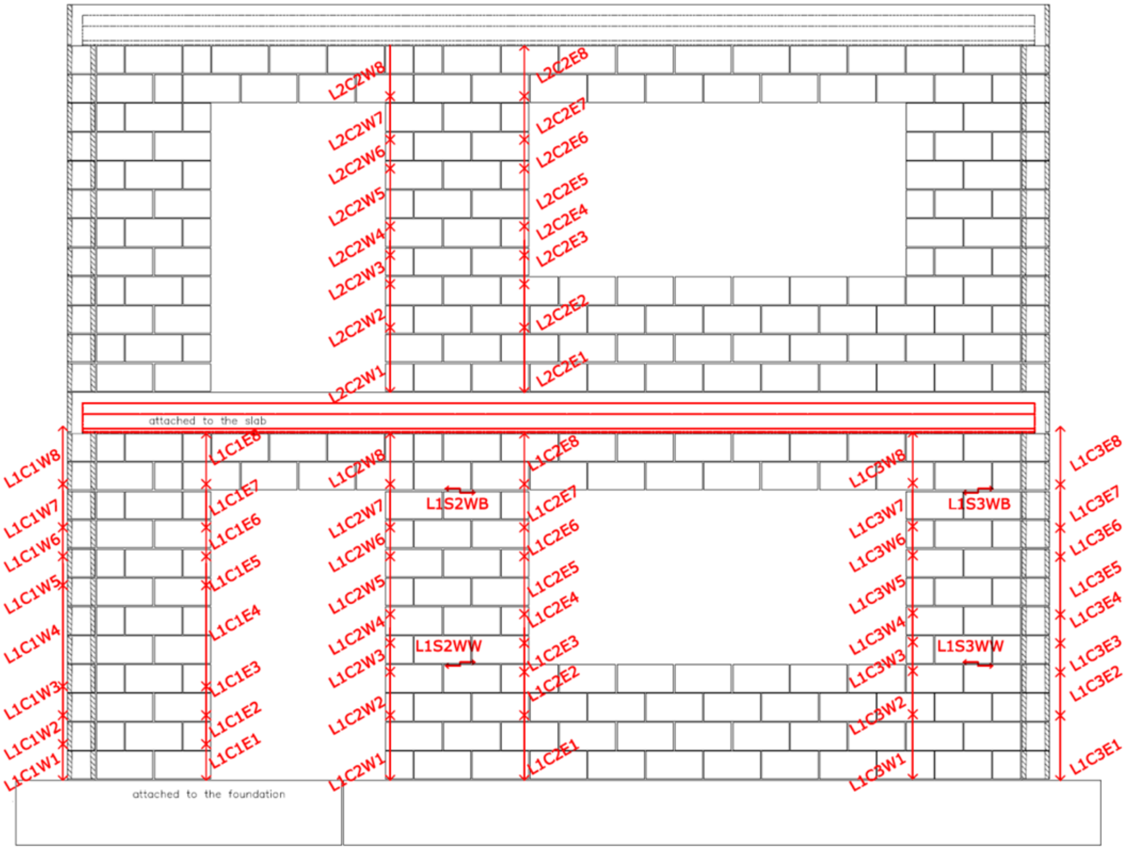

Figure J.7 Locations of displacement transducers on Walls W-1, W-2, and W-3

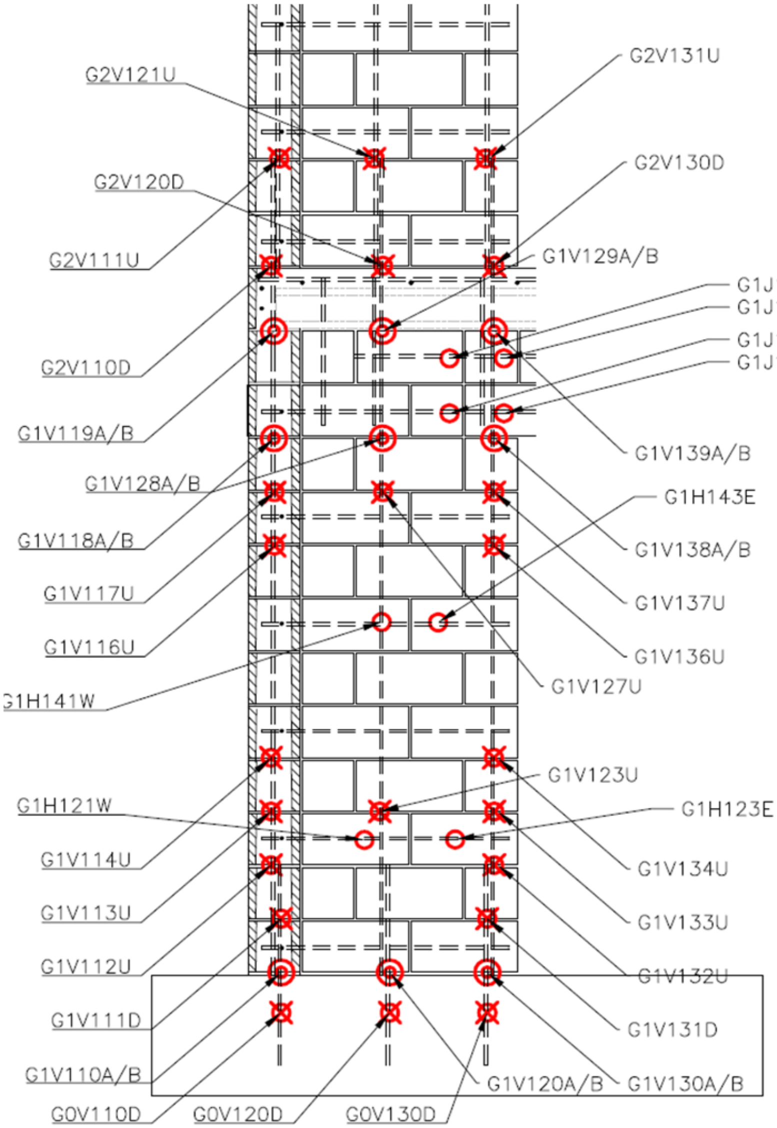

Figure J.8 Locations of strain gages on Wall W-1

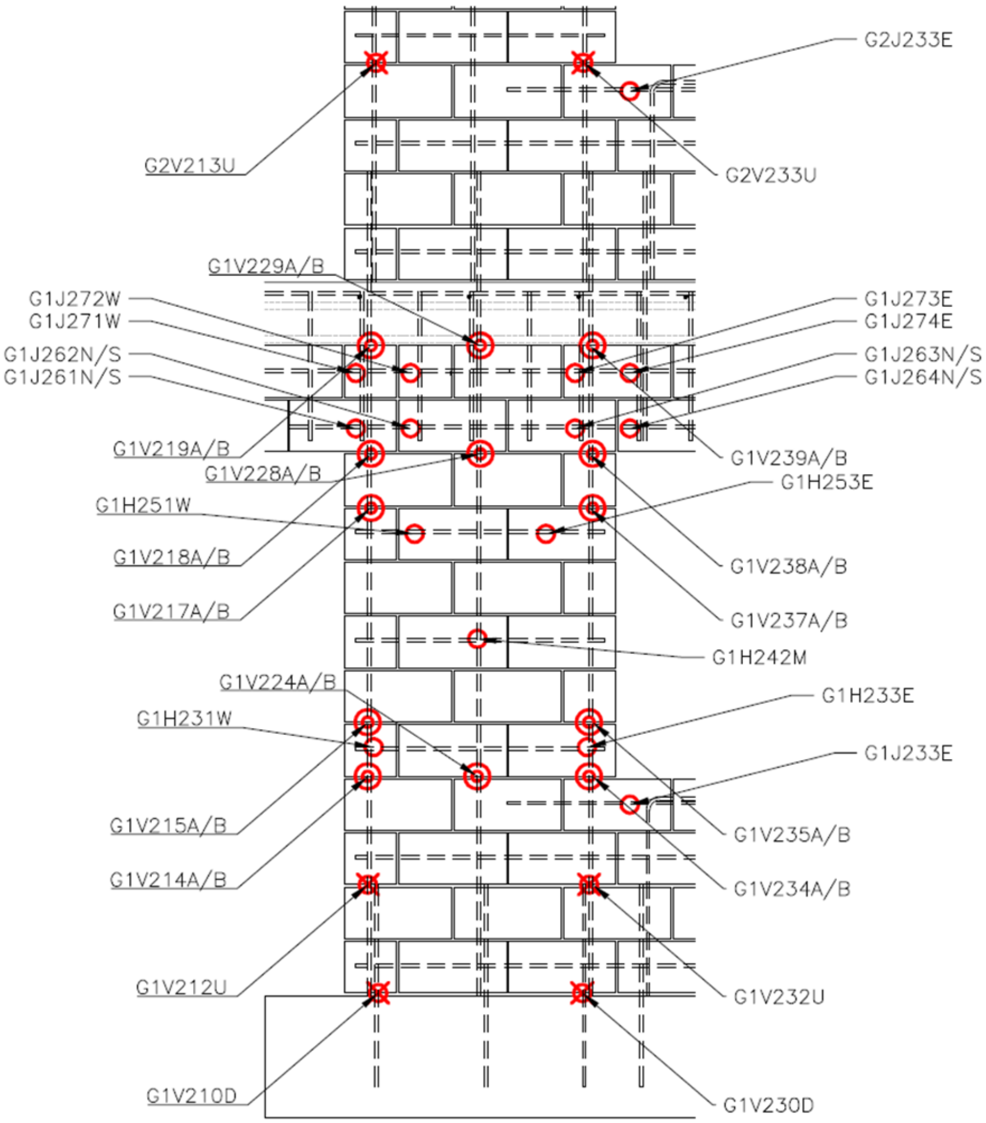

Figure J.9 Locations of strain gages on Wall W-2

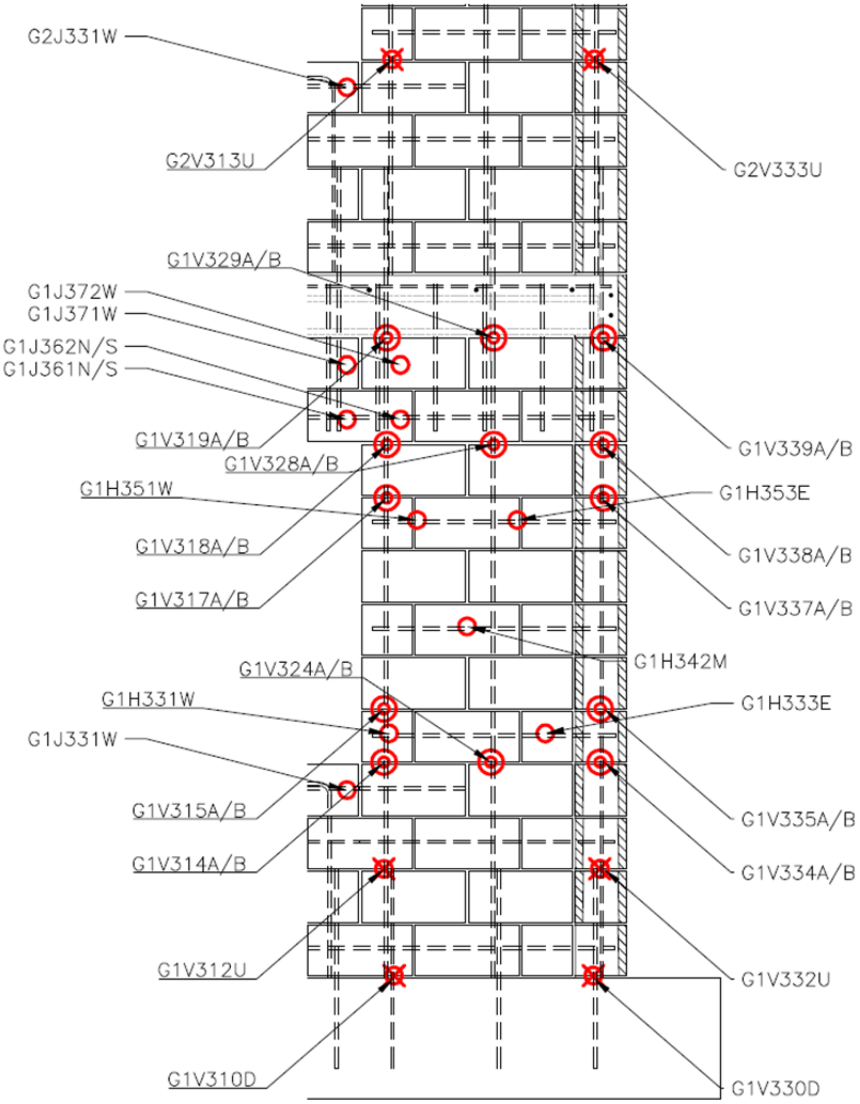

Figure J.10 Locations of strain gages on Wall W-3

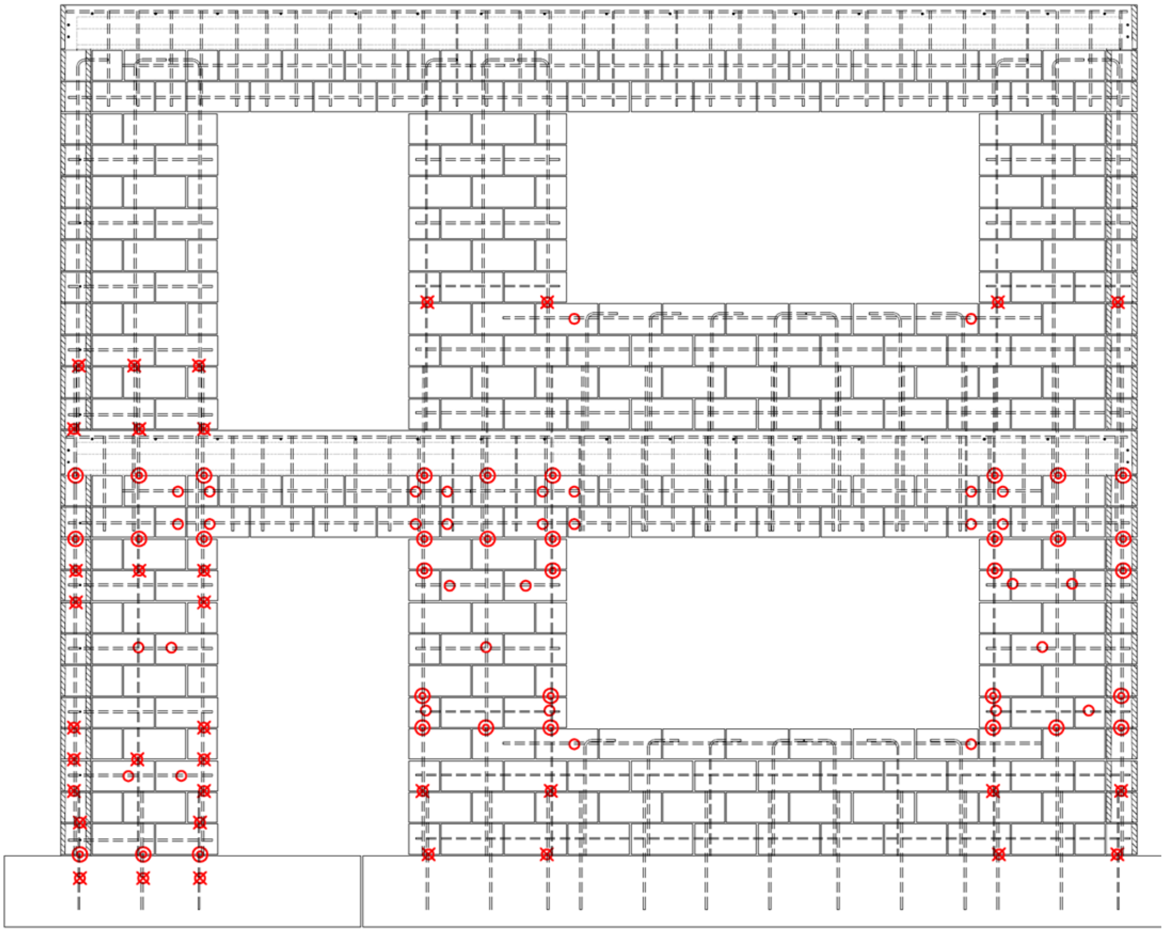

Figure J.11 Locations of strain gages on Walls W-1, W-2, and W-3

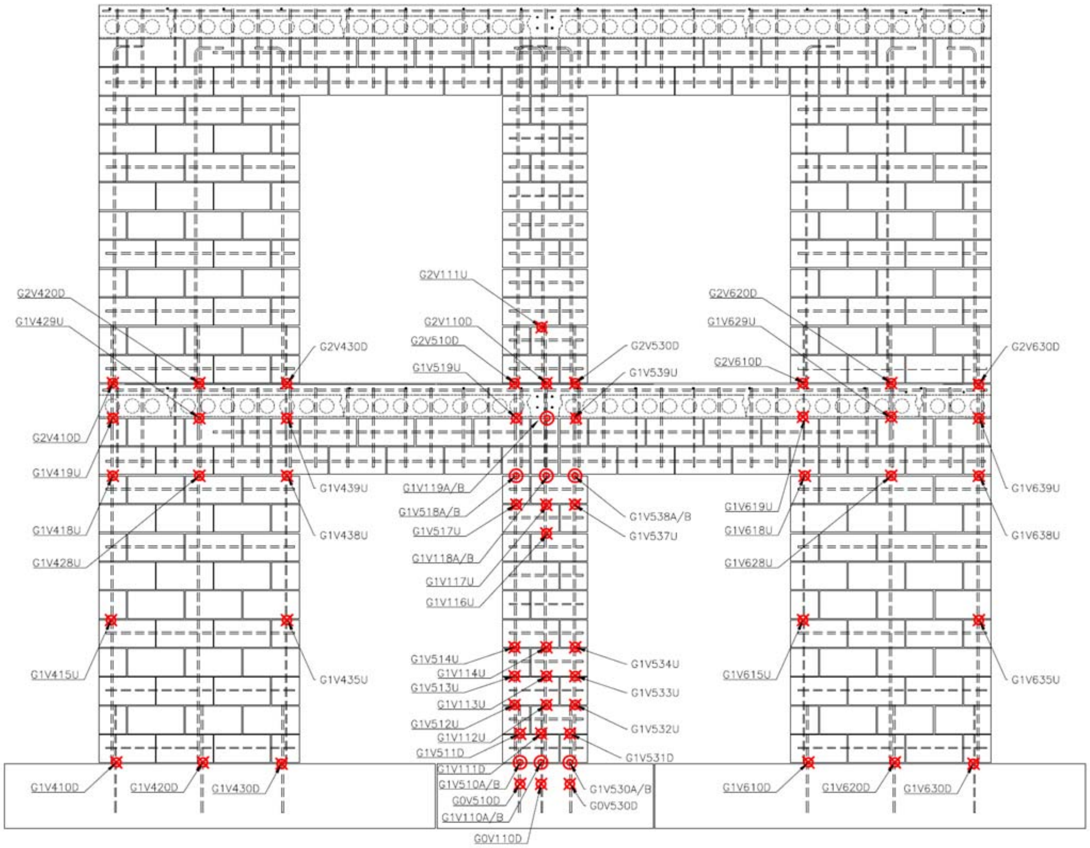

Figure J.12 Locations of strain gages on west Walls W-4 and W-5

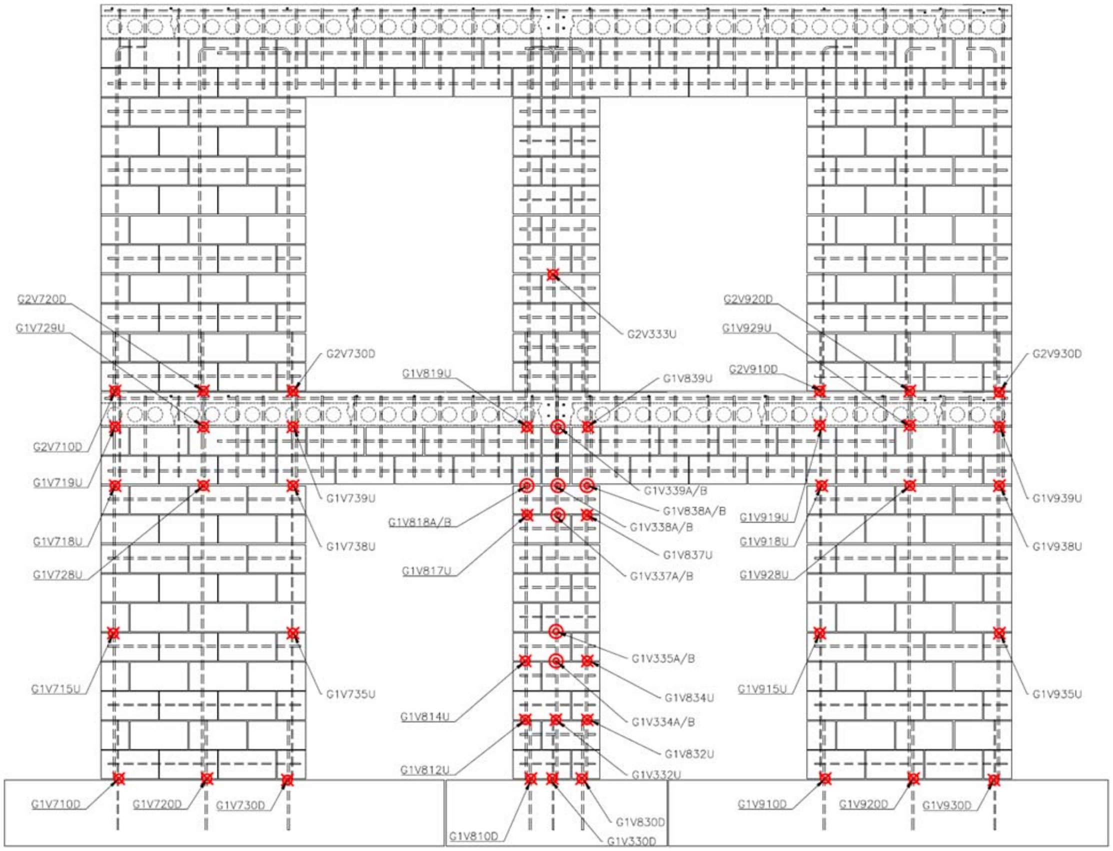

Figure J.13 Locations of strain gages on east Walls W-4 and W-5

APPENDIX K

Proposed Code Changes to Permit Displacement-Based Design of Masonry Shear-Wall Structures

In order for the information in this dissertation and in the other work products that will result from this research project to be effectively implemented, it is useful for the displacement-based design method proposed here to be extended in the form of specific draft language for consideration by US building codes. That is the purpose of this appendix.

In the US, structural design requirements are provided in model codes (almost universally, the *International Building Code*, which references ASCE7 and the MSJC *Code* for masonry design). For this reason, the proposed draft language addresses the 2012 IBC, the draft 2013 MSJC *Code,* and ASCE 7-10.

K.1 PROPOSED CHANGES TO THE 2012 IBC

The requirements of the 2012 IBC for structural design are shown in Figure K.1.

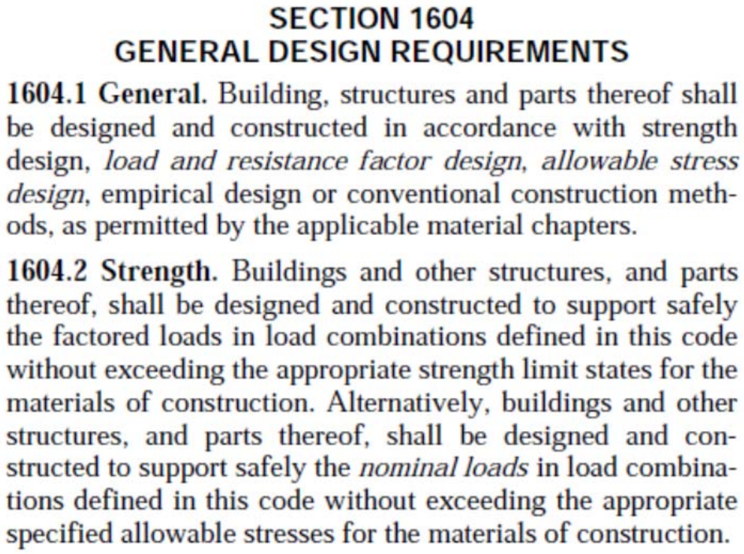

SECTION 1604
GENERAL DESIGN REQUIREMENTS

1604.1 General. Building, structures and parts thereof shall be designed and constructed in accordance with strength design, *load and resistance factor design*, *allowable stress design*, empirical design or conventional construction methods, as permitted by the applicable material chapters.

1604.2 Strength. Buildings and other structures, and parts thereof, shall be designed and constructed to support safely the factored loads in load combinations defined in this code without exceeding the appropriate strength limit states for the materials of construction. Alternatively, buildings and other structures, and parts thereof, shall be designed and constructed to support safely the *nominal loads* in load combinations defined in this code without exceeding the appropriate specified allowable stresses for the materials of construction.

Figure K.1 2012 IBC requirements for structural design

The requirements of the 2012 IBC for seismic design of masonry are shown in Figure K.2.

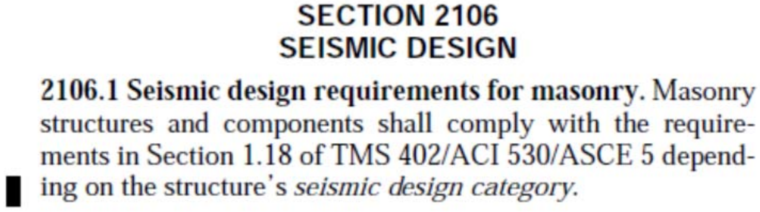

SECTION 2106
SEISMIC DESIGN

2106.1 Seismic design requirements for masonry. Masonry structures and components shall comply with the requirements in Section 1.18 of TMS 402/ACI 530/ASCE 5 depending on the structure's *seismic design category*.

Figure K.2 2012 IBC requirements for seismic design of masonry

The corresponding requirements in the draft 2013 MSJC Code are given in Figure K.3, using the section numbers corresponding to the re-numbered (current) version of that draft.

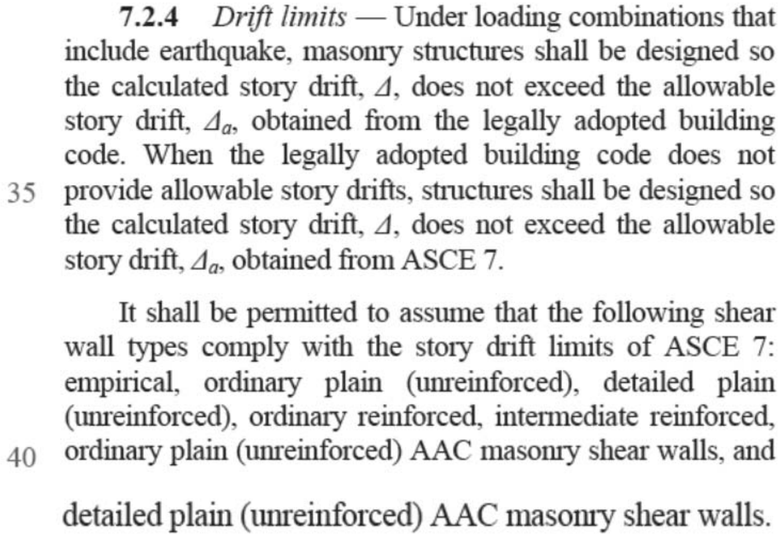

7.2.4 *Drift limits* — Under loading combinations that include earthquake, masonry structures shall be designed so the calculated story drift, Δ, does not exceed the allowable story drift, Δ_a, obtained from the legally adopted building code. When the legally adopted building code does not provide allowable story drifts, structures shall be designed so the calculated story drift, Δ, does not exceed the allowable story drift, Δ_a, obtained from ASCE 7.

It shall be permitted to assume that the following shear wall types comply with the story drift limits of ASCE 7: empirical, ordinary plain (unreinforced), detailed plain (unreinforced), ordinary reinforced, intermediate reinforced, ordinary plain (unreinforced) AAC masonry shear walls, and detailed plain (unreinforced) AAC masonry shear walls.

Figure K.3 Cited seismic design requirements for masonry

The draft 2013 MSJC *Code* require that non-participating elements be isolated under the calculated drift, that participating elements be classified (ordinary, intermediate, special), and that those elements meet requirements for strength and detailing. This process implicitly requires that each participating element be designed for the forces calculated according to ASCE7-10. It would probably be better to be explicit in this regard. Interestingly enough, ACI 318-11 is no better.

CODE	CODE COMMENTARY
7.2.5 ***Forces*** **—** Under loading combinations that include earthquake, masonry structures shall be designed to resist the forces calculated according to ASCE7.	

Because the 2012 IBC is so general, displacement-based design would require no change to it.

K.2 PROPOSED CHANGES TO ASCE7-10

ASCE7-10 would have to be augmented to permit the steps of a specific displacement-based seismic design procedure, such as that proposed here. The proposed approach, given below for DBE and MCE levels, should be added to Section 12.6 of ASCE7-10.

Table 12.6-1 of ASCE7-10 should be augmented by one more column, "Displacement-based Seismic Design (Chapter XX)."

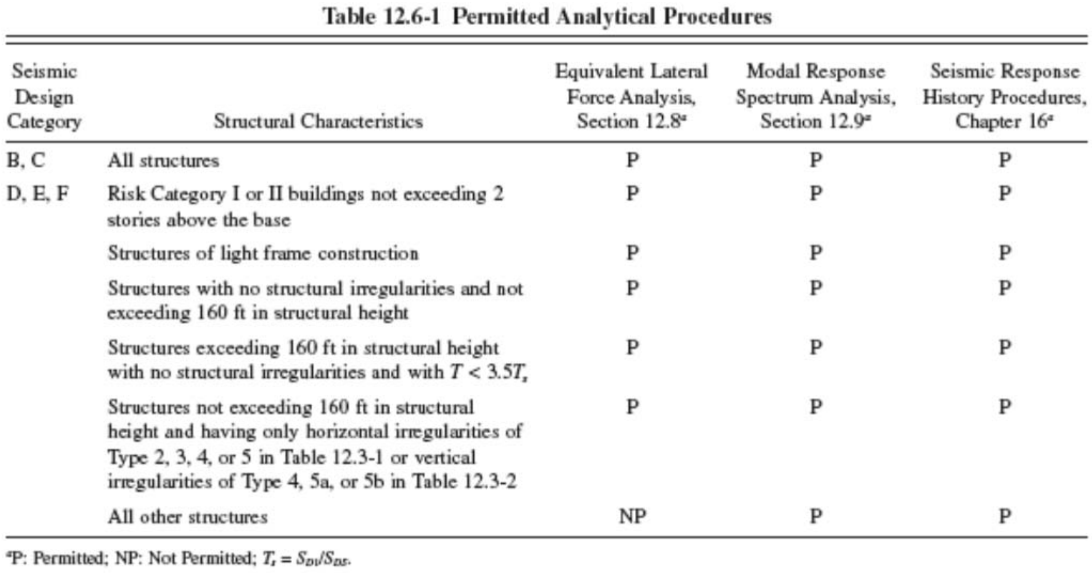

Table 12.6-1 Permitted Analytical Procedures

Seismic Design Category	Structural Characteristics	Equivalent Lateral Force Analysis, Section 12.8[a]	Modal Response Spectrum Analysis, Section 12.9[a]	Seismic Response History Procedures, Chapter 16[a]
B, C	All structures	P	P	P
D, E, F	Risk Category I or II buildings not exceeding 2 stories above the base	P	P	P
	Structures of light frame construction	P	P	P
	Structures with no structural irregularities and not exceeding 160 ft in structural height	P	P	P
	Structures exceeding 160 ft in structural height with no structural irregularities and with $T < 3.5T_s$	P	P	P
	Structures not exceeding 160 ft in structural height and having only horizontal irregularities of Type 2, 3, 4, or 5 in Table 12.3-1 or vertical irregularities of Type 4, 5a, or 5b in Table 12.3-2	P	P	P
	All other structures	NP	P	P

[a] P: Permitted; NP: Not Permitted; $T_s = S_{D1}/S_{DS}$.

CHAPTER XX

DISPLACEMENT-BASED SEISMIC DESIGN

XX.1. ***Design seismic hazard*** — A structure shall be designed for the seismic hazard levels of this section.

XX.1.1 Seismic hazard levels shall be Design Basis Earthquake (DBE) and a Maximum Considered Earthquake (MCE), as established in Chapter 21 (“Site-specific Ground Motion Procedures for Seismic Design”).

XX.1.2 Design intensity for a specified hazard level shall be expressed in terms of an elastic displacement response spectrum corresponding to an elastic damping ratio of 5%.

XX.1.3 Design spectral accelerations for the assigned seismic design category $S_{A\ Code}$ shall be transformed into corresponding design spectral displacement values $S_{D\ Code}$.

$$\boldsymbol{S_{D\ Code} = \frac{T_{eq}^2}{4\pi^2} S_{A\ Code}} \quad (\boldsymbol{Equation\ 1})$$

XX.1.4 The spectral displacement values corresponding to the total equivalent viscous damping of the structure including inelastic response, $S_{D\ \xi eq}$, shall be calculated using Equation 2.

$$\boldsymbol{S_{D\ \xi eq} = \sqrt{\frac{0.07}{0.02 + \xi_{eq}}} S_{D\ Code}} \quad (Equation\ 2)$$

XX.1.5 Equivalent hysteretic damping, ξ_{eq}, shall be taken as 10% for the DBE hazard level, and 15% for the MCE hazard level.

XX.2. *Design seismic performance criteria* — Inter-story drift ratios shall not exceed 0.3% for the DBE hazard level, and shall not exceed 0.7% for the MCE hazard level.

XX.3. *Develop Design Mechanism* — A design mechanism consistent with target displacements shall be developed. It shall be permitted to use push-over analysis to determine the controlling design mechanism and its corresponding local and global deformations at target displacements. The following aspects shall be considered in developing the design mechanism.

XX.3.1 Elastic and inelastic structural elements shall be detailed and reinforced appropriately for the strengths and deformation demands associated with the mechanism displacement.

XX.3.2 Locations of intended plastic hinges shall be selected to ensure a satisfactory mechanism of inelastic deformations. It shall be permitted to consider elements with "shear hinging" and elements with flexural hinging.

XX.3.3 Appropriate combination of gravity loads and seismic effect shall be considered to determine the strength of plastic hinges at the target displacement and designed mechanism, except that axial loads due to horizontal seismic forces shall be permitted to be neglected.

XX.3.4 The strength assigned to flexural and shear plastic hinges shall be based on nominal strengths.

XX.*4. Equivalent SDOF Structure* — The structural parameters of the equivalent SDOF structure to be used for determining the target displacement and required stiffness and base shear shall be defined by Equations 3 through 6.

XX.4.1 The effective mass of the equivalent SDOF structure shall be defined by

$$W_{eff} = \frac{(\sum W_i u_i)^2}{W_i {u_i}^2} \quad (Equation\ 3)$$

XX.4.2 The target displacement used for design shall be calculated by

$$\delta_d = \frac{\sum W_i {u_i}^2}{W_i u_i} \quad (Equation\ 4)$$

XX.4.3 The effective period of the SDOF structure, T_{eq} shall be calculated from the response spectrum, modified in Section XX.1 using target displacement.

XX.4.4 The effective stiffness of the SDOF structure shall be taken as:

$$\left(k_{eq}\right)_r = \frac{4\pi^2 W_{eff}}{gT_{eq}^2} \quad (Equation\ 5)$$

XX.4.5 The required base shear capacity V_b of the SDOF structure shall be

$$\boldsymbol{V_b = \left(k_{eq}\right)_a \delta_d} \quad (Equation\ 6)$$

XX.5. ***Actual equivalent lateral stiffness***— The capacity curve from a static pushover analysis and target displacements shall be used to calculate actual equivalent lateral stiffnesses (at the target displacements) at DBE and MCE levels.

XX.6. ***Verify lateral stiffness*** — the actual stiffness values shall be compared to the required equivalent lateral stiffness corresponding to each hazard level If these two stiffness values differ by more than 10% of the required equivalent lateral stiffness, the seismic resistance system of the structure shall be modified.

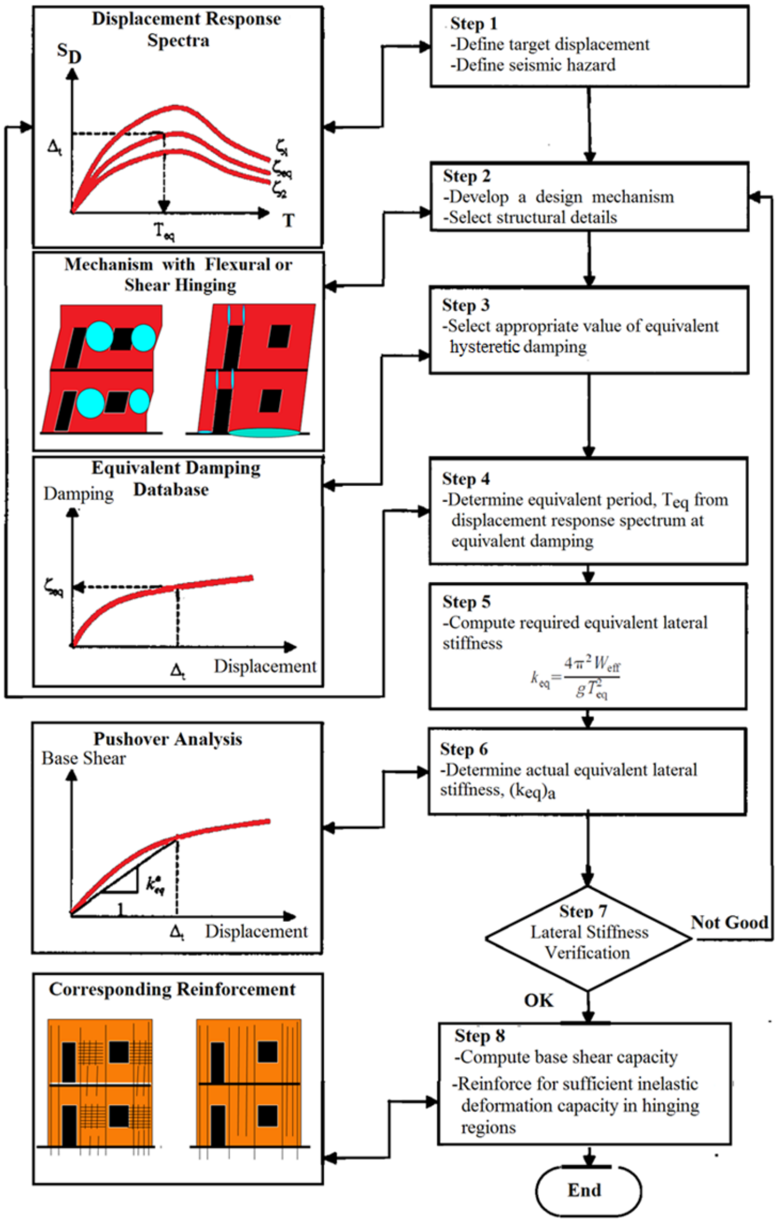

Figure K.4 Modified flowchart of displacement-based seismic design method for reinforced masonry shear-wall structures

K.3 PROPOSED CHANGES TO THE DRAFT 2013 MSJC CODE

To incorporate displacement-based design into the MSJC *Code*, Appendix D is proposed, and is referenced from the MSJC sections for special reinforced masonry shear walls.

APPENDIX D DISPLACEMENT-BASED DESIGN METHOD	
CODE	**CODE COMMENTARY**
D. *General* — The Displacement-based Design Method shall be permitted to be applied to Special Reinforced Masonry Shear Wall structures that are designed per the Strength Design provisions of Chapter 9, except that the provisions of Section 9.3.3.5 and Section 9.3.6.5 shall not apply.	***D. General*** — This section provides alternative design provisions for special reinforced masonry shear walls subjected to in-plane seismic loading. The displacement-based design method is presented as an alternative to the requirements of 9.3.3.5 and 9.3.6.5. All other sections in Chapter 9 are applicable.
D.1 *Design mechanism* — It shall be permitted to use mechanism analysis to determine the controlling mechanism and its corresponding base-shear strength, V_{base}, at target displacement for lateral load resistance system, provided that (a) through (d) are satisfied:	**D.1 *Design mechanism*** — This section defines the basic conditions for allowing the use of displacement-based design to determine the base shear strength of a line of resistance subjected to seismic loading.
(a) The relative magnitude of lateral seismic forces applied at each floor level shall correspond to the loading condition producing the maximum base shear at the line of resistance in accordance with displacement-based design procedure permitted in Section 12.6 of ASCE 7.	Item (a) allows the use of displacement-based design as permitted in ASCE 7 to determine the distribution of lateral loads.

APPENDIX D
DISPLACEMENT-BASED DESIGN METHOD

CODE	CODE COMMENTARY
(b) In the investigation of potential design mechanisms induced by seismic loading, locations of intended plastic hinges shall be selected to ensure a satisfactory mechanism of inelastic deformations. In the investigation of potential design mechanisms induced by seismic loading For perforated wall structures, elements with “shear hinging” and elements with flexural hinging are possible.	Item (b) allows the location of yielding regions at the interfaces between wall segments and their supporting members.
(c) The axial forces associated with Load Combination 7 of Section 2.3.2 of ASCE 7 shall be used when determining the strength of plastic hinges, except that axial loads due to horizontal seismic forces shall be permitted to be neglected.	Item (c) prescribes the use of the loading condition that induces the lowest axial force due to gravity loads. For wall segments loaded with axial forces below the balanced point, this loading condition gives the lowest flexural and shear strength and therefore leads to lower mechanism strengths. Axial loads from seismic overturning are permitted to be neglected only in the initial process of establishing the plastic capacity of the selected mechanism. Axial loads from seismic overturning are required to be considered subsequently, in determining the deformation capacity of plastic hinges.
(d) The strength assigned to and flexural plastic hinges and “shear hinging” regions shall be based on the nominal flexural strength, M_n , and nominal shear strength,	

CODE	CODE COMMENTARY
V_n , calculated using MSJC Section 9.3.4.1.2.	
(e) At locations other than the plastic hinges identified in D.1(b), shear and moments shall not exceed the strengths assigned in D.1(d) using the assumptions of D.1(c).	Item (e) requires the designer to verify that the selected design mechanism is the critical one. If hinging is detected away from the selected plastic hinge locations, the designer has the choice of changing the selected plastic hinge location to recognize that possible hinging, or of placing additional reinforcement at the section where hinging is detected.
D.2 ***Mechanism strength*** — The design mechanism associated with the displacement-based base-shear strength at target displacement, V_{base} , shall satisfy the following: $\phi V_{base} \geq V_{ub}$ (Equation D-1) The value of ϕ assigned to the mechanism strength shall be taken as 0.8. The base-shear demand, V_{ub} , shall be determined from the displacement-based design procedure permitted in Section 12.6 of ASCE 7. The elastic wall segments shall be controlled as force-controlled components, and shall be reinforced for sufficient strength at the target displacements with capacity design principles.	**D.2** ***Mechanism strength*** — Because the controlling yield mechanism is investigated using nominal strengths, an overall strength reduction factor of $\phi = 0.8$ is applied to the limiting base shear strength. For simplicity, a single value of ϕ is adopted.
D.3 ***Mechanism deformation*** — The	**D.3** ***Mechanism deformation*** —Structural

CODE	CODE COMMENTARY
rotational deformation demand on plastic hinges shall be determined by imposing the target displacement, δ_d , at the roof level of the design mechanism. The rotational deformation capacity of plastic hinges shall satisfy D.3.1 to D.3.3.	local deformation demands at target displacements, at locations of plastic hinges are determined by imposing the calculated design roof displacement to the controlling yield mechanism.
D.3.1 Flexure-controlled wall segments should be assigned a maximum local deformation capacity ratio of 0.8% at the DBE level, and 1.5% at the MCE level.	
D.3.2 The rotational deformation capacity of flexural plastic hinges shall be less than $0.5(l_w\varepsilon_{mu})/c$ for DBE level, and $(l_w\varepsilon_{mu})/c$ for MCE level. The value of c shall be calculated for the P_u corresponding to Load Combination 5 of Section 2.3.2 of ASCE 7.	**D.3.2** At DBE and MCE hazard levels, the rotational deformation capacities are calculated assuming an ultimate curvature of $(\varepsilon_{mu})/c$ and $(2\varepsilon_{mu})/c$, respectively, over a plastic hinge length of $0.5l_w$. The resulting expressions are similar to that used in 9.3.6.5.3(a) to determine the need for special boundary elements. In the latter case, it is multiplied by wall height. The value of P_u includes earthquake effects, and may be calculated using a linearly elastic model.
D.3.3 Shear-controlled wall segments should be assigned a maximum local deformation capacity ratio of 0.5% at the DBE level, and 1.0% at the MCE level for masonry components satisfying the	

CODE	CODE COMMENTARY
following requirements: (a) Transverse and longitudinal reinforcement ratios shall each not be less than 0.001; (b) Spacing of transverse and longitudinal reinforcement shall not exceed the smallest of 24 in., $l_w/2$, and $h_w/2$. (c) Reinforcement ending at a free edge of masonry shall be anchored around perpendicular reinforcing bars with a standard hook.	
D.3.4 The axial load in inelastic shear- and flexure-controlled wall segments shall be controlled as force-controlled components, to confirm their structural stability. The P_u corresponding to load combination 5 of Section 2.3.2 of ASCE 7 shall not exceed a compressive stress of 0.3 $f_m' A_g$ at plastic hinges in the controlling mechanism.	**D.3.4** The limit of 30% of f_m' is intended to ensure that all yielding components respond below the balanced point of the *P-M* interaction diagram.

REFERENCES

Abrams and Paulson (1991): Abrams, D. and Paulson, T., “Modeling earthquake response of concrete masonry building structures,” *ACI Struct. J.*, 88(4), 475–485.

ACI 318-08 (2008): *Building Code Requirements for Structural Concrete* (ACI 318-08) and *Commentary* (ACI 318R-08), American Concrete Institute, Farmington Hills, Michigan.

ACI 318-11 (2011): *Building Code Requirements for Structural Concrete* (ACI 318-11) and *Commentary* (ACI 318R-11), American Concrete Institute, Farmington Hills, Michigan.

Alogla (2012): Alogla, Saleh., “Evaluation of 2011 MSJC Strength-Design Shear Provisions for Reinforced Masonry Shear Walls,” Master’s report, University of Texas, Austin, Texas.

Aristizabal (1983): Aristizabal-Ochoa. J. D., “Cracking and shear effects of structural walls,” *ASCE Journal of Structural Engineering*, 109(5): 1267–1275.

ASCE 41-06 (2006): *Seismic Rehabilitation of Existing Buildings*, American Society of Civil Engineers, Reston, Virginia, 2006.

ASCE 7-05 (2005): *Minimum Design Loads for Buildings and Other Structures* (ASCE 7-05) (with Supplement), American Society of Civil Engineers, Reston, Virginia.

ASCE 7-10 (2010): *Minimum Design Loads for Buildings and Other Structures* (ASCE 7-10), American Society of Civil Engineers, Reston, Virginia.

Assis (1989): Assis, G. F., Hamid, A. A., and Harry, H. G., "Material Models for Grouted Block Masonry," U.S.-Japan Coordinated Program for Masonry Building Research, *Report No. 1.2(a)-2*, Drexel University, Philadelphia, Pennsylvania.

ASTM A370-05 (2005): “Standard Test Methods and Definitions for Mechanical Testing of Steel Products,” American Society for Testing and Materials, West Conshohocken, PA.

ASTM A476-10 (2010): “Standard Specification for Grout for Masonry,” American Society for Testing and Materials, West Conshohocken, PA.

ASTM C1019-11 (2011): “Standard Test Method for Sampling and Testing Grout,” American Society for Testing and Materials, West Conshohocken, PA.

ASTM C109-05 (2005): “Standard Test Method for Compressive Strength of Hydraulic Cement Mortars (Using 2-in. or [50-mm] Cube Specimens),” American Society for Testing and Materials, West Conshohocken, PA.

ASTM C1314-11a (2011): “Standard Test Method for Compressive Strength of Masonry Prisms,” American Society for Testing and Materials, West Conshohocken, PA.

ASTM C140-07 (2007): “Standard Test Methods for Sampling and Testing Concrete Masonry Units and Related Units,” American Society for Testing and Materials, West Conshohocken, PA.

ASTM C1552-03a (2003): “Standard Practice for Capping Concrete Masonry Units, Related Units and Masonry Prisms for Compression Testing,” American Society for Testing and Materials, West Conshohocken, PA.

ASTM C270-12 (2012): “Standard Specification for Mortar for Unit Masonry,” American Society for Testing and Materials, West Conshohocken, PA.

ASTM C780-11 (2011): “Standard Test Method for Preconstruction and Construction Evaluation of Mortars for Plain and Reinforced Unit Masonry,” American Society for Testing and Materials, West Conshohocken, PA.

ASTM C90-11a (2011): “Standard Specification for Loadbearing Concrete Masonry Units,” American Society for Testing and Materials, West Conshohocken, PA.

ATC-40 (1996): “Seismic Evaluation and Retrofit of Concrete Buildings,” *Report No. ATC-402*, Applied Technology Council, Redwood City, California.

ATC-63 (2009): “Quantification of Building Seismic Performance Factors,” *Report No. FEMA P695/ATC-63*, June 2009, prepared by the Applied Technology Council, Redwood City, California, for the Federal Emergency Management Agency, Washington, DC.

Atkinson *et al.* (1988): Atkinson, R.H., Kingsley, G. R., Saeb, S., B. Amadei, B., and Sture, S., "A Laboratory and In-situ Study of the Shear Strength of Masonry Bed Joints," *Proceedings* of the 8th International Brick/Block Masonry Conference, Dublin.

Bazant and Oh (1983): Bazant, Z. P. and Oh, B.H., "Crack Band Theory for Fracture of Concrete," Materials and Structures, 31, RILEM, 16(93), 155-177.

Bohl and Adebar (2011): Bohl, A. and Adebar, P., "Plastic Hinge Lengths in High-rise Concrete Shear Walls," *ACI Structural Journal*, March-April 2011.

Bozorgnia and Bertero (2004): Bozorgnia, Y. and Bertero, V., *Earthquake Engineering: From Engineering Seismology to Performance-Based Engineering*, CRC Press LLC, Boca Raton, Florida.

Calvi and Kingsley (1995): Calvi G. M., Kingsley G. R., "Displacement-based seismic design of multi-degree-of-freedom bridge structures." *Earthquake Engng. Struct. Dyn.*, 1995;24.

Calvi and Sullivan (2009): Calvi, G. M., Sullivan, T. J., "A Model Code for the Displacement-Based Seismic Design of Structures," *DBD09 – Draft Issued for Public Enquiry*, IUSS Press, 80 pp.

Centeno *et al.* (2012): Centeno, J., Ventura, C.E., and Brzev, S., "Modeling of Sliding Shear Resistance of Reinforced Masonry Squat Walls," *Proc.* of 15th World Conference on Earthquake Engineering, Lisbon, 2012.

Clough and Penzien (2003): Clough, R. W., and Penzien, J., *Dynamics of Structures*, 3rd ed., Computers and Structures, Inc., Berkeley, California.

Cohen (2001): Cohen, G.L., "Seismic Response of Low-Rise Masonry Buildings with Flexible Roof Diaphragms," Master's thesis, University of Texas, Austin, Texas.

Coleman and Spacone (2001): Coleman, J. and Spacone, E., "Localization Issues in Forced-Based Frame Elements," *J. of Struct. Engrg.*, Vol. 1127(11), 1257-1265.

CSI (2007): *PERFORM 3D V5, Nonlinear Analysis and Performance Assessment for 3D Structures*, Computer and Structures, Inc., Berkeley, California.

Cyrier (2012): Cyrier, W. B., “Performance of Concerete Masonry Shear Walls with Integral Confined Concerete Boundary Elements,” Master’s thesis, Whashington State University, Pullman, Washington.

Davis (2008): Davis, C. L., “Evaluation of Design Provisions for In-Plane Shear in Masonry Walls,” Master’s thesis, Washington State University, Pullman, Washington.

Davis *et al.* (2010): Davis, C.L., McLean, D.I., and Ingham, J. M., “Evaluation of Design Provisions for In-Plane Shear in Masonry Walls,” *TMS Journal*, The Masonry Society, Boulder, Colorado, vol. 28, no. 1, July.

Dazio (2009): Dazio, A., Beyer, K. and Bachmann, H., “Quasi-static cyclic tests and plastic hinge analysis of RC walls,” *Engineering Structures* 31(7): 1556-1571.

Eikanas (2003): Eikanas, I. K., “Behavior of Concrete Masonry Shear Walls with Varying Aspect Ratio and Flexural Reinforcement,” Master’s thesis, Washington State University, Pullman, Washington.

FEMA 273 (1997): “NEHRP Guidelines for the Seismic Rehabilitation of Buildings,” Building Seismic Safety Council, Federal Emergency Management Agency, Washington, D.C.

FEMA 306 (1999): “Evaluation of earthquake damaged concrete and masonry wall buildings, basic procedures manual,” The partnership for response and recovery, for the Federal Emergency Management Agency, Washington, DC.

FEMA 356 (2000): “Prestandard and Commentary for the Seismic Rehabilitation of Buildings,” prepared by the American Society of Civil Engineers, for the Federal Emergency Management Agency, Washington, DC.

FEMA 440 (2005): “Improvement of Nonlinear Static Seismic Analysis Procedures,” prepared by Applied Technology Council (ATC-55 Project), Redwood City, California, for Federal Emergency Management Agency, Washington, DC.

Filiatrault (2002): Filiatrault, A., and Folz, B., “Performance-Based Seismic Design of Wood Framed Buildings,” *ASCE Journal of Structural Engineering*, American Society of Civil Engineers, Reston, Virginia, Vol. 128, No. 1, 39-47.

Freeman *et al.* (1975): Freeman, S. A., Nicoletti, J. P., and Tyrell, J. V., ‘‘Evaluations of existing buildings for seismic risk—A case study of Puget Sound

Naval Shipyard, Bremerton, Washington,'' *Proc., 1st U.S. Nat. Conf. on Earthquake Engrg.*, 113–122.

Ghobarah (2001): Ghobarah, A., "Performance-based design in earthquake engineering: State of development," *Engineering Structures*, Vol. 23, No. 8, 878-884.

Gulkan and Sozen (1974): Gulkan, P. and Sozen, M.A., " In-elastic Responses of Reinforced Concrete Structures to Earthquake Motions," *Proceedings* of the ACI, Vol. 71, No. 12, Dec. 1974, pp 605-610.

Gulkan *et al.* (1990a): Gulkan, P., Clough, R.W., Mayes, R.L., and Manos, G., "Seismic testing of single-story masonry houses, Part I," *J. Struct. Eng.*, 116(1), 235–256.

Gulkan *et al.* (1990b): Gulkan, P., Clough, R.W., Mayes, R.L., and Manos, G., "Seismic testing of single-story masonry houses, Part II", *J. Struct. Eng.*, 116(1), 257–274.

He and Priestley (1992): He, L. and Priestley, M. J. N., "Seismic Behavior of Flanged Masonry Walls," *Report No. SSRP-92/09*, University of California, San Diego, Department of Applied Mechanics and Engineering Sciences.

Hernandez (2012): Hernández, J. F., "Quasi-Static Testing of Cantilever Masonry Shear Wall Segments," Master's thesis, University of Texas, Austin, Texas.

Humar et al .(2011): Humar, J.M, Fazileh, F; Ghorbanie-Asl, M., Pina, F.E., "Displacement-based seismic design of regular reinforced concrete shear wall buildings," *Canadian Journal of Civil Engineering*,, Vol. 38 Issue 6, p616.

Jo (2010): Jo, Seongwoo, "Seismic Behavior and Design of Low-rise Reinforced Concrete Masonry with Clay Masonry Veneer" Ph.D. dissertation, Dept. of Civil Engineering, The University of Texas at Austin, May 2010.

Kabeyasawa *et al.* (1983): Kabeyasawa, T., Shiohara H., Otani S. and Aoyama H., "Analysis of the full-scale sevenstory reinforced concrete test structure," *Journal of the Faculty of Engineering*, The University of Tokyo 37(2): 431–478.

Kapoi (2011): Kapoi, C. M., "Experimental Performance of Concrete Masonry Shear Walls Under In-Plane Loading," Master's thesis, Washington State University, Pullman, Washington.

Keshavarzian and Schnobrich (1984): Keshavarzian, M. and Schnobrich, W. C., “Computed nonlinear response of reinforced concrete wall-frame structures,” *Report No. SRS 515*, University of Illinois. Urbana-Champaign.

Klingner (1994): Klingner, R. E., editor, “Performance of Masonry Structures in the Northridge, California Earthquake of January 17, 1994,” Technical Report 301-94, The Masonry Society, Boulder, Colorado, June 1994, 100 pp.

Klingner *et al.* (2010): Klingner, R. E., P. Benson Shing , W. Mark McGinley , David I. McLean, Hussein Okail , and Seongwoo Jo, “Seismic Performance Tests of Masonry and Masonry Veneer,” *Journal of ASTM International*, Vol. 7, No. 3, American Society for Testing and Materials, West Conshohocken, PA January 2010. Also published as part of ASTM STP 1512, J. Farny and B. Behie, eds., American Society for Testing and Materials, West Conshohocken, PA (2010).

Koutromanos and Shing (2009): Koutromanos, I. and Shing, P.B., “Trial Application Reinforced Masonry Shear Wall Structures,” Chapter for *ATC 76-Trial Application of FEMA P695 (ATC-63) Methodology*, submitted to the Applied Technology Council, Redwood City, California.

Leborgne (2012): Leborgne, M. R., “Modeling the Post Shear Failure Behaviour of Reinforced Concerete Columns,” Ph.D. dissertation, Dept. of Civil Engineering, The University of Texas at Austin, May 2012.

Leiva and Klingner (1990): Leiva, G., Merryman, M., Antrobus, N. and Klingner, R. E., “In-Plane Seismic Resistance of Two-Story Coupled Concrete Masonry Walls,” *MASONRY - Components to Assemblages*, ASTM STP 1063, Philadelphia, PA.

Leiva and Klingner (1991): Leiva, G. and Klingner, R. E., "In-Plane Seismic Resistance of Two-Story Concrete Masonry Shear Walls with Openings," U.S.-Japan Coordinated Program for Masonry Building Research, *Report No. 3.1(c)-2, PMFSEL Report No. 91-2*, The University of Texas at Austin, Austin, Texas.

Lepage et al. (2011): Lepage, A., Dill, S., Haapala, M., and Sanchez, R., “Seismic Design of Reinforced Masonry Walls: Current Methods and Proposed Limit Design Alternative,” *Proceedings*, Eleventh North American Masonry Conference, Minneapolis, Minnesota, June 5-8, 13 p.

Lotfi and Shing (1991): Lotfi, H.R. and Shing, P. B., "An Appraisal of Smeared Crack Models for Masonry Shear Wall Analysis," *Computers & Structures*, Vol. 41(3), 413-425.

Marini and Spacone (2006): Marini, A. and Spacone, E., "Analysis of Reinforced Concrete Elements Including Shear Effects," *ACI Structural Journal*, Vol. 103(5), 645-655.

Massone and Wallace (2004): Massone, L. M. and Wallace, J. W., "Load-Deformation Responses of Slender Reinforced Concrete Walls," *ACI Structural Journal*, Vol.101, No. 1, 103-113.

Mehrabi and Shing (2003): Mehrabi, A.B. and Shing, P.B., "Seismic Analysis of Masonry-Infilled Reinforced Concrete Frames," *The Masonry Society Journal*, pp. 9-22.

Moehle (1992): Moehle J. P., "Displacement-based design of RC structures subjected to earthquakes," *Earthquake Spectra* 8(3):403–428.

MSJC 2008a (2008): *Building Code Requirements for Masonry Structures* (TMS 402-08 / ACI 530-08 / ASCE 5-08), The Masonry Society, Boulder, Colorado, the American Concrete Institute, Farmington Hills, Michigan, and the American Society of Civil Engineers, Reston, Virginia.

MSJC 2008b (2008): *Specification for Masonry Structures* (TMS 602-08 / ACI 530.1-08 / ASCE 6-08), The Masonry Society, Boulder, Colorado, the American Concrete Institute, Farmington Hills, Michigan, and the American Society of Civil Engineers, Reston, Virginia.

MSJC 2011a (2011): *Building Code Requirements for Masonry Structures* (TMS 402-11 / ACI 530-11 / ASCE 5-11), The Masonry Society, Boulder, Colorado, the American Concrete Institute, Farmington Hills, Michigan, and the American Society of Civil Engineers, Reston, Virginia.

MSJC 2011b (2011): *Specification for Masonry Structures* (TMS 602-11 / ACI 530.1-11 / ASCE 6-11), The Masonry Society, Boulder, Colorado, the American Concrete Institute, Farmington Hills, Michigan, and the American Society of Civil Engineers, Reston, Virginia.

Newmark and Hall (1982): Newmark, N.M. and Hall, W.J., *Earthquake Spectra and Design*, Earthquake Engineering Research Institute, Berkeley, California.

Noland (1987): Noland, J. L., “A Review of the US Coordinated Program for Masonry Building Research,” *Proc.* of the 4th North American Masonry Conference, The Masonry Society, The University of California, Los Angeles.

Orakcal *et al.* (2006): Orakcal, K., Massone, L. M., and Wallace J. W., “Analytical Modeling of Reinforced Concrete Walls for Predicting Flexural and Coupleld-Shear-Flexural Responses,” *PEER Report 2006/2007*, University of California, Berkeley, California, October.

Park and Paulay (1975): Park, R. and Paulay, T., Reinforced Concrete Structures, John Wiley & Sons.

Paulay and Priestley (1992): Paulay, T., and Priestley, M. J. N., *Seismic Design of Reinforced Concrete and Masonry Builidings*, John Wiley & Sons, Inc., New York.

Paulay, Priestley, and Synge (1982): Paulay, T., Priestley, M. J. N., and Synge A. J., “Ductility in Earthquake Resisting Squat Shear walls,” *ACI Journal,* Vol. 79, No. 4, pages 257-269.

PEER (2006): *OpenSees, Open System for Earthquake Engineering Simulation*, Pacific Earthquake Engineering Research Center, University of California, Berkeley, California.

Petrangeli *et al.* (1999a): Petrangeli, M., Pinto P. E., and Ciampi V., “Fiber Element for Cyclic Bending and Shear of RC Structures, I: Theory,” *J. Eng. Mech.*, Vol. 125, 994-1001.

Petrangeli et al. (1999b): Petrangeli, M., “Fiber element for Cyclic Bending and Shear of RC structures, II: verification,” *ASCE Journal of Engineering Mechanics*, 125(9): 1002–1009.

Priestley (1986): Priestley, M.J.N. “Seismic Design of Concrete Masonry Shear Walls.” *ACI Journal*, Vol. 83, No. 8, 58-68.

Priestley (1993a): Priestley M. J. N., “Myths and fallacies in earthquake engineering—Conflicts between design and reality,” *Proceedings* of the Tom Paulay symposium—Recent developments in lateral force transfer in buildings, ACI SP-157, pp 229–252.

Priestley (1993b): Priestley, M. J. N., "Seismic Design of Concrete Masonry Shearwalls," *ACI Structural Journal*, Vol. 83, No. 1, 58-68.

Priestley (1997): Priestley, M.J.N, "Displacement-Based Seismic Assessment of Reinforced Concrete Buildings," *Journal of Earthquake Engineering*, Vol. 1, No.1, 1997, pp 157-192.

Priestley (2003): Priestley, M. J. N., "Myths and Fallacies in Earthquake Engineering," Revisited. Pavia: IUSS Press.

Priestley and Bridgeman (1974): Priestley, M. J. N. and Bridgeman, D.O., "Seismic Resistance of Brick Masonry Walls," *Bulletin of the New Zealand National Society for Earthquake Engineering*, Vol. 7, No. 4, pages 167-187.

Priestley and Grant (2005): Priestley, M.J.N. and Grant, D.N., "Viscous Damping in Seismic Design and Analysis," *Journal of Earthquake Engineering,* 9, (Special Issue 2), 229-255.

Priestley *et al.* (2007): Priestley, M. J. N., Calvi, G. M., and Kowalsky, M. J., *Direct Displacement-Based Seismic Design of Structures*, IUSS, University of Pavia, Pavia, Italy.

Rose *et al.* (2002): Rose, B., Shing, P.B., Spacone, E., and Willam, K., "Modeling of the Shear Behavior of RC Members," *Proc.* of 7th National Conference on Earthquake Engineering, Boston, MA.

Seible *et al.* (1992): "The U.S.-TCCMAR 5-Story Full Scale Masonry Research Building Test-Preliminary Report," Report No. TR-92/01, University of California, San Diego, Department of Applied Mechanics and Engineering Sciences.

Seible *et al.* (1994a): Seible, F., Hegemier, A., Igarashi, A., and Kingsley, G., "Simulated seismic-load tests on full-scale five-story masonry building," *J. Struct. Eng.*, 120(3), 903–924.

Seible *et al.* (1994b): Seible, F., Priestley, N., Kingsley, G., and Kurkchubashe, A., "Seismic response of full-scale five-story reinforced-masonry building," *J. Struct. Eng.*, 120(3), 925–947.

Shedid *et al.* (2008): Shedid, M. T., Drysdale, R. G., and El-Dakhakhni, W. W., "Behavior of Fully Grouted Reinforced Concrete Masonry Shear Walls Failing in

Flexure: Experimental Results," *Journal of Structural Engineering*, ASCE, Vol. 134, No. 11, 1754-1767.

Shedid *et al.* (2010): Shedid, M. T., Drysdale, R. G., and El-Dakhakhni, W. W. (2010): "Seismic Performance Parameters for Reinforced Concrete-Block Shear Wall Construction," *Journal of Performance of Constructed Facilities*, Vol. 24, No. 1, 4-18.

Sherman (2011): Sherman, J. D., "Effects of Key Parameters on the Performance of Concrete Masonry Shear Walls Under In-Plane Loading," Master's thesis, Whashington State University, Pullman, Washington.

Shibata and Sozen (1976): Shibata, A. and Sozen, M., "Substitute Structure Method for Seismic Design in R/C," *Journal of the Structural Division*, ASCE, Vol.102, No. ST1, January 1976, pp1-18.

Shing *et al.* (1989): Shing, P. B., Noland, J. L., Klamerus, E., and Spaeh, H., "Inelastic Behavior of Concrete Masonry Shear Walls," *Journal of Structural Engineering*, ASCE, Vol. 115, No. 9, 2204-2225.

Shing *et al.* (1990a): Shing, P. B., Schuller, M., and Hoskere, V. S., "In-Plane Resistance of Reinforced Masonry Shear Walls," *Journal of Structural Engineering*, ASCE, Vol. 116, No. 3, 619-640.

Shing *et al.* (1990b): Shing, P. B., Schuller, M., Hoskere, V. S., and Carter, E., "Flexural and Shear Response of Reinforced Masonry Walls," *ACI Structural Journal*, Vol. 87, No. 6, 646-656.

Shing *et al.* (1993): Shing, P.B., Carter, E.W., and Noland J. L., "Influence of Confining Steel on Flexural Response of Reinforced Masonry Shear Walls," *The Masonry Society Journal*, Vol. 11(2), 72-85.

Stavridis (2009): Stavridis, A., "Analytical and Experimental Study of Seismic Performance of Reinforced Concrete Frames Infilled with Masonry Walls," Ph.D. Dissertation, University of California, San Diego, La Jolla, CA.

Stavridis and Shing (2008): Stavridis, A. and Shing, P.B., "Calibration of a Numerical Model for Masonry Infilled RC Frames," *Proc.* of 14th World Conference on Earthquake Engineering, Beijing, China.

Sullivan *et al.* (2006): Sullivan, T. J., Priestley, M. J. N., and Calvi G. M., "Direct displacement-based design of frame-wall structures," *J Earthquake Eng* 10(1), 91–124.

Takayanagi and Schnobrich (1976): Takayanagi, T. and Schnobrich. W. C.,. "Computed behavior of reinforced concrete coupled shear walls," *Report No. SRS 434*, University of Illinois, Urbana-Champaign.

Tanner (2003): Tanner, J. E., "Design Provisions for Autoclaved Aerated Concrete (AAC) Structural Systems," Ph.D. dissertation, Dept. of Civil Engineering, The University of Texas at Austin, May 2003.

Thomsen and Wallace (1995): Thomsen, J. H. and Wallace, J. W., "Displacement-Based Design of RC Structural Walls: An Experimental Investigation of Walls with Rectangular and T-Shaped Cross Sections," *Report No. CU/CEE–95/06,* Department of Civil Engineering, Clarkson University, Postdam, New York.

Vaughan (2010): Vaughan, T. P.,"Evaluation of Masonry Wall Performance Under Cyclic Loading," Master's thesis, Washington State University, Pullman, Washington.

Voon and Ingham (2006): Voon, K. C. and Ingham, J. M., "Experimental In-Plane Shear Strength Investigation of Reinforced Concrete Masonry Walls," *Journal of Structural Engineering*, ASCE, Vol. 132, No. 3, 400-408.

Voon and Ingham (2007): Voon, K. C., Ingham, J. M., "Design Expression for the In-Plane Shear Strength of Reinforced Concrete Masonry," *Journal of Structural Engineering*., Vol. 133, No. 5, 706 713.

Voon and Ingham (2008): Voon, K. C. and Ingham, J. M., "Experimental In-Plane Strength Investigation of Reinforced Concrete Masonry Walls," *J. of Struct. Engrg.*, Vol. 134(5), 758-768.

Yanez (1991): Yanez, F. V., Park, R., and Paulay, T., "Seismic Behavior of Reinforced Concrete Structural Walls with Irregular Openings," *Proc.* of Pacific Conference on Earthquake Engineering, New Zealand, 3303-3308.

VITA

Farhad Ahmadi Koutalan was born in Urmia, Iran on June 10, 1980. After graduating from NODET High School in Urmia in 1998, he entered Khajeh Nasir University in Tehran, Iran, from which he received the degree of Bachelor of Science in August 2002. He started his graduate studies at Sharif University in 2002, and completed his Master of Science degree in Structural Engineering there in December 2005. From 2003 to 2009, he was a structural engineer and project manager in TSP Engineers in Tehran, Iran, where he performed and directed a wide variety of design projects. He entered the PhD program in structural engineering at The University of Texas at Austin in January 2010.

Permanent address: 267 Shahid Mostafazadeh Dr., Bahonar Boulevard
Urmia, West Azerbaijan, 57158
Iran

This dissertation was typed by the author.